THE UNIVERSITY *of* EDINBURGH

PILOT-SCALE TESTING OF DYNAMIC OPERATION AND MEASUREMENT OF INTERFACIAL WAVE DYNAMICS IN POST-COMBUSTION CARBON DIOXIDE CAPTURE

Paul Tait

THE UNIVERSITY *of* EDINBURGH

Thesis submitted for the degree of
Doctor of Philosophy

The University of Edinburgh
School of Engineering

2017

Lay Summary

Coal and natural gas-fired power stations are expected to remain an important source of electricity generation for much of the 21st century, If burned unabated, currently-proven fossil fuel reserves will release enough CO2 to exceed the +2^{o}C limit set by 2015's Paris agreement, resulting in catastrophic global warming. Existing and future coal and gas power plants must be equipped with carbon capture & storage (CCS) technology.

The output of renewable energy sources is variable and reliant on changing weather conditions. Thermal power stations are flexible in their output and when equipped with CCS technology, which uses solvents to absorb carbon dioxide from the exhaust gas stream, can provide dispatchable, low carbon electricity to match variable demand.

A lab-scale test rig is designed and constructed to investigate gas-liquid interactions between absorbing solvent and counter-current gas flow. Measurements of liquid wave formation are made with absorbing and non-absorbing systems using a high-speed camera. These measurements can be used to validate computational fluid dynamic (CFD) models of gas-liquid interactions in absorption columns for CCS.

Two pilot-scale test campaigns are carried out to investigate the effects of varying power plant output on CO_2 capture facility. The first test campaign is carried out on flue gas from a natural gas combined cycle (NGCC) plant, the second on flue gas from pulverised coal (PC). Finally, knowledge of plant hydrodynamics and response times are used to demonstrate, for the first time, control of the plant using in-situ online measurements of solvent composition. A mathematical scale up of pilot plant results is used to investigate the potential effect of dynamic plant operations on CO_2 emissions and associated penalties.

Abstract

Flexible carbon capture and storage (CCS) has the potential to play a significant part in the decarbonisation of electricity generation portfolios which have significant penetration from intermittent renewable sources. Post-combustion capture (PCC) with amine solvents is a mature technology and is currently the state-of-the-art for CO2 emissions reduction from power stations. However, knowledge of the dynamic capture process is currently limited due to a dearth of dynamic datasets which reflect real plant operation, lack of a robust in-situ solvent analysis method for plant control and uncertainty about how changing plant design affects the response to dynamic operations. In addition, the nature of interfacial gas-liquid dynamics inside the absorber column are not well known and rely on correlations for effective mass transfer area and liquid holdup which may have uncertainties of up to +/- 13%. This could result in absorption columns being improperly sized for CCS operations.

Two pilot-scale test campaigns are implemented in order to gain an understanding of how the capture plant responds to dynamic operations, the first on natural gas combined cycle (NGCC)-equivalent flue gas, the second on pulverised coal (PC)-equivalent. Changes in flue gas flow rates and steam supply which are designed to be representative of PCC operation on real NGCC and PC plant are implemented, using 30%wt monoethanolamine (MEA) as absorbent in both cases. Dynamic datasets are obtained for 5 scenarios with NGCC and 8 with PC flue gas. The test campaigns are carried out using two separate pilot-scale facilities and highlight the effect of plant design on hydrodynamics and hence, the response of the capture plant to dynamic operations. Finally, a novel solvent sensor is used to demonstrate, for the first time, control of the capture facility using in-situ measurements of solvent composition, combined with knowledge of test facility hydrodynamics and response times. Results from the pilot-scale test campaign are then used along with a mathematical NGCC capture plant scale-up to investigate the potential effects of dynamic operations on total yearly CO_2 emissions and the associated environmental penalties, depending on CO_2 price.

Manufacturers of column internals for CCS often rely on computational fluid dynamic (CFD) software tools for design, but existing commercial codes are unable to handle complex two-phase flows such as those encountered in the absorber column of a CO2 capture plant. An open-source direct numerical simulation (DNS) tool which will be capable of rigorously modelling two-phase flow with turbulence and mass transfer has been developed and could eventually replace the empirical methods currently used in packing design. The DNS code requires validation by experiment. For the purpose of validation a dual-purpose wetted-wall column is constructed, which in addition to mass transfer measurements can be used to determine liquid film thickness using an optical method. Measurements of average film thickness, wave amplitude, frequency, velocity and growth rate are provided for three liquid flow rates of fresh 30%wt MEA solution. Wave measurements are made with quiescent, laminar and turbulent gas flow, with and without mass transfer. These measurements can be used to validate the DNS code at its existing level of complexity, and in the future when turbulence and mass transfer are added.

Acknowledgements

First, I'd like to thank my supervisors Mathieu Lucquiaud and Prashant Valluri, who were always (okay, usually) available to give me advice and guidance on any number of issues. Mathieu always pushed me to apply for funding to go on placements which led to me spending time at Masdar Institute, Ferrybridge power station and a particularly enjoyable & useful one at the University of Texas. Thanks to both for all the advice you gave to a confused chemist who didn't have a clue what he was doing.

I'd also like to say a special thank you to Dr Marc Wehrli and Dr Ilja Ausner of Sulzer Chemtech, who allowed me full use of their absorption/desorption test facility for three weeks. You both went out of your way to make me feel welcome in Winterthur and accommodate our mad academic ideas. Similarly, thanks to Dr Kris Milkowski and Dr Muhammad Akram of the UKCCSRC'S PACT amine pilot for frequently working overtime to modify the facility on the fly and to allow me to finish off my test campaign. I hope our paper was worth it!

I'd be remiss not to mention the assistance I've had from the technical support staff at Edinburgh, not just in building things for me, but in helping me to develop my own practical skills from being just about able to wire a plug when I started. George Cairns and Gordon Paterson walked me through the design of my test rig and Derek Watson modified it multiple times for me, sometimes in the same day. Steve Gourlay and Paul Aitken from the mechanical workshop were also a massive help with the design of my wetted-wall column contactor which must have gone through, at a conservative estimate, four or five different design iterations. Cheers folks!

I also learned a huge amount from my fellow PhD students and postdocs, either by discussing problems with them or via osmosis from listening on other conversations. Bill Buschle and I collaborated on a few projects over the course of my PhD and I owe him and Roger Watson big-time for help with Labview programming and digital communications. Olivia, Laura, Maria, Thomas, Erika, Nacho and all the others also deserve a shout out for being more than willing to discuss problems with me or just chill out and chat some nonsense every once in a while.

Finally, you don't get through a PhD without *some* kind of distraction from the academic bubble so I'm eternally grateful to all the folks from back home who kept me sane over the years. There are too many of you to list but going to Wick Academy games, camping trips, playing guitars and singing karaoke in the Camps Bar were all hugely welcome distractions whether I was feeling fine or like hell with regard to my PhD work. Last but by absolutely no means least, my Mam and Dad who have offered me nothing but support through what is now eleven years of higher education.

This thesis isn't dedicated to anyone in particular, but if it were it'd be to my family and friends, and my dog Ted. A great bunch of lads.

Declaration

Unless explicitly stated the work presented in this thesis is the work of the author, and has not been submitted for the partial or full completion of any other professional qualification.

Parts of this work have previously been published in:

1. The International Journal of Greenhouse Gas Control, Issue 48, Pages 216-233.
2. The International Journal of Greenhouse Gas Control, Issue 71, Pages 253-277.

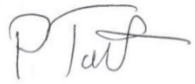

Paul Tait

Contents

List of Figures

List of Tables

Chapter 1 - Introduction

1.1 Climate Impacts in the 21st Century

Atmospheric levels of CO_2 and other greenhouse gases, including N_2O and CH_4, have risen consistently since the industrial revolution as a direct result of human industrial and agricultural activity. The average daily atmospheric CO_2 concentration was recorded, for the first time, at greater than 400ppm on May 9th, 2013, at the Mauna Loa observatory in Hawaii. Global averages are expected to remain above this concentration year-round by 2017 (Jones, 2013), an increase of approximately 40% since pre-industrial times. The effect of CO_2 on global temperatures is net positive and is well documented, with anthropogenic CO_2 emissions resulting in an additional 1.33 – 2.03 W/m^2 of radiative forcing since 1750 (IPCC, 2013). This is a considerable proportion of the total anthropogenic contribution to radiative forcing since 1750, which – including all other greenhouse gases and negative effects due to aerosol emissions – is around 2.29 W/m^2. This has resulted in a net increase in average global surface temperatures of 0.85°C from 1880-2012 (IPCC, 2013). While each individual CO_2 molecule emitted has a lifetime in the atmosphere of approximately 5 years, natural CO_2 sinks and the atmosphere exist in equilibrium, resulting in an additional CO_2 molecule being present in the atmosphere for up to 100 years (IPCC, 2007). After 100 years, 80% of emitted CO_2 molecules will be absorbed by a sink, with the remaining 20% potentially lingering for millennia. Thus, all past and present CO_2 emissions have long-lasting impacts on the climate.

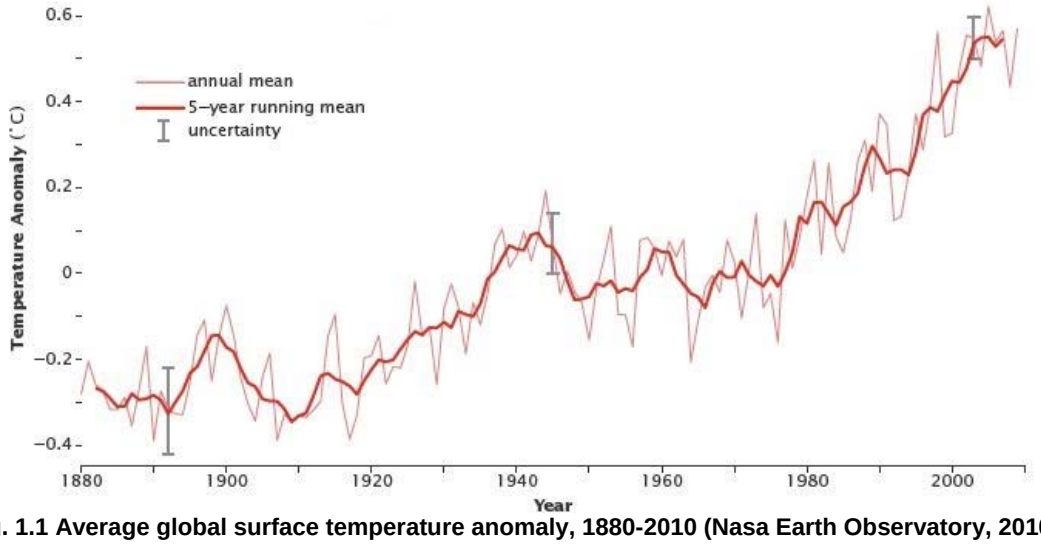

Fig. 1.1 Average global surface temperature anomaly, 1880-2010 (Nasa Earth Observatory, 2010).

Current trends suggest that the world is, at the time of writing, locked into an average temperature increase of around +1.5oC relative to the pre-industrial era even with immediate, drastic action to curb emissions (World Bank, 2014). Even this level of warming is likely to have considerable impacts on both the natural world and human society, with the developing world being particularly at risk (World Bank, 2014).

Global climate talks at the 2015 UN Climate Change Conference in Paris have resulted in the adoption of a global +1.5oC target with an absolute limit of +2oC, which will require rapid, deep decarbonisation to limit the release of greenhouse gases. For 2oC of warming to take place the total carbon budget since pre-industrial times is estimated as 1000 Gt of CO2, with a confidence level of 66% (IPCC, 2013). If only the warming effect of CO2 is taken into consideration, this means that 80% of currently proven coal reserves, 50% of gas reserves and 30% of oil reserves must either remain unburned or have their associated CO2 emissions captured (Jakob & Hilaire, 2015) to avoid catastrophic warming. Emissions of other greenhouse gases including CH4 and N2O reduce the budget yet further.

1.2 Future Energy Demand

Current greenhouse gas emissions by sector and gas type are shown in Figure 1.2.

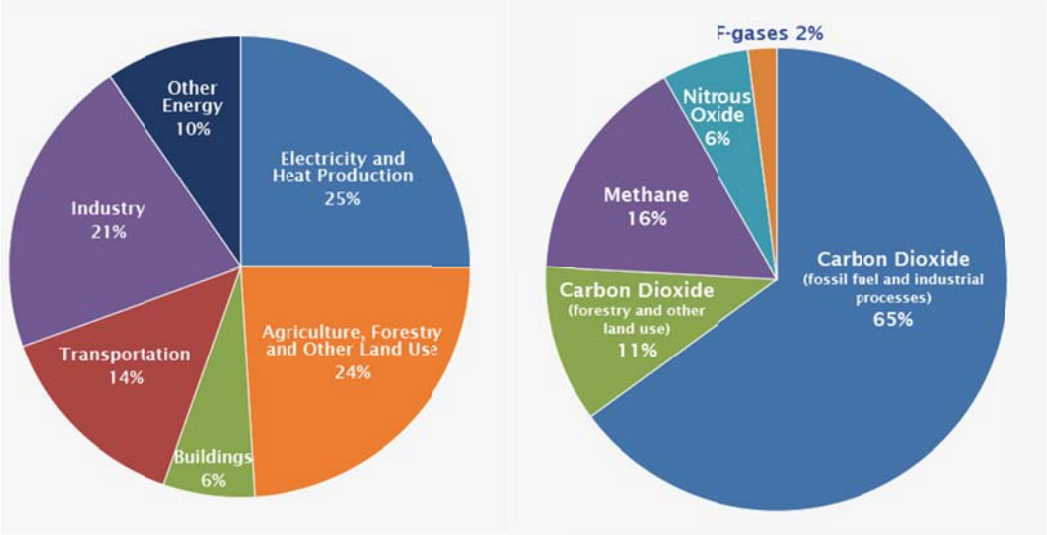

Fig. 1.2a – Global greenhouse gas emissions by sector (IPCC, 2014).
Fig. 1.2b – Global greenhouse gas emissions by gas (IPCC, 2014).

As electricity and heat generation comprises 25% of total greenhouse gas emissions, the decarbonisation of this sector is essential if catastrophic warming is to be avoided. Current trends suggest that worldwide electricity demand will continue to increase over the next century, with sources of energy such as coal and natural gas remaining important to economically-developing regions and those which rank among the worst polluters per capita, as fossil fuels remain relatively cheap, can be deployed rapidly and are dispatchable on demand (IEA, 2012). Despite the rapid growth of renewable energy sources they remain a small fraction of total electricity generation capacity worldwide (fig. 1.3).

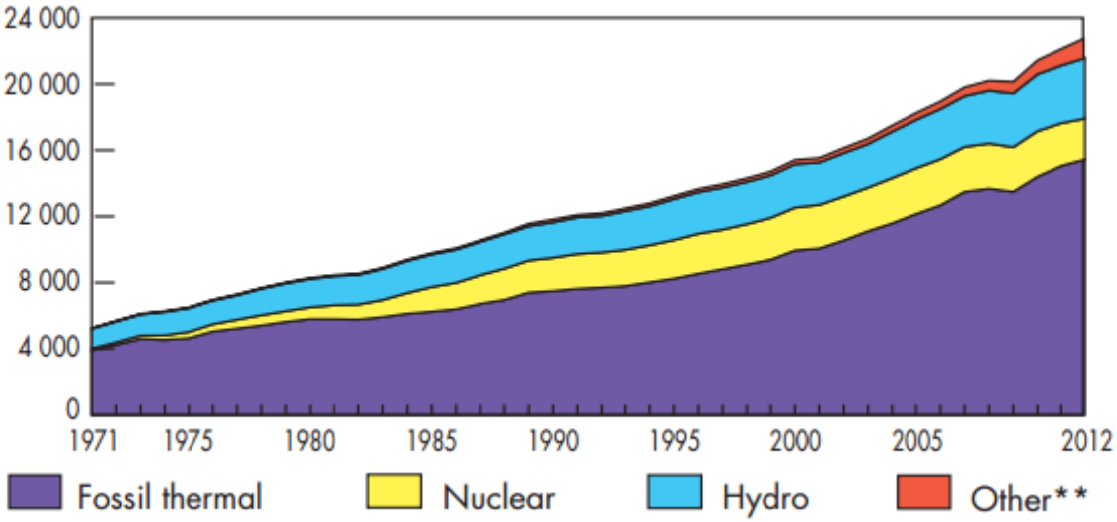

Fig. 1.3. World electricity generation by fuel source, TWh, 1971-2012. (IEA, 2014)
"Other" comprises geothermal, solar, wind and other renewables.

Renewable sources of energy such as solar and wind bring with them the issue of intermittency. Although the use of smart grids can potentially mitigate some of the impact of intermittent generation, as of 2016 the only current solution for dealing with the problem of renewable intermittency is to ramp up the output from thermal sources. It is clear that in any energy portfolio which has significant penetration from intermittent, renewable sources, peaking plants which are able to rapidly respond to changes in electricity demand will be required. A

study which assumes a hypothetical 43GW of installed wind capacity on the UK electricity grid illustrates how intermittency can affect the dispatch patterns of other energy sources (Pöyry, 2009).

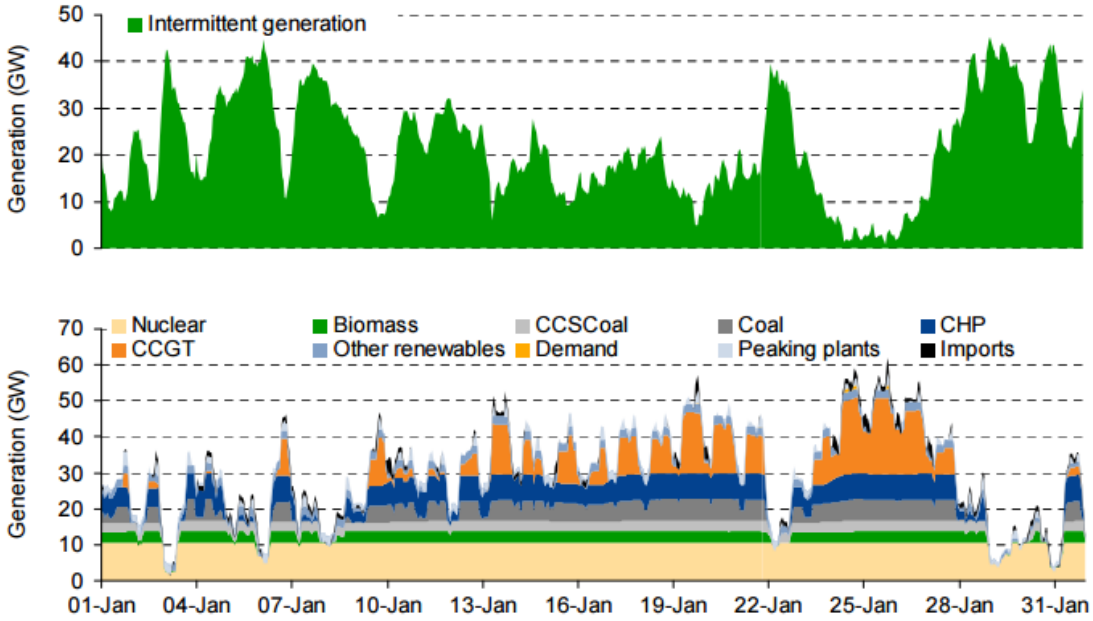

Fig. 1.4. Generation from 43GW installed wind capacity* (top), and UK energy demand (bottom) over the course of 1 month (Pöyry, 2009).
Model uses weather patterns from January 2000

Barring a technological breakthrough resulting in mass deployment of large-scale energy storage technology, combined with massive deployment of renewables worldwide, thermal power stations will continue to play a significant role in power generation throughout the 21st century. If any meaningful progress is to be made on decarbonising the power generation sector, their emissions must be eliminated. Carbon capture and Storage (CCS) can be used as a bridging technology over the course of the 21st century until truly sustainable, clean energy systems can be developed. CCS on coal, gas or biomass-fired power generation facilities can also provide dispatchable, low-carbon energy on demand, filling in for intermittent renewable sources when they are unavailable (fig. 1.4). The 5th assessment report of the IPCC states that without CCS, only 4/10 potential scenarios will succeed in limiting warming to within the +2°C limit (IPCC, 2014).

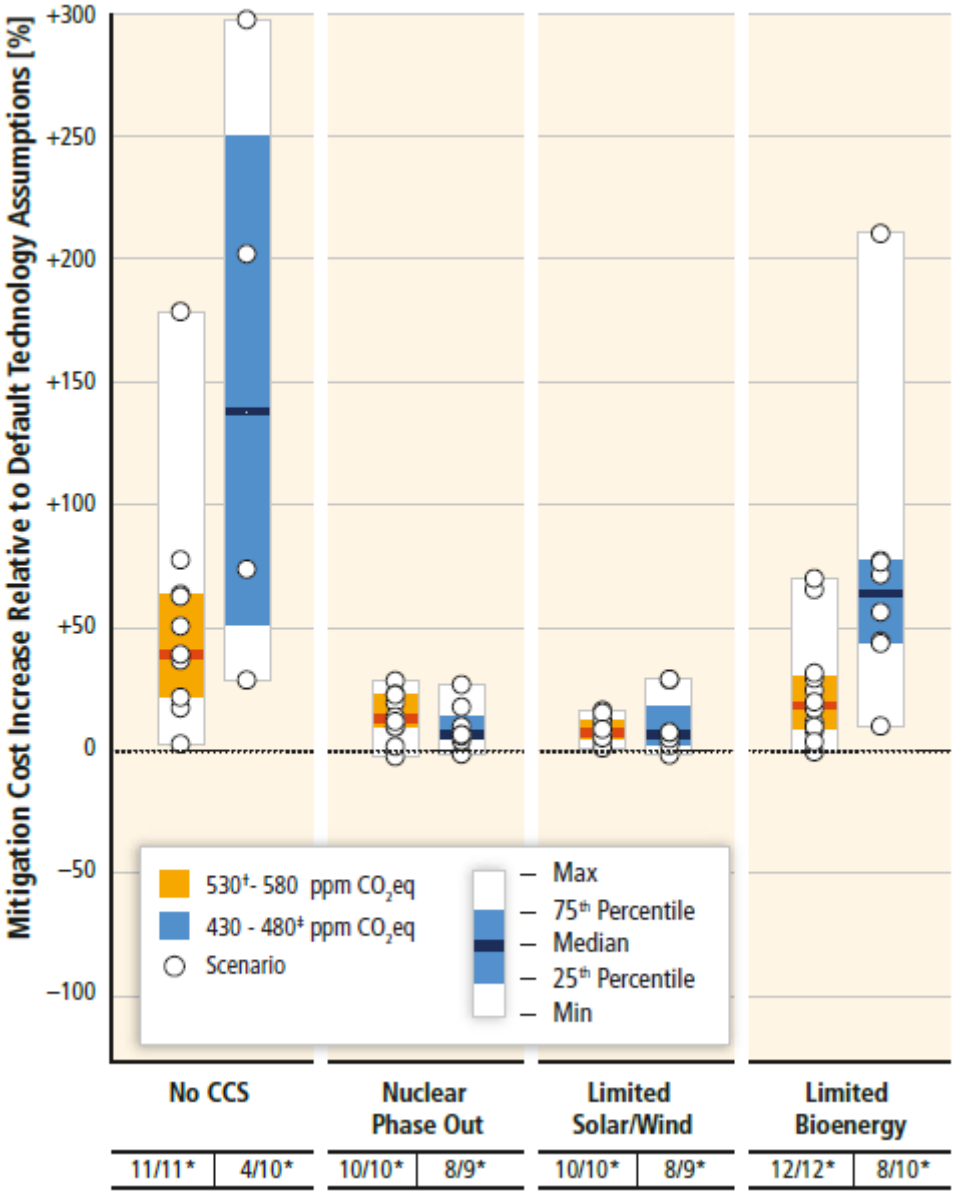

Fig. 1.5: Costs of mitigation relative to default technology assumptions, in the absence of one low-carbon technology (IPCC, 2014)

The report also shows that for the 480ppm CO_2 limit, the median mitigation cost in the absence of CCS is approx. 140% higher than when all available technologies are considered (fig. 1.5). If policy is able to successfully drive the mass-deployment of CCS on coal and natural gas plant, chances of meeting the 2°C target affordably will be significantly increased.

1.3 CCS Technology

Carbon Capture and Storage (CCS) as applied to electricity generation allows the majority of harmful CO_2 emissions from the burning of coal, biomass and natural gas to be eliminated. The challenge lies in obtaining a pure outlet stream of CO_2 for compression from an exhaust flue gas of approx. 3-4% for natural gas and 10-14% for coal-fired power stations. At present there are several proven technologies which can achieve this.

Although other technologies including pre-combustion and oxyfuel capture exist and have been proven at pilot-scale, this work focuses on post-combustion capture using amines. This is a mature and proven method of capturing CO_2. In post-combustion capture (PCC) the exhaust gas from the generation plant is pre-treated to remove particulates, sulphates (SO_x) and nitrates (NO_x). The treated flue gas is introduced counter-currently to the amine solvent in an absorber column which removes the majority of the CO_2 from the flue gas.

The desired percentage of CO_2 capture rate is dependent on economic factors such as electricity selling price and carbon price, but most PCC studies aim for between 80-90% removal of CO_2 from the flue gas stream. The absorbing solvent, now loaded with CO_2, is pumped into a desorber column via a rich/lean solvent heat exchanger, the purpose of which is to minimise the heating duty required for rich solvent entering the desorber and cooling duty for lean solvent entering the absorber. The solvent is heated in the reboiler using steam taken from the crossover pipe between the intermediate and low-pressure turbines of the steam cycle (Lucquiaud and Gibbins, 2011), liberating gaseous CO_2. A condenser removes water from the gas stream before the CO_2 is compressed and pumped off-site for storage or utilisation.

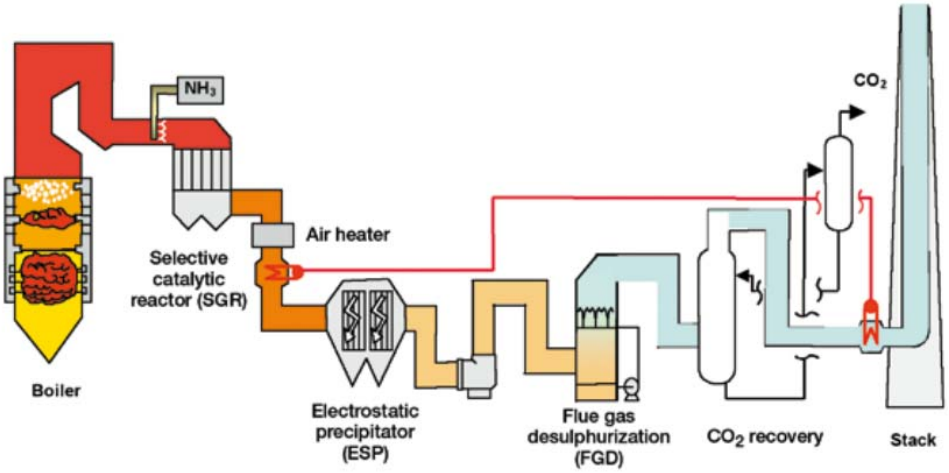

Fig. 1.6 – Schematic diagram of PC plant fitted with amine-based CCS (IPCC, 2005)

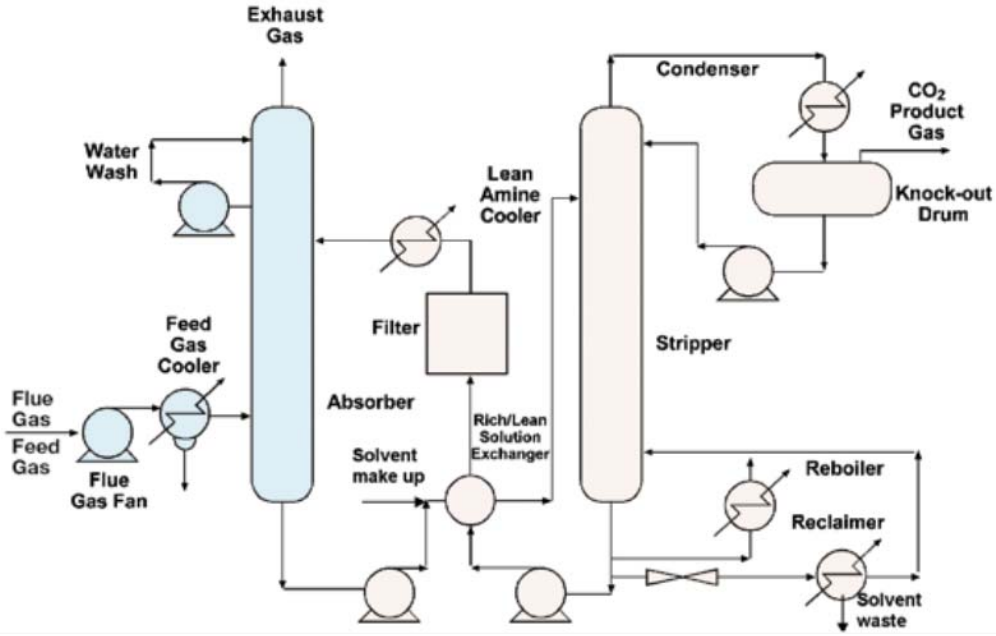

Fig. 1.7 – Schematic diagram of post-combustion capture amine plant (IPCC, 2005)

Figure 1.7 is a generic schematic diagram of a post-combustion capture (PCC) plant. Flue gas which has passed through a flue gas desulfurization (FGD) and in the case of coal flue gas, an electrostatic precipitator to remove particulates, is cooled and enters the bottom of the absorber column. In the absorber it comes into contact counter-currently with a solvent which absorbs the majority of CO_2 from the flue gas stream, in general the target is 80-90% removal efficiency. The scrubbed flue gas exits through the top of the absorber to atmosphere. The absorbing solvent, which is now rich in CO_2, is pumped through a rich/lean heat exchanger to increase its temperature and into the top of the stripper column. The stripper column uses steam, usually extracted from the inlet of the low-pressure steam turbine, to feed the reboiler and strip CO_2 from the rich solvent. The gaseous

mixture of CO_2/H_2O passes through a condenser to remove water, producing a CO_2 product gas with >99% purity. The regenerated lean solvent is pumped from the stripper outlet back to the absorber inlet to absorb more CO_2 from flue gas.

At the time of writing, post-combustion capture (PCC) using amines is only technology with an operational demonstration-scale project; the 120MW SaskPower Boundary Dam project in Saskatchewan, Canada which became operational in late 2014 (GCCSI, 2014). Although the plant has experienced outages due to generation plant shutdowns and design flaws with the capture facility, the knowledge and experience gained from the construction and operation of this first-of-a-kind (FOAK) facility will be crucial for the continued deployment of CCS. A continually-updated database of CCS projects (MIT, 2015) suggests that several further demonstration-scale PCC facilities are due to become operational by 2020 in the Netherlands (ROAD CCS Project, PC, 250MW), Texas (Petra Nova, PC, 240MW), the United Arab Emirates (Taweelah, NGCC, TBC) and China (Sinopec Shengli, PC, 101-250MW). Although demonstration-scale projects for amine-based PCC exist, research into the improvement of the process is ongoing among academics and industry.

1.4 Research Questions and Scope

Increased grid capacity from non-dispatchable, intermittent sources including wind and solar power will require fossil thermal power stations to change the way they operate, with flexibility of generation plant output being of increased importance. To increase its attractiveness to operators and facilitate deployment on the massive scale required, post combustion CCS must be able to respond to changing generation plant output in a manner which is economically, environmentally and operationally optimised.

Several gaps in existing knowledge must be addressed for the successful deployment of flexible post-combustion capture. At present, it is not well understood how the capture plant can most effectively respond to changes in process variables which are representative of real fossil thermal plant operation, or how differences in capture plant construction affect its optimal operation. A robust method for the rapid determination of solvent CO_2 loading, an important plant control variable for dynamic operation, does not yet exist. On a smaller scale, the interfacial dynamics of gas-liquid interactions in the absorber must be more comprehensively understood as at present, the empirical correlations used for the sizing of absorption columns contain large uncertainties (up to +/- 30%). Direct numerical simulations (DNS) of gas-liquid flows have the potential to model the complex interactions inside the absorber rigorously to facilitate more accurate sizing, but these models must be validated by experiment.

The work described in this thesis uses experimental studies at lab and pilot-plant scale to:

- Design and construct a test rig which can be used to observe the development of the interface for counter-current gas-liquid flows.
- Confirm the suitability of the test rig for DNS model validation by making interfacial wave measurements with laminar and turbulent gas flows, both with and without mass transfer.
- Implement test campaigns at pilot-plant scale to observe the effect of changes in plant parameters which are representative of real coal and natural gas plant operation.
- Identify any potential barriers to dynamic operation capture plant operation.
- Test the functionality of a novel online solvent sensor designed by Buschle (2015) in its ability to provide in-situ, continuous measurements of solvent CO_2 capacity.
- Identify potential new metrics for plant control, during dynamic operation.

1.5 Original Contribution

The experimental work in this thesis is separated into two areas, the first of which involves the design, construction and operation of a wetted-wall column for the future validation of DNS code, the second of which describes two pilot-scale dynamic test campaigns. A clear contribution to existing literature is Tait et al. (2016), which describes a pilot-scale test campaign on natural gas combined cycle (NGCC) equivalent flue gas with parameter changes which are designed to represent NGCC operation. The thesis expands on and refines the conclusions reached via the implementation of another test campaign on pulverised coal (PC)-equivalent flue

gas at a second pilot-scale test facility. The following could be considered original contributions to knowledge of dynamic PCC operations:

- Wave Measurement Experiments
    - Development of an experimental method which will allow DNS modelling practitioners to validate their code at its current level of complexity, and with the addition of mass transfer and turbulence in the future.
    - The measurement of wave velocity, length, frequency and growth rate with a relevant solvent for CCS operations (30%wt monoethanolamine) in the presence of quiescent, laminar and turbulent counter-current gas flows.
    - Validation of a low-dimensional thin film model using experimentally measured wave film profile data.
- Pilot-Scale Testing
    - Thirteen datasets in total are obtained for scenarios which are designed to be representative of real capture plant operation – five on NGCC and eight on PC-equivalent flue gas.
    - The use of two pilot-scale test facilities allows for qualitative comparisons to be made between how their respective designs affect their response to dynamic operations.
    - Active management of solvent inventory and reboiler heat input, combined with continuous in-situ measurements of solvent CO_2 loading and knowledge of future changes in generation plant output are identified as key metrics for the achievement of optimised capture plant operation.
    - Continuous online solvent measurements are used to predict solvent CO_2 loading at the absorber inlet. This is used to demonstrate, for the first time, control of the CO_2 capture rate using an online solvent sensor.
    - A mathematical plant scale-up based on the proposed Peterhead CCS project is performed and the effect of plant design and operating solvent volume on response times at full-scale are investigated. Plant operators can use active control of lean solvent inventory to optimise plant response times based on the operating environment of the capture facility.
    - Pilot-scale results are used to make a first-order estimation of how much additional CO_2 is released during a start-up operation if plant response times are increased due to having a large lean solvent inventory. The total CO_2 per year for a plant operating in a two-shifting or double two-shifting operating regime is calculated, and an indication of the associated additional emissions costs are provided. This is intended to highlight the importance of plant response time on operating costs.

1.6 Thesis Overview

The thesis comprises eight chapters. Their contents are summarised below.

Chapter 2 provides a review of existing literature on the dynamic operation of post-combustion CO_2 capture, including dynamic modelling, plant control and the current state-of-the-art for rapid solvent composition measurement. A critique of our current understanding of gas-liquid interactions between amine solvents and flue gas is provided and the reasons for large uncertainties in the sizing of absorption columns are discussed.

Chapter 3 describes the design and construction of the wetted-wall column apparatus.

Chapter 4 describes wave measurements using the wetted-wall camera and a high-speed camera. The method is discussed in detail. A “base case” is established, in which the wetted surface is observed at 4 locations along the column length using unloaded 30% w/w MEA, three liquid flowrates and no counter-current gas flow. This process is repeated with both counter-current N_2 and counter-current CO_2 at two flow rates. The length, velocity, frequency and growth rate of the waves at each gas-liquid condition is provided.

Chapter 5 describes a pilot-scale test campaign carried out using an absorption/desorption test facility at Sulzer Chemtech. Changes in flue gas flow rate and reboiler steam flowrate which are designed to be representative of

a natural gas combined cycle (NGCC) power station operating in an electricity generation portfolio with significant penetration from intermittent renewable sources are implemented, and the response of critical plant parameters is observed. These scenarios include a shutdown-startup coupling and three enhanced flexibility scenarios – two capture bypass events and one frequency response. Solvent circulation times and mixing are found to have a significant effect on plant response to dynamic operation. The test campaign also demonstrates real-time measurement of lean solvent CO_2 loading using a device designed by Buschle (2015).

Chapter 6 describes a subsequent pilot-scale test campaign which is implemented at the UK Carbon Capture Research Centre's PACT amine pilot facility, on coal-equivalent flue gas, which utilises the lessons learned from the previous test campaign to inform the direction of the experimental programme. Nine dynamic scenarios are implemented, including two shutdown-startup couplings, a load-following scenario, a frequency response and two capture bypass scenarios. Where available, two online solvent sensors are used to provide continuous measurements of solvent composition. Finally, control of the plant using continuous lean solvent loading measurements in conjunction with knowledge of plant hydrodynamics and response times is demonstrated.

Chapter 7 discusses the potential impact of plant design and construction on its ability to respond to dynamic operations. Two cases are considered – a compact capture plant in which the absorber and desorber are located close to each other, and a non-compact plant where due to planning considerations, there is some considerable distance between the two. Via control of the working volume of solvent in the main solvent tank, plant operators are able to adjust lean solvent circulation times to optimise the response of the capture facility.

Chapter 8 provides a summary of the work and recommendations for future research.

References

Department of Energy and Climate Change (2014). Life Cycle Impacts of Biomass Energy in 2020. DECC: London, United Kingdom.

Hoegh-Guldberg, O. (1999). Climate change, coral bleaching and the future of the world's coral reefs. *Marine Freshwater Research,* 50, 839-866.

Harvey, L.D.D and Huang (1995). Evaluation of the potential impact of methane clathrate destabilization on future global warming. *Journal of Geophysical Research,* 100, 2905-2926.

International Energy Agency (2012).*World Energy Outlook 2012*. OECD/IEA: Paris,France.

International Energy Agency (2012). *CO_2 Emissions from Fuel Combustion Highlights.* OECD/IEA: Paris, France.

International Energy Agency (2013). *Workshop Report 2013 – CCS in Industrial Applications*. OECD/IEA: Paris, France.

International Energy Agency (2014). *Key World Energy Statistics*. OECD/IEA: Paris, France. IPCC (1995). *Climate Change 1995: Second Assessment Report of the Intergovernmental Panel on Climate Change*. Cambridge University Press: Cambridge, UK

IPCC (2007). *Climate Change 2007: Fourth Assessment Report of the Intergovernmental Panel on Climate Change.* Cambridge University Press: Cambridge, UK

IPCC (2013). *Climate Change 2013: The Physical Science Basis. Fifth Assessment Report of the Intergovernmental Panel on Climate Change.* Cambridge University Press: Cambridge, UK

IPCC (2014). *Climate Change 2014: Fifth Assessment Report of the Intergovernmental Panel on Climate Change*. Cambridge University Press: Cambridge, UK

Jakob, M. and Hilaire, J. (2015). Climate Science: Unburnable fossil-fuel reserves. *Nature,* 517, 150-152.

Jones, N. (2013). Troubling milestone for CO2. *Nature Geoscience*, *6*(8), 589-589.

Nasa Earth Observatory (2010). *Global Warming* [online]. Available at: http://earthobservatory.nasa.gov/Features/GlobalWarming/page2.php [Accessed Dec 2015]

Pöyry, 2009. *Impact of Intermittency, How Wind Variability Could Change the Shape of British and Irish Energy Markets*. [.pdf] Available at: <www.poyry.co.uk/sites/www.poyry.uk/files/IntermittencyMethodologyv1_0.pdf> [Accessed Jan 2016]

World Bank (2012). *Turn Down The Heat: Why a 4°C Warmer World Must Be avoided.* World Bank: Washington D.C., United States of America.
World Bank (2014). *Turn Down The Heat: Confronting the New Climate Normal.* World Bank: Washington D.C., United States of America.

Chapter 2 – Literature Review

2.1 CCS Cost Reduction

Along with the initial capital expenditure related to building the capture plant, the most significant cost associated with building a new CCS power plant or retrofitting an older one is the loss of generation capacity. The addition of PCC using 30% w/w monoethanolamine (MEA) as a base-case scenario is predicted to result in a percentage point loss in efficiency of 9% for coal and 8%for natural gas, as of 2020 (Mac Dowell and Staffell, 2016). If CCS is ever to be deployed on the scale necessary to avoid dangerous warming the technology must be made more attractive to potential operators by reducing the energy penalty.

In post-combustion capture the energy penalty is strongly tied to the choice of absorbing solvent. Early efforts into developing alternatives to MEA focused on obtaining a low heat of absorption. One may anticipate that a low ΔH_{abs} would require less energy for regeneration, reducing the reboiler heat duty and therefore, the energy penalty. However, focusing only on the heat of absorption does not take into account the other thermodynamic processes involved with the liberation of CO_2. Oexmann and Kather (2010) describe the mass-specific reboiler heat duty (i.e. GJ/tCO_2) using three separate terms.

$$q_{reb} = q_{sens} + q_{vap,H_2O} + q_{abs,CO_2} \tag{2.1}$$

Where the total reboiler energy required is made up of 3 terms, the sensible heat required to bring the solvent up to temperature, the heat required to vapourise of H_2O and the heat required to desorb CO_2 from the amine. The authors conclude that solvents which have low energy of absorption can benefit from desorption at lower temperatures and pressures, meaning lower-quality steam can be taken from the generation cycle. However, low-pressure regeneration has the added effect of increasing the energy required for CO_2 compression. It is important to consider the effects on the entire process when selecting or designing an absorbing solvent. In practice, solvents with relatively high heat of absorption and fast kinetics such as 30% w/w MEA or 40% w/w Piperazine (Rochelle et al., 2011) tend to be regarded as the benchmark against which other solvents are evaluated.

The nature of the absorbing solvent can have a significant effect on costs related to solvent degradation, which can account for up to 22% of the total operational costs with 30% MEA (Abu Zahra et al., 2007). Exposure to O_2 and acidic trace species in the flue gas stream including NO_x, SO_x and HCl can lead to the formation of heat-stable salts (Supap et al., 2011; Dumée et al., 2012), some of which are capable of corroding the plant construction materials (Tanthapanichakoon and Veawab, 2006). This can lead to the liberation of metal cations which will further increase the rate of degradation. Prolonged exposure to reboiler temperatures greater than 100^{o}C also contributes to the thermal degradation of amines (Rochelle, 2012).

The addition of degradation inhibitors can further prolong the life of solvents (example: Sexton and Rochelle, 2009) and heat-stable salts can be partially recovered using specialised ion-exchange resins, electrodialysis or distillation (Dumée et al., 2012). The oxidative and thermal degradation rates of amine solvents have been studied in the lab and at pilot scale at steady state, (Nielsen, 2013; Namjoshi, 2013) but the effects of repeated dynamic plant operations including start-up and shut-down are not well known, as most pilot-scale facilities operate at steady state and the operating time typically required to obtain degraded solvent samples is significant (>1000hrs).

Novel process configurations such as absorber intercooling (Li, 2016) and advanced stripper configurations (Frailie et al., 2013) can further reduce the energy penalty. In addition to operating economically at steady-state baseload conditions, the ability to operate flexibly and adapt to changing grid requirements, electricity prices and power plant output is likely to be critical in making PCC with amines an attractive technology for emissions mitigation.

The work presented in this thesis attempts to provide guidelines for cost reduction of CCS in terms of both operational and capital costs. Operational costs can be reduced via ensuring that the capture facility can operate flexibly, and allow the generation plant operator to tap into additional revenue streams. These include providing supplementary services to the grid such as primary or secondary frequency response, and increasing generation plant output during times where electricity selling price is high via CO_2 capture bypass. Capital costs can be

reduced via the development of new packings which promote gas-liquid interactions and CO_2 absorption rate, reducing the volume and construction cost of the absorber column.
The work presented in this thesis contributes to the advancement of operating cost reduction via pilot-scale testing to more fully understand the factors affecting dynamic operation, and to identify any serious physical barriers which may prevent capture facilities from doing so. A more complete understanding of gas-liquid interactions on structured packings via the use of computational fluid dynamic (CFD) models can allow packing developers to maximise the available contact area between liquid and gas via novel designs, enhancing absorption rate. This work describes the design, construction and initial evaluation of a wetted-wall column device which supports CFD model development by providing validation via thin-film measurements.

2.2 Flexible Post-Combustion Capture Operation

Until recently, the majority of research carried out on PCC at the time of writing has assumed that the vast majority of CCS would be deployed on baseload plant, operating at steady-state with a consistent power plant output and flue gas flowrate/composition. When plant dispatch patterns for electricity generation portfolios which include significant penetration from intermittent renewable sources are considered, it is increasingly obvious that dynamic and flexible operation will be highly relevant. Chapter 1, Fig, 1.4 (Pöyry, 2009) illustrates potential plant dispatch patterns for an example situation in which the UK has 43GW of installed wind capacity. As the deployment of low-carbon renewable technologies continues, the dispatch patterns of both gas and coal power stations become less regular, with rapid ramping, startup & shutdown operations based on variable demand and changing weather patterns becoming commonplace (Murray, 2013).
Post-combustion CCS practitioners have the ability to control capture plant process variables, adjusting the CO_2 capture rate (η_{CO2}) to a level which is optimal for current electricity selling price, fuel cost and carbon price conditions. The value in operating the CO_2 capture plant at off-design conditions in reference to a CO_2 capture rate design value of 90% is illustrated by Errey et al (2014). Depending on the nature of the market, the cost of CO_2 emissions and the electricity selling price, it may be possible to increase short-term operational profits by up to $30,000/hr via off-design operation or bypass of the capture facility.
This inherent flexibility makes PCC an attractive option for deployment on plants which may have to change their output rapidly. Although both are based on thermal fossil fuel generation, PC and NGCC plants have different operating capabilities and can provide different services to the grid, so the potential impacts and opportunities for each of them to operate flexibly, while similar, are not the same.

2.2.1 Non-steady state operations for coal and gas plant

Coal plants in general have slower ramp rates and take longer to start up and shut down than NGCC, so they are unlikely to act as peaking plants or respond to rapid changes in demand. Chalmers & Gibbins (2007) identified the three operating modes which are of foremost interest to flexible CCS operations on coal as plant startup, shutdown and load following.
The potential impacts, both advantageous and disadvantageous of flexible CCS operations on coal-fired power plants were considered by Chalmers & Gibbins (2007). Coal plants require 1.5-2.5 hours to reach their full generation capacity on a hot start (IEAGHG, 2012) and during this time will release a not-insignificant proportion of their total daily emissions. While capture at the beginning of the startup operation is not possible due to the presence of chemical species in the flue gas which will contaminate the solvent, capture should be possible in most cases once the plant has reached minimum stable generation. The addition of the capture plant can also enhance coal plant operational flexibility, as varying the rate of steam abstraction from the LP/IP crossover to the solvent reboiler allows for rapid changes in output to be made without interfering with the operation of the main generation facility.
In another paper, Chalmers et al. (2009) describe two potential hardware options which could increase the operational flexibility of CCS. The first is in the addition of a flue gas bypass valve. All or a proportion of the flue gas is redirected away from the absorber column and emitted directly to atmosphere via a secondary stack. In practice, an absorber bypass valve will be mandatory for safety reasons and to avoid contamination of the solvent below minimum stable generation, but it can also be used to implement flexible capture modes. Capture bypass can be beneficial during times when it is economically preferable to emit the CO2 and pay the carbon price rather than operate the capture system, for example, when the selling price of electricity is high. In this scenario, which is possible where the capture unit has been retrofitted or the integrated generation plant is fitted

with an oversized low pressure turbine, the steam flow to the reboiler is redirected to the low-pressure steam turbine to maximise the amount of electricity available for export. Capture bypass is shown to increase plant profitability when CO_2 price is ≤ \$40/ton during normal daytime operation, ≤ \$60/ton at peak times when the electricity selling price is double that of normal daytime operation, and with carbon prices well above \$100 for a "super-peak" when electricity selling price is 4x that of normal daytime operation.

The second hardware upgrade involves adding storage tanks which can keep a supply of solvent in reserve. This approach adds complexity to the process and will incur extra capital costs via the construction of additional hardware (Chalmers & Gibbins, 2007), but can add flexibility in a number of different ways. In the eventuality that emissions legislation prohibits extended periods of total capture bypass, or the carbon price is too high to make it advantageous, the rich solvent could be redirected to a storage tank at the base of the absorber. This allows the regeneration steam to be redirected to the low-pressure steam turbine instead, maximising the power output of the plant. A second storage tank at the top of the absorber contains a backup supply of lean solvent to ensure continual solvent flow and CO_2 capture over an extended period of time (e.g. Cohen et al., 2011; Van Peteghem and Delarue, 2014). The stored rich solvent can then be regenerated when the selling price of electricity is low, or when the plant is shut down overnight.

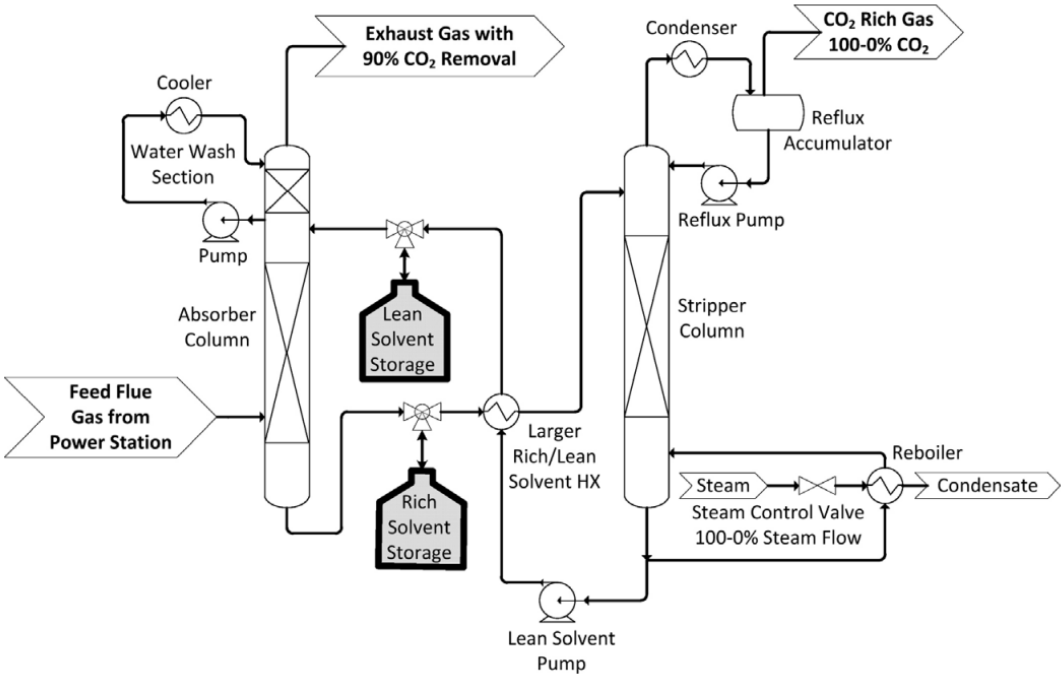

Fig. 2.1 PFD of post-combustion capture plant with solvent storage (Cohen et al., 2011)

NGCC power plants can also provide baseload energy, but have advantages over coal in that their cycling rates are much faster, since they do not require the speed of the coal grinders to be adjusted to change generation plant output. This means they can rapidly change their power output in response to variable demand. NGCC plants are likely to be used as a means of rapidly responding to changes in weather patterns in a marketplace which has heavy penetration from intermittent wind or solar power. State-of-the-art gas turbines can perform a full hot startup operation in 30 minutes (Eisfeld & Feldmüller, 2013). Using weather patterns and generation portfolio for the UK, Bruce et al. (2014) predicted that with 30GW of installed wind capacity, CCGT plants would be required to execute between 18.6 and and 85.0 hot startup operations per year, on average, depending on their position in the merit order. If these plants were to be equipped with PCC, the capture plant must be able to cope with startup, shutdown and ramping operations which would incur rapid changes in flue gas flowrate.

NGCC plants equipped with PCC can benefit from capture bypass, solvent storage and variation of steam abstraction similarly to PC plant (Domenichini et al., 2013). As oil burners are not required during NGCC startup, CO_2 capture is possible once NO_x concentration in the flue gas is sufficiently reduced by scrubbing. This offers additional flexibility in how the plant is operated during startup and shutdown.

Since the identification of the potential benefits of capture plant flexibility, researchers have used dynamic modelling techniques to investigate the impacts of flexible operation on the capture plant for coal and NGCC cases. Some pilot-scale studies have also attempted to implement dynamic scenarios, highlighting the growing relevance of this field of CCS research.

2.2.2 Modelling and implementation of dynamic operating scenarios

Researchers have used dynamic process simulation software to model the effects of flexible operation on post-combustion capture for both coal and NGCC cases. As pulverised coal plants have slower ramp rates and are more likely to operate at baseload, dynamic modelling efforts for coal cases have focused heavily on maximising profits via innovative capture plant operation, rather than reacting to changing plant output. Errey et al. (2014) describes the effect of changing electricity prices and carbon prices on the optimal capture rate, affirming that their inherent volatility requires the capture plant to be flexible in order to operate most economically. MacDowell and Shah (2014) and Flø et al. (2015) consider how solvent storage, flue gas venting (i.e. capture bypass) and variable solvent regeneration can be used to maximise operating profits during load-following operations, while maintaining an average daily CO2 capture rate close to 90%. The most effective operating strategy appears at to be dependent on the specific nature of future emissions regulations – for example, harsh penalties for sudden spikes in CO2 emissions could limit the use of flue gas venting, even if the emitted CO2 were recouped over the course of the day. Continuing uncertainty about the specifics of emissions regulations highlights the necessity for CCS plants to be constructed with flexible operation in mind.

As mentioned in section 2.2.1, for slow-ramping coal plants the addition of CCS can be used as a method to enhance operating flexibility. Wiley et al. (2010) describe how modifying the CO2 capture rate between 90-20% can be used as a means of ramping coal plant output in order to meet variable demand, while maintaining an average CO2 capture rate of around 50% over the course of 24hrs. Davison & Haines (2014) propose the use of a "stripper stop" operation to provide a rapid (<10sec) increase in power plant output in response to grid frequency demands. For NGCC plant an increase or decrease in firing rate is normally used to provide frequency response to the grid, but for PCC-equipped plants this can also be achieved by increasing or decreasing the flow of steam to the reboiler, so the plant operator has more options at their disposal. During ramping events and at part load the operator has several options available – they may choose to maintain a constant flow of steam to the reboiler, or maintain a 90% capture rate by either varying either the stripper pressure and allowing the solvent loading to change, or varying the solvent flow rate at the absorber inlet to maintain a constant absorber inlet CO2 loading (Lucquiaud et al., 2014).

The technical aspects of varying the CO2 capture level and responding to changing plant output must be considered, and there exists a considerable body of work on the dynamic modelling of the energetics and control of the capture process itself. This kind of study is highly relevant for CCS on gas plant, since modern NGCC plants are highly flexible and large changes in output (and hence flue gas flow rate) are likely to impact the capture process significantly. Changing gas and/or liquid flowrate will have knock-on effects for the entire capture process and may also lead to undesirable hydrodynamic phenomena in the absorber, such as flooding or insufficient wetting of the packing (Kvamsdal et al., 2009). The quantification of these effects is essential for the optimal operation of CCS on both gas and coal plant, and due to the complexity of dynamic events, researchers will often simplify by focusing on only one aspects of the process in great detail. Some examples of this approach include: Kvamsdal et al. (2009), which observes the evolution of CO2 partial pressure, solvent temperature and solvent CO2 loading across the absorber cross-section during start-up and load reduction. Enaasen et al. (2013) models the response of the stripper to increasing rich solvent flowrate and decreasing rich solvent loading. Examples of models which simulate the entire capture process dynamically include Ceccarelli et al. (2014) who investigate the effect of realistic dynamic operations for NGCC on plant performance, and Lawal et al. (2012) who simulate two dynamic scenarios at full scale - reducing power output and increasing capture rate to 95%. Mac Dowell and Shah (2015) and Flø et al. (2016) provide analysis on the most cost-effective method of maintaining an average 90% capture rate over a 24hr period while still capitalising on short-term increases in electricity selling price, which appears to be highly dependent on the time period over which CO2 emissions are penalised. A comprehensive discussion of recent dynamic modelling studies in PCC is presented by Bui et al (2014a), who concludes that a significant failing of current dynamic modelling efforts is a lack of real dynamic plant data against which these models can be validated. Of the 29 dynamic modelling

papers discussed by Bui et al., only 3 are validated using dynamic pilot plant data, with the majority being validated against steady-state data and several remaining unvalidated. These are: Bilyok et al. (2012), validated using step-changes in lean solvent flow rate, CO2 concentration in flue gas and inlet flue gas temperature; Lawal et al. (2012), who validate the power plant model using dynamic frequency-following events, but the capture plant with steady state data from a smaller facility than the one modelled and Posch & Haider (2013), validated using an increase in both lean solvent and flue gas inlet temperature.

It is clear that there is a lack of existing dynamic data against which researchers can validate their dynamic models. High-quality dynamic pilot data can be difficult to obtain and reproduce due to externalities such as ambient weather conditions, and differences in the timing of events due to human error. Validation via implementing scenarios which are representative of real capture plant operation is even more difficult, as these may involve changing multiple process variables with precise timing. Modelling practitioners must also have highly detailed knowledge of the capture plant, as the column and sump dimensions, surface area for heat transfer, circulation times and packing type all have a significant effect on plant performance and must be factored into the model. This makes validation of full-scale models difficult as plant data from such large facilities is not generally available for academic use. Instead, data from pilot-scale facilities is used (Kvamsdal, 2011).

Reproducible data for validation can be obtained by introducing a series of step-changes to a single plant variable (e.g. flue gas flow rate), and observing the effect on other plant parameters as it returns to steady state (Bui, 2014b). The Validation of Carbon Capture (VOCC) test rig at the Norwegian University of Science and Technology (NTNU) is specifically designed for this purpose and has been used for both dynamic and steady-state validation (e.g. Tobiesen, 2012; Kvamsdal, 2011; Enaasen Flø, 2015). Step-changes in individual (flue gas flow; lean solvent flow) and multiple simultaneous plant parameters (flue gas flow, lean solvent flow and reboiler energy input) have been investigated using the Esbjerg pilot-scale facility (Faber et al., 2011).

While process parameters such as absorber inlet and outlet CO2 concentration, stripper pressure, flue gas and solvent flow rates can all be measured in real time using widely available sensors, continuous measurement of solvent CO2 loading in real-time remains difficult. This prevents it from being used as a control variable and makes it difficult to come to definitive conclusions about how lean and rich solvent loading react to dynamic operations. Efforts to develop sensors for the real-time measurement of solvent composition are discussed further in section 2.2.3.

2.2.3 Capture plant control strategies for dynamic operation

While step-changes in single plant control variables are highly reproducible and therefore useful for the validation of dynamic models, they are not truly representative of how the plant would operate in response to changes in plant output. Optimal dynamic and part-load operation is likely to be achieved via manipulation of one or more control variables in response to changes in flue gas flow rate. Potential options include modifying the solvent flow rate and reboiler heat input to maintain a constant solvent lean loading, with sliding stripper pressure, or a constant stripper pressure with variable lean loading (Lucquiaud et al., 2014).

Advanced process control system architectures such as Model-predictive control (MPC) and fuzzy logic control are a promising alternative to single input-single output PID or cascading-PID control systems in maintaining plant operation within environmental, economic and operational boundaries (Luu et al., 2015; Mechleri, 2015). Optimisation of pilot plant operation via such strategies will require a highly detailed understanding of plant dynamics including solvent circulation times, temperature changes and the degree of solvent mixing in sumps (Tait et al., 2016). Implementing realistic dynamic operating scenarios at pilot-scale can enhance knowledge of plant-specific dynamics and gain insight into how PCC plants react to dynamic operation in general. The datasets generated may also prove useful for model validation.

Solvent amine concentration and loading have been identified as critical process variables for plant control, but the majority of pilot-scale facilities are not equipped with an online measurement system for amine concentration and CO_2 loading, instead using offline lab-based measurements which are labour-intensive and slow (Buschle, 2015; van Eckeveld et al., 2014).

Online auto-sampling with titration is less labour-intensive but anecdotal evidence suggests that it may require up to 20 minutes for analysis, during which time the solvent composition at this location may change significantly in response to dynamic operation. Taking the UK's electricity generation system as an example, response times for dispatchable energy services are: within 30mins for a load following operation, 20mins for

short-term operating reserve balancing, 2mins for fast reserve balancing and 10-30sec for a mandatory frequency response. Hypothetically, all of these services could be provided by either NGCC or PC plant fitted with PCC, via a change in firing rate or by temporarily increasing or decreasing the level of steam abstraction to the reboiler. With generation capture plant flow conditions potentially changing an order of magnitude more rapidly than solvent loading measurements can be made with the current state-of-the-art, it becomes apparent that online sensing devices for the rapid determination of solvent composition must be developed for the realisation of optimised post-combustion capture.

Online density meters have been used to provide some indication of solvent CO_2 loading (Seibert et al., 2011) but this is susceptible to changes in amine concentration via water losses, and changes in density due to amine decomposition or other impurities. Current research focuses on using multiple chemical and physical analysis methods in conjunction with a suitable multivariate model to predict solvent composition rapidly and accurately. Analysis methods may include density, viscosity, UV/visible spectroscopy, conductivity, refractive index and pH (van der Ham et al., 2014; Fandiño et al., 2016). There have also been promising developments in using Raman spectroscopy for the speciation of loaded amine solutions (Samarakoon et al., 2013; Idris et al., 2014), but Raman-based sensing devices are yet to be evaluated via deployment in a pilot-facility setting. These methods are all affected by the presence of amine degradation products and before online solvent measurement is fit for application on full-scale PCC an effective method of compensation must be devised.

2.3 Interfacial gas-liquid dynamics

The effective surface area of structured packings for mass transfer absorption depends on the nature of liquid distribution and behaviour on the packed bed. In general, the effective surface in m^2/m^3 of packing is determined experimentally using very fast reactions which can be approximated as instantaneous, for example, the absorption of CO_2 into sodium hydroxide (Puranik and Vogelpohl, 1973). The presence of semi-stagnant solvent pools in packed beds for absorption and distillation is well-established (Astarita, 1963). These regions may or may not contribute significantly to the effective interfacial mass transfer area.

2.3.1 Effect of semi-stagnant regions

Taking the absorption of dilute CO2 into NaOH as an example, Puranik and Vogelpohl (1973) posits that these semi-stagnant pools may be as effective for CO2 absorption as the moving liquid, provided the free absorbent concentration in the liquid phase is high enough so that saturation is not reached. The concentration of CO2 in the gas phase also affects the absorption effectiveness of these pools – a higher CO2 concentration results in the semi-stagnant area becoming saturated with CO2 more rapidly than the liquid in the semi-stagnant region can be replenished. The effectiveness of these pools for mass trransfer can be quantified as being proportional to the ratio of reactive to purely physical mass transfer, kL/kL0 (Pigford, 1952).

In absorbing systems where chemical reaction takes place, part of the absorbed reactant exists unreacted in solution, in equilibrium with the partial pressure in the gas phase, with the rest being converted to products as per the chemical equilibrium. The maximum absorbate capacity is dependent on the total concentration of reacted and unreacted absorbate at equilibrium and the thickness of the semi-stagnant layer (Last and Stichlmair, 2002). Chemical reaction allows the semi-stagnant pool to continue contributing to the effective surface area for absorption past the time at which it would have become physically saturated. The time required to reach chemical saturation relative to physical saturation is dependent on the reaction enhancement factor E and the Hatta number, which compares the rate of reaction to the rate of reactant diffusion through the liquid film (fig. 2.2, Last and Stichlmair, 2002).

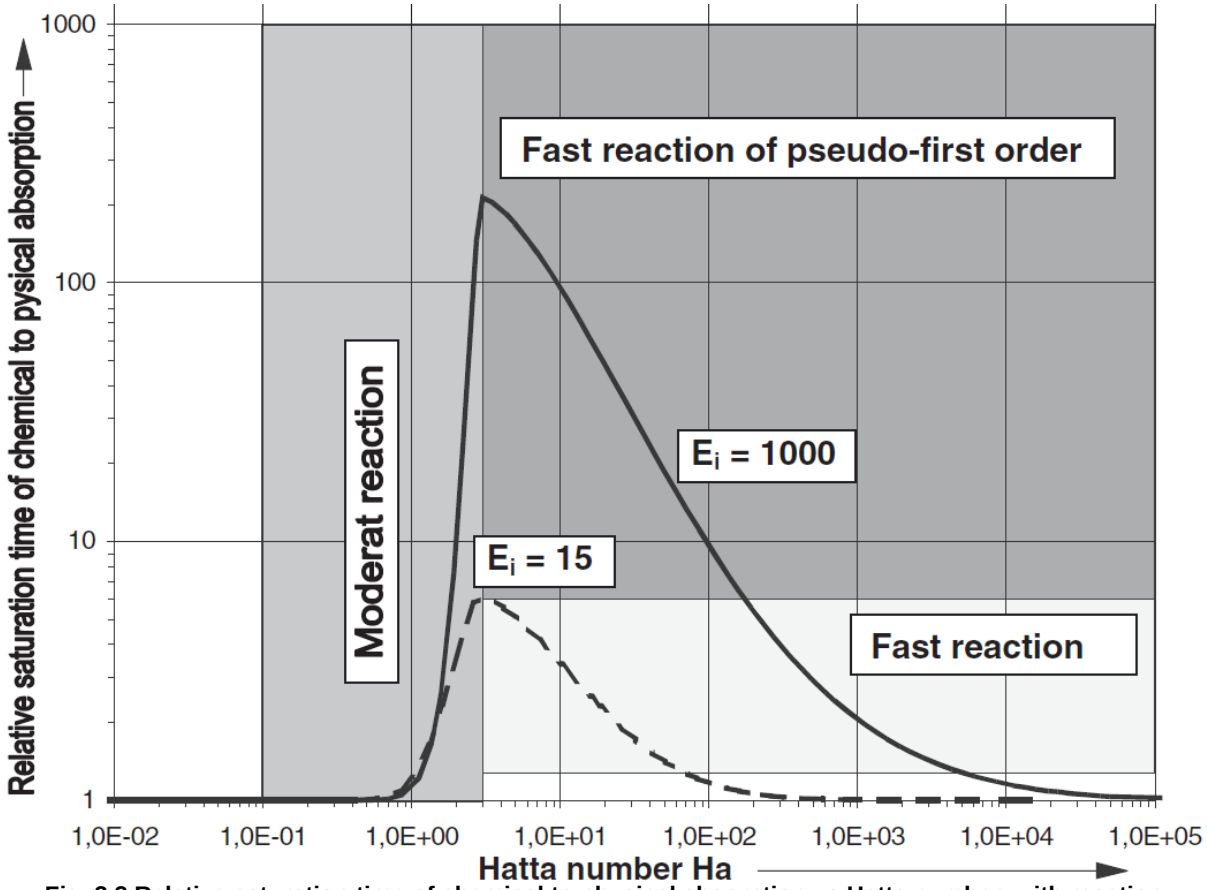

Fig. 2.2 Relative saturation time of chemical to physical absorption vs Hatta number, with reaction regimes (Last and Stichlmair, 2002)

The additional time provided by chemical reaction is greatest with large enhancement factors and a Hatta number of around 2, i.e. a pseudo-first order, fast reaction. Last & Stichlmair (2002) suggest that the fast, pseudo-first order reactions which are commonly used to characterise the effective surface area of structured packings are precisely in the range where stagnant liquid elements contribute most significantly to mass transfer, thus a large effective transfer area is determined. This may not apply to all mass transfer applications, including the absorption of CO2 by amines in CCS. This is illustrated in fig. 2.3, a comparison between the absorption of dilute CO2 from air into KOH solution (pseudo-first order reaction, large enhancement factor), and pure CO2 into 30% w/w MDEA (moderately fast reaction, lower enhancement factor). The kinetic parameter, Ki (x-axis) is a dimensionless number and is the ratio of the reaction rate constant (k2), the square of the thickness of the stagnant region (S2) and the concentration of reactants at the interface (CAI) to the diffusion coefficient of reactants through the liquid phase.

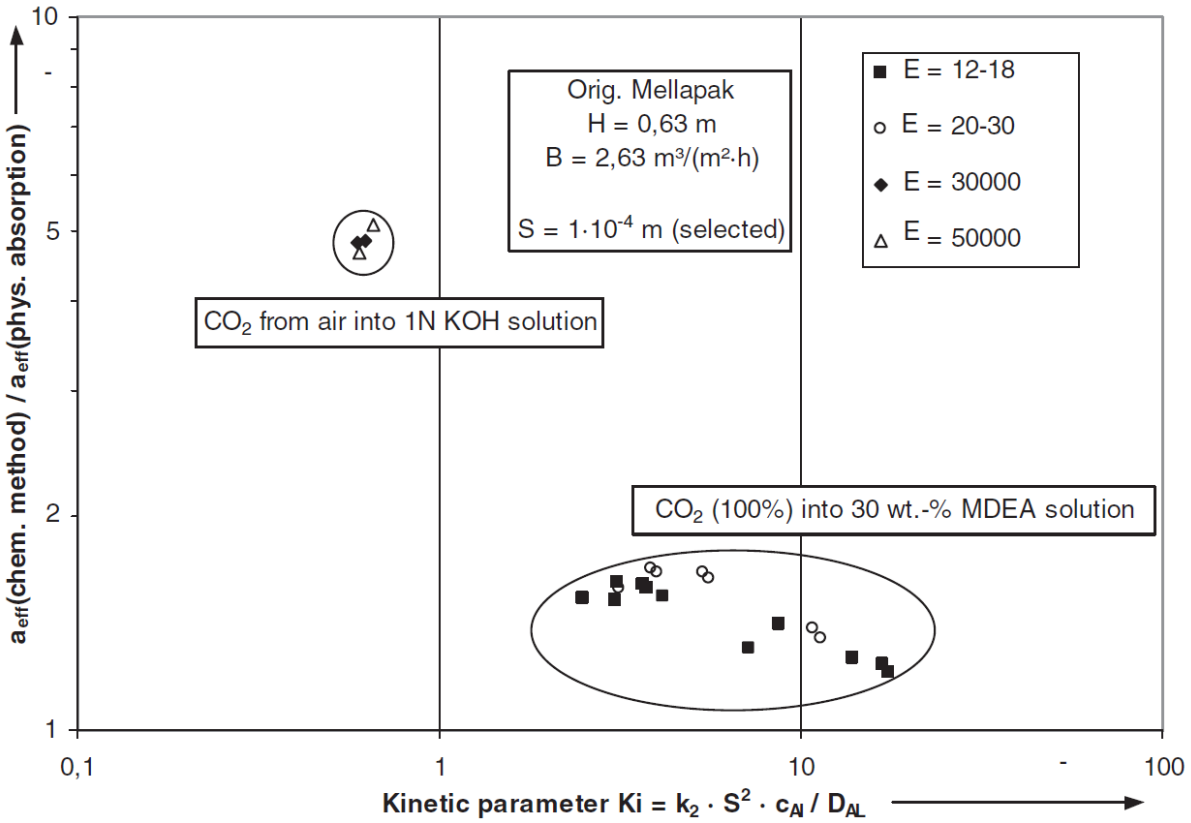

Fig. 2.3 Effective surface area vs kinetic parameter Ki (Last and Stichlmair, 2002)

The ratio of effective surface area with chemical absorption to that with only physical absorption increases by a factor of around 5 for the absorption of CO_2 from air, and a factor of around 1.5 for the absorption of pure CO_2 by MDEA. In the former case, stagnant liquid areas provide additional effective surface area for mass transfer. For gas-liquid systems in which CO_2 is absorbed using amines the nature and prevalence of these semi-stagnant areas in absorbers using structured packing is not well understood. Considering the example of CO_2 absorption from flue gas using 30% w/w MEA solution, the pseudo-first order approximation holds when the concentration of one of the reactants (free MEA in the liquid film) is in great excess and its concentration is effectively constant (Last & Stichlmair, 2002; Dang and Rochelle, 2003). However, in lower regions of the absorber the solvent becomes highly loaded with CO_2 and significant depletion of free MEA at the interface is expected (Putta et al, 2016), so the order of the reaction shifts. Moving away from this pseudo-first order reaction regime, these semi-stagnant pools become less effective for CO_2 absorption as they are more rapidly chemically saturated. The effective surface area of structured packings may be significantly over-estimated when used for CCS operations with MEA and other amines, and in other industrial processes which do not exhibit pseudo-first order kinetics, leading to the mis-sizing of packed columns for CCS operations.

2.3.2 Existing correlations for effective interfacial area

A review of previous correlations for the determination of interfacial mass transfer area is provided by Razi et al. (2012). Fig. 2.4, compares predicted effective interfacial area (y axis) against superficial liquid velocity (x axis) for a number of empirical, semi-empirical and theoretical models. The results vary greatly and are dependent on the assumptions and packing type used.

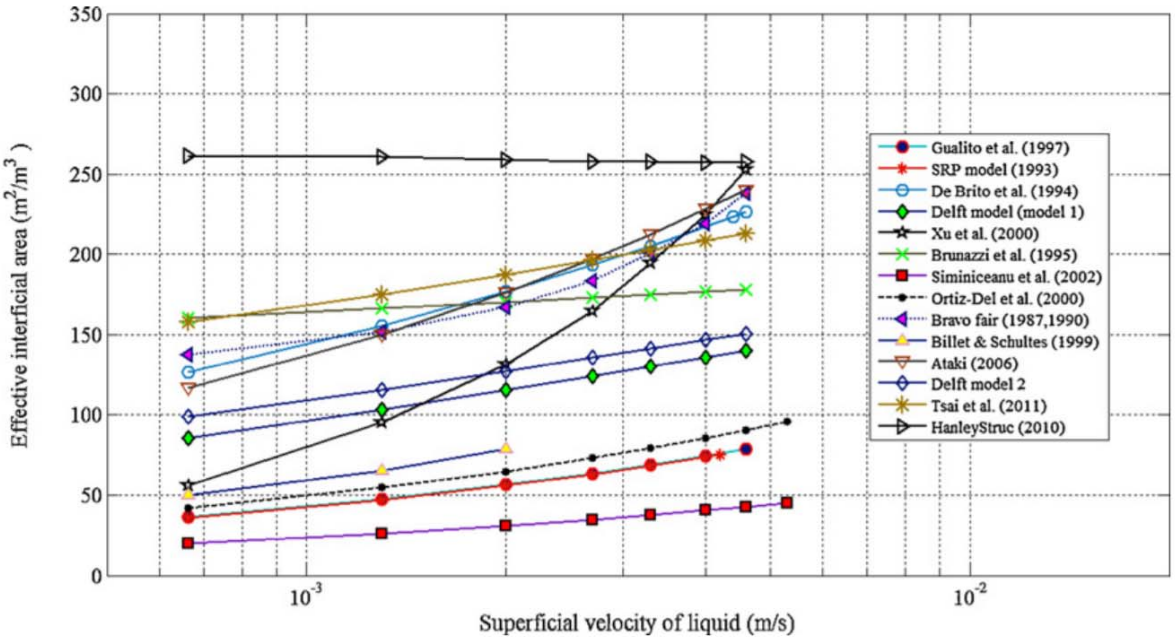

Fig. 2.4. Effective interfacial surface area correlations for flue gas from gas-fired power plant (Razi et al., 2012)

There can be large uncertainties associated with these existing models. For example, Xu et al. (2000), report +/- 20% uncertainty for a model designed to predict interfacial area for a wide range of structured packings and operating conditions. Tsai et al (2011) investigate the effect of liquid properties, packing surface area and texture on effective interfacial area for Sulzer Mellapak packings, reporting an uncertainty of +/-13%. In addition, experimental absorption data is obtained using columns which measure between 0.1-1m in diameter and there is uncertainty about the applicability of these correlations to larger absorption columns, such as those which may be constructed on a full-scale PCC plant (Razi, 2012).

The use of correlations for the sizing and construction of absorption and scrubbing columns is a well-established engineering discipline, having been studied extensively and used in industrial processes for many decades. However, absorber columns for CCS could potentially be an order of magnitude larger in diameter than those used in in comparable industrial processes, such as gas sweetening. When the comparatively huge size of these absorber columns is taken into consideration, an uncertainty in effective interfacial surface area of +/- 10% could increase the required packing volume by hundreds of cubic metres, incurring significant additional construction costs. More effective tools could provide accurate prediction of interfacial surface area for absorbing systems specific to CO_2 absorption using amines, while accounting for the potential effects of semi-stagnant pools. A greater understanding of gas-liquid interactions in amine solvent/CO_2 systems may also lead to the development of novel packings for CO_2, which maximise effective surface area and reduce the packing volume required to achieve a desired capture efficiency. Computational fluid dynamic (CFD) models could provide the solution.

2.3.3 Direct numerical simulations

Currently available commercial CFD simulation tools such as ANSYS do not incorporate mass transfer, so are insufficient to predict the rate of replenishment and mixing in these semi-stagnant pools. Current research efforts focus on developing code which implements mass transfer using existing commercial CFD packages (Saez, et al. 2015) and direct numerical simulation (DNS) of the gas-liquid flow system (O Naraigh et al., 2014; Schmidt et al., 2016). At present, due to high computational costs DNS is limited to observing wave formation in gas-liquid cells in which no mass transfer takes place and the gas flow is laminar (see fig 2.5), but in future it could be used to model a 3d cell of structured packing with turbulent gas flow and mass transfer, in order to determine the replenishment rate and effect of the previously-discussed semi-stagnant pools and the true effective surface area for mass transfer. This will allow packed columns for industrial applications, including CCS, to be more accurately sized.

Ongoing research efforts involve adding turbulence and purely physical mass transfer models to open-source DNS code (TPLS, 2015). Due to the high computational power required at present, work is also ongoing to produce efficient integral models which can replicate the results of DNS at reduced computational cost (Lavalle et al., 2015; Lavalle et al., 2017). This approach is suitable for gas-liquid flow conditions where the liquid film depth is low in comparison to the wavelength, and may be applicable to the case of amine solvent flowing over structured packing.

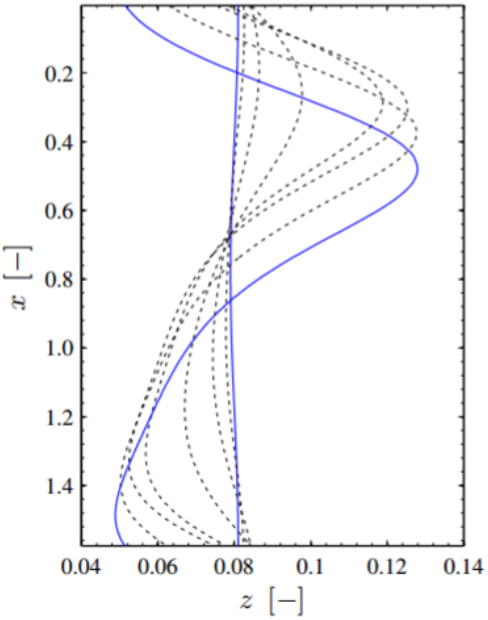

Fig. 2.5. DNS of wave growth in a 2D cell with laminar counter-current gas flow (Schmidt, 2016)

As with all models, direct numerical simulations must be validated. While it is possible to validate DNS code via an analytical solution (O Naraigh et al., 2014), there may exist no analytical solution for flow systems with turbulent hydrodynamics and/or mass transfer and so the simulation must be validated against experimental data. This data may include wave length, growth rate, amplitude or frequency. To ensure that the validation of more complex models is possible in the future, an experimental rig which can be used to make wave profile measurements with turbulent counter-current gas flows and mass transfer must be developed.

2.3.4 Optical measurement of liquid film thickness

The practice of using experimental methods to determine the thickness of liquid films is well established and there are a large number of techniques available, and can generally be categorised as film average, localised, point or spatial methods (Clark, 2002). In this work a localised, non-invasive method using a high-speed CMOS camera is used. This method is selected for several reasons. Unlike invasive techniques which use contact or conductivity probes, a non-invasive optical method allows the liquid film to develop unimpeded. Optical methods are also relatively simple to implement and do not require additional considerations to be made when designing the gas-liquid contactor, since as long as the liquid film can still be observed the camera can be an entirely separate device.

Previous work in the field of wave measurements has involved a variety of contactor types. Mouza et al (2002; 2003) use a high-speed camera to investigate flooding points and film height for liquid flowing down the inside of vertical and inclined small-diameter tubes. Georgantaki et al. (2016) use a conductivity method to measure the stabilisation effect of surfactants on an angled plate. Negny et al. (2001) use a CCD camera to observe the liquid flow down the outside of a structured, wavy column. In this work the gas-liquid contactor is a wetted-wall column, which allows liquid to flow down the outside of a vertical tube against a flow of counter-current gas. The design of the device and the measurement method are described in detail in Chapters 3 and 4, respectively.

2.4 Summary and overview of this work

This chapter has discussed the present state of research on the flexible operation of post-combustion capture. Several gaps in our current knowledge must be filled so that CCS can operate flexibly and in a fashion which can be optimised in terms of economic and/or environmental performance.

- Uncertainty about how changes in capture plant size and configuration will affect the response of the capture plant to changing generation plant output.
- A limited number of existing datasets for dynamic scenarios which are representative of real generation plant operation.
- Difficulty in repeating "high-impact" dynamic operations for the validation of dynamic models.
- Interactions between gas and absorbing solvent in the absorber column, leading to uncertainty about the true effective surface area for mass transfer.
- Lack of a well-developed, robust method for rapid online solvent composition measurements. This is a necessity for the implementation of future advanced control systems which will allow operators to optimise capture plant operation.

Through experiments at pilot-plant scale, this work investigates the effect of dynamic operating scenarios for NGCC and PC plant which are intended to be representative of real plant operation. Two pilot-scale facilities are used for this purpose and the effect of differences in plant design on the response to dynamic scenarios is discussed. An online solvent sensor designed by Buschle (2015) is used to passively monitor solvent composition. Once its performance has been assessed, continuous measurement of lean solvent CO_2 loading, combined with discrete knowledge of plant hydrodynamics are used to determine when the flow of steam should be reintroduced to the reboiler following a steam decoupling event, to achieve a minimum CO_2 capture rate of around 30%. Having highlighted the effect of solvent inventory and circulation times on dynamic response, a mathematical scale-up of a plant based on the proposed full-scale Peterhead CCS project is performed to investigate the effects of plant construction on dynamic operations. Experimental data is then used to estimate to a first-order approximation, the potential effect of plant response times and solvent inventory on the total CO_2 emitted during start-up and the associated emissions costs per year for a two-shifting NGCC plant.

A lab-scale test rig, a wetted-wall column, is designed and built at Edinburgh University. The device is designed to be used for the observation and measurement of how the liquid film develops as it runs down the outside of a stainless steel tube, while also being suitable for mass transfer experiments. The optical wave measurement method is discussed further in Chapter 4. Such a device can be used to provide validation for DNS code which is used to model gas-liquid interactions. The optical measurement method is tested with quiescent and countercurrent, non-reactive laminar gas flow regimes, which is the maximum level of complexity achievable with current DNS code. Wave measurements are also made using turbulent non-reactive gas, and with laminar and turbulent systems which incorporate mass transfer, demonstrating that the device can be used for the validation of reactive systems when the DNS models become sufficiently advanced. Measurements made using the device are then used to validate a low-dimensional model simulation of a thin liquid film flowing against laminar, non-absorbing counter-current gas. This will lead to a more comprehensive understanding of gas liquid interactions in the absorber and potentially allow for the design of novel structured packings which are specialised for flexible CCS operations.

References

Abu Zahra, M., Schneiders, L., Niederer, J., Feron, P. and Versteeg, G. (2007). CO_2 capture from power plants, Part II. A parametric study of the economical performance based on monoethanolamine. *Int. J. Greenh. Gas Cont.,* 1, 135-142.

Al-Qayim, K., Nimmo, W. and Pourkashanian, M. (2015). Comparative techno-economic assessment of biomass and coal with CCS technologies in a pulverized combustion power plant in the United Kingdom. *Int. J. Greenh. Gas Cont.,* 43, 82-92.

Astarita, G. (1963).Absorption of carbon dioxide into alkaline solutions in packed towers. *Inorganic and Engineering Chemistry Fundamentals,* 2, 294-296.

Biliyok, C., Lawal, A., Wang, M., & Seibert, F. (2012). Dynamic modelling, validation and analysis of post-combustion chemical absorption CO2 capture plant. *International Journal of Greenhouse Gas Control*, 9, 428–

445.Bruce, A.R.W., Harrison, G.P., Gibbins, J. and Chalmers, C. (2014). Assessing operating regimes of CCS power plants in high wind and energy storage scenarios. *Energy Procedia*, 63, 7529-7540.
Bui, M., Gunawan, I., Verheyen, V., Feron, P., Meuleman, E. and Adeloju, S. (2014a). Dynamic modelling and optimisation of flexible operation in post-combustion CO_2 capture plants – A review. *Computers and Chemical Engineering*, 61, 245-265.
Bui, M., Gunawan, I., Verheyen, V., Meuleman, E. and Feron, P. (2014b). Dynamic operation of post-combustion CO_2 capture in Australian coal-fired power plants. *Energy Procedia,* 37, 2694-2702.
Buschle, B. (2015). Solvent analysis instrumentation options for the control and flexible operation of post-combustion carbon dioxide capture plants. PhD Thesis, The University of Edinburgh.
Ceccarelli, N., van Leeuwen, M., Wolf, T., van Leeuwen, P., van der Vaart, R., Maas, W. and Ramos, A. (2014). Flexibility of low-CO_2 gas power plants: Integration of the CO_2 capture unit with CCGT operation. *Energy Procedia*, 63, 1703-1726.
Committee on Climate Change (2013). *Fourth Carbon Budget Review*. London, United Kingdom.
Chalmers, H. and Gibbins, J. (2007). Initial evaluation of the impact of post-combustion capture of carbon dioxide on supercritical pulverised coal power plant part load performance. *Fuel,* 86, 2109-2123.
Chalmers, H., Leach, M., Lucquiaud, M. and Gibbins, J. (2009). Valuing flexible operation of power plants with CO_2 capture. *Energy Procedia,* 1, 4289-4296.
Clark, W.W. (2002). Liquid film thickness measurement. *Multiphase Science and Technology*, 14, 1-74.
Cohen, S.M., Rochell, G.T. and Webber, M.E. (2011). Optimal operation of flexible post-combustion CO_2 capture in response to volatile electricity prices. *Energy Procedia*, 4, 2604-2611.
Dang, H. and Rochelle, G.T. (2003). CO_2 absorption rate and solubility in monoethanolamine/piperazine/water. *Separation Science and Technology,* 38, 337-357.
Department for Energy and Climate Change (2014). *Technical Assessment of the Operation of Coal & Gas Fired Plants*. DECC, London, United Kingdom.
Domenichini, R., Mancuso, L., Ferrari, N. and Davison, J. (2013). Operating Flexibility of Power Plants with Carbon Capture and Storage (CCS). *Energy Procedia,* 37, 2727-2737.
Dumée, L., Scholes, C., Stevens, G. and Kentish, S. (2012). Purification of aqueous amine solvents used in post-combustion CO_2 capture: a review. *Int. J. Greenh. Gas Cont.*, 10, 443-455.
Eisfeld, T. and Feldmüller, A. (2013). Fast cycling and Fast Start Capability of Combined Cycle Power Plants with SGT5-4000F Gas Turbines. *IMechE Seminar: Demand Response and Flexible Operation in UK Power Stations,* Nottingham, 28 November 2013.
van Eckeveld, A.C., van der Ham, L.V., Geers, L.F.G., van der Broeke, L.J.P., Boersma, B.J. and Goetheer, E.L.V. Online Monitoring of the Solvent and Absorber Acid Gas Concentration in a CO_2 capture Process Using Monoethanolamine. *Industrial and Engineering Chemistry Research*, 5515-5525.
Enaasen, N., Tobiesen, A., Kvamsdal, H.M. and Hillestad, M. (2013). Dynamic modelling of the solvent regeneration part of a CO_2 capture plant. *Energy Procedia,* 37, 2058-2065.
Errey, O., Chalmers, H., Lucquiaud, M. and Gibbins, J. (2014). Valuing responsive operation of post-combustion CCS power plants in low carbon electricity markets. *Energy Procedia,* 63, 7471-7484.
Faber, R., Köpcke, M., Biede, O., Knudsen, J.N. and Andersen, J. (2011). Open-loop step responses for the MEA post-combustion capture process: Experimental results from the Esbjerg pilot plant. *Energy Procedia,* 4, 1472-1434.
Flø, N.E., Kvamsdal, H.M. and Hillestad, M. (2015). Dynamic simulation of post-combustion CO_2 capture for flexible operation of the Brindisi pilot plant. *International Journal of Greenhouse Gas Control,* 48, 204-215.
Enaasen Flø, N., Knuutila, H., Kvamsdal, H.M. and Hillestad, M. (2015). Dynamic model validation of the post-combustion CO2 absorption process. *International Journal of Greenhouse Gas Control,* 41, 127-141.
Fandiño, O., Yacyshyn, M., Cox, J. S. and Tremaine, P. R. (2016) Speciation in Liquid-Liquid Phase-Separating Solutions of Aqueous Amines for Carbon Capture Applications by Raman Spectroscopy. In Acid Gas Extraction for Disposal and Related Topics (eds Y. Wu, J. J. Carroll and W. Zhu), John Wiley & Sons Inc., Hoboken, NJ, USA.
Frailie, P.T., Madan, T., Sherman, B.J. and Rochelle, G.T. (2013). Energy performance of advanced stripper configurations. *Energy Procedia*, 37, 1696-1705.

Georgantaki, A., Vlachogiannis, M. and Bontozoglou, V. (2016). Measurements of the stabilisation of liquid film flow by the soluble surfactant sodium dodecyl sulfate. *International Journal of Multiphase Flow,* 86, 28-34.
Global CCS Institute (2015). *Kemper County Energy Facility* [online]. Available at: https://www.globalccsinstitute.com/projects/kemper-county-energy-facility [Accessed Jan 2016].
Global CCS Institute (2015). *Shanxi International Energy Group CCUS Project* [online]. Available at: https://www.globalccsinstitute.com/projects/shanxi-international-energy-group-ccus-project [Accessed Jan 2016].
Global CCS Institute (2014). *The Global Status of CCS*: *2014*. Melbourne, Australia.
van der Ham, L., Bakker, D.E., Geers, L. and Goetheer, E.L.V. (2014).Inline Monitoring of CO_2 Absorption Processes Using Simple Analytical Techniques and Multivariate Modeling. *Chemical Engineering Technology*, 37, 221-228.
Haines, M.R. and Davison, J. (2014). Enhancing dynamic response of power plant with post-combustion capture using "Stripper stop". *Int. J. Greenh. Gas Cont.,* 20, 49-56.
Idris, Z., Jens, K.J. and Eimer, D.A. (2014). Speciation of MEA-CO_2 adducts at equilibrium using Raman spectroscopy. *Energy Procedia,* 63, 1424-1431.
IEAGHG (2012). Operating Flexibility of Power Plants with CCS, 2012/6. IEAGHG, Oxford, UK.
International Energy Agency (2012).*World Energy Outlook 2015.* OECD/IEA: Paris,France.Kvamsdal, H.M., Chikukwa, A., Hillestad, M., Zakeri, A. and Einbu, A. (2011). A comparison of different parameter correlation models and the validation of an MEA-based absorber model. *Energy Procedia,* 4, 1526-1533.
Kvamsdal, H.M., Jakobsen, J.P. and Hoff, K.A. (2009). Dynamic modelling and simulation of a CO_2 absorber column for post-combustion CO_2 capture. *Chemical Engineering and Processing: Process Intensification*, 48, 135-144.
Last, W. and Stichlmair, J. (2002). Influence of Stagnant Liquid Elements on the Effective Interfacial Area During Chemical Absorption in Packed Columns. *Chemical Engineering and Technology,* 25, 1075-1079.
Lavalle, G., Vila, J.P., Laurent, C. and Charru, F. (2015). Integral modelling of liquid films sheared by a gas flow. *22ème Congrès Français de Mécanique,* Lyon, 24th-28th August 2015.
Lavalle, G., Vila, J.P., Lucquiaud, M. and Valluri, P. (2017). Ultraefficient reduced model for countercurrent two-layer flows. *Physical Review Fluids,* 2, 0104001.
Lawal, A., Wang, M., Stephenson, P., & Obi, O. (2012). Demonstrating full-scale postcombustion CO2 capture for coal-fired power plants through dynamic modelling and simulation. *Fuel*, 101, 115–128.
Li, K., Leigh, W., Feron, P., Yu, H. and Tade, M. (2016). Systematic study of aqueous monoethanolamine (MEA)-based CO_2 capture process: Techno-economic assessment of the MEA process and its improvements. *Applied Energy,* 165, 648-659.
Lucquiaud, M. and Gibbins, J. (2011). Effective retrofitting of post-combustion CO_2 capture to coal-fired power plants and insensitivity of CO_2 abatement costs to base plant efficiency. *Int. J. Greenh. Gas Cont.,* 5, 427-483.
Lucquiaud, M., Sanchez Fernandez, E., Chalmers, H., Mac Dowell, N. and Gibbins, J. (2014). Enhanced operating flexibility and optimised off-design operation of coal plants with post-combustion capture. *Energy Procedia,* 63, 7494 – 7507.
Luu, M.T., Manaf, N.A. and Abbas, A. (2015). Dynamic modelling and control strategies for flexible operation of amine-based post-combustion CO2 capture systems. *International Journal of Greenhouse Gas Control,* 39, 377-389.
Mac Dowell, N. and Shah, N. (2014). Optimisation of post-combustion CO_2 capture for flexible operation. *Energy Procedia*, 63, 1525-1535.
Mac Dowell, N. and Shah, N. (2015). The multi-period optimisation of an amine-based CO_2 capture process integrated with a super-critical coal-fired power station for flexible operation. *Computers and Chemical Engineering*, 74, 169-183.
Mac Dowell, N. and Staffell, I. (2016). The role of flexible CCS in the UK's future energy system. *International Journal of Greenhouse Gas Control,* 48, 327-344.
Mechleri, E. (2015). Controllability analysis of a post-combustion CO2 capture plant integrated with a coal and natural gas-fired power plan. 3rd Post Combustion Capture Conference, 9th September 2015, Regina, Canada.

Massachusetts Institute of Technology (2015). *Large scale power plant CCS projects worldwide* [online]. Available at: https://sequestration.mit.edu/tools/projects/index_capture.html [Accessed Jan 2016].
Mouza, A.A., Paras, S.V. and Karabelas, A.J. (2002). The influence of small tube diameter on falling film and flooding phenomena. *International Journal of Multiphase Flow,* 28, 1311-1331.
Mouza, A.A., Paras, S.V. and Karabelas, A.J. (2003). Incipient flooding in inclined tubes of small diameter. *International Journal of Multiphase Flow,* 29, 1395-1412.
Murray, S. (2013). Why whole portfolio modelling is essential. *IPA 5th Annual Conference,* East Kilbride, 12 March 2013.
Negny, S., Meyer, M. and Prevost, M. (2001). Study of a laminar falling film flowing over a wavy wall column: Part II. Experimental validation of hydrodynamic model. *International Journal of Heat and Mass Transfer,* 44, 2147-2154.
Namjoshi, O., Li, L., Du, Y. and Rochelle, G. (2013). Thermal degradation of piperazine blends with Diamines. *Energy Procedia, 37*, 1904-1911.
O Naraigh, L., Valluri, P., Scott, D.M., Bethune, I. and Spelt, P.D.M. (2014). Linear instability, nonlinear instability and ligament dynamics in three-dimensional laminar lwo-layer liquid/liquid flows. *Journal of Fluid Mechanics,*
National Energy Technology Laboratory (2013), *Cost and Performance Baseline for Fossil Energy Plants Volume 1: Bituminous Coal and Natural Gas to Electricity* [online]. Available at: http://www.netl.doe.gov/File%20Library/Research/Energy%20Analysis/OE/BitBase_FinRep_Rev2a-3_20130919_1.pdf [Accessed Jan 2016]
Nielsen, P.T., Li, L. and Rochelle, G.T. (2013). Piperazine degradation in pilot plants. *Energy Procedia,* 37, 1912-1923.
Oexmann, J. and Kather, A. (2010). Minimising the heat duty of post-combustion CO_2 capture by wet chemical absorption: The misguided focus on low heat of absorption solvents. *Int. J. Greenh. Gas Cont.*, 4, 36-43.
Partnership to Advance Clean Energy (2014), *Best Practices Manual for Indian Supercritical Plants* [online], Available at: http://www.pace-d.com/wp-content/uploads/2013/03/BP-MANUAL-FOR-PRINTING.pdf [Accessed Jan 2016]
Pigford, R.L. and Sherwood, T.K. (1952). Absorption and Extraction, p317, McGraw-Hill, New York.
Puranik, S.S. and Vogelpohl, A. (1973). Effective interfacial area in irrigated packed columns. *Chemical Engineering Science,* 29, 501-507.
Putta, K.R., Pinto, D.D.D., Svendsen, H.F. and Knuutila, H.K. (2016). CO_2 absorption into loaded aqueous MEA solutions: Kinetics assessment using penetration theory. *International Journal of Greenhouse Gas Control,* 53, 338-353.
Razi, N., Bolland, O. and Svendsen, H. (2012). Review of design correlations for CO_2 absorption into MEA using structured packings. *International Journal of Greenhouse Gas Control,* 9, 193-219.
Rochelle, G.T. (2012). Thermal degradation of amines for CO_2 capture. *Current Opinion in Chemical Engineering,* 1, 183-190.
Rochelle, G., Chen, E., Freeman, S., van Wagener, D., Xu, Q. and Voice, A. (2011). Aqueous piperazine as the new standard for CO_2 capture. *Chem. Eng. J.,* 171, 725-733.
Samarakoon, G.L., Andersen, N.H., Perinu, C. and Jens, K.J. (2013). Equilibria of MEA, DEA and AMP with Bicarbonate and Carbamate: A Raman Study. *Energy Procedia,* 37, 2002-2010.
Sebastia-Saez, D., Gu, S., Ranganathan, P. and Papadikis, K. (2015). Micro-scale CFD modelling of reactive mass transfer in falling liquid films within structured packing materials. *International Journal of Greenhouse Gas Control*, 33, 40-50.
Schmidt, P., Ó Náraigh, L., Lucquiaud, M. and Valluri, P. (2016). Linear and nonlinear flow instability in vertical counter-current laminar gas-liquid flows. *Physics of Fluids,* 28, 042102.
Seibert, F., Chen, E., Perry, M., Briggs, S., Montgomery, R. and Rochelle, G. (2010). UT/SRP CO_2 capture pilot plant - operating experience and procedures. *Energy Procedia,* 4, 1616-1623.
Sexton, A.J. and Rochelle, G.T. (2009). Catalysts and inhibitors for oxidative degradation of monoethanolamine. *Int. J. Greenh. Gas Cont.,* 3, 704-711.
Supap, T., Idem, R. and Tontiwachwuthikul, P. (2011). Mechanism of formation of Heat Stable Salts (HSSs) and their roles in further degradation of monoethanolamine during CO_2 capture from flue gas streams.

Tait, P., Buschle, B., Ausner, A., Valluri, P., Wehrli, M. and Lucquiaud, M. (2016). A pilot-scale study of dynamic response scenarios for the flexible operation of post-combustion CO2 capture. *International Journal of Greenhouse Gas Control,* 48, 216-233.
Tanthapanichakoon, W. and Veawab, A. (2006). Electrochemical investigation on the effect of heat-stable salts on corrosion in CO_2 capture plants using aqueous solution of MEA. *Ind. Eng. Chem. Res.,* 45, 2586-2593.
Tobiesen, F.A., Hillestad, M., Kvamsdal, H. and Chikuwa, A. (2012). A general column model in CO2SIM for transient modelling of CO_2 absorption processes. *Energy Procedia*, 23, 129-139.
TPLS (2015). High Resolution Direct Numerical Simulation of Two-Phase Flows. Available at: http://sourceforge.net/projects/tpls/
Tsai, R.E., Seibert, F., Elridge, R.B. and Rochelle, G.T. (2011). A Dimensionless Model for Predicting the Mass-Transfer Area of Structured Packing. *American Institute of Chemical Engineers Journal,* 57, 1173-1184.
Van Peteghem, T. and Delarue, E. (2014). Opportunities for applying solvent storage to power plants with post-combustion carbon capture. *Int. J. Greenh. Gas Cont.*, 21, 203-123.
Wiley, D.E., Ho, M.T. and Donde, L. (2010) Technical and economic opportunities for flexible CO_2 capture at Australian black coal fired power plants. *Energy Procedia,* 4, 1893-1900.
Xu, Z.P., Afacan, A. and Chuang, K.T. (2000). Predicting mass transfer in packed columns containing structured packings. *Transactions of the Institution of Chemical Engineers,* 78, 91-98.

Chapter 3. Wetted-Wall Column Design

3.1 Introduction

As discussed in chapter 2, DNS of counter-current gas-liquid flow systems must be validated by experiment. The construction of a test rig which can be used for validation at Edinburgh University is of considerable benefit to DNS practitioners, allowing models to be validated in-house, with full control over flow conditions and gas & liquid physical properties. Existing contactor types for the measurement of interfacial wave phenomena include flat inclined channels (e.g. Georgantaki et al., 2016) and vertical and inclined tubes (e.g. Mouza et al., 2002; Mouza et al., 2003). In this work, the contactor used is a wetted-wall column. This type of device is selected because, in addition to its potential to provide validation for DNS code via wave measurements, wetted-wall columns are widely used to determine the mass transfer properties of solvents for use in CCS applications. This is a useful capability for the lab to possess and could be used to complement future research projects.

This chapter describes the design of a dual-purpose wetted-wall column which can be operated in two configurations, one which is suited to wave measurement experiments, the other to mass transfer. This is achieved by making it possible to vary the length of the column and contact chamber, with an exposed column length of 250mm in wave measurement configuration and 100mm in mass transfer configuration. Wave measurements are made using a high-speed camera with a shutter rate of 300 frames per second (fps) to observe the falling liquid film at a number of locations along the length of the column. The method is described in detail in chapter 4. Although the determination of solvent properties using the WWC is not explicitly related to process or interfacial wave dynamics and is therefore outside the scope of this thesis, a brief overview of their use in mass transfer is provided below.

3.1.1 Mass Transfer measurements using Wetted Wall Columns

The screening of solvents for use in post-combustion capture using wetted-wall columns was first described by Pacheco (1998) using a WWC designed by Mshewa (1995) and the practice is now well-established. The wetted-wall column can be used for the initial evaluation of solvent kinetic and thermodynamic properties.

Fast reaction kinetics are favoured for the absorption of CO_2 into amine solvents. If CO_2 is rapidly absorbed a smaller volume of packing is required to achieve a high level of capture, reducing construction costs and making CCS more attractive to plant operators. The wetted-wall column is used to determine the liquid-side mass transfer coefficient (k_g') of the solvent over a range of solvent CO_2 loadings. This is an effective way of comparing the absorption rates of different solvents and thus their viability for PCC. The overall mass transfer coefficient K_G and the gas-side mass transfer coefficient k_g can be determined by experiment, so the liquid-side mass transfer coefficient is determined using the following expression. A detailed description of the determination of K_G and k_g is provided by Dugas (2009).

$$\frac{1}{K_G} = \frac{1}{k_g} + \frac{1}{k_g'} \tag{3.1}$$

Solvent CO_2 absorption capacity (ΔC) is defined as the difference in loading between rich and lean solvent. Solvents with high capacity are favoured as the flow rate of solvent required to capture CO_2 is reduced, which reduces the reboiler heat input requirement for regeneration. Secondary benefits include the reduction of the power required to run solvent pumps and the size of the cross-flow heat exchanger.

$$\Delta C = \frac{(\alpha_{rich} - \alpha_{lean}) * mol\ alkalinity}{kg\ solvent} = \frac{mol\ CO_2}{kg\ solvent} \tag{3.2}$$

The rich-lean loading difference ($\Delta\alpha$) can be calculated from the VLE curve, in which the equilibrium partial pressure of CO_2 (PCO_2*) above the solvent is plotted against solvent loading in mol CO_2/mol alkalinity. α_{rich} is often taken to be to that which has PCO_2* of 5000Pa, and α_{lean} to that which has PCO_2* of 500Pa at a temperature of 40°C. These two partial pressures approximate a 90% CO_2 capture rate, and provide a useful indication of the solvent's operating capacity.

The wetted-wall column can be used to determine the equilibrium PCO_2* above the amine solvent over a range of solvent loadings. An empirical model is used to relate PCO_2* (Pa) to temperature T (K) and solvent CO_2 loading α (mol CO_2/mol MEA), and takes the form below (Xu, 2011), where a…f are constants dependent on the amine or mixture of amines used:

$$ln(P^*_{CO2}) = a + \frac{b}{T} + c * \alpha + d * \alpha^2 + e * \frac{\alpha}{T} + f * \frac{\alpha^2}{T} \quad (3.3)$$

VLE data can also be used to determine the heat of absorption for the solvent. It is now widely accepted that when the entire process is considered, a high heat of absorption is favourable. Oexmann and Kather (2010) modelled desorber thermodynamics rigorously and conclude that solvents with high heat of absorption benefit more greatly from the temperature swing between the absorber and desorber, resulting in a higher desorber operating pressure and less water vapour (and hence increased CO_2 concentration in the vapour phase) at the top of the absorber. A higher desorber operating pressure also reduces the compression duty required. Heat of absorption is determined using the Gibbs-Helmholtz equation and is dependent on the solvent CO_2 loading. For comparison between solvents, a CO_2 loading which corresponds to an equilibrium partial pressure of 1500Pa is sufficient as an average, and can be determined from the VLE curve (Chen, 2011). Terms b and d are solvent-dependent empirical constants, R is the ideal gas constant.

$$\Delta H_{abs} = -R \frac{d(ln\, P^*_{CO2})}{d(1/T)} = -R(b + d\alpha) \quad (3.4)$$

VLE and k_g' measurements are essential for the development of kinetic and thermodynamic models of solvent behaviour, which are frequently used in process modelling and in the design of full-scale absorption and stripping columns (Sherman, 2016). However, as discussed in chapter 2 of this thesis (section 2.2.4) more sophisticated models are required for the correct sizing and design of absorption equipment.

3.2 Existing Column designs

The wetted wall column described in this work is based on existing designs and is intended to be suitable for both liquid film thickness and mass transfer measurements. Although various designs have been constructed and implemented, at its most basic level a wetted-wall column consists of an annular gas-liquid contact chamber with a column of well-defined surface area in the centre for the absorbing or desorbing liquid to flow over. The column is encased in a glass or perspex tube which creates a sealed enclosure for gas-liquid interactions to take place. Gas flows counter-currently from the base of the column and exits the top of the chamber. Existing designs on which the WWC used in this work are summarised in section 3.2.1. Although none of these devices have been used to make film thickness or wave profile measurements, some of their features are well suited to this purpose and are incorporated into the design.

3.2.1 Danckwerts

The use of wetted-wall columns as a method of determining solvent kinetics and vapour-liquid equilibrium is first described by Danckwerts (1962), who used the absorption of CO_2 into alkaline solutions as a means of validating the surface renewal theory of mass transfer. The design of this column incorporates two design aspects which ensure highly accurate mass transfer measurements can be made.

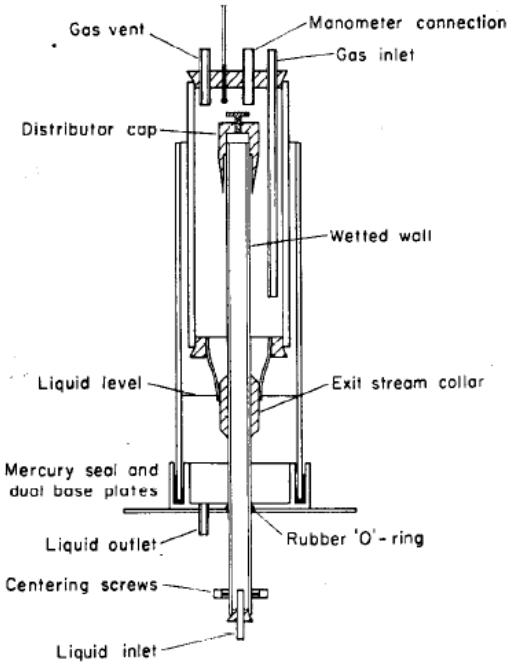

Fig. 3.1 Diagram of the wetted-wall column used by Danckwerts (1962)

Assuming that the liquid surface is at its terminal velocity over its entire surface could introduce an error in the effective surface area. To rectify this, a distributor cap which is longer than the predicted maximum thermal and hydrodynamic length was fitted at the top of the column. This allows the liquid film to approach terminal velocity before coming into contact with the gas.

A rigid film of surface-active material is believed to build up on the liquid surface at the bottom of the column, reducing the rate of absorption close to the outlet. The absorption rate reduction is not negligible and the height of this inactive film tends to vary depending on the solvent used. The Danckwerts design minimises this effect by installing a polyethylene exit collar with three 2.5mm grooves through which solvent could escape at the base of the column. The stagnant film is confined to these grooves, which comprise no more than 2% of the entire exposed area.

Neither the distributor cap nor the exit collar are incorporated into the design of the wetted-wall column used in this work. The distributor cap is unsuitable for wave measurements as it may constrain the liquid flow at higher liquid flow rates, preventing the film profile from developing naturally. In the Danckwerts design, gas enters through a tube which descends from the top plate through the annular space, with the gas exiting close to the base of the column (see fig. 3.1). This is unsuitable for wave measurements as the presence of the inlet tube may affect the countercurrent flow of gas, potentially creating disturbances in the liquid film which would otherwise not be present. Therefore the gas must enter though the column base plate.

3.2.2 University of Texas at Austin

The WWC designed in this work is most similar to a device used at the University of Texas at Austin. Designed by Mshewa (1995), it has been used extensively in the screening of amine solvents for CO_2 capture (e.g. Pacheco, 1998; Cullinane, 2004; Li, 2013) with a focus on aqueous piperazine and its blends with other amines (Rochelle, 2011).

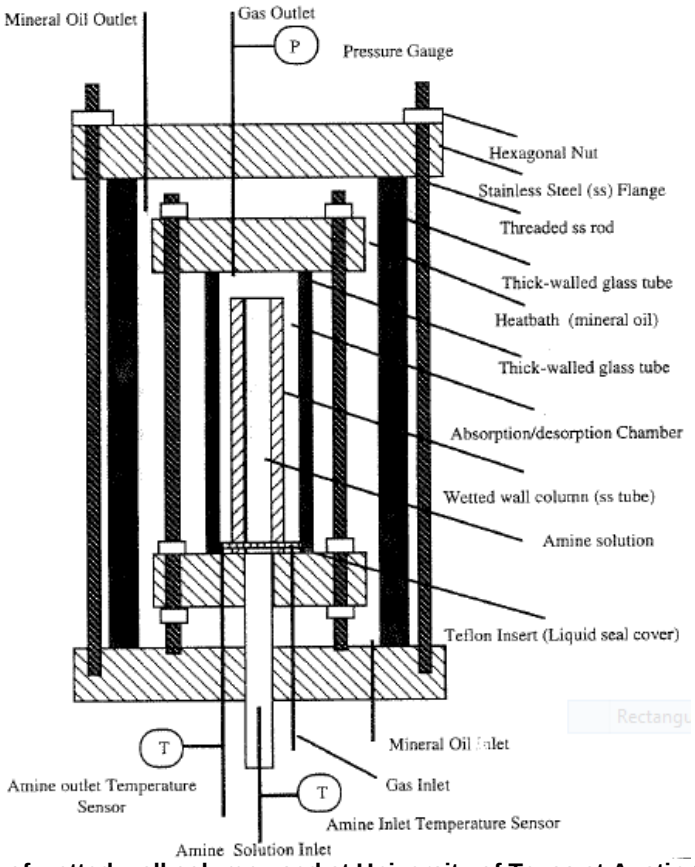

Fig. 3.2 Diagram of wetted-wall column used at University of Texas at Austin (Mshewa, 1995)

The column at UT Austin is designed for use at high temperatures, and is contained in an oil jacket so the inside temperature can be modified to match that of the absorption process (40^{o}C) and beyond. Precise temperature control is not possible due to the exothermic reaction between amine and CO_2. Chapter 4 of this work describes an extreme case in which unloaded MEA absorbs pure CO_2, resulting in a temperature change between liquid inlet and of no more than 2^{o}C. However as ΔH_{abs} increases with temperature (Kim et al., 2009), $\Delta T_{outlet\text{-}inlet}$ may be considerably greater at higher temperatures. The column itself is a stainless steel tube with an exposed length of 9.1cm and a diameter of 1.26cm. An exit collar or distributor cap are not used since its primary function is to compare the properties of different solvents as part of a screening process, and all solvents tested will be susceptible to the same systematic errors. Gas enters the chamber through a single inlet in the baseplate.

3.2.3 Commonwealth Scientific and Industrial Research Organisation

A WWC with very similar design has been used at Australia's Commonwealth Scientific and Industrial Research Organisation (CSIRO) to investigate solvents based on ammonia (Puxty, 2010) and proprietary solvents (Artanto, 2012).

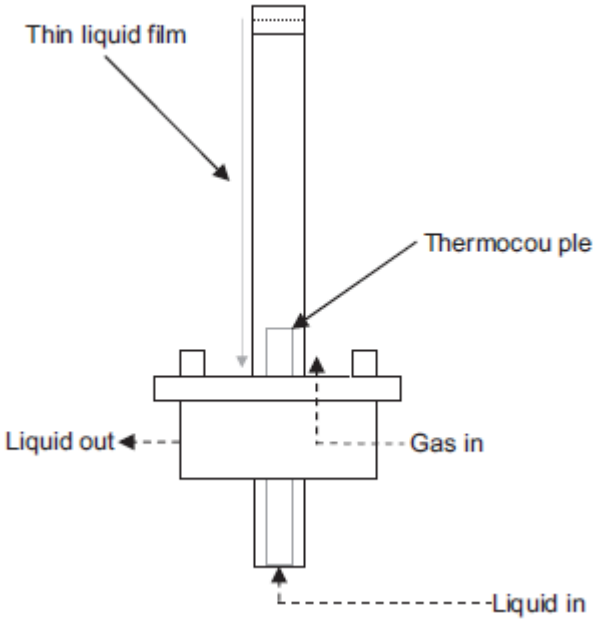

Fig. 3.3. Diagram of wetted-wall column at CSIRO (Puxty, 2010)

The contactor design and dimensions are similar to that of the column at the Universty of Texas, with a single gas inlet and no distributor cap or exit collar. Here, the apparatus is heated using water rather than oil. While it is not a problem for mass transfer experiments, a single gas inlet is not suitable if wave measurements are to be made, which require much higher gas flow rates to achieve superficial velocities similar to those encountered in the absorber. A single inlet and short column length does not give the gas flow ample time to develop, and could result in significant differences in the forces acting on the falling film around the column circumference.

3.2.4 Norwegian University of Science and Technology

A wetted-wall column has been used in conjunction with a string-of-discs column at the Norwegian University of Science and Technology (NTNU) to provide more complete kinetic data for the CO_2-MEA-H_2O system (Luo, 2012). In this design, the gas first enters an inlet chamber before entering the contact chamber through an annulus, ensuring that the gas flow regime is circumferentially uniform. A similar approach is used in the design of the WWC described in this work.

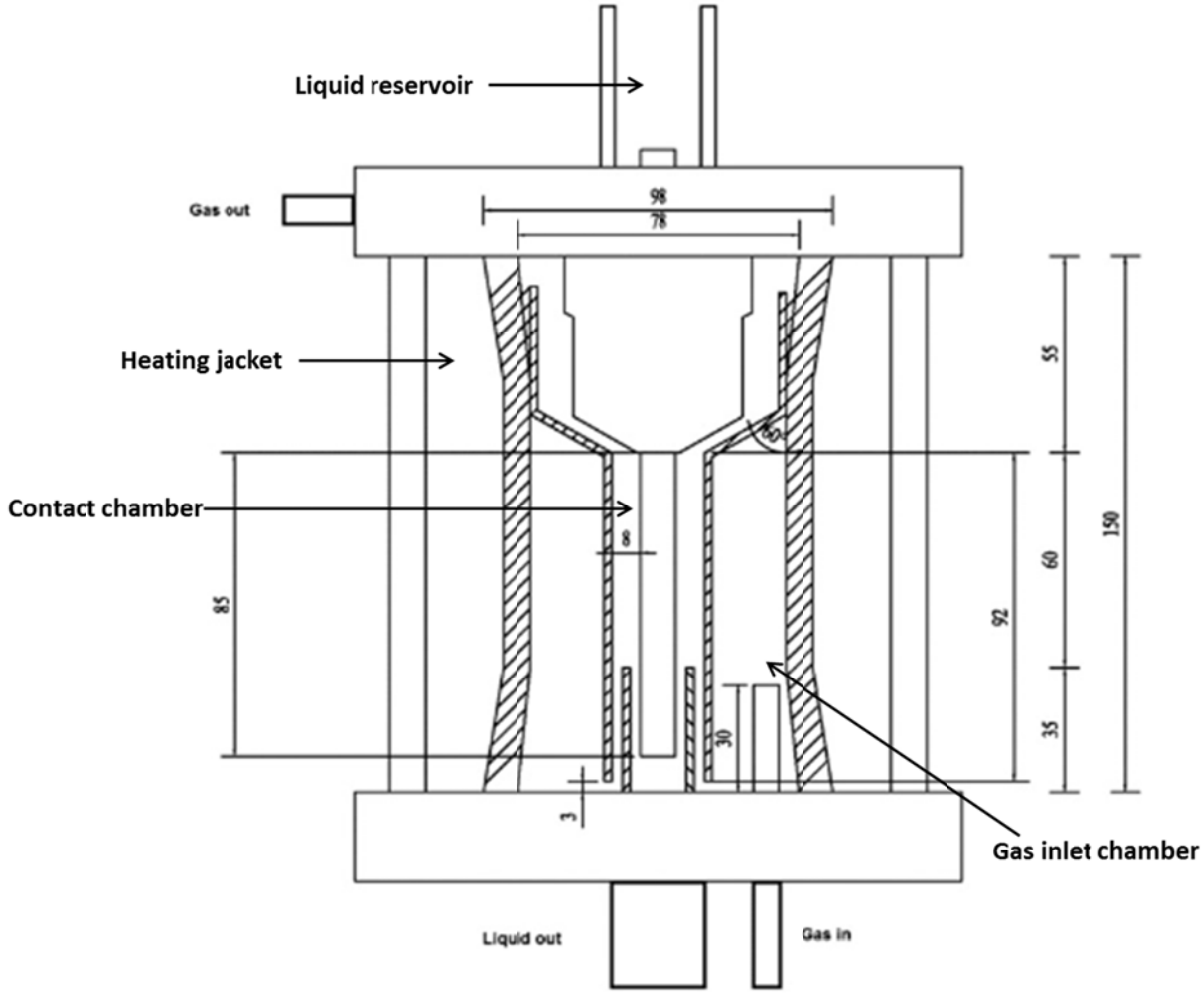

Fig. 3.4. Diagram of wetted-wall column at NTNU (Luo, 2012)

Liquid enters from a reservoir located at the top of the column. While this works well for mass transfer, the increased pressure from the liquid head may influence the development of the liquid film and produce unrepresentative wave measurement results. The column at NTNU is around 50mm in length as opposed to those at CSIRO and the University of Texas, which are 8.21 and 9.10mm in diameter, respectively. The shortening of the column is to minimise changes in solvent CO_2 loading between the inlet and outlet, as mass transfer measurements typically assume α is constant.

3.3 Wetted-Wall Column Design

3.3.1 Contactor and column dimensions

The wetted-wall column has been designed with two different configurations in mind, the first for the measurement of the thickness of the liquid film and waves on the wetted wall, the second for the determination of mass-transfer properties. Wave measurements require a column length which is sufficient to allow gas and liquid flows ample time to develop hydrodynamically. For mass transfer measurements, the contact area must be long enough that enough mass transfer occurs for a change in CO_2 concentration between the gas inlet and outlet is observed by the CO_2 analyser but also short enough to avoid absorbing sufficient CO_2 that significant changes in solvent CO_2 loading are observed. Based on previous work using other columns a length of around 100mm is sufficient for mass transfer.

For wave measurements, the recommended column length is based on the hydrodynamic entrance length for gas and liquid. In an annular space this is dependent on the hydraulic diameter (D_h) and the Reynolds number of the fluid (Re).

$$L_{h,laminar} = 0.05 * Re * D_h \quad (3.5)$$

$$L_{h,turbulent} = 1.359 * D_h * Re^{0.25} \quad (3.6)$$

The maximum liquid flow achievable using the solvent pump is approx. 470ml/min for which Re = 74.92 and L_h = 1.939mm. However, this assumes a ripple-free liquid film when in reality waves will develop over a significantly longer distance. The maximum gas flow achievable is 100l/min for which Re = 14603 and L_h = 183.9mm for pure CO_2, and Re = 7881 and L_h = 157.6mm for pure N_2. Both of these values of L_h are greater than the length of the ideal column for mass transfer, and would risk significant changes in CO_2 loading.

An exposed column length of 250mm is selected for wave measurements and 100mm for mass transfer. The 250mm length allows both gas flow and waves to fully develop for the majority of flow conditions, while keeping the device short enough that its construction and assembly are not impractical. A length of 100mm for mass transfer is in line with other, established wetted wall column designs. Column length is changed by switching out the column and glass casing with those of different size.

The column diameter is 12.7mm with contact chamber inner diameter of 26.0mm. A small contact chamber diameter allows higher superficial gas flow rates to be achieved with the mass flow controllers available, so that the effect of turbulent gas flow on wave formation can be observed. This also reduces the dependence of the overall mass transfer resistance $1/K_G$ on the rate of diffusion of reactants from the gas bulk to the interface, $1/k_g$. This reduces the uncertainty associated with measurements of the liquid phase mass transfer resistance, $1/k_g$' (equation 3.1) and hence the determination of the liquid-side mass transfer coefficient.

3.3.2 Gas and liquid inlets

To approximate a uniform circumferential gas flow regime, the gas inlet chamber approach is adopted from the column described in Luo (2012). A ring of twelve holes, 3mm in diameter, evenly spaced around the base of the column allow gas to enter the contact chamber from an inlet chamber located below. This ensures that the forces acting on the liquid film due to the countercurrent flow of gas are, roughly, circumferentially symmetrical. Wave measurements are made by observing the shape and evolution of the outer edge of the liquid film profile, as observed by the high-speed camera. If the forces acting on the liquid film are similar around its the entire circumference, it is reasonable to assume that the film profile observed by the stationary camera is representative of film behaviour around the circumference of the column.

Liquid flows up the inside of the stainless steel tube and spills over the edge. The inside of the tube acts as a weir and allows the liquid film to develop naturally and uniformly around the column circumference, without being constrained by a distributor cap.

3.3.3 Wave Measurement Configuration

The wetted-wall column can be assembled either with or without a second, outer piece of glass/Perspex casing. This second piece forms a cavity between itself and the inner Perspex casing into which hot water can be pumped, to act as a heating jacket and to allow for greater control over contact chamber temperature. In wave measurement configuration, this outer glass casing is not present so that the liquid film is not obscured or distorted by a layer of water and two layers of curved glass. For this reason, all wave measurement experiments are carried out at room temperature.

A cross-section of the device is shown in fig. 3.5.The contactor is held together by three 12mm threaded rods with "feet" on the end, which provide support and allow the column to sit on the workbench. Three nuts are screwed down tightly against the top of the base plate (part 1) to ensure the feet are held flush against the underside, and that the threaded rods are held firmly in place to eliminate any wobbling. Two more pieces (parts 2 and 3) sit on top of the baseplate to form a gas inlet chamber and the surface on which the glass casing sits. An evenly-spaced ring of 12 holes, 3mm in diameter are located at a radius of 10.7mm from the centre of part 3 – these act as gas inlets to the contact chamber. During the start of operation, while the flow of liquid is stabilising it is possible that some may spill into the gas inlet chamber via these holes, so Part 2 contains a liquid outlet which can be used to drain the chamber.

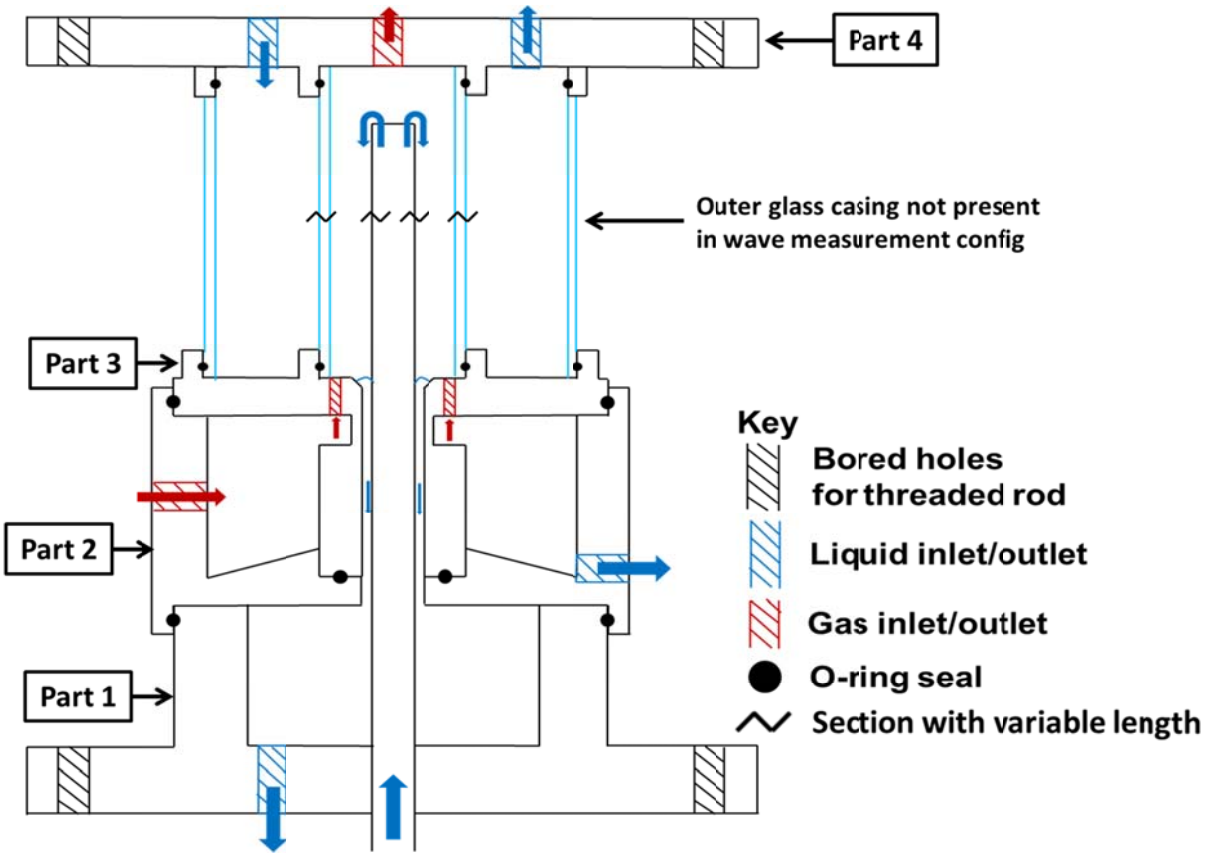

Fig. 3.5 Cross-section of wetted wall column

Two glass cylinders sit inside raised ridges on the upper face of part 2, creating the contact chamber and heating jacket. The inner diameter of the contact chamber is 26.0mm. A ½" tube fitting in the top plate (part 4) acts as a gas outlet, with aperture diameter 10mm. Two ¼" tube fittings in the top plate act as an inlet and outlet for heating water.

The column itself is made of ½" stainless steel Swagelok tubing, and is held perpendicular to the workbench using a bored-through half-inch compression fitting which sits flush against the underside of part 1. Once the glass pieces are in place, the top plate (part 4) is lowered over the threaded rod supports and allowed to rest in position on top of the glass plate. Three nuts are screwed down carefully, ensuring that the Perspex tubing does not crack, until the entire assembly is pulled together.

Radial and axial o-ring seals are used to keep the gas and liquid phases separate before they enter the contact chamber. Liquid flows down the outside of the column and through an annular channel which separates it from the gas entrance chamber. It flows into a liquid exit chamber which is created by the space between parts 1 and 2, then out through a ¼" outlet in the baseplate.

Fig. 3.6. Solid Edge assembly of wetted wall column in wave measurement configuration

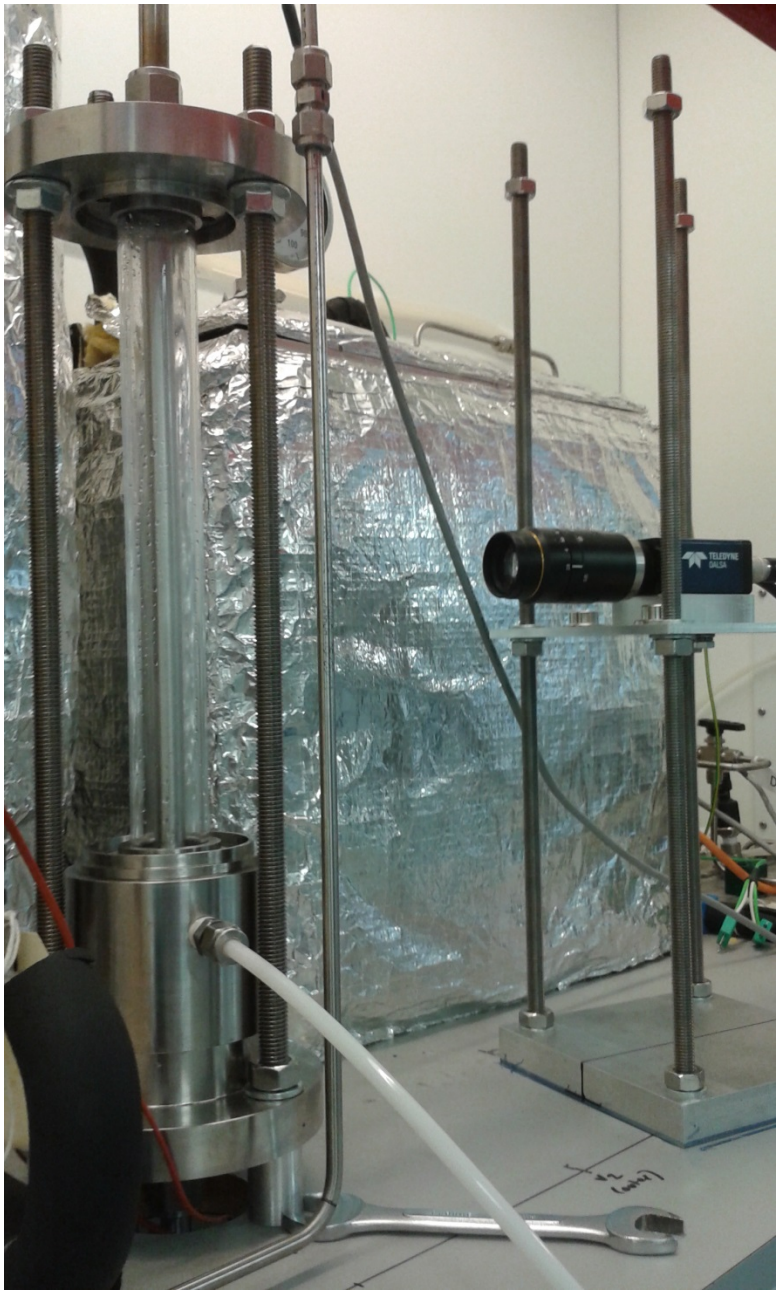

Fig. 3.7. Photo of column in wave measurement configuration

3.3.4 Mass Transfer Configuration

For mass transfer experiments the contact chamber and column length can be shortened by 150mm. This is achieved by unscrewing the three nuts which hold the top plate in place, replacing the stainless steel column and inner Perspex casing with those which are 150mm shorter and adding an outer glass borosilicate glass tube which acts as a heating jacket. This provides temperature control up to 80^{o}C. If the solvent to be tested is likely to react with the inner Perspex casing it can also be exchanged for one which is made of glass. The exposed column length is 100mm and the column area is 4114.41mm^2. The effective interfacial area is dependent on the liquid film thickness, which is calculated using equation 3.7 (Kapitza, 1965).

$$\delta = \sqrt[3]{\frac{2.4 \cdot \nu \cdot Q_l}{g \cdot W \cdot cos\beta}} \tag{3.7}$$

Q_l is the volumetric flowrate in m^3/s, ν is the kinematic viscosity of the fluid in m^2/s, g is acceleration due to gravity in m/s^2, W is the channel width in m and β is the angle of the channel. In this case, the channel is vertical so $cos\beta = 0$. The effective interfacial area can then be determined via equation 3.8.

$$a_e = (\pi * (d_{column} + (2 * \delta) * h_{column}) + \frac{\pi * (d_{column} + (2 * \delta))^2}{4} \qquad (3.8)$$

Where A_e is the effective surface area in mm^2, d_c is the diameter of the column in mm, h_c is the column height in mm and δ is the theoretical film thickness in mm.

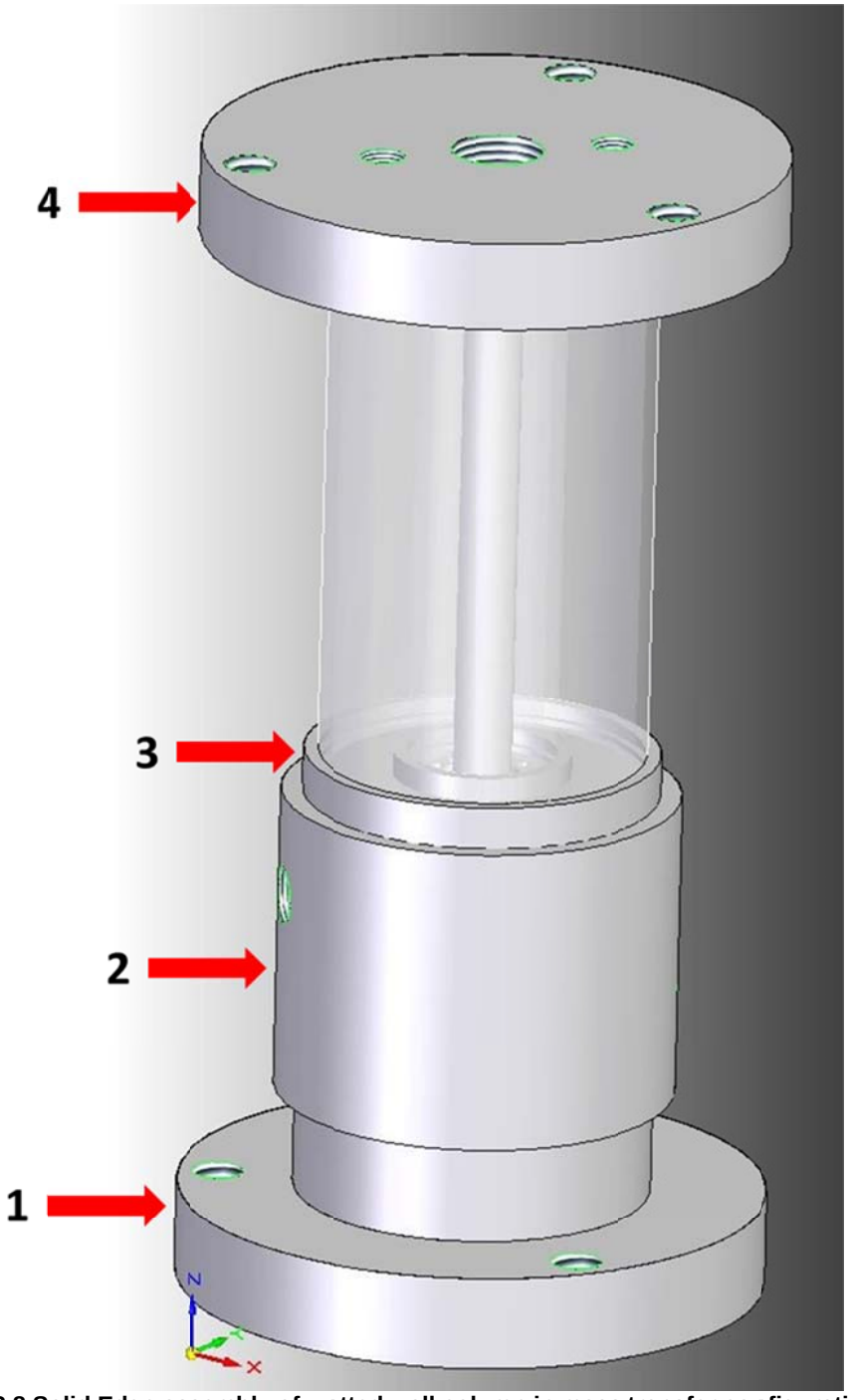

Fig. 3.8 Solid Edge assembly of wetted wall column in mass transfer configuration

The individual design of the four parts which comprise the completed device: base plate (part 1), gas inlet chamber (part 2), base upper section (part 3) and top plate (part 4) are catalogued in section 3.3.4.

3.4 Individual parts listing

3.4.1 Part 1 – Base plate

Liquid flows down into this section through the annular space between the outside of the column and the wall which separates the liquid exit channel from the gas inlet chamber (see fig. 3.5). It collects in the space between this part and the underside of part 2, before exiting the WWC apparatus through a ¼in NPT Swagelok tube fitting which can be seen just to the left of the central threaded hole. The hole in the centre is for a bored-through 1/2in Swagelok tube fitting, which holds the stainless steel column in place. The fitting sits flush to the underside of part 1 and allows the column to be securely fastened by tightening a nut, ensuring that it is held perpendicular to the baseplate. The three outer holes are sized to accommodate 12mm threaded rod, which will be used to affix legs which hold the apparatus together.

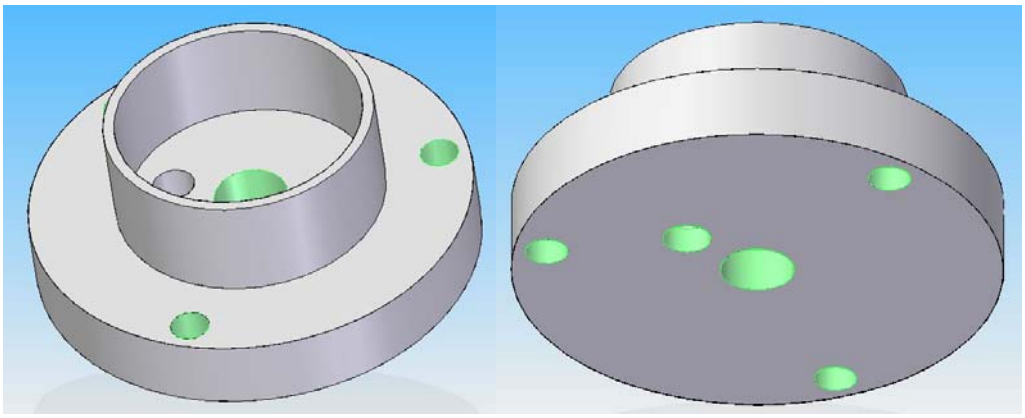

Fig. 3.9 a, b. Wetted wall column baseplate rendering, upper (left, a) and lower (right, b) faces

3.4.2 Part 2 – Gas inlet chamber

This part acts as an inlet for the gas stream, an outlet for any liquid which may have spilled over into the gas inlets and as a way of keeping the gas and liquid streams separate. The baseplate (part 1) and the base upper section (part 3) slot into the space created by the ridges on the lower and upper faces, of part 2. Radial o-ring seals in these ridges isolate the gas inlet chamber and liquid outlet chamber from the surrounding atmosphere. Gas enters the chamber through a 1/2in Swagelok tube fitting. Any liquid which may have spilled over into the gas entrance chamber during column startup can be drained through a 1/4in Swagelok tube fitting which is located on the opposite side.

The recess in the base of the part 2 contains a groove for an axial o-ring seal. Part 3 sits in this recess, with the o-ring seal keeping the gas separate from the liquid flow exit channel (see fig. 3.5)

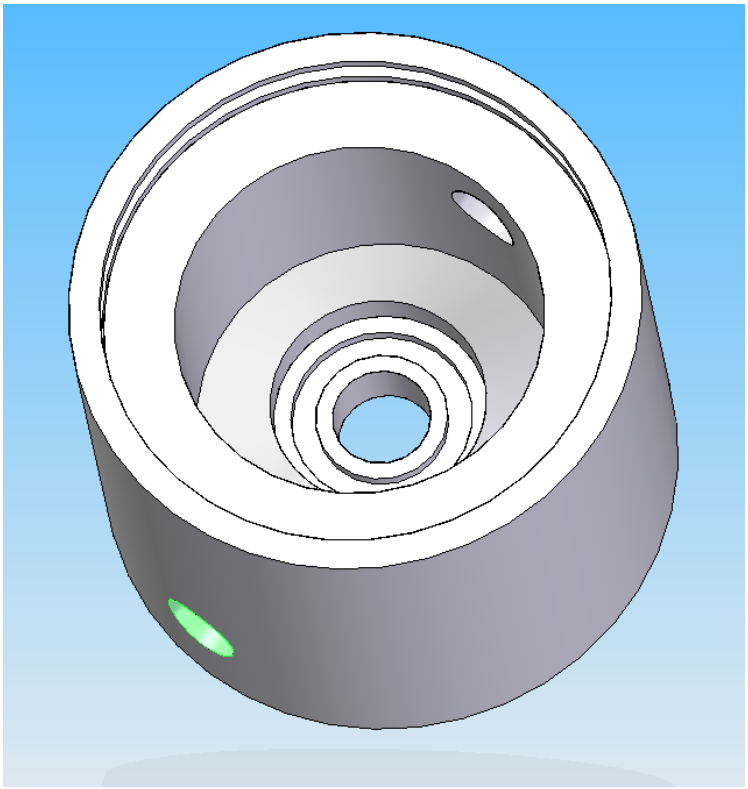

Fig. 3.10 Wetted wall column gas inlet chamber rendering

3.4.3 Part 3 – Base upper section

Gas travels from the inlet chamber up through the twelve 3mm holes surrounding the central liquid exit channel to enter the contact chamber. This allows the gas velocity profile to develop more rapidly and with less uncertainty than with a single liquid inlet. The column itself extends through the middle of the central hole, creating a 1mm annulus through which liquid can exit the contact chamber. O-ring grooves in the inner and outer ridges create a seal between the contact chamber and the heating jacket, and between the heating jacket and the surrounding atmosphere. A 45^{o} countersink around the central hole ensures liquid is directed towards the exit channel and minimises overspill into the gas side. The section extending from the underside of the plate slots into the recess in the base of part 2, isolating the liquid exit channel from the gas via an o-ring seal.

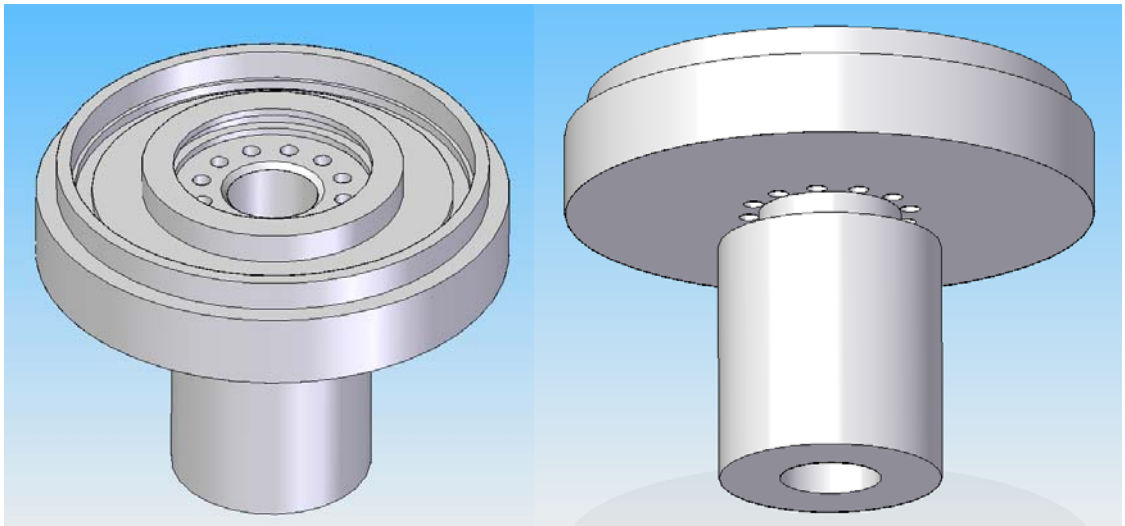

Fig. 3.11a, b. Base upper section upper (left, a) and lower (right, b) faces

3.4.4 Part 4 – Top plate

The top plate has a central gas outlet (1/2in NPT fitting), an inlet and outlet for heating water (1/4in NPT fittings) and three holes for threaded supports which and with 12mm pipe thread screwed through the baseplate of the apparatus. The ridges on the lower face contain grooves for radial o-ring seals to fit the piece snugly to the inner and outer glass casing, similarly to part 3.

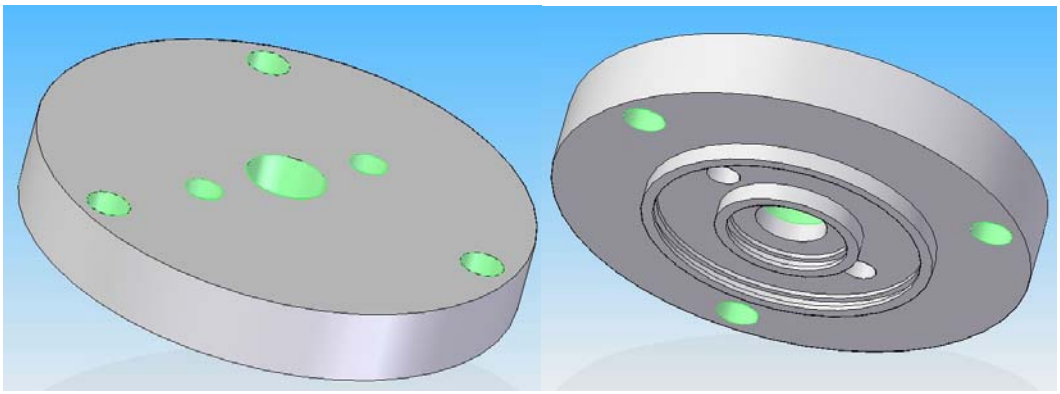

Fig. 3.12a, b. Top plate upper (left, a) and lower (right, b) faces

3.5 – Wetted Wall Column External Setup

3.5.1 Gas loop

Nitrogen and carbon dioxide flow rates are controlled using Cole-Parmer MC series differential pressure mass flow controllers. A contactor bypass allows the CO_2 concentration in the inlet flue gas to be confirmed prior to gas entering the column. Gas is heated to the required temperature for the experiment in a water bath and saturated by sparging through 500mm of water in a heated pressure vessel. A second contactor bypass allows the inlet CO_2 concentration to be double-checked at this stage, as some may be absorber by the water during saturation. Inlet and outlet gas temperatures and the pressure inside the column are measured using thermocouples. An ADC 3000 series infra-red CO_2 detector is used to detect the CO_2 concentration in the gas phase. The analyser has a flow limit of 100ml/min, pressure limit of 0.3bar_g and may be affected by water vapour in the gas phase, so after leaving the contactor the gas stream passes through a condenser, pressure reducing valve and a bleed valve to vent a proportion of the flow.

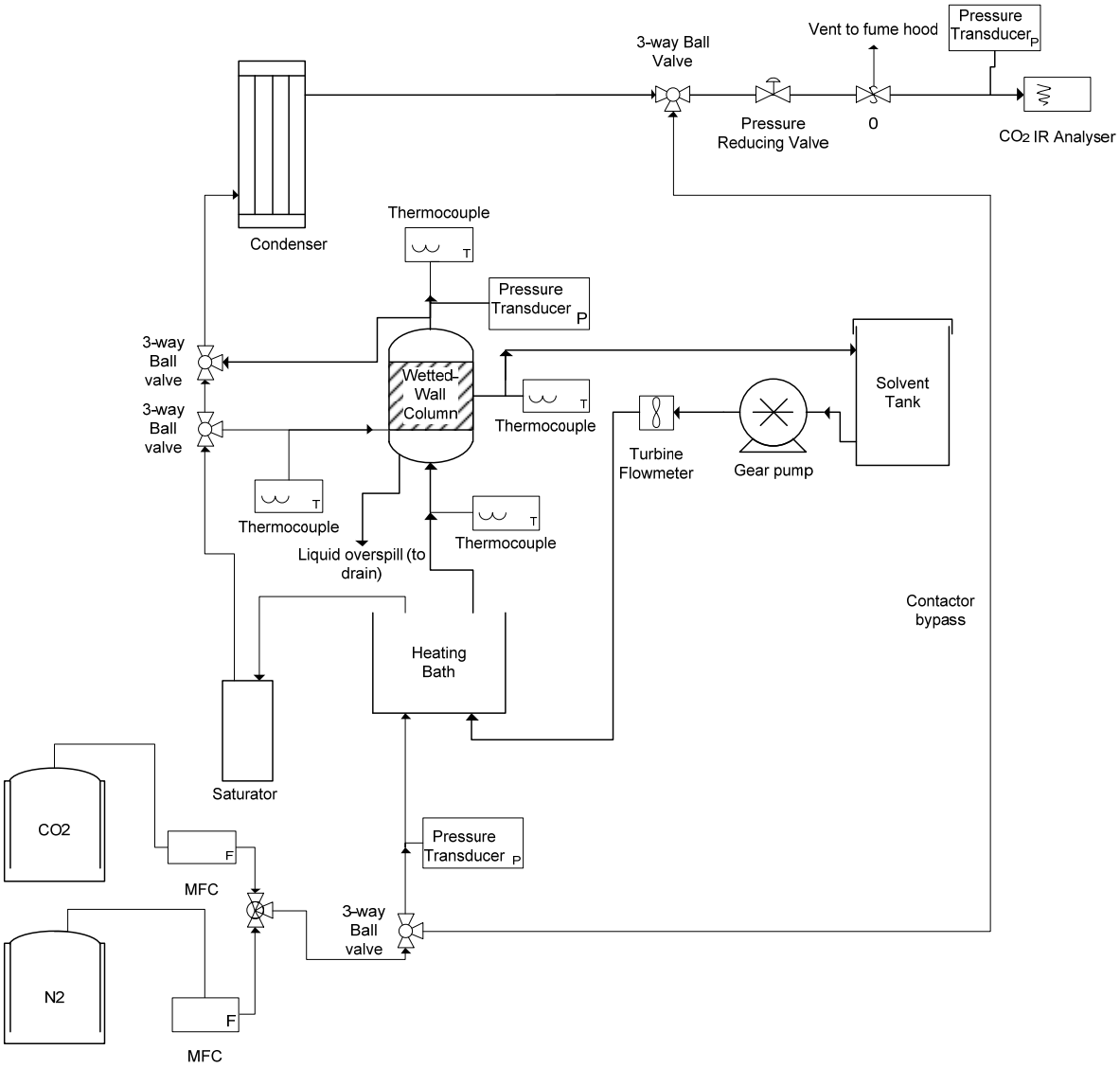

Fig. 3.13 External Setup of wetted-wall column apparatus

3.5.2 Liquid loop

The total solvent inventory of the system is 2.2 litres, most of which resides in a solvent tank with an approx. 1.8l capacity. It is circulated using a gravity-fed, Cole-Parmer Masterflex digital gear pump. The pump setpoint is related to the real liquid flow rate by the following equation (see section 4.4.2).

$$Ql = 0.23514 * Ql_{setpt} \tag{3.9}$$

Liquid is pumped through a heating bath and up through the centre of the stainless steel column before spilling over the top. Inlet and outlet temperatures are measured and recorded using thermocouples. The liquid system is a closed loop and after passing through the contact chamber it returns to the solvent tank.

3.6 Conclusions

A wetted-wall column device for the purpose of wave measurements for DNS validation has been designed and constructed. It has dual functionality in that it can also be operated in a second configuration to determine the properties of absorbing solvents, which is achieved by exchanging the casing which forms the contact chamber and the central column with ones which are shorter in length, and adding a second outer glass casing to create a heating jacket.

The validation via experiment of direct numerical simulations is an important step in ensuring they accurately predict interfacial wave dynamics, allowing for a greater understanding of gas-liquid interactions in industrial processes and the correct sizing of packed columns. The wetted-wall column rig can allow DNS modellers to validate their code with and without mass transfer and with either laminar or turbulent gas flow. Initial wave measurement experiments which demonstrate these capabilities are detailed in Chapter 4.

References

Amundsen, T.G.,Øi, L.E. and Eimer, D.A. (2009). Density and Viscosity of Monoethanolamine + Water + Carbon Dioxide from (25 to 80)°. *Journal of Chemical Engineering Data,* 54*,* 3096–3100.

Artanto, Y., Jansen, J., Pearson, P., Do, T., Cottrell, A., Meuleman, E. and Feron, P. Performance of MEA and amine-blends in the CSIRO PCC pilot plant at Loy Yang Power in Australia. *Fuel,* 101, 264-275.

Cullinane, J.T. and Rochelle, G.T. (2004). Carbon dioxide absorption with aqueous potassium carbonate promoted by piperazine. *Chemical Engineering Science,* 59, 3619-3630.

Chen, X., Closmann, F. and Rochelle, G.T. (2011). Accurate screening of amines by the wetted wall column. *Energy Procedia,* 4, 101-108.

Danckwerts, P.V. and Roberts, D. (1962). Kinetics of CO_2 absorption in alkaline solutions. *Chemical Engineering* Science, 17, 961-969.

Dugas, R.E. (2009). Carbon Dioxide Absorption, Desorption and Diffusion in Aqueous Piperazine and Monoethanolamine. Ph.D. Dissertation. University of Texas at Austin.

Freeman, S.A., Davis, J. and Rochelle, G.T. (2010). Degradation of aqueous piperazine in carbon dioxide capture. *International Journal of Greenhouse Gas Control,* 4, 756-761.

Georgantaki, A., Vlachogiannis, M. and Bontozoglou, V. (2016). Measurements of the stabilisation of liquid film flow by the soluble surfactant sodium dodecyl sulfate. *International Journal of Multiphase Flow,* 86, 28-34.

Goto, K., Yogo, K. and Higashii, T. (2013). A review of efficiency penalty in a coal-fired power plant with post-combustion CO_2 capture. *Applied Energy,* 111, 710-720.

Kim, I., Hessen, E.T., Haug-Warberg, T. and Svendsen, H.F. (2009). Enthalpies of absorption of CO_2 in aqueous alkanolamine solutions from e-NRTL model. *Energy Procedia*, 1, 829-835.

Li, L., Voice, A.K., Li, H., Namjoshi, O., Nguyen, T., Du, Y. and Rochelle, G.T. (2013). Amine blends using concentrated piperazine. *Energy Procedia,* 37, 353-369.

Luo, X., Hartono, A. and Svendsen, H.F. (2012). Comparative kinetics of carbon dioxide absorption in unloaded aqueous monoethanolamine solutions using wetted wall and string of discs columns. *Chemical Engineering Science,* 82, 31-43.

Mouza, A.A., Paras, S.V. and Karabelas, A.J. (2002). The influence of small tube diameter on falling film and flooding phenomena. *International Journal of Multiphase Flow,* 28, 1311-1331.

Mouza, A.A., Paras, S.V. and Karabelas, A.J. (2003). Incipient flooding in inclined tubes of small diameter. *International Journal of Multiphase Flow,* 29, 1395-1412.

Mshewa, M.M., 1995. *Carbon dioxide desorption/absorption with aqueous mixtures of methyldiethanolamine and diethanolamine at 40 to 120°C.* Ph. D. The University of Texas at Austin.

Oexmann, J. and Kather, A. (2010). Minimising the regeneration heat duty of post-combution CO_2 capture by wet chemical absorption: The misguided focus on low heat of absorption solvents. *International Journal of Greenhouse Gas Control,* 4, 36-43.

Pacheco, M.A., 1998. *Mass-Transfer, kinetics and rate-based modelling of reactive absorption.* Ph. D. The University of Texas at Austin.

Perry, R.H., Green, D.W. and Maloney, J.O. eds, 1997. *Perry's Chemical Engineering Handbook, 7th Ed.* New York: McGraw-Hill

Puxty, G., Rowland, R. and Attalla, M. Comparison of the rate of CO_2 absorption into aqueous ammonia and monoethanolamine.*Chemical Engineering Science,* 65, 915-922.

Rochelle, G., Chen, E., Freeman, S., Van Wagener, D., Xu, Q., and Voice, A. (2011). Aqueous piperazine as the new standard for CO_2 capture technology. *Chemical Engineering Journal*, 171, 725-733.

Sherman, B.J., Ciftja, A.F. and Rochelle, G.T. (2016). Thermodynamic and mass transfer modelling of carbon dioxide absorption into aqueous 2-piperidineethanol. *Chemical Engineering Science*, 153, 295-307.
Vevelstad, S.J., Eide-Hagumo, I., da Silva, E.F. and Svendsen, H.F. (2011). Degradation of MEA; a theoretical study. *Energy Procedia* 4, 1608-1615.
Xu, Q. and Rochelle, G. (2011). Total Pressure and CO_2 Solubility at High Temperature in Aqueous Amines. *Energy Procedia*, 4, 117-124.
Yu, H., Qi, G., Xiang, Q., Wang, S., Fang, M., Yang, Q., Wardhaugh, L. and Feron, P. (2013). Aqueous ammonia based post combustion capture: Results from pilot plant operation, challenges and further opportunities. *Energy Procedia,* 37, 6256-6264.
Zhang, S., Ye, X. and Lu, Y. (2014). Development of a Potassium Carbonate-Based Absorption Process with Crystallization-Enabled High-Pressure Stripping for CO2 Capture: Vapor–Liquid Equilibrium Behavior and CO2 Stripping Performance of Carbonate/Bicarbonate Aqueous Systems. *Energy Procedia*, 63, 665-675.
Zoannu, K.-S., Sapsford, D.J. and Griffiths, A.J. (2013). Thermal degradation of monoethanolamine and its effect on CO_2 capture capacity. *International Journal of Greenhouse Gas Control,* 17, 423-430.

Chapter 4. Wave Measurements Using a Wetted-Wall Column Apparatus

4.1 Introduction

In the design of specialized equipment for mass transfer applications in chemical processing an understanding of gas-liquid interactions is critical for the correct sizing and construction of process apparatus, particularly in absorption and distillation operations using structured packing. Mass transfer, heat transfer and operational limits such as load and flood points are dependent on the interaction between the gas and liquid phases. As discussed in section 2.2.4 there currently exists some uncertainty about the effective mass transfer area of packed columns for CO2 absorption using amines, due to possible deviation from pseudo-first order reaction kinetics. This deviation causes semi-stagnant pools which act as effective surface area for mass transfer to become chemically saturated with more rapidly (Last & Stichlmair, 2002). An understanding of gas-liquid interactions is critical for design and operation, as it allows for the prediction of loading and flooding points and for the correct sizing and design of absorber columns. It could also be used in the development of specialised structured packings which maximise the effective surface area for CCS operations.

Direct numerical simulations can be used to obtain a rigorous understanding of gas-liquid flow interactions. At present, DNS is able to simulate two-dimensional, non-turbulent gas-liquid flow in a vertical geometry (Schmidt, 2016) but once the cost of computational power becomes sufficiently reduced they could be used to simulate 3D cells of structured packing with turbulent gas flow and mass transfer. This will allow the rate at which these semi-stagnant pools are replenished to be determined and their effect on interfacial area for mass transfer across the absorber to be quantified. DNS could also be used to study the growth and propagation of interfacial waves and their effect on mass transfer in a 3D cell.

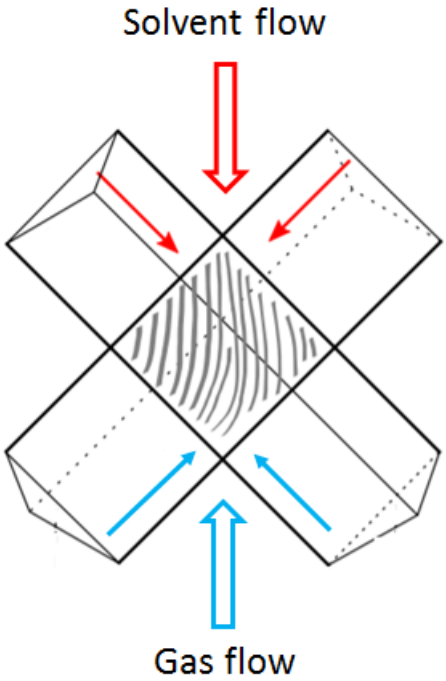

Figure 4.1 Unit cell of structured packing for counter-current absorption, showing net direction of fluid flows and discrete flows into the unit cell via channels.

Direct numerical simulations which solve the full Navier-Stokes equations can be used to obtain a rigorous understanding of gas-liquid flow interactions. At present, DNS is able to simulate two-dimensional, non-turbulent gas-liquid flows (Schmidt, 2016) and has the potential to provide insights into the incitement and development of interfacial instability dynamics which remain poorly understood, and which may have a

significant effect on operational limits and mass and heat transfer processes between the liquid and gas phases. However, DNS requires significant computational power for more complex flow systems and is currently limited to laminar/laminar cases.

An alternative to DNS is low-dimensional modelling, which can be applied when the wavelength of interfacial waves is long in comparison to the depth of the liquid film, as is often the case when gravity-driven films or channel flows are considered (Lavalle et al., 2015). This technique utilises the shallow-water theory (Benney, 1966; Shkadov, 1967; Lavalle, 2017) in which a film parameter term measures the film thickness in comparison to the wavelength. The reduction of the liquid phase to this low-dimensional model significantly reduces the computational cost in comparison to full DNS, which is likely to be particularly expensive when flow conditions relevant to industrial processes are analysed.

In order for DNS or low-dimensional models of liquid film development and wave propagation over a surface to be validated, it is necessary to compare results against analytical solutions (e.g. Schmidt, 2016; O Naraigh, 2014) or if no analytical solution exists, as is likely for cases with turbulent flow conditions, carry out experimental studies of the film. The wetted-wall column can be used to investigate the behaviour of free-falling films over a wide range of gas-phase Reynolds numbers for both reactive and non-reactive flow conditions, if a suitable film measurement method is selected.

Clark (2002) provides a comprehensive review of the development of film-thickness measurement methods over the years, .Intrusive point methods which use conductance or capacitance probes will disturb the flow of counter-current gas, and their introduction to the wetted wall through the outer tubing is not easily achieved. The most suitable option is a non-intrusive, optical method. Dietze (2010) employs a suite of optical methods for the measurement of falling film properties on the inside of a section of glass tube, with separate methods being used to obtain highly accurate properties of the liquid film. Film thickness is measured via confocal chromatic imaging (CCI), which uses the spectral intensity of light reflected from the interface back through a pair of convex lenses and a semi-reflecting mirror to determine the location of the interface in space. Velocity is measured via particle image velocimetry (PIV), which uses a laser to illuminate tracer particles whose positions are then captured with a high-speed camera. While the measurements are highly precise, these methods are complex to implement and in addition, the tracer species are shown to be present at the liquid surface and may affect the liquid film physical mass transfer coefficient, k_l^0, if combined mass transfer/wave measurement experiments are to be carried out at a later date. High-speed CCD camera methods have been employed to make film profile measurements (Negny et al., 2001; Mouza et al., 2002) and to plot the position of the film height as a time series (Kofman et al., 2017) allowing wave frequency to be determined. The contrast between the liquid film and a white screen located behind it defines the gas-liquid interface.

While these are existing optical methods, the novelty of the apparatus lies in that it can be rapidly switched between configurations to facilitate mass transfer experiments on absorbing solvents, or wave measurement experiments for the validation of numerical models of film dynamics. In addition, measurements are made using 30%wt monoethanolamine (MEA) as the liquid phase, for which no thin film measurements of this type are currently published in the literature.

Wave profile data, frequency, length, velocity and growth rate are provided for nonreactive systems at three liquid flow conditions in the absence of countercurrent gas flow, and again with laminar and turbulent countercurrent N_2. Film profile data for cases with reactive absorption of countercurrent CO_2 are also provided. Experimental film profile data is used to validate a low-dimensional two-phase flow model, demonstrating that the test rig can provide validation for DNS and low-dimensional models at their current level of complexity.

4.2 Scope of this work

The experimental work described in this section acts as a proof of concept for the dual-purpose wetted-wall column described in Chapter 3. Using three different liquid flow rates of unloaded, fresh 30%wt MEA solution, wave measurements are taken using a high-speed camera at 10mm intervals from the top of the column until 160mm along its length. This allows the growth and eventual saturation of wave amplitude and velocity to be observed. Wave measurements are made at these liquid flow conditions without counter-current gas flow initially, to establish a reference scenario against which others can be compared. Subsequent experiments use N_2 at 20l/min and 80l/min to observe the effect of laminar and turbulent counter-current gas flow on wave propagation. Counter-current CO_2 at similar Reynolds numbers to the non-reacting cases is absorbed into

unloaded 30%wt MEA so that the effect of reactive absorption on the liquid film can be observed. Finally, a low-dimensional two-phase flow model developed by Lavalle et al. (2015) is validated against film profile, height, and frequency for one of the non-absorbing systems.

4.3 Experimental Apparatus

The wetted-wall column is set up in its extended configuration, as described in chapter 3. An HM640 Dalsa Genie high-speed camera (maximum speed 300 frames per second) is set up so that it views the wetted surface directly, and fixed to a bracket which allows it to be moved up and down along the length of the wetted surface.

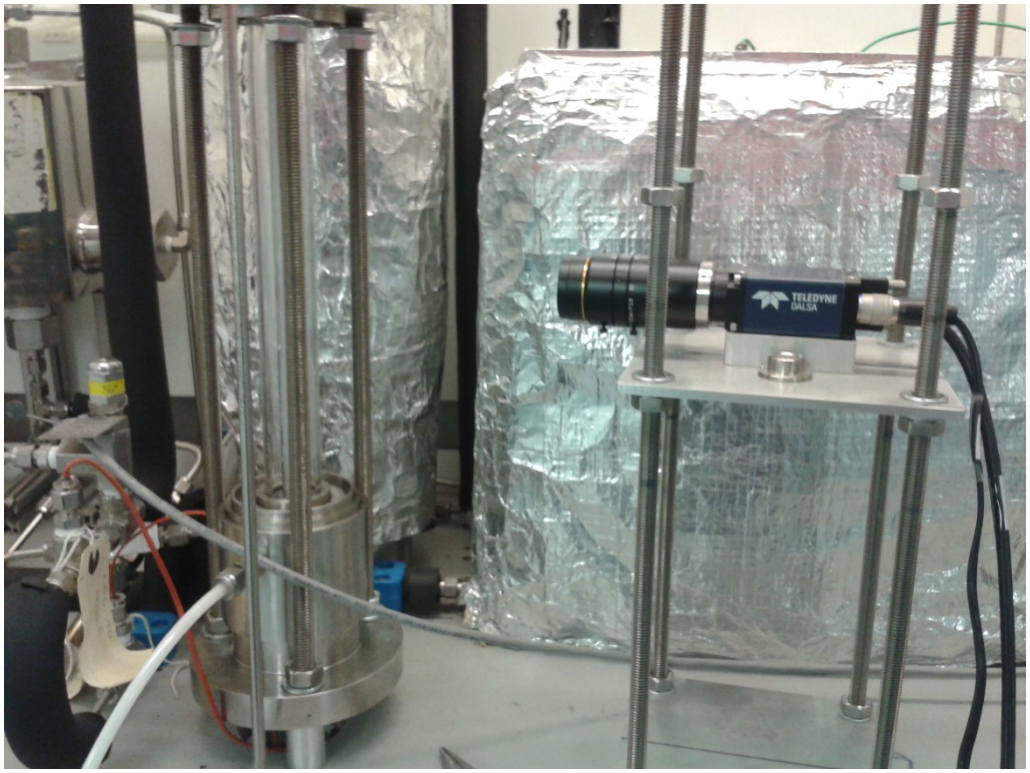

Figure 4.2 High-speed camera observing the wetted surface of the column

A non-intrusive optical method which utilises an HM640 Dalsa Genie high-speed camera to observe the two-dimensional film profile as it travels down the outside of the steel tube is used. The observation of interfacial waves using a high-speed camera is well-established (Mouza, 2005) and with a sufficiently large field of view can be used to determine wave velocity, frequency and wave growth rate in addition to film thickness. A potential disadvantage of the optical measurement technique is that the accuracy of measurements is limited by the resolution and framerate of the camera. The camera used in this work has a resolution of 640x480 pixels, which results in a measurement uncertainty which does not exceed 10% of the mean film thickness. This is in line with or better than similar studies in the existing literature which report a relative uncertainty of 10-20% (Mouza, 2002).

The high-speed camera is set up so that it views the wetted surface directly. A bracket allows it to be moved axially along the length of the wetted surface. All sources of fluorescent lighting in the immediate vicinity are switched off, and the surface is illuminated using an LED desk lamp. A white screen placed behind the experimental setup provides further contrast between the liquid surface and its surroundings. The white screen is marked at 10mm intervals so that the camera's field of view can be centred on the desired measurement location.

Nitrogen and carbon dioxide flow rates are controlled using Cole-Parmer MC series differential pressure mass flow controllers with range 0-100 standard litres per minute. Mass flow controllers are calibrated to NIST standard with a flow accuracy of 0.2% of their full scale (0.2l/min) or 0.8% of the setpoint, whichever is larger.

All experiments are made at ambient temperature and pressure, with thermocouples in place to record gas inlet & outlet and liquid inlet & outlet temperatures. The total recirculating solvent inventory of the system is 2.2 litres, the majority of which resides in a solvent tank with an approx. 1.8l capacity. It is circulated using a gravity-fed, Cole-Parmer Masterflex digital gear pump. Three liquid flow rates are used over the course of the experimental programme, corresponding to 141, 188 and 235 ml/min. These are referred to for the remainder of this work as flow condition 1, 2 and 3 respectively.

4.4 Calibration and theoretical calculations

4.4.1 Camera Calibration

Camera calibration is carried out at the beginning of each set of experiments to relate the number of pixels in each recorded image to distance in real space. The camera is raised or lowered to the desired location along the length of the column and a spirit level is used to ensure it is not viewing the surface at an incline. The diameter of the stainless steel column is known (12.70mm) and can be used to relate pixels to distance. For example, if the left edge of the column is located at co-ordinate x_1 and the right edge is located at co-ordinate x_2 the distance per pixel (d) is calculated as follows:

$$d = \frac{12.70mm}{x_2 - x_1} \tag{4.1}$$

Once the flow of liquid has started, the camera is used to determine the x co-ordinate of the edges of the falling liquid film. Due to lighting conditions in the lab the leftmost edge has greater contrast between the film and the white backing screen, so it is used to determine film height δ for all flow conditions.

$$\delta = d(x_1 - x_{film}) \tag{4.2}$$

Due to imperfect focusing of the camera, in some cases the gas-liquid interface may be as many as three pixels wide. The measurement uncertainty is therefore conservatively estimated to be +/- 1 pixel, or +/- d in other words. Optical measurement uncertainty is discussed in detail in section 4.4.5.

4.4.2 Pump Calibration

There is approx. 1200mm of static head between the pump outlet and the liquid inlet at the top of the wetted-wall column, plus a considerable number of bends and fittings in the liquid line which contributes to dynamic head when the pump is in operation. To account for the effect of static and dynamic head on the liquid flowrate at the top of the column a pump curve must be obtained.

The liquid line is broken as close to the wetted wall liquid inlet as possible and a T-piece and drain valve are added at this location. The drain valve is initially closed and the liquid inventory is circulated at a given setpoint. Once the flow has stabilised, the drain valve is opened and liquid flows preferentially into a vessel for collection. The sampling duration (around 60sec) is recorded via stopwatch and the mass of collected liquid is measured using a digital scale.

For consistency with experiments, 30%wt MEA solution is used for calibration. The measured mass values are converted to volume using the solution density at current lab ambient temperature.

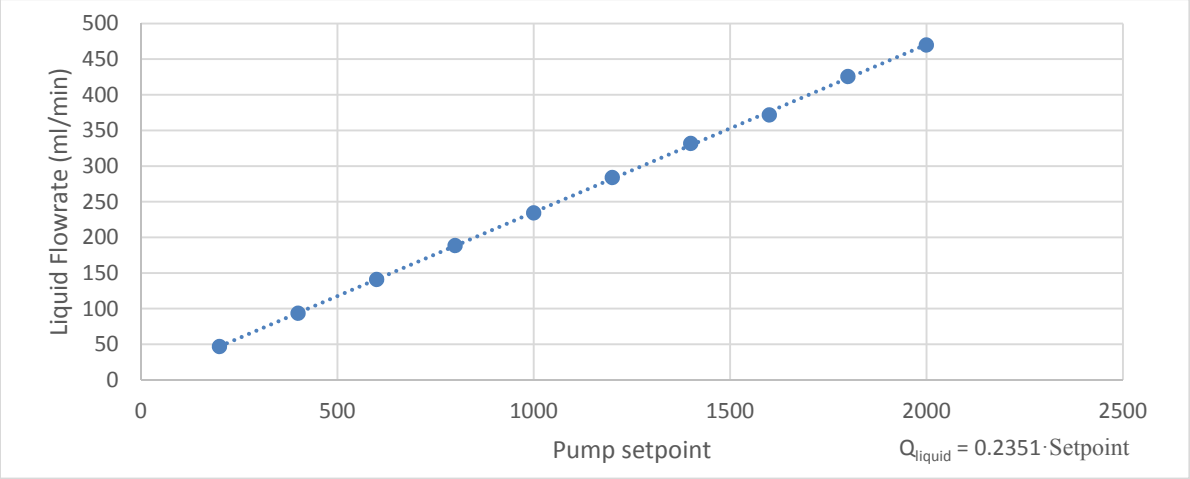

Figure 4.3 Pump calibration curve

Solvent flowrate in ml/s is equivalent to the setpoint multiplied by 0.235. Pump setpoints used in experiments are 600, 800 and 1000, corresponding to 141, 188 and 235 ml/min respectively. These are referred to for the remainder of this document as liquid flow conditions 1, 2 and 3 as indicated by subscripts. These flow conditions are selected for practical reasons - they are large enough that a consistent solvent film with no dry patches is formed on the column wall, but small enough that the liquid film is able to easily flow into the annulus which acts as the solvent outlet channel without spilling over into the gas inlets.

Flow condition	Pump Setpoint	Liquid flow rate (ml/s)
1	600	2.35
2	800	3.13
3	1000	3.91

Table 4.1 Solvent flow conditions used in this work

There existed some concern that the action of the gear pump could result in a "pulsed" liquid flow which influences wave formation. To determine if this were the case, the number of revolutions per second at each liquid flowrate were calculated and compared with the wave frequency range.

Pump RPM at liquid flow condition 1 = 512.8RPM, 8.547 rev/sec
Pump RPM at liquid flow condition 2 = 683.8RPM, 11.40 rev/sec
Pump RPM at liquid flow condition 3 = 854.7RPM, 14.24 rev/sec

These values are outside the bounds of the calculated frequency range for each flowrate (see section 4.5.3), so are not considered to be significant as a source of wave formation.

4.4.3 Liquid Physical Properties

Inlet and outlet liquid temperatures are determined using thermocouples at the liquid inlet and outlet of the wetted-wall column contactor. These are logged using Labview and used to determine the average liquid temperature. Liquid density, dynamic viscosity and kinematic viscosity are dependent on temperature and are determined using correlations devised by Weiland et al. (1998). Fresh 30% w/w MEA solution, unloaded with CO_2, is used for all experiments. For comparison with experimental results the average film thickness at each liquid flow condition can be calculated using the Nusselt expression (equation 4.3).

$$\delta_N = \sqrt[3]{\frac{3\nu Q_l}{gW\cos\beta}} \tag{4.3}$$

Where Q_l is the volumetric flowrate, ν is the kinematic viscosity of the fluid, g is acceleration due to gravity, W is the channel width and β is the angle of the channel. The Nusselt equation may over-estimate the film thickness for thin wavy films (Kapitza, 1965), so when compared with theoretical results the position of the interface is normalised with respect to both the Nusselt and Kapitza film thickness (equation 4.4)

$$\delta_K = \sqrt[3]{\frac{2.4\nu Q_l}{gW cos\beta}} \tag{4.4}$$

In this experimental apparatus, the column is vertical so β = 0°. Channel width (W) is analogous to the wetted circumference of the stainless steel tube.
Liquid surface tension is calculated using the empirical correlation of Jayarathna et al (2013). Wave measurements were made at 20-25°C which is outside the range of experimental data used to develop this correlation, but other work in this area does not cover temperatures below 40°C.

$$\sigma = p00 + (p10.\alpha) + (p01.T) + (p20.\alpha^2) + (p11.\alpha.T) + (p02.T^2) + (p30.\alpha^3) + (p21.\alpha^2.T) + (p12.\alpha.T^2) + (p40.\alpha^4) + (p31.\alpha^3.T) + (p22.\alpha^2.T^2) \tag{4.5}$$

Where σ is surface tension in N/m, α is solvent loading in mol CO_2/mol MEA, T is the temperature of the liquid in K and p numbers are constants (see Appendix B).

The theoretical average film velocity at each liquid flow condition is calculated by dividing the volumetric liquid flowrate by the average liquid cross-sectional area.

$$OD_{film} = 12.70mm + (2\delta)$$

$$A_{film} = \frac{\pi OD_{film}2}{4} - \frac{\pi OD_{tube}2}{4}$$

$$\bar{v}_l = \frac{Q_l}{A_{film}} \tag{4.6}$$

Where OD_{film} is the outer diameter of the film in m, OD_{tube} is the outer diameter of the tube in m, A_{film} is the cross-sectional area of the film in m^2, $\bar{v}_l$ is the mean film velocity in m/s and Q_l is the volumetric liquid flow rate in m^3/s.
The liquid phase Reynolds number is defined by Equation 4.7 (Dietze et al., 2007):

$$Re_l = \frac{\bar{v}_l \delta_l \rho_l}{\mu_l} \tag{4.7}$$

Where $\bar{v}_l$ is the mean velocity of the liquid film in m/s, δ_l is the theoretical mean film thickness in m, ρ is density in kg/m^3 and μ_l is dynamic viscosity in m^2/s.
Experiments without gas flow, with countercurrent N_2 and countercurrent CO_2 are carried out on separate days, so solvent properties may vary due to ambient temperature changes. Measured average liquid temperature for a set of experiments ranged between 21.7°C – 23.4°C. The measurement uncertainty of the J-type thermocouples used to measure liquid temperature is +/- 1.1°C. With this uncertainty, the temperature range of experiments is 20.6°C to 24.5°C. Physical properties for fresh, unloaded 30% MEA solution with uncertainty due to temperature variation are summarised in table 3.

Physical Property	Value
Liquid Density (kg/m^3)	1010.5 ± 0.8
Liquid Dynamic Viscosity (mPa.s)	2.65 ± 0.16
Surface Tension mN/m	64.73 ± 0.26

Table 4.2. Liquid Physical Properties of unloaded 30% w/w Monoethanolamine (MEA) solution.

Film thickness Reynolds number and velocity are functions of density and viscosity and are therefore sensitive to variations in liquid temperature. The range of values encountered over the course of the experimental programme are summarised in tables 4.3a and b.

Liquid flow condition	Liquid flow rate (ml/min)	Nusselt film thickness (mm)	Mean film velocity (m/s)	Liquid Reynolds no.
1	141	0.361 ± 0.007	0.158 ± 0.003	21.8 ± 1.3
2	188	0.398 ± 0.008	0.191 ± 0.004	29.1 ± 1.7
3	235	0.437 ± 0.008	0.221 ± 0.004	36.2 ± 2.2

Liquid flow condition	Liquid flow rate (ml/min)	Kapitza film thickness (mm)	Mean film velocity (m/s)	Liquid Reynolds no.
1	141	0.335 ± 0.007	0.171 ± 0.003	21.9 ± 1.3
2	188	0.369 ± 0.008	0.206 ± 0.004	29.1 ± 1.7
3	235	0.405 ± 0.008	0.239 ± 0.005	36.3 ± 2.2

Table 4.3a Mean liquid film thickness, velocity and Reynolds number based on Nusselt equation
Table 4.3b Mean liquid film thickness, velocity and Reynolds number based on Kapitza equation

4.4.4 Gas Physical Properties

The two gases used in this experimental test campaign are CO_2 and N_2 with >99.9% purity. Ideal gas properties are assumed. Gas density is calculated as follows:

$$\rho_g = \frac{[(M_{N2}x_{N2})+(M_{CO2}x_{CO2})]P}{RT} \tag{4.8}$$

Where M is the molar mass of the gas in kg/mol, x is the mole fraction of each gas, P is absolute pressure in Pa, R is the universal gas constant in J/K*mol and T is the average gas temperature at the inlet in K.
Gas viscosity is calculated via Sutherland's equation (Sutherland, 1893) using reference gas viscosities for N_2 and CO_2 at 298.15K:

$$\mu = \mu_{ref}\left(\frac{T}{T_{ref}}\right)^{3/2}\frac{T_{ref}+S}{T+S} \tag{4.9}$$

$$\mu_g = \frac{(\mu_{N2}*x_{N2})+(\mu_{CO2}*x_{CO2})}{R*T} \tag{4.10}$$

Where S is the Sutherland's coefficient for the gas in question, μ_{ref} is the reference dynamic viscosity in m^2/s, T is temperature in K, T_{ref} is the reference temperature in K, $\mu_g$is the viscosity of the gas mixture in m^2/s and R is the universal gas constant in J/K*mol.
To calculate the average gas velocity and Reynolds number, the cross-sectional area available for the gas to flow into and gas hydraulic diameter are initially calculated.

$$A_g = (\pi * r_{glass\ ID}^2) - (\pi(\delta_l + r_{column})^2) \tag{4.11}$$

$$D_{H,g} = r_{glass\ ID} - (\delta_l + r_{column}) \tag{4.12}$$

$$\bar{v}_l = \frac{Q_g}{A_g} \tag{4.13}$$

$$Re_g = \frac{\bar{v}_g D_{H,g} \rho_g}{\mu_g} \tag{4.14}$$

Where A_g is the cross-sectional area in m^2, r is the radius in m, δ is the film thickness in m, $\bar{v}$ is the average film velocity in m/s, Q is the volumetric flow rate of the fluid in m^3/s, DH is hydraulic diameter in m, Re is the Reynolds number, ρ is density in kg/m3 and μ is dynamic viscosity in m^2/s. Subscripts g, l, column and glass ID refer to the gas phase, liquid phase, stainless steel column outer diameter and glass inner diameter, respectively. Gas Reynolds number is similarly affected by variations in lab ambient temperature and the flow uncertainty of the mass flow controller.

Gas Composition	Gas flow setpoint	Re_g
Pure N_2	20 ± 0.2	1563 ± 23
Pure N_2	80 ± 0.6	6254 ± 82
Pure CO_2	10.6 ± 0.2	1564 ± 39
Pure CO_2	43.2 ± 0.3	6256 ± 89

Table 4.4 Gas flow conditions and Reynolds numbers, with uncertainty

4.4.5 Optical Measurement Uncertainty

Raw footage is processed using National Instruments Vision Assistant, which uses pixel intensity values between 0 (pure black) and 1 (pure white) to interpret each individual image. The gas-liquid interface is located at the intersection of two pixels which have the greatest difference in pixel intensity for the region of the image specified. To illustrate this, figure 4.4 shows an example of the software tool detecting the edge of the liquid film.

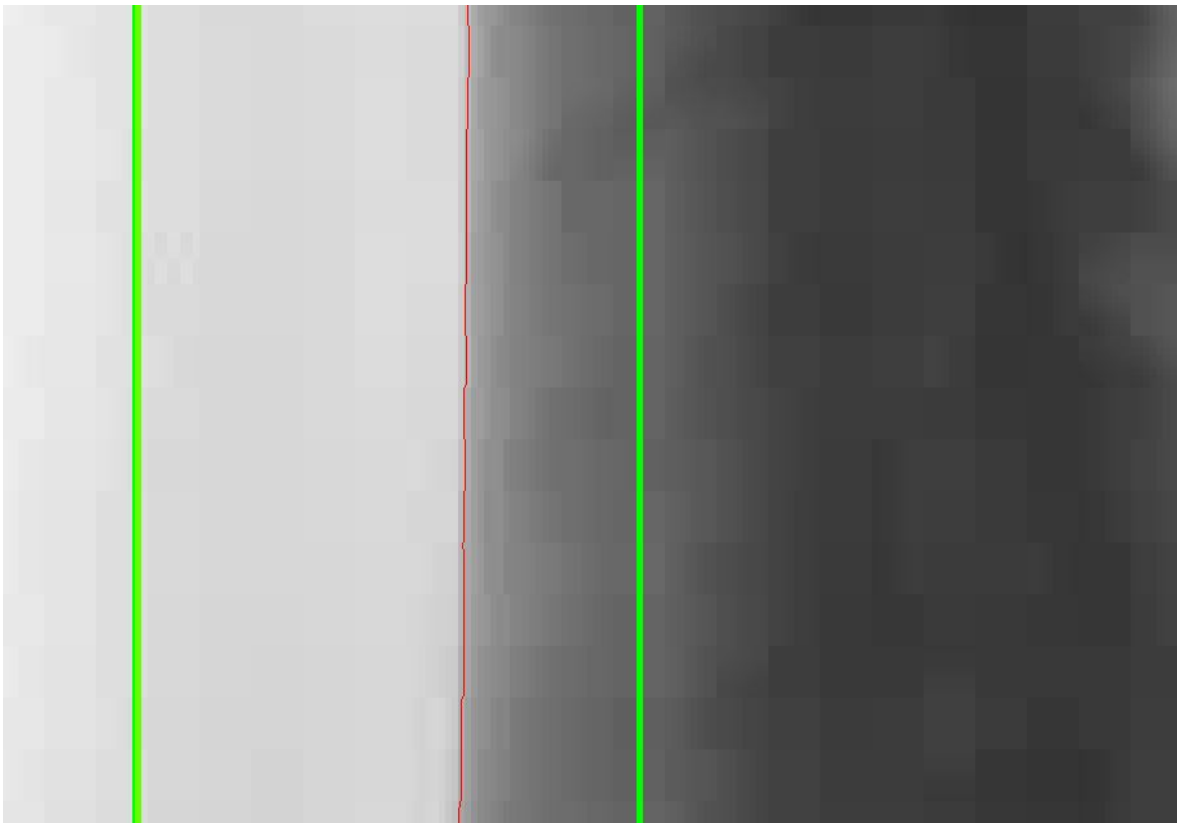

Figure 4.4 Detection of gas-liquid interface in a single frame of footage using National Instruments Vision Assistant.

The outer green lines specify the area of the image to be analysed, while the red line shows the calculated location of the gas-liquid interface. Due to imperfect focusing of the camera lens the observed gas/liquid interface may be conservatively assumed to be as wide as 3 pixels. The calculated interface location is shown as a red line, but over some of its length there exists a 1-pixel wide region to its left which is a slightly darker grey and is distinguishable from the region where there is no liquid film. Similarly, immediately to the right of the red line it may be slightly lighter than the region where liquid exists. For this reason a measurement uncertainty of +/- 1 pixel is assumed in all experiments, so if the interface is observed at x co-ordinate 82, it may in fact exist at x=81 or x=83.
Using equations 4.1 and 4.2, an example in which the edges of the steel column are located at x = 93, x = 538 during calibration and the liquid film is detected at x = 82 is considered.

$$x_1 = 93$$
$$x_2 = 538$$
$$d = \frac{12.70mm}{x_2 - x_1} = 2.854 \times 10^{-2} mm/pix$$
$$x_{film} = 82 \pm 1pix$$
$$\delta_{film} = d(x_1 - x_{film})$$
$$\delta_{film} = 0.3139 \pm 0.0029mm$$

The initial calibration is made using the edges of the steel column, so uncertainty in the measured colulmn diameter contributes to the total uncertainty. The diameter of the column is determined to be 12.70 +/- 0.01mm using calipers.

$$d = \frac{12.70 \pm 1mm}{x_2 - x_1} = 2.854 \times 10^{-2} \pm 2.247 \times 10^{-5}\ mm/pix$$

The additional contribution to the uncertainty is:

$$(x_1 - x_{film}) 2.247 \times 10^{-5}\ mm/pix = 2.4717 \times 10^{-4} mm$$

So the film height, δ_{film} = 0.3139 +/- 0.0288mm. In this case and in the rest of this work, the contribution to the uncertainty from the interface location is 2 orders of magnitude greater than the contribution from calibration.
The inner stainless steel column is surrounded by a Perspex tube. To determine if the tube has any effect on measurements due to refraction, an insert with well-defined ridges of known radius is used.

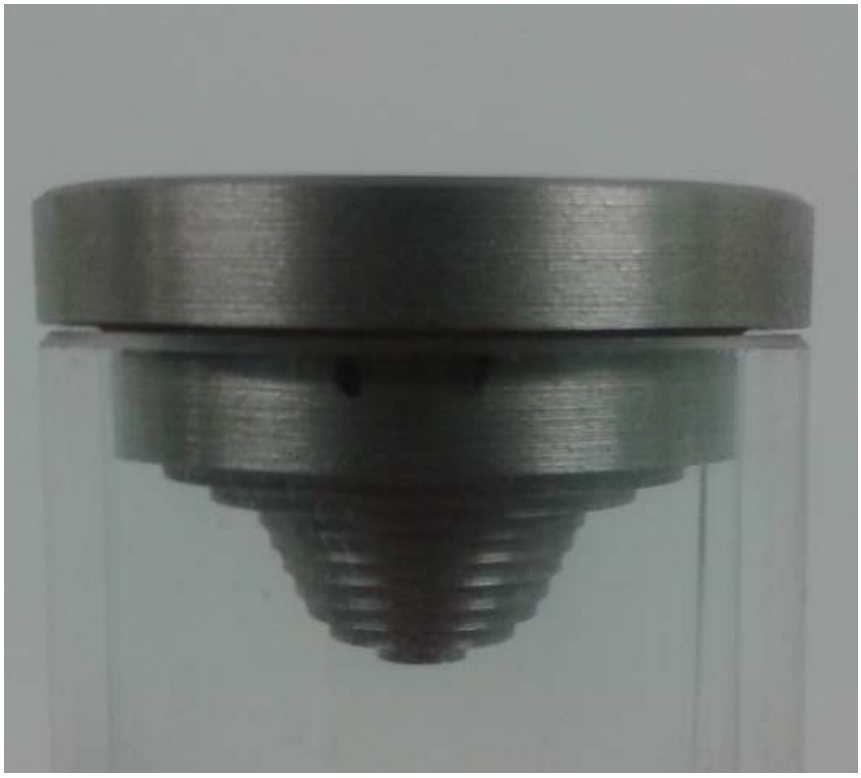

Figure 4.5 Ridged stainless steel insert used for uncertainty analysis

The radius of each of the insert's ridges is calculated. If there is any significant distortion due to the curvature of the glass, a curved profile should be observed when the known distance in mm is plotted against the measured distance in pixels when observed through the high-speed camera lens.

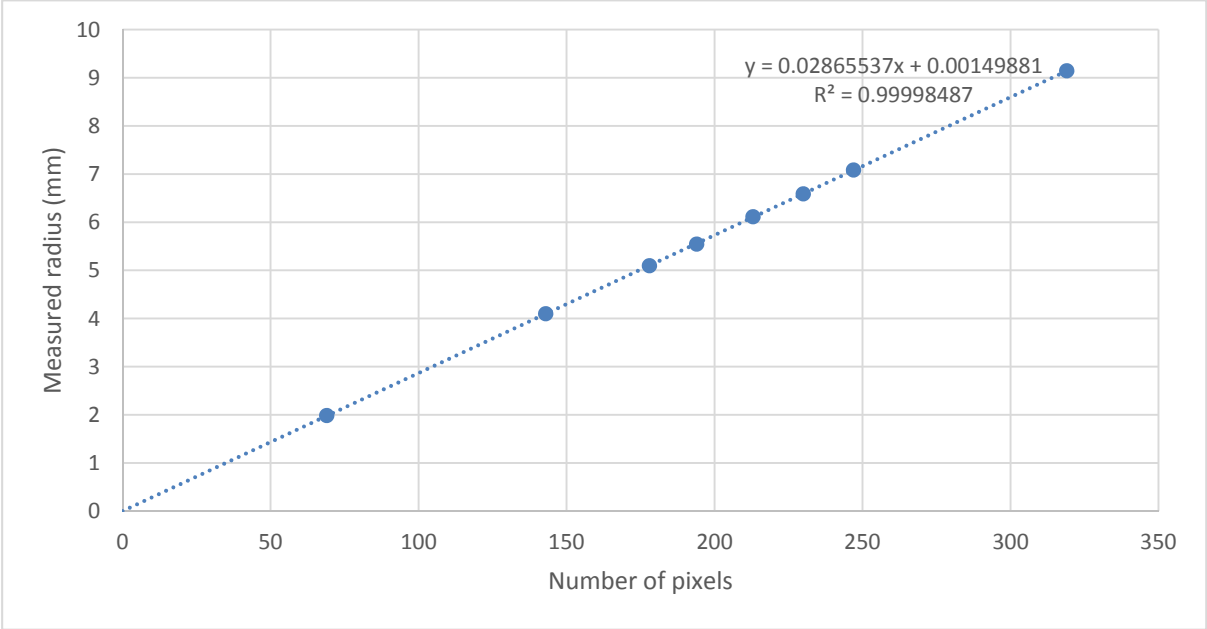

Figure 4.6 Fig. Measured Radius vs no. pixels for column insert

A regression analysis of the data points shows that the line of best fit is linear and within 1 pixel's distance (0.02871 +/- 0.00002mm) of going through the origin, indicating that any distortion is not significant. As a second check, the edges of the ridge which is closest in diameter to that of the steel column is used as a calibration point.

$$d = \frac{12.23 \pm 1mm}{531 - 105} = 2.871 \times 10^{-2} \pm 0.002 \times 10^{-2}\ mm/pix$$

The radii of the other ridges were then calculated by measuring their horizontal distance in pixels in reference to the calibration point at x=105. If tube curvature affects the measurement significantly, the difference between the calculated values and those measured with calipers should increase as the distance from the calibration point increases. At least one of the differences should also be greater than the mm/pixel distance d.

Measured radius of ridge(mm)	Distance of ridge from calibration point (mm)	Calculated radius of ridge (mm)	Difference between calculated and measured values (mm)
1.985	4.130	1.980915	0.004084507
4.100	2.015	4.105376	0.005375587
5.090	1.025	5.081479	0.008521127
5.545	0.570	5.540822	0.004178404
6.600	0.485	6.603052	0.003051643
7.085	0.970	7.091103	0.006103286
9.155	3.040	9.158146	0.00314554

Table 4.5 Difference between measured and calculated radii of calibration insert ridges

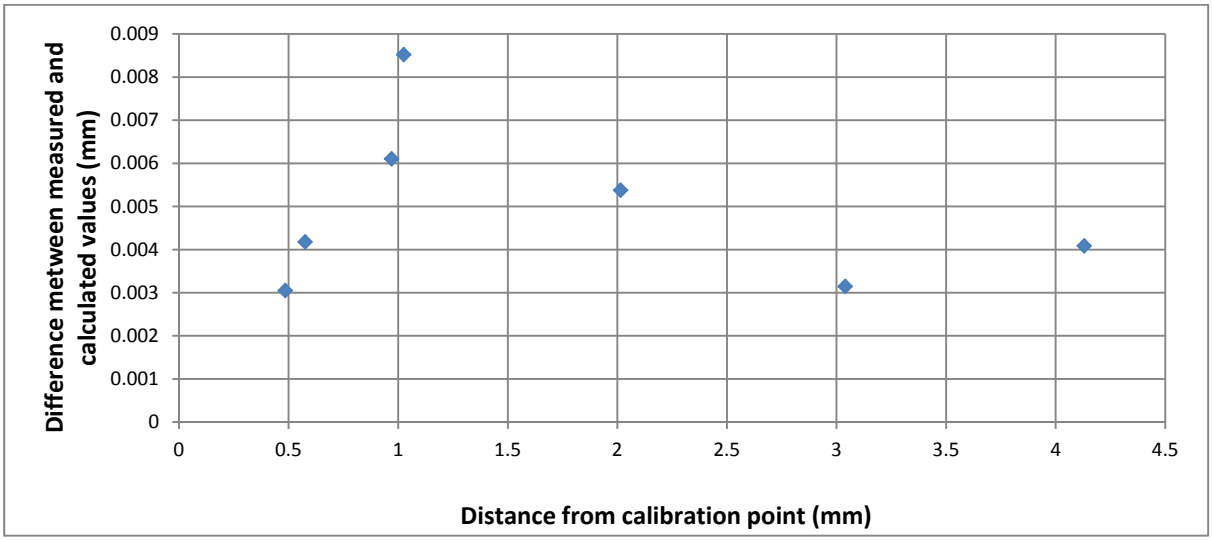

Figure 4.7 Difference between measured and calibrate values vs distance from calibration point

The plot shows no increasing trend as the distance from the calibration point increases and the largest deviation from the calculated value is 0.0085mm. Since the distance per pixel in this case is 0.02871 +/- 0.00002mm it is safe to assume that any distortion due to the curvature of the outer tube is negligible.

4.5 Experimental Results

At each flow condition and location, footage is captured at a shutter speed of 300fps for 10s. Footage is recorded in triplicate, with lighting conditions and camera gain modified slightly in each case to ensure that the gas-liquid interface is well-defined for each flow condition. Camera artefacts occasionally appear in the video feed as the camera is operating at its maximum shutter speed, but for each condition at least 1950 uninterrupted frames (6.5 sec) of artefact-free footage are obtained from which film properties can be determined.

For flow systems with no countercurrent gas flow, laminar countercurrent N_2, and turbulent countercurrent N_2, wave measurements are made at 10mm intervals along the length of the column from 10mm to 160mm. Film profile analysis is used to determine mean film thickness, wave velocity, wavelength, and growth rate for non-absorbing flow systems.

Gas flow rates of N_2 are selected to be representative of flow conditions in structured packings for CO_2 capture. Structured packings are, in general, characterised in terms of the range of gas-phase F-factors they are operational over, a function of gas velocity and density ($v_{gas} \cdot \rho_{gas}^{0.5}$). Anecdotal evidence based on experience and correspondence with Sulzer Chemtech suggests that for CCS applications using 30% MEA and packing based on Mellapak Y, a range of F-factors between 0.7 – 1.5 $Pa^{0.5}$ are likely to be the design point. A volumetric N_2 flow rate of 20l/min results in an F-factor of 0.95 $Pa^{0.5}$. Other packing types, absorber configurations and solvents may be optimised for greater f-factors, so an 80l/min flowrate of N_2 (F-Factor = 3.8) is also used to investigate the effect of fully turbulent flow on wave development. This also proves that the test rig is suitable for use over a wide range of gas flowrates.

The effect of reactive absorption on film profile is observed via comparison of the wave film profile for non-absorbing systems and those with 30% MEA and counter-current CO_2. To ensure comparisons with non-absorbing systems are valid, flow rates of CO_2 are selected to have the same Reynolds number as those of the two N_2 cases, with 11.4l/min and 43.1/min equating to approximately 1560 and 6250, respectively. All flow conditions tested are summarised in table 4.6.

Liquid flow condition	Liquid Reynolds number	Gas composition	Gas flow rate (l/min)	Gas Reynolds Number
1	21.9	N/A	0	0
2	29.1	N/A	0	0
3	36.3	N/A	0	0
1	21.9	Pure N_2	20	1563
2	29.1	Pure N_2	20	1563
3	36.3	Pure N_2	20	1563
1	21.9	Pure N_2	80	6254
2	29.1	Pure N_2	80	6254
3	36.3	Pure N_2	80	6254
1	21.9	Pure CO_2	10.8	1564
2	29.1	Pure CO_2	10.8	1564
3	36.3	Pure CO_2	10.8	1564
1	21.9	Pure CO_2	43.2	6256
2	29.1	Pure CO_2	43.2	6256
3	36.3	Pure CO_2	43.2	6256

Table 4.6 List of gas-liquid flow conditions tested

4.5.1 Mean Film Thickness Measurement

Mean film thickness measurements are made at a distance of 40mm from the top of the column for three liquid flow conditions, in the absence of gas flow, for comparison with Nusselt and Kapitza film thicknesses. The high-speed camera is positioned so that the vertical field of view is centred at 40mm from the top of the stainless steel column. At this distance the waves are still beginning to develop, so there is less variation in film thickness and the measurement error due to averaging will be minimised. National Instruments Vision Assistant is used to rapidly determine the location of the gas-liquid interface in the centre of the vertical field of view for each frame of footage captured. Film thickness is determined using the interface on the left side of the stainless steel column, as lighting conditions provide a better contrast here than on the right.. As the distance per pixel (d_{pix}) and x co-ordinate of both the interface (x_i) and the column edge (x_1) are now known, the film thickness δ in mm can be calculated using equation 4.2.

Figure 4.8 Sample footage of liquid flowing down stainless steel column

Film thickness vs time is plotted for each flow condition.

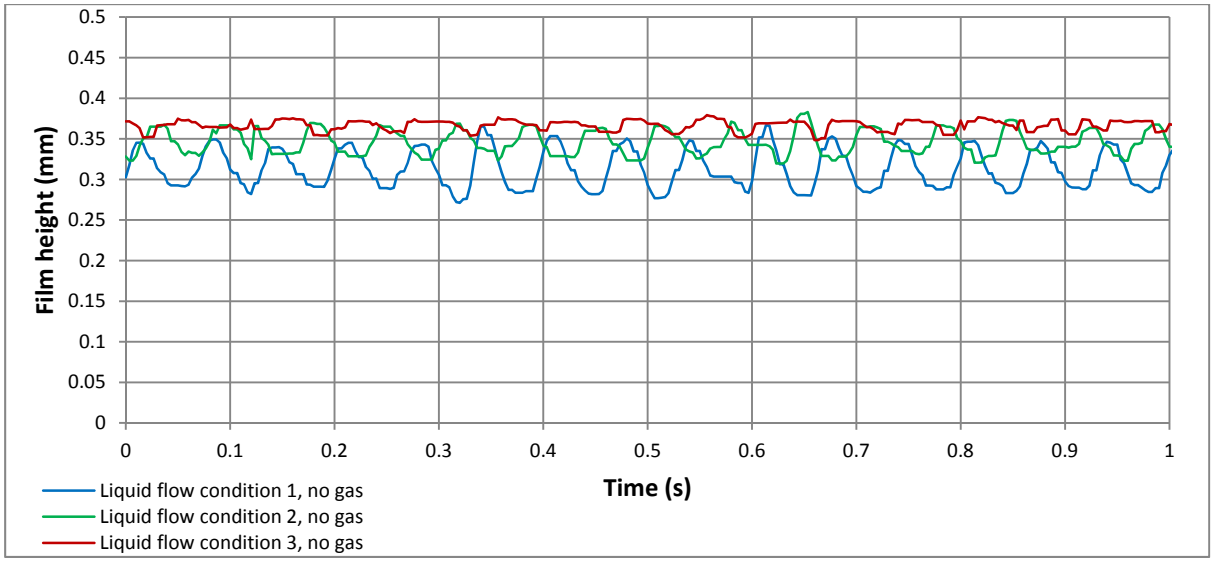

Figure 4.9 Film height vs time, 40mm from top of column, no countercurrent gas

The uncertainty in the film height measurement is +/- 1 pixel, in this case 0.029mm. The magnitude of the uncertainty for each liquid flow condition is shown in figure 4.10. To enhance the clarity of the figure, liquid flow condition 2 is offset by +0.1mm, while liquid flow condition 3 is offset by +0.2mm.

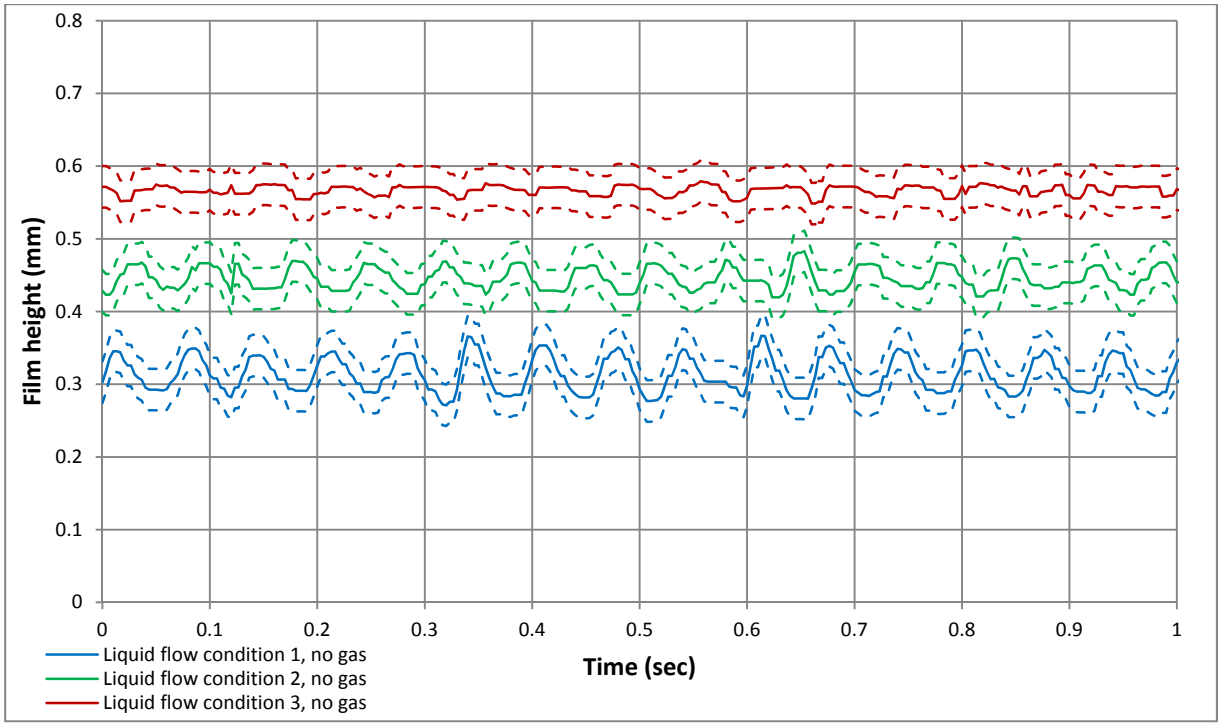

Figure 4.10 Liquid film profile with uncertainty, 40mm from top of column, no countercurrent gas

A comparison between theoretical and measured film thickness for flow conditions without counter-current gas is provided in table 4.6. The results show good agreement with the Kapitza film thickness, which falls within the bounds of the measurement uncertainty for all three cases, but the discrepancy between the measured value and the Nusselt film thickness is considerably larger.

Liquid flow condition	Liquid Re	Nusselt film thickness (mm)	Kapitza film thickness (mm)	Measured film thickness (mm)	Deviation of measured value from Nusselt (%)	Deviation of measured value from Kapitza (%)
1	21.3	0.364	0.329	0.313 ± 0.029	14.00	4.91
2	28.3	0.401	0.363	0.345 ± 0.029	13.84	4.74
3	35.3	0.432	0.391	0.368 ± 0.029	14.75	5.76

Table 4.7. Comparison of theoretical film thickness as predicted by Nusselt and Kapitza expressions, with measurements

4.5.2 Wave Velocity

Wave velocity is calculated by plotting wave traversal profiles through the field of view as a function of time in Matlab. The wave profile is smoothed as described in section 6 below. As it travels along the column length, the film maintains a characteristic local minimum which precedes the crest of the wave. Shown below is an example for flow condition 1, with the minima indicated by black arrows. For clarification, x=0 is the top of the vertical field of view and the first frame visible is at t=0s.

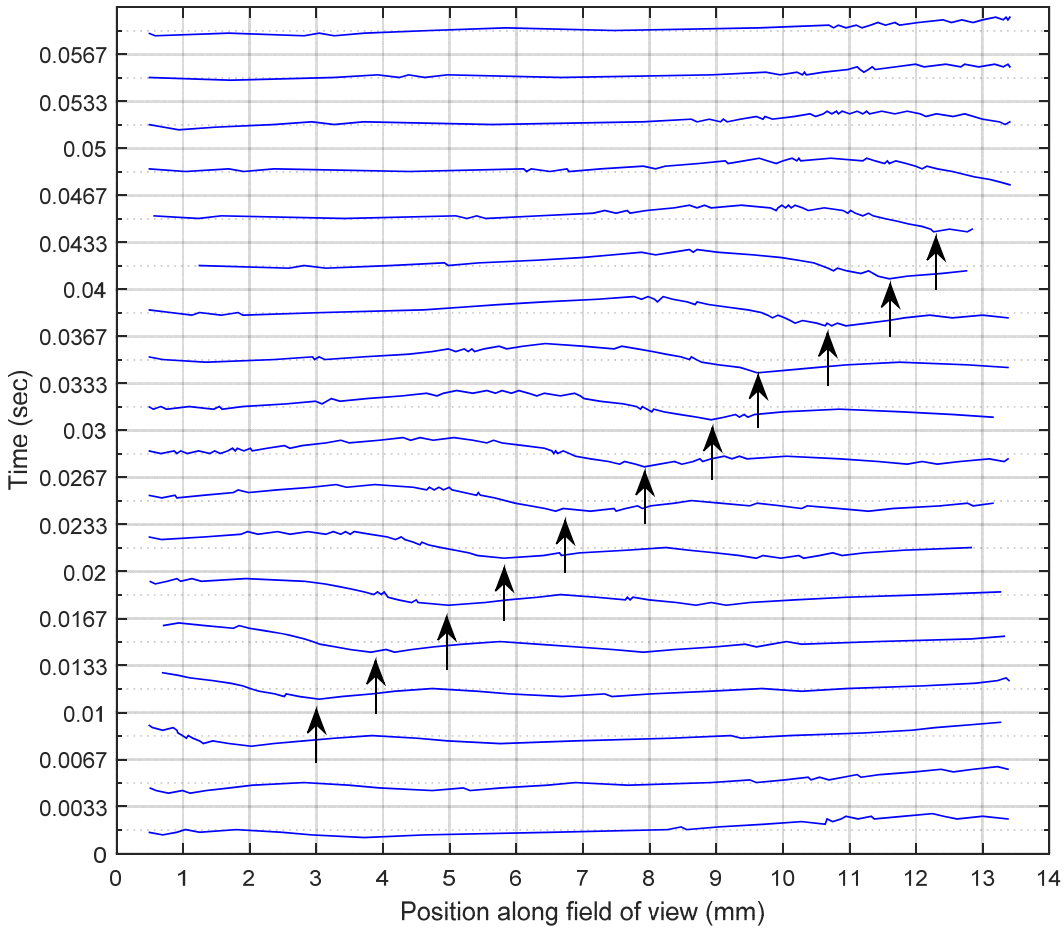

Figure 4.11. Evolution of wave profile across field of view, liquid flow condition 1, no gas flow

It is possible to extract the location of this local minimum for each frame as the wave passes through the camera's field of view. A linear regression of this dataset, plotted as vertical position along the field of view vs time has gradient equal to the wave velocity in mm/s. However, the location of the local minimum is not precise

to within one pixel, thus there is a positional uncertainty regarding its location. This is illustrated using example footage (figure 4.11) and associated raw text data for a single frame.

Figure 4.12 Contour analysis of the wetted surface. Green lines indicate the area to be analysed for the liquid surface. Local minimum location is indicated by the red box.

Curve X Position	91	91	91	91	91	91	91	91	91	91	91
91	91	91	91	91	91	91	91	91	91	91	91
Curve Y Position	297	298	299	300	301	302	303	304	305	306	307
308	309	310	311	312	313	314	315	316	317	318	319

Table 4.8 Raw text data from contour analysis

The local minimum is located at an x co-ordinate of 91 pixels and runs vertically from y = 297 to y = 319 pixels. The location of the local minimum in this frame is therefore located at 308±12 pixels. The location of the local minimum along the y-axis is tracked as it travels along the field of view, then positional data in pixels is converted into real distance using equation 4.1. Distance along the field of view is plotted against elapsed time for each liquid-gas flow condition, with the line of best fit through the datapoints providing the calculated wavelength.

To account for any short-term, transient interruptions in the normal film flow pattern, the mean positional uncertainty is calculated using contour profile data for three non-consecutive waves at each gas-liquid flow condition. The mean uncertainty, rounded to the nearest pixel for each gas-liquid flow condition, is provided in table 4.9

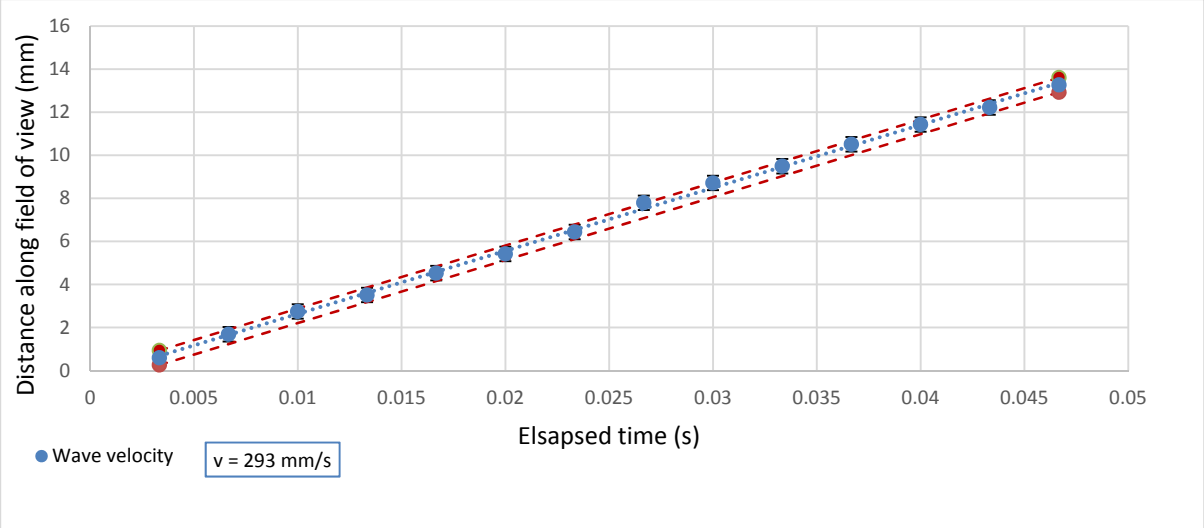

Figure 4.13 Local minimum location vs time, 120mm from top of column. Wave velocity lies somewhere in the region defined by the red dashed lines.

The region between the red lines in figure 4.12 defines the range of possible velocities for the wave. In this case the calculated velocity, i.e. the line of best fit, is 293mm/s (0.293m/s). There is also some uncertainty in elapsed time along the x-axis, equivalent to the exposure time per frame of the high-speed camera. However, these are of the order of 10^{-6} s, at least three orders of magnitude lower than the time between subsequent datapoints. The time uncertainty can therefore reasonably be considered to be negligible.

The range of velocities in mm/s is calculated using the maximum and minimum velocities for the defined region, as shown in figure 4.13. Further examples are provided for the other two liquid flow conditions (figure 4.14, 4.15). Results for all non-absorbing gas-liquid flow conditions are provided in table 4.9.

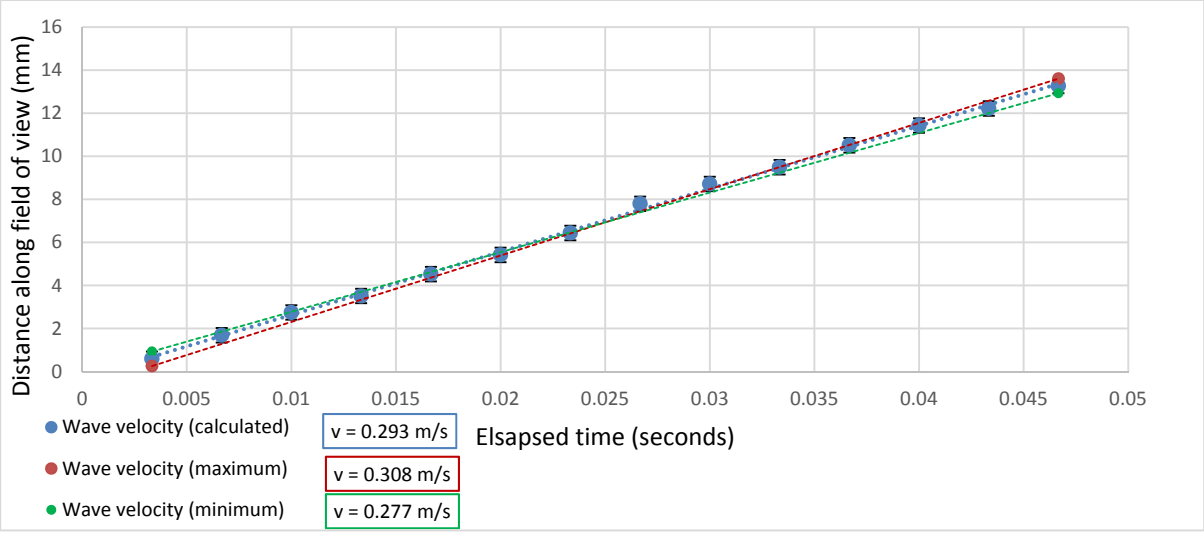

Figure 4.14. Local minimum location vs time, 120mm from top of column, liquid flow condition 1 (Re = 21.9), no gas flow

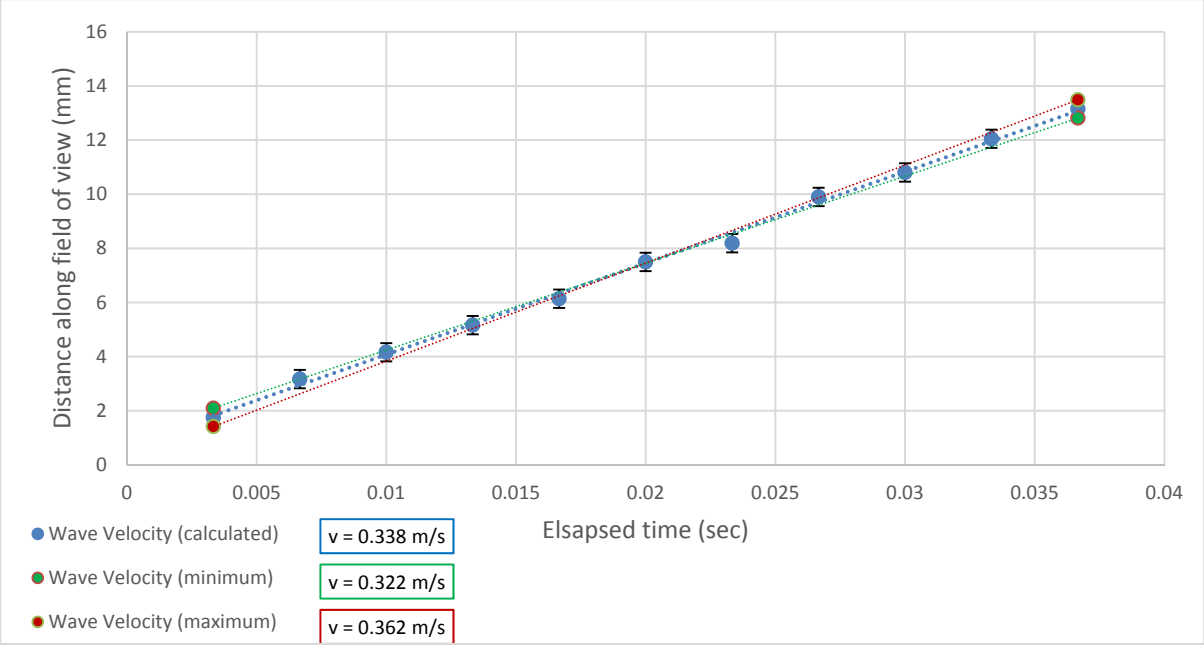

Figure 4.15. Local minimum location vs time, 120mm from top of column, liquid flow condition 2 (Re = 29.1)

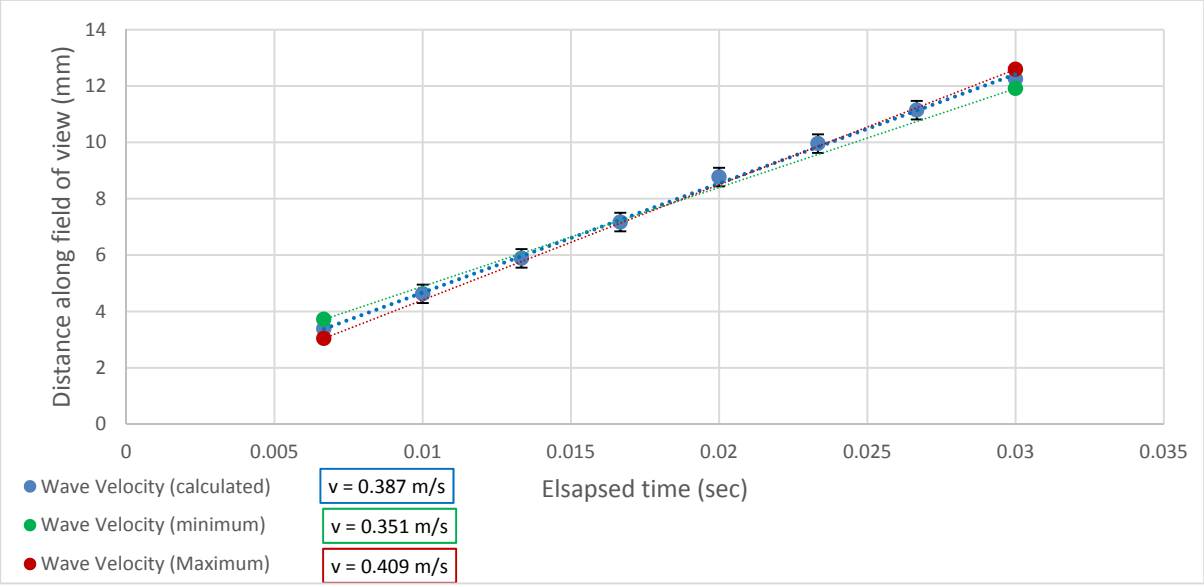

Figure 4.16. Local minimum location vs time, 120mm from top of column, liquid flow condition 3

For each flow condition, three non-consecutive waves are used to calculate the mean maximum and velocity. This midpoint of the velocity range is taken to be the wave velocity at this flow condition. Wave velocity results for all conditions are given in table 4.9. All measurements are made at a distance of 120mm from the top of the column, as waves have fully developed and are well defined for all flow conditions at this point (See section 4.5.4 on wave growth rate).

Mean film velocity is also provided to allow comparison with wave velocity to be made. These are based on the volumetric flow rate and the liquid film cross-sectional area as defined by the Kapitza film thickness, which is found to be in close agreement with measured values (Table 4.7). All liquid flows are in the laminar region so the hydraulic entrance length ($L_{h,laminar}$) can be calculated using equation 4.15, in which Re is the Reynolds number and D_H is the hydraulic diameter of the film. The hydraulic entrance length never exceeds 1mm at these low Reynolds numbers, so the velocity profile

$$L_{h,laminar} = 0.05ReD_H \tag{4.15}$$

Liquid flow condition	Liquid Reynolds number	N_2 flow rate (l/min)	N_2 Reynolds number	Wave velocity (m/s)	Theoretical mean film velocity (m/s)
1	21.9	0	0	0.292 ± 0.016	0.171
2	29.1	0	0	0.342 ± 0.020	0.206
3	36.3	0	0	0.380 ± 0.030	0.239
1	21.9	20	1563	0.295 ± 0.018	0.171
2	29.1	20	1563	0.338 ± 0.020	0.206
3	36.3	20	1563	0.388 ± 0.025	0.239
1	21.9	80	6254	0.276 ± 0.025	0.171
2	29.1	80	6254	0.319 ± 0.027	0.206
3	36.3	80	6254	0.376 ± 0.025	0.239

Table 4.9. Wave velocity results for all flow conditions

There may be a slight trend towards lower wave velocity at higher counter-current gas flows, but the effect on velocity is small and lies within the bounds of the measurement uncertainty. This indicates that wave velocity in these flow systems is not a strong function of gas flow rate. The uncertainty in wave velocity measurement, while never exceeding 9% of the absolute value, becomes highly significant in the determination of wave growth rate.

4.5.3 Frequency and wavelength

Wave frequency can be calculated by counting the number of definite wave peaks appearing in a "slice" of high-speed camera footage. An example for liquid flow condition 1 with no counter-current gas is shown below.

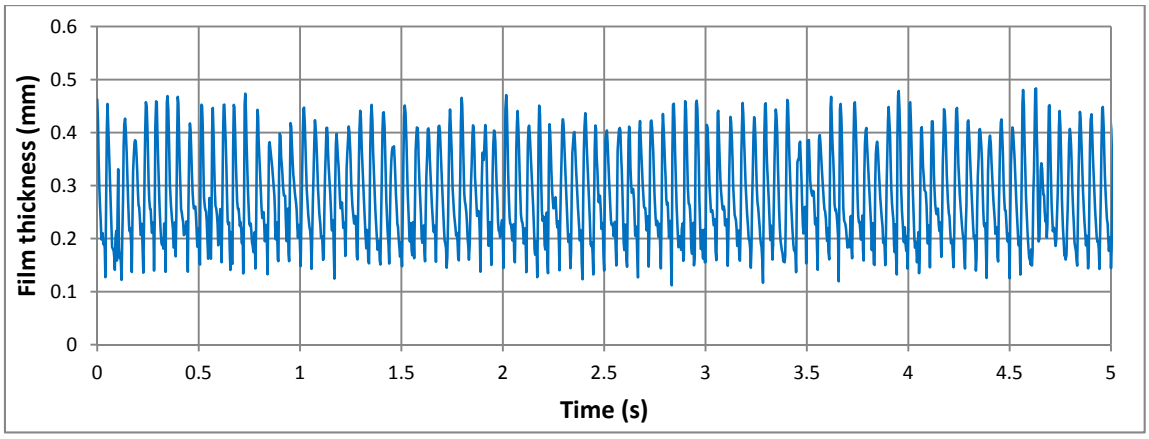

Figure 4.17. Film thickness vs time, liquid flow condition 1 (Re = 21.9), no counter-current gas

Over a period of 5 seconds, 90 definite peaks are observed. However, there is a short period of time which elapses between t=0s and the first peak appearing. Similarly, there is a short period of time between the final peak appearing and t=5s. The sum of these two periods of time are at most, equal to 2x the mean wave period. Therefore the time required for 90 full waves to pass through the field of view is 5s ± (2×wave period).s

The wave period can be reasonably approximated as $\frac{5}{90}s$. The time required for 90 waves to pass through the field of view is therefore 5s ± $\frac{10}{90}s$. Frequency is then determined using equation 4.16.

$$\nu = \frac{waves}{time} = \frac{90}{(5 \pm \frac{10}{90})s} \tag{4.16}$$

$$\nu = 18 \pm 0.4 s^{-1}$$

Wavelength is calculated by dividing the velocity by the frequency, accounting for the relative measurement uncertainty in each case. Using the frequency calculated above and associated wave velocity of 0.292 ± 0.016m/s:

$$\lambda = \frac{0.292 \pm 0.016\ m/s}{18 \pm 0.4\ s^{-1}}$$

$$\lambda = \frac{0.292 m/s \pm 5.5\%}{18 s^{-1} \pm 2.2\%}$$

$$\lambda = 0.016 m\ \pm 7.7\%$$

Full frequency results for all flow conditions with are shown in table 4.10. All calculations are made using high-speed camera footage recorded at 120mm from the top of the column, as this allows ample time for the waves to develop while reducing the risk of liquid spraying up from the gas inlet and obscuring the field of view.

Liquid flow condition	N_2 flow rate (l/min)	Frequency (s^{-1})	Wavelength (m)
1	0	18.0 ± 0.4	0.016 ± 7.7%
2	0	18.0 ± 0.4	0.019 ± 8.1%
3	0	18.2 ± 0.4	0.021 ± 10.1%
1	20	15.6 ± 0.4	0.019 ± 8.7%
2	20	16.2 ± 0.4	0.021 ± 8.4%
3	20	16.2 ± 0.4	0.024 ± 8.9%
1	80	13.4 ± 0.4	0.020 ± 12.0%
2	80	14.6 ± 0.4	0.022 ± 11.2%
3	80	16.5 ± 0.4	0.022 ± 9.1%

Table 4.10. Wave frequency and wavelength for all non-absorbing flow conditions

Once gas flow is introduced the wave pattern becomes less regular and the presence of occasional, brief periods without well-defined waves (see between t=1 and t=1.5s in fig. 4.18 below) reduces the frequency. Between t=3.5 and 4.5s the wave pattern is regular, but a short-term transient disturbance can be observed around t=1s, when the regular wave pattern breaks down and distinct peaks are not observable. This results in a lower average frequency (and higher wavelength). In cases such as this, when model validation is the goal, the frequency and wavelength should be determined over periods where the wave period is regular.

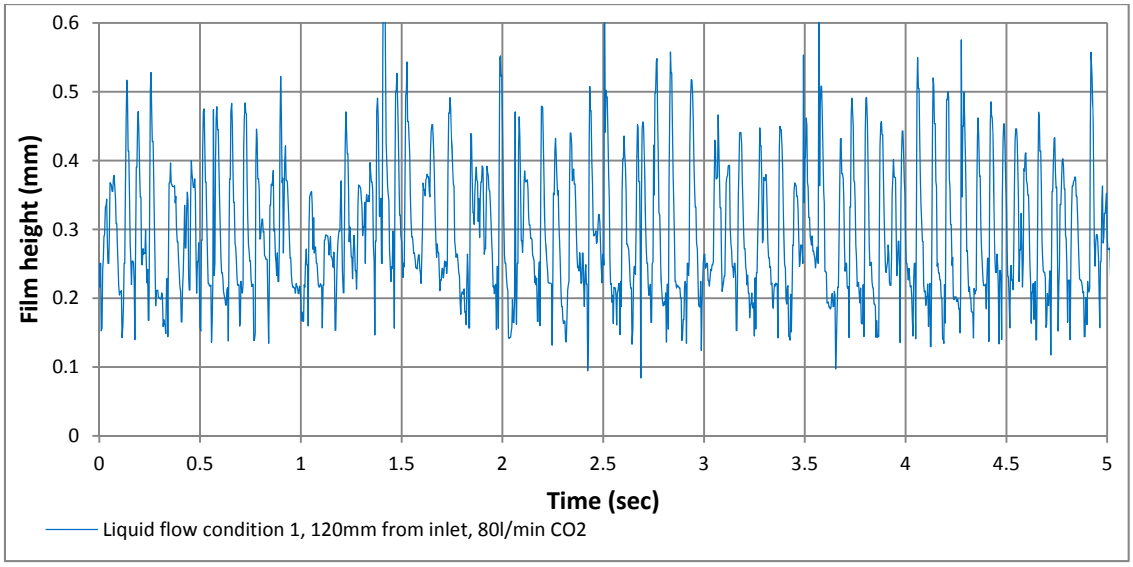

Figure 4.18. Film height vs time, liquid flow condition 1 (Re = 21.9), 80l/min N2

The wavelength in particular must be known. The purpose of using this test rig for wave measurement analysis is to support modelling efforts of thin films flowing over structured packing. The reduced-order numerical SWANS model (Lavalle et al, 2017), currently under development by collaborating researchers, is suitable for counter-current flow systems in which the film thickness is much smaller than the wavelength. In all flow cases presented, the wavelength is two orders of magnitude greater than the maximum liquid film height. The test rig therefore satisfies this criterion for the validation of numerical models.

4.5.4 Wave Growth Rate

As waves travel down the outside of the tube, they grow in size until the wave peak amplitude reaches its saturation point. Using optical measurements it is possible to determine the saturation point and the growth rate of these waves for each flow condition. The amplitude of a wave can be expressed as:

$$a = a_o e^{\omega^{temp} t} \tag{4.17}$$

Where a is the wave amplitude in mm, a_o is the film amplitude at t=0 (in this case, the average film thickness determined previously), ω^{temp} is the temporal wave growth rate and t is the time the wave has been travelling for. In theory, the temporal wave growth rate can be determined by plotting $\ln(a/a_0)$ vs t for the period during which the wave is growing.

$$ln\frac{a}{a_0} = \omega^{temp} t \tag{4.18}$$

The vertical field of view of the high-speed camera is limited to around 13mm, if it were positioned any further away the resolution is not high enough to avoid incurring large measurement uncertainties in film height. Over this distance it is not possible to observe the growth of a single wave, so instead the mean wave peak amplitude at 10mm intervals from 0 to 160mm from the top of the column are calculated. The average of 10 non-consecutive wave peak heights are used to determine an average for each location. Only non-absorbing cases with no counter-current gas, 20l/min N_2 and 80l/min N_2 are considered as the

For each liquid flow condition the time the mean film thickness is taken as the amplitude at t=0. The wave velocity is known, so the time required for it to travel between camera locations can be calculated. The absolute uncertainty in wave velocity propagates and increases as a function of time.

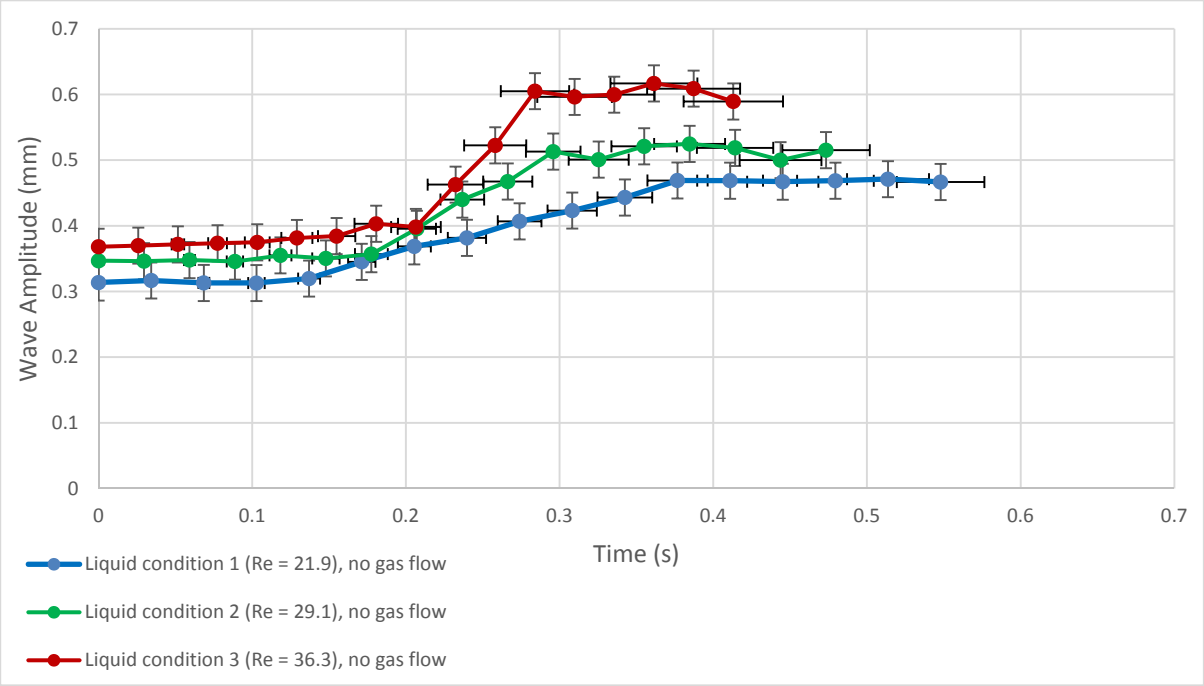

Figure 4.19. Wave amplitude plotted against time, all liquid flow conditions (Re = 21.9, 29.1, 36.3), no gas flow

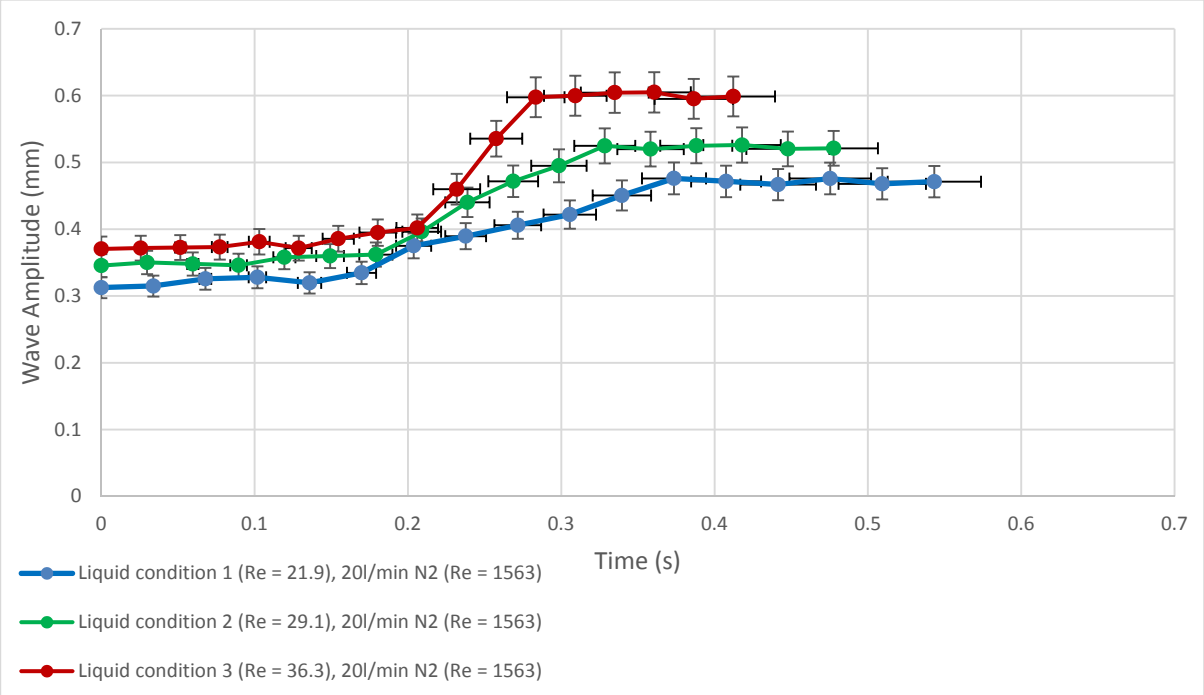

Figure 4.20. Wave amplitude plotted against time, all liquid flow conditions (Re = 21.9, 29.1, 36.3), 80l/min N2 (Re = 1564)

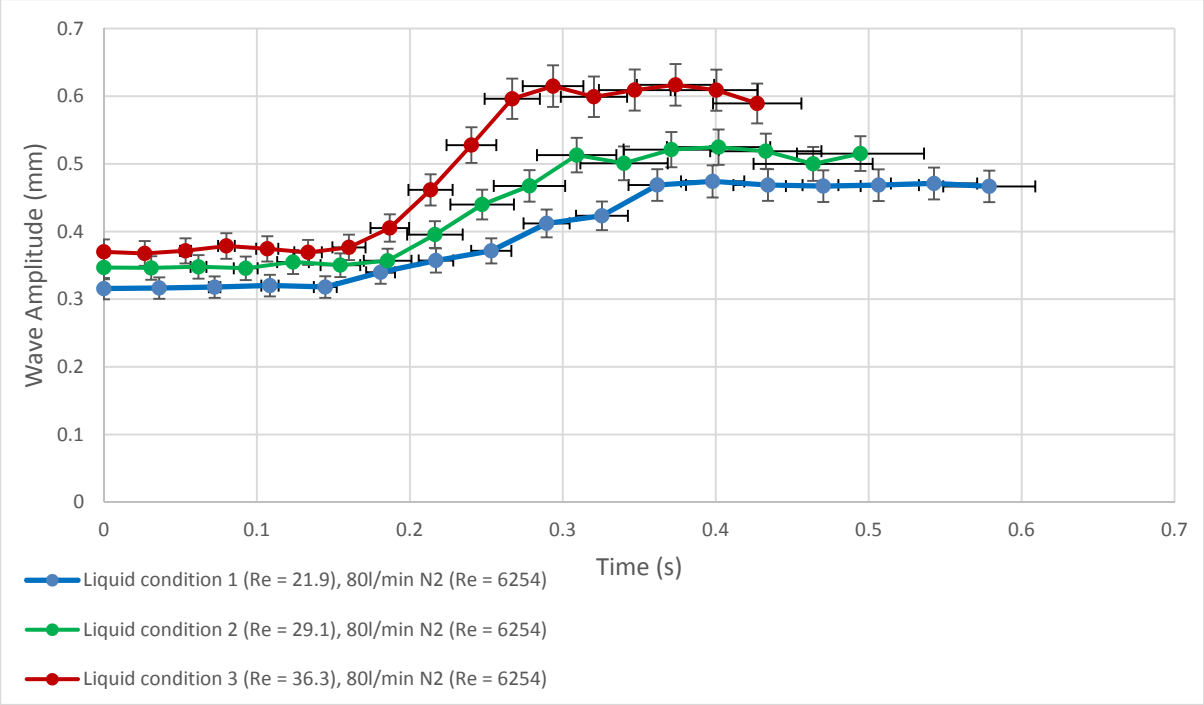

Figure 4.21. Wave amplitude plotted against time, all liquid flow conditions (Re = 21.9, 29.1, 36.3), 80l/min N2 (Re = 6254)

Plotting ln (a/a_0) vs time over regions where the wave is increasing in amplitude allows the temporal wave growth rate to be determined from the gradient of the region in which the wave is growing. The case without gas flow is plotted in figure 4.22. For clarity, error bars are not included in this diagram.

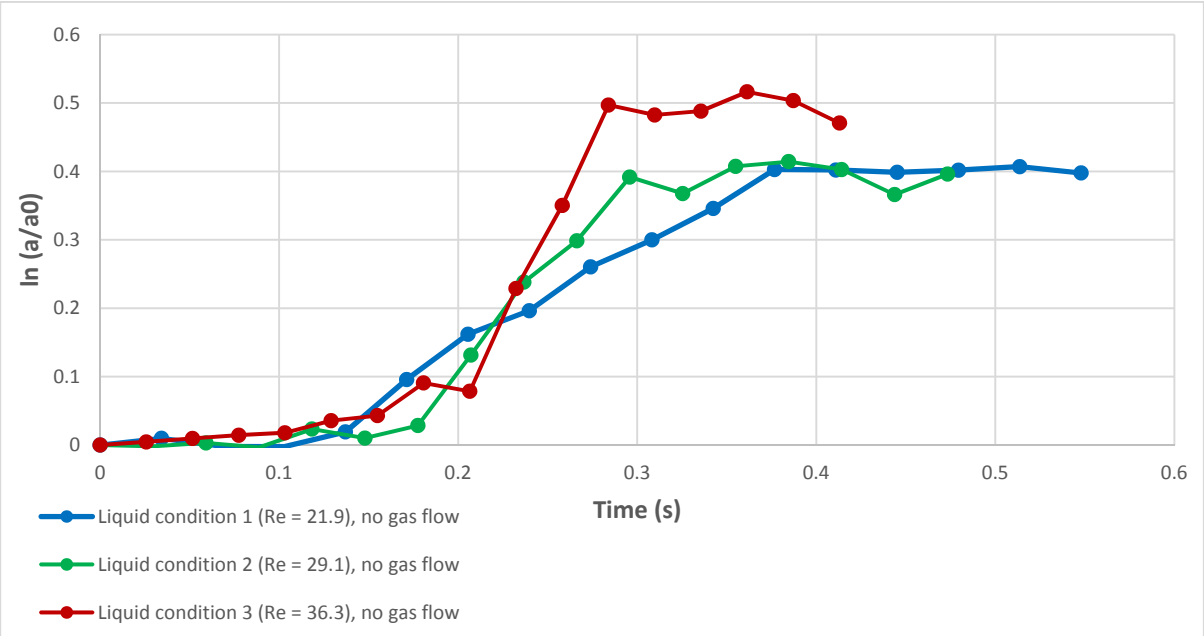

Figure 4.22 ln(a/a0) plotted against time, all liquid flow conditions (Re = 21.9, 29.1, 36.3), no gas flow, error bars omitted for clarity

The regions which appear approximately linear are extracted and plotted individually in figures 4.23a, b and c. A linear regression of the data points produces a line whose gradient is the calculated wave growth rate in s^{-1}. The growth rate exists somewhere in the region defined by the uncertainty, which is significant. The growth rate calculated by linear regression and the growth rate range are shown for each flow condition.

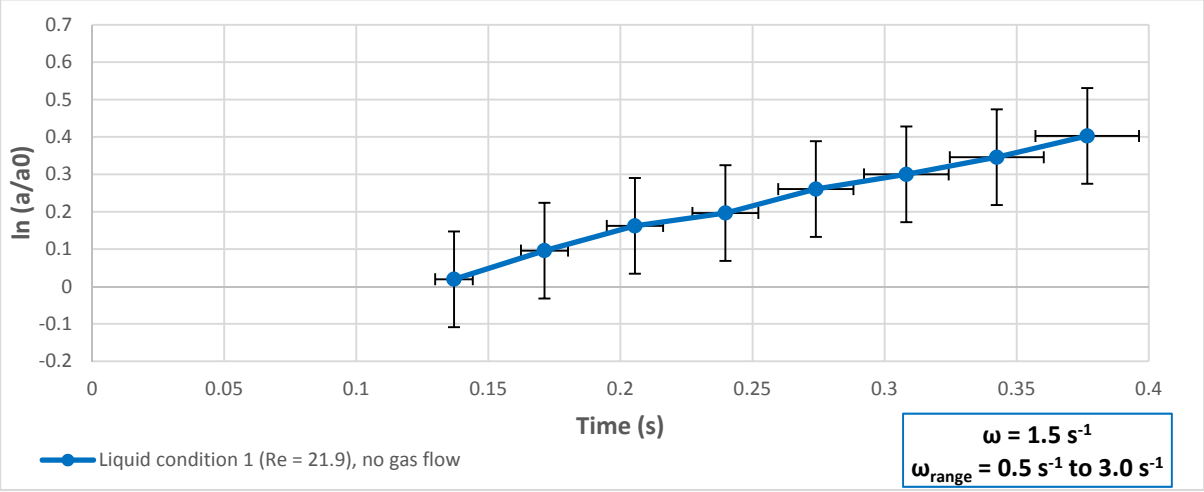

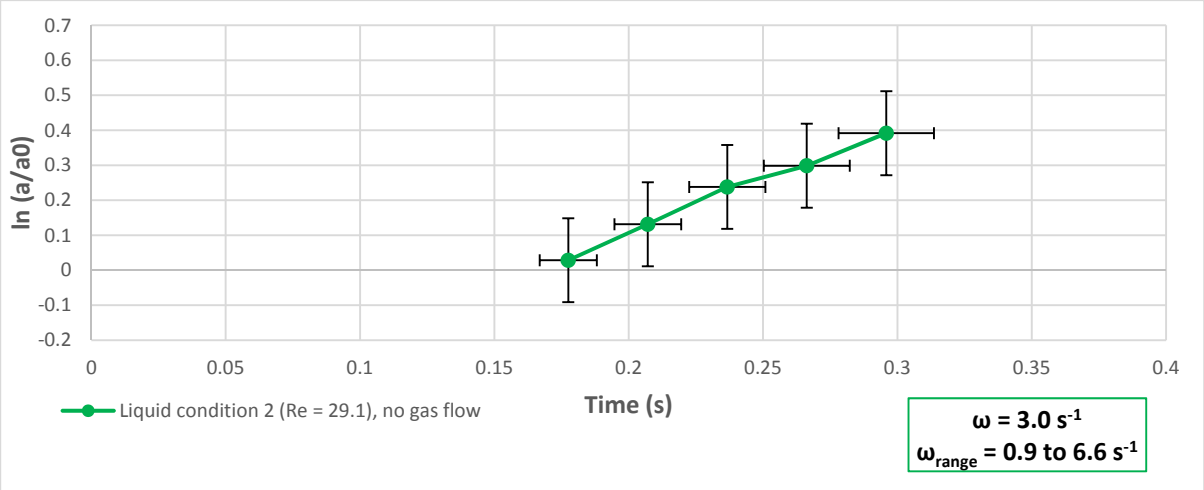

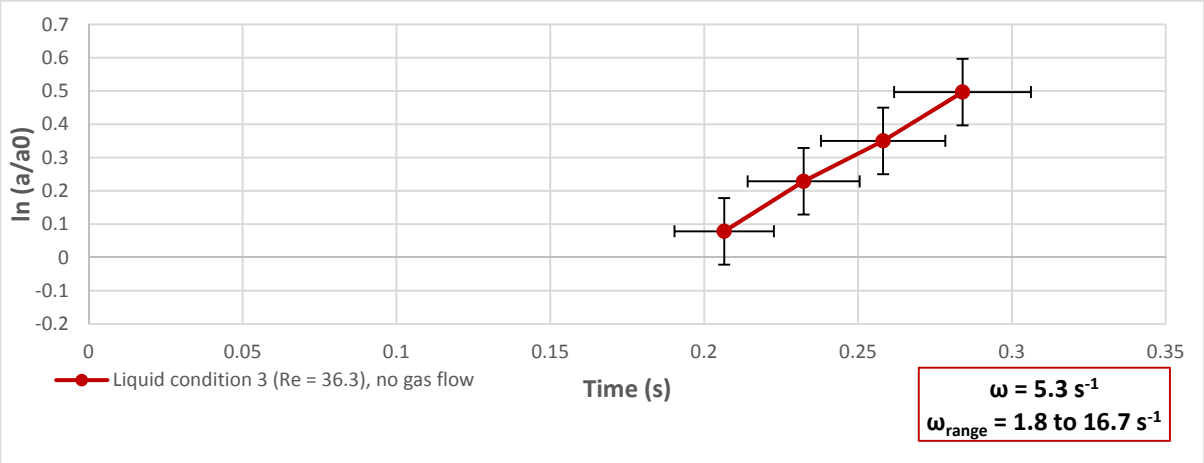

Figure 4.23a. ln(a/a0) plotted against time, liquid flow condition 1 (Re = 21.9), no gas flow
Figure 4.23b ln(a/a0) plotted against time, liquid flow condition 1 (Re = 29.1), no gas flow
Figure 4.23c. ln(a/a0) plotted against time, liquid flow condition 1 (Re = 36.3) no gas flow

While the possible range of wave growth rates is large for each flow condition, the general trend is of increasing ω as the liquid phase Reynolds number increases and the flow becomes more unstable.
Data is also collected for the three liquid flow conditions with countercurrent gas. This is presented in figures 4.24, 4.25a, b and c for 20l/min N_2, and 4.26, 4.27a, b and c for 80l/min N_2.

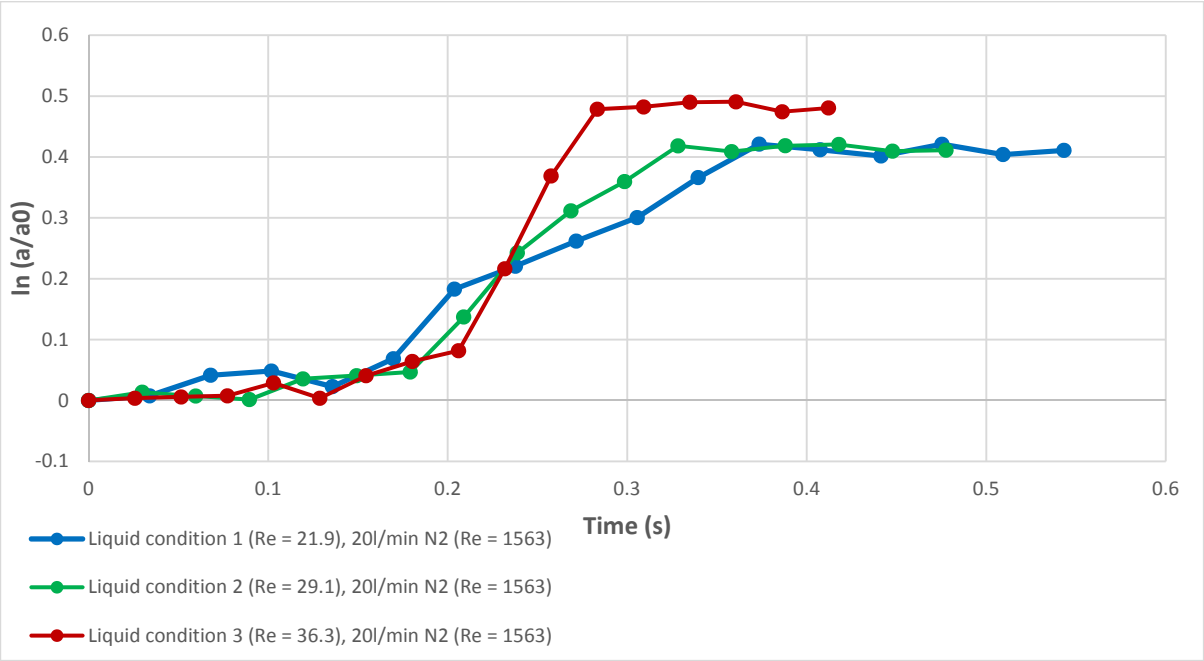

Figure 4.24 ln(a/a0) plotted against time, all liquid flow conditions (Re = 21.9, 29.1, 36.3), 20l/min N2 (Re = 1564)

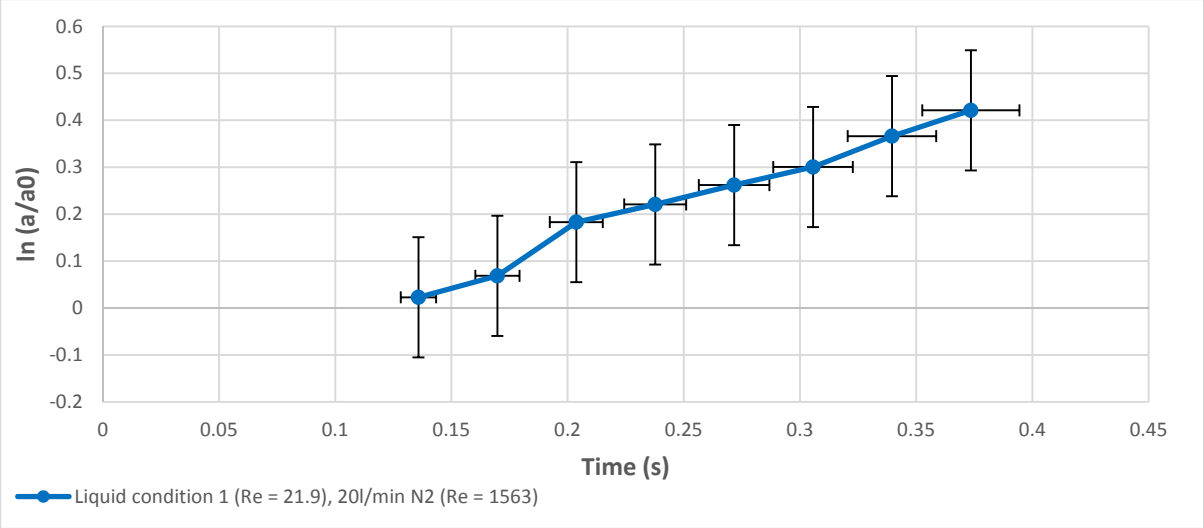

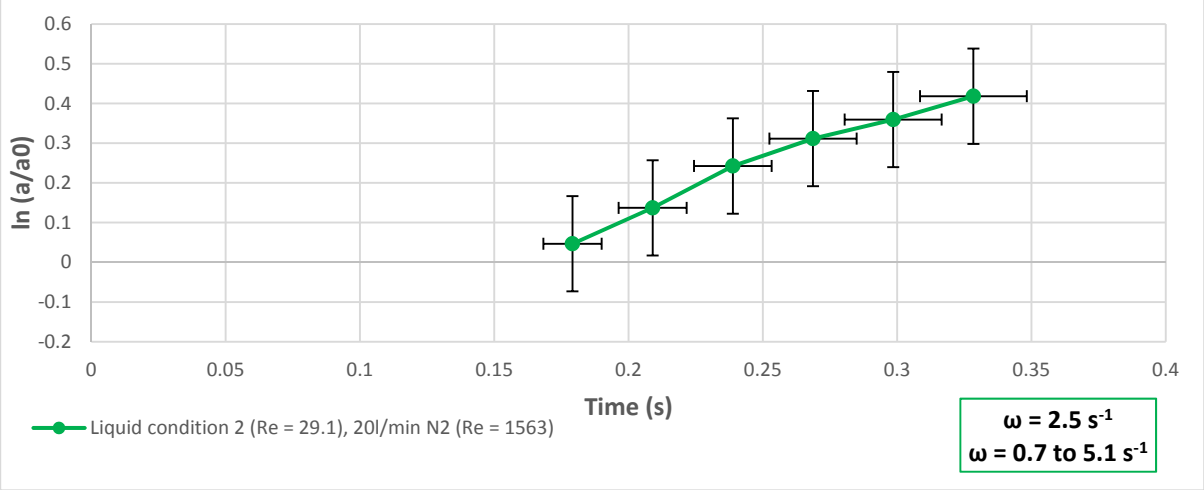

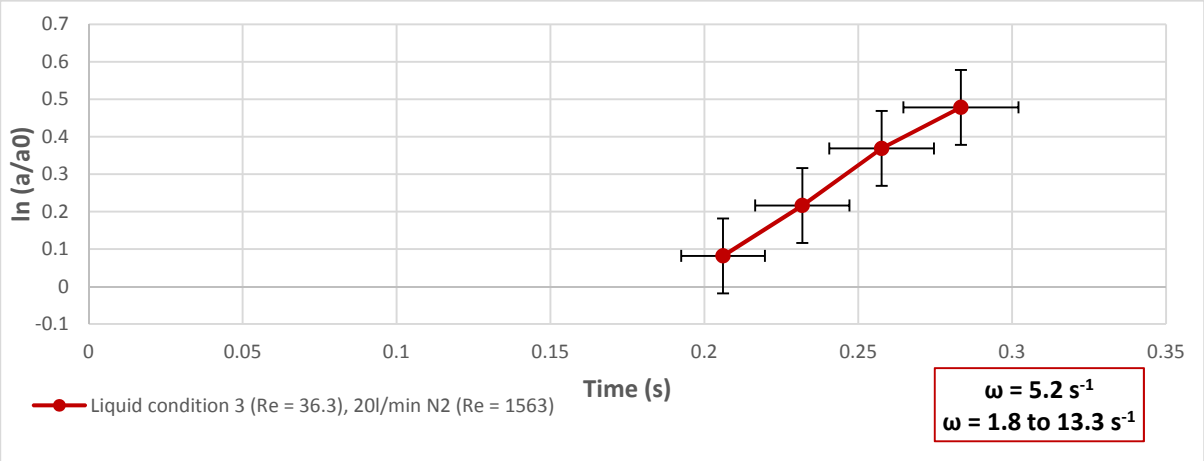

Figure 4.25a. ln(a/a0) plotted against time, 20l/min N2
Figure 4.25b ln(a/a0) plotted against time, 20l/min N2
Figure 4.25c ln(a/a0) plotted against time, 20l/min N2

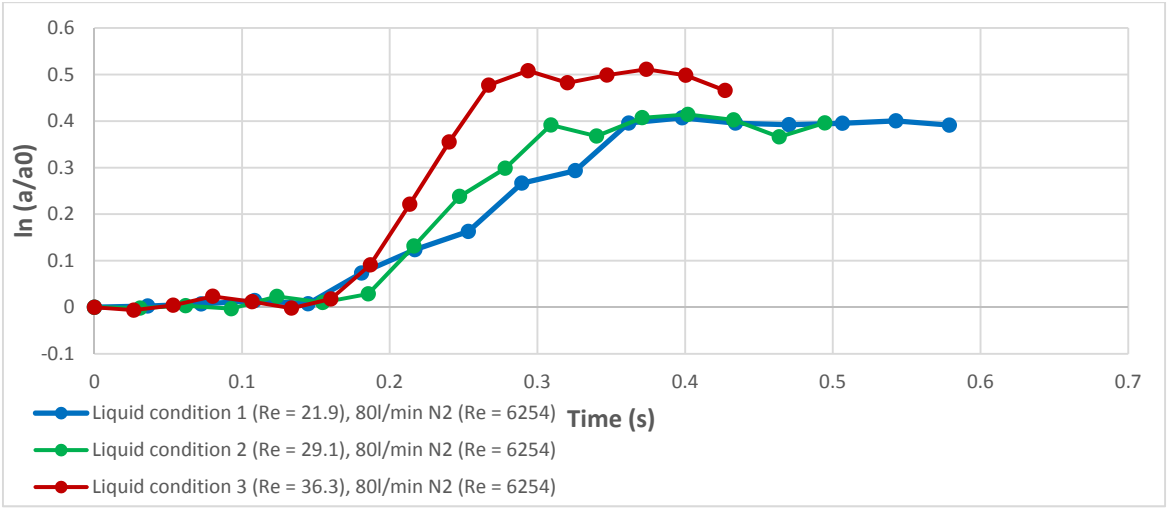

Figure 4.26 ln(a/a0) plotted against time, all liquid flow conditions (Re = 21.9, 29.1, 36.3), 80l/min N2 (Re = 6254)

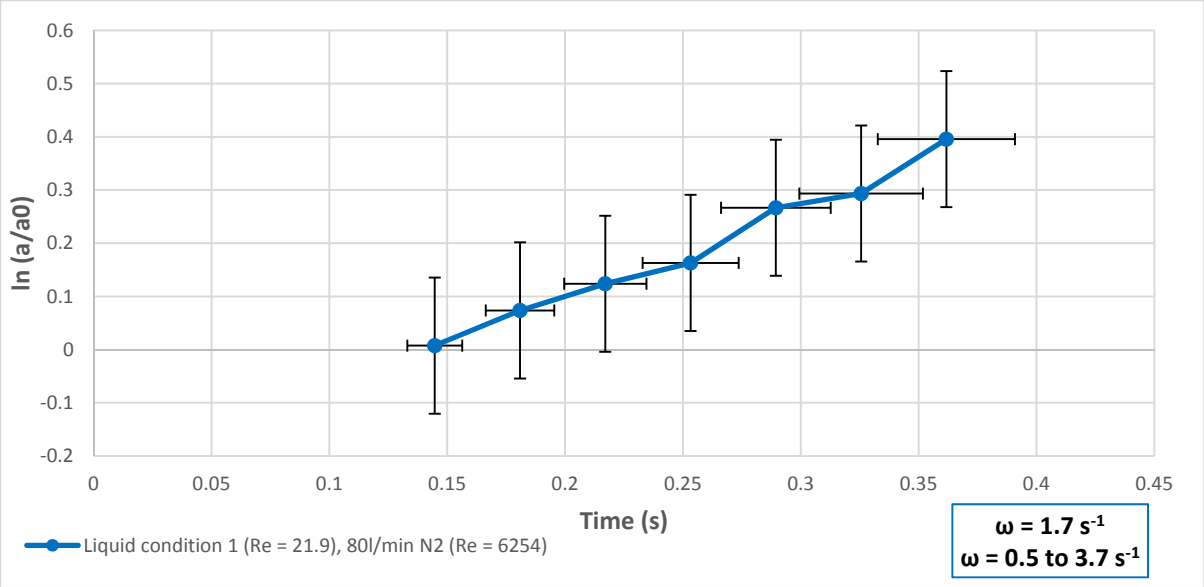

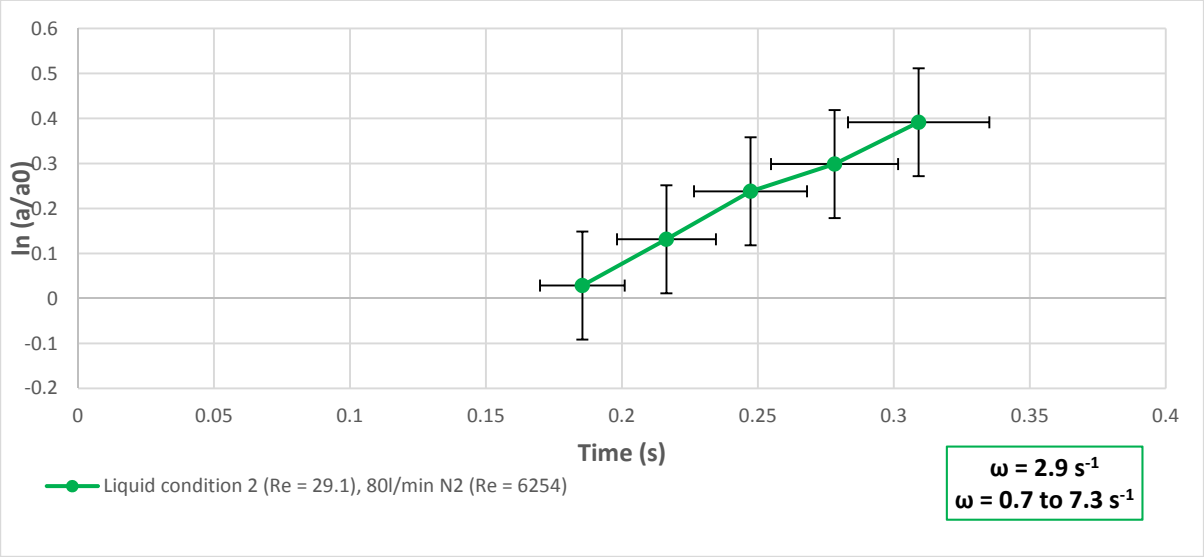

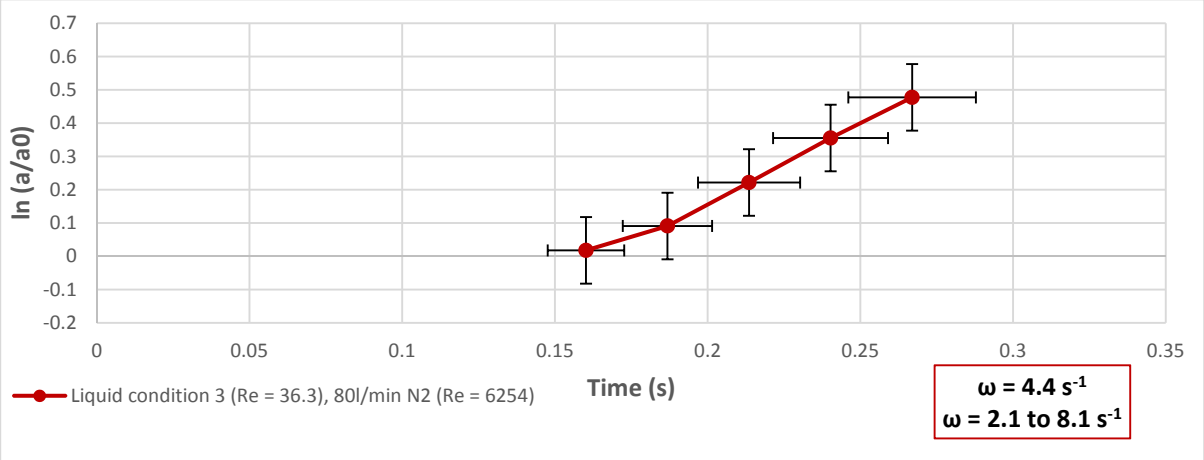

Figure 4.27a ln(a/a0) plotted against time, 80l/min N2
Figure 4.27b. ln(a/a0) plotted against time, 80l/min N2
Figure 4.27 c. ln(a/a0) plotted against time, 80l/min N2

The results are summarised in Table 4.11.

Liquid flow condition	N_2 flow rate (l/min)	Reynolds no. (liquid phase)	Reynolds no. (gas phase)	Wave growth rate (best fit, s^{-1})	Wave growth rate (range, s^{-1})
1	0	21.5+/-0.7	N/A	1.5	0.5 – 3.0
2	0	28.6+/-1.0	N/A	3.0	0.9 – 6.6
3	0	35.7 ± 1.2	N/A	5.3	1.8 – 17.6
1	20	21.5+/-0.7	1563 ± 23	1.6	0.5 – 3.1
2	20	28.6+/-1.0	1563 ± 23	2.5	0.7 – 5.1
3	20	35.7 ± 1.2	1563 ± 23	5.2	1.8 – 13.3
1	80	21.5+/-0.7	6254 ± 82	1.7	0.5 – 3.7
2	80	28.6+/-1.0	6254 ± 82	2.9	0.7 – 7.3
3	80	35.7 ± 1.2	6254 ± 82	4.4	2.1 – 8.1

Table 4.11 Summary of wave growth rate results

Although it is not possible to make definitive claims about the wave growth rate due to the large uncertainty, ω shows an indicative trend of increasing with higher liquid Reynolds number for all gas flow conditions. Changes in growth rate with the addition of laminar and turbulent counter-current gas are small, verging on negligible when the uncertainty is considered, indicating that it is not a strong function of countercurrent gas flow rate.
The uncertainty in wave growth could be reduced by using a high-speed camera which has a higher resolution than 640x480, reducing the distance per pixel for a similarly sized vertical field of view. This would reduce the uncertainty in film amplitude and therefore ln(a/a0). The length of the local minimum in real space may also be smaller, reducing the uncertainty in velocity and therefore time. While these wave growth rate measurements are unlikely to be able to provide model validation alone, they can act as part of a larger suite of validation criteria, which also includes comparisons with normalised film height and wave period.

4.5.5 Effect of countercurrent gas and CO_2 absorption

The mean wave peak amplitude increases as the liquid flows down the outside of the steel column. No further increase in mean wave peak height outwith the bounds of the measurement uncertainty is observed below the 120mm location (figures 4.22, 4.24 and 4.36), so it can be assumed that the waves stop growing and become saturated in amplitude between 80mm and 120mm from the top of the column. Wave film profile data for cases with no countercurrent gas, 20l/min N_2 and 80l/min countercurrent N_2 are shown in figures 4.28, 4.29 and 4.30. To improve readability, for all figures in this section the wave amplitude at liquid flow condition 2 is increased by 0.4mm and the amplitude at flow condition 3 by 0.8mm.

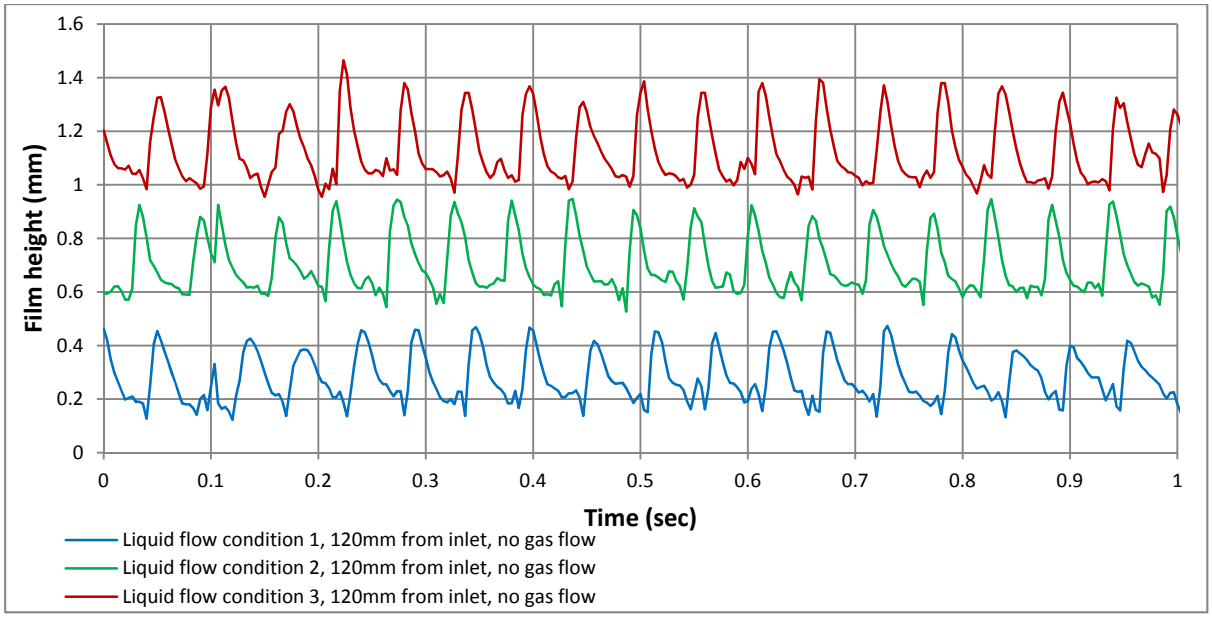

Figure 4.28 Film thickness at 120mm from top of steel column, no gas flow

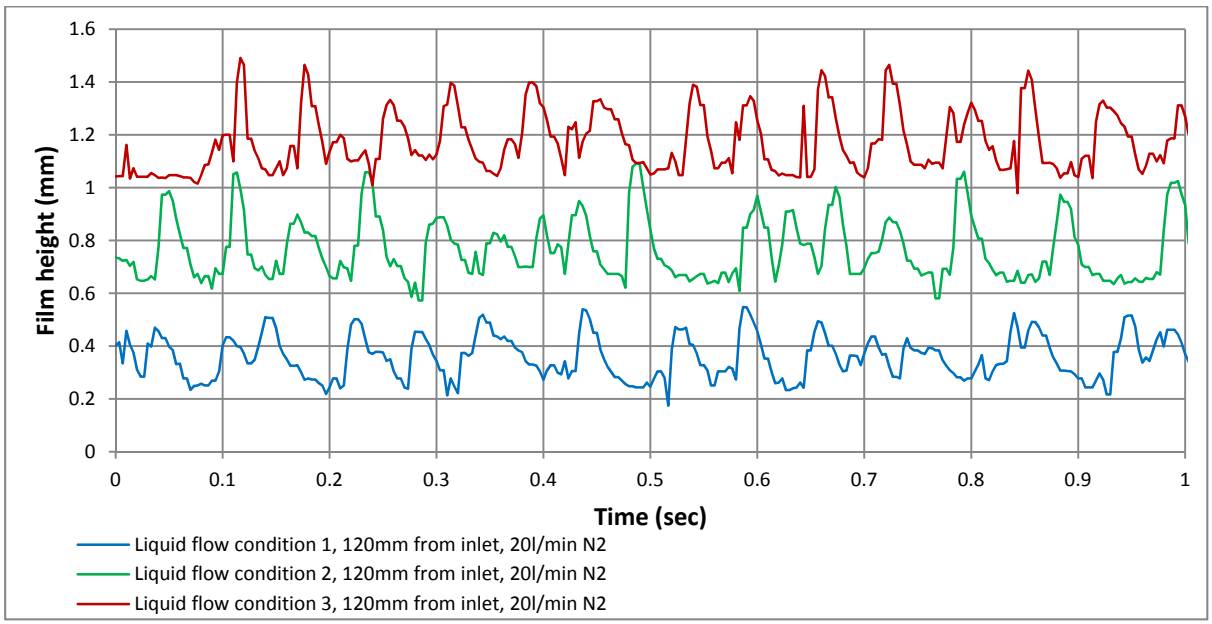

Figure 4.29 Film thickness at 120mm from top of steel column, 20l/min N2

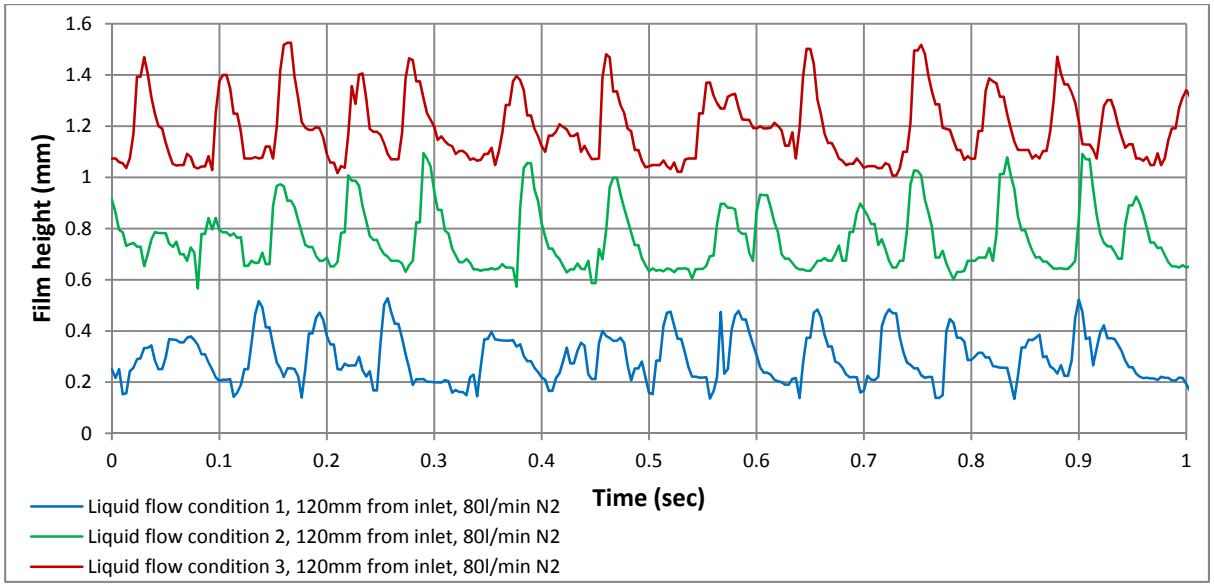

Figure 4.30 Film thickness at 120mm from top of steel column, 80l/min N2

Although the wave amplitude and frequency become less regular with the addition of counter-current N_2 there are still well-defined waves which can be analysed and it is possible to determine the average wave length, velocity and frequency. For all three liquid flow conditions, the addition of counter-current N2 results in increased irregularity of film profile as the turbulence of the gas flow increases. Validation of models against experimental film profile data requires at least three subsequent waves of regular period and amplitude, and while this may be more difficult to find as the gas turbulence increases it is not anticipated to be a serious problem.

Preliminary experiments counter-current CO_2 suggested that wave formation may be suppressed by reactive absorption, the proposed mechanism being an increase in solvent surface tension. This was a potentially critical finding, as wave suppression effects with 30% MEA solution which has been loaded with CO_2 could have serious implications for the flow of solvent over structured packing, and the development of novel packings for CCS. However, the predicted increase in surface tension based on solvent loading measurement (an increase of around 5% relative compared to unloaded MEA, Jayarathna et al., 2013) seemed unlikely to produce the kind of significant wave suppression observed, in which all regular wave structure is lost. An example is shown in figure 4.31.

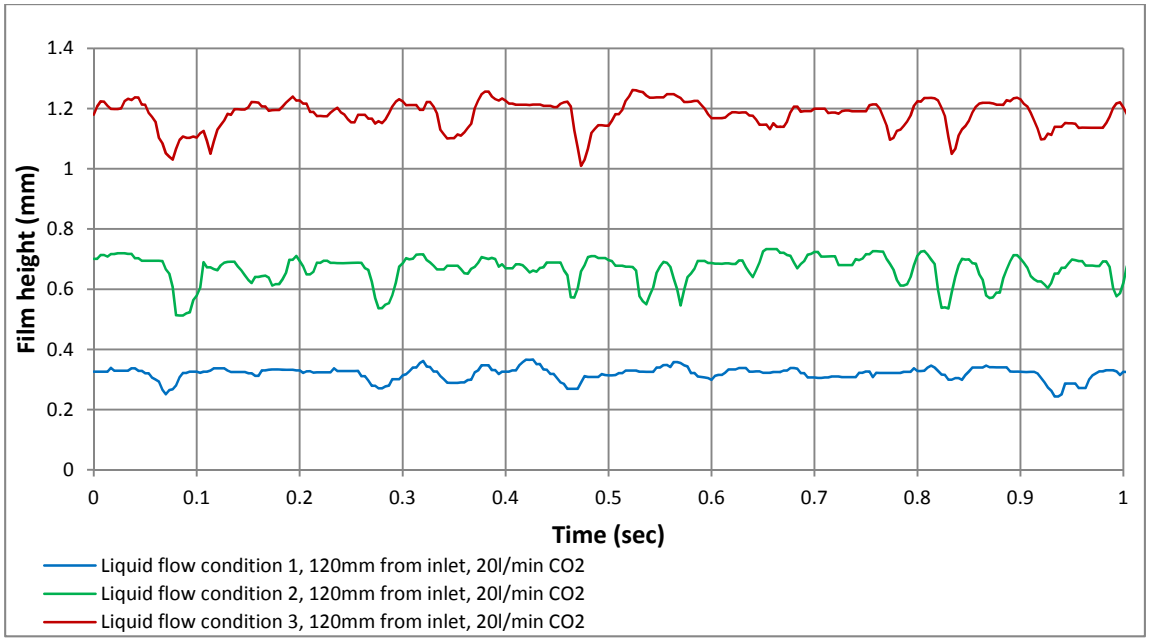

Figure 4.31 Preliminary experiments with countercurrent CO_2

A reappraisal of the raw footage suggests an experimental error – a misalignment of the central stainless steel column with respect to the vertical, leading to a distortion of the liquid film. Experiments with counter-current CO_2 are repeated in triplicate for each liquid flow condition to ensure the column is properly aligned and that liquid flow develops naturally. CO_2 flowrates are also selected so that they have the similar gas-phase Reynolds numbers as the flows of N_2 tested. Results are shown in figures 4.32a and b.

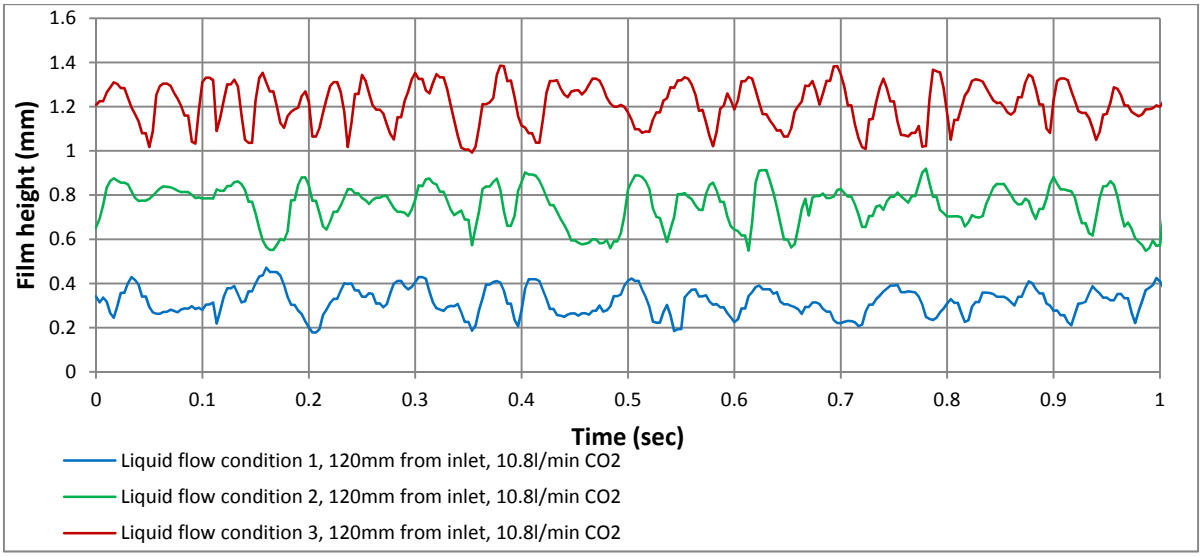

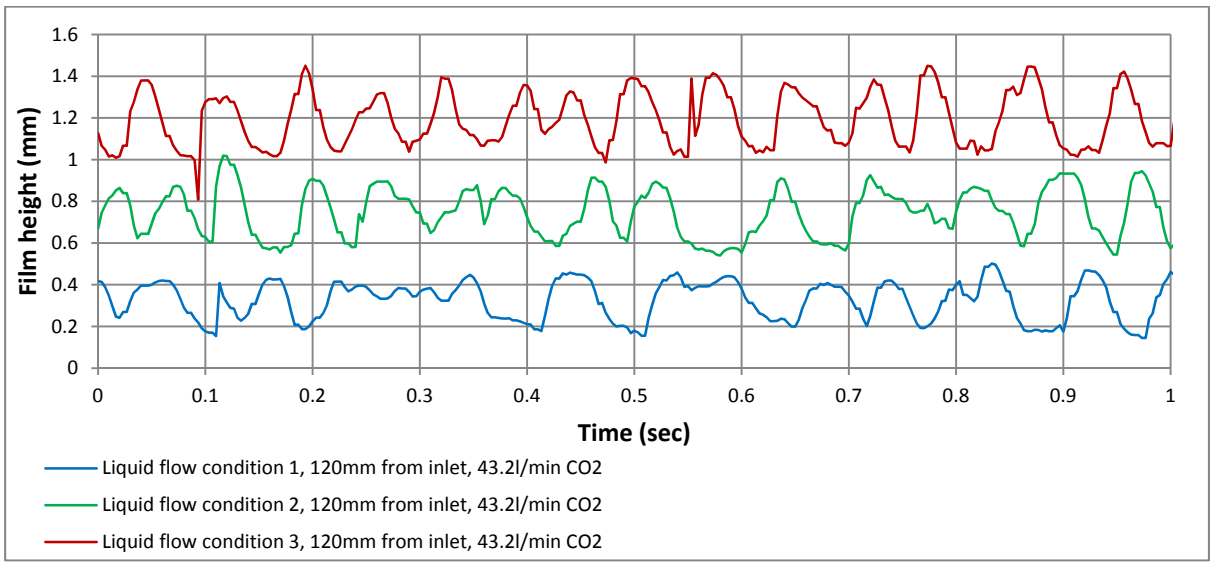

Figure 4.32a. Film profiles at 120mm from top of steel column, 10.8l/min CO2 (Re = 1654)
Figure 4.32b. Film profiles at 120mm from top of steel column, 43.2l/min CO2 (Re = 6256)

Any wave suppression effect is significantly less prominent than initially thought. While there is potentially some suppression – wave peaks with CO_2 appear to consistently be between 0.01-0.05mm lower than cases with N_2 at similar gas-phase Reynolds numbers – there is still a well-defined wave structure. 0.01 to 0.05mm is also of similar magnitude to the measurement uncertainty in liquid film position, so it is not possible to definitively say if a significant suppression effect exists or not. Again, use of a high-speed camera which has higher resolution than 640x480 pixels could reduce the measurement uncertainty. The wave pattern with countercurrent gas is also more irregular, resulting in a wider spread of wave peak heights being observed.

Further experiments with 30% MEA over with a range of CO_2 loadings, combined with a more powerful camera, could allow any wave suppression effects to be either nailed down or discounted as insignificant.

4.6 Comparison with thin-film models

To complete the evaluation of the test rig and demonstrate that it is fit for purpose, the evolution of the film over time is compared with a low-dimensional film model. The SWANS film model is a reduced-order model which has the advantage of requiring considerably less computational power than direct numerical simulations (Lavalle et al., 2015). It has been used to predict the dynamics of falling films with co- and counter-current laminar gas flows, for systems in which the fluid film height is small in comparison to its wavelength (Lavalle et al., 2017).

Film profile data is compared against modelling data for liquid flow condition 1 (2.35ml/s, Re = 21.9), normalised via division by both the Nusselt and Kapitza film thicknesses. The comparison of the normalised wave profiles is depicted in Figure 4.33a. Film profile data with measurement uncertainty, both normalised with respect to the Kapitza film thickness, are shown in figure 4.33b.

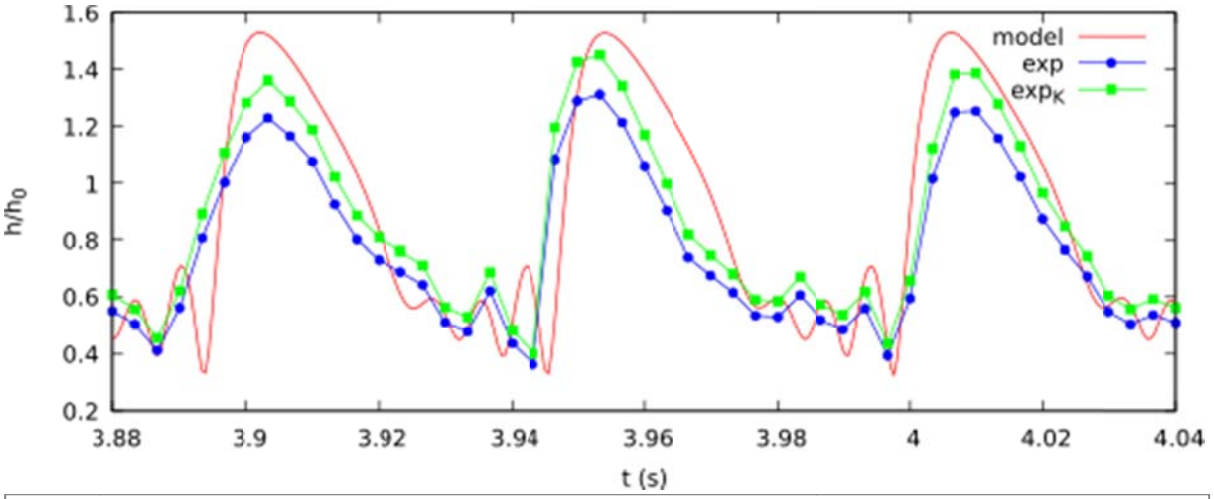

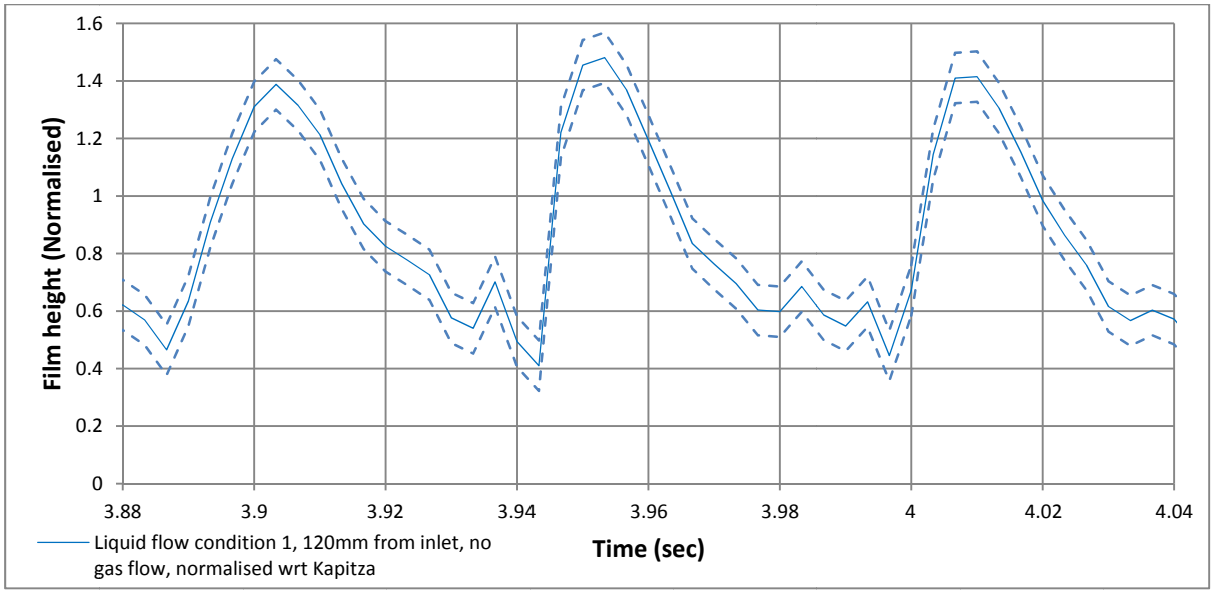

Figure 4.33a Comparison between theoretical and measured wave profile
Figure 4.33b Measured wave profile with uncertainty

First, it is noted that the model and the experimental data have similar behaviour and wave period. The model appears to overpredict the wave peaks, but the over-prediction is less significant when the experimental data is normalised with respect to the Kapitza film thickness. When the uncertainty is taken into consideration (figure 4.33, dashed lines) the discrepancy is lowered further. However, the optical measurements do not pick up some of the fine detail in the capillary region. The wave period in s^{-1} of each capillary wave is of a similar magnitude to the framerate of the camera, and the propagated measurement uncertainty is of the same order of magnitude as the capillary wave amplitude. Only the largest capillary waves immediately preceding the main wave peak

are likely to be detected by the optical method. While observation of fine detail in capillary waves would act as a bonus and could potentially be achieved with an upgrade to the test rig's high-speed camera, these initial results show good agreement with model film behaviour and highlight the potential of the test rig to provide validation for thin-film models.

4.7 Conclusions

Wave measurement experiments using a modified wetted-wall column and high-speed camera are made at three different liquid flow and five different gas flow conditions, using unloaded 30%wt MEA solution, no gas flow, pure N_2 at two flowrates and pure CO_2 at two flowrates. The average film thickness at each liquid flow condition is in agreement with the value predicted by the Kapitza equation (Kapitza, 1965) when the measurement uncertainty is taken into account. The uncertainty does not exceed +/-10% of the mean film thickness, which is in line with or better than similar studies in this field (Mouza, 2002). Film observations for non-absorbing systems are made at 10mm intervals along the column length from 0mm to 160mm.

Average wave length, velocity, frequency, temporal growth rate and temporal growth rate are determined for all non-absorbing systems, i.e. with no countercurrent gas, N_2 at 20l/min and N_2 at 80l/min. Increasing the flow of N_2 may reduce the terminal velocity of the wave due to greater inertial forces acting on its down-coming face, but as the reduction is within the bounds of the measurement uncertainty in all cases it is not possible to be certain. Wavelength shows increases with greater liquid flowrate, but no significant sensitivity to gas flow conditions outside the bounds of the measurement uncertainty can be determined.

Wave frequency shows a small sensitivity to liquid or gas flowrate, however, this is due to the frequency being determined via counting the total number of waves in a 5-second period. Countercurrent gas flow results in the wave pattern being more likely to be subject to random flow perturbations; these cause the regular wave profile to be disturbed, reducing the number of peaks for a short period of time. When the flow pattern is regular, the wave period and frequency are not affected significantly. These occasional periods of flow irregularity are the major effect of counter-current gas flow, the evolution of the film does not appear to be affected strongly by it.

Temporal wave growth rate measuerments are made for all non-absorbing systems

Experiments with CO_2 absorption may have an effect on wave formation as the increased solvent surface tension results in a flatter overall profile, but the change in average wave peak height is small if it exists, being of the same order of magnitude as the uncertainty in wave peak height.

For a case with no counter-current gas flow and a liquid Reynolds number of 21.9, experimental data is normalised with respect to the Kapitza and Nusselt mean film thickness and compared with the low-dimensional model of Lavalle et al (2015). The general shape of the experimental wave profile matches that of the model, and the wave period is in close agreement. When the experimental data is normalised with respect to the Kapitza mean film thickness the wave amplitude is also close to that predicted by the model, especially if the propagated uncertainty is take into account. Unfortunately the high-speed camera is unable to detect fine detail in the capillary wave region, in most cases detecting one large capillary wave immediately before the main crest, but the model and experimental detail are in good agreement otherwise. Next steps should be to compare experimental data for cases with laminar counter-current gas with that of the model.

Measurements of temporal wave growth rate again show no significant sensitivity to increasing the flowrate of counter-current gas, indicating that it is not a strong function of gas-phase Reynolds numebr. Uncertainties in wave growth rate measurements are high as the uncertainty from film height and velocity measurements propagates through, but there is an indicative trend of increasing growth rate as the Reynolds number of the liquid phase increases and the flow becomes less stable. These measurements could be combined with the film profile comparison to provide secondary validation for modelled liquid films.

Future work in collaboration with CFD modelling practitioners could allow for model validation of another model which requires lower computational power than DNS; the TPLS code developed by O'Naraigh et al. (2014), which is a high-resolution 3D flow solver for multiphase systems (TPLS, 2015). Validation could be achieved via the observation of three subsequent, regular, fully-developed waves using a laminar counter-current N2 flow regime and a single liquid flow rate of unloaded 30%wt MEA, or some other fluid with well-known physical properties; for example, silica oil. Improvement of the precision of experimental wave growth

rate measurements via, for example, the purchase of a camera with considerably higher resolution and framerate, may allow models based on linear stability theory (Schmidt et al, 2016)

Models are commonly validated against wave features such as amplitude and frequency, both of which have been measured in this work at multiple flow conditions. If more reliable measurements of temporal growth rate using additional measurement locations can be obtained, these could also be used for validation. Finally, it has been demonstrated that wave measurements are possible with turbulent gas flows and with absorbing systems, allowing for the potential validation of DNS with turbulent gas flow and integrated mass transfer when such models are developed.

The continuing development of DNS so that gas-liquid interactions in packed columns can be rigorously modelled is an important part of the continuing development of flexible CCS, and other industrial processes. With the addition of turbulence and mass transfer prediction capabilities and complex geometries, codes such as TPLS have the potential to replace empirical trial-and-error design strategies for column internals, leading to the development of structured packings which are optimised for CCS operations. The development of specialised packings can make CCS more attractive via increasing absorption efficiency, thereby reducing the volume of absorber packing required and hence the capital cost associated with construction, However, it is also important to consider how the entire capture plant can operate most effectively. Chapters 5 and 6 use pilot-scale test campaigns on NGCC and PC-equivalent flue gas to investigate the effect of dynamic operation on the entire capture process.

References

Benney, D.J. (1966). Long waves on liquid films. *Journal of Mathematical Physics*, 45, 150-155.

Bird, R.B., Stewart. W.E. and Lightfoot, E.N. (1960). Transport Phenomena. Wiley, New York.

Clark, W.W. (2002). Liquid film thickness measurement. *Multiphase Science and Technology,* 14, 1-74.

Dietze, G.F. (2010). Flow Separation in Falling Liquid Films. Doctoral Thesis, Aachen University.

Dietze, G.F., Leefken, A. and Kneer, R. (2007). Investigation of the Backflow Phenomenon in falling liquid films. *Journal of Fluid Mechanics*, 595, 435-459.

Dugas, R.E. (2009). Carbon Dioxide Absorption, Desorption, and Diffusion in Aqueous Piperazine and Monoethanolamine. Doctoral Thesis, The University of Texas at Austin.

Jayarathna, S.A., Weerasooriya, A., Dayarathna, S., Eimer, D.A. and Melasen, M.C. (2013). Densities and Surface Tensions of CO2 Loaded Aqueous Monoethanolamine Solutions with r = (0.2 to 0.7) at T = (303.15 to 333.15) K. *Journal of Chemical Engineering Data,* 58, 986-992.

Kapitza P.L. (1965). Wave Flow of Thin Layers of a Viscous Fluid. Collected Papers of P.L. Kapitza, 2, 662-708.

Kofman, N., Mergui, S., Ruyer-Quil, C. (2017). Characteristics of solitary waves on a falling liquid film sheared by a turbulent counter-current gas flow. *International Journal of Multiphase Flow*, 95, 22-34.

Lavalle, G., Vila, J.-P., Blanchard, G., Laurent, C. and Charru, F. (2015). A numerical reduced model for thin liquid films sheared by a gas flow. *Journal of Computational Physics,* 301, 119-140.

Lavalle, G., Vila, J.P., Lucquiaud, M. and Valluri, P. (2017). Ultraefficient reduced model for countercurrent two-layer flows. *Physical Review Fluids,* 2, 0104001.

Mouza, A.A., Paras, S.V. and Karabelas, A.J. (2002). The influence of small tube diameter on falling film and flooding phenomena. *International Journal of Multiphase Flow*, 28, 1311-1331.

Mouza, A.A., Pantzali, M.N. and Paras, S.V. (2005). Falling film and flooding phenomena in small diameter vertical tubes: The influence of liquid properties. *Chemical Engineering Science,* 60, 4981-4991.

Negny, S., Meyer, M., & Prevost, M. (2001). Study of a laminar falling film flowing over a wavy wall column: Part II. Experimental validation of hydrodynamic model. *International Journal of Heat and Mass Transfer*, 44, 2147-2154.

Schmidt, P., Lucquiaud, M. and Valluri, P. (2016). Linear and nonlinear instability in vertical counter-current laminar gas-liquid flows. *Physics of Fluids,* 28, 042102.

Shkadov, V.Y. (1967). Wave flow regimes of a thin layer of viscous fluid subject to gravity. Fluid Dynamics, 2,

Sutherland, W. (1893). The viscosity of gases and molecular force. *Philosophical Magazine* 5, 36, 507-531

TPLS (2015). High Resolution Direct Numerical Simulation of Two-Phase Flows. Available at: http://sourceforge.net/projects/tpls/

Weiland, R.H., Dingman, J.C., Cronin, D.B. and Browning, J. (1998). Density and Viscosity of Some Partially Carbonated Aqueous Alkanolamine Solutions and Their Blends. *Journal of Chemical Engineering Data,* 43, 378-382.

Chapter 5. Pilot Scale Testing 1 – Dynamic operation of Post-Combustion Capture as applied to natural gas-fired power stations

Note on self-plagiarism

This chapter re-uses material from a previous publication co-authored by the author of this thesis: Tait, P., Buschle, B., Ausner, A., Valluri, P., Wehrli, M. and Lucquiaud, M. (2016). A pilot-scale study of dynamic response scenarios for the flexible operation of post-combustion CO2 capture. *International Journal of Greenhouse Gas Control,* 48, 216-233.

5.1 Introduction

Chapters 5 and 6 describe two pilot-scale test campaigns which aim to fill several of the existing gaps in knowledge of how dynamic PCC operates. The two pilot facilities – one based at Sulzer Chemtech facilities in Winterthur, Switzerland, the other at the UKCCSRC PACT facilities in Sheffield, United Kingdom – are similar in size but have certain unique design features which affect the way they respond to dynamic operating scenarios.

The first test campaign investigates changes in the flowrate of solvent, flue gas and steam supply which are designed to be representative of the operation of a natural gas combined cycle (NGCC) plant fitted with PCC. NGCC plants offer favourable dynamic operating capability, with shorter times for startup, ramping and load response compared to coal-fired thermal plants, and are likely to play a significant role in providing dispatchable electricity infills for intermittency management in future energy generation mixes.

The second test campaign investigates scenarios based on PCC with pulverised coal. PCC on coal is a similar process to PCC on gas but with less stringent ramping requirements and higher CO_2 concentration in the flue gas. Although current carbon budgets suggest that a gradual phase-out of coal generation is necessary between now and 2030 in order to meet emissions targets (CCC, 2013), it seems likely to remain an important source of electricity in Asia, Africa and the Americas through 2040 and beyond (IEA, 2015). Furthering our understanding of dynamic PCC operations on coal is therefore highly relevant to the electricity generation systems of these countries.

Dynamic scenarios are combined with the online measurement of solvent CO_2 loading, using a novel sensor designed by Buschle (2015). The first test campaign, described in this chapter, provides insights about capture plant response to dynamic scenarios, highlights the importance of plant circulation times and solvent mixing and demonstrates the operation of a novel online solvent sensor. These learning outcomes inform the direction of the second test campaign, described in Chapter 6.

5.2 Description of pilot-scale test faciliity

The absorber has inner diameter 159mm and contained 6.92m of Sulzer Mellapak 250.X packing. The desorber has inner diameter 350mm and contained 5.00m Sulzer Mellapak 500.X packing. Absorber dimensions are comparable to other pilot plants (Table 5.1). Test conditions for steady-state baseload operation are determined prior to dynamic testing, and are provided in section 5.3.1.

Pilot Facility	Absorber inner diameter (mm)	Height of packed bed (m)	Packing type	Has Cross-heat exchanger Y/N	Reference
University of Texas at Austin, Separations Research Program	427	3.07 x 2	Raschig Super-Pak 250	Y	Seibert et al. (2011)
NTNU/SINTEF, VOCC (Validation Of Carbon Capture)	500	5.4	Sulzer Mellapak 2X	Y	Kvamsdal et al. (2011)
University of Stuttgart	125	4.2	Sulzer Mellapak 250.Y	Y	Notz et al. (2012)
CO_2SEPPL pilot, Dürnrohr power station	150	12	Raschig Super-Pak 250	Y	Rabensteiner et al. (2014)
Sulzer Chemtech absorption/desorption facility	158	6.92	Sulzer Mellapak 250.X	N	Tait et al. (2016)
UKCCSRC PACT Pilot Plant	300	6.50	Sulzer Mellapak CC	Y	Akram et al. (2016)

Table 5.1 Comparison of pilot-scale test facilities

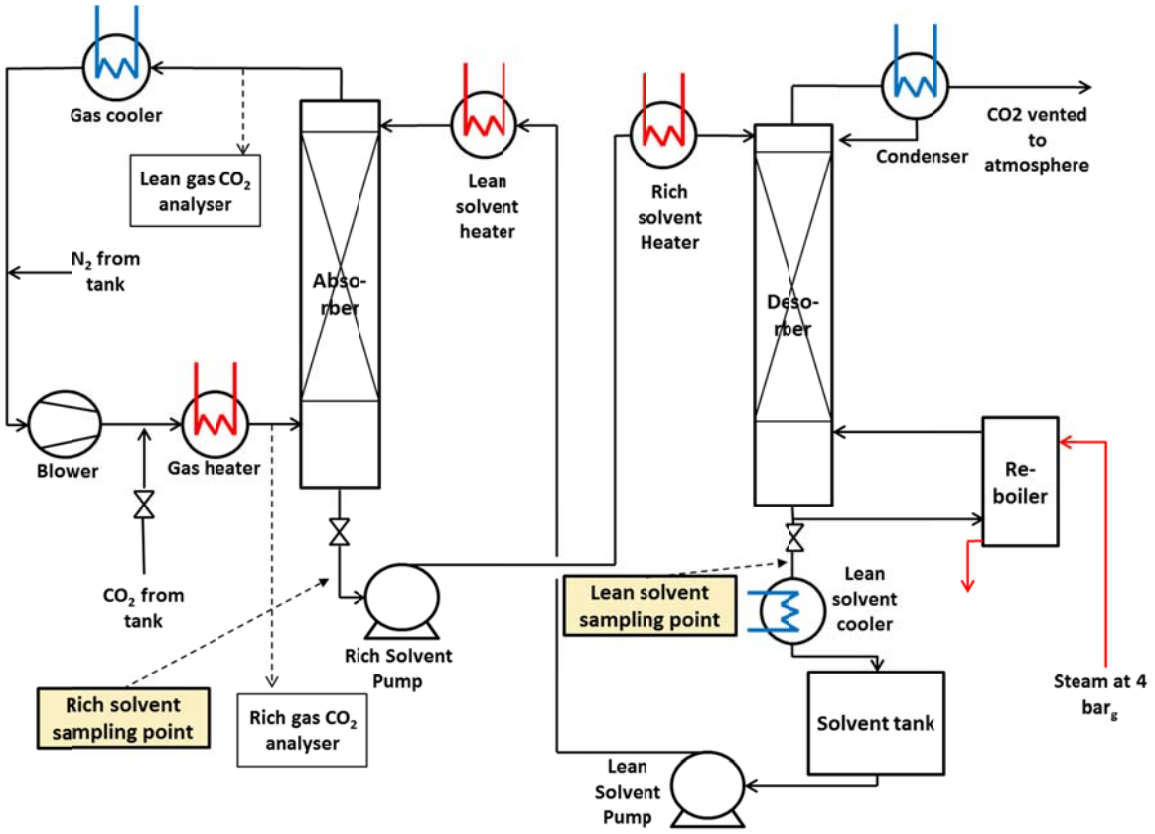

Fig. 5.1 Absorption/desorption test facility process flow diagram

5.2.1 Flue Gas

A blower with PID setpoint controls the flow rate of flue gas. Synthetic flue gas is composed of N_2 and CO_2, with a target CO_2 concentration which is representative of NGCC exhaust (4.3% v/v). The flue gas is recycled after exiting the absorber, and the required CO_2 concentration at the inlet is maintained by feeding additional CO_2 to the stream of gas via an inlet just after the blower. As the non-reacting flue gas is recycled it becomes saturated due to contact with the solvent, so water losses due to absorption or entrainment in the gas stream are negligible.

A PID cascade controller was designed in Labview to maintain the make-up flow of CO_2 so that its concentration at the inlet is maintained at 4.3%. However, due to a delay of approx. 90sec between CO_2 passing through the control valve and flue gas reaching the inlet CO_2 content analyser, CO_2 concentration tended to fluctuate between 3 and 6% when a perturbation to the system was introduced. Adjusting the setpoint of the CO_2 mass flow controller in kg/s manually proved a more reliable and consistent method of maintaining CO_2 inlet concentration at 4.3%. Infra-red (IR) CO_2 analysers are located at the absorber gas inlet and outlet, and are used to determine the capture rate of CO_2.

5.2.2 Liquid Inventory

116.8kg MEA and 270.5kg H2O were mixed in a tank to produce a solution of 30.16% w/w MEA. Of this, 366.0l were pumped into the main solvent tank of the DRABS plant. This volume of solvent inventory is sufficient to stop the solvent pump from running dry, and the main solvent tank level remained approx. 10% full during plant operation. With the imperfect assumption of plug flow, each individual "packet" of solvent requires 37min to circulate once through the entire plant during operation at baseload liquid flowrate.

When the liquid inventory was measured at the end of the test campaign, approx. 10kg (2.73%) had been lost due to evaporation, spillage or sampling. Titration measurements indicated that the solvent nominal amine concentration had changed by a maximum of +0.8%, to 30.96% w/w. Significant amine losses due to degradation are not expected over the 4-week duration of the test camapaign since the plant operates with CO2-enriched nitrogen.

5.2.3 – Reboiler heat input

Rich solvent is regenerated using steam which is fed to the reboiler at $4bar_g$. The steam flow setpoint required to represent post-combustion capture from NGCC plant (around 20kg/hour) approaches the limit of the turndown ratio of the solenoid valve used to control steam flow. As a result the flowrate of steam tends to fluctuate, so the reported values are averaged over a 30 second period.

5.2.4 – Plant Control and Modifications

Plant parameters are manipulated via PID controllers in Labview. Several minor modifications were made to the Labview control panel in order to accommodate dynamic operations. A mathematical function was added to calculate the CO_2 capture rate in real-time. The Labview code is modified for gas turbine shutdown and startup operations, using stacked sequence structures to ramp gas, liquid and steam flowrates automatically. This allows a single operator to control the entire process.

5.2.5 – Approximation of cross-flow heat exchanger

The Sulzer pilot facility is used for a range of applications and is not designed specifically for post-combustion capture at atmospheric pressure. Unlike other pilot plants reported in Table 5.1, which utilise a cross-heat exchanger to increase the temperature of the rich solvent, the pilot plant used in this study does not have this capability so the effect is simulated using separate heat exchangers. With a setpoint of 20^oC below the outlet temperature, a rich solvent heater increases the liquid temperature at the desorber inlet. The solvent is cooled to room temperature before entering the main solvent tank, then heated to approx. 40^oC before entering the absorber. A PID control loop with steam supply is used to control the solvent temperature at absorber and desorber inlets. Temperature settings are selected to be representative of the typical temperature pinch of a cross flow heat exchanger.

5.2.6 – Desorber Pressure

Desorber pressure is held at 1.8bar_a during all times at which steam was fed to the reboiler for solvent regeneration. If steam flow is shut down during a dynamic operation, a manual valve is opened to release the pressure, which decays rapidly. It was not possible to observe a natural decay in absorber pressure.

5.3 Test Campaign Methodology and Preparation

5.3.1 Determination of baseload operating conditions

The purpose of the test campaign is to implement dynamic post-combustion capture scenarios using a test facility configuration which approximates a PCC pilot plant. A reference "baseload" operation scenario, which all other scenarios are carried out in comparison to, is first determined.

30% w/w MEA solution is used as a liquid absorbent, since it is commonly used as a benchmark for pilot-scale facilities worldwide (Fitzgerald, 2014; Hamborg, 2014; Artano, 2012). A desired baseload capture rate of 90% is selected in order to remain consistent with other pilot-scale studies (Rabensteiner, 2014; Carey, 2013; Mejdell, 2011).

Previous work on natural gas flue gas capture (Ystad, 2012) indicates that for 30% w/w MEA, the liquid to gas flow ratio (L/G) which results in the lowest energy expenditure per ton CO_2 captured is approx. 1.5l solvent per m^3 gas. This L/G ratio is not achievable for this test campaign, as a lack of packing volume in the absorber requires the L/G flow ration to be increased to compensate and achieve 90% capture. This is likely to result in a reboiler duty in GJ/tCO_2 which is higher than that of a fully optimised plant.

Baseload flow conditions are determined by the author of this thesis with assistance from an experienced Sulzer plant operator. Flue gas flowrate is kept constant at 115m^3/h. With further addition of CO_2 at a rate of approx. 8.1kg/h an inlet CO_2 concentration of 4.3% v/v (moist), an f-factor of 1.85$Pa^{0.5}$ is obtained. Liquid flowrate is varied to obtain L/G ratios between 2.4 and 3.6 l/Nm^3. For each ratio, at a desorber pressure of 0.8bar_g, the flowrate of steam to the reboiler at 4bar_g is increased until a CO_2 capture rate of 90% is achieved. A minimum reboiler duty of 3.96GJ/tCO_2 for this plant is observed at an L/G ratio of 2.858l/m^3. Typical reboiler duty values for NGCC base case studies have been reported between 3.4 – 4.04 GJ/tCO_2 (Jordal, 2012).

Both lean and rich solvent CO_2 loadings are low in comparison to capture plants which are purpose-built and optimised for NGCC flue gas, due to a lack of packing height in the absorber (Biliyok, 2014; Rabensteiner, 2013). In order to compensate and achieve 90% capture, the liquid flowrate is increased. This results in a similarly low rich loading, with the effect being exacerbated as the increased liquid flowrate results in a smaller difference in loading between the liquid inlet and outlet. An alternative strategy would be to accept a lower CO_2 capture rate while maintaining more representative values of L/G ratio, lean loading and rich loading, but due to equipment limitations caused by the turndown ratio of the liquid pump and steam inlet valve, further reductions in flowrate would result in considerable flow instability. Increasing the gas flowrate is also not an option as the blower has a maximum flowrate of around 130Nm^3/h due to the pressure drop of the packing and liquid holdup.

The energy input to the absorber and desorber solvent trim heaters is not accounted for due to the absence of steam flowrate measurement to each heat exchanger. It is possible that the reboiler inlet liquid temperature is unrepresentatively high of that which could be achieved using a cross-flow heat exchanger, so the reboiler is required to provide less energy as sensible heat. This seems likely, as the figure of 3.96GJ/tCO_2 is still within the reported range of typical values, with a liquid flowrate which is much higher than optimal.

A full list of conditions is summarised below.

Controlled Variable	Value
Gas Flowrate at absorber inlet (Nm^3/h)	120.5
Gas inlet temperature (^oC)	46.14
Inlet gas CO_2 concentration (% v/v)	4.27
Steam flowrate (kg/h)	19.5
Liquid flowrate (l/h)	344.4
Steam pressure (bar_a)	4.0
Desorber pressure (bar_a)	1.80
Liquid inlet temperature, Absorber (^oC)	40.05
Liquid inlet temperature, Desorber (^oC)	104.07
Measured Parameter	**Value**
CO_2 capture rate (%)	89.7
Reboiler duty (GJ/tCO_2)	3.96
L/G ratio (l/m^3)	2.86
Lean Solvent Loading (mol amine/mol CO_2)	0.232
Rich Solvent Loading (mol amine/mol CO_2)	0.345

Table 5.2. Summary of baseload operating conditions

To allow for comparison with real plant ramping events and future pilot plant campaigns, all flowrates and ramp rates in the dynamic scenarios investigated are subsequently referred to as percentages of this baseload condition.

Due to the low loadings, the solvent retains unused capacity of approximately 0.155 mol CO_2/mol free amine at the bottom of the absorber. This results in a significant driving force in this location during baseload operation. During dynamic scenarios which involve shutdown or reduction of stripping steam, this additional capacity will allow the plant to continue to capture CO_2 for longer periods of time than if the plant were operated with a rich loading which is closer to equilibrium with the inlet gas CO_2 concentration.

5.3.2 Solvent circulation times

The mass inertia of the solvent inventory has an effect on the dynamic response of the plant. Solvent circulation time is obviously dependent on total solvent inventory, which is limited in this study to as little as practically possible. Circulation times at several different liquid flowrates are estimated by inducing a step-change in main pump output, and observing the time required for this to produce a liquid level change of 10% at several points in the liquid line. The solvent pump reaches its new setpoint within approx. 10 seconds and does not contribute significantly to the overall circulation time. The results are summarised in Table 3. Circulation times between each individual section of the plant, and relevant circulation times at 50% of solvent baseload flowrate are estimated using the measured values and indicated by *. Circulation times through sumps are estimated by dividing the liquid holdup by the volumetric flow rate.

Liquid flowrate (as % of baseload)	Circulation time from main solvent pump to top of Absorber sump (min:sec)	Circulation time from top of absorber sump to top of desorber sump (min:sec)	Circulation time from top of desorber sump to top of 500l liquid tank (min:sec)	Circulation time from top of liquid tank to main solvent pump (min:sec)	Total circulation time required (min:sec)	Circulation time from lean sample point to rich sample point* (min:sec)
100	1:07	6:03	8:35	21:10	36:55	30:17*
75	1:20	7:25	10:36	32:17	51:38	43:38*
50*	1:49*	8:40*	14:25*	48:58*	73:52*	63:11*
30	2:20	12:18	19:40	79:35	113:08	97:50*

Table 5.3. Summary of plant solvent circulation times (* indicates estimated values based on other measurements)

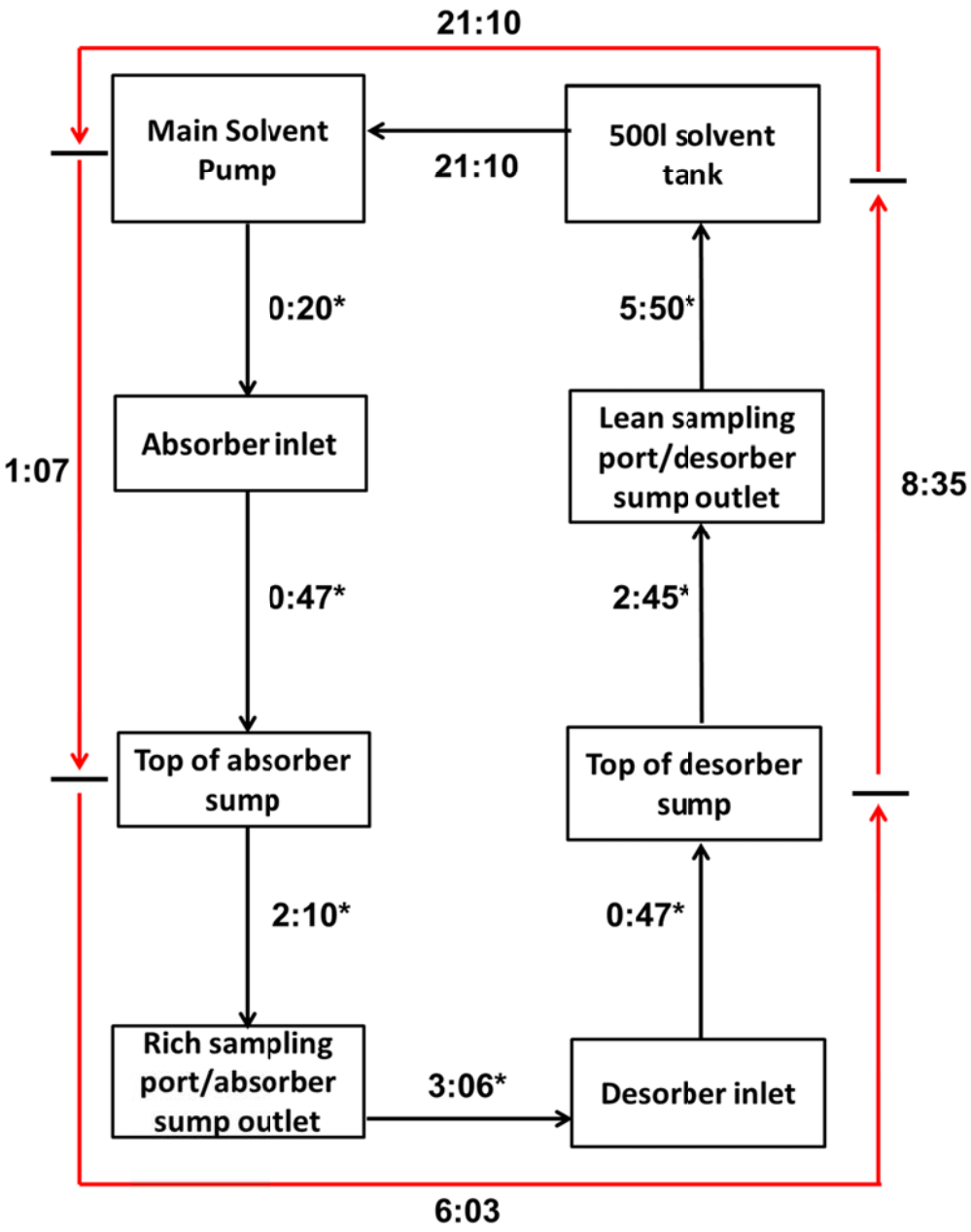

Fig. 5.2. Block diagram of plant solvent circulation times (in min:sec) for baseload solvent flowrate. * indicates estimated value based on other measurements

	100% baseload	75% baseload	50% baseload	30% baseload
Main solvent pump – Absorber inlet	0:20*	0:27*	0:40*	0:55*
Absorber inlet – Top of absorber sump	0:47*	0:53*	1:09*	1:25*
Top of absorber sump – Rich sampling port (absorber sump outlet)	2:10*	2:55*	3:24*	5:08*
Rich sampling port (absorber sump outlet) – Desorber inlet	3:06*	3:37*	4:07*	5:45*
Desorber inlet – Top of desorber sump	0:47*	0:53*	1:09*	1:25*
Top of desorber sump – Lean sampling port (desorber sump outlet)	2:45*	3:30*	5:25*	9:03*
Lean sampling port (desorber sump outlet) – Top of 500l solvent tank	5:50*	7:06*	9:00*	10:37*
Top of 500l solvent tank – Main solvent pump	21:10*	32:17*	48:58*	79:35*
Total circulation time	36:55	51:38	73:52*	113:53

Table 5.4. Estimated circulation times (in min:sec) between relevant plant locations

Solvent circulation times have a direct impact on the response of the capture plant and affect the time delay between when a process parameter is changed and when the impact of that change is observed in solvent loading and plant capture rate. For example, after a change in steam flow rate to the reboiler, it takes approximately 30 minutes (Table 5.4) at liquid flow for the change in lean solvent loading to be observed at the rich solvent sampling point. The importance of solvent circulation times and mixing is apparent when observing the response of the pilot plant of UKCCSRC PACT in comparison to this facility. This is discussed further in Chapter 6.

5.3.3 Rationale for selection of dynamic scenarios

Five dynamic scenarios are selected, with the intention of representing real plant operation as much as is practically possible in order to gain insights about plant response and identify important metrics for future advanced control systems. This also allows any bottlenecks to dynamic operation to be identified. A brief description of each scenario tested is provided in sections 5.3.3.1 to 5.3.3.5.

5.3.3.1 Gas turbine shutdown

The shutdown sequence represents a realistic scenario based on the shutdown sequence of a modern NGCC plant. Gas and steam ramp rates are characteristic of a SIEMENS STG5-4000F (Eisfeld and Feldmuller, 2013), and are detailed in sections 5.5.1 and 5.5.2 respectively. The method by which the plant is shut down directly impacts its performance upon restart. Cecarelli et al. (2014) model two generation/capture plant shutdown cases, one of which is implemented in this work. After the shutdown sequence has been completed liquid flow is maintained at 30% to make use of the plant's cooling duty, resulting in a cooler solvent upon startup to promote CO_2 absorption. There is, however, some tradeoff in in implementing this strategy, as the continued circulation causes lean and rich solvent loadings to converge due to mixing effects. This may affect CO_2 absorption performance when the plant is restarted.

5.3.3.2 Gas turbine startup

Plant startup is simulated to follow a shutdown event in which the flow of solvent has been maintained at 30% of baseload, causing solvent temperature to be reduced to $<35^{O}C$, and lean and rich loading to begin to converge due to mixing. Before the startup sequence is initiated, liquid flowrate is stabilised at 30% of baseload flowrate. Gas and steam flow rates for the startup operation are based on an NGCC plant using a state-of-the-art SIEMENS STG5-4000F gas turbine (Eisfeld and Feldmuller, 2013), as with the gas-turbine shutdown scenario, and are provided in section 5.2. Liquid flowrate is ramped with gas to maintain a constant L/G flow ratio.

5.3.3.3 Power output maximisation via capture plant decoupling

This represents a scenario for a NGCC with a by-pass of the capture plant, where steam for solvent regeneration is redirected to the combined cycle, the CO_2 compressors are shut down and the flue gas is vented directly to

atmosphere after the HRSG. Solvent flowrate is also reduced to 50% to reduce the power consumption of the pumps. This mode of operation increases flowrate of steam to the turbine and hence power plant electricity output. It is a useful capability during instances when the selling price of electricity is high, rapidly increasing the amount of energy available for dispatch to the grid (Haines and Davison, 2014). It should be noted that the viability of this scenario depends on carbon cost, electricity selling price and specific regulations regarding emissions costs. Flue gas venting will be uneconomical when CO_2 prices are high in comparison to the selling price of electricity.

5.3.3.4 Power output maximisation by reboiler heat input decoupling

This scenario rapidly stops the flow of steam to the reboiler, while flue gas continues to flow through the absorber. This method of operation is similar to capture plant decoupling, but could also be utilised in power plants, where the ability to bypass the absorber has not been implemented or if some level of capture is still desirable. Again, solvent flowrate is reduced to 50% to reduce the power consumption of pumps.

5.3.3.5 Frequency response increase via rapid reboiler steam flow increase

In this operation, the flow of steam to the reboiler is rapidly increased to 200% of baseload. This is a complementary method of rapidly decreasing plant electricity output in response to a requirement to maintain grid frequency within acceptable limits. A doubling of steam extraction from the combined cycle of a gas power plant is consistent with maintaining a minimum steam flow rate at the inlet of the low pressure turbine for blade cooling. With the increase in steam flowrate there exists a risk of accelerating solvent thermal degradation due to the creation of "hot spots" on the heat exchanger, but this will be plant/solvent specific and could be mitigated via plant design or solvent control methods.

5.3.4 Solvent circulation times and estimation of real-time solvent working capacity

To effectively understand the impact of dynamic scenarios on solvent CO_2 loading at the absorber inlet and outlet, it is necessary to estimate the time at which each "packet" of lean or rich solvent sampled for analysis will reach the absorber inlet or outlet, respectively. The continuous online solvent measurement is also time-shifted using the same method. It is possible to estimate when each packet of solvent sampled at the lean inlet reaches the absorber, by estimating the total solvent inventory between the lean sampling port and the absorber inlet and dividing by the flowrate. It is also possible to determine when each rich solvent sample reached the base of the packed bed by estimating the time required to flow through the absorber sump. This time-shifting approach is imperfect as it does not account for potential mixing effects in the main solvent tank, nor does the backwards time-shifting of rich loading measurements account for mixing effects in the absorber sump, as both rely on the assumption of plug flow. However, the approximation allows the reader to more easily relate changes in CO_2 capture rate to changes in solvent lean loading.

After time-shifting, there is no guarantee that a lean sample which is time-shifted forward to time *t* will have a corresponding rich sample at time *t* from which the solvent capacity can be calculated. The significance of solvent circulation times was not identified until after the test campaign had been completed, so there was no opportunity to modify the sampling times or install new sampling ports closer to the absorber inlet and outlet. The real-time solvent working capacity (defined as the difference in solvent loading between the absorber inlet and absorber outlet at any given point in time) is estimated using the capture rate and flowrates of CO_2 and MEA. This can be done using two methods:

Each lean loading bench measurement is time-shifted forward to the time where it enters the absorber inlet, rich loading at the base of the packing is then estimated using the average capture rate and flowrates of CO_2 and MEA over the following minute. $\dot{N}$ is the molar flow rate, η_{CO2} is the CO_2 capture rate.

$$\alpha_{rich,calculated} = \alpha_{lean,measured} + (\dot{N}_{CO2} * \eta_{CO2} / \dot{N}_{MEA}) \quad (5.1)$$

Each rich loading bench measurement is time-shifted backwards to the time where it reaches the base of the absorber packing, lean loading at the absorber inlet is then estimated using the average capture rates and flowrates of CO_2 and MEA over the previous minute.

$$\alpha_{\text{lean. calculated}} = \alpha_{\text{rich,measured}} + (\dot{N}_{CO2} * \eta_{CO2} / \dot{N}_{MEA}) \quad (5.2)$$

5.3.5 Titration Measurement Uncertainty

Based on the analysis of 14 lean and rich solvent samples measured in triplicate (42 measurements in total) the repeatability is estimated to be +/-4.54% relative. The accuracy estimate is +/-0.63% relative, based off a single measurement of a 1.110 wt% CO2 standard. Therefore, the expanded uncertainty estimation for the method is +/-5.2% relative (rounded to 2 significant figures). This could be improved by utilising multiple measurements of CO_2 standards which have a range of different CO_2 concentrations. Additionally, it is assumed that the nominal amine concentration remains constant throughout the test campaign, when in reality it may vary due to water losses and/or solvent degradation.

5.3.6 Online solvent sensor

A novel liquid sensor which differs from previous online measurement techniques (e.g. van Eckeveld et al., 2014) has been developed in-house at Edinburgh University. The sensor is used for continuous measurement of solvent lean loading in four of the dynamic scenarios. In-situ measurements of solvent physical properties are used to determine solvent loading and amine concentration, using proprietary intellectual property which is under development at the time of writing. The necessity for rapid, online solvent composition measurements for the implementation of advanced control systems is discussed in the literature review section of this thesis (section 2.1.3.3). An in-depth account of sensor development can be found in Buschle (2015).

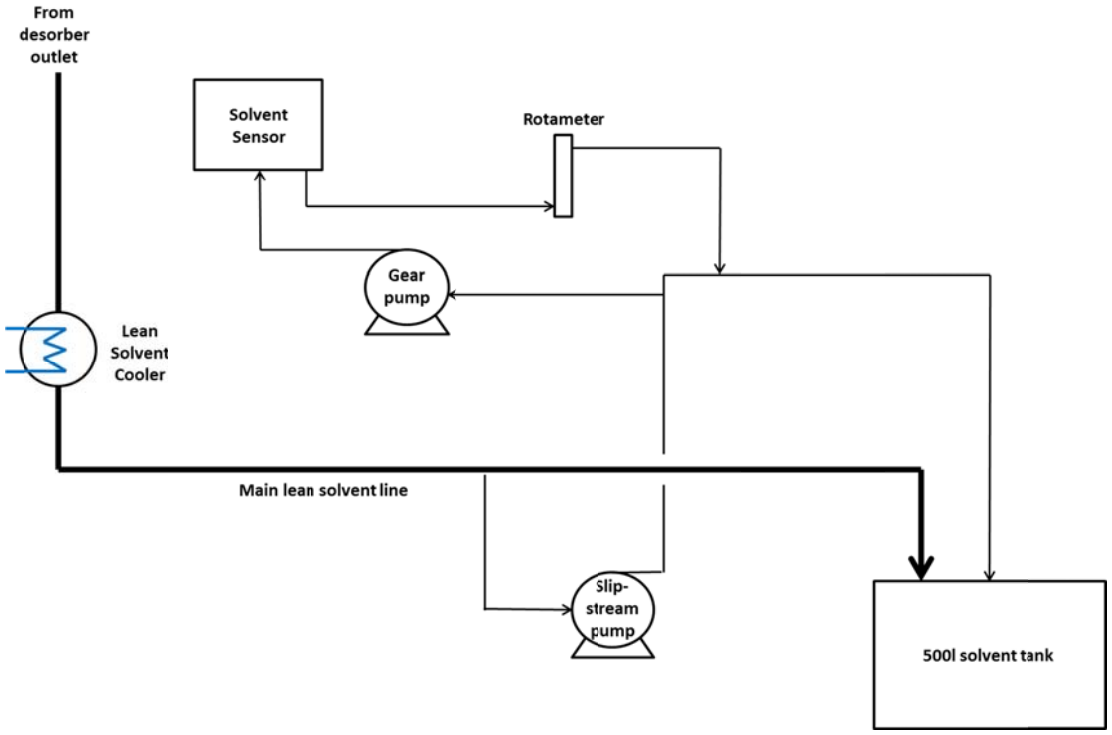

Fig. 5.3. Liquid loop for online solvent sensor – location upstream of solvent tank

Two sensor locations are tested in this study, as illustrated in Figure 5.3 and Figure 5.4.
For the "gas turbine startup" and "power output maximisation by capture plant decoupling" scenarios the sensor is located in the lean solvent line upstream of the solvent tank, between the desorber sump outlet and the main solvent tank. For the scenarios "power output maximisation by reboiler steam decoupling" and "frequency response" it is located downstream of the solvent tank and the main solvent pump. The sensor output is time-

shifted to the point at which each ”packet” of lean solvent analysed exits the desorber sump, for comparison with titration measurements. The sensor was unavailable for the “gas-turbine shutdown scenario”.

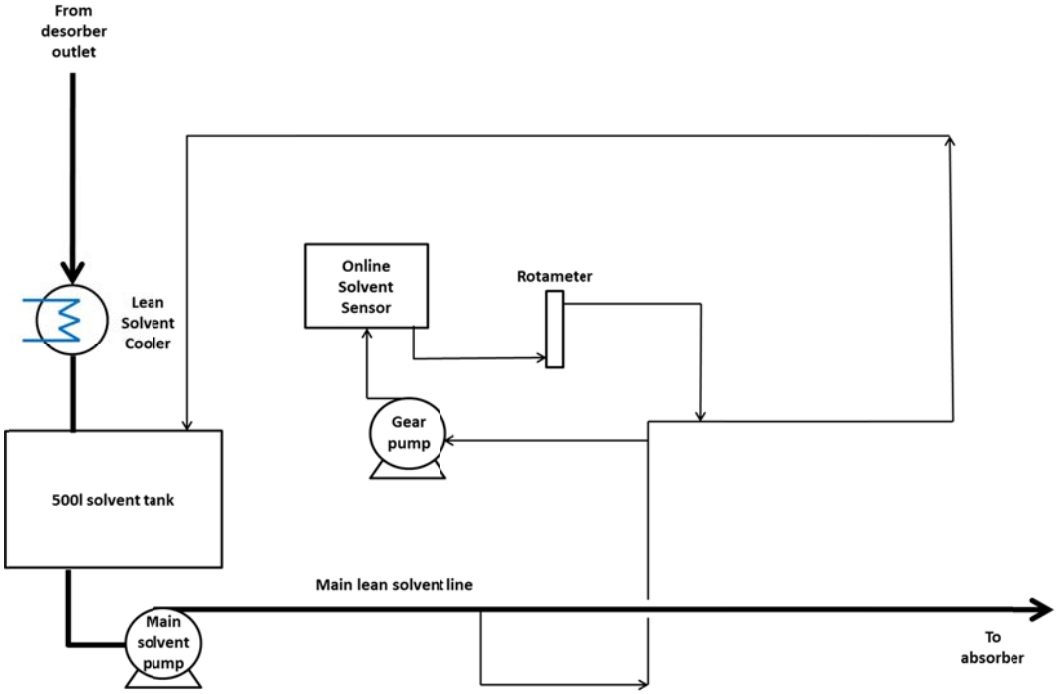

Fig. 5.4 Liquid loop for online solvent sensor – downstream of solvent tank

5.4 Dynamic Scenarios

This section provides an overview of each of the five dynamic scenarios implemented during this test campaign.

5.4.1 Gas Turbine Shutdown

Ramp rates for this and the subsequent start-up scenario are based on those of a Siemens SGT5-4000F turbine with a power output of 329MW. For this turbine, the maximum ramp rate during load turndown is 50MW/min (Eisfeld and Feldmuller, 2013). Mass flow rate of gas through the column is approximated as being proportional to GT load.

The shutdown sequence is initiated at t=0min as shown on fig. 5.6a. Steam flowrate is ramped down to zero over 10 minutes at a rate of 10% of baseload/min, as is representative of state-of the art gas turbine operation. Liquid and gas flowrates are ramped down simultaneously at a rate of 2.5%/min (8.2MW/min equivalent) for a period of 16 minutes, maintaining a constant L/G flow ratio throughout. At t=16min, the shutdown rate of liquid and gas is changed to 7.5% of baseload/min (24.7MW/min equivalent). At t=20min, liquid and gas flowrates both reach 30% of baseload. The liquid flowrate is held at this value, while the gas flow is further reduced at a rate of 15%/min (49.3MW/min) until it reaches zero. Gas flowrate reaches zero at t=22min, while liquid flow is maintained at 30% of baseload until the absorber temperature bulge has subsided (Fig. 5.7).

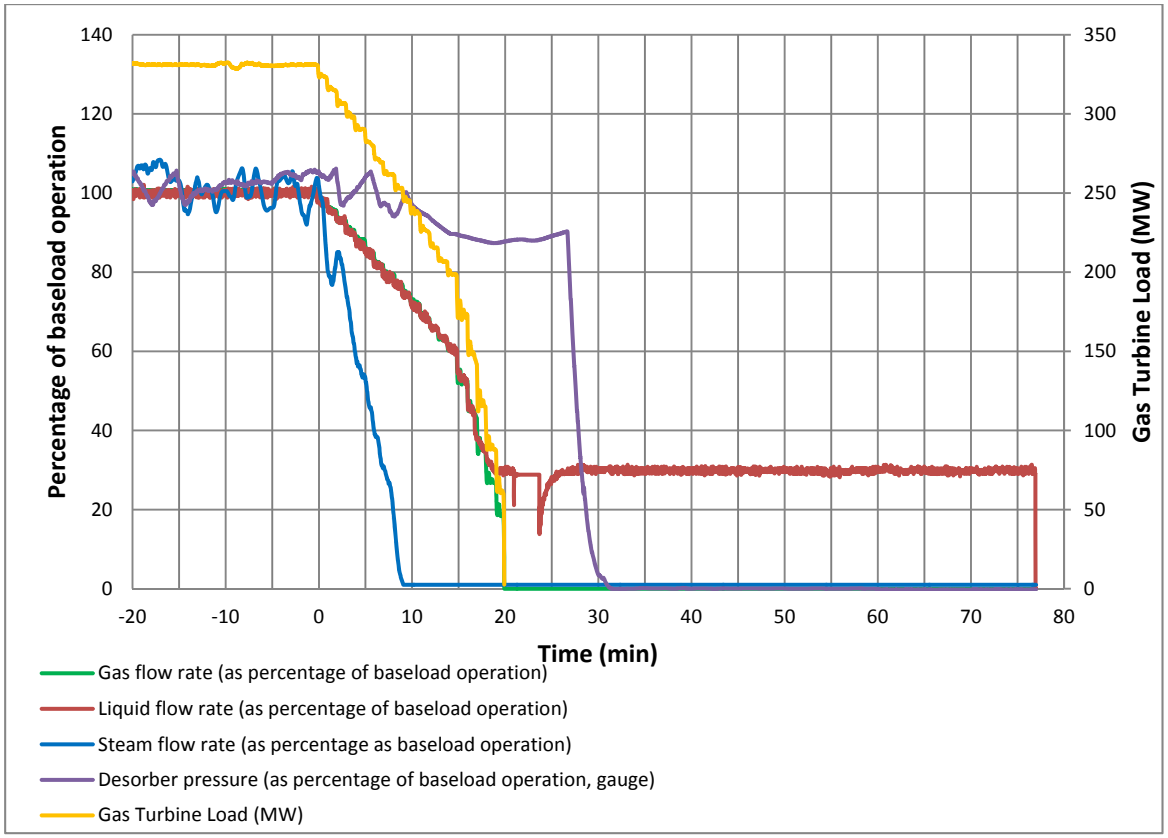

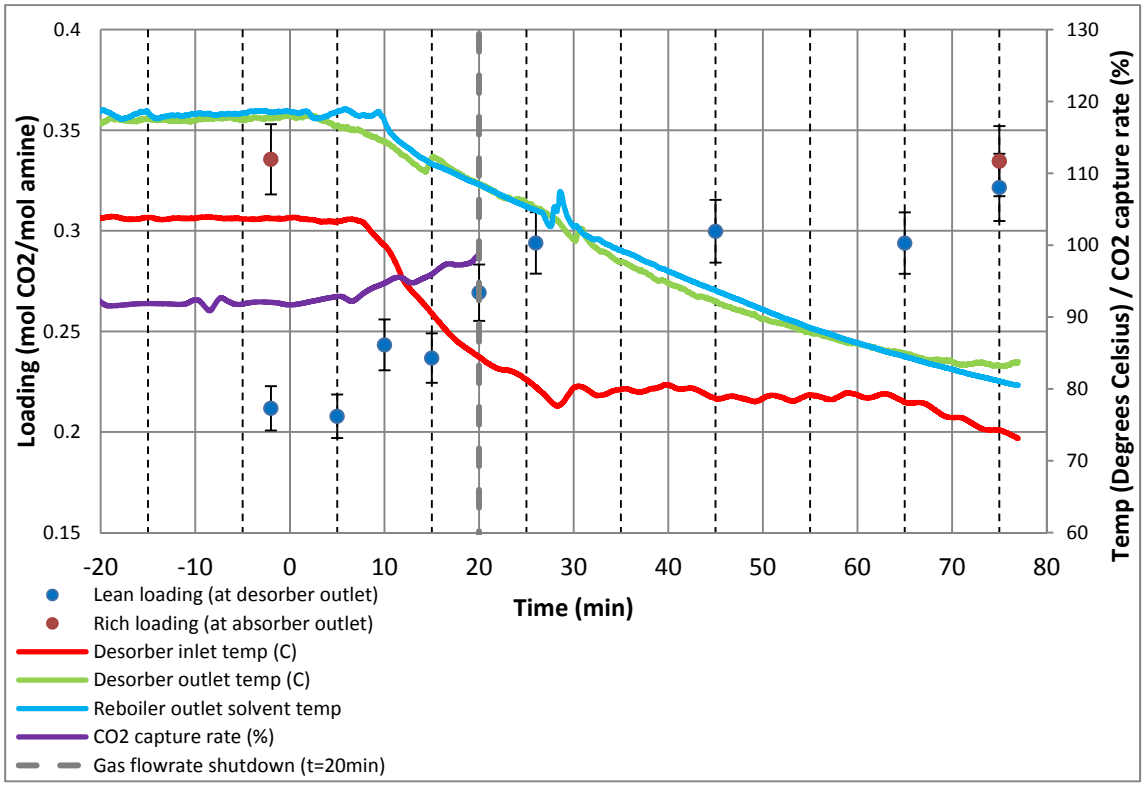

Fig. 5.6a. Gas, liquid and steam flowrates as percentage of previously-defined baseload operation, for Gas Turbine Shutdown sequence

Fig. 5.6b. Rich and lean solvent CO_2 loading, CO_2 capture rate, desorber and reboiler temperatures for Gas Turbine Shutdown sequence

The solvent lean loading at the desorber outlet begins to rise sometime between t=5min and t=10min due to the reduction in steam flow to the reboiler. Assuming plug flow and no mixing in the solvent tank, the more CO_2-

rich "packet" of solvent sampled at t=10min does not reach the absorber inlet before the gas flowrate reaches zero, using the estimated solvent circulation times as described in section 3.4. Lean loading at the desorber outlet increases throughout the shutdown operation, but has no significant effect on capture rate as this "richer" lean solvent is not predicted to reach the absorber inlet before of the flow of gas reaches zero..

Capture rate is observed to increase from 90% to 97.5% as gas and liquid flow is reduced (fig. 5.6b). Since the solvent flow rate is gradually ramped down, the liquid holdup in the absorber requires additional time (compared to baseload) to flow over the packing and into the absorber sump. Although the L/G flow ratio is controlled to remain constant, the flowrate of gas passing through the absorber decreases more rapidly than the liquid holdup on the packing it comes into contact with, so a greater proportion of the CO_2 in the flue gas may be absorbed as the gas flowrate approaches and eventually drops to zero. Furthermore, the increased residence time of liquid and gas in the absorber column could result in this increased capture rate.

Although capture rate increases, the temperature profile of the absorber (fig. 5.7) decreases in magnitude, as the exothermic absorption of CO_2 decreases as the gas as the flowrate approaches zero. After the flow of gas is stopped at t=20min, the location of the temperature bulge decreases in magnitude and moves down the packing height. Figure 5.7 illustrates the evolution of the absorber temperature profile as hot solvent flows down the packed bed and into the absorber sump, with the packing hold up being replaced by slow flowing, semi-stagnant cooler solvent. J-type thermocouples used for temperature measurement have been calibrated by plant operators before the beginning of the test campaign and have an uncertainty of +/- 1.5^{o}C.

Although no exothermic absorption reaction is taking place, residual heat in the metal elements of the absorber column combined with additional insulation to prevent heat loss, result in the absorber requiring some time to cool down.

It should be noted that the values of temperature at a height of 7.1m in fig. 5.7 and all other figures which represent the temperature profile, refer to a temperature measured directly before the absorber inlet.

Rich and lean solvent CO_2 loading measurements are not time-shifted in this instance (See section 5.3.4), but in all other dynamic scenarios they are. It was discovered in post-processing that the first lean titration measurement requires longer than the entire duration of the event to reach the absorber inlet. In an ideal situation the plant would be allowed to run until the entire solvent inventory becomes well mixed, so the full response of the plant can be observed. In the subsequent test campaign described in Chapter 6, the plant continues to be monitored for as long as possible so that the full extent of the plant response can be observed.

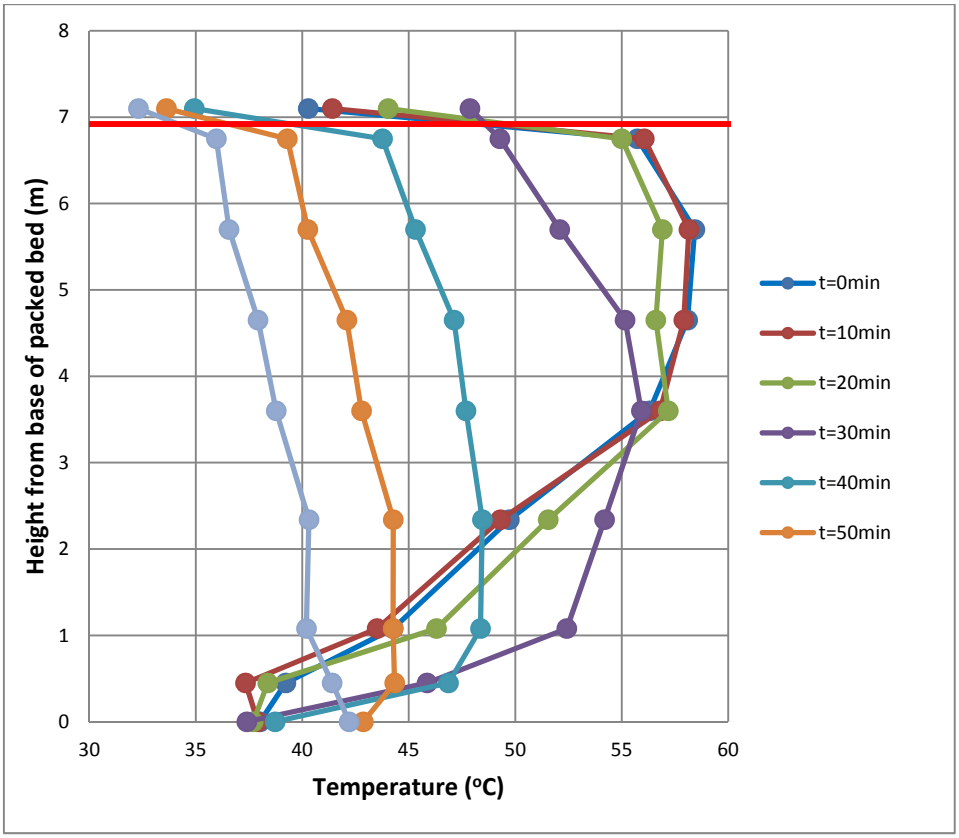

Fig. 5.7. Evolution of absorber temperature profile during gas turbine shutdown operation

5.4.2 Gas Turbine Startup

Due to the nature of the shutdown sequence which involves a continued circulation of solvent at 30% of baseload flow in order to lower solvent temperature more rapidly, rich and lean loadings have begun to converge due to solvent mixing at the beginning of the experiment. Gas flow is initiated at t=0 and increased at a rate of 5.7% of baseload/min. This is equivalent to a gas turbine ramp rate of approx. 18.75MW/min for the Siemens SGT5-4000F turbine, which has a maximum ramp rate of 30MW/min for fast start (Eisfeld & Feldmuller, 2013). Once the flow of gas reaches 30%, at approx. t=5min 15s, the flowrate of liquid commences ramping at 5.7%/min in order to maintain a constant L/G flow ratio.

As suggested by the models of Ceccarelli et al (2014), the CO2 capture rate (fig. 5.8c) is initially higher than that of baseload operation between t=0 and approximately t=5min, as the gas flowrate is ramped up to reach the operating L/G flow ratio. The liquid holdup on the packing is established before gas is introduced, and a cool solvent results in a higher driving force for CO2 absorption. Once the target liquid/gas flow ratio is established at t=5min and the absorber temperature profile increases in magnitude (fig. 5.9a), the capture rate begins to drop as lean solvent loading increases (Fig. 5.8c).

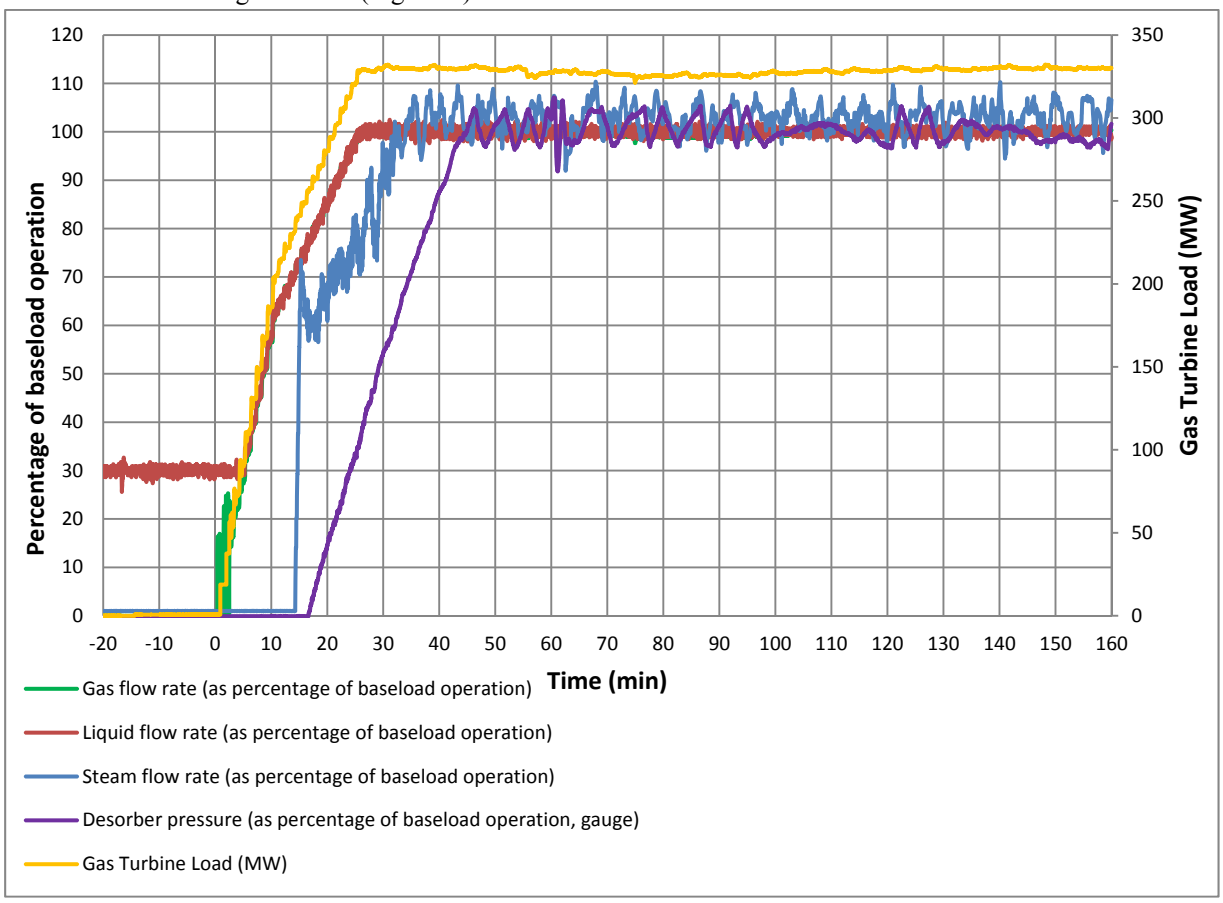

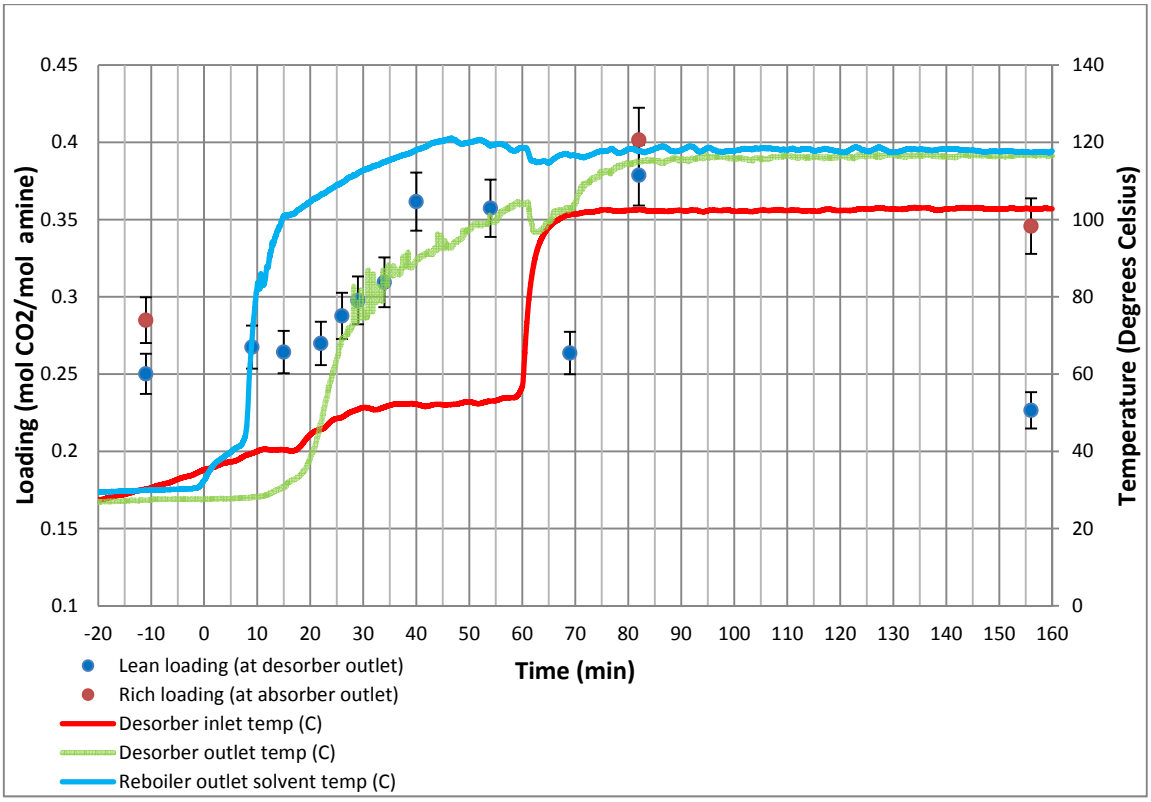
Loading (mol CO2/mol amine)
Temperature (Degrees Celsius)
Time (min)
Lean loading (at desorber outlet)
Rich loading (at absorber outlet)
Desorber inlet temp (C)
Desorber outlet temp (C)
Reboiler outlet solvent temp (C)

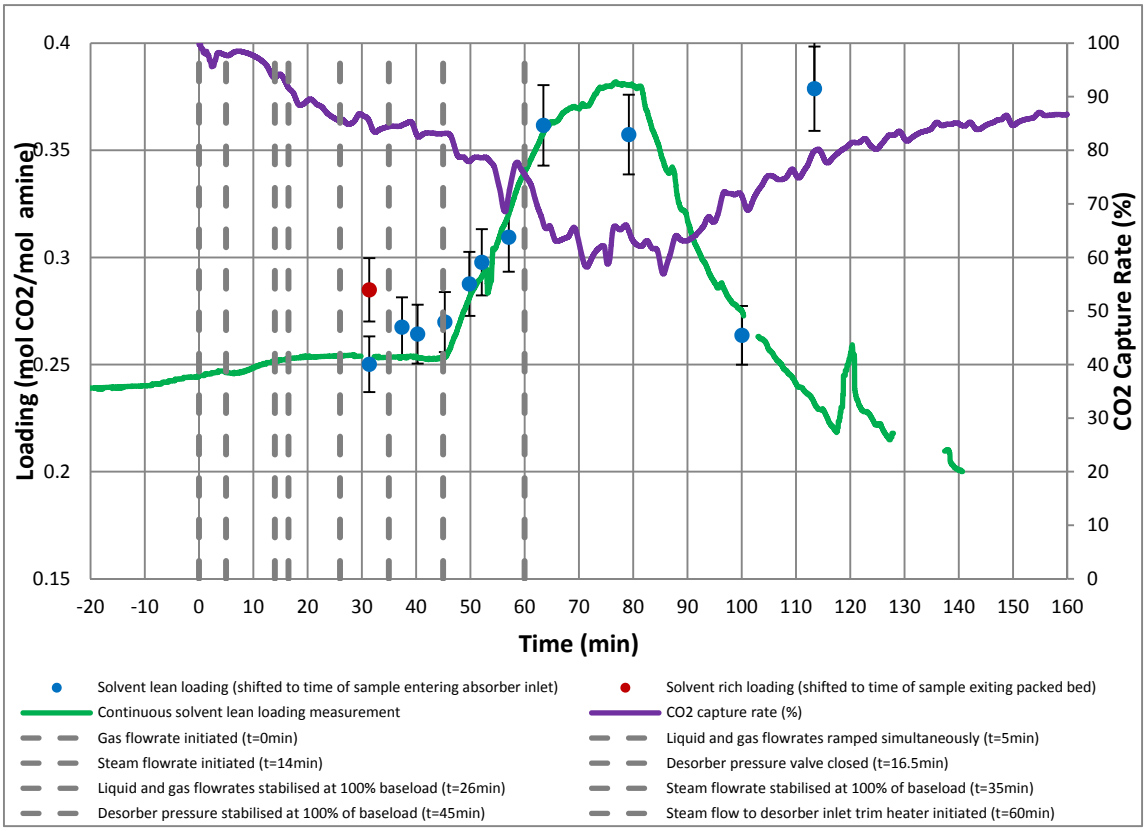
Loading (mol CO2/mol amine)
CO2 Capture Rate (%)
Time (min)
Solvent lean loading (shifted to time of sample entering absorber inlet)
Solvent rich loading (shifted to time of sample exiting packed bed)
Continuous solvent lean loading measurement
CO2 capture rate (%)
Gas flowrate initiated (t=0min)
Liquid and gas flowrates ramped simultaneously (t=5min)
Steam flowrate initiated (t=14min)
Desorber pressure valve closed (t=16.5min)
Liquid and gas flowrates stabilised at 100% baseload (t=26min)
Steam flowrate stabilised at 100% of baseload (t=35min)
Desorber pressure stabilised at 100% of baseload (t=45min)
Steam flow to desorber inlet trim heater initiated (t=60min)

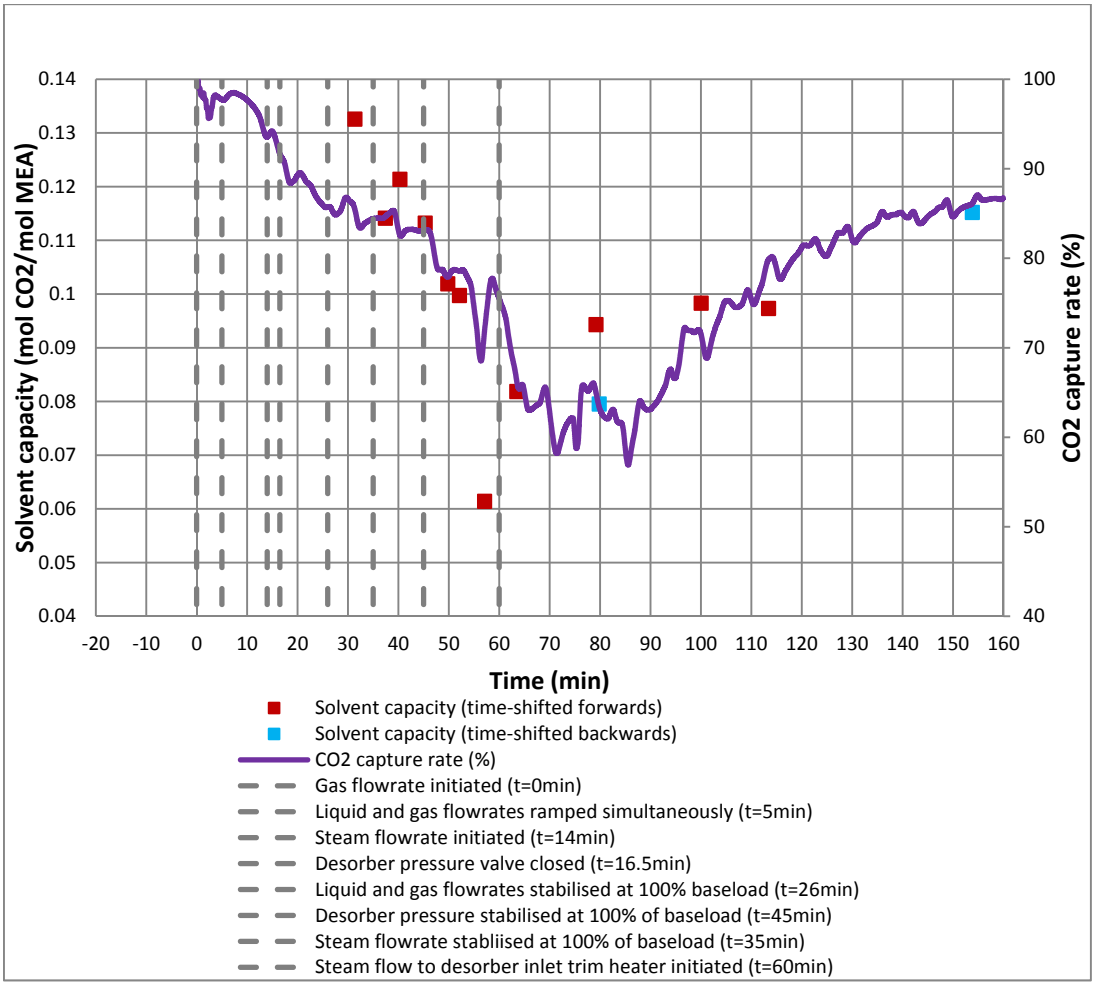

Fig. 5.8a. Gas, liquid and steam flowrates as percentage of previously-defined baseload operation, gas turbine startup scenario

Fig. 5.8b. Rich and lean solvent CO_2 loading at sampling ports, desorber and reboiler temperatures, gas turbine startup scenario

Fig. 5.8c. Lean and rich solvent loading titration measurements, shifted to time of absorber inlet entry and outlet exit respectively, continuous lean loading measurement, CO_2 capture rate, gas turbine startup scenario

Fig. 5.8d. Predicted real-time solvent capacity and CO_2 capture rate, gas turbine startup scenario

At t=11min, ramp rates of both liquid and gas flowrate are reduced to approx. 2.45% of baseload/min (8MW/min equivalent) and remain at this value until both reach 100% of baseload (t=26min). Steam flowrate is ramped at a rate of 18.0%/min from t=15 to t=18min, before the ramp rate is decreased to approx. 2.55%/min. The manual valve controlling desorber pressure is closed at t=17min. Although the flow of steam to the reboiler is established and stabilised at 100% of baseload by t=35min, the steam flow to the desorber inlet trim heater, which is used to simulate the effect of the cross-flow heat exchanger, is not initiated until t=60min (fig. 5.8b) due to an error. As a significant proportion of the energy from the stripping steam must be used as sensible heat to raise rich solvent temperature by 50-60^{o}C, solvent loading continues to increase and the capture rate continues to decrease. Around 25-30 minutes after the establishment of baseload absorber conditions, which is the approximate circulation time between desorber outlet and absorber inlet, the capture rate begins to increase once again (t=85min, figure 5.8d).

The decrease in absorber temperature profile (fig. 5.9b) can be directly linked to this decrease in capture rate, both of which reach a minimum at t=80min. Leaner solvent which has been exposed to baseload desorber and reboiler operation is returned to the absorber after t=80min (fig. 5.8c, 5.8d), resulting in a higher driving force for CO_2 absorption and a steady increase in capture rate (fig. 5.8c, 5.8d) and absorber temperature (fig. 5.9c). The capture rate, predicted solvent capacity and continuous lean solvent loading

measurement all suggest a steady decrease in solvent lean loading at the absorber inlet after t=80min, so it is believed that the bench lean loading measurement of 0.3787 at t=113min (fig. 5.8c) is the result of an abnormal or unrepresentative titration measurement. The sample may be an example of abnormal "noise" and therefore unrepresentative of overall change, or the result of unknown mixing effects in the desorber sump. Several similar measurements are encountered throughout the test campaign, and unfortunately it is not possible to know definitively the source of the error without more regular sampling.

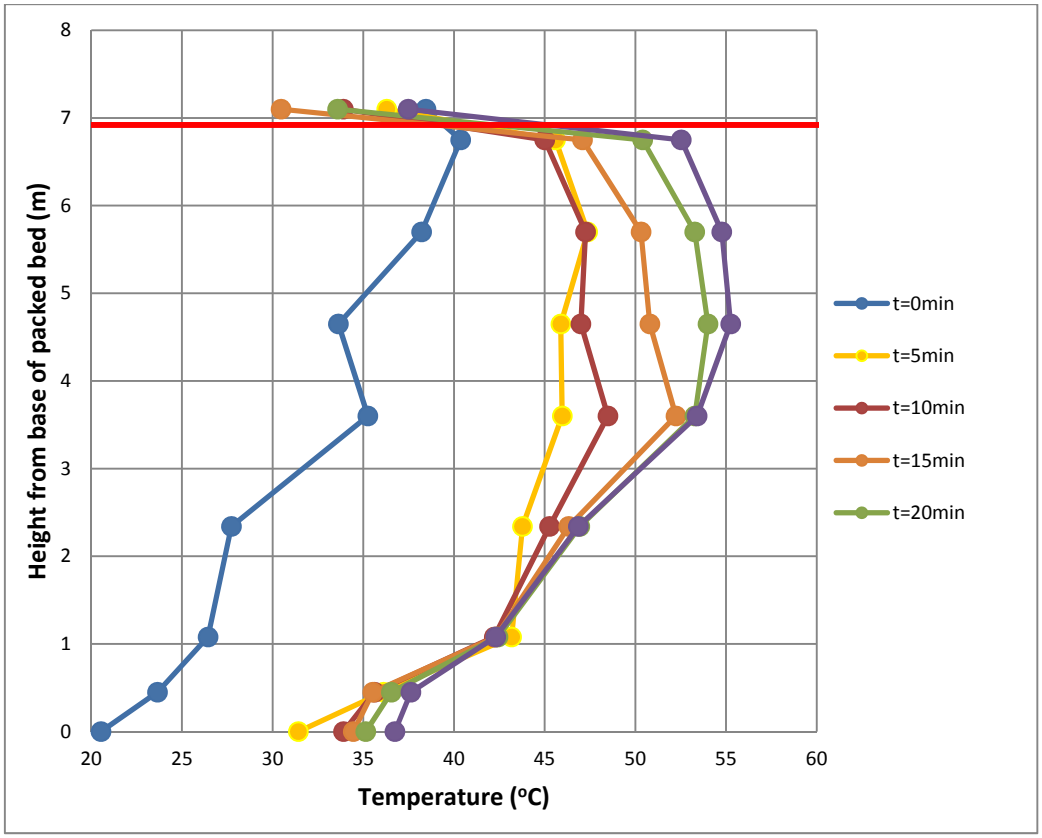
Height from base of packed bed (m)
Temperature (°C)
t=0min
t=5min
t=10min
t=15min
t=20min

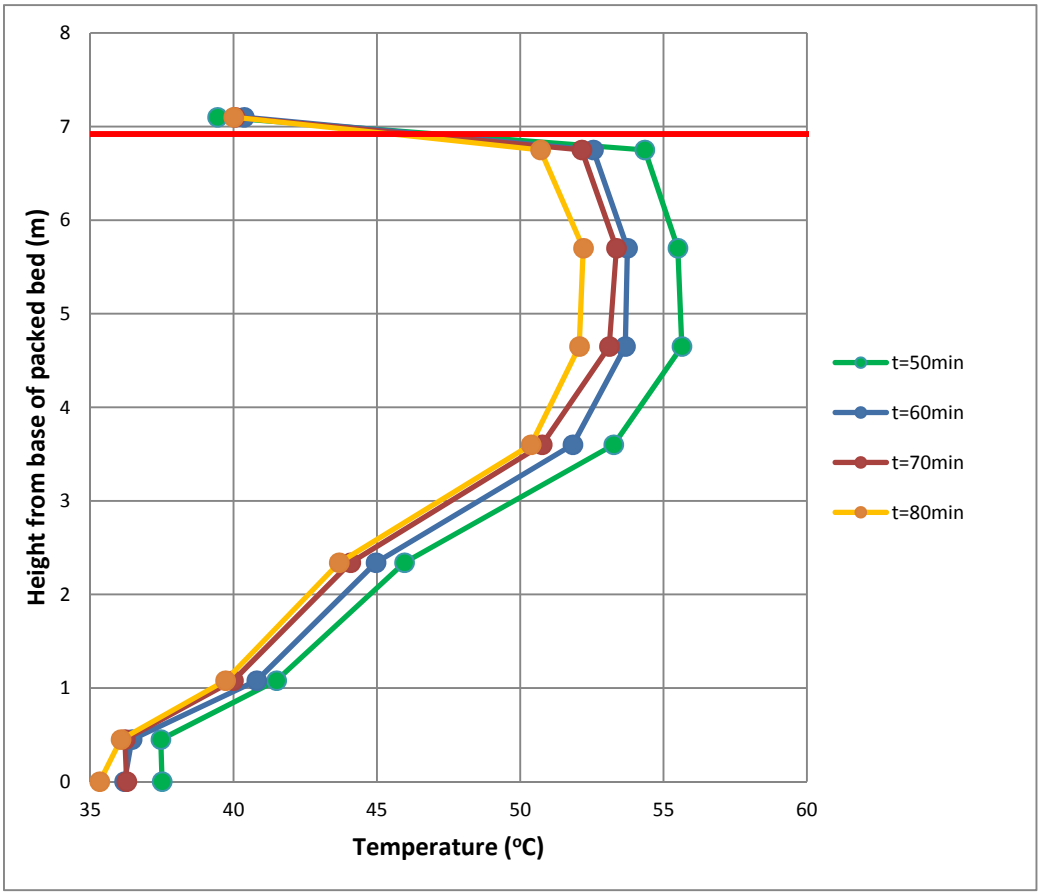
Height from base of packed bed (m)
Temperature (°C)
t=50min
t=60min
t=70min
t=80min

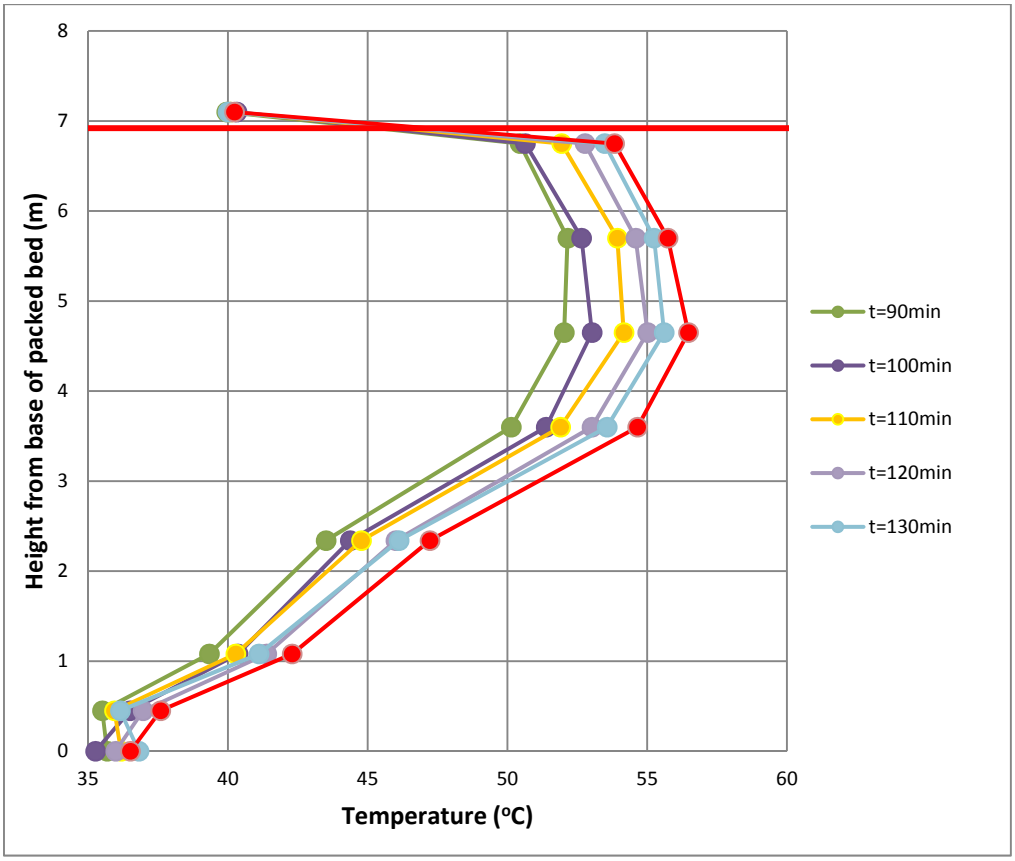

Fig. 5.9a. Evolution of absorber temperature profile, t=0min – t=30min, gas turbine startup scenario
Fig. 5.9b. Evolution of absorber temperature profile, t=50min – t=80min, gas turbine startup scenario
Fig. 5.9c. Evolution of absorber temperature profile, t=90min – t=140min, gas turbine startup scenario

The outcomes from this experiment suggest that a decrease in capture rate following startup is inevitable as plant parameters stabilise, in cases where some solvent flowrate has been maintained between the shutdown and startup to use the cooling capacity available. If maintaining a high capture rate is of critical importance, interim solvent storage has been proposed as a method to increase capture flexibility from coal plants, by ensuring that a large separate reserve of lean solvent is available until the plant is stabilised at baseload (Lucquiaud et al., 2014). In the absence of solvent storage, minimisation of CO_2 emissions could be achieved by prioritising the use of steam for solvent regeneration rather than sending it through the low-pressure steam turbine. This approach is explored in the context of PCC on coal in the subsequent test campaign described in chapter 6.

5.4.3 Power output maximisation via capture plant decoupling

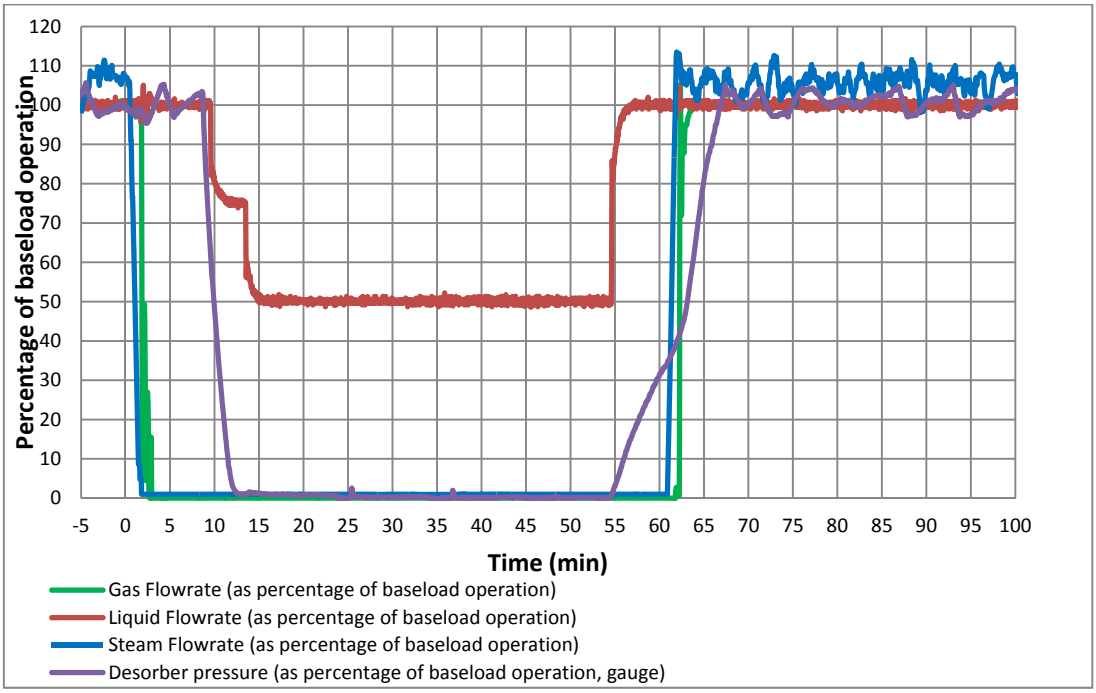

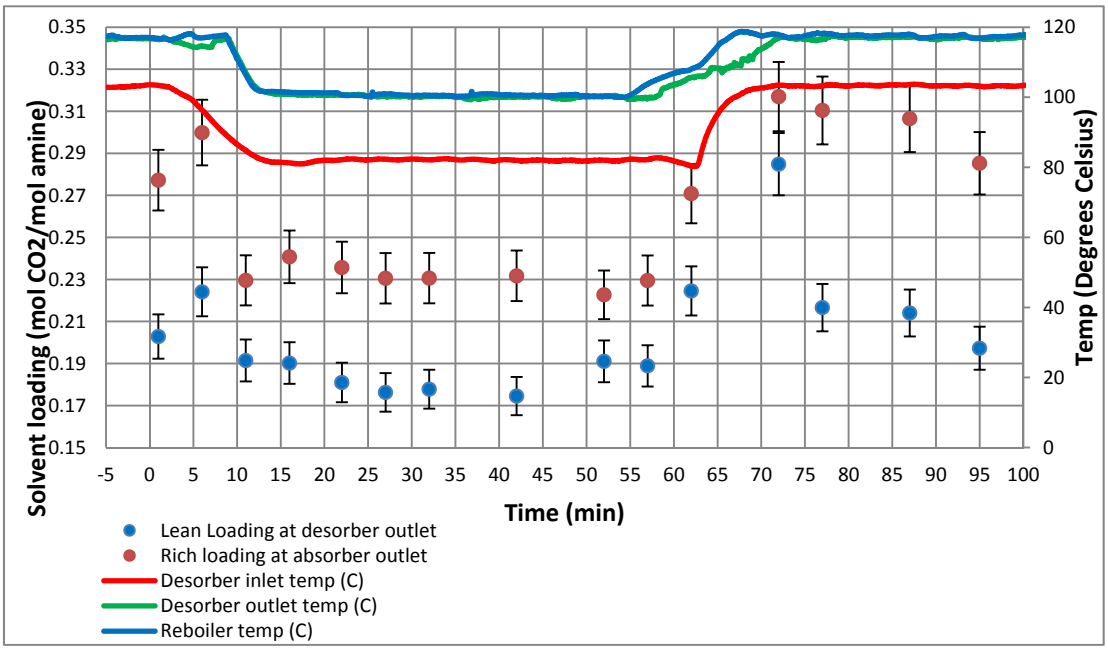

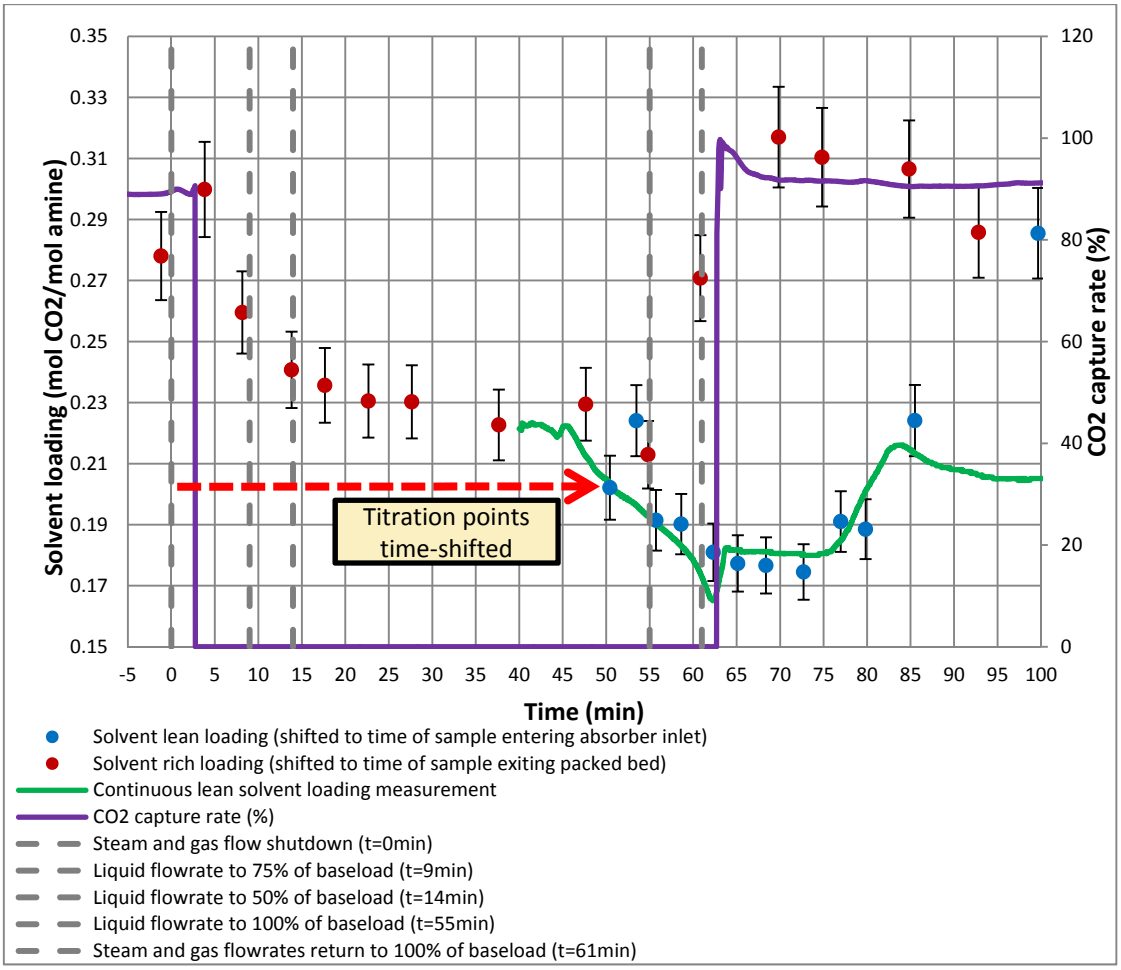
Solvent loading (mol CO2/mol amine)
CO2 capture rate (%)
Time (min)
Titration points time-shifted
Solvent lean loading (shifted to time of sample entering absorber inlet)
Solvent rich loading (shifted to time of sample exiting packed bed)
Continuous lean solvent loading measurement
CO2 capture rate (%)
Steam and gas flow shutdown (t=0min)
Liquid flowrate to 75% of baseload (t=9min)
Liquid flowrate to 50% of baseload (t=14min)
Liquid flowrate to 100% of baseload (t=55min)
Steam and gas flowrates return to 100% of baseload (t=61min)

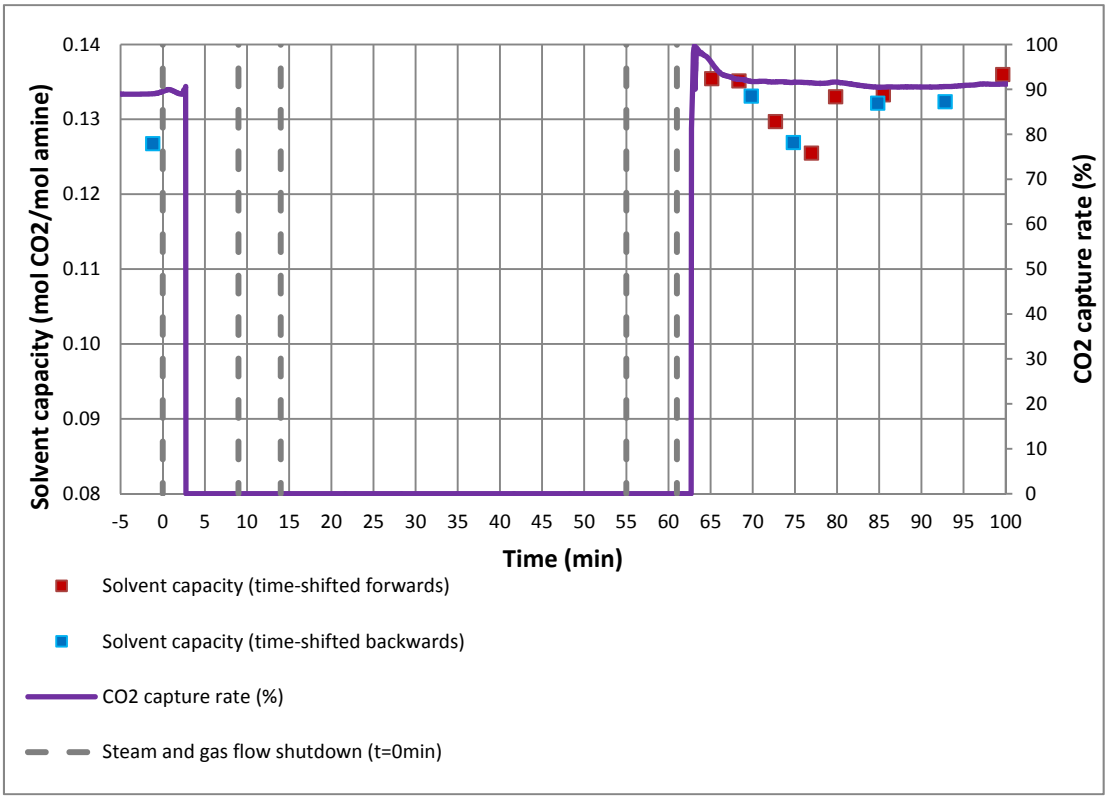
Solvent capacity (mol CO2/mol amine)
CO2 capture rate (%)
Time (min)
Solvent capacity (time-shifted forwards)
Solvent capacity (time-shifted backwards)
CO2 capture rate (%)
Steam and gas flow shutdown (t=0min)

Fig. 5.10a. Gas, liquid and steam flowrates as percentage of baseload, power output maximisation by capture plant decoupling scenario

Fig. 5.10b. Rich and lean solvent CO_2 loading at sampling ports, desorber and reboiler temperatures, power output maximisation by capture plant decoupling scenario

Fig. 5.10c. Lean and rich solvent loading titration measurements (time-shifted), continuous lean loading measurement (time-shifted) and CO_2 capture rate, power output maximisation by capture plant decoupling scenario

Fig. 5.10d. Predicted real-time solvent capacity and CO_2 capture rate, power output maximisation by capture plant decoupling scenario

Before the capture plant decoupling scenario is initiated, the plant operates at steady state baseload. The flowrates of steam and gas are reduced to zero at t=0min and t=1min, respectively (figure 5.10a), with the capture rate dropping to zero shortly thereafter since gas no longer passes through the absorber (figure 5.10b). The manual valve maintaining pressure in the desorber is released at t=8min to allow the pressure to decay. The flow of liquid is turned down in two steps, to 75% of baseload at t=9min, then 50% at t=14min (figure 5.10a). Solvent flow is maintained at 50%, reproducing likely operating conditions where power for solvent circulation is reduced to a minimum to maximise electricity power output. Continued circulation of solvent also allows for rapid capture plant startup as the pumps are already running. This lower solvent flowrate ensures that a substantial reserve of solvent capacity is available when flue gas is reintroduced to the absorber column.

Lean solvent loading measured with by titration at the desorber outlet appears to rise between t=1min and t=6min, before dropping once again at t=11min (figure 5.10c). The rise in lean loading around t=6min is not observed in the continuous measurement which indicates that this sample may be unrepresentative of plant trends. The liquid flowrate remains at 100% until t=9min, and by the time the sample at t=11 is taken, solvent which has not been exposed to CO_2 in the absorber begins to reach the desorber outlet. This is consistent with the circulation time between the top of the absorber sump and top of the desorber sump at baseload liquid flow being approx. 8min in total, allowing 6min from absorber outlet to desorber, plus an additional 2min to pass through the desorber sump.

After the flow of gas has been shut down, the absorber temperature bulge decreases in magnitude and moves down the column as hot solvent in the upper region of the absorber flows down the packed bed, being replaced by cooler solvent (fig. 5.11a). The absorber is insulated and requires some time to cool down as heat is transferred from the packing to the incoming cool solvent.

Assuming that the lean titration measurement at t=6min is unrepresentative of true plant trends, lean loading at the desorber outlet decreases from 0.202 mol/mol to 0.174 mol/mol from t=0min until around t=50min (fig 5.10b) as residual heat in the desorber continues to liberate small amounts of CO_2, from solvent not exposed to CO2 in the absorber.

Lean loading titration measurements are shifted forward to the time at which they should reach the absorber inlet (blue markers) on Fig. 5.10c. The continuous online solvent measurement shows good agreement with the titration data until t=85min. Based on the liquid flowrate and volume of liquid in the pipework between the desorber outlet and absorber inlet, solvent which has lean loading of 0.204 mol/mol at t=1min (fig 10b), is predicted to reach the absorber inlet at t=54min (fig. 5.10c). This appears very close to the rich loading value of 0.213 mol/mol which reaches the absorber outlet at t=54min. Given that there is no CO_2 flow into the absorber between t=1min and t=54min, this indicates that the time-shifting method provides a moderately accurate estimation of solvent circulation time of 53min.

The temperature profile of the absorber (fig. 5.11a) decreases in magnitude after t=0min, as the exothermic absorption of CO_2 stops after the flowrate reaches zero. The absorber temperature bulge shows a similar response to that observed during simulated gas turbine shutdown, decreasing in magnitude and moving down the packing height as hot solvent flows down the packed bed and is replaced by slow flowing incoming cooler solvent. By t=15min there is no observable bulge, and the temperature across the entirety of the packed bed decreases until flue gas is reintroduced.

The desorber manual release valve is closed and pressure begins to rise at t=55min. At t=60min, the bypass event ends and the flowrates of gas and steam are ramped back up to 100% (fig. 5.10a).

Rich loading increases rapidly upon reintroduction of CO_2 to the absorber at t=62min. The capture rate is initially higher than the baseload value as a batch of cool solvent promotes CO_2 absorption, and this is reflected

in the rich loading titration measurements of 0.316, 0.313, 0.306 mol/mol at t=72, 77 and 87min respectively (fig 5.10b). The lean loading at the desorber outlet follows a similar trend once the desorber has reached operational temperature, with the circulation time from the absorber sump to the desorber sump being around 6min at 100% baseload solvent flowrate. A temperature bulge is observed in the absorber at t=65min, 3min after the reintroduction of gas flow, and is fully established by t=95min (fig. 5.11b).

Fig. 5.10c shows the lean and rich solvent measurements time-shifted to the absorber inlet and outlet. It should be noted that the time-shifting method detailed in section 5.3.4 contains a level of uncertainty due to the hydraulic response of the plant, and in this case predicts an increase in solvent loading at the base of the absorber packing at t=61min, 60 seconds before the flow of gas is reintroduced. A batch of richer lean solvent which is predicted to reach the inlet between t=85 and t=99min appears not to be detected by the online solvent sensor, and has no real effect on the capture rate. It is possible that there is sufficient mixing with leaner solvent between the sampling port and the absorber inlet, that the increase in loading is dampened.

The time shifting method is used to show the solvent working capacity in the absorber in mol/mol (fig. 5.10d), and how it relates to capture level. Solvent working capacity is calculated as described in section 5.3.3.

In this scenario there is no observable reduction in capture rate upon reintroduction of flue gas. However, it is worth noting that the effect on capture rate upon reintroduction of flue gas will be highly dependent on the length of the shutdown operation, the circulation time, total solvent inventory and extent of mixing in the liquid loop for each individual capture plant. Potential detrimental effects on capture rate upon restart could be mitigated by using interim solvent storage (Lucquiaud et al., 2014). Aside from this this reduced capture rate and the associated additional cost of CO_2 emissions, no severe operational barriers to capture bypass such as column flooding are encountered. The CO_2 capture rate rapidly returns to normal operation upon baseload flow conditions being re-established, and the decision to operate in this fashion is likely to be based entirely on economic factors, i.e. the trade-off between increased electricity selling price and potential penalties for emissions.

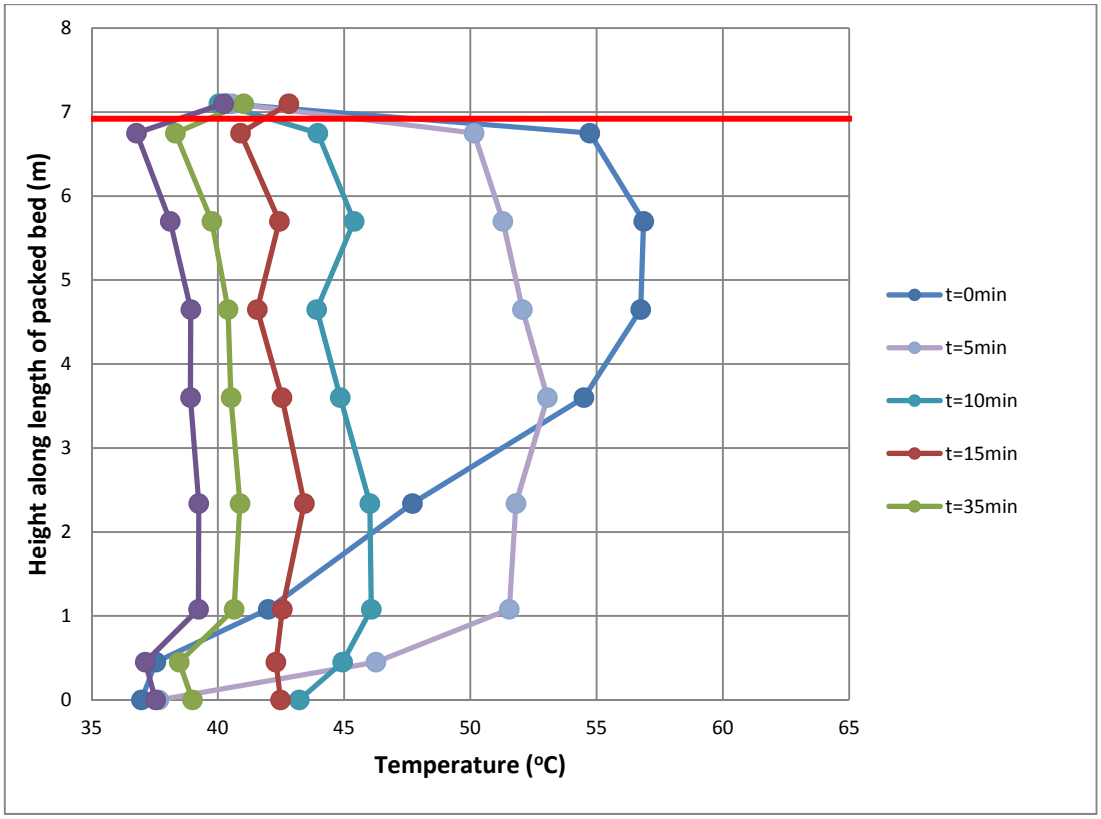

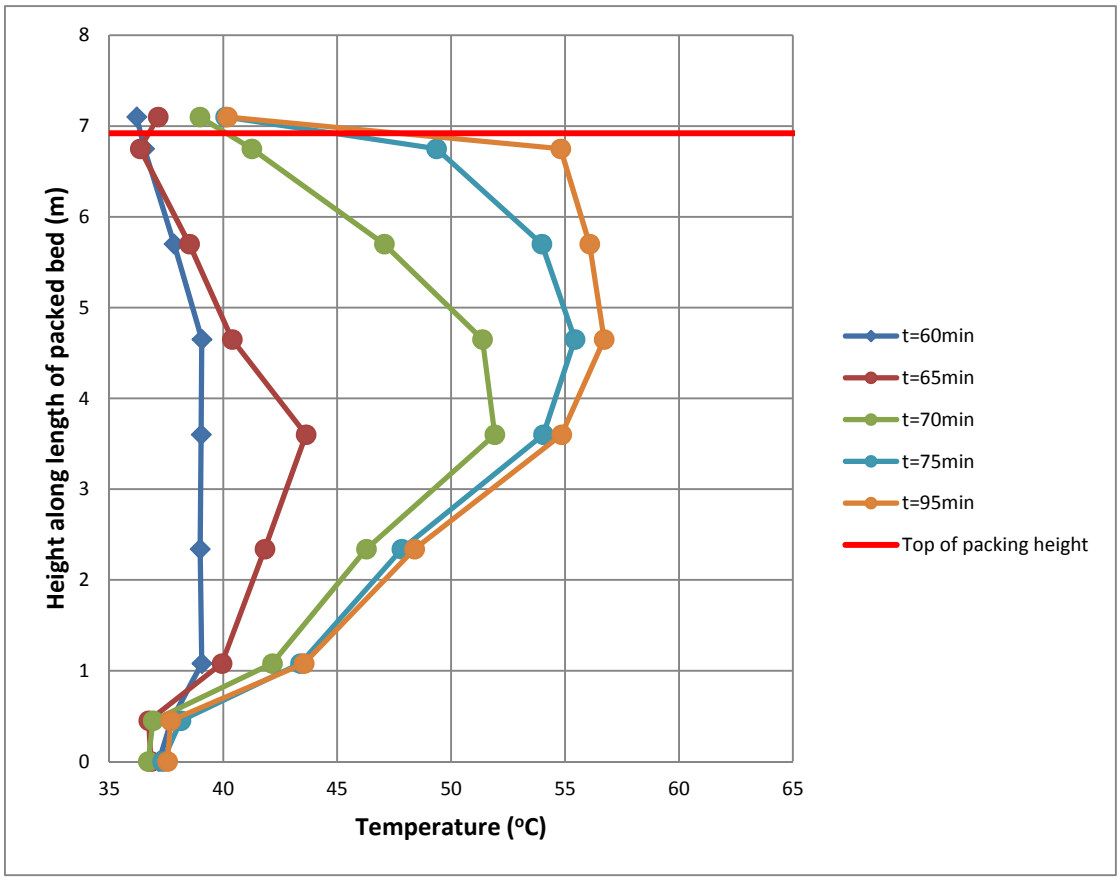

Fig. 5.11a. Evolution of absorber temperature profile during power output maximisation by capture plant decoupling scenario– temperature decrease

Fig. 5.11b. Evolution of absorber temperature profile during power output maximisation by capture plant decoupling scenario – temperature increase

5.4.4 Power output maximisation via reboiler steam decoupling

Although similar to the previous scenario, a significant difference is that synthetic flue gas is continuously fed to the absorber column during reboiler steam shutdown. Steam flow to the reboiler is reduced to zero at t=0min, followed by the opening of the desorber pressure release valve at t=1min (fig. 5.12a). Solvent flowrate is turned down to 75%, then 50% at t=8min and t=15min respectively. The capture rate begins to drop at t=8min after the initial decrease in solvent flow, but does not decrease sharply until t=17min (fig. 5.12c).

Lean loading at the desorber outlet appears to fluctuate between t=6 and t=31min, based on the titration measurements taken (fig 5.12c). When the flowrate of solvent is reduced rapidly, the PID control system may fully close the desorber outlet valve for several minutes in an attempt to maintain desorber sump level. Solvent which has not been exposed to steam flow will have ample opportunity to mix with fully regenerated solvent in the desorber sump. This mixing effect makes it very difficult to predict what will happen to the lean loading at the desorber outlet, although based on the results from the online solvent sensor, it is possible that the titration measurements at t=11 and t=21min (fig. 5.12b) are erroneous or not representative of lean solvent loading which will be seen by the solvent sensor or at the absorber inlet. Short-term fluctuations in CO_2 loading at the desorber outlet are likely to be dampened by solvent mixing in the large solvent tank.

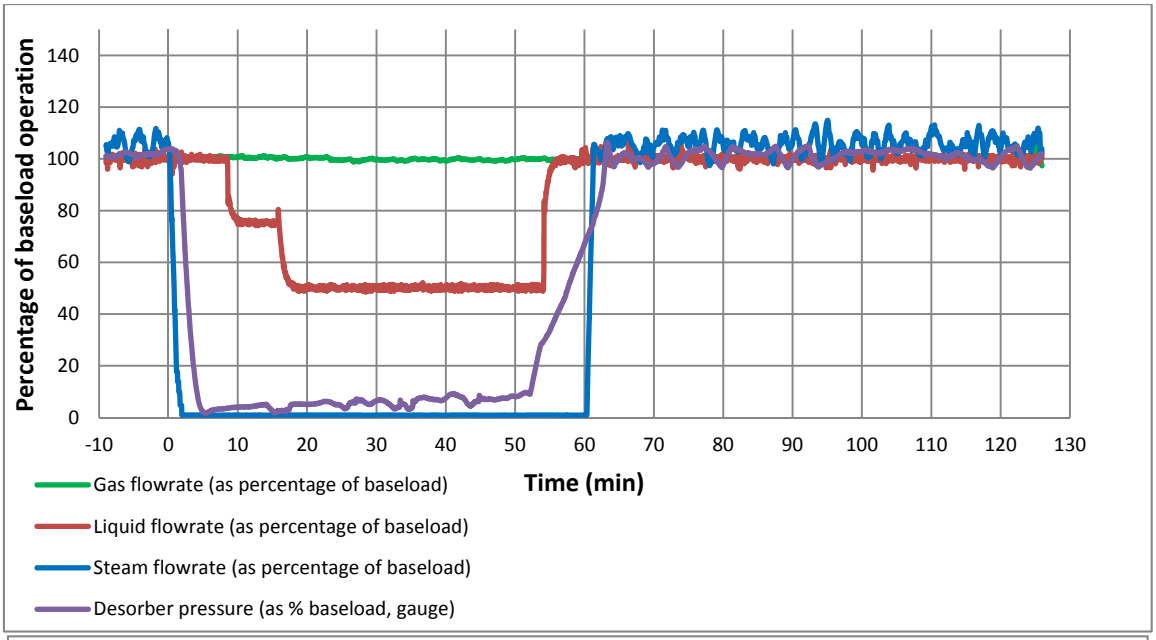
Percentage of baseload operation
140
120
100
80
60
40
20
0
-10
0
10
20
30
40
50
60
70
80
90
100
110
120
130
Time (min)
Gas flowrate (as percentage of baseload)
Liquid flowrate (as percentage of baseload)
Steam flowrate (as percentage of baseload)
Desorber pressure (as % baseload, gauge)

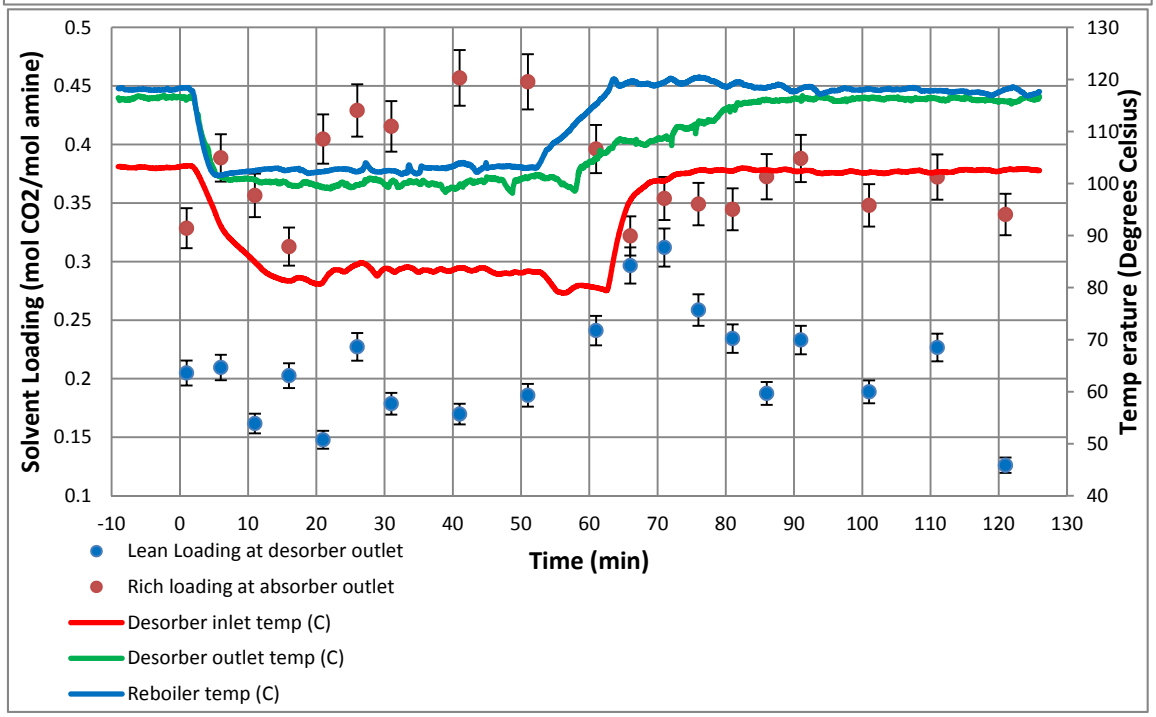
Solvent Loading (mol CO2/mol amine)
0.5
0.45
0.4
0.35
0.3
0.25
0.2
0.15
0.1
Temp erature (Degrees Celsius)
130
120
110
100
90
80
70
60
50
40
-10
0
10
20
30
40
50
60
70
80
90
100
110
120
130
Time (min)
Lean Loading at desorber outlet
Rich loading at absorber outlet
Desorber inlet temp (C)
Desorber outlet temp (C)
Reboiler temp (C)

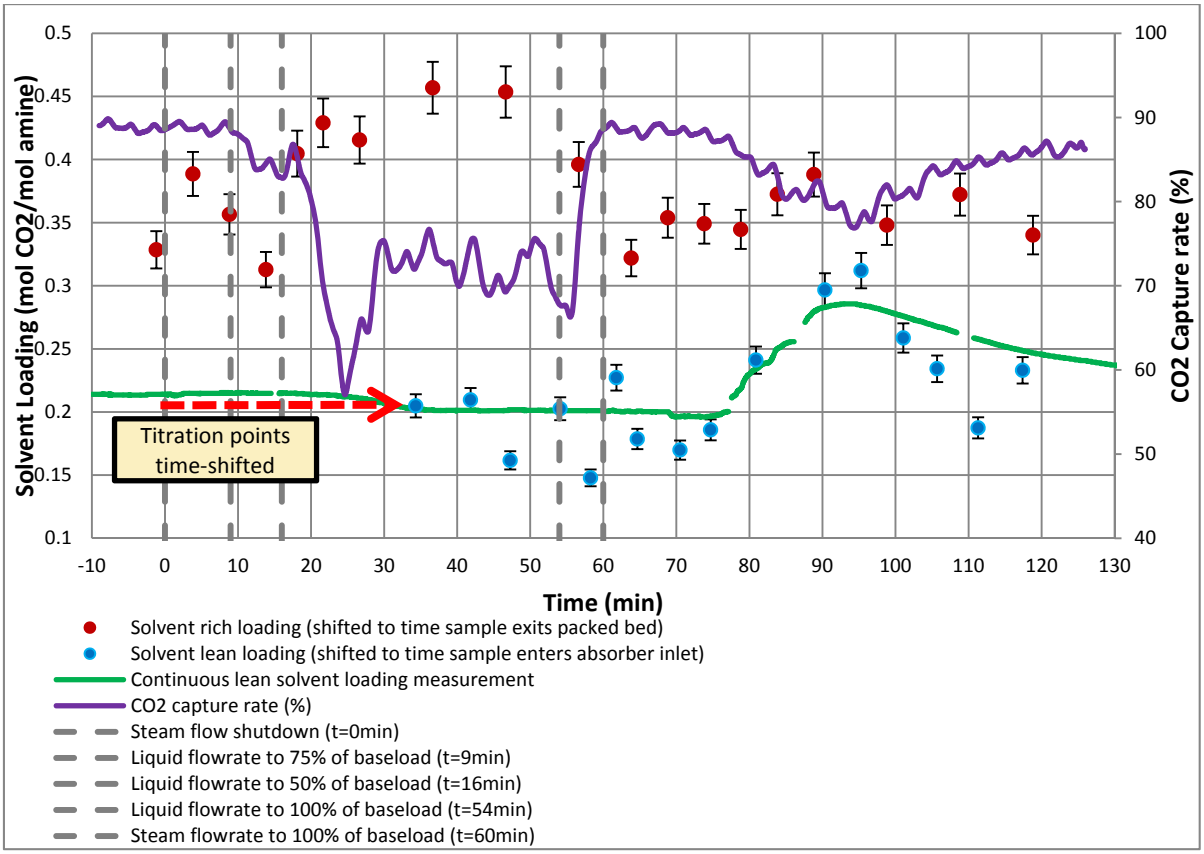

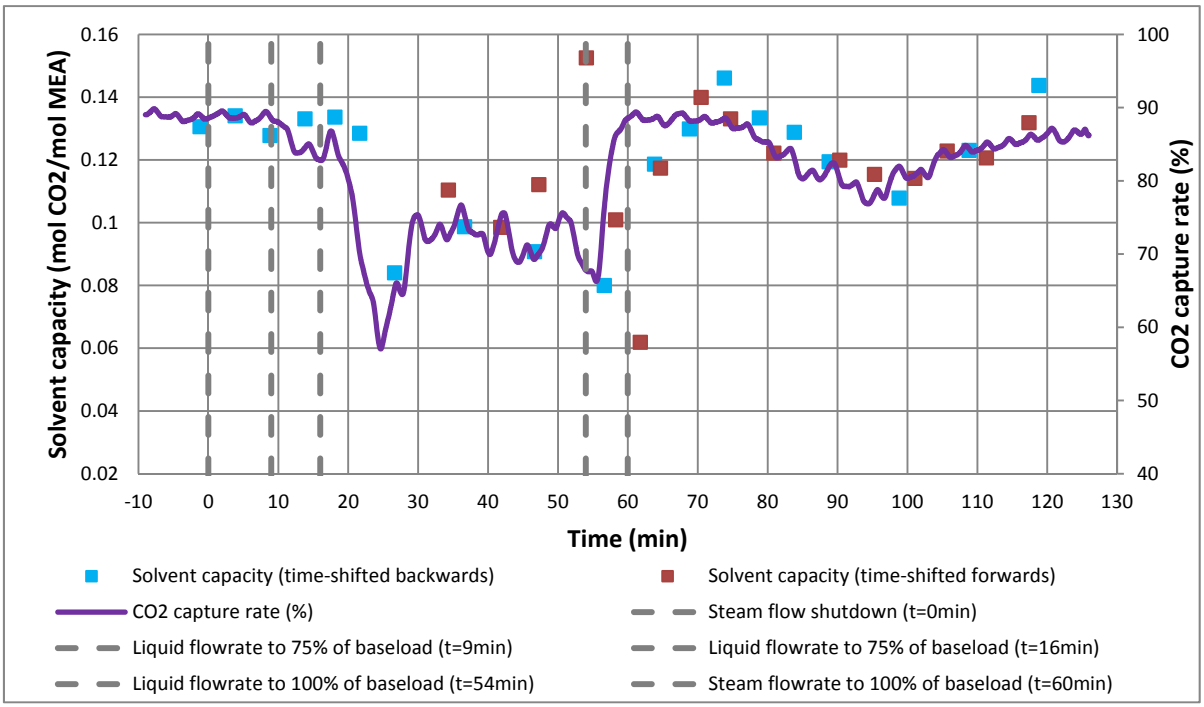

Fig. 5.12a. Gas, liquid and steam flowrates as percentage of baseload operation, for power output maximisation by reboiler steam decoupling scenario

Fig. 5.12b. Rich and lean solvent CO_2 loading at sample points, desorber and reboiler temperatures, power output maximisation by reboiler steam decoupling scenario

Fig. 5.12c. Rich and lean solvent loading measurements (time-shifted), continuous lean loading measurement (time-shifted), CO_2 capture rate, power output maximisation by steam decoupling scenario

Fig. 5.12d. Predicted real-time solvent capacity and CO_2 capture rate, power output maximisation by steam decoupling scenario

In this and the final dynamic scenario (section 5.4.5), the online solvent sensor is relocated to just downstream of the main solvent pump, just before the absorber inlet. When the titration values are shifted to the time at which each packet of solvent would reach the absorber inlet (fig. 5.12c), this fluctuating lean loading behaviour is not observed in the continuous measurement or CO_2 capture rate response. This may suggest that the fluctuations in lean solvent loading at the desorber are dampened due to mixing in the solvent tank, and will not have a considerable impact on the lean loading at the absorber inlet.

There is an increasing trend in rich loading at the absorber outlet before the flowrate from t=17min, and the increased liquid residence time on the packing. Although the rich solvent loading at the bottom of the absorber increases, the liquid flow rate is low enough that the mass of CO2 captured is reduced overall. The absorber temperature bulge decreases in magnitude (fig 5.13a), consistent with the decrease in capture rate, and moves upwards. The upwards shift may be due to diminished working capacity, capture rate and L/G ratio, which results in higher concentrations of CO_2 in the upper regions of the absorber. The solvent becomes loaded with CO_2 more rapidly upon entry, decreasing the driving force for CO_2 absorption in lower regions of the packed bed. Higher CO_2 concentration in the upper regions of the packing also results in a higher driving force for CO_2 absorption on the gas-side.

The desorber pressure release valve is closed and liquid flow ramped back up at t=52 and 53min, respectively, in anticipation of the plant returning to normal operating conditions. Steam flow is ramped back up to 100% at t=60min. In total the steam shutdown operation lasts 60min, a plausible duration for a bypass event in response to an evening peak in electricity selling price. Lean loading at the desorber outlet decreases between t=71 and t=76min, once the desorber has reached operational temperature (fig. 5.12b). The estimated real-time solvent loading capacity (fig. 5.12d) appears to follow the capture rate for the majority of the scenario, except for two points at t=54.07 and 61.08. This may be due to the fact that the lean loading titration measurements, which the calculations are based on, are erroneous or that the CO_2 flowrate into the absorber is not entirely stable during this time.

Capture rate is observed to decrease between t=75 and t=95min, corresponding to the time where solvent which has not been fully regenerated in the desorber is predicted to reach the absorber inlet (fig. 5.12c).

There is good agreement around t=95min between solvent working capacity and capture rate, yet, on Figure 5.12c, the lean loading value of 0.312 mol/mol, time shifted to t=95min, is close to the rich loading value of 0.348 mol/mol while a capture rate of >75% is achieved. This is considerably higher than the baseload lean loading value of 0.232mol MEA/mol CO_2 (section 5.3.1) As mentioned in section 5.3.4, the time shifting method is not able to account for mixing effects since it relies on the assumption of plug flow. Therefore it is likely that mixing effects in the solvent tank, located between the lean and the rich sampling points, play an important role to maintain solvent working capacity and capture rate around 75-80% for from t=75 until t=95min.

The batch of richer lean solvent passing through the absorber, indicated by online measurement readings at around t=95min (fig. 5.12c) is then followed by a rise in capture rate before the plant returns to steady state baseload operation. The absorber temperature bulge reflects capture rate trends, increasing in magnitude and moving down the packing height after t=60min (fig. 5.13b). The temperature profile decreases slightly around t=100 min, coinciding with the drop in capture rate, before increasing as the plant reaches steady state operation at t=120min.. Innovative strategies which involve switching between partial capture and capture rates >90% depending on electricity selling price have been suggested as a method of increasing daily revenue without severely compromising environmental standards (Mac Dowell and Shah, 2014).

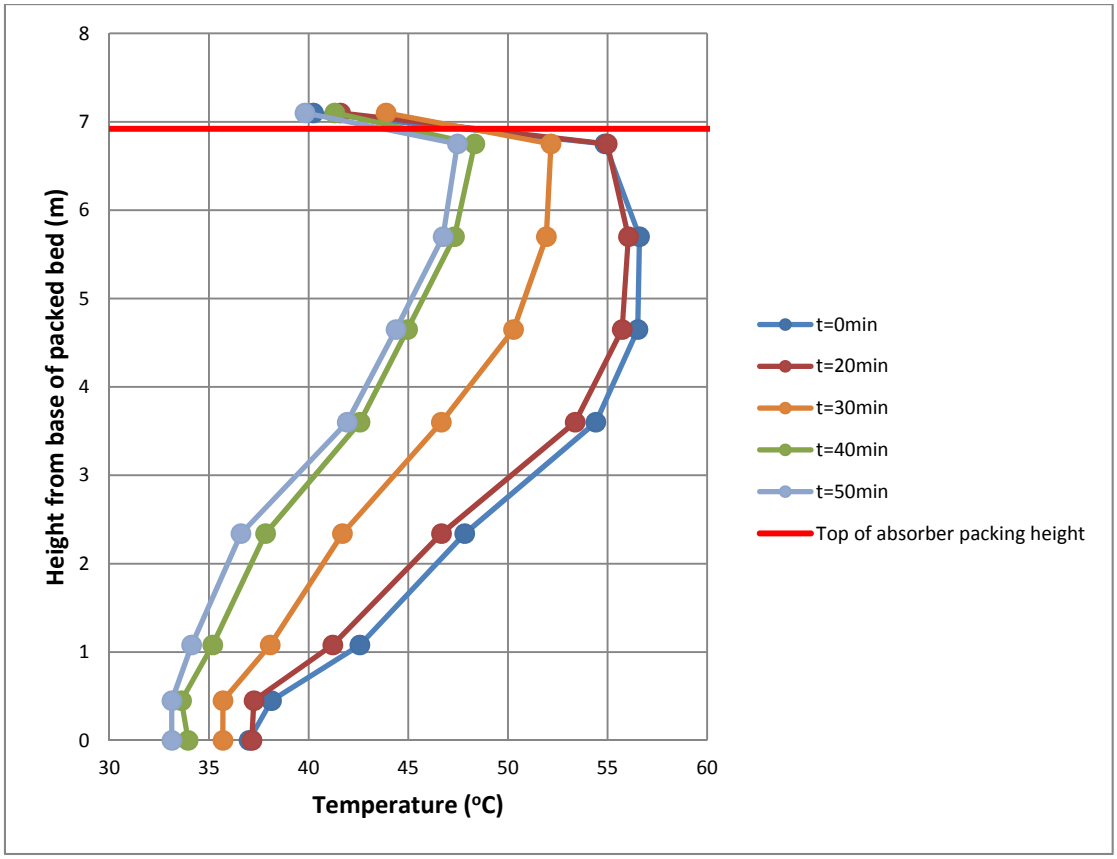

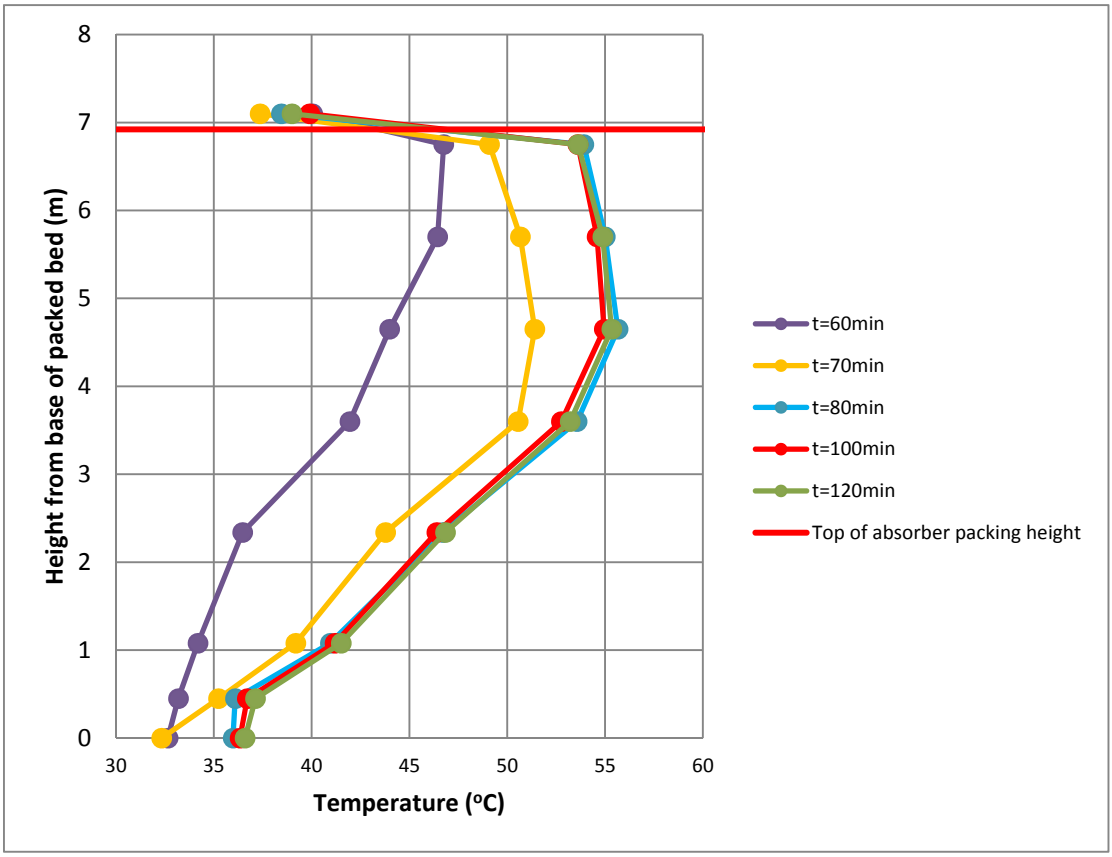

Fig. 5.13a. Evolution of absorber temperature profile, power output maximisation by reboiler steam decoupling scenario – temperature decrease

Fig. 5.13b. Evolution of absorber temperature profile, power output maximisation by reboiler steam decoupling scenario – temperature increase

5.4.5 Frequency Response via rapid reboiler steam flow increase

The flowrate of steam to the reboiler is increased rapidly to 200% at t=0 and remains at this value for 41 minutes, while all other plant parameters remain at steady state (fig. 5.14a). Plant data continues to be obtained for an additional 50 minutes after steam flow returns to its baseload value, in order to observe any further effects on the response of the plant.

Please note that the plant may not have fully reached steady-state before the start of this scenario, with the initial capture rate at 85% and a lean loading of 0.250mol/mol. Nevertheless, valuable insights about how the plant reacts to a frequency response operation can be gained from the results and are discussed below.

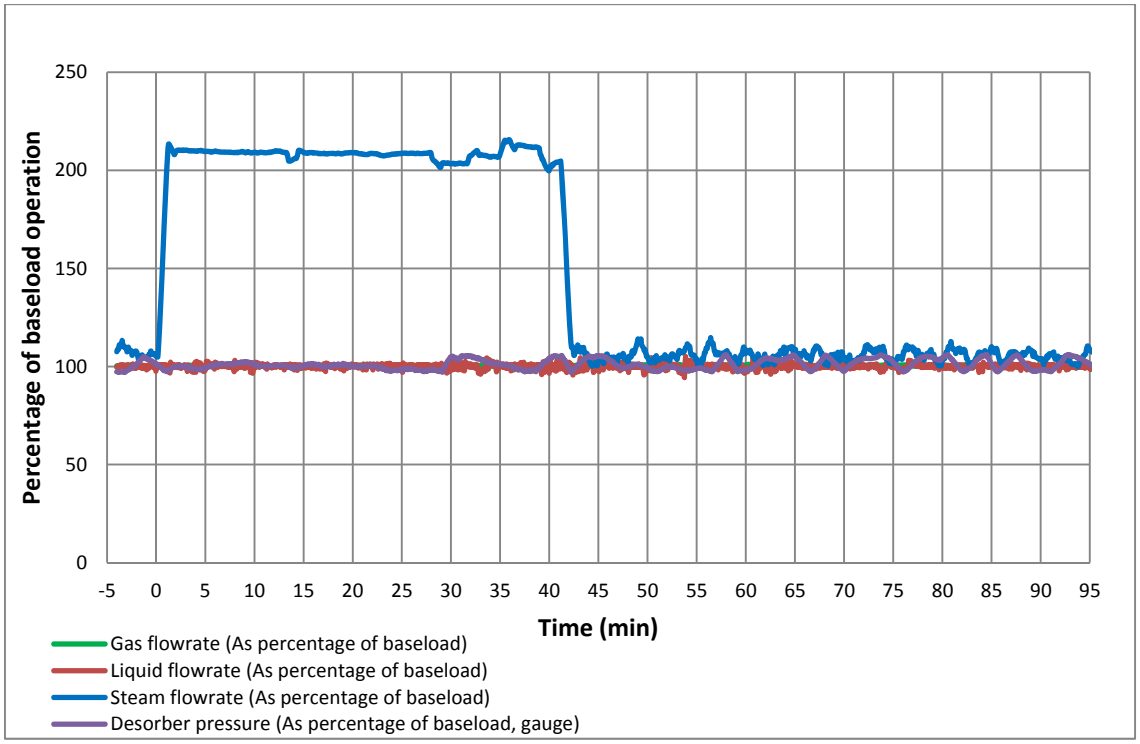
Percentage of baseload operation
250
200
150
100
50
0
-5 0 5 10 15 20 25 30 35 40 45 50 55 60 65 70 75 80 85 90 95
Time (min)
Gas flowrate (As percentage of baseload)
Liquid flowrate (As percentage of baseload)
Steam flowrate (As percentage of baseload)
Desorber pressure (As percentage of baseload, gauge)

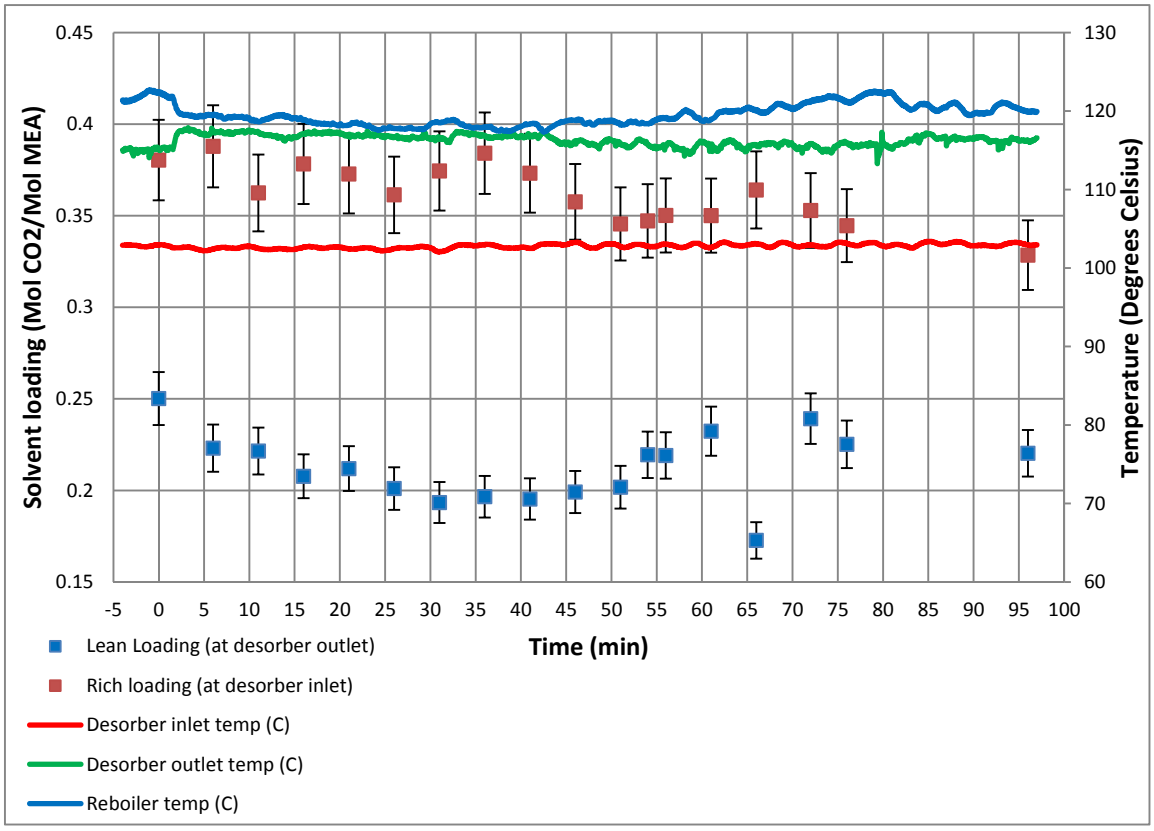
Solvent loading (Mol CO2/Mol MEA)
0.45
0.4
0.35
0.3
0.25
0.2
0.15
Temperature (Degrees Celsius)
130
120
110
100
90
80
70
60
-5 0 5 10 15 20 25 30 35 40 45 50 55 60 65 70 75 80 85 90 95 100
Time (min)
Lean Loading (at desorber outlet)
Rich loading (at desorber inlet)
Desorber inlet temp (C)
Desorber outlet temp (C)
Reboiler temp (C)

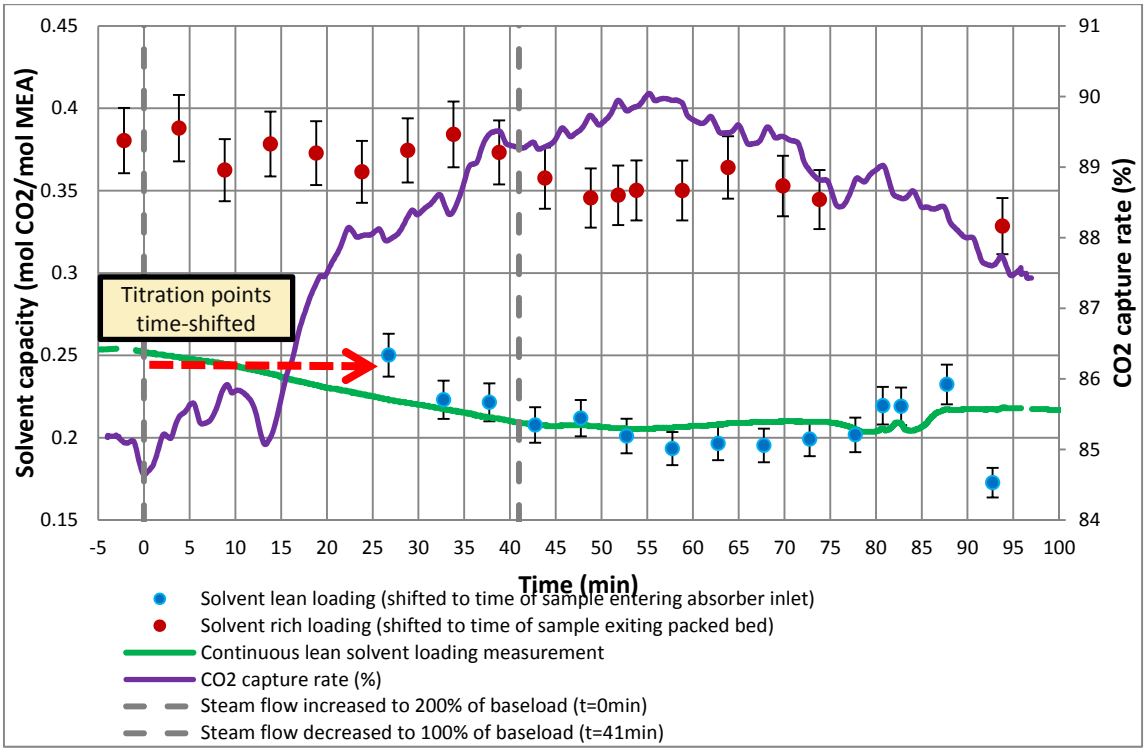

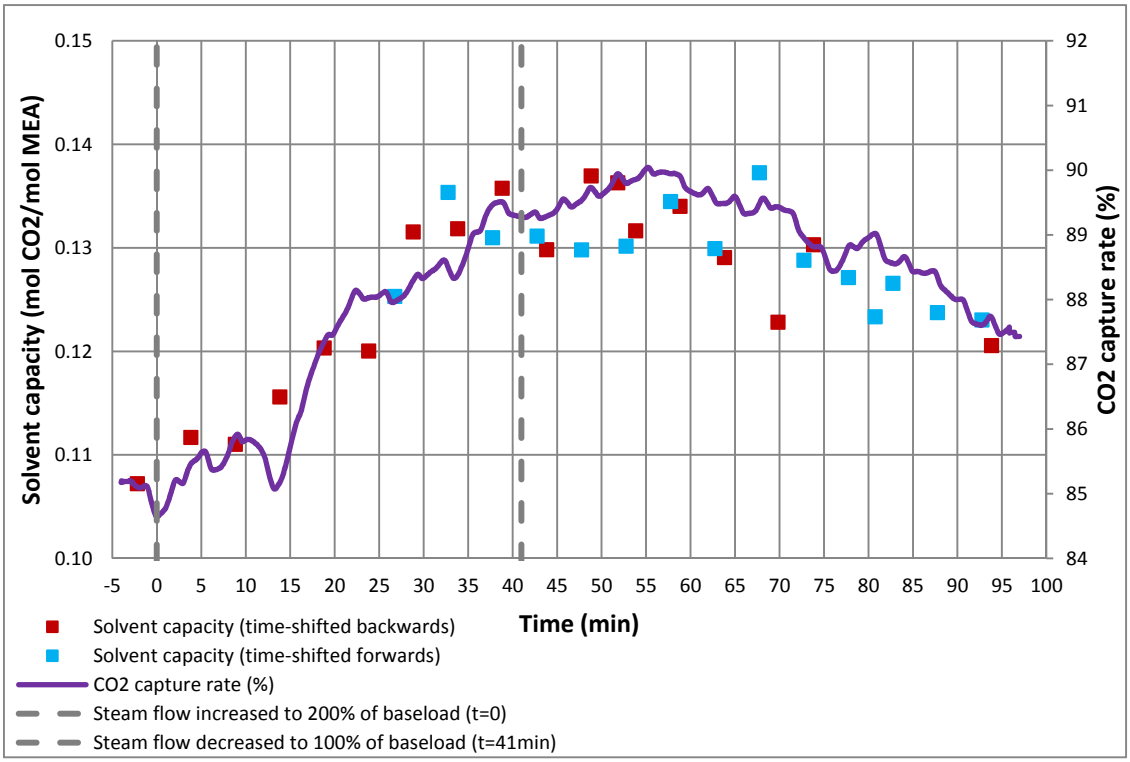

Fig. 5.14a. Gas, liquid and steam flowrates as percentage of baseload operation, frequency response scenario

Fig. 5.14b. Rich and lean solvent CO_2 loading, desorber and reboiler temperatures, frequency response scenario

Fig. 5.14c. Lean and rich solvent loading bench measurements (time-shifted), continuous lean loading measurement (time-shifted), CO_2 capture rate, frequency response scenario

Fig. 5.14d. Predicted real-time solvent capacity and CO_2 capture rate, frequency response scenario

Lean loading at the desorber outlet decreases steadily from 0.250 mol/mol after the flowrate of steam is increased at t=0, eventually stabilising at around 0.2mol CO_2/mol amine (fig. 5.14b). These titration data points

are shifted to the time at which each sample would reach the absorber inlet (fig. 5.14c). The online solvent sensor output displays similar behaviour, but the decrease in lean loading appears less rapid. As the sensor is located after the main solvent tank, any rapid changes in lean loading at the desorber outlet are dampened when that packet of solvent reaches the sensor, due to mixing in the solvent tank. The continuous measurement suggests that the lean loading at the absorber inlet begins to decrease before any solvent which has undergone a greater degree of regeneration due to increased steam flow is expected to reach the absorber inlet. As the plant is not initially at baseload, it is not possible to attribute the observed increase in capture rate and decrease in lean loading at the absorber inlet between t=0 and t=25min to the frequency response operation.

Figures 5.14c and 5.14d show that, when solvent which has undergone a greater degree of regeneration due to increased steam flow starts entering the absorber from t=26min onwards, the increase in solvent working capacity results in an increase in capture rate from 88% to 90%. Steam flow is turned down to 100% of baseload at t=41min. The response of the capture rate, starting at t=70min, corresponds to an increase in lean solvent loading at the absorber inlet (fig. 5.14c).

A titration lean loading measurement at t=66min (fig. 5.14b)/t=93min (fig. 5.14c) appears to be anomalous as there is no significant change in the capture rate, and it deviates significantly from the online lean loading measurement at this point in time..

The calculated real-time solvent working capacity (fig 5.14d) follows the trend of the capture rate over the course of the whole experiment. Accurate monitoring and prediction of real-time working capacity via continuous loading measurements at the absorber inlet and outlet could prove to be a key metric in future advanced control systems for dynamic post-combustion capture.

As there is no significant change in absorber temperature profile, the maximum temperature change over the course of the experiment being an increase of 1.68^{o}C at a height of 3.6m, absorber temperature data are not reported for this scenario.

5.5 Conclusions

Five enhanced operational flexibility scenarios of an amine post-combustion capture process treating flue gas from a state of the art combined cycle gas turbine plant are investigated.

The outcomes of this test campaign directly informed the direction of research in the subsequent test campaign at the UKCCSRC PACT facility. No significant hardware or operational barriers to flexible operation are observed, but the question remains of how PCC can respond most effectively to rapid changes in generation plant output. As long as unwanted hydrodynamic phenomena such as flooding or foaming in the absorber column can be avoided, it was determined that the focus of the next test campaign should be on observing the effects of a different plant configuration on dynamic operation. The significance of circulation times and solvent mixing also necessitates an understanding of plant hydrodynamics to be developed before any dynamic scenarios are implemented. The effect of plant circulation times ay appear obvious, but it has not been widely discussed in the literature as a major factor affecting plant response to dynamic operations.

The volume of active solvent inventory plays a part in how the plant reacts to dynamic scenarios. A large solvent inventory implies longer circulation times, resulting in the plant requiring additional time to return to steady-state following a perturbation. A reduction of solvent inventory may reduce delays due to circulation times, but there are positive effects to having a large solvent inventory – this increases the solvent capacity of the plant so a high capture rate can be maintained for longer if steam supply to the reboiler is reduced or turned off. The design and construction of the CO_2 capture facility, in particular the volume of solvent present between the desorber outlet and absorber inlet, should be carefully considered within the energy generation portfolio within which the plant will operate. The use of interim solvent storage as initially suggested by (Chalmers and Gibbins, 2007) and widely studied since by others, e.g. (Chalmers, 2009; Oates, 2014) could allow PCC operators to retain a large reserve of available capacity while operating with a small solvent inventory during steady state operations.

Solvent working capacity is identified as a potential metric for future advanced plant control systems. An automated control system must perform feedback control loop operations at least 10x faster than the time frame required to change state. Therefore, if the capture plant changes state once every 30 minutes, the feedback operation must be performed at least once every 3 minutes. Obtaining a solvent loading measurement within this timeframe is not possible with existing methods - manual sampling followed by loading analysis at regular

intervals is time-consuming and labour-intensive, while anecdotal evidence regarding the use of automated titration systems indicates that each loading measurement procedure can take up to 20 minutes. Accurate, continuous solvent CO_2 loading measurements at the absorber inlet and outlet are likely to be key control variables (Seibert, 2011; van der Ham, 2014). The efficacy of this approach and further thoughts on plant control using continuous solvent composition measurements are provided in the conclusions to Chapter 6.

The prototype online solvent sensor performs adequately during this test campaign but rapid changes in solvent CO_2 loading result in software errors. Solvent loading occasionally has to be recalculated from the raw sensor output with reference to current plant conditions. In the intervening time between this campaign and the subsequent test campaign, a second sensor is constructed and the existing one is modified to improve stability.

In addition to investigating dynamic scenarios which are representative of real coal plant operation, addtional key research goals for test campaign 2 are identified:

- To obtain real-time, stable measurements of lean and rich solvent amine concentration and CO_2 loading during dynamic operations.
- To obtain knowledge of plant hydrodynamics prior to the start of the test campaign, so the full response of the plant to dynamic scenarios can be obtained and interpreted without ambiguity.
- To investigate the effect of differences in plant construction and circulation times on its response to dynamic operations.

Chapter 6 describes this second test campaign and its outcomes.

References

Akram, M., Ali, U., Best, T., Blakey, S., Finney, K.N. and Pourkashanian, M. (2016). Performance evaluation of PACT Pilot-plant for CO_2 capture from gas turbines with Exhaust Gas Recycle. *International Journal of Greenhouse Gas Control,* 47, 137-150.

Artanto, Y., Jansen, J., Pearson, P., Do, T., Cottrell, A., Meuleman, E. and Feron, P. (2012). Performance of MEA and amine-blends in the CSIRO PCC pilot plant at Loy Yang Power in Australia. *Fuel*, 101, 264-275.

Biliyok, C., Mechleri, E.D. and Thornhill, N.F. (2014). Dynamic Simulation and Control of Post-combustion CO_2 Capture with MEA in a Gas Fired Power Plant. *Computer Aided Chemical Engineering,* 33, 619-624.

Bui, M., Gunawan, I., Verheyen, V., Artanto, Y., Meuleman, E. and Feron, P. (2013). Dynamic modelling and validation of post-combustion CO_2 capture plants in Australian coal-fired power stations. *Energy Procedia,* 37, 2694-2702.

Carey, J., Damen, K., Fitzgerald, F.D. and Gardiner, R.A. (2013). CCPilot 100+ Operating experience and test results. *Energy Procedia*, 37, 6170-6178.

Ceccarelli, N., van Leeuwen, M., van Leeuwen, P., Maas, W., Ramos, A., van der Vaart, R. and Wolf, T. (2014). Flexibility of low-CO_2 gas power plants: Integration of the CO_2 capture unit with CCGT operation. *Energy Procedia,* 63, 1703-1726.

Chalmers, H. and Gibbins, J. (2007). Initial evaluation of the impact of post-combustion capture of carbon dioxide on supercritical pulverised coal power plant part load performance. *Fuel*, 86, 2109-2123.

Chalmers, H., Lucquiaud, M., Gibbins, J. and Leach, M. (2009). Flexible operation of coal fired power plants with postcombustion capture of carbon dioxide. *Journal of Environmental Engineering*, 135, 449-458.

Committee on Climate Change (2013). *4th Carbon Budget Review Part 2,* [.pdf], Available at: https://www.theccc.org.uk/publication/fourth-carbon-budget-review/ [Accessed October 2015].

van Eckeveld, A. C., van der Ham, L. V., Geers, L. F. G., van den Broeke, L. J. P., Boersma, B. J. & Goetheer, E. L. V. (2014). Online monitoring of the solvent and absorbed acid gas concentration in a CO2 capture process using monoethanolamine*. Industrial & Engineering Chemistry Research*, 53, 5515-5523.

Eisfeld, T. and Feldmüller, A. (2013). Fast cycling and Fast Start Capability of Combined Cycle Power Plants with SGT5-4000F Gas Turbines. *IMechE Seminar: Demand Response and Flexible Operation in UK Power Stations,* Nottingham, 28 November 2013.

Faber, R., Köpcke, M., Biede, O., Knudsen, J.N. and Andersen, J. (2011). Open-loop step responses for the MEA post-combustion capture process: Experimental results from the Esbjerg pilot plant, *Energy Procedia*, 4, 1427-1434.

Fitzgerald, F.D., Hume, S.A., McGough, G. and Damen, K. (2014). Ferrybridge CCPilot100+ Operating Experience and Final Test Results. *Energy Procedia*, 63, 6239-6251.
Flø N E., Zangrilli, L., Mangiaracina, A., Mejdell, T., Kvamsdal, H.M. and Hillestad, M. (2014). Validation of a Dynamic Model of the Brindisi Pilot Plant. *Energy Procedia*, 63, 1040-1054.
Flø, N.E.,Knuutila, H., Kvamsdal, H.M. and Hillestad, M (2015). Dynamic model validation of the post-combustion CO_2 absorption process, *International Journal of Greenhouse Gas Control,* 41, 127-141.
van der Ham, L.V., van Eckeveld, A.C. and Goetheer, E.L.V. (2014). Online monitoring of dissolved CO_2 and MEA concentrations: Effect of solvent degradation on predictive accuracy. *Energy Procedia*, 63, 1223-1228.
Hamborg, E.S., Smith, V., Cents, T., Brigman, N., Falk-Pedersen, O., De Cazenove, T., Chhaganlal, M., Feste, J.K., Ullestad, Ø., Ulvatn, H., Gorset, O., Askestad, I., Gram, L.K., Fostås, B.F., Shah, M.I., Maxson, A. and Thimsen, D. (2014). Results from MEA testing at the CO_2 Technology Centre Mongstad. Part II: Verification of baseline results. *Energy Procedia*, 63, 5994-6011.
IPCC (2014). *Climate Change 2014: Fifth Assessment Report of the Intergovernmental Panel on Climate Change*. Cambridge University Press: Cambridge, UK
Jordal, K., Ystad, P. A. M., Anantharaman, R., Chikukwa, A. and Bolland, O. (2012). Design-point and part-load considerations for natural gas combined cycle plants with post combustion capture. International Journal of Greenhouse Gas Control, 11, 271-282.
Kvamsdal, H.M., Chikuwa, A., Hillestad, M., Zakeri, A. and Einbu, A. (2011). A comparison of different parameter correlation models and the validation of an MEA-based absorber model. Energy Procedia, 4, 1526-1533.
Lucquiaud, M., Fernandez, E.S., Chalmers, H., Mac Dowell, M., and Gibbins, J. (2014). Enhanced operating flexibility and optimised off-design operation of coal plants with post-combustion capture. Energy Procedia, 63, 7495-7507.
Mac Dowell, N., Shah, N. (2014). Optimisation of post-combustion CO_2 capture for flexible operation. Energy Procedia, 63, 1525 – 1535.
Mechleri, E. (2015). Controllability analysis of a post-combustion CO_2 capture plant integrated with a coal and natural gas-fired power plan. 3rd Post Combustion Capture Conference, 9th September 2015, Regina, Canada.
Mejdell, T., Vassbotn, T., Juliussen, O., Tobiesen, A., Einbu, A., Knuutila, H., Hoff, K.A., Andersson, V. and Svendsen, H. (2011). Novel full height pilot plant for solvent development and model validation. Energy Procedia, 4, 1753-1760.
Murray, S. (2013). Why whole portfolio modelling is essential. IPA 5th Annual Conference, East Kilbride, 12 March 2013.
Oates D.L.,Versteeg, P., Hittinger, E. and Jaramillo P. (2014) Profitability of CCS with flue gas bypass and solvent storage. International Journal of Greenhouse Gas Control, 27, 279–288
Pöyry, 2009. Impact of Intermittency, How Wind Variability Could Change the Shape of British and Irish Energy Markets. [.pdf] Available at:
www.poyry.co.uk/sites/www.poyry.uk/files/IntermittencyMethodologyv1_0.pdf [Accessed March 2015]
Notz, R., Mangalapally, H.P. and Hasse, H. (2012). Post combustion CO_2 capture by reactive absorption: Pilot plant description and results of systematic studies with MEA. International Journal of Greenhouse Gas Control, 6, 84-112
Rabensteiner, M., Kinger, G., Koller, M., Gronald, G. and Hochenhauer, C. (2014). Pilot plant study of ethylenediamine as a solvent for post combustion carbon dioxide capture and comparison to monoethanolamine. International Journal of Greenhouse Gas Control, 27, 1-14.
Seibert, F., Chen, E., Perry, M., Briggs, S., Montgomery, R., and Rochelle, G. (2011). UT/SRP CO_2 Capture Pilot Plant – Operating Experience and Procedures. Energy Procedia, 4, 1616-1623
Ystad, M.P.A., Bolland, O. and Hillestad, M. (2012). NGCC and hard-coal power plant with CO_2 capture based on absorption. Energy Procedia, 23, 33-44.

6. Pilot-Scale Testing 2 – Dynamic operation of Post-Combustion Capture as applied to coal-fired power stations

6.1 Introduction

Despite the continuing phase-out of coal power generation in Europe it is likely to remain an important source of electricity in Asia, Africa and the Americas through 2040 and beyond (IEA, 2015) Carbon capture and storage (CCS) has the potential to significantly limit the emissions from coal and gas-fired power stations, reducing the cost and mitigating the worst effects of dangerous climate change (IPCC, 2014). Post-combustion capture (PCC) applied to coal-fired power stations is a proven technology for the reduction of CO2 from flue gas, but there are outstanding questions regarding how the process responds to changes in generation plant output.

Coal-fired plants are less likely to provide dispatchable services for rapid response to spikes in electricity demand due to their slower ramp rate than modern NGCCs. However, the plants are capable to do so if needs be, and are increasingly likely to participate in load-following operations or operate in a two-shifting regime. In this regime the plant is shut down at night due to reduced demand and restarted in the morning when the demand is higher. Flexibility in capture plant operation is critical if it is to respond to these dynamic generation events effectively.

Capture plant flexibility also allows coal-fired power stations to maximise the electricity available for transmission while the plant is operating at baseload. Errey et al (2014) demonstrates the value of CO2 capture plants varying their capture efficiency in response to changes in electricity selling price. Mac Dowell (2015) and Flø (2016) use dynamic models to investigate various capture plant operation strategies to capitalise on volatile electricity selling price while maintaining an average CO2 capture efficiency which is close to 90% over 24 hours. The model used by Flø (2016) is validated against flexibility tests done at the Brindisi pilot published previously by Mangiaracina et al. (2014). However, the availability of dynamic plant performance data in open literature in very limited and the lack of public-domain dynamic plant data makes the validation of these strategies problematic (Bui, 2014), especially for dynamic scenarios which are more complex than a step-change in a single plant parameter.

Furthermore, the implementation of these operational strategies requires a robust process control system to achieve optimised performance when manipulating reboiler steam input to capitalise on fluctuating electricity selling price, or responding to a dynamic generation plant event (Mac Dowell, 2015; Flø 2016). The previous chapter, based on Tait et al (2016) suggests that active control of the real-time solvent capacity via manipulation of solvent flow rate and/or reboiler heat input, combined with continuous measurement of lean and rich solvent CO2 loading could be used to control CO2 capture efficiency during dynamic operations.

This chapter details the implementation of dynamic scenarios at pilot plant scale for a coal plant. Coal-fired power stations operating flexibly will most frequently engage in hot startup operations, requiring up to 2 hours to reach baseload generation capacity. The test campaign shares some similarity with the previous chapter but with several key differences. This work focuses on coal generation; the dynamic scenarios are based on operating data from real coal plant and on operating modes which are most relevant to post-combustion capture on coal. The test facility is purpose-built for CO2 capture and the reboiler design is significantly different to that described in Chapter 5, allowing comparisons to be made between how different pilot-plant design and configuration affects the response to dynamic operations. Circulation times between absorber and desorber are significantly reduced for this facility. The deployment of two online solvent sensors allows for continuous measurement of both rich and lean loading to be made.

Seven dynamic operating scenarios are implemented. This includes two different shutdown-startup couplings, frequency response, load-following and two capture bypass events. These scenarios are used to provide insights about plant hydrodynamics and response to dynamic scenarios while passively monitoring changes in solvent loading with the online solvent sensors. The knowledge of plant dynamics gained over the course of the test campaign is used in a final scenario in which online lean solvent loading measurements are used to demonstrate control of CO2 capture efficiency following a steam decoupling event.

6.2 Description of Test Facility

6.2.1 Overview

The UKCCSRC PACT Amine Pilot facility was previously installed at Aberthaw power station by RWE is purpose-built for CO2 capture operations and has been upgraded several times since 2012. The absorber contains 6.50m of 300mm diameter Sulzer Mellapak CC3 packing, while the desorber contains 7m of Intalox IMTP 25 random packing and is 460mm in diameter (fig. 6.1). There are several options for flue gas injection – the facility can be connected to a biomass burner, a gas turbine or a gas mixing skid which can create synthetic flue gas from air/$N_2$and CO_2. For the duration of the test campaign, a mixture of ambient air with approx. 12% CO_2 from the gas mixing skid is used to simulate flue gas from a coal-fired power station. Gas ordinarily flows through an FGD wash column prior to entering the absorber (Akram, 2016), but due to consistent problems with water condensation and buildup in the pipework between the FGD and absorber inlet, the FGD is bypassed for the duration of the test campaign. For all tests, the flue gas entering the absorber is unsaturated and has water content approx. 1% of total volume. This causes the plant to lose water through the absorber gas outlet, resulting in an increase in nominal amine concentration of 2-3% w/w per day. The effect of this on plant reboiler duty is discussed in section 6.3.3.

The water wash at the top of the absorber periodically introduces a batch of water to the plant if significant water losses are detected, indicated by the absorber sump level sensor falling below a certain threshold. There is currently no way to control when this will occur, and the introduction of a slug of pure water into the top of the absorber (see water wash top-up valve, fig. 6.1) during a dynamic operation will have a significant effect on the results. To avoid these additional perturbations during operation, the water wash top-up valve is kept closed for the duration of the test campaign and the plant is topped up with water manually at the beginning of each operating day.

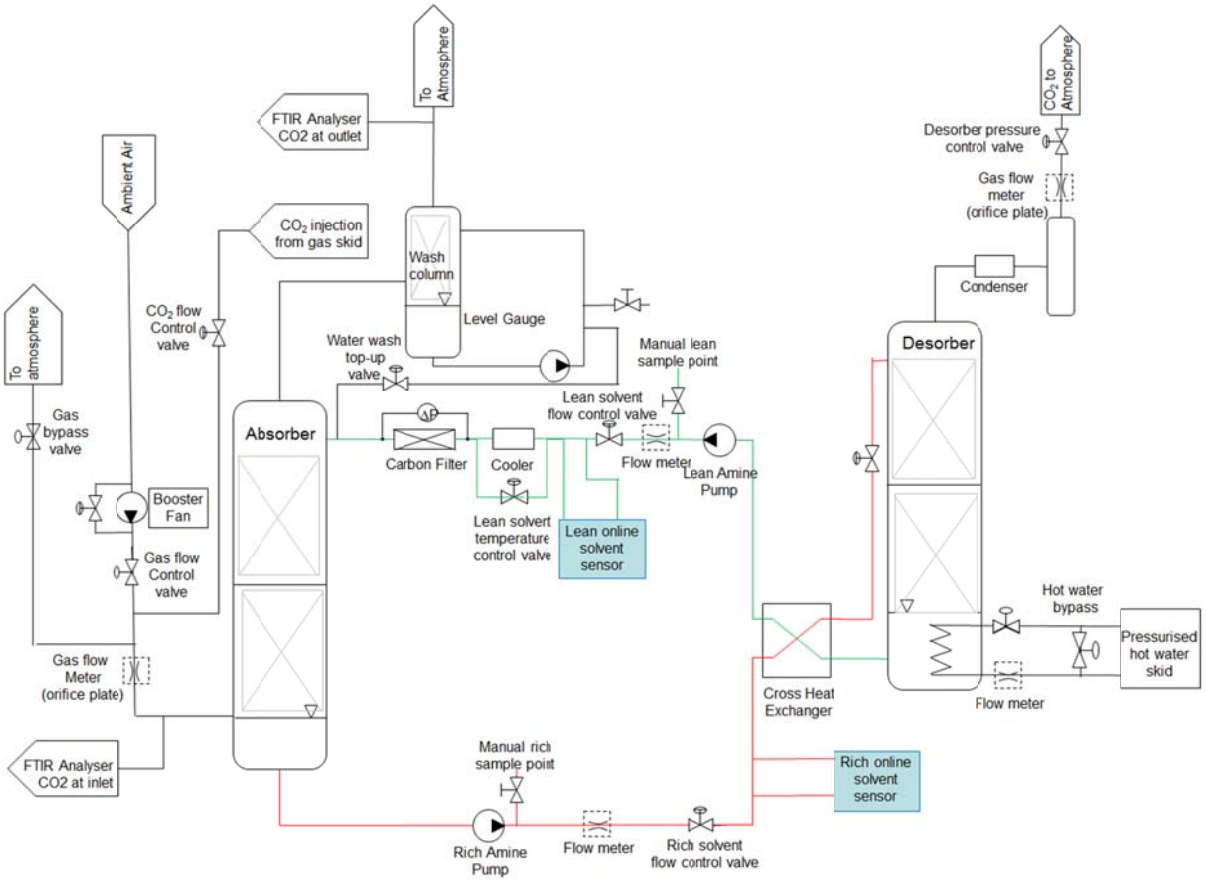

Fig. 6.1. Process flow diagram of amine plant (Akram, 2015)

Instead of using steam to regenerate solvent the plant uses hot water (fig. 6.1). The reboiler consists of a large overspill tank containing a heating element, through which pressurised water at approx. 124°C is pumped. At the end of the reboiler tank furthest from the desorber, solvent spills over a baffle to feed the lean solvent pump, which is protected by a sensor which will trip if the liquid level in this section falls below a given threshold (fig. 6.2). This shuts down the plant. The total solvent inventory of the plant is approx. 600l, the majority of which resides in the reboiler during operation. The absorbing solvent used for the duration of the test campaign is 30% MEA, though the nominal amine concentration varies between 28% and 35% for the reasons mentioned previously.

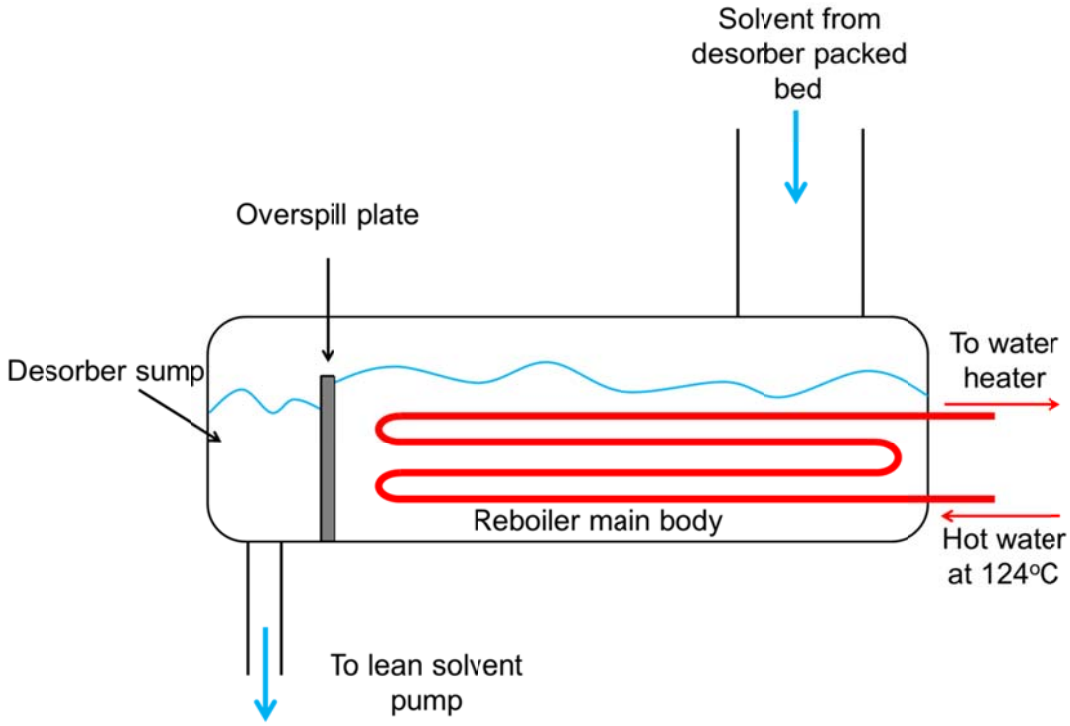

Fig. 6.2. Reboiler design at UKCCSRC PACT

6.2.2 Plant Modifications and Control

Prior to the commencement of the test campaign a thorough evaluation of the plant control system and its suitability for dynamic operation was carried out by researchers at the universities of Edinburgh and Sheffield. The following modifications were recommended by the author of this thesis, and implemented jointly with Dr Kris Milkowski, the business director and occasional plant operator at PACT.

Plant variable	Original control system	Current control system	Hardware modifications
Gas flow rate	Siemens PLC	Siemens PLC/Labview	Addition of flue gas bypass, allows flow control via Labview over a limited range
CO_2 injection flow rate	Siemens PLC	Siemens PLC	Second FTIR machine installed at absorber inlet
Hot water flow rate	Siemens PLC	Labview	Bypass valve added, allows full control via Labview
Solvent flow rate	Siemens PLC	Siemens PLC	None
Desorber pressure	Siemens PLC	Siemens PLC	None

Table 6.1. Plant control modifications

6.2.2.1 Gas flow and CO_2 injection rate

The gas flow is comprised of ambient air which is enriched with CO_2 to the required concentration via injection. Gas flow rate was originally controlled using a valve located downstream of the booster fan (see fig. 6.1). However, CO_2 injection takes place downstream of this location, so any modification of the gas flowrate means the CO_2 flowrate, which is controlled from a different location, would also need to be changed & checked via an inlet FT-IR spectroscopy analyser. To simplify the process of changing gas flowrate during dynamic operations a bypass with control valve connected to Labview was installed downstream of the CO_2 injection port. Hypothetically, the bypass should be the preferential path for the gas, allowing the flow rate to be controlled via Labview with CO_2 concentration remaining constant. The FT-IR at the inlet could then be used to determine the concentration of CO_2 in the desorber gas outlet stream and hence, close the CO_2 mass balance.

The bypass did not work as planned. The absorber inlet remained the preferential path for flue gas and even with the bypass valve fully open, only a 40% reduction in flow was achieved. For all scenarios which require a reduction in flue gas flow below 60% of baseload, the original control method using the PLC system was used, with a second operator monitoring the CO_2 concentration at the inlet via FT-IR and adjusting the injection rate if necessary. As the two available FT-IR systems are required at the absorber inlet and outlet for the determination of CO_2 capture rate, it is not possible to determine the CO_2 mass flow at the desorber outlet.

6.2.2.2 Solvent flow

Solvent flow rate is controlled via rich and lean solvent control valves located after their respective pumps, using the PLC system. The valves can be controlled via a flow rate setpoint or opened and closed manually. There is a considerable risk of plant shutdown due to solvent levels in the absorber sump falling below the low level limit switch during flow rate changes.. As fine control and ramping are not possible without considerable effort only large step-changes in solvent flow are possible.

6.2.2.3 Pressurised hot water flow

A bypass valve allows the flow of pressurised hot water to the reboiler to be adjusted using a PID controller in Labview. The hot water pump has an operating range of 0-10m^3/hr and while the flowmeter is unable to detect any flow below approx. 3.0m^3/hr, below this value the PID controller can be switched off allowing the valve position to be adjusted manually.

6.2.2.4 Desorber pressure

Desorber pressure setpoint is adjusted via a PID controller in the PLC system, by opening or closing the valve at the top of the desorber. For all scenarios in this work, the desorber pressure setpoint was 0.4 bar_g. Desorber pressure fluctuates between around 0.37-0.47 bar_g (gauge) even at baseload flow conditions. This could be improved by re-tuning the PID controller for the desorber pressure control valve.

6.2.2.5 Data Logging

Lean and rich solvent flow rates and absorber inlet temperature are logged on via the PLC system, absorber inlet and outlet CO_2 concentrations are logged on their respective FTIR machines, and all other plant parameters including gas flow, hot water flow, desorber pressure and all other temperatures are logged in Labview.

6.2.2.6 Cross heat exchanger

At baseload conditions the cross-heat exchanger provides a temperature increase of approx. +47^oC to the rich solvent entering the desorber and a decrease of approx. -47^oC to the lean solvent entering the absorber.

This is sufficient to bring the lean solvent down from 99^oC to around 52^oC, so further cooling is required to reduce the temperature to 40^oC at the absorber inlet.Solvent enters the desorber at approx. 98^oC.

Absorber inlet temperature is maintained at 40^oC using a PID-controlled cooler and bypass valve which is connected to the PLC system. There is very little variation in temperature once the temperature of lean solvent coming from the cross-heat exchanger is greater than 40^oC.

6.2.3 Comparison of test facilities – Key design differences

The major difference between the PACT and Sulzer pilot facilities is in the design of the reboiler. The Sulzer test facility uses steam to regenerate solvent and the volume of the reboiler and desorber sump combined is small in comparison to the total solvent inventory. The majority of the solvent inventory during operation exists in the pipework and solvent tank between the desorber sump outlet and the absorber inlet. Any changes made to the flow of steam to the reboiler are not observed at the absorber inlet for an estimated 15-25min (ref. section 5.4.5, Frequency Response scenario). Since the majority of the solvent inventory is contained in pipework or tanks which do not promote rapid solvent mixing, the plant may require up to 3 full circulations of its entire solvent inventory (around 120min) before the capture rate stabilises following a dynamic event (ref. section 5.4.2, gas turbine startup scenario).

In contrast to this, around 400l of the 600l total solvent inventory of the PACT pilot plant is contained in the large container which contains the heating element used for solvent regeneration (fig. 6.2). Thus the majority of the solvent inventory is contained within a single vessel which is continually being agitated by downcoming solvent from the bottom of the packed bed and the heating action of the coil. Solvent mixing tests using conductivity measurements were carried out before the beginning of the test campaign to determine how the PACT pilot plant may react to perturbations. The results and implications for dynamic operation are discussed in section 6.3.1.

The second key design difference is that the PACT plant has a cross-heat exchanger so there is no need to simulate the effect using additional heating at the desorber inlet. However, it may be undersized as the dT provided is around 20^{o}C less than would be ideal at the selected baseload solvent flow rate. This contributes to the relatively high reboiler duty in MJ/tCO_2 captured. (see section 6.3.2).

6.3 Methodology and Preparation

6.3.1 Solvent Mixing Experiments

Solvent circulation times and mixing effects have been shown to affect plant response to dynamic operations (Tait et al, 2016), so prior knowledge of plant hydrodynamics is required to fully account for changes in capture rate, absorber temperature profile, lean loading and rich loading over the course of each dynamic scenario.

Four conductivity probes were installed at the absorber inlet and outlet and the desorber inlet and outlet. Ideally the conductivity probes would have been installed as close to the absorber/desorber inlet and outlet as possible, but due to difficulties installing the conductivity probes at height the desorber outlet/absorber inlet and the absorber outlet/desorber inlet pairs are installed very close to each other in the solvent line. For this reason it is not possible to determine the circulation between the lean solvent pump > absorber inlet or rich solvent pump > desorber inlet, but valuable information about solvent mixing and total circulation time was still obtained. Modelling of solvent mixing in sumps is a complex fluid-dynamic problem. The

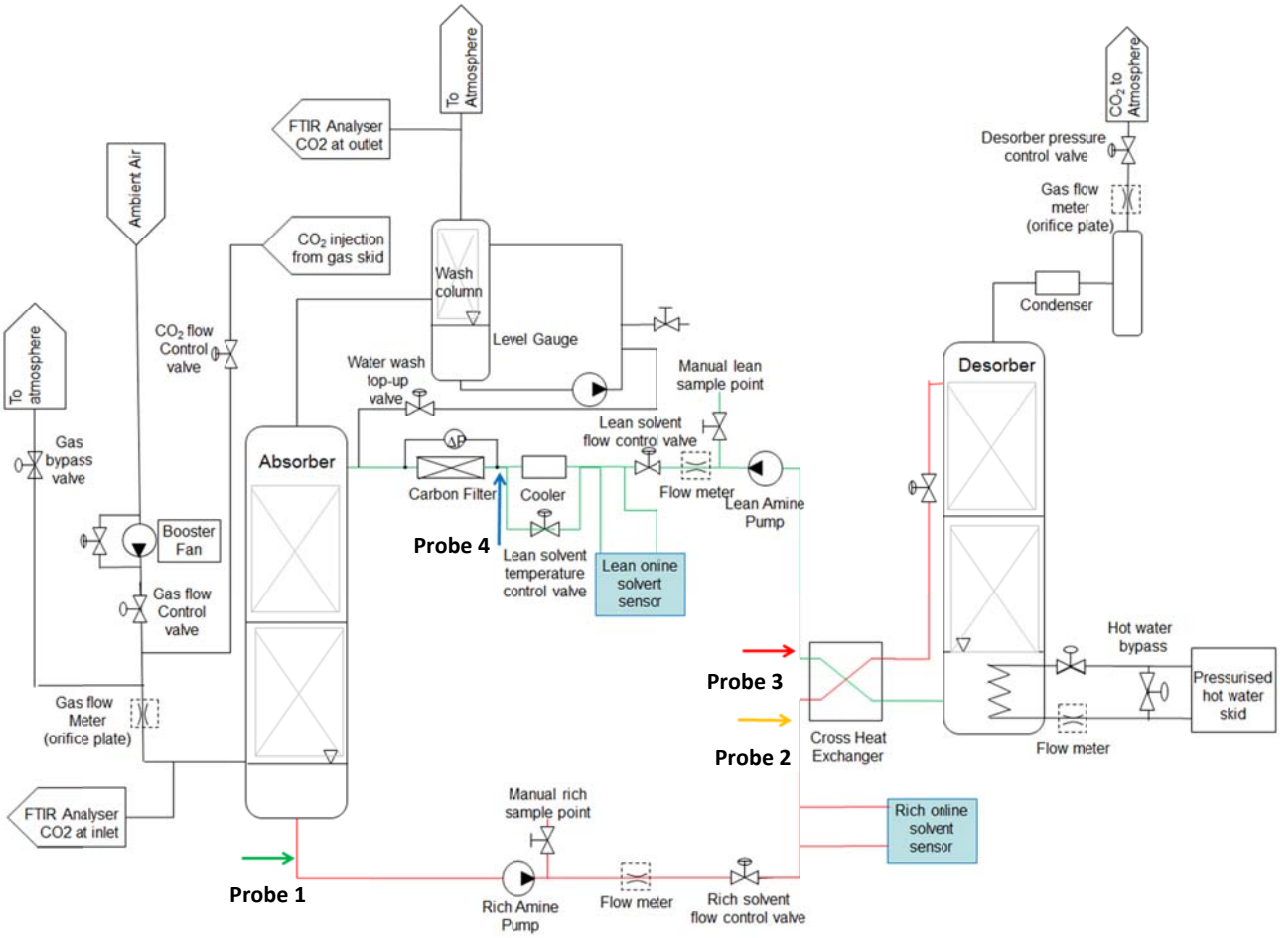

Fig. 6.3 Plant PFD with conductivity probe locations

A batch of amine solvent (between 30-40%wt MEA, approx. 400l) is isolated in the desorber sump. Deionised water (approx. 70l) is added to the absorber sump. The solvent pumps are started at t=0. As pure water mixes with amine solvent, the conductivity decreases. By observing the conductivity at each of these points it is possible to estimate the circulation time between them and the duration required for the solvent inventory to become fully mixed.

Tests were carried out at the initially proposed baseload flowrate (1200l of solvent/hr), but a flow rate of only 1000l/hr was necessary to achieve >90% capture (see section 6.3.2).

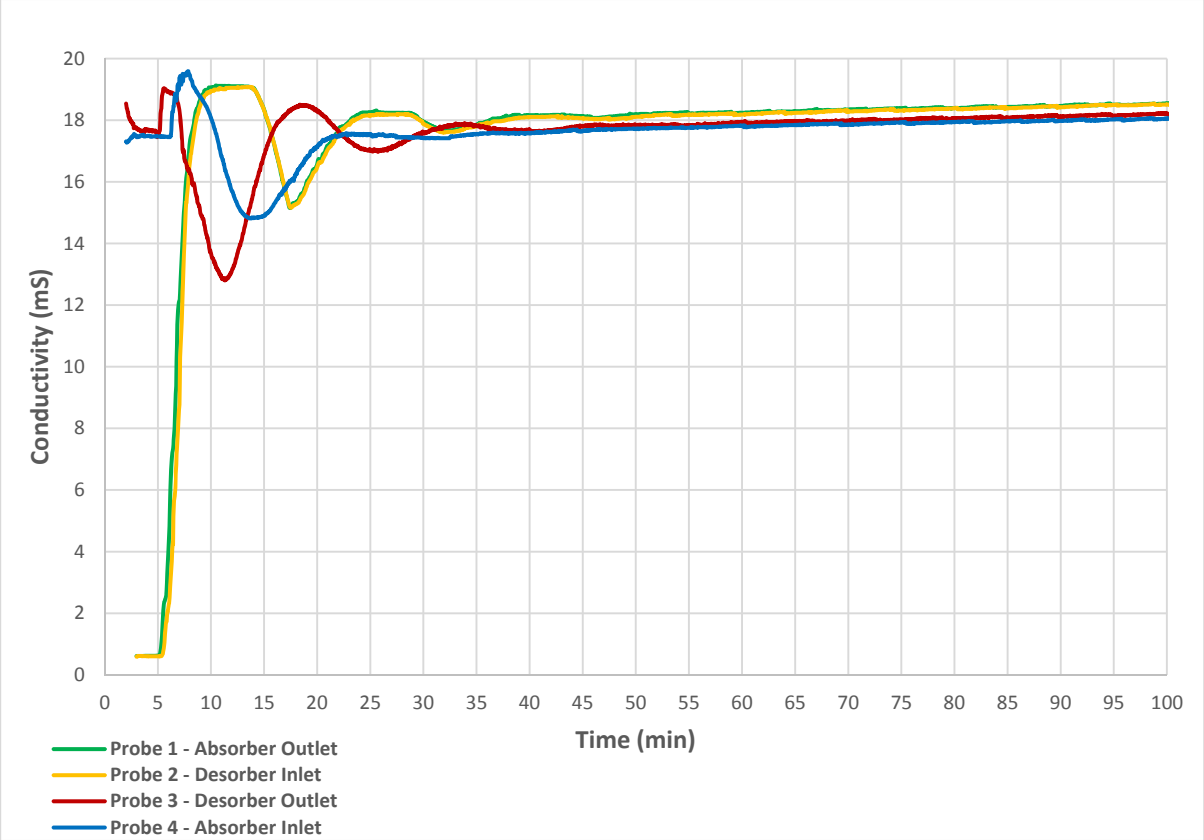

Fig. 6.4. Liquid circulation experiments

Due to their close proximity in the liquid line, probes 1 and 2 (absorber outlet/desorber inlet pair) follow each other closely. There is a noticeable difference between probes 3 and 4 (desorber outlet/absorber inlet pair) which may indicate a small amount of solvent mixing taking place within the line, or may be due to the lean solvent pump starting up and stabilising more slowly than the rich.

Conductivity at the absorber outlet (probe 1) begins to increase at t=5min. This indicates that the time required for a batch of solvent to circulate from the desorber outlet (probe 3) to the absorber sump and begin to mix with the sump's existing solvent inventory is 5min. Conductivity at the desorber outlet (probe 3) begins to decrease at t=5min 30sec, indicating that the time required for a batch of solvent to circulate from the absorber outlet (probe 1) to the reboiler and begin mixing with the solvent inventory is 5min 30sec. The entire solvent inventory requires 37-38min to become fully mixed, which is 7min more than the estimated time of 30 min required for a batch of solvent to fully circulate the plant at this flow condition, based on vessel volumes and total solvent inventory. The implications for dynamic operations are:

1. During operation, the solvent spends approx. 2/3 of the time residing in the reboiler or absorber sump. This allows ample time for the solvent to become well mixed. Therefore it is not anticipated that large additional fluctuations in solvent loading or capture rate will be observed following a return to baseload flow conditions, as observed in the previous test campaign at Sulzer Chemtech (see section 5.4.4, capture bypass scenario).
2. The solvent becomes fully mixed within approx. 1.25 circulations of the entire solvent inventory. This reduces the amount of time required for the plant to return to steady state conditions following a dynamic event.
3. The circulation time between desorber outlet and absorber inlet is less than 5min. Any changes in solvent loading at the desorber outlet due to step-changes in reboiler heat input should induce a CO_2 capture rate response within 5min.

As this test was carried out at a solvent flowrate of 1200l/hr and the eventual baseload condition has a flow rate of 1000l/hr, a reasonable approximation is to multiply the circulation times obtained in this test by 1.2 to obtain

circulation times at 1000l/hr. Repeating the experiment at the correct baseload flowrate was not possible due to time constraints.

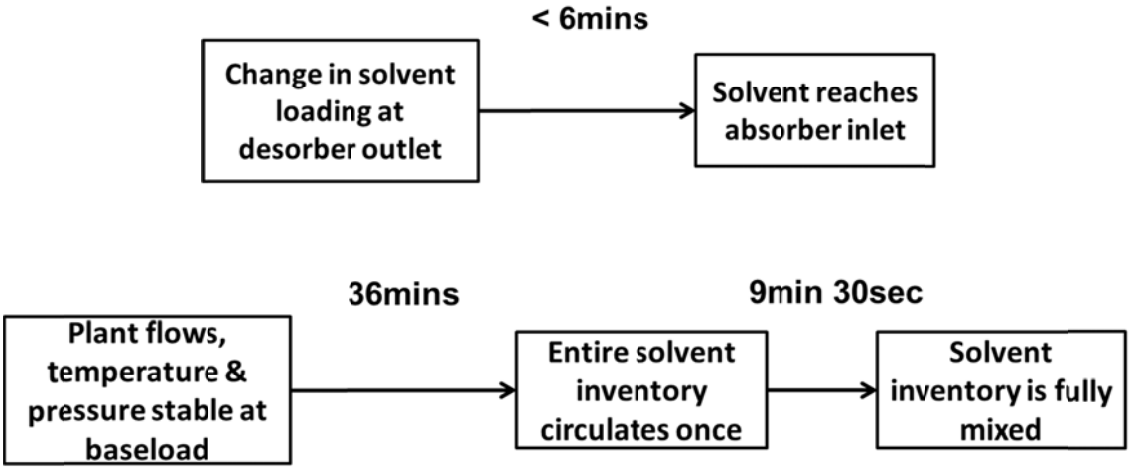

Fig. 6.5. Important solvent circulation times for dynamic operation, scaled to 1000m^3/hr

These circulation tests provide a reasonable estimate of solvent circulation times, and are useful in the planning of experiments and analysis of plant response early in the test campaign. However, as demonstrated in section 5 it is possible to use online solvent sensors, plant temperatures and capture rate to build on this initial analysis and construct a much clearer picture of plant response.

6.3.2 Baseload Operating Conditions

Due to changes in ambient conditions, general flow variability and varying nominal MEA concentration due to water losses these baseload conditions should be regarded as approximate.

Controlled Variable	**Value**
Gas Flowrate at absorber inlet (Nm^3/h)	200
Gas inlet temperature (^{o}C)	42
Inlet gas CO_2 concentration (% v/v)	12
Pressurised hot water flow rate (m^3/hr)	10
Solvent flowrate (l/h)	1000
Pressurised hot water inlet temperature (^{o}C)	124
Pressurised hot water outlet temperature (^{o}C)	118.5
Liquid inlet temperature, Absorber (^{o}C)	40
Liquid inlet temperature, Desorber (^{o}C)	98
Measured Parameter	
CO_2 capture rate (%)	91.5-95
Reboiler duty (GJ/tCO_2)	6.2-6.8
L/G ratio (l/m^3)	5.0
Nominal amine concentration (% w/w)	28-34
Lean Solvent Loading (mol amine/mol CO_2)	0.36-0.40
Rich Solvent Loading (mol amine/mol CO_2)	0.13-0.17

Table 6.2. Baseload Operating Conditions

The baseload liquid-to-gas flow ratio (L/G) is established as 5 l/m^3. The minimum solvent flow rate achievable without risking damage to solvent pumps is 400l/hr so a flow rate of 1000l/hr allows solvent flow to be reduced to 50% of its baseload value (500l/hr) while affording the operators a reasonable margin for error. The gas flow is operating close to its maximum for this plant at 200m^3/hr.

It is worth noting that the baseload operating conditions reported here correspond to a necessary reference point, which allow for large changes in amplitude of key operating variables, such as solvent flowrate, gas flow rate,

etc. It does not necessarily correspond to the optimised conditions for minimising reboiler duty. This is one reason explaining why the reboiler duty is higher than reported for other comparable facilities.

The other reason is due to the small size of the cross-flow heat exchanger. In most CO_2 capture facilities the approach temperature for the cross-heat exchanger is approx. 10°C. For this pilot facility the process fluid (rich solvent) exits the heat exchanger at approx. 98°C while the working fluid (lean solvent) enters the heat exchanger at approx. 118°C, for an approach temperature of 20°C. A lower desorber inlet temperature requires more energy input from the reboiler as sensible heat to bring the incoming solvent up to stripping temperature. The additional contribution to the reboiler duty due to the undersized heat exchanger (ΔQ_{reb}) can be calculated as follows.

$$\Delta Q_{reb} = \frac{m_{rich} Cp_{rich} \Delta T_a}{m_{CO2}} \quad (6.1)$$

Where m_{rich} is the mass flow rate of rich solvent in kg/s, Cp_{rich} is the specific heat capacity of the rich solvent in J/kg.K, ΔT_a is the difference in approach temperature between this facility and one with an optimised heat exchanger in K and m_{CO2} is the CO_2 capture efficiency in kg/s. With ΔT_a = 10K the additional contribution to the reboiler duty ranges between 1.033GJ/tCO_2 and 1.084GJ/tCO_2, accounting for changes in capture efficiency and nominal MEA concentration.

Due to water losses through the absorber and desorber gas outlets the nominal MEA concentration of the solvent increases over time. An automatic, batch-wise water topup system exists, but to avoid additional perturbations during dynamic testing it is not used over the duration of the test campaign. Instead, water levels are topped up in a single large batch at the start of each test day if MEA concentration becomes too high.

This variation in amine concentration appears to reduce the reboiler duty as the solvent becomes more concentrated in amine (see fig. 6). Increased amine concentration may also have the effect of lowering the lean and rich solvent CO2 loading and increasing the capture efficiency. Although the volumetric flow of solvent remains constant, the molar flow rate of lean amine into the absorber increases thus decreasing the lean solvent CO2 loading. Additionally, the baseload plant conditions are such that the solvent never reaches a saturated rich CO2 loading (around 0.5 mol MEA/mol CO_2), therefore a reduction in lean solvent CO2 loading entering the absorber can also correspond to a reduction of rich solvent CO2 loading leaving the absorber. The mass ratio of CO_2 in reaction products to H_2O in the rich solvent is increased, reducing the energy lost into the water as sensible or latent heat per mole of CO_2 liberated. Finally, leaner solvent entering the absorber results in a larger driving force for CO_2 absorption and therefore a higher capture efficiency.

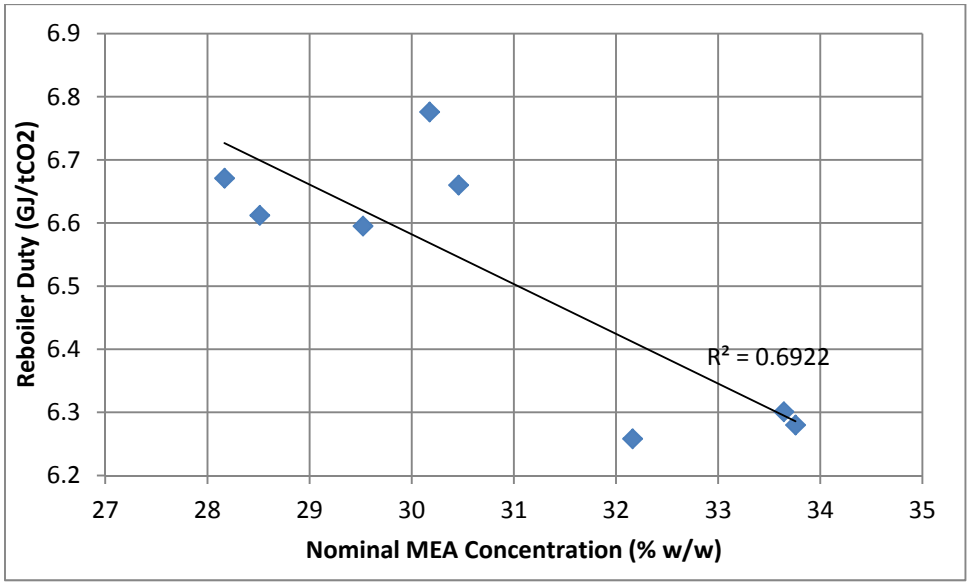

Fig. 6.6 Reboiler Duty Variance with amine concentration

Figure 6 shows how the reboiler duty appears to decrease with nominal amine concentration at steady-state, baseload flow conditions. To minimise uncertainty due to short-term variations in temperature, capture efficiency and flow, the reboiler duties are calculated using the average hot water inlet/outlet temperature, CO_2

capture efficiency and hot water flow rate over a 20 minute period. The nominal amine concentration is the average of four measurements (2x lean, 2x rich) taken at the beginning and end of this 20 minute period.
Previous studies describe a poor water balance initially having an initially negative effect on the CO_2 capture rate, reaching a minimum at an MEA mass fraction of around 0.62 before increasing as more water is lost (Lawal, 2010). In this pilot-scale study water this negative effect was not observed, only an increase in CO_2 capture rate from around 92% to 95% on a mass basis over an approx. 16hr period of operation. This may be due to differences in plant configuration and rate of water loss, or because this "minimum" capture rate period coincides with dynamic operations.

Test Facility	L/G Ratio (l/m^3)	Reboiler Duty (GJ/tCO_2)	CO_2 conc. In flue gas (%)	Packing Height (m)	Reference
CSIRO Pilot, Loy Yang	2.3 – 4.2	3.4 – 6.3	10-11	9.4 x 2 (two absorbers in series)	Artanto et al. (2012)
CO_2SEPPL Pilot, Dürnrohr	2.2-4.6	3.6-4.5	12	12.0	Fraubaum (2013)
CASTOR Pilot Plant, Esbjerg	3.6-3.9	2.2-4.0	12	18.0	Knudsen et al. (2007)
UKCCSRC PACT Pilot, Beighton	5	6.2-6.8	12	6.5	Akram et al. (2016)

Table 6.3 Comparison of reboiler duty and L/G with other pilot facilities using 30% MEA with coal-equivalent flue gas

6.3.3 Titration measurements and uncertainty

Lean and rich solvent samples were taken at regular intervals during dynamic testing and analysed for MEA and CO_2 content using a Mettler Toledo T90 auto-titrator. Samples were titrated against 0.2M HCl to determine total amine concentration, then 0.5M NaOH to determine CO_2 concentration.
To determine the the uncertainty of titration measurements a solution of 29.40%wt MEA (nominal) and 8.04%wt CO_2 equivalent was made up gravimetrically by bubbling CO_2 through MEA solution in a dreschel flask. The loaded solution was titrated for MEA and CO_2 content in triplicate. The uncertainty in bench CO_2 loading measurements was found to be +/- 3.15% relative.

MEA concentration (% wt)	CO2-Equivalent (%wt)	MEA concentration (% wt nominal)	CO2 loading
27.068	7.876	29.38	0.403
26.942	7.936	29.26	0.409
27.307	7.751	29.60	0.395

Table 6.4 Titration measurements for determination of uncertainty

6.3.4 Online solvent sensors

Two online solvent composition sensors are located in the lean and rich solvent lines (see fig. 6.1). In-situ measurements of solvent physical properties are used to determine amine concentration and CO_2 loading in real-time. The sensor used at Sulzer Chemtech was modified to comply with site safety regulations and to allow it to be operated remotely. It was deployed along with a second device which has the same design. A detailed account of sensor development is provided by Buschle (2015). Continuous rich solvent measurements are provided for 8 of 9 dynamic scenarios and continuous lean solvent measurements for 7 of 9.

6.3.5 Selection of dynamic scenarios

Dynamic operations were selected to be representative of scenarios which may be encountered during the operation of a supercritical coal power unit fitted with post-combustion CCS. This section provides a brief overview.

6.3.5.1 Generation plant shutdown

This scenario is designed to be a realistic representation of how a post-combustion capture plant would respond to generation plant shutdown, with flue gas and regeneration "steam" (in this case pressurised hot water) ramp rates based on real operating procedures for supercritical coal units with stated power outputs of 500 MW or greater (NETL, 2014). In this scenario and all others, flue gas flow is approximated as being proportional to generation plant output. Flue gas flow is ramped down until it reaches 30% of baseload, which is defined as minimum stable generation (MSG). Below MSG the flue gas contains too many impurities due to incomplete combustion (DECC and Parsons Brinckerhoff, 2014), so to avoid polluting the solvent the gas flow is reduced to zero at this time. Hot water (i.e. "steam") is fed to the reboiler for as long as possible so the solvent is lean in preparation for startup. Once gas flow reaches zero, solvent flow is reduced to 50% of baseload and for practical reasons is allowed to circulate until rich and lean loading have converged, simulating a scenario in which solvent flow is left running overnight to make use of the plant site's cooling water. A similar shutdown procedure is described in Ceccarelli et al. (2014) as applied to PCC on NGCC plant – in this case it is applied to coal. The comparative benefits of continuing to circulate solvent overnight as opposed to immediate shutdown as soon as the flue gas flow has stopped are discussed in section 6.5.3.3.1. The shutdown method has a direct impact on capture plant response on the next startup. Two plant startup methods were investigated, both of which were preceded by this method of shutdown.

6.3.5.1.1 Generation plant startup 1

Ramp rates for plant startup were taken from PACE (2014), with minimum stable generation once again defined as 30% of baseload. Two startup scenarios are simulated, both preceded by the shutdown method described in 3.5.1 and intended to simulate a "hot start" of a coal plant, in which the plant is shut down in response to falling demand (DECC and Parsons Brinckerhoff, 2014). The first startup scenario simulates a situation in which the low-pressure steam turbine is allowed to reach full load before any steam is introduced to the reboiler. This results in an extended period during which the CO_2 capture rate is low and the plant requires several hours to reach the desired capture rate.

6.3.5.1.2 Generation plant startup 2

In the second startup scenario steam (i.e. hot water) is introduced to the reboiler as soon as it becomes available, resulting in a smaller drop in capture rate and the plant reaching steady state more rapidly. This kind of operating mode may be useful in cases where there are restrictive laws on large, short-term spikes in CO_2 emissions from point sources.

6.3.5.2 Frequency response via pressurised hot water flow reduction

A coal power station which is equipped with post-combustion capture can provide additional flexibility in output via manipulation of the steam flow to the reboiler (Lucquiaud, 2009; Haines, 2014). In this scenario the flow of hot water to the reboiler is reduced to 50% of baseload as the other 50% is redirected to the LP steam turbine. In a real power plant equipped with PCC this would result in a rapid, but marginal increase in plant output which would allow the coal plant to be used in grid balancing operations such as frequency response. After the hot water flow has been at 50% of baseload for 2 hours it is ramped back up to baseload.

6.3.5.3 Capture bypass via pressurised hot water flow decoupling

This scenario simulates the plant operator taking actions at the capture plant level in order to maximise electricity power output and capitalise on high electricity selling price. Two capture bypass scenarios are implemented – Bypass scenario 1 maintains both solvent and gas flow rates at baseload while reducing the hot water flow rate to zero. Bypass scenario 2 maintains gas flow rate at baseload, but reduces the solvent flow to 50% of baseload while reducing the hot water flow rate to zero. This is to reduce the power consumption of the pumps, and to reduce the power consumption of the flue gas booster fan via minimisation of absorber pressure drop. The period of this event lasts 2 hours.

6.3.5.4 Capture plant ramping

This scenario simulates the operation of a load-following plant, which is identified as one of the five typical modes of operation for coal-fired power stations in the UK as of 2012 (Mac Dowell and Shah, 2015). The generation plant ramps down its output from 100% of baseload to 70% for a period of 2 hours, then ramps back up. Hot water flow and solvent flow are matched as closely as possible to the gas flowrate to maintain the baseload L/G flow ratio, and to maintain consistency with the conclusion of Mac Dowell and Shah (2015) that less steam is available for solvent regeneration during these events.

6.3.5.5 Capture rate control using online solvent measurements

Future advanced control systems for both coal and gas CCS plants are likely to require real-time measurements of solvent composition to anticipate changes in capture rate and respond in a manner which is optimised in terms of environmental, economic and operational boundaries (Luu, 2015). For example, there could be a situation in which the operator wishes to maximise revenue by providing an ancillary service such as fast reserve balancing by reducing the level of steam abstraction to the reboiler, but at the same time wishes to minimise CO_2 emissions charges for the duration. Optimised capture plant operation in such a scenario is not possible without discrete knowledge of capture plant dynamics (process gain, dead time, time constants), so a simplified version is implemented.

This scenario envisions a situation in which the operator has to drive the CO2 capture rate to 30% via a steam decoupling event and immediately return to the baseload capture rate of 90% or higher. With flue gas and solvent flow kept constant at baseload, the hot water flow to the reboiler is shut down. The lean solvent sensor is used in combination with knowledge of plant hydrodynamics and response times to predict when the flow of hot water must be turned back on to achieve a minimum capture rate of 30%.

6.4 Discussion of dynamic operating scenarios

In this section, plant trends from the dynamic scenarios are discussed in detail. Rich and lean titration measurements are based on solvent samples taken from the absorber outlet and desorber outlet, respectively. At baseload conditions the circulation time from lean solvent sampling port to absorber inlet and rich solvent sampling port to desorber inlet is approximately 3 minutes. The circulation time between the lean solvent sensor and the absorber inlet is also around 3 minutes at baseload flow conditions. These short circulation times make relating changes in solvent concentration to changes in CO_2 capture rate simple, so there is no need to time-shift the titration points as in test campaign 1 (Chapter 5). Full datasets for each scenario are available in the UKCCSRC's data archive under the heading: "Towards more flexible power generation with CCS: pilot plant test campaigns for best practice guidelines for post-combustion capture". In some scenarios, regular downward "spikes" in CO_2 capture rate are observed. This is a result of gas being periodically purged from the FTIR analyser which measures absorber inlet gas composition.

6.4.1 Shutdown/Startup coupling 1

6.4.1.1 Shutdown

Plant shutdown is initiated at t=0min. Gas flow is ramped down at a rate of 5% of baseload (10 m^3/hr) per minute until it reaches 30% (60m^3/hr), then reduced to zero. At t=9min, the flow of pressurised hot water to the reboiler is ramped down at a rate of around 10% of baseload (1m^3/hr) per minute until it reaches zero at t=19min. The hot water flowmeter is unable to detect any flow below approx. 3m^3/hr, which accounts for the apparent immediate reduction of hot water flow to zero once it reaches 30% of baseload at t=16min, however considering the flow of hot water was controlled by the position of a proportional control valve, it is assumed the hot water flow continued on a similar trajectory between t=16 mins and t=19 mins. Once the flow of gas has been reduced to zero, solvent flow is reduced to 50% of baseload (500kg/hr) and allowed to continue circulating until the reboiler has cooled to under 80^oC and lean & rich loadings have converged. This simulates a scenario in which the plant operator has allowed the solvent inventory to continue circulating so that the plant is cool for the subsequent startup event.

The CO_2 capture rate increases slightly over the course of the shutdown operation until the flow of gas is switched off (see fig. 7b). This is expected, since the gas flow is decreasing while the liquid flow remains constant, resulting in a gradually increasing L/G ratio. This also results in a decrease in rich solvent CO_2 loading

which, due to effective solvent mixing within the plant, rapidly converges with lean loading and eventually stabilises at around 0.18mol CO_2/mol amine as seen in figure 7b. The volume of rich solvent contained in the absorber sump is around 70l while the desorber contains around 400l of lean solvent, so the loading of the fully mixed solvent inventory is closer to that of the lean. Continuous lean solvent measurement was not available during this scenario.

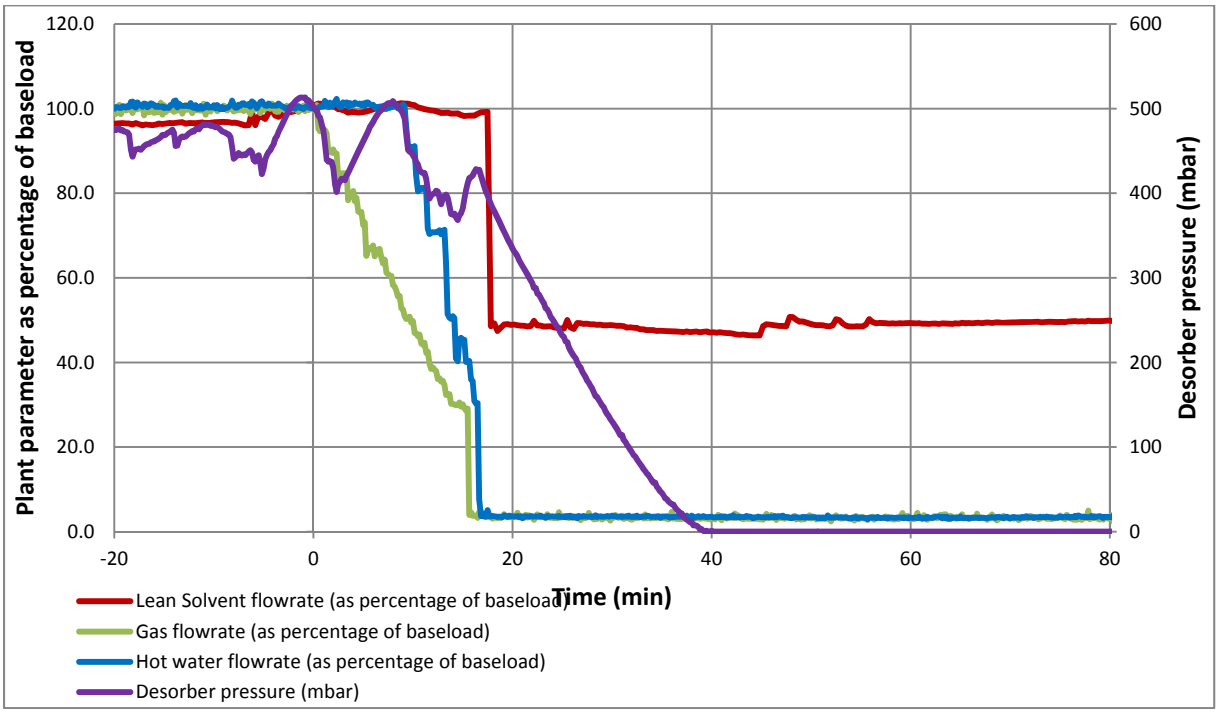

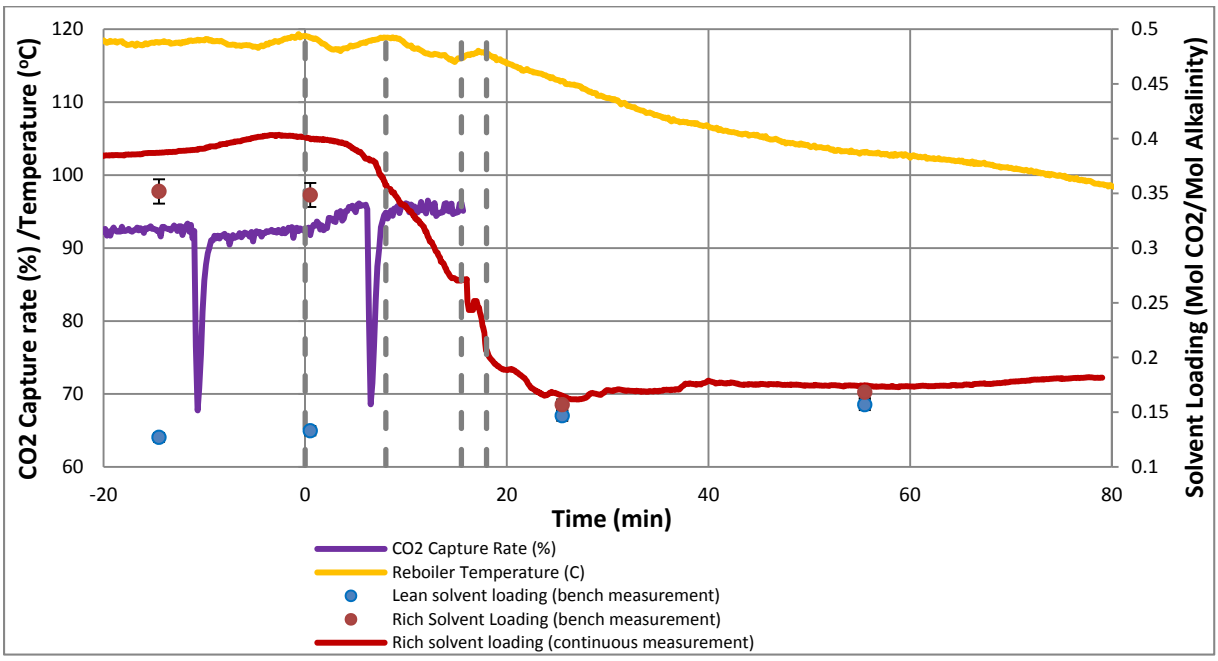

Fig. 6.7a. Gas, solvent hot water flow rate and desorber pressure as percentage of baseload operation, shutdown scenario 1

Fig. 6.7b. Rich and lean solvent loading, reboiler temperature and CO_2 capture rate, shutdown scenario 1

The absorber temperature bulge decreases in magnitude and moves towards the base of the packed bed over the course of the shutdown operation as seen in figure 6.8. This is to be expected because the molar flow rate of CO_2 absorbed is decreasing due to the decrease in gas flow rate, and a proportionally larger amount of CO_2 is

being absorbed close to the gas inlet. Hot solvent residing in the upper regions of the packed bed will also flow down the packing as time progresses, increasing the temperature closer to the base.

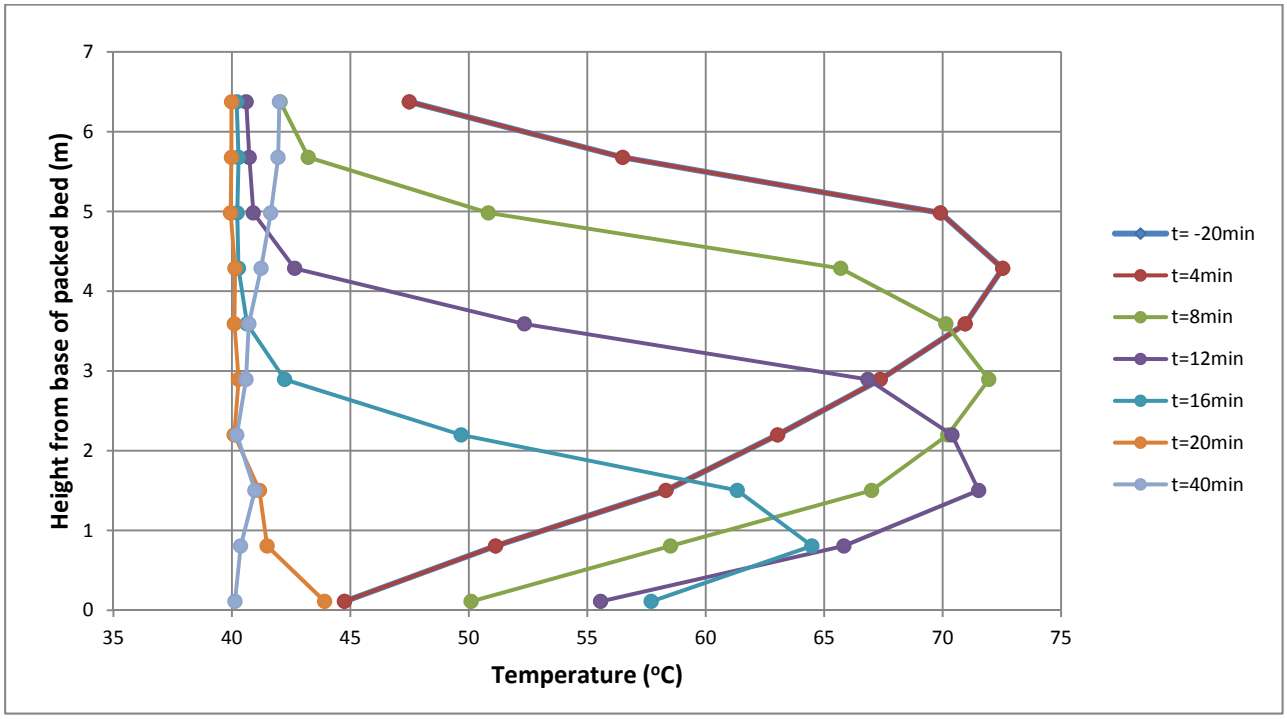

Fig. 6.8 Absorber temperature profile during plant shutdown scenario #1

6.4.1.2 Startup – standard procedure

This plant startup scenario intends to simulate a situation in which the low-pressure steam turbine achieves full power output before the introduction of steam to the reboiler. In anticipation of plant startup, the flow of solvent is stabilised at 50% of baseload. Titration measurements show that the lean and rich loadings remain at approximately 0.18 mol CO_2/mol amine from the previous shutdown event. The

Gas is introduced to the absorber at t=0min (fig. 6.9a), when the hypothetical generation plant reaches minimum stable generation (30% of its stated power generation capacity). The startup procedure is based on real pulverised coal plant data (NETL, 2014). Once the flow of gas is stabilised at 50% of baseload (100m^3/hr) at t=20min, the solvent flow is increased to 100% of baseload (1000 l/hr) in anticipation of the next gas flow ramp, which is initiated at t=28min. Pressurised hot water is ramped at a rate of approx. 0.4m^3/hr per minute from t=29min to t=54min. As mentioned previously, the hot water flow meter does not detect flow below around 30% of baseload (3m^3/hr), but the hot water flow rate increase is assumed to have the same rate throughout the ramp. Hot water and gas flowrates both reach 100% of baseload at t=54min.

CO_2 capture rate is initially higher than desired as seen in figure 6.9b due to the plant's large reserve of lean solvent but drops off rapidly at t=35min. At this time, lean solvent CO_2 loading at the absorber inlet becomes high enough to diminish the driving force for CO_2 absorption, reducing the capture rate. Solvent lean loading reaches a maximum at t=69min, while capture rate reaches a minimum at t=72min. If it is assumed that mixing effects in the pipework between the desorber sump outlet and absorber inlet are negligible, solvent which is analysed by the lean solvent sensor at t=x min will reach the absorber inlet at t=x+3 min.

Due to an error with the data-logging programme at t =200min, certain datasets after this time is unavailable. There is also a large spike in the rich solvent CO_2 loading online measurement at t=260-280min, but since the measured value exceeds 0.5mol/mol and a similar spike in titration measurements is not observed, this may be attributed to sensor instability.

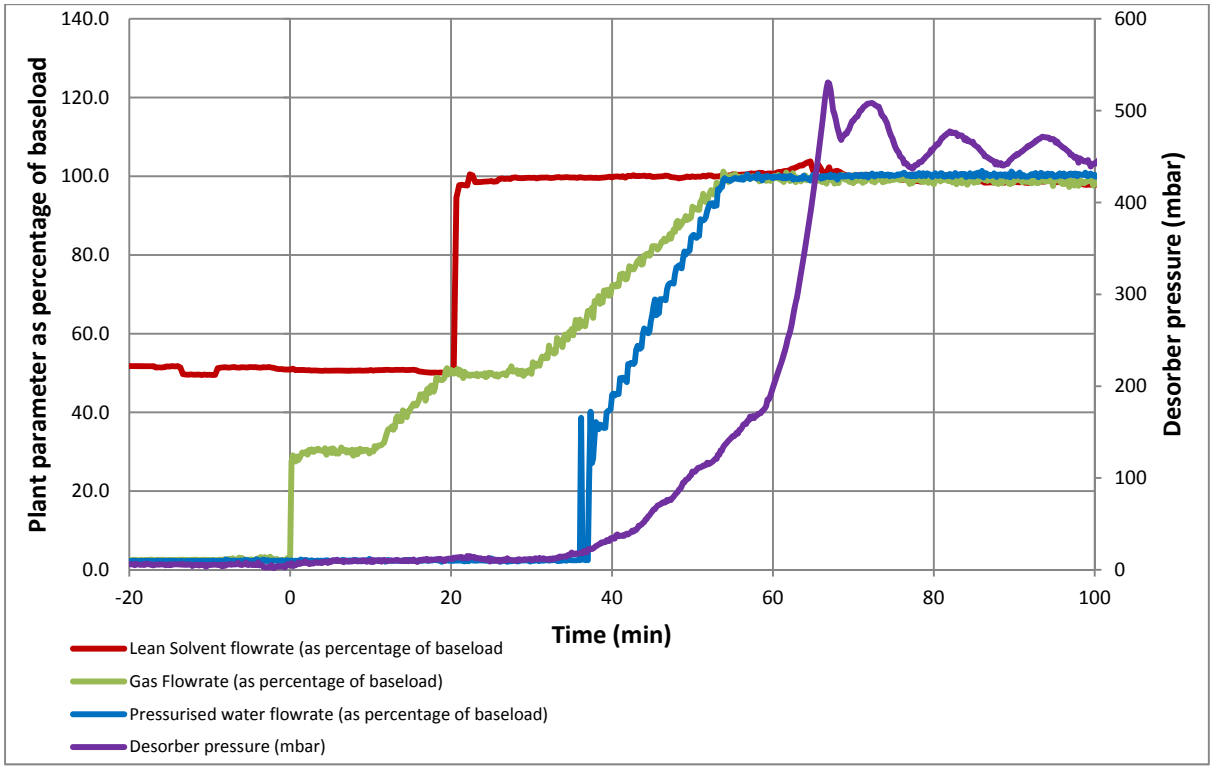

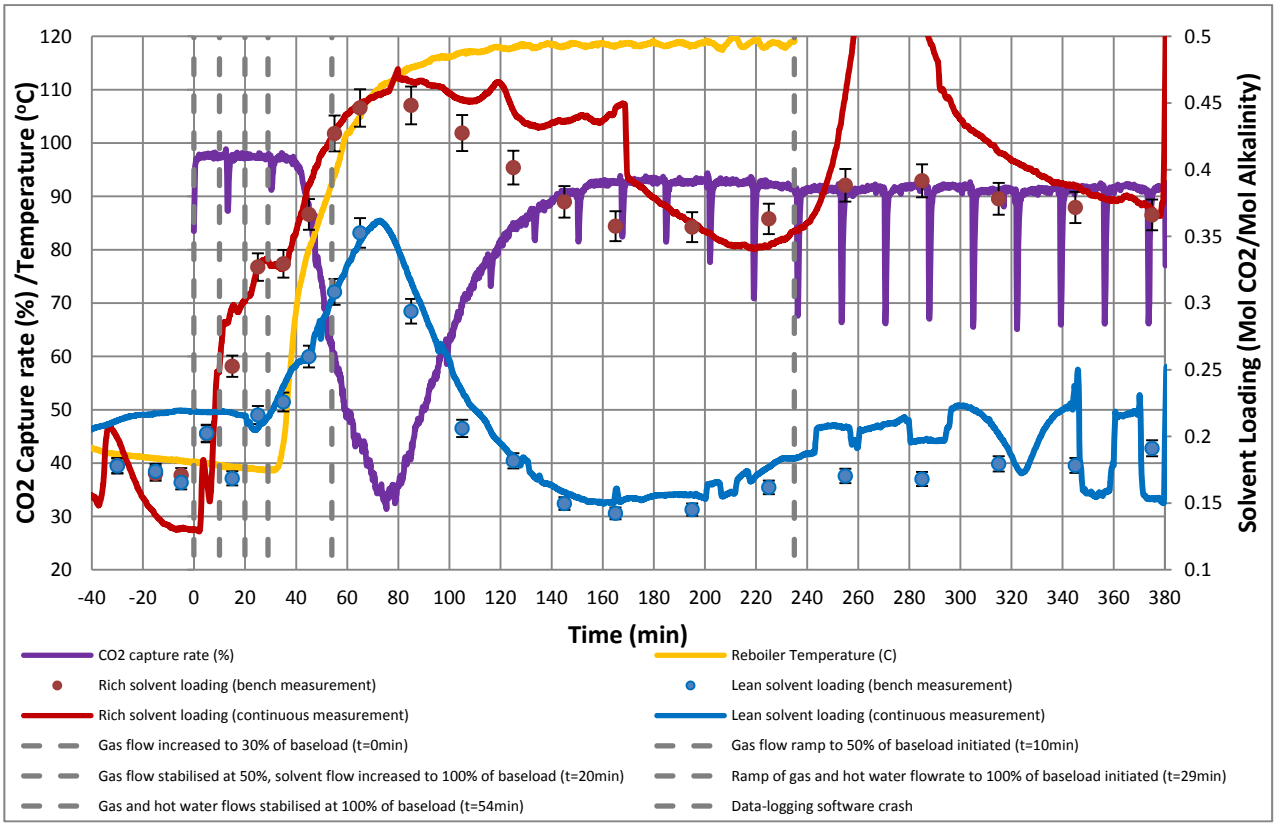

Fig. 6.9a Gas, solvent hot water flow rate and desorber pressure as percentage of baseload operation, startup scenario 1

Fig. 6.9b Rich and lean solvent loading, reboiler temperature and CO_2 capture rate, startup scenario 1

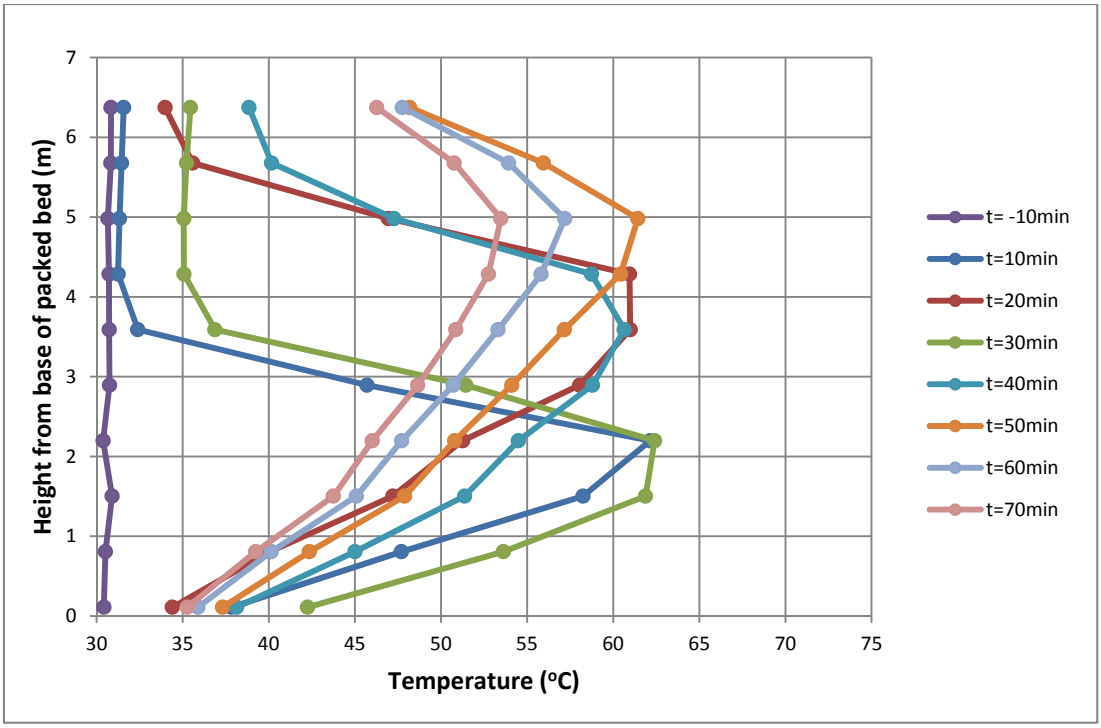

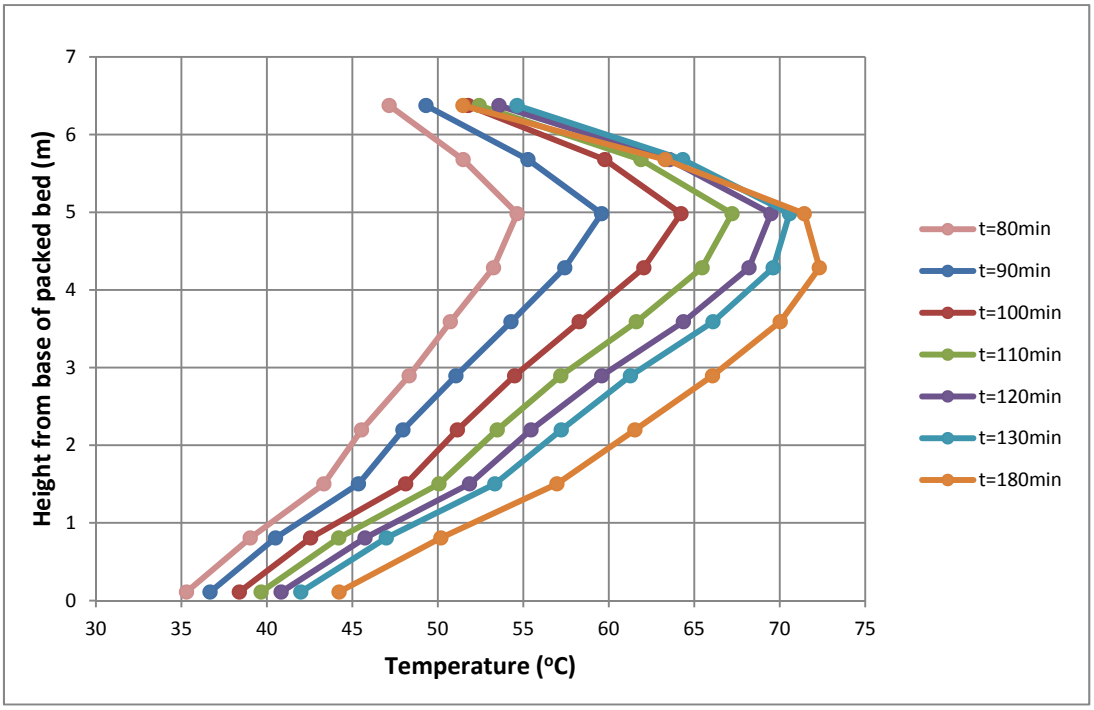

Fig. 6.10a Absorber temperature profile, startup scenario 1, t= -10min to t=70min
Fig. 6.10b Absorber temperature profile, startup scenario 1, t= 80min to t=180min

The absorber temperature bulge increases in magnitude and rises up the packed bed as the gas flow rate increase, until t=20min. Just after t=20min there is a step-change in solvent flow rate from 500l/hr to 1000l/hr. This rapid increase in L/G ratio results in a larger proportion of the CO_2 being absorbed close to the gas inlet, so the temperature bulge migrates to a lower location in the packed bed. As the flow of gas continues to increase, the L/G ratio decreases and the temperature bulge moves further up the packed bed. After t=50min it begins to decrease in magnitude as the lean loading at the absorber inlet increases and the capture rate falls. Between t=70min and t=80min the capture rate begins to rise again, as does the magnitude of the temperature bulge until it is fully established at t=180min.

6.4.2 Shutdown/Startup coupling 2

6.4.2.1 Shutdown

This shutdown scenario was carried out similarly to shutdown scenario #1. Lean and rich solvent sensors were experiencing stability issues prior to the initiation of this scenario, so manual solvent samples were taken at more regular intervals so that the effect of the shutdown operation on solvent loading could still be observed. A marginal increase is again observed in CO_2 capture rate before the flow of gas is shut down, and rich & lean solvent loadings rapidly converge and stabilise at around 0.18 mol CO_2/mol amine. Plant trends are similar to the previous shutdown operation (see 4.1.1) with no significant differences.

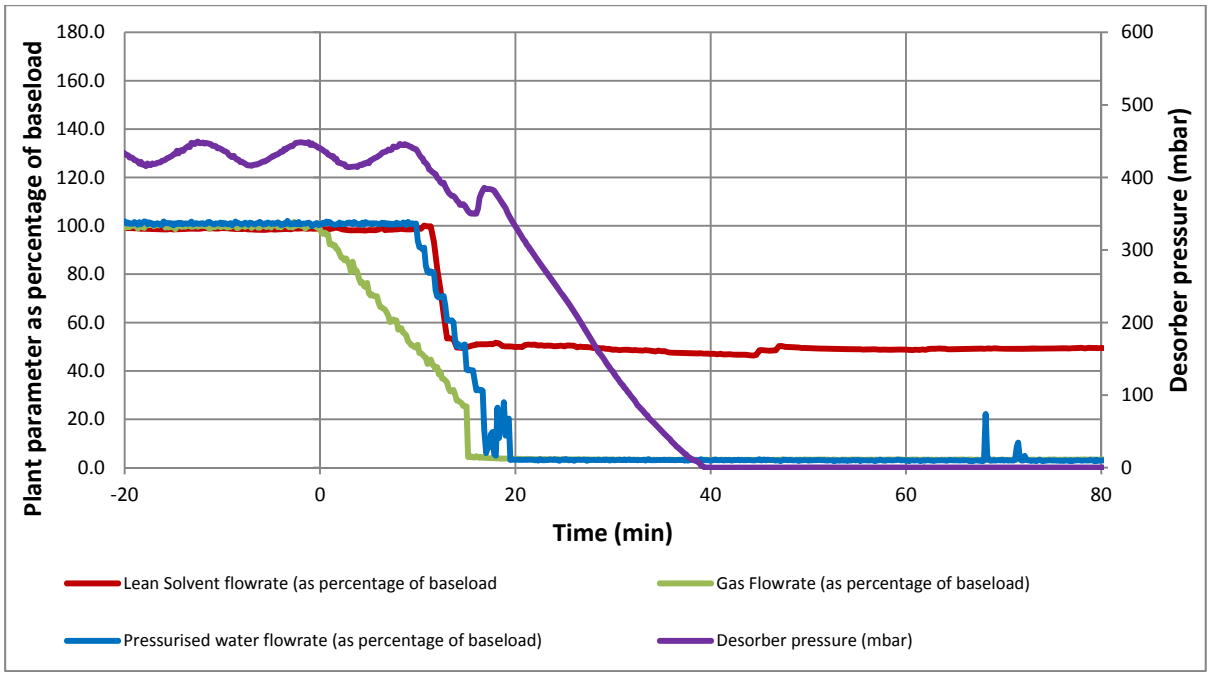

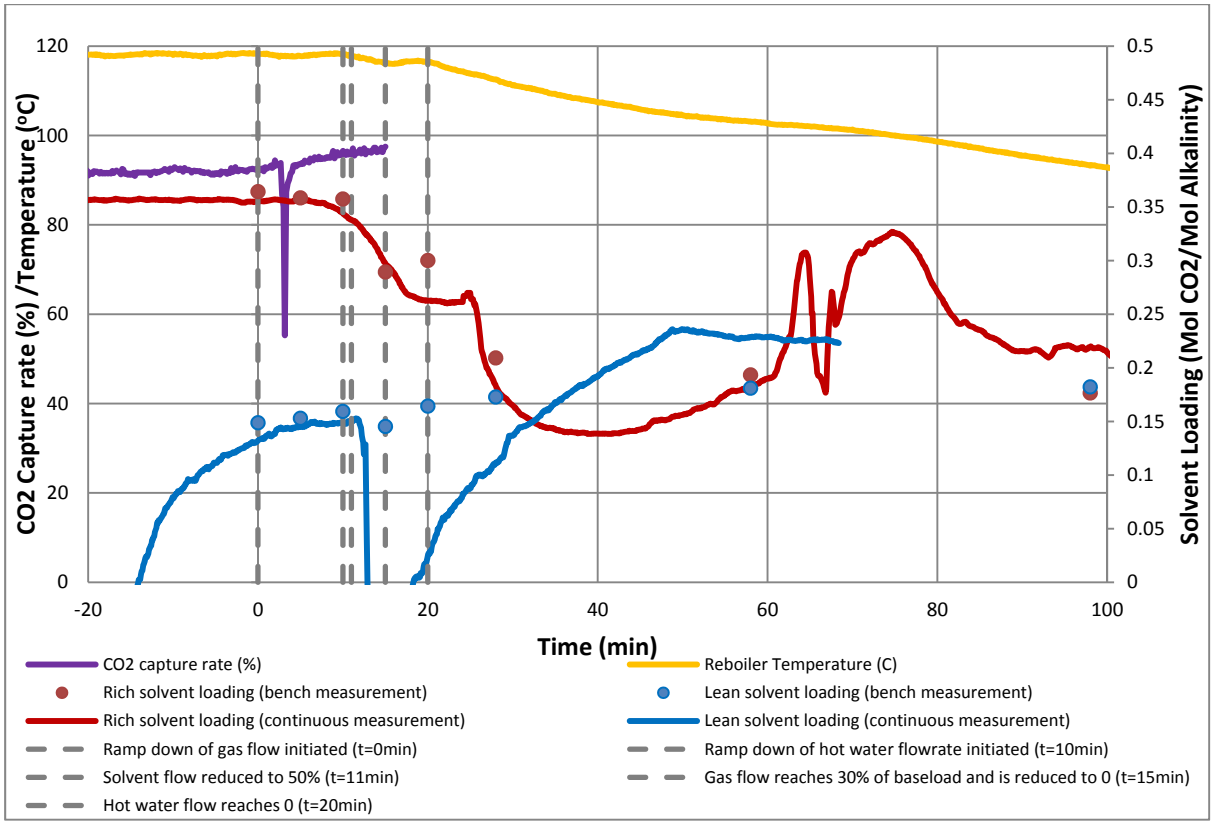

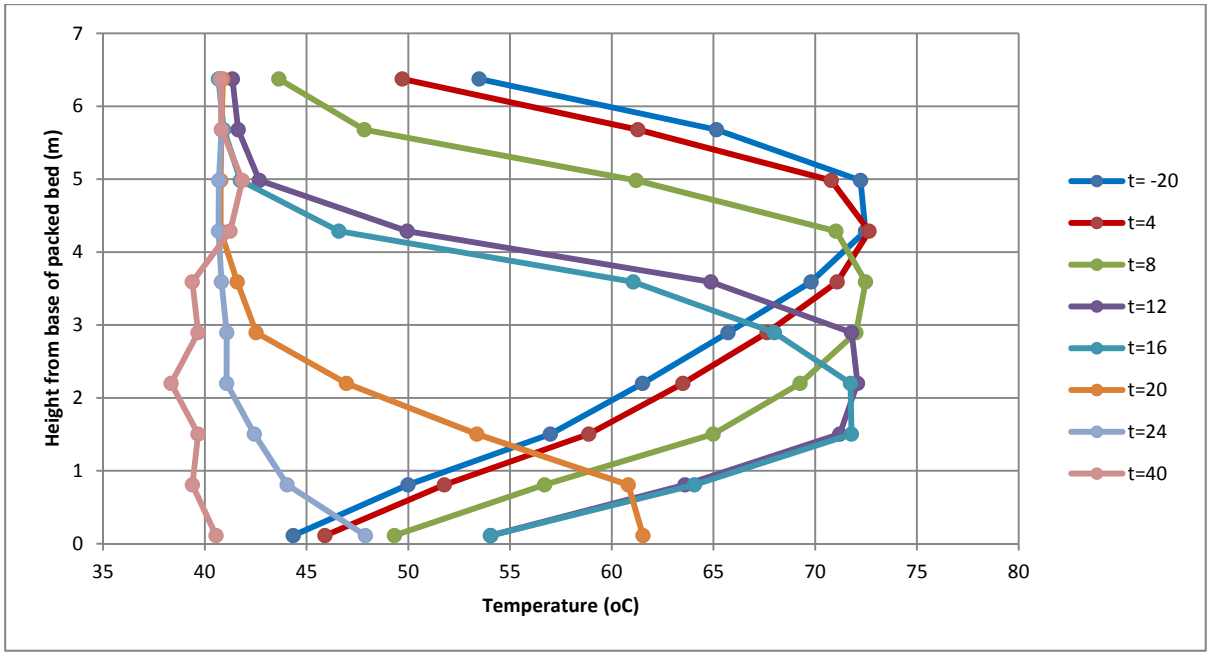

Fig. 6.11a. Gas, solvent hot water flow rate and desorber pressure as percentage of baseload operation, shutown scenario 2

Fig. 6.11b. Rich and lean solvent loading, reboiler temperature and CO_2 capture rate, shutdown scenario 2

Fig. 6.11c Absorber temperature profile, startup scenario 2, t= -20min to t=40min

6.4.2.2 Startup – with prioritisation of CO_2 emissions minimisation

In the subsequent startup operation, steam is introduced to the reboiler as soon as it becomes available instead of after 35 minutes as was the case in the previous shutdown/startup coupling. This may be useful in situations where the plant operator may be subject to significant emissions penalties in the case of large spikes in CO_2 emissions from a point source. Pressurised hot water is ramped up to 30% of baseload ($3m^3$/hr) at t=0 and is subsequently ramped up at 1.75% of baseload ($0.175m^3$/hr) per minute until it reaches $10m^3$/hr. All other flow rates remain similar to startup scenario #1.

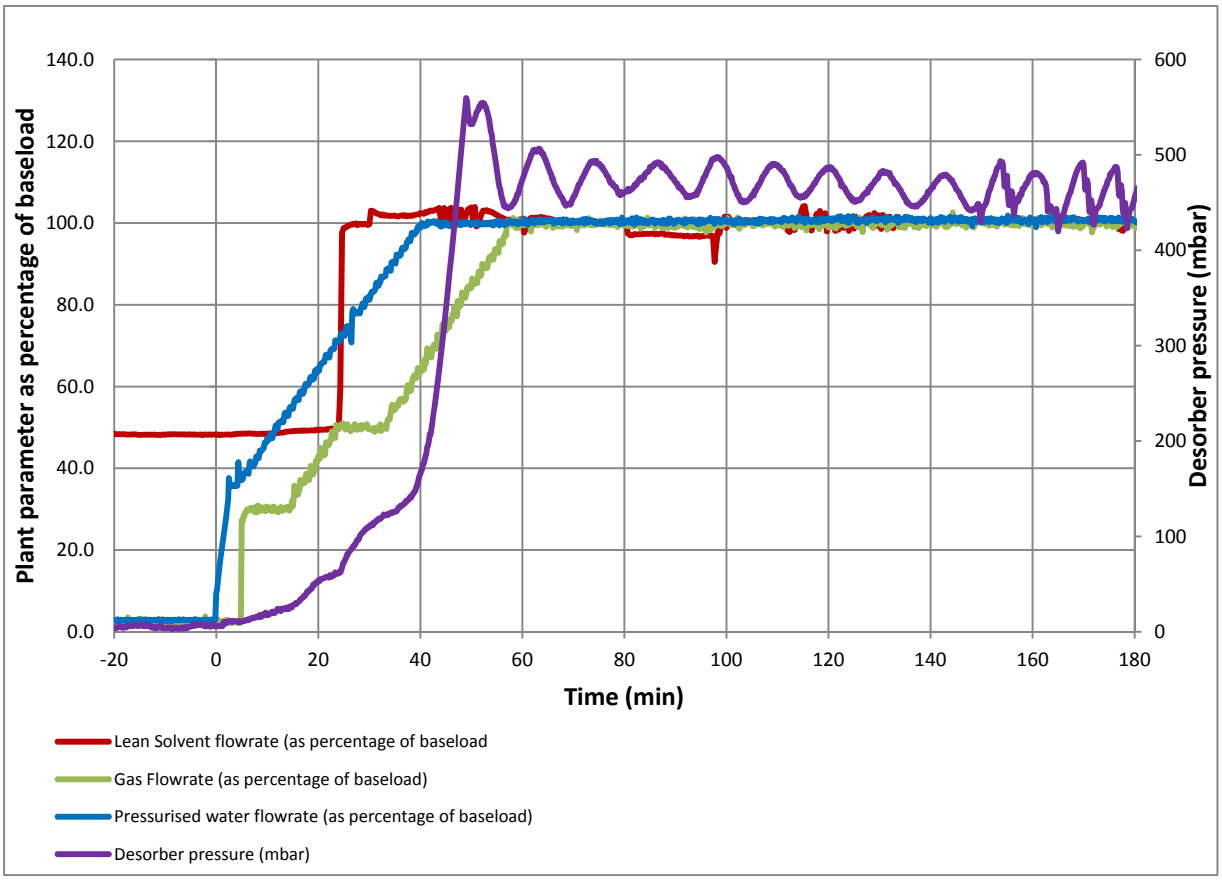

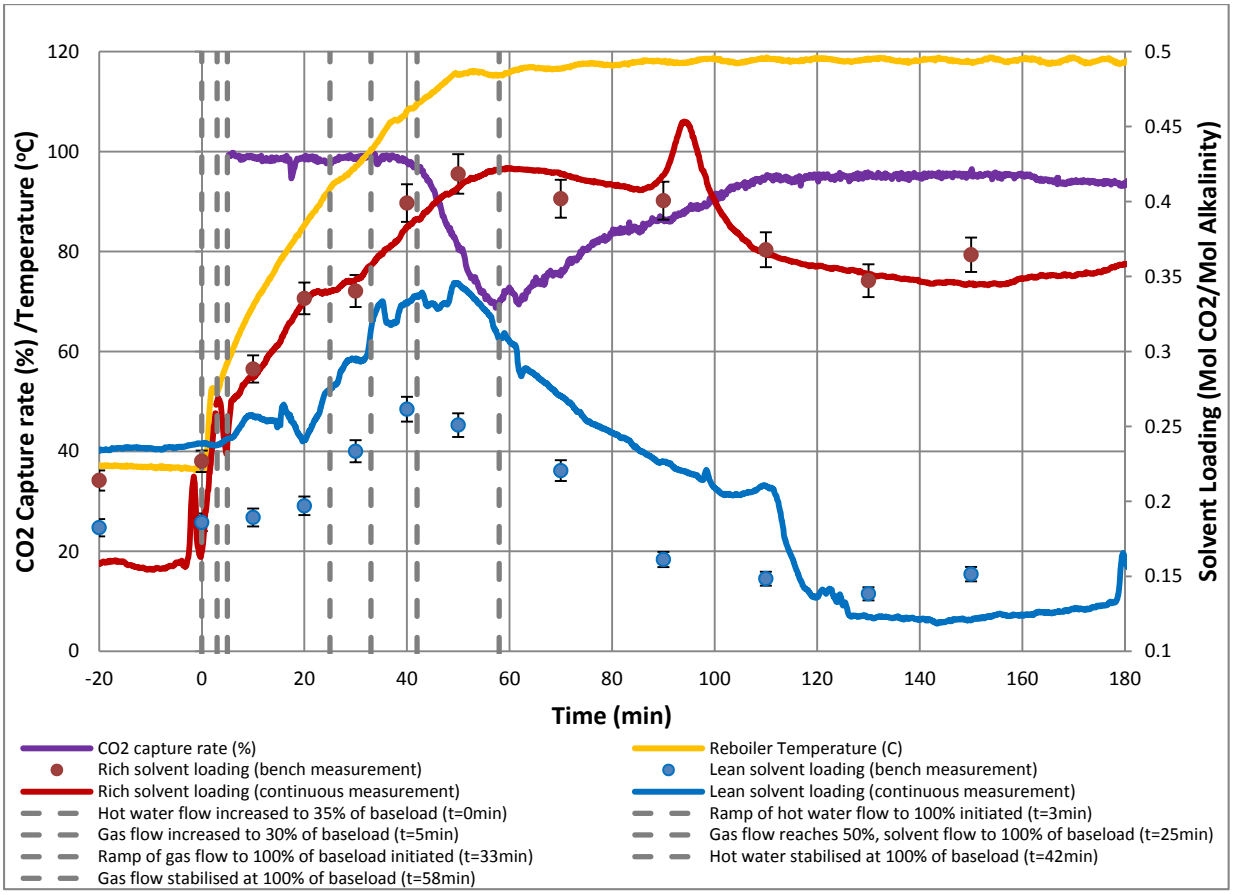

Fig. 6.12a. Gas, solvent hot water flow rate and desorber pressure as percentage of baseload operation, startup scenario 2

Fig. 6.12b. Rich and lean solvent loading, reboiler temperature and CO_2 capture rate, startup scenario 2

The reboiler reaches operational temperature much more rapidly than in scenario 6.4.1.2, so the drop-off in CO_2 capture efficiency is less sharp and reaches a minimum of approx. 70% (fig. 6.12b) instead of 33%. If a similar approach were to be attempted during real plant startup operation, it could proceed by synchronising the turbine shaft while abstracting the maximum possible flow of steam from the IP/LP crossover, allowing the remainder to flow through the LP turbine to remove the resultant frictional heat. It may also be possible to extract additional steam from the HP turbine outlet during start-up, if maintaining a capture efficiency as close to 90% as possible were critical.

For comparison with the startup scenario described in 6.4.1.2 the total CO_2 emissions over the first 160mins of gas being introduced to the absorber are calculated. This length of time is selected as it is the duration required for the plant in scenario 6.4.1.2 to stabilise at baseload operating conditions (fig. 9b).

$$mCO_2 = \int_{0min}^{160min} \left(\frac{Q_{gas,t}}{60} \cdot \varphi_{CO2,t} \cdot \rho_{CO2,t}\right)\left(1 - \frac{\eta_{CO2,t}}{100}\right) \qquad (6.2)$$

mCO_2 is the total mass of CO_2 emitted, Q_{gas} is the volumetric flow rate of gas in m^3/hr, φ_{CO2} is the volume fraction of CO_2 in the gas phase, ρ_{CO2} is the density of CO_2 at the gas inlet temperature and η_{CO2} is the percentage CO_2 capture efficiency. mCO_2 for startup scenario 4.1.2 is 25.1kg. mCO_2. For startup scenario 4.2.2 is 10.3kg, a saving of 14.8kg CO_2 over the same time period.

To determine the potential effect on total daily CO_2 emissions this result is considered in the context of a coal-fired power station, equipped with CCS and operating under a two-shifting dispatch pattern. In this operating mode a hot startup is initiated at 6am, then operates at steady-state baseload with 90% capture efficiency until 10pm, for a total daily operating time of 16 hours.

Operating Scenario	Duration (mins)	Total startup CO_2 emissions (kg)	Total daily CO_2 emissions (kg)
Startup with prioritization of grid synchronization	160	25.1	79.4
Startup with prioritization of emissions minimization	160	10.3	64.6

Table 6.4. Total CO_2 emissions in total kg per scenario

The saving of 14.8kg CO_2 during startup is approx. 18.6% of the total emissions for a day under two-shifting operation. As steam is introduced more rapidly in scenario 2 the total mass of steam used during the startup period increases by 23.6%. However, as stripping steam is extracted before the inlet of the low-pressure steam turbine the impact on overall plant energy output is likely to be small. Depending on the future emissions cost of CO_2, this analysis shows that it may be economical to implement advanced control strategies to begin capturing CO_2 as rapidly as possible during a start-up event. A comparison of two similar scenarios at large-scale via, for example, dynamic modelling would be an interesting follow-up study.

6.4.3 Power output maximisation via hot water decoupling

It can be advantageous for plant operators to stop the flow of steam to the reboiler, redirecting it instead to the low-pressure steam turbine to capitalise on high electricity selling price. This scenario demonstrates how the capture plant responds to the decoupling of steam flow from the reboiler. It also provides valuable insights about plant circulation times and dynamics, which prove useful when controlling the plant using solvent measurements in real-time.

Flow of hot water to the reboiler is switched off at t=0min. The online solvent sensor detects a change in lean loading is at t=5min, with the CO_2 capture rate responding at approximately t=8min. The CO_2 capture rate decreases steadily as both rich and lean solvent become more concentrated in CO_2. Hot water is reintroduced to the reboiler at t=118min 30sec. The lean solvent sensor detects a reduction in lean loading around 5mins after the step-change in reboiler heat input, at t=123min 30sec. The capture rate responds between t=126 and 127mins. The observed plant response suggests that, at baseload solvent flow conditions, inducing a step-change in hot water flowrate results in a response in lean online solvent measurement after 5mins, and a response in capture rate after around 8mins.

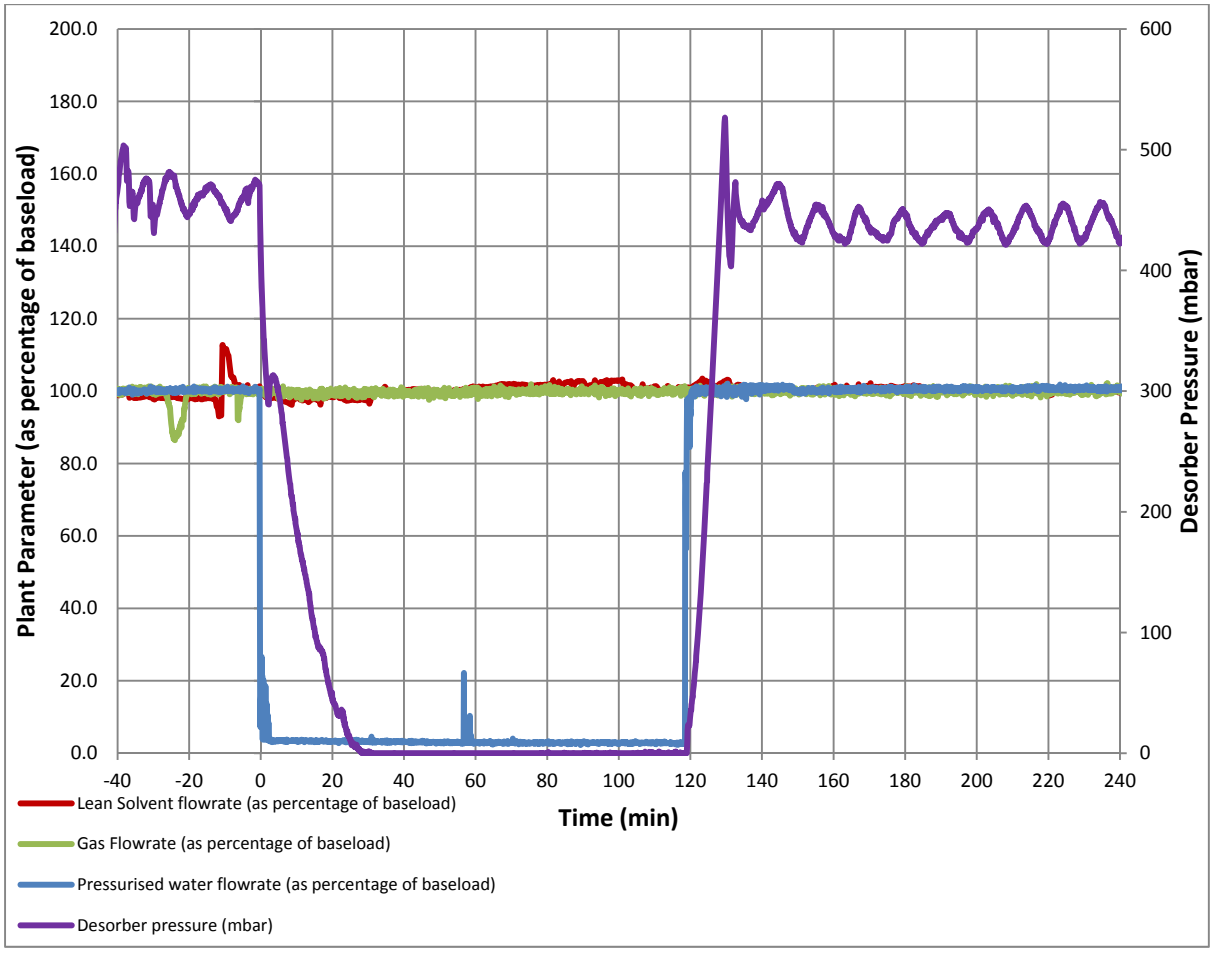

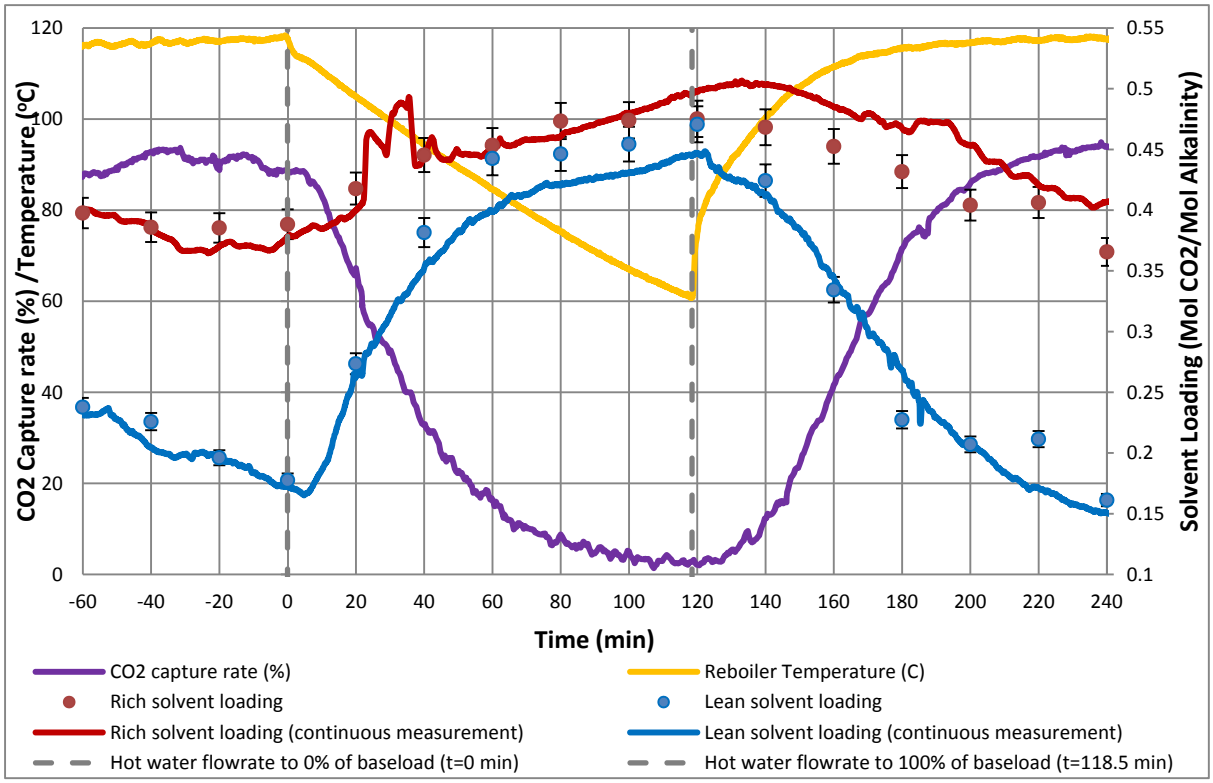

Fig. 6.13a. Gas, solvent hot water flow rate and desorber pressure as percentage of baseload operation, capture bypass scenario 1

Fig. 6.13b. Rich and lean solvent loading, reboiler temperature and CO_2 capture rate, capture bypass scenario 1

Event	Cause of event	Approximate elapsed time since hot water flow is reintroduced (min)
Hot water flow increased from $0m^3/hr$ to $10m^3/hr$	Step-change in setpoint from operator.	0
Response in online lean loading measurement	Solvent which is leaner as a result of hot water step-change reaches the lean online solvent sensor.	5
Response in CO_2 capture rate	Leaner solvent reaches the absorber inlet.	8

Table 6.6. Response of plant parameters to reintroduction of reboiler heat input

The absorber temperature profile gradually decreases in magnitude along with the capture rate, as can be seen in fig. 14a. When the flow of hot water is reintroduced to the reboiler at 118min 30sec as seen in figure the capture rate increases and the absorber temperature increases in magnitude until the plant reaches steady state, baseload operating conditions.

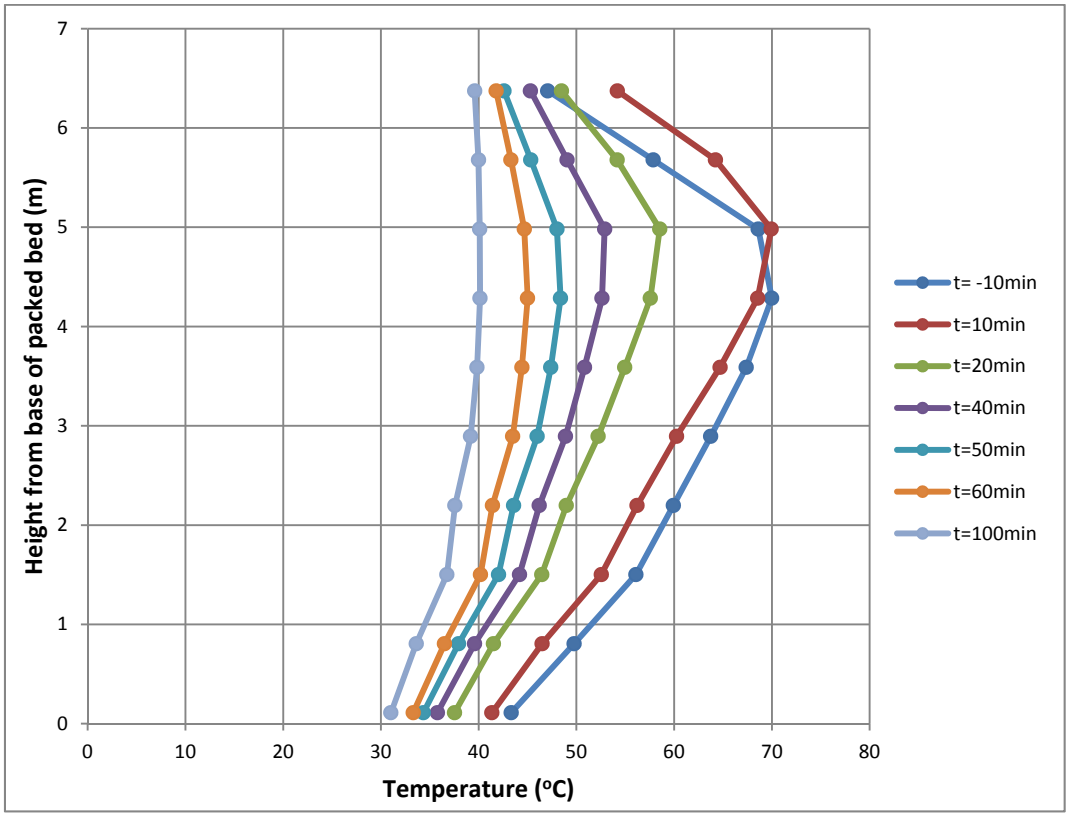

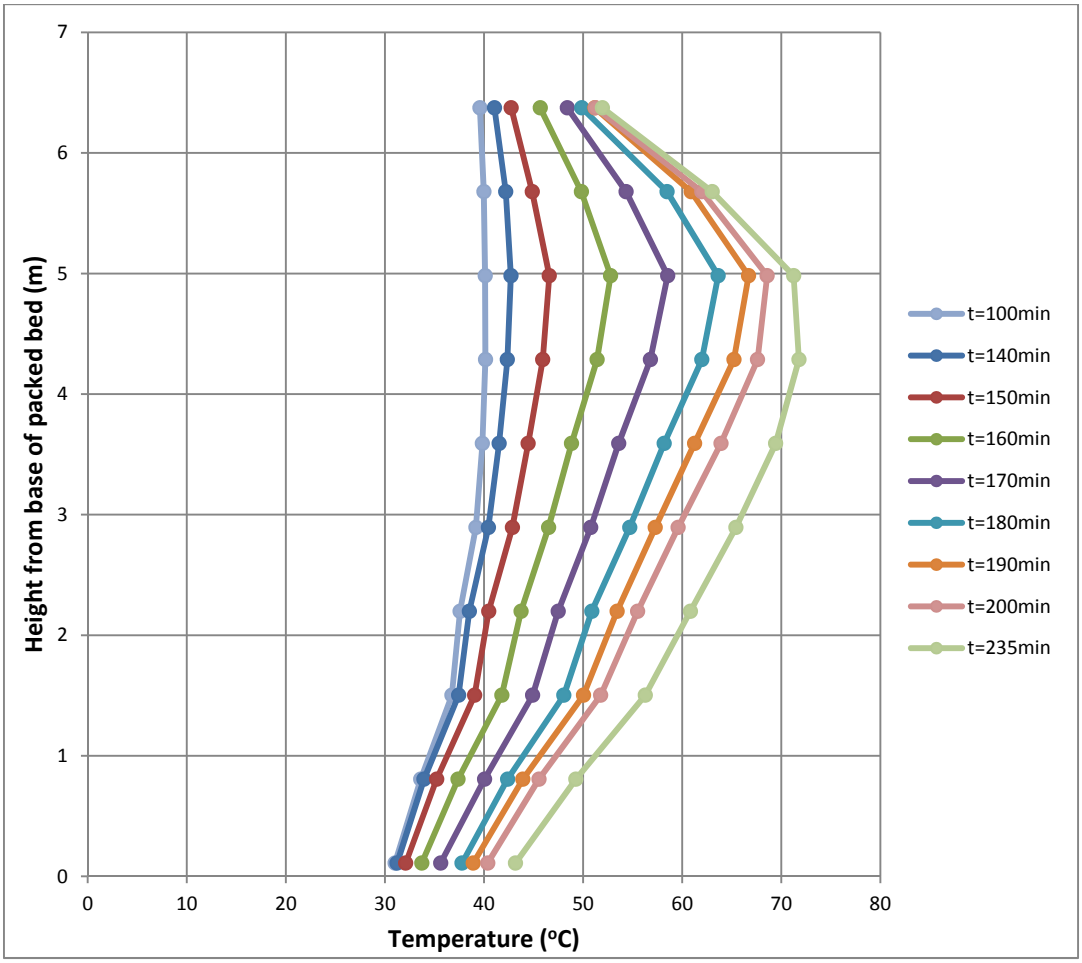

Fig. 6.14a. Absorber temperature profile, capture bypass scenario 1, t= -10min to t=100min
Fig. 6.14b. Absorber temperature profile, capture bypass scenario 1, t= 100min to t=235min

6.4.4 Power output maximisation via hot water decoupling, solvent flow reduced by 50%

This scenario is similar to the previous hot water decoupling event (section 6.4.3), but the flow of solvent to the absorber is reduced to 50% in addition to the reduction of hot water flow to zero. In a real CO_2 capture plant, this would reduce both the power consumption of the pumps and the power consumption of the booster fan, via reduction of the pressure drop across the absorber.

Hot water flow to the reboiler is both reduced to zero and solvent flow is reduced to 50% of baseload at t=0min. Due to the rapid decrease in L/G flow ratio the capture rate drops off rapidly, reaching 60% within 4 minutes. Capture rate continues to decrease over the course of the hot water decoupling event. At t=118min the flow of solvent and hot water are both increased to 100% of baseload, but due to an error with the Labview control system the hot water flow is not stabilised at baseload until t=125min. CO_2 capture rate begins to increase noticeably at around t=130mins, the plant response being slower than in scenario 4.3 due to the error with hot water flow stabilisation at t=118min.

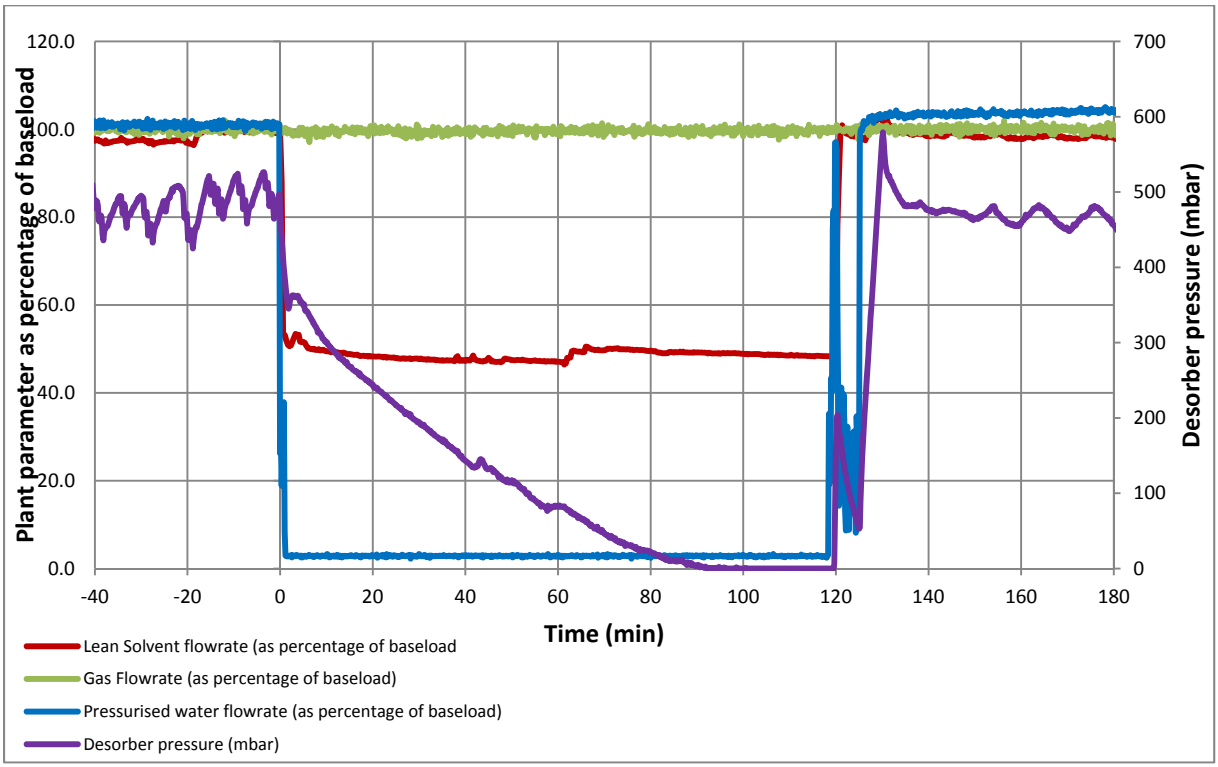

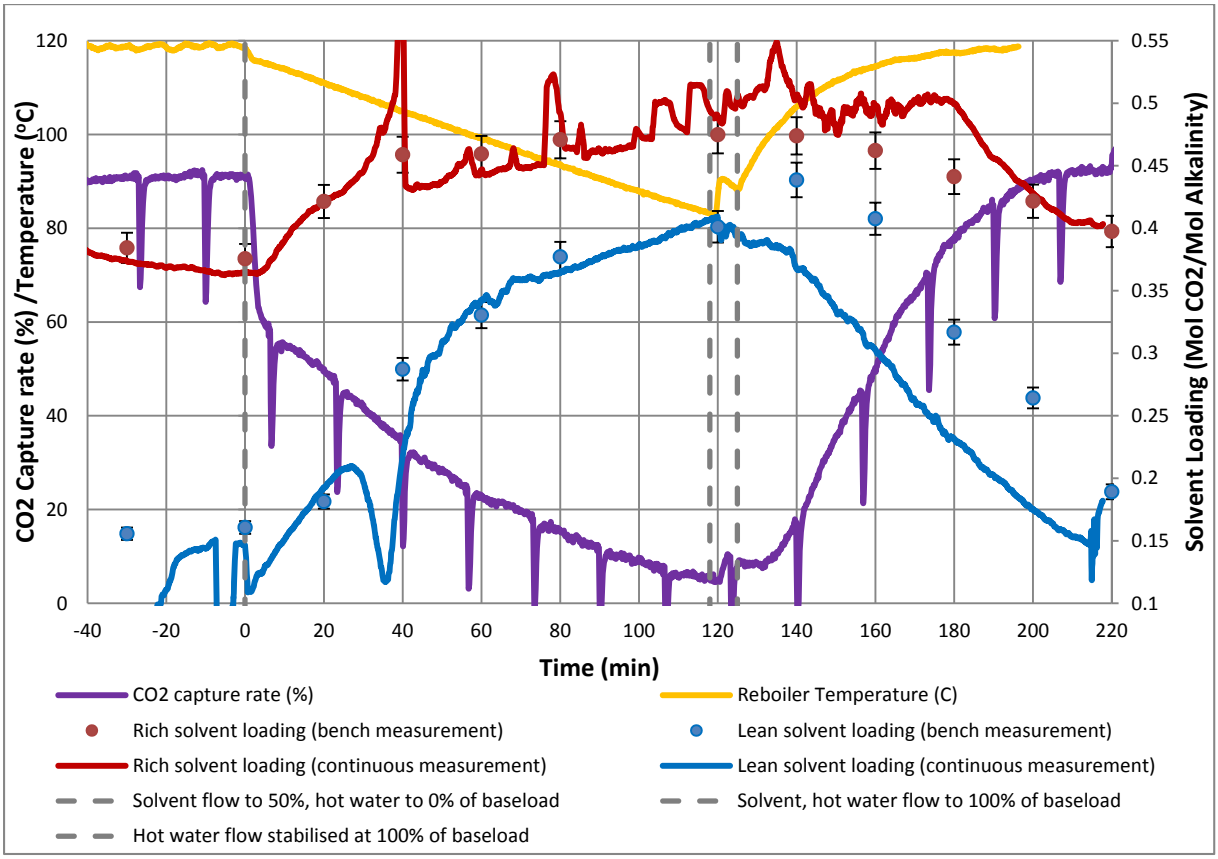

Fig. 6.15a. Gas, solvent hot water flow rate and desorber pressure as percentage of baseload operation, power output maximisation event 2.

Fig. 6.15b. Rich and lean solvent loading, reboiler temperature and CO_2 capture rate, power output maximisation event 2

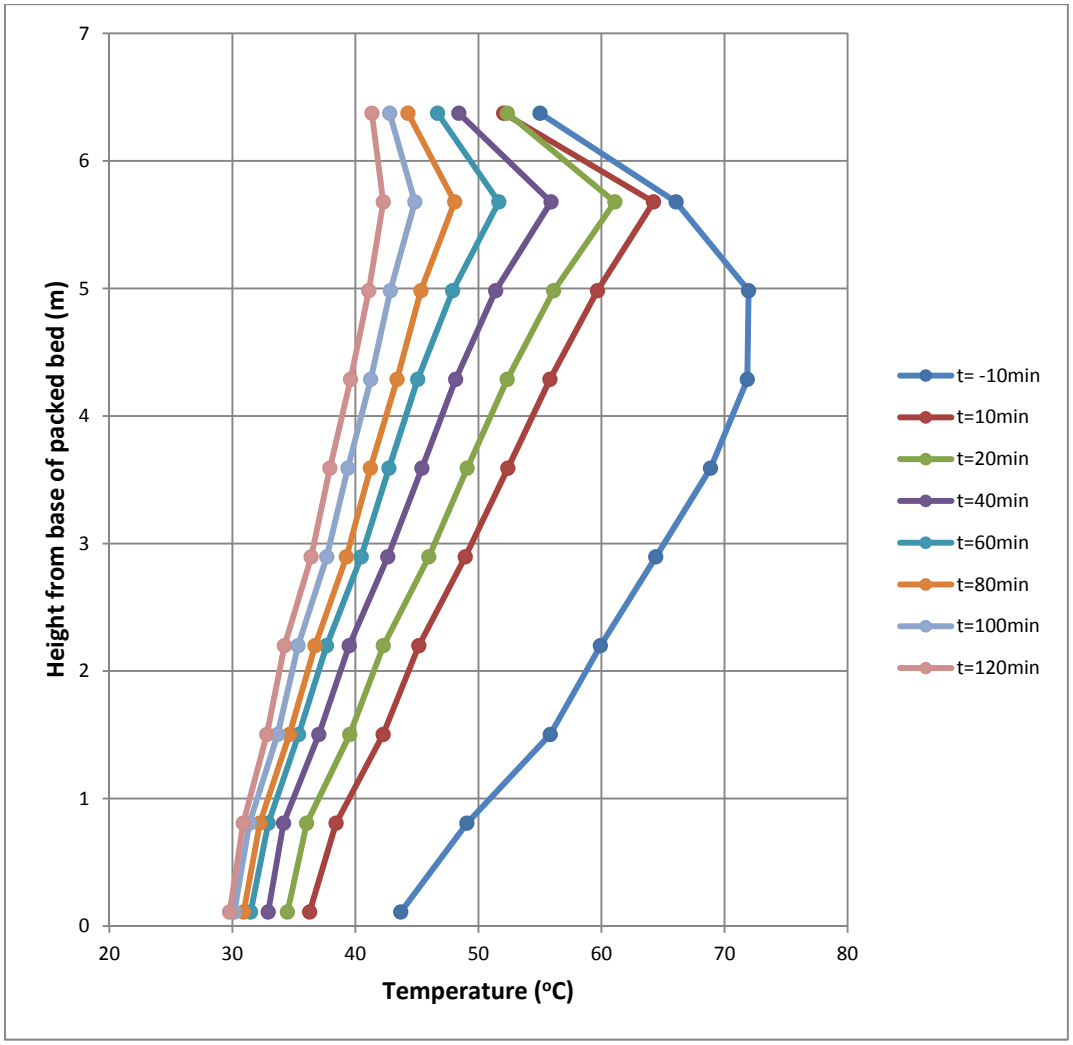
Height from base of packed bed (m)
0
1
2
3
4
5
6
7
20
30
40
50
60
70
80
Temperature (°C)
t= -10min
t=10min
t=20min
t=40min
t=60min
t=80min
t=100min
t=120min

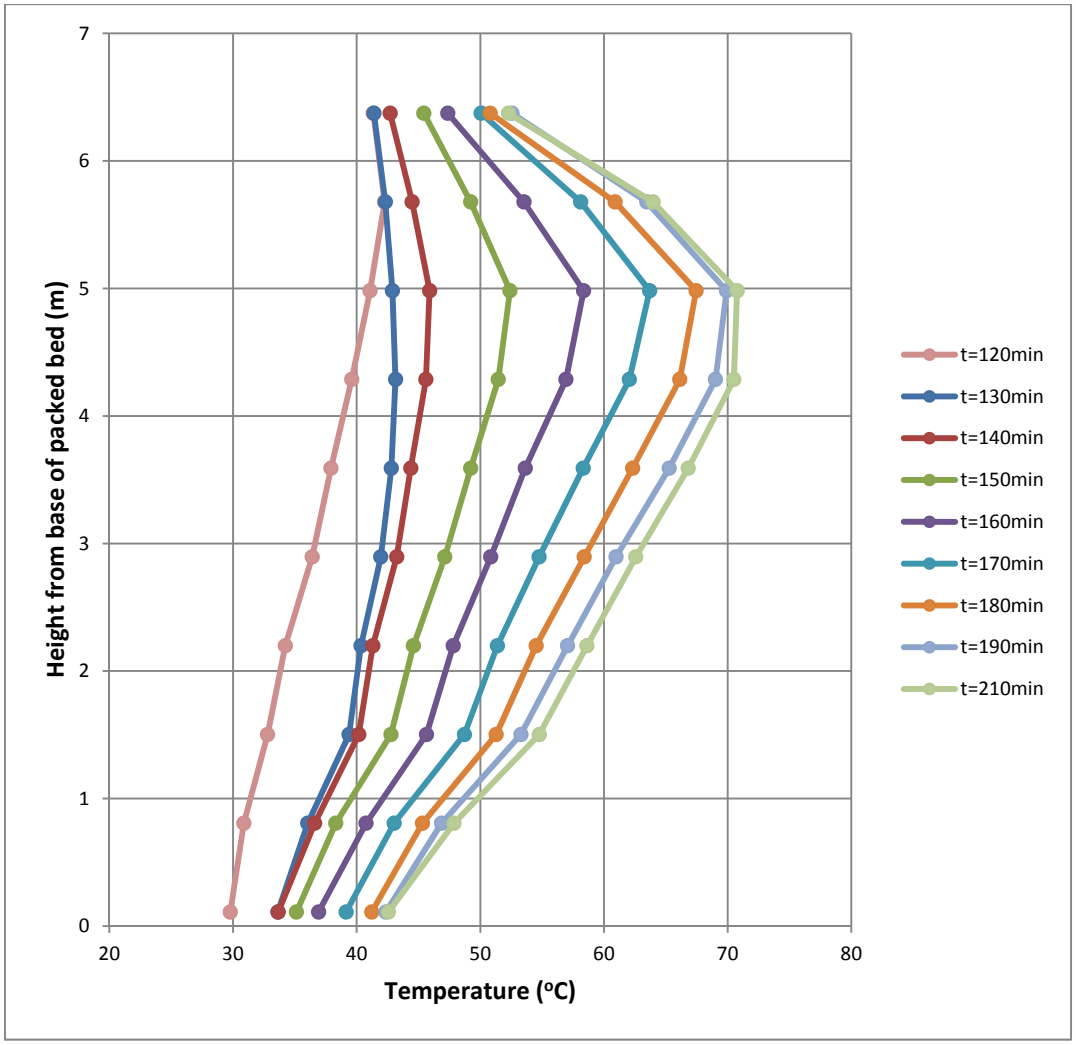

Fig. 6.16a. Absorber temperature profile, capture bypass scenario 2, t= -10min to t=120min
Fig. 6.16b. Absorber temperature profile, capture bypass scenario 2, t= 120min to t=210min

In comparison to the previous hot water decoupling scenario the absorber temperature profile follows a roughly similar trajectory, but with a much more rapid initial decrease in temperature bulge magnitude due to the reduced solvent flow rate and hence, reduced capture rate.

6.4.5 Frequency response via hot water flow reduction

Coal-fired power stations can enhance their flexibility via the addition of post-combustion capture, which allows them to rapidly increase plant output via redirection of steam flow from the reboiler to the low pressure steam turbine (Haines, 2014). In this scenario the flow of hot water to the reboiler is reduced by 50% at t=0. All other plant flow rates remain at baseload throughout. A decrease in CO_2 capture rate is observed over the course of t=20min to t=100min, stabilising at around 75% This results in an 8°C decrease in absorber temperature bulge magnitude over this time period.

At t=141min the flow of hot water to the reboiler is increased to 100% of baseload. A response in capture rate is observed at approx. t=149min which is consistent with the plant response observed in scenario 6.4.3. The capture rate requires 70mins to increase to its original value, stabilising at around 93% at t=210min. The absorber temperature bulge increases to its original magnitude as the capture rate increases.

The rich solvent online measurement is in close agreement with bench titration measurements, but the lean online measurement suffers from severe measurement instability until approx. t=122min.

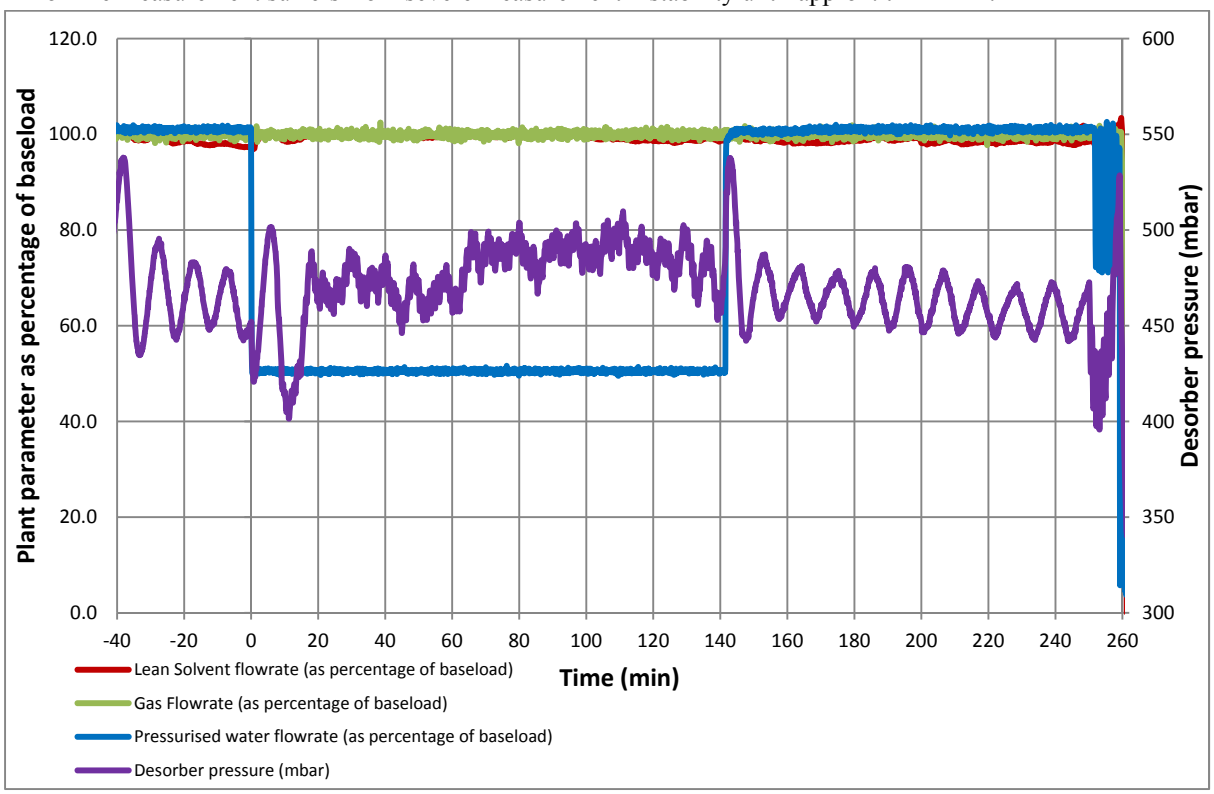

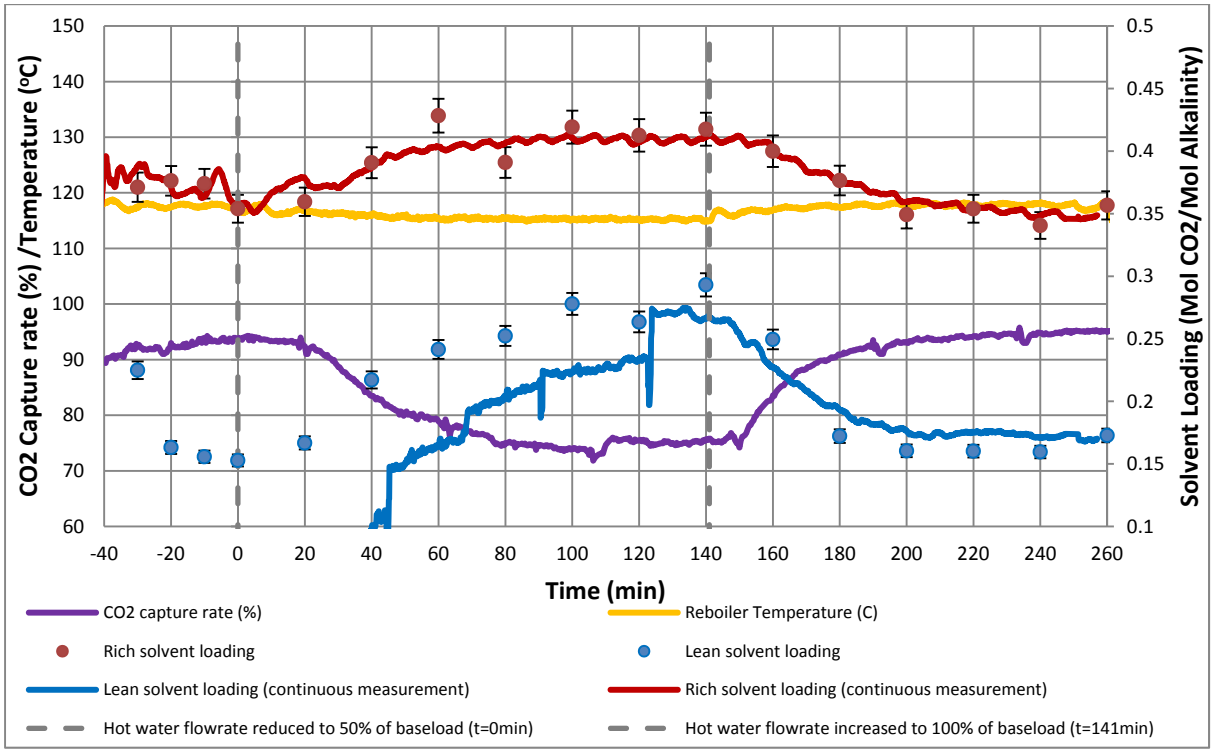

Fig. 6.17a. Gas, solvent hot water flow rate and desorber pressure as percentage of baseload operation, frequency response scenario

Fig. 6.17b. Rich and lean solvent loading, reboiler temperature and CO_2 capture rate, frequency response scenario

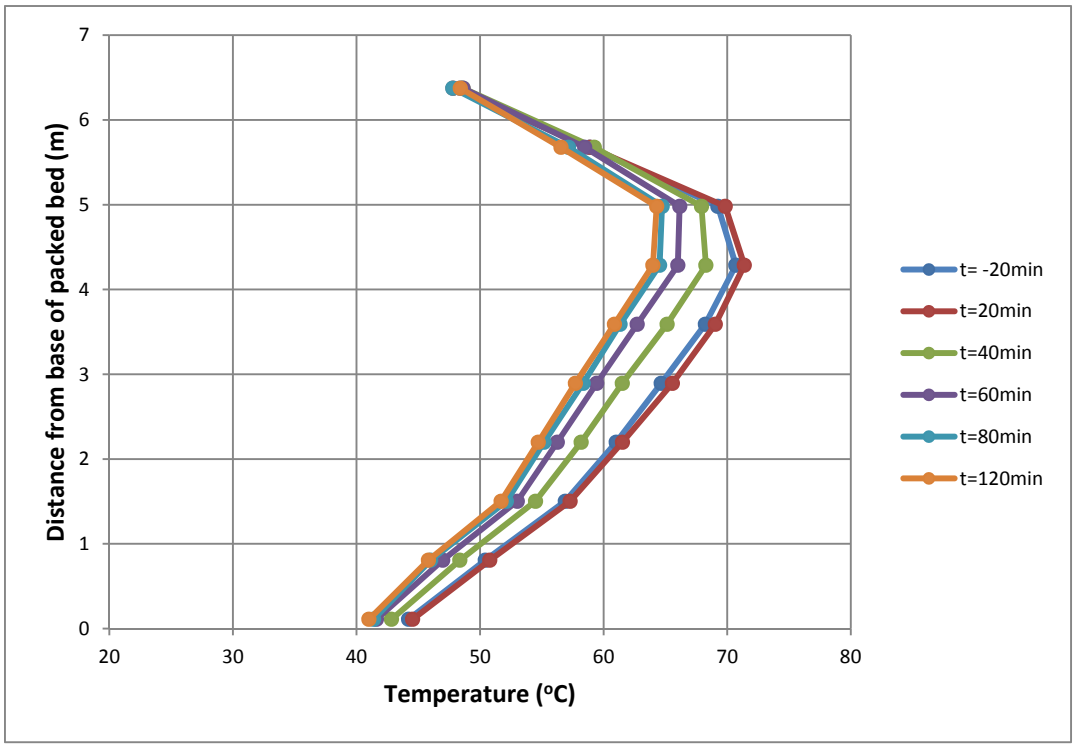

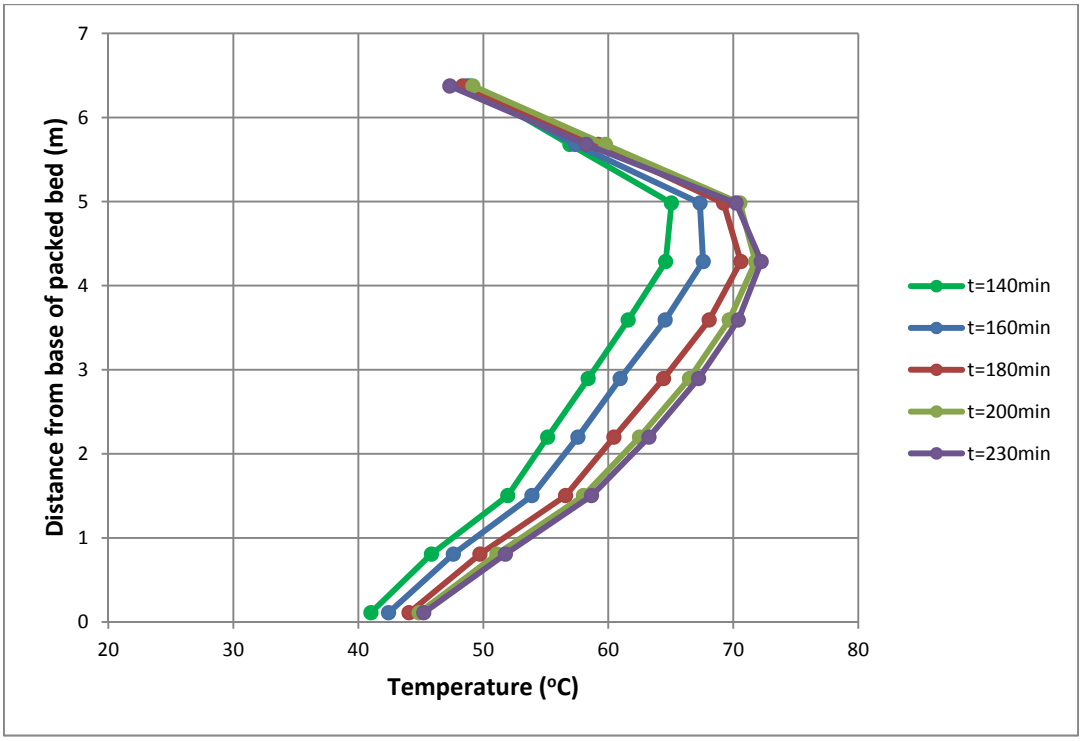

Fig. 6.18a. Absorber temperature profile, frequency response scenario, t= -10min to t=100min
Fig. 6.18b. Absorber temperature profile, frequency response scenario, t= -100min to t=235min

6.4.6 Capture plant ramping

With increasing contribution to an electricity generation portfolio from intermittent renewable sources it is likely that some coal-fired power stations will operate in a load-following regime for a significant proportion of their operational lifetime (Mac Dowell and Shah, 2014; Mac Dowell and Staffell, 2016). This scenario simulates the capture plant reducing its output from baseload to 70%, then ramping back up to baseload after 2 hours. This relatively small ramp is selected in order to compare with dynamic modelling data. Gas flow is ramped down at 2.5% of baseload ($5m^3$/hr) per minute to represent a coal unit cycling rate of 2.5% of its output per minute (DECC, 2014). Hot water flow is also ramped down at 2.5% of baseload ($0.25m^3$/hr) per minute. Once gas and hot water flows have been stabilised at 70% of baseload at t=12min a step-change in solvent flow from 100% to 70% of baseload (1000l/hr to 700l/hr) is made to keep the L/G ratio constant for as much of the operation as possible.

At t=119min the flow of solvent is increased to 100% of baseload operating conditions (1000l/hr) in anticipation of the gas and hot water ramp operation. At t=120min, gas and hot water flow are both ramped up at a rate of 2.5% of baseload per minute, then stabilised at baseload at t=132min.

A slight increase in CO_2 capture rate from 90% to 96% is observed while the plant is operating at 70% capacity. This is the opposite of what is observed in the simulation of Mac Dowell and Shah (2015), who report a small decrease. The reason for this becomes clear if the gas and liquid flow rate during the load-following operation are inspected closely (fig. 6.19c). In the modelling study, the L/G flow ratio and both lean and rich loading are kept constant throughout. Due to the imperfect control system of the pilot plant, for a significant proportion of the real operation the L/G ratio is greater than at baseload, with liquid flow varying between 71-71% and gas flow at around 68-69%. The lean solvent loading also appears to decrease slightly over the duration of the event which may account for the higher capture rate during t=78-93min, when the L/G ratio is almost the same as at baseload flow conditions. However, the change is small (around 0.01-0.02 mol/mol) and there is some variation in titration measurements both at baseload and during the ramping operation (titration points at t=-23min, t=77min). In the absence of accurate continuous lean loading measurements it is not possible to come to definitive conclusions about how it affects the capture rate in this case, highlighting the importance of capturing this behaviour via dynamic modelling.

The lean solvent sensor was not available during this operation. Small transient decreases in rich loading are observed between t=5min to t=25min and t=120 to t=140min. Allowing for several minutes time delay for leaner solvent to circulate through the absorber sump and pipework to the rich solvent analyser corresponds to time periods during which the L/G ratio is higher than at baseload. The temperature bulge increases in magnitude slightly and moves down the packed bed, indicating that a relatively higher proportion of CO_2 is being absorbed per unit of solvent at the absorber inlet, and that more of this CO_2 is being absorbed lower in the packed bed. Once the plant is stabilised at baseload flow conditions after t=132min the capture rate decreases back to around 90%.

There remains scope for the implementation of flexible load-following operations which utilise strategies such flue gas venting, varying degrees of solvent regeneration and solvent storage to maximise the electricity available for export during peak selling times, while retaining an average level of CO_2 capture close to 90% over the course of a single day (Enaasen et al, 2016; Mac Dowell & Shah, 2015). These could be investigated in future pilot-scale test campaigns on flexible CCS.

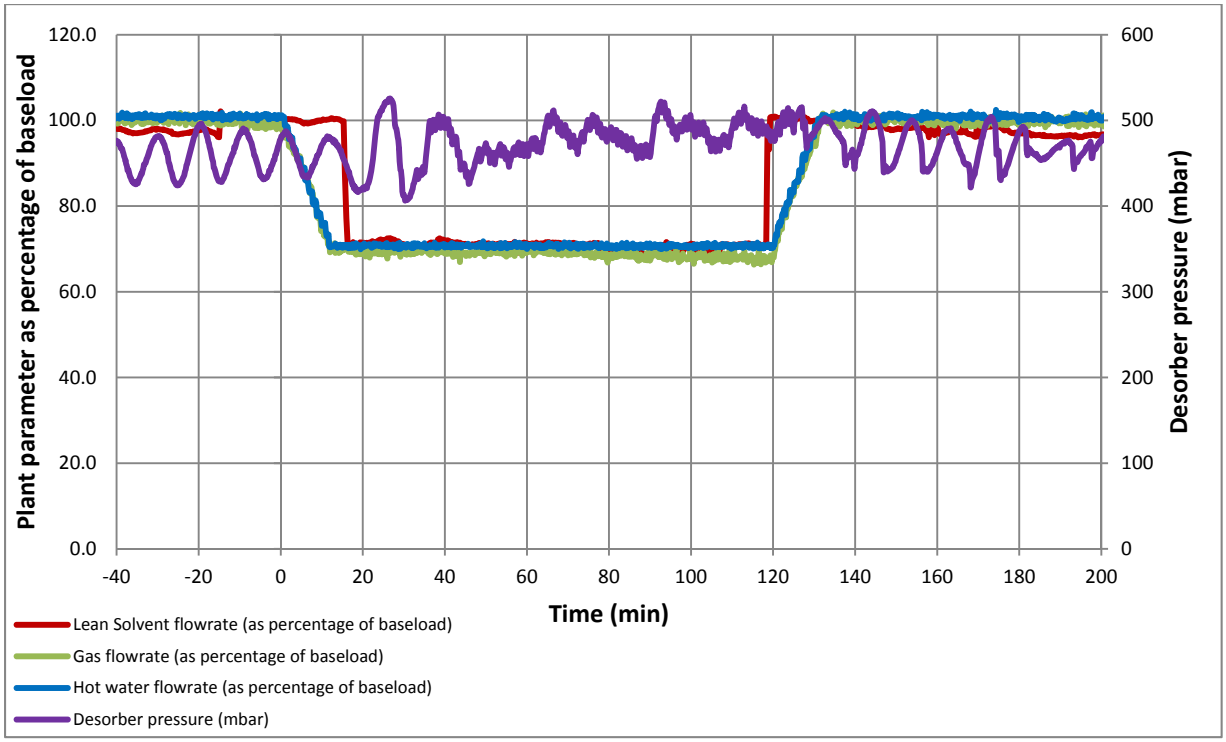
Plant parameter as percentage of baseload
Desorber pressure (mbar)
Time (min)
120.0
100.0
80.0
60.0
40.0
20.0
0.0
600
500
400
300
200
100
0
-40
-20
0
20
40
60
80
100
120
140
160
180
200
Lean Solvent flowrate (as percentage of baseload)
Gas flowrate (as percentage of baseload)
Hot water flowrate (as percentage of baseload)
Desorber pressure (mbar)

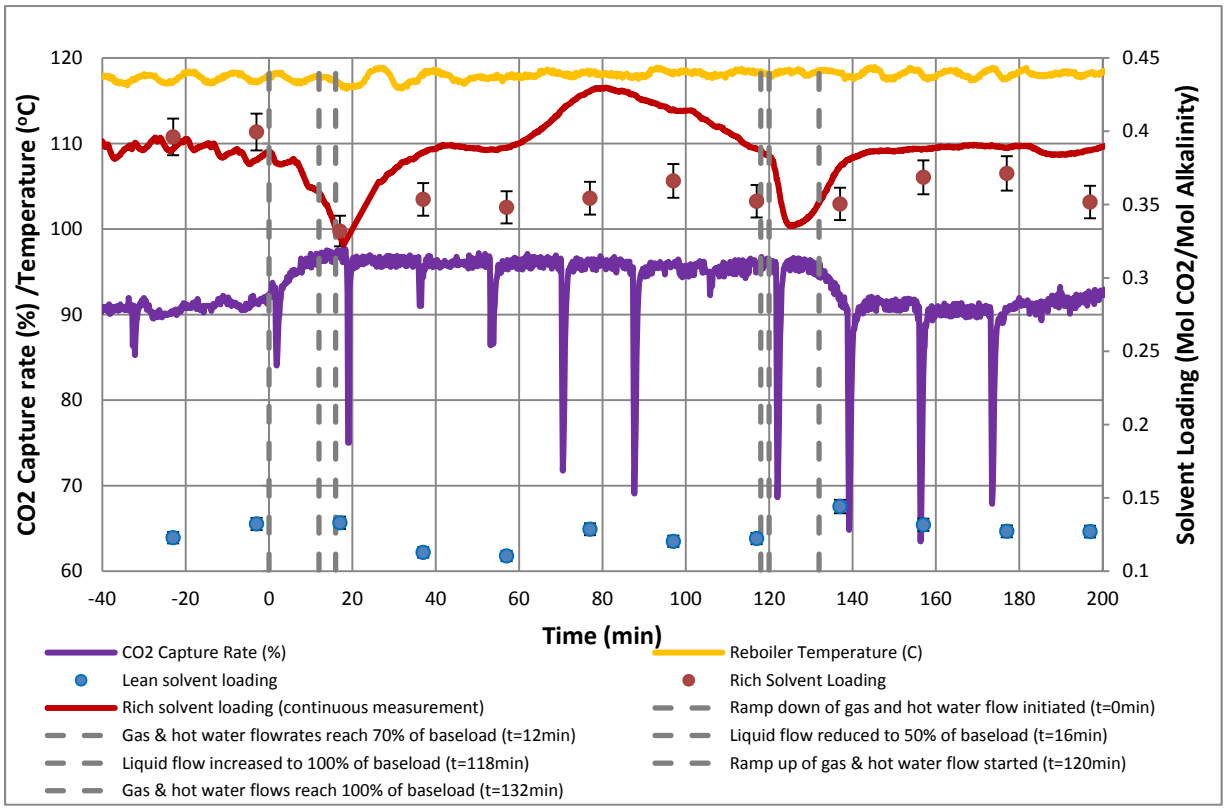
CO2 Capture rate (%) /Temperature (°C)
Solvent Loading (Mol CO2/Mol Alkalinity)
Time (min)
120
110
100
90
80
70
60
0.45
0.4
0.35
0.3
0.25
0.2
0.15
0.1
-40
-20
0
20
40
60
80
100
120
140
160
180
200
CO2 Capture Rate (%)
Lean solvent loading
Rich solvent loading (continuous measurement)
Gas & hot water flowrates reach 70% of baseload (t=12min)
Liquid flow increased to 100% of baseload (t=118min)
Gas & hot water flows reach 100% of baseload (t=132min)
Reboiler Temperature (C)
Rich Solvent Loading
Ramp down of gas and hot water flow initiated (t=0min)
Liquid flow reduced to 50% of baseload (t=16min)
Ramp up of gas & hot water flow started (t=120min)

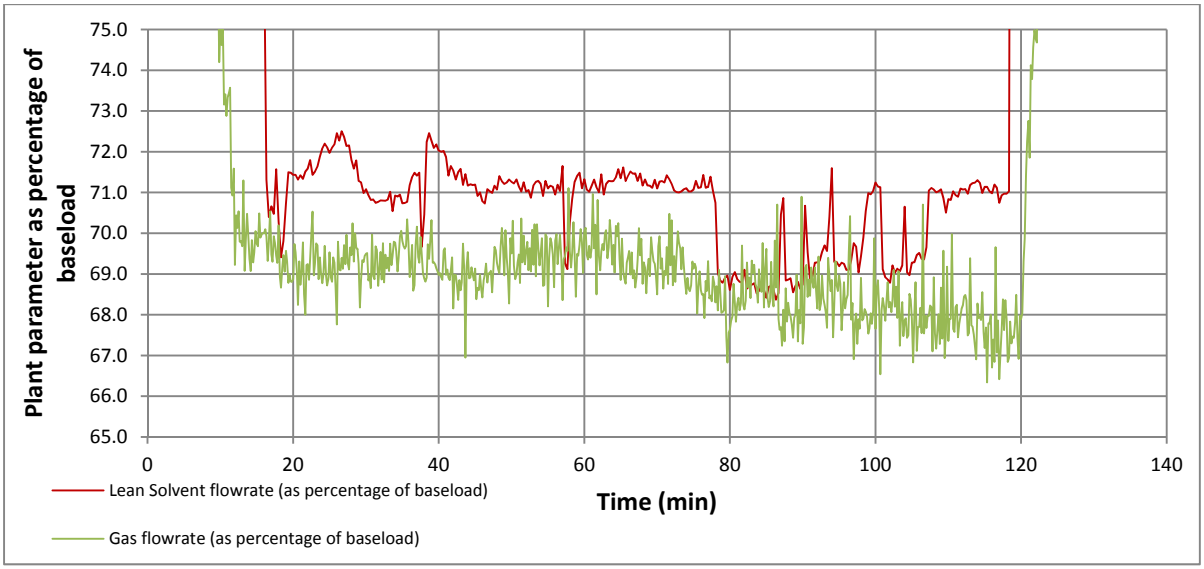

Fig. 6.19a. Gas, solvent hot water flow rate and desorber pressure as percentage of baseload operation, load following scenario

Fig. 6.19b. Rich and lean solvent loading, reboiler temperature and CO_2 capture rate, load following scenario

Fig. 6.19c Gas and solvent flow rate as percentage of baseload operation, load following scenario

There is very little change in the absorber temperature bulge profile over the course of the event. The magnitude of the bulge increases by around 2.5°C after the ramp down, corresponding to the slightly higher capture rate. The capture rate is also slightly higher than at the beginning of the event when it returns to "baseload" steady state conditions at t=180min. This may be due to water losses increasing the nominal amine concentration in the solvent.

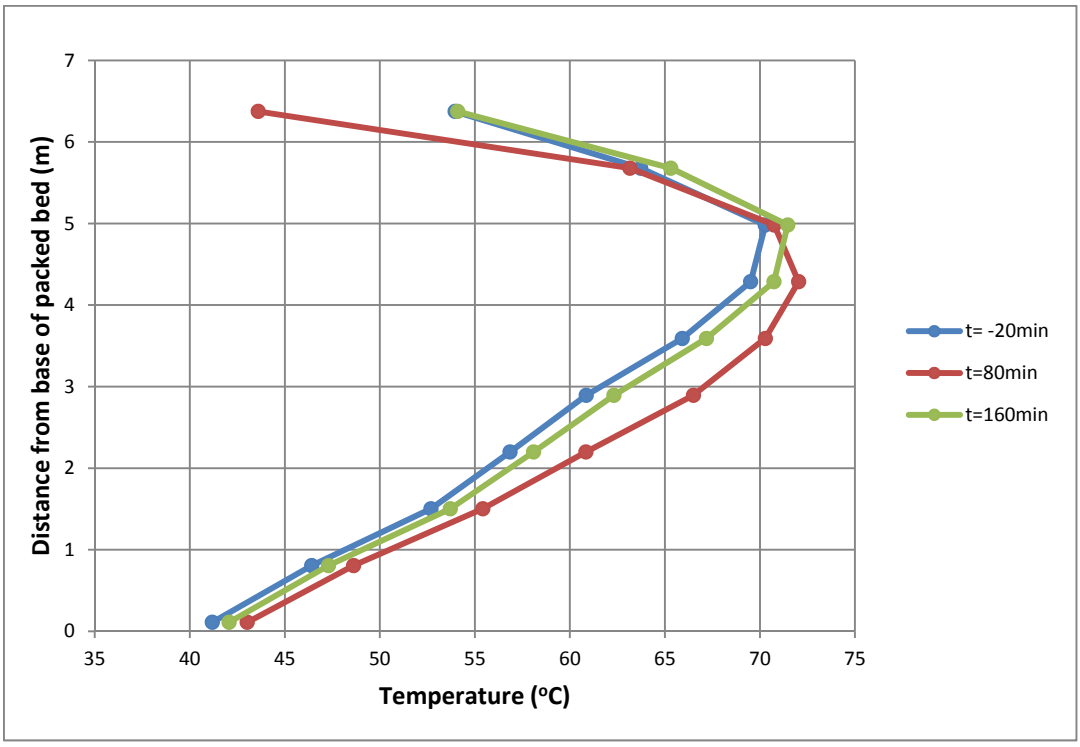

Fig. 6.20 Absorber temperature profile, load following scenario

6.4.7 Real-time control using online solvent measurement

In this scenario control of the plant in real-time using online solvent measurements is demonstrated. It has already been demonstrated (section 6.4.3) that at baseload solvent and gas flow rates, a response in lean loading online measurement is observed approx. 5min after a step-change change in reboiler heat input. The CO_2 capture rate responds after a further 3min (see table 6.6).

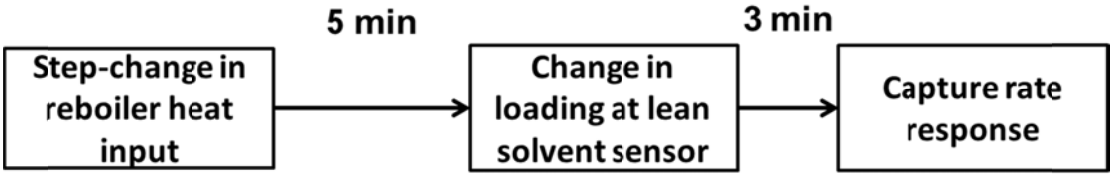

Fig. 6.21 Capture rate and lean solvent response times at baseload solvent flow conditions

This knowledge can be used to estimate the lean solvent loading which will result in a desired capture rate by observing plant trends from previous scenarios. For the purpose of demonstration, a capture rate of 30% was selected. In scenario 6.4.3 the capture rate reaches 30% at t=44min, this allows ample time for the rate of change in lean CO_2 solvent loading to be estimated and recalculated if necessary.

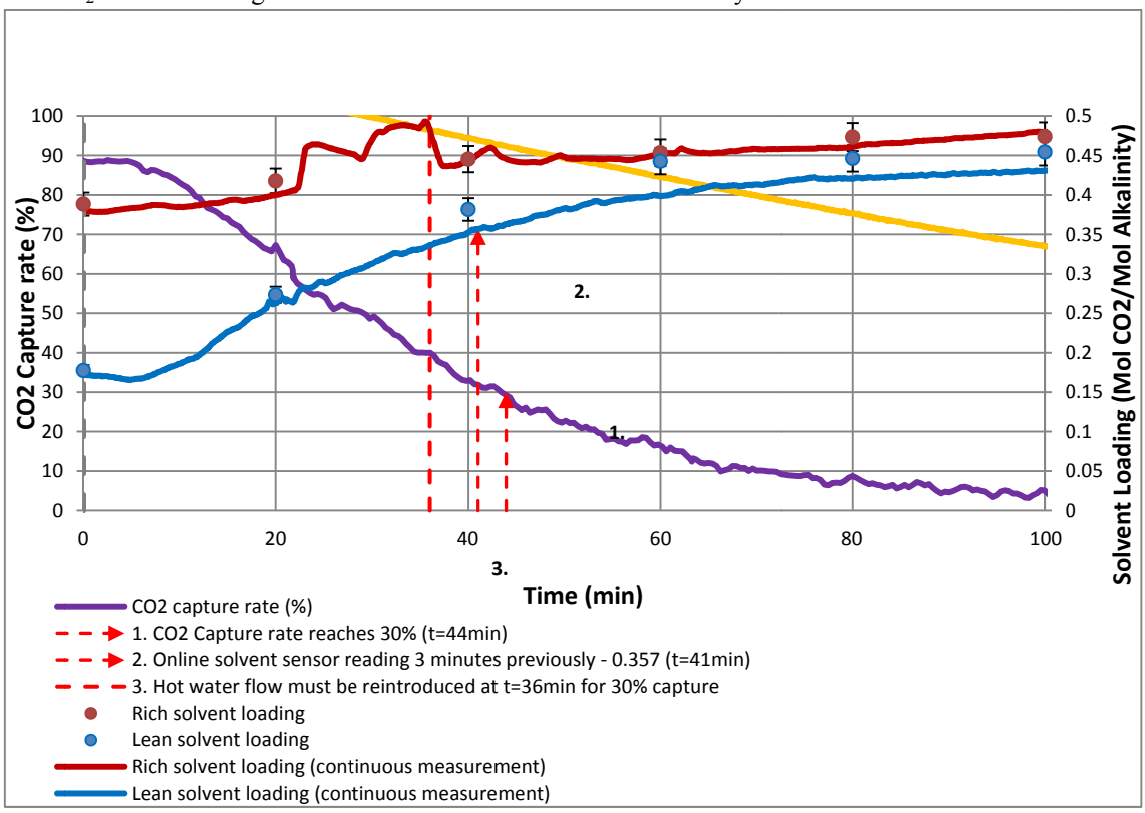

Fig. 6.22 Section of data between t=0 and t=100min from scenario 6.4.3

With reference to a section of data from scenario 6.4.3 (see fig. 6.22) and table 6.6, it is possible to retroactively calculate when the flow of hot water to the reboiler should be reintroduced using the time CO_2 capture rate reaches 30%.

1. CO_2 capture rate reaches 30% at t=44min.
2. The solvent loading which corresponds to 30% capture passes through the lean solvent loading analyser 3 minutes previously, at t=41min. At this time, lean loading is 0.357 mol MEA/mol CO_2.
3. To achieve a maximum solvent loading of 0.357 mol MEA/mol CO_2 and hence a CO_2 capture rate of 30% the flow of hot water to the reboiler must be reintroduced 5 minutes before (2.), at t=36min.

The lean loading can be used to control the plant by calculating the rate of change of lean solvent based on current trends and predicting its value in 5 minutes time. If this value exceeds the "target" lean loading of

0.357mol CO_2/mol MEA the flow of hot water to the reboiler should be restarted. A simple Boolean expression for the method in more general terms could look as follows:

$$If\ \left(\alpha_{current} + \left(\Delta t_{desorber-sensor} * \frac{\Delta\alpha}{\Delta t}\right) > \alpha_{target}\right) Then$$
$$(PV = 0)$$
$$Else (PV = 1)$$

Where $\alpha_{current}$ is the current online lean loading measurement, $\Delta t_{desorber-sensor}$ is the time delay between making a change in reboiler heat input and a response being observed in lean loading measurement, $\frac{\Delta\alpha}{\Delta t}$ is the lean loading's rate of change (based on t=15min – t=25min in this case) and α_{target} is the previously-determined "target" lean loading. PV refers to the position of the hot water bypass valve, 0 being completely open (all flow goes through the bypass), 1 being completely closed (all flow goes to the reboiler).

This is a fairly rudimentary method of lean loading and capture rate prediction, it could be improved by taking into account dependencies on current plant temperatures (especially in the absorber), variations in nominal amine concentration and planned changes in solvent flow rate. In future studies, rich online solvent measurements could also be used as a predictor of how the lean loading's rate of change will vary in the future. Since the response of the lean loading upon reboiler shutdown is non-linear the rate of change should be recalculated at regular intervals. This would require more plant data to be acquired than practical in the limited experimental time available, but future control efforts should consider these dependencies and attempt to integrate the method with the plant control system.

Hot water flow to the reboiler is reduced to zero at t=0min. The capture plant has no continual capture rate measurement as absorber gas inlet and outlet CO_2 concentrations are recorded on separate FTIR machines, so plant control is dependent entirely on lean solvent measurements and the prediction method. It is predicted that the loading will reach the target of 0.357 mol CO_2/mol MEA at t=46min 30sec, so the flow of hot water is redirected to the reboiler at t=41min 30sec (allowing 10sec for the plant operator to respond).

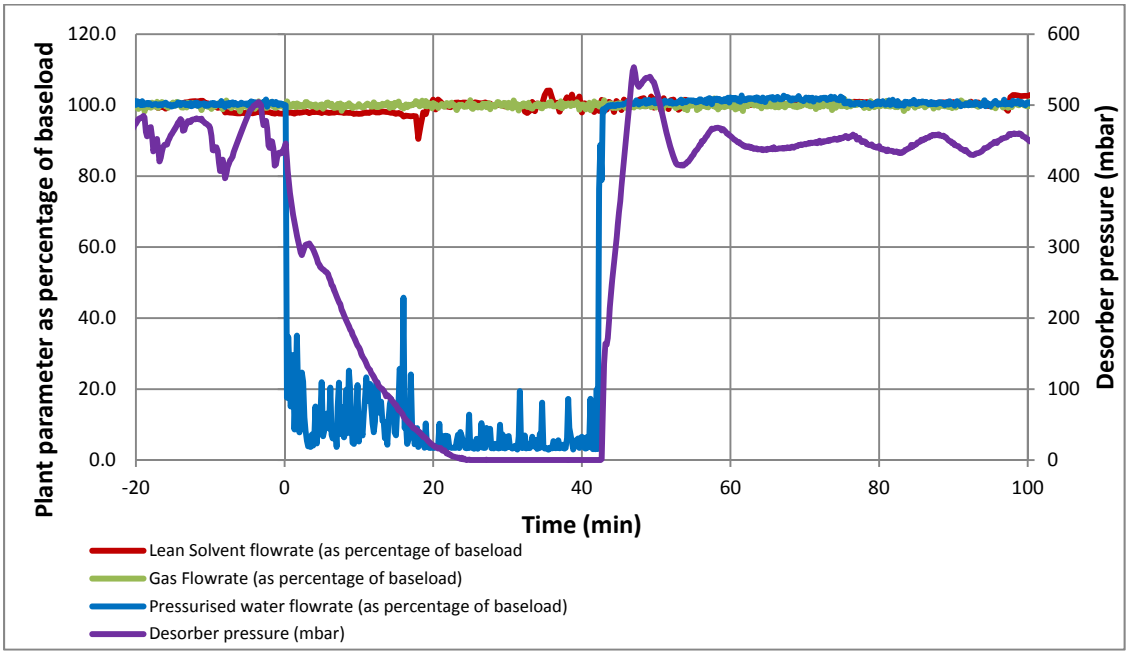

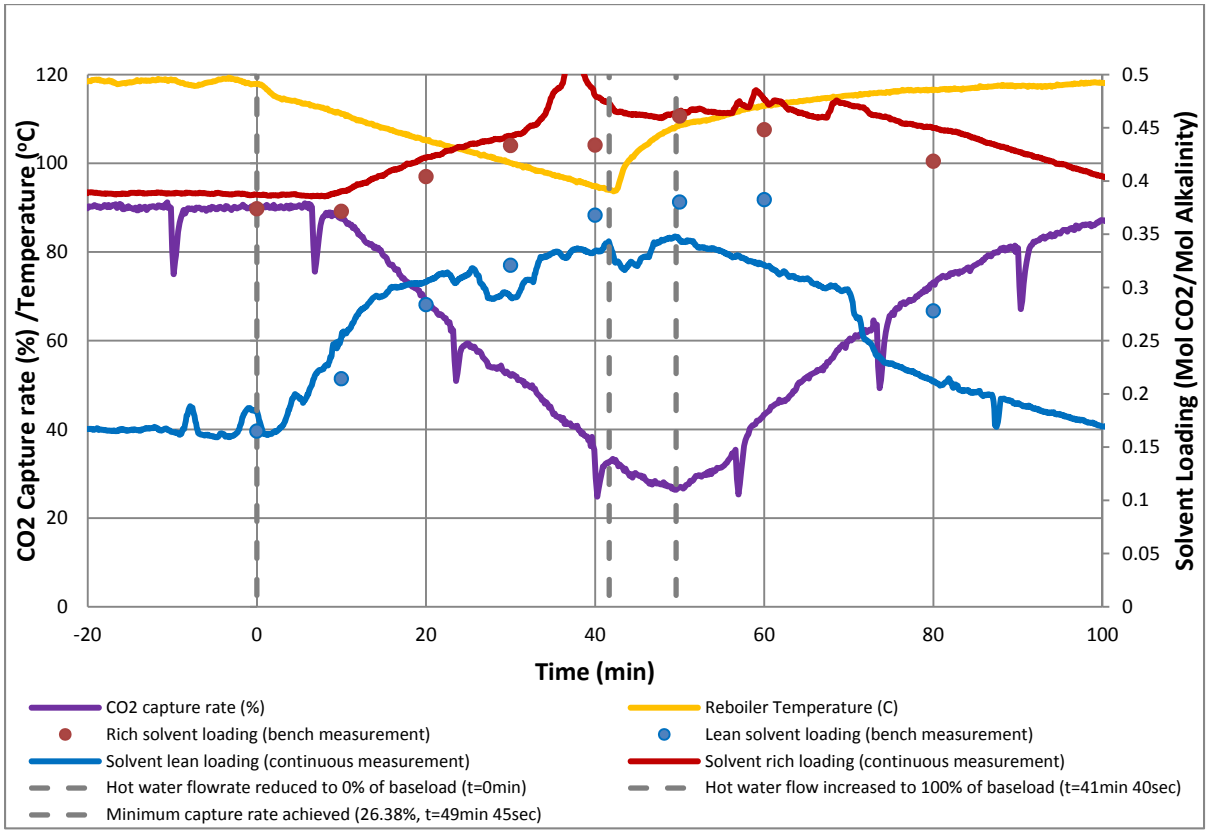

Fig. 6.23a. Gas, solvent hot water flow rate and desorber pressure as percentage of baseload operation, real time control with online solvent measurement

Fig. 6.23b. Rich and lean solvent loading, reboiler temperature and CO_2 capture rate, real time control via online solvent measurement

The target minimum capture rate was 30% and the actual capture rate achieved was 26.38%, displaying that while plant control using continuous online solvent measurements is possible there remains scope for improvement. The rate of change of lean loading was estimated using the values at t=15 and t=25min. Titration measurements suggest that this may have resulted in an underestimation of $\frac{\Delta\alpha}{\Delta t}$, leading to the optimum time for reintroduction of hot water being overshot.

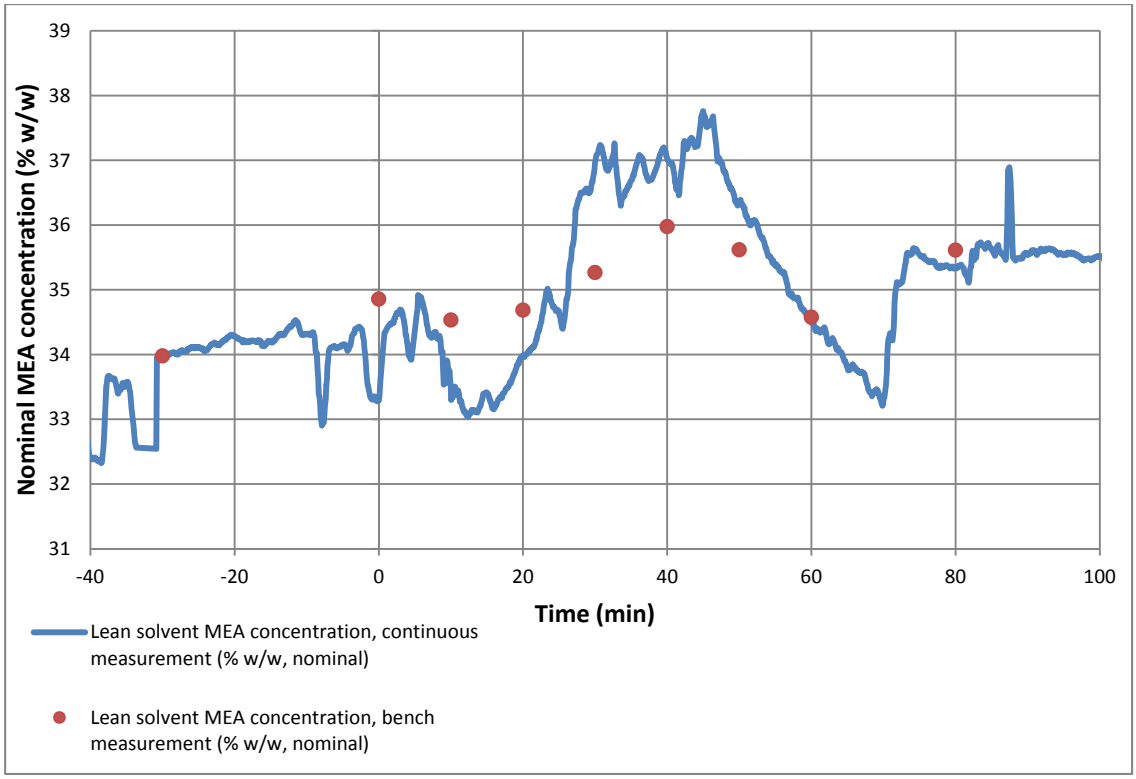

Fig. 6.24 Continuous and bench measurements of nominal amine concentration

The data shows that the lean solvent sensor under-estimates solvent amine concentration from around 7min to 25min, then over-estimates it from around 25min to 55min. This explains why the online solvent loading measurement is over-estimated before t=25min then under-estimated after t=25min, making it difficult to calculate the rate of change of solvent loading over the most critical part of the operation. Adjustment of the sensor's algorithm which is used to calculate solvent CO_2 loading could produce a result which is closer to 30% capture in the future.

Nevertheless, given the non-ideal operating environment and fairly basic prediction method the sensor performed sufficiently well to achieve a minimum CO_2 capture rate within 4% of the target. This is the first ever implementation PCC plant control combined with in-situ online loading measurements and opens the door for the development of fit-for-purpose tools for dynamic operation, with further work focusing on the improvement of sensor performance and refinement of the prediction method.

6.5 Conclusions

Six flexible operating scenarios which could be encountered by operators of PCC as applied to coal-fired power plant are demonstrated. Via comparison of different methodologies for plant start-up, rapid introduction of steam to the reboiler is found to provide CO_2 emissions savings equivalent to 18.6% of the total daily emissions for a similar plant operating in a two-shifting dispatch pattern with 90% capture following startup (Table 6.3). Differences in plant construction are found to have a direct effect on solvent circulation times and as a result, how the plant reacts to dynamic operations. In contrast to the absorption/desorption facility described in chapter 5, which has a desorber outlet to absorber inlet solvent circulation time of 15-25mins, the PACT pilot facility used in this work has a circulation time of approx. 8mins. Changes in capture efficiency are observed after a relatively short period of time after making changes to reboiler heat input at the PACT pilot, but the increase or decrease is gradual and no significant additional fluctuations are observed following the initial return to baseload flow conditions, as the solvent becomes more rapidly mixed in the large desorber tank and sump. Steady state data and full datasets from these six dynamic tests are available via open access on the UKCCSRC data archive, for the potential validation of dynamic models. Tables of information which detail plant dimensions and packing types are also provided.

A final dynamic operating scenario demonstrates plant control uses real-time measurement of solvent loading to attempt to hit a "target" CO_2 capture efficiency following a steam shutdown event. A capture efficiency of 26.4% is achieved for a target of 30%. While not possible during this campaign due to time constraints, the next immediate steps for development of CO_2 capture efficiency control using online solvent measurements are as follows:

- Write Labview code (or other control software) which allows the existing prediction method to be implemented programmatically, with rate of change in solvent loading ($\Delta\alpha/\Delta t$) being recalculated on a regular basis.
- Refine the sensor algorithm which calculates solvent loading to make measurements more reliable, accurate and less prone to instability. Additional studies at pilot-facilities and large-scale commercial CCS plants which are not published at the time of writing show considerable improvements in sensor stability, and consistent close agreement with offline measurements. These results are to be presented at the GHGT-14 conference.
- Continue to develop knowledge of plant hydrodynamics at PACT so that the prediction method can be scaled to account for changes in solvent flow rate.

Achievement of these objectives at the UKCCSRC PACT amine pilot can form a basis for the development of an enhanced plant control system, which uses continuous solvent measurements as control variables to maintain plant parameters within pre-defined boundaries. Differences in plant construction are found to significantly affect response to dynamic operation, so a step-by-step methodology for the development of similar control systems at other plants is likely to be a useful tool.

Solvent working capacity as a potential control variable was discussed in chapter 5 but it is now obvious that this is too simplistic an approach. Discrete knowledge of plant hydrodynamics, response times based on current plant conditions, knowledge of upcoming changes in generation plant output and continuous monitoring of rich and lean solvent loading will be required to optimise operation. Advanced process control system architectures such as Model-predictive control (MPC) and fuzzy logic control applied to the control of post-combustion capture are a promising alternative to single input-single output PID or cascading-PID control systems in maintaining plant operation within environmental, economic and operational boundaries via active control of solvent flow, desorber pressure and reboiler energy input (Luu et al., 2015; Mechleri, 2015). The successful demonstration of the sensor represents a significant practical step toward combining online solvent measurements with novel control strategies to optimise plant operation.

To summarise, the key findings of this work are:

- Six dynamic pilot-scale datasets are generated.
- Two plant startup modes are implemented at pilot-scale.
    - Startup method 1: The low pressure steam turbine is powered up before stripping steam is sent to the reboiler.
    - Startup method 2: Low pressure steam is immediately introduced to the reboiler as soon as it becomes available.

  Total CO_2 emissions during startup are 25.1kg for method 1 and 10.3kg for method 2, a saving of 14.8kg. To quantify these potential savings, the case of a two-shifting coal plant which initiates a hot startup at 6am, operates with 90% capture efficiency for the rest of the day and shuts down at 10pm is considered. Total residual CO_2 emissions for a plant of this scale over the 16hr period are 79.4kg with startup method 1, and 64.6kg with startup method 2. This represents a potential 18.6% reduction in daily emissions, at the cost of increased low-pressure steam consumption during startup.
- A steam shutdown event is used to determine response times critical plant response times, with the intent of using continuous online solvent measurements as an input parameter for the control of CO_2 capture efficiency.
- In the final dynamic scenario, the use of an online solvent sensor combined with knowledge of plant response times to achieve an arbitrarily chosen "target" capture efficiency following a steam shutdown event is demonstrated. For a target of 30%, a minimum capture efficiency of 26.4% is achieved.

The following chapter will attempt to crystallise some of the findings detailed in this chapter regarding the effect of plant construction and configuration on response. This will be achieved via the identification of "desirable" aspects of plant design for the facilitation of flexible operation, practical operating constraints, and determination of the effects of plant construction on plant response times.

References

Akram, M. (2017). Amine Plant Layout. Personal communication, 28/03/17.

Akram, M., Ali, U., Best, T., Blakey, S., Finney, K.N. and Pourkashanian, M. (2016). Performance evaluation of PACT Pilot-plant for CO2 capture from gas turbines with Exhaust Gas Recycle. International Journal of Greenhouse Gas Control, 47, 137-150.

Bui, M., Gunawan, I., Verheyen, V., Feron, P., Meuleman, E. and Adeloju, S. (2015). Dynamic modelling and optimisation of flexible operation in post-combustion CO2 capture plants – a review. Computers and Chemical Engineering, 61, 245-265.

Buschle, W. (2015). Solvent analysis instrumentation options for the control and flexible operation of post combustion carbon dioxide capture plants. PhD thesis, The University of Edinburgh.

Ceccarelli, N., van Leeuwen, M., van Leeuwen, P., Maas, W., Ramos, A., van der Vaart, R. and Wolf, T. (2014). Flexibility of low-CO2 gas power plants: Integration of the CO2 capture unit with CCGT operation. Energy Procedia, 63, 1703-1726.

Chalmers, H., Leach, M., Lucquiaud, M. and Gibbins, J. (2009). Valuing flexible operation of power plants with CO2 capture. Energy Procedia, 1, 4289-4296.

Davison, J. (2006). Performance and costs of power plants with capture and storage of CO2. Energy, 32, 1163-1176.

Department for Energy and Climate Change and Parsons Brinckerhoff. 2014. Technical Assessment of the Operation of Coal & Gas Fired Plants. Retrieved from https://www.gov.uk/government/uploads/system/uploads/attachment_data/file/387566/Technical_Assessment_of_the_Operation_of_Coal_and_Gas_Plant_PB_Power_FIN....pdf

Errey, O., Chalmers, H., Lucquiaud, M. and Gibbins, J. (2014). Valuing responsive operation of post-combustion CCS power plants in low carbon electricity markets. Energy Procedia, 63, 7471-7484.

Flø, N.E.,Kvamsdal, H.M. and Hillestad, M. (2016). Dynamic simulation of post-combustion CO2 capture for flexible operation of the Brindisi pilot plant. International Journal of Greenhouse Gas Control, 48, 204-215.

Haines, M.R. and Davison, J. (2014). Enhancing dynamic response of power plant with post-combustion capture using "Stripper stop". International Journal of Greenhouse Gas Control, 20, 49-56.

IPCC (2014). Climate Change 2014: Fifth Assessment Report of the Intergovernmental Panel on Climate Change. Cambridge University Press: Cambridge, UK

International Energy Agency (2015). World Energy Outlook 2015. OECD/IEA: Paris,France.

Lawal, A., Wang, M., Stephenson, P. Koumpouras, G. and Yeung, H. (2010). Dynamic modelling and analysis of post-combustion CO2 chemical absorption process for coal-fired power plants. Fuel, 89, 2791-2801.

Lucquiaud, M., Chalmers, H. and Gibbins, J. (2009). Capture-ready supercritical coal-fired power plants and flexible post-combustion CO2 capture. Energy Procedia, 1, 1411-1418.

Luu, M.T., Manaf, N.A. and Abbas, A. (2015). Dynamic modelling and control strategies for flexible operation of amine-based post-combustion CO2 capture systems. International Journal of Greenhouse Gas Control, 39, 377-389.

Mac Dowell, N. and Staffell, I. (2016). The role of flexible CCS in the UK's future energy system. International Journal of Greenhouse Gas Control, 48, 327-344.

Mac Dowell, N. and Shah, N. (2014). Optimisation of post-combustion CO2 capture for flexible operation. Energy Procedia, 63, 1525-1535.

Mangiaracinaa A., Zangrillib L., Robinsonc L.*, Kvamsdald H.M., Van Ose P. (2014). OCTAVIUS: Evaluation of flexibility and operability of amine based post combustion CO2 capture at the Brindisi Pilot Plant, Energy Procedia 63 (2014) 1617 – 1636.

Mechleri, E. (2015). Controllability analysis of a post-combustion CO2 capture plant integrated with a coal and natural gas-fired power plan. 3rd Post Combustion Capture Conference,9th September 2015, Regina, Canada.

National Energy Technology Laboratory (2013, September 2013), Cost and Performance Baseline for Fossil Energy Plants Volume 1: Bituminous Coal and Natural Gas to Electricity, retrieved from: http://www.netl.doe.gov/File%20Library/Research/Energy%20Analysis/OE/BitBase_FinRep_Rev2a-3_20130919_1.pdf

Partnership to Advance Clean Energy (2014, February 2014), Best Practices Manual for Indian Supercritical Plants, retrieved from: http://www.pace-d.com/wp-content/uploads/2013/03/BP-MANUAL-FOR-PRINTING.pdf

Tait, P, Buschle, W, Ausner, I, Wehrli, M, Valluri, P and Lucquiaud, M. (2016). A pilot-scale study of dynamic response scenarios for the flexible operation of post-combustion CO2 capture. International Journal of Greenhouse Gas Control, 216-233.

van Eckeveld, A. C., van der Ham, L. V., Geers, L. F. G., van den Broeke, L. J. P., Boersma, B. J. & Goetheer, E. L. V. (2014). Online monitoring of the solvent and absorbed acid gas concentration in a CO2 capture process using monoethanolamine. Industrial & Engineering Chemistry Research, 53, 5515-5523.

Wonder, D.K., Blake, R.J., Fager, J.H. and Tierney, J.V. (1959). An Approach to Monoethanolamine Solution Control: Chemical Analysis and its Interpretation. In Laurance Reid Gas Conditioning Conference. Norman, Oklahoma, USA, pp. 42–59.

7. Scale-up of a post-combustion capture facility

7.1 Introduction

The pilot-scale test campaigns described in chapters 5 and 6 provide useful insight into how post-combustion CO_2 capture facilities may respond to changing plant output. To come to meaningful conclusions about the effect of these operations for a full-size capture facility it is necessary to scale up the generation and capture plant, mathematically.

This chapter considers how plant construction and operating specifications for a full-scale capture plant affect solvent circulation times and hence, the response of the plant to changes in reboiler heat input. The two pilot-scale test campaigns indicate that for a flexibly operating CCS plant, having a short circulation time between the desorber outlet and absorber inlet may be beneficial or detrimental to minimising emissions depending on the type of dynamic scenario.

- In a scenario in which the plant operator provides primary reserve power to the grid via redirection of reboiler steam to the low-pressure (LP) turbine (section 5.4.4 for gas, section 6.4.3 for coal), it is beneficial to have a large total solvent inventory with long circulation times between the reboiler outlet and absorber inlet. This ensures there is always a large reserve of lean solvent which can continue to capture CO_2 and avoid a spike in emissions while the reboiler is un-operational.
- Conversely, in hot startup events (section 5.4.1 for gas, sections 6.4.1.2 and 6.4.2.2 for coal) it is beneficial to have a small lean solvent inventory resulting in a short circulation time between reboiler outlet and absorber inlet. Lean solvent can reach the absorber inlet more rapidly after the flow of steam is introduced, ensuring that the plant can rapidly return to baseload operating conditions and minimising the additional emissions associated with plant startup.

The case of a gas-fired power station equipped with CCS is considered. State-of-the-art NGCC plants can provide rapid hot start-up capability and as such are the preferred option for future energy generation portfolios which contain a significant proportion of intermittent renewables. When equipped with CCS these plants are also well suited to provide, via adjustment of steam flow to the reboiler, fast reserve power for a duration of up to 15 minutes, primary frequency response for a duration of up to 20 seconds, or secondary frequency response for a duration of up to 30 minutes.

An authoritative study on the design of the recently-cancelled Peterhead capture plant has been released to the public domain as part of the UK government's CCS knowledge sharing programme (Shell UK Ltd., 2015a; Shell UK Ltd., 2015b). The Front End Engineering Design (FEED) study for this facility, designed to capture 90% of emissions from a 385MW NGCC plant is used to scale-up the absorber, desorber, sumps and pipework to full size. Assumptions are made where certain construction details are unavailable. The effect of plant design features which are likely to affect dynamic operation are considered for both a bespoke new-build plant and a retrofit where planning considerations may require the capture facility to be located some considerable distance from the generation plant.

While the work presented in this chapter is based on a number of estimates and assumptions, it aims to provide guidelines and highlight the issues which should be considered by those involved in the planning, design, operation and construction of flexible post-combustion capture facilities.

7.2 Sizing of CO_2 capture facility

The engineering design package and equipment list for the Peterhead power station CCS project (Shell UK Ltd., 2015a & 2015b) provides details of the majority of process equipment used in construction. The basic layout of the plant is similar to that of the Sulzer facility described in Chapter 5, with a conventional reboiler and large lean solvent tank situated between the reboiler outlet and absorber inlet. As discussed later in this chapter, the volume of solvent contained in this tank will affect solvent circulation times and hence, the response of the plant to dynamic operations. Figures 7.1 provides an overview of the retrofitted capture plant layout relative to the generation facility.

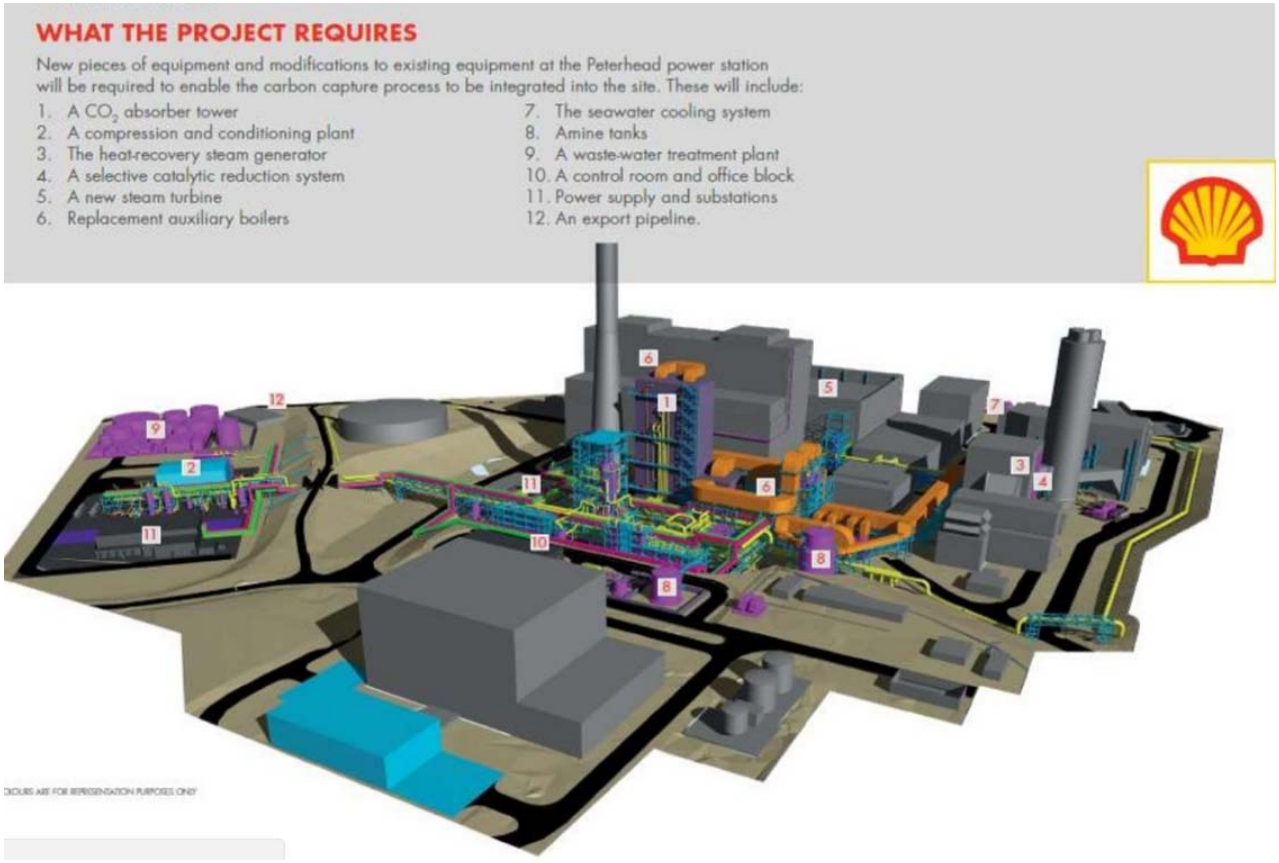

Figure 7.1 Proposed layout of the retrofitted PCC plant at Peterhead Power Station (Spence, 2015)

This section details the sizing of equipment including absorber, desorber, sumps, pipework and lean solvent storage tank for a plant of this scale. These are used to calculate the volume of total solvent inventory, total circulation time and crucially, the circulation time between desorber inlet and outlet. Two cases are considered

7.2.1 Flue gas flow and composition

The composition and flow rate of flue gas after passing through the direct contact cooler (i.e., at the absorber flue gas inlet) are provided in Table 7.1.

Plant Variable	Value	Units
Flue gas throughput after Direct Contact Cooler (DCC)	663	kg/s
Flue gas CO_2 concentration (vol/vol)	3.97	%
Flue gas H_2O concentration (vol/vol)	3.98	%
Flue gas O_2 concentration (vol/vol)	13.32	%
Flue gas N_2 concentration (vol/vol)	77.79	%
Flue gas Ar_2 concentration (vol/vol)	0.94	%
Flue gas CO_2 throughput	40.092	kg/s
CO_2 capture rate	90	%

Table 7.1 Flue gas and capture rate specifications

As composition data for flue gas composition at part-load are not provided it is assumed that the composition remains constant regardless of current plant output. As in the pilot-scale test campaigns described in chapters 5 and 6, the flue gas flow rate is approximated as being directly proportional to generation plant output.

7.2.2 Absorber, desorber and packing dimensions

The volume of absorber and desorber packing must be known for the estimation of solvent holdup in the absorber/desorber and hence, the total solvent circulation time. The proposed plant at Peterhead uses a proprietary solvent which has unknown kinetics and solvent capacity, so the absorber and desorber dimensions provided may not be suitable for 90% capture with 30%w/w MEA. A case study described by Herraiz (2016) is used to provide realistic packing dimensions for a full-scale capture plant on NGCC flue gas using 30%wt MEA. The absorber of this plant contains two packed beds of Sulzer Mellapak 250Y packing, each with a volume of 4190m^3, to achieve a 90% capture rate from a flue gas flow of 658kg/s. These values are used to scale the total packing volume required for a plant with flue gas flow 663kg/s.

$$Absorber\ Packing\ Volume = \frac{663\ kg/s}{658\ kg/s} \cdot 2 \cdot 4190m^3 \tag{7.1}$$

The estimated packing volume required, based on the dimensions of Herraiz and the relative gas mass flowrates is 8444m^3. The packing volume is then increased by a further 10% as a fail-safe against under-sizing, bringing the total packing volume to 9288m^3. Mass flow rates of gas are similar for both cases, so the packing diameter of Herraiz, 12.0m, can be maintained. The total height of the packed bed is therefore 82.17m, or 82.2m approximately.

Sizing of desorber packing volume is based on a 1st-order approximation, the ratio of desorber to absorber volume at the proposed Peterhead plant. This ratio is used as a scaling factor to determine desorber packing dimensions for a capture plant with absorber packing volume 9288m^3. Consider also that the absorber contains a water wash section above the packed bed, and that this may take up around 30% of the total absorber height. From equation 7.2, the scaling factor is 0.059

$$Scaling\ Factor = \frac{H_{des} \cdot W_{des} \cdot L_{des}}{70\% \cdot H_{abs} \cdot W_{abs} \cdot L_{abs}} = \frac{34.6m \cdot 5.4m \cdot 6m}{70\% \cdot 64.25m \cdot 29m \cdot 14.5m} = 0.059 \tag{7.2}$$

$$Desorber\ Packing\ Volume = 0.059 \cdot 9288m^3 \tag{7.3}$$

The total volume of packing in the desorber is estimated to be 548m^3. Desorber packing dimensions are approx. 6.40m in diameter and 17m in height.

In addition to the packing volume the desorber will contain some solvent inventory in the reboiler itself. The design documents for the Peterhead project describe six heat exchangers working in parallel, with dimensions 3.166m x 1.5m x 2.59m. Each reboiler is a heat exchanger, with the total volume split approximately halfway between hot fluid (steam) and cool fluid (solvent) The total volume of solvent in the six reboilers is therefore 36.9m^3.

There is also a significant volume of solvent present in the absorber and desorber sumps, but these are discussed in the following section as they are sensitive to the baseload solvent flow rate. Absorber and desorber dimensions are provided in table 7.2.

Absorber Dimension	**Value**	**Units**
Absorber Packing Height	82.2	m
Absorber Packing Diameter	12.0	m
Absorber Packing Volume	9288	m^3
Desorber Dimension	**Value**	**Units**
Desorber Packing Height	17.0	m
Desorber Packing Diameter	6.40	m
Desorber Packing Volume	548	m^3
Reboiler Volume	6.15 (6x)	m^3

Table 7.2 Absorber and Desorber dimensions

7.2.3 Sizing of solvent pumps and sumps

To come to valid conclusions about plant response at full scale using the experimental data obtained at the Sulzer pilot the same absorbing solvent, 30%wt MEA, must be considered in the scaled-up plant. Literature values for optimum L/G flow ratio for 30% w/w MEA on NGCC flue gas range between 1.0 to 1.47 kg_{solv}/kg_{gas} (Rezazadeh et al., 2015; Gonzalez Diaz, 2016). For consistency with the calculated volume of packing in the absorber, the value of 1.29kg/kg as used by Herraiz (2016) is selected for this work.

$$Q_{solv} = \frac{m_{gas} \cdot 1.29 kg/kg}{\rho_{MEA,30\%wt}} = 3.052 \times 10^3 \, \frac{m^3}{hr} \tag{7.4}$$

Where Q_{solv} is the baseload volumetric flow rate of solvent, m_{gas} is the mass flowrate of gas at the absorber inlet and $\rho_{MEA,30\%wt}$ is the density of MEA solution at 40°C. This baseload flowrate can be used to determine solvent circulation times between critical plant locations as a function of solvent inventory.

The equipment list for the proposed Peterhead capture plant specifies that pump flow output can be increased from baseload flow by up to 10% if necessary (Shell UK Ltd., 2015b). Solvent pumps for the scaled-up facility are rated at a maximum volumetric flow rate ($Q_{solv,max}$) which is 10% greater than that of baseload, 3.357x10^3 m^3/hr. Three main pumps circulate solvent through the facility; one at the absorber outlet, one at the desorber outlet and one at the outlet of the main solvent tank. A simplified PFD of the solvent circulation loop is shown in figure 7.2.

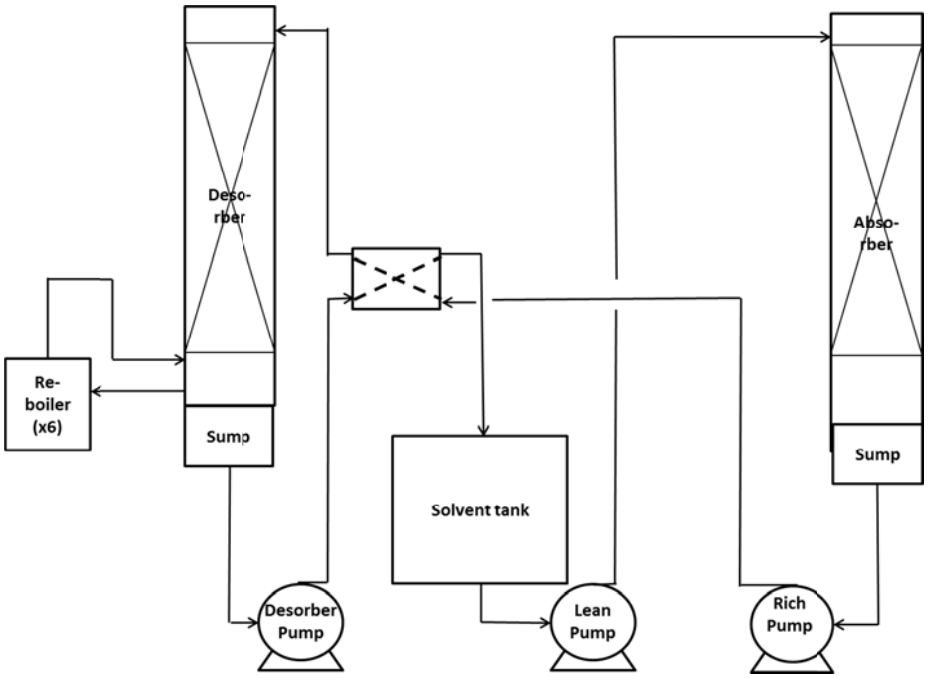

Figure 7.2 Simplified PFD of solvent circulation loop

To protect the pumps and avoid cavitation a certain volume of solvent, the net positive suction head, must remain upstream of the pump inlet. This is used to determine the minimum safe working volume of sumps and solvent tanks. In the absence of detailed pump specifications, and dimensions and configuration of pipework required to calculate the minimum suction head, a rule of thumb based on pilot plant operations can be used.

At the UKCCSRC PACT pilot facility described in Chapter 6, pumps are protected by a level sensor which will trip and stop all plant operations if the absorber liquid level falls below a certain point. At a baseload flow setpoint of 1000l/min, the volume of solvent in the absorber sump and pipework upstream of the rich pump inlet is maintained at around 70l. This provides sufficient head to avoid tripping the plant in the event of small disturbances in flow rate. At baseload flowrate, the pump requires 4.2min to run the absorber sump and pipework's reserve of solvent completely dry. This figure of 4.2min worth of head at normal flow conditions can be used as a metric to determine the operating sump volume for the scaled-up plant.

The operating volume of head for the scaled-up plant is determined by multiplying the volumetric flow rate by what is determined to be a "safe" duration before the pump runs dry. To account for potential situations in which the pumps may be operating at their maximum output, $Q_{solv,max}$ ($3.357x10^3$ m^3/hr) is used as an operating. The pipework of the scaled-up capture plant is likely to be considerably more complex than that of a pilot-scale facility, so to account for potential pressure losses due to friction an additional 20% is added to the "safe" time, increasing it to 5 minutes. The operating volume of absorber and desorber sumps is calculated by equation 7.5.

$$SumpVol = \frac{Q_{solv,max} \cdot 5min}{60min/hr} = 297.7m^3 \quad (7.5)$$

The volume of the lean solvent tank is variable, but should also contain at least $297.7m^3$ of solvent during operation to protect the feed pump to the absorber.

7.2.4 Sizing of pipework

Pipe diameters are sized based on a personal email conversation with an engineer involved with the design of the Ferrybridge CCPilot 100+ project, which used 30% MEA as the absorbing solvent for a significant proportion of its operating life (Hume, 2017). Pipework dimensions at CCPilot were based on solvent velocity, a similar approach to that used for water and steam systems. A velocity of 2m/s at maximum pump output was selected to minimise frictional erosion or corrosion of the pipework.

$$A_{pipe} = \frac{Q_{solv,max}}{2m/s \cdot 3600\ sec/hr} = 0.466m^2 \quad (7.6)$$

$$D_{pipe} = \sqrt{\frac{4A_{pipe}}{\pi}} = 0.77m \quad (7.7)$$

In which A_{pipe} is the cross-sectional area of the pipework and D_{pipe} is its inner diameter. The length of pipework will vary depending on planning considerations. For example, the planning permission document for the Peterhead retrofit shows a fairly compact site, with absorber, desorber and solvent tank all in close proximity to each other (Aberdeenshire Council Infrastructure Services, 2015). The absorber and desorber in this case require around 90m and 40m of pipework to transport solvent from ground level to their respective inlets. A rough estimate of approx. 40m of additional ground-level pipework connecting absorber outlet to desorber inlet, and 40m connecting the desorber outlet to absorber inlet can be made based on the area of the capture plant construction site. Shorter pipework lengths between plant locations are beneficial for rapid plant response to changes in reboiler steam supply, as circulation times are reduced.

However, not all CO_2 capture facilities will be so compact. The absorber and desorber may be a significant distance apart depending on the availability of space, or planning regulations. Cases in which the length of pipework between absorber outlet to desorber inlet (and vice versa) are varied between 40m up to 500m are considered to observe the potential effect on solvent circulation times.

Plant Variable	Value	Units
Solvent mass flow rate	885.3	kg/s
Solvent volumetric flow rate	0.8476	m^3/s
Absorber sump operating volume	297.7	m^3
Desorber sump operating volume	297.7	m^3
Minimum lean solvent tank operating volume	297.7	m^3
Solvent pipe diameter	0.466	m
Maximum solvent velocity in pipework	2.0	m/s

Case 1 – Compact capture plant		
Total pipework length (absorber outlet – desorber inlet)	40 (vertical) + 40 (horizontal)	m
Total pipework length (desorber outlet – absorber inlet)	90 (vertical) + 40 (horizontal)	m
Case 2 – Non-compact capture plant		
Total pipework length (absorber outlet – desorber inlet)	40 (vertical) + up to 500 (horizontal)	m
Total pipework length (desorber outlet – absorber inlet)	90 (vertical) + up to 500 (horizontal)	m

Table 7.3a Shared pump, sump and flow specifications for compact and non-compact plant
Table7.3b Pipework lengths for compact and non-compact capture plant

Section 7.3 investigates the effect of varying pipework length and solvent tank operating volume on solvent circulation times between key plant locations.

7.3 Solvent inventory and circulation times

Circulation times between plant locations are determined based on the solvent inventory. The most important of these for dynamic operation is the circulation time between the desorber outlet and absorber inlet, as this will determine:

- How rapidly the CO_2 capture rate is affected by changes in steam flow to the reboiler.
- The total lean solvent inventory available to continue capturing CO_2 in the event of a reboiler steam shutdown event.

In this section the total non-variable solvent inventory of the plant is calculated. This is used to determine the circulation time of solvent through the absorber, desorber, sumps, and pipework for a compact capture facility plant with short lengths of connecting pipework. Solvent circulation time is then plotted as a function of pipework length to determine how dynamic operations may affect a capture facility for which compact construction is not an option.

7.3.1 Non-variable solvent inventory

In the case of the compact capture plant, whether new-build or retrofitted, it is assumed that 40m of horizontal pipework connect the absorber inlet to desorber outlet and vice versa. 90m of vertical pipework is required to reach the top of the absorber, and 40m to reach the top of the desorber. Solvent inventory in pipework is calculated via equation 7.8.

$$I_{pipe} = L_{pipe} \cdot A_{pipe} \tag{7.8}$$

Working solvent inventory in absorber and desorber sumps are equivalent to 5mins of the maximum output of solvent pumps. Solvent inventory in the six parallel reboilers is assumed to be the total of their internal dimensions on the cool fluid (solvent) side.

7.3.2 Absorber and Desorber packing holdup

The total volume of packing in the absorber and desorber is 9288m^3 and 548m^3, respectively. To estimate the solvent holdup on the packing and hence, the circulation time from inlet to the top of the respective sump, experimental data are taken from literature and used to define an empirical correlation.

The packing type selected is Sulzer Mellapak 250Y, which has similar corrugation angle and specific surface area in m^2/m^3 to current advanced packings designed specifically for CCS applications. The volume fraction of solvent on a section of packing can be estimated using correlations based on the solvent load. Solvent load is a measurement of the volume of solvent which flows through a cross-sectional area of packing per unit of time, and in general has units of $m^3_{solvent}/m^2_{packing}$.hr. For the scaled-up plant, the cross sectional area of the absorber and desorber packed bed are known, as is the baseload flow rate of solvent.

Measurements of solvent volume fraction as a function of solvent load are taken from datasets based on X-ray tomography (Green et al., 2007), Neutron radiography (Basden et al., 2013) and gravimetric measurements (Basden et al., 2013). The linear correlation obtained from these data points is shown in figure 7.3.

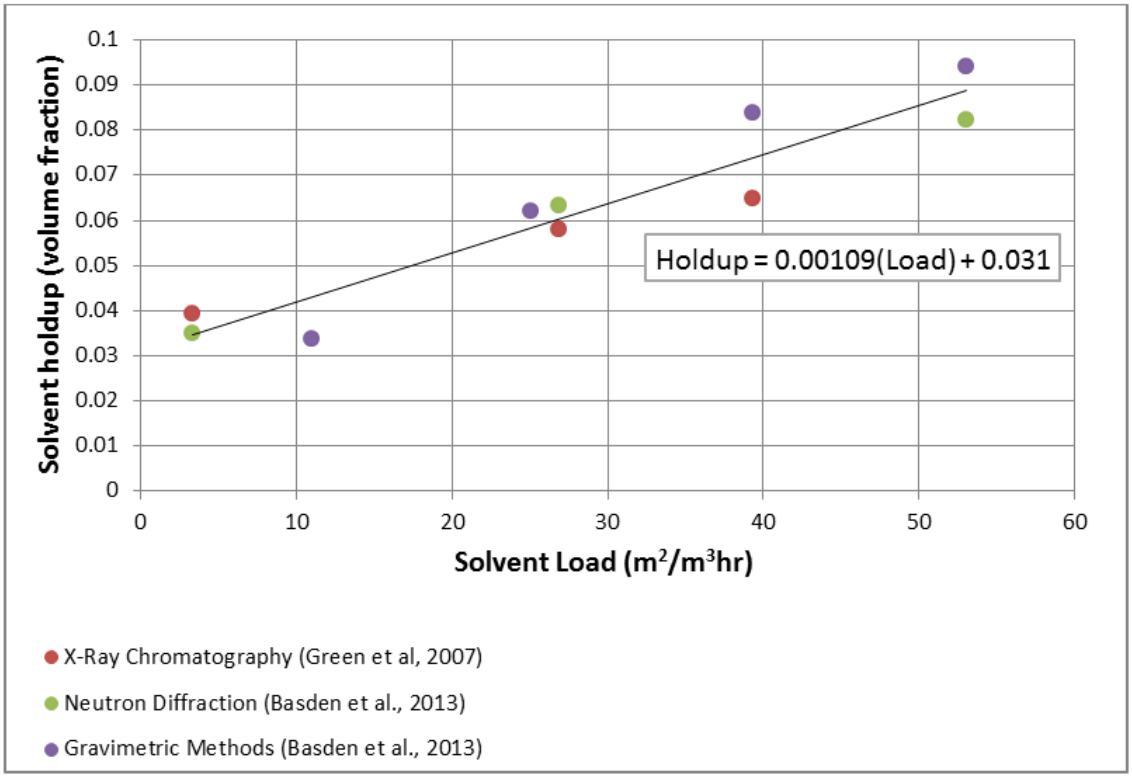

Figure 7.3 Solvent holdup vs Solvent load for Sulzer Mellapak 250Y structured packing

$$Holdup = (0.00109 \cdot Load) + 0.031 \tag{7.9}$$

Solvent load for absorber and desorber are calculated as follows:

$$Load = \frac{Q_{solv}}{A_{packing}} \tag{7.10}$$

In which $A_{packing}$ is the cross-sectional area of the packed bed (absorber = 113m^3, desorber = 32.4m^3) and Q_{solv} is the baseload solvent flowrate (3052m^3/hr). At baseload flow conditions, the absorber solvent load is 27.0 m^3/m^{2}hr while the desorber load is 94.2 m^3/m^{2}hr.

The empirical correlation yields values of 560.6m^3 of holdup in the absorber packing, and 149.6m^3 of holdup in the desorber packing. The total non-variable solvent inventory for a compact capture plant is summarised in table 7.4.

Section of plant	Solvent Inventory (m^3)
Absorber sump	297.7
Desorber sump	297.7
Absorber packing holdup	560.6
Desorber packing holdup	149.6
Lean solvent pipework	60.6
Rich solvent pipework	37.3
Reboilers	12.3 (x6)

Table 7.4 Non-variable solvent inventory for compact post-combustion capture plant

7.3.3 Working lean solvent tank inventory for a compact PCC plant

The designer of the CO_2 capture plant has a degree of freedom in the sizing of the working inventory of the lean solvent tank which is located in the lean solvent line, downstream of the lean/rich heat exchanger (figure 7.2). This can be modified to achieve the desired solvent lean solvent inventory of the plant.

The circulation time of lean solvent inventory, from reboiler outlet to absorber inlet, can be calculated by dividing the total volume lean solvent inventory by volumetric solvent flowrate as in equation 7.11, while the total solvent circulation time is determined using equation 7.12. Note that the solvent inventory of only one reboiler (6.15m^3) is included in the calculation, as the six of them work in parallel.

$$CircTime_{Lean} = \frac{I_{DesSump}+I_{LeanPipe}+I_{LeanTank}}{Q_{solv}} \quad (7.11)$$

$$CircTime_{Total} = \frac{I_{DesSump}+I_{LeanPipe}+I_{LeanTank}+I_{AbsPacking}+I_{AbsSump}+I_{RichPipe}+I_{DesPacking}+\frac{I_{Reb}}{6}}{Q_{solv}} \quad (7.12)$$

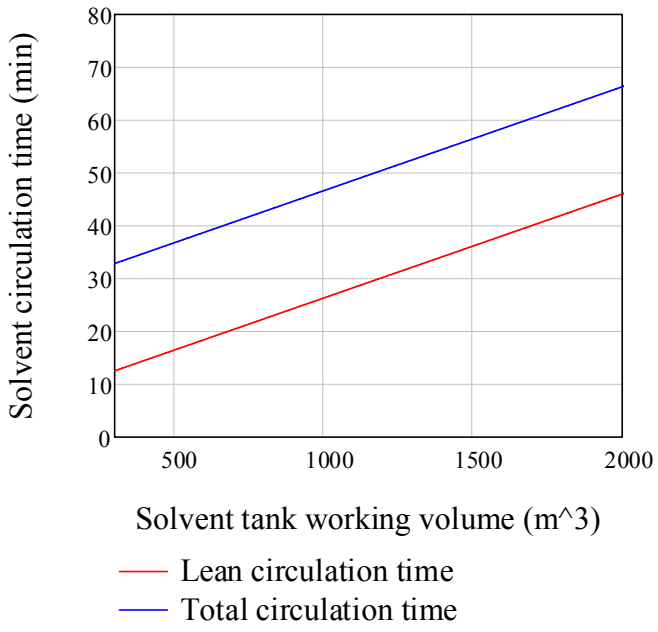

Figure 7.4 Sensitivity analysis of total and lean solvent circulation times as a function of solvent tank working volume

In a working CO_2 capture facility it is unlikely that the working inventory of the lean solvent tank will be the safe minimum of 297.7m^3. A lean solvent circulation time of approx. 30min can allow the plant operator to continue capturing CO_2 for the duration of a short reboiler steam decoupling event, for example, for the provision of secondary frequency response, without seriously compromising flexibility. Solving equation 7.11 for a target lean solvent circulation time of 30mins yields a lean solvent tank working inventory of 1185m^3. The total solvent circulation time for the compact capture plant, with a lean solvent circulation time of 30min, is 50min 18sec.

7.3.4 Influence of pipework length

Longer horizontal distances between the absorber and desorber appear intuitively to have a detrimental effect on plant response to dynamic operations. Increased pipework length as a result of planning and construction constraints could significantly increase the lean solvent circulation time.

While the working volume of solvent in sumps and pipework cannot be changed, plant operators have a degree of freedom in the working inventory of the main solvent tank, down to a minimum of 297.7m^3. Mitigation of increased lean circulation times due to longer pipework length could be achieved via reduction of the working solvent inventory in the lean solvent tank. To quantify the delay incurred by increasing pipework length and to determine if mitigation of this type is necessary and/or possible, lean circulation time is plotted as a function of desorber outlet > absorber inlet pipework length for a range of solvent tank working volumes (figure 7.5).

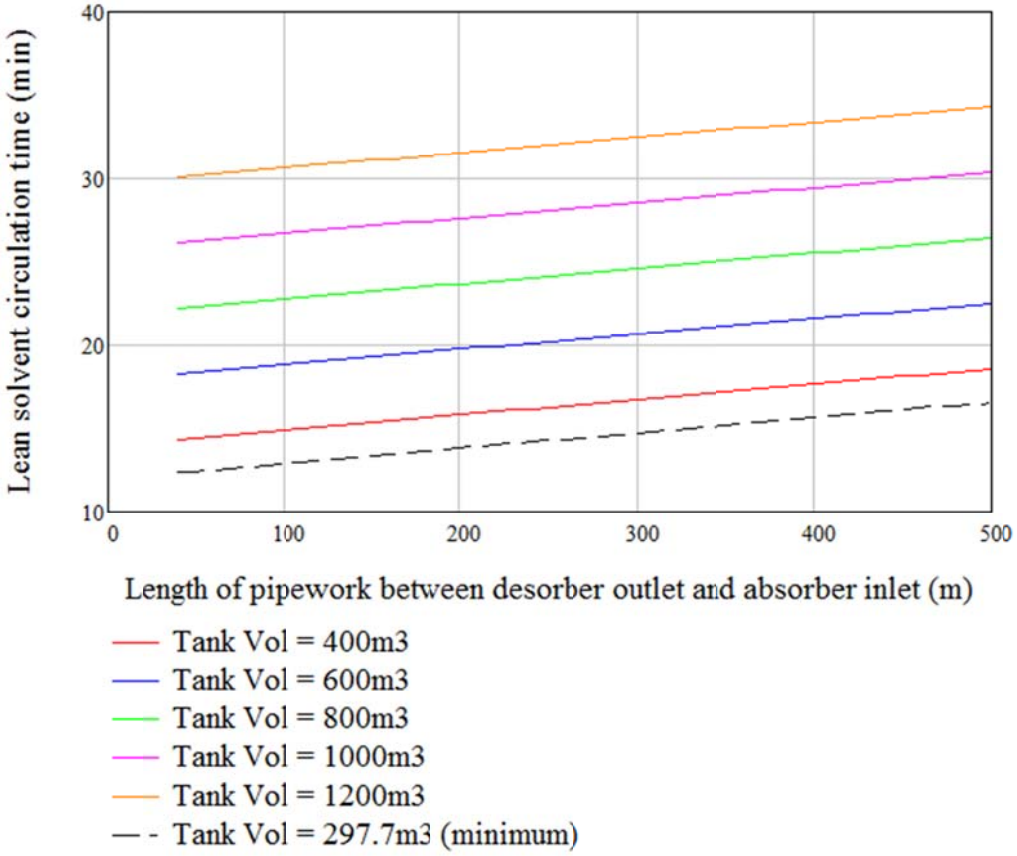

Figure 7.5 Effect of pipework length on lean solvent circulation time

Even in the most extreme case in which the desorber and absorber are located 500m apart, the resulting additional time is only 4mins 13sec. This is also a case in which the solvent velocity is limited to 2m/s, so if plant designers are confident that frictional erosion of the pipework will not occur, the velocity could be increased up to 4m/s, further diminishing the significance of additional pipework length. The bottom trace in chart 7.5, for the minimum lean solvent tank inventory, shows that even with 500m of lean solvent pipework the lean circulation time could be as short as 16min 30sec, allowing capture plant designers and operators considerable freedom in selecting a working lean solvent inventory which best suits the generation plant's probable dispatch pattern. By these metrics, a retrofitted, non-compact capture facility should suffer no greater barriers to flexible operation than a bespoke new-build.

7.4 Impact of plant design on CO_2 emissions

In Chapter 6 it is determined that changing the method of capture plant startup for a coal-fired facility can reduce total CO_2 emissions over a 16hr operating shift by up to 18.6%. To determine if startup emissions for PCC on a full-scale NGCC plant are similarly significant, and to determine the effect of changing plant design and solvent circulation times, the total CO_2 released during startup can be quantified.

This section aims to determine the effect of changing the operating solvent tank volume on CO_2 emissions during a hot startup operation. Experimental results from the startup scenario described in Chapter 5 are used to determine the rate of change in CO_2 capture rate during startup. This is used to determine the total CO_2 released during startup, between the gas flow rate being initiated and the CO_2 capture rate returning to 90%. Note that this analysis is based on plant data from a single pilot-scale plant, and is intended only to illustrate the potential scale of monetary and CO_2 costs per startup. Plants which respond differently during startup, e.g. those which have a different rate of change in CO_2 capture rate

7.4.1 Quantifying CO_2 emissions during hot startup

In the absence of a validated, full-scale dynamic plant model, total startup CO_2 emissions are estimated calculated via the scale-up of experimental data. The plant start-up dataset from the pilot-scale facility described in chapter 5 can be used to estimate the rate of change in CO_2 capture rate, and the capture rate response time for a scaled-up test facility following the introduction of steam to the reboiler during a hot start-up event. Several assumptions are made to ensure the comparison is valid and to compensate for errors in the startup procedure which are unrepresentative of real capture plant behaviour.

- Assumption 1: At the beginning of the startup event it is assumed that the solvent inventory has been continuously circulated at low-level following the previous shutdown event (Ceccarelli et al., 2014) to cool down the solvent overnight, resulting in a uniform solvent loading throughout the plant.
- Assumption 2: In the pilot-scale experiment an error was made in which the rich solvent trim heater, intended to mimic the operation of the rich/lean heat exchanger, is not switched on until 60min into the experiment. This results in a delayed capture rate response. CO_2 capture rate begins to increase around 25mins after the trim heater is switched on, which is approximately the lean solvent circulation time of the pilot facility. Therefore, at full scale it is assumed that capture rate begins to increase at after the flow of steam to the reboiler reaches 100% of baseload.
- The trim heater error results in the true CO_2 capture rate response not being observed until after t=60min. The energy provided to the solvent by the desorber steam is approximately 0.75 times that which is provided by the trim heater to raise the temperature of the solvent to 90^{o}C at the desorber inlet. It is reasonable to assume that before the trim heater is switched on the vast majority of the energy provided by the desorber is used as sensible heat, and the amount of CO_2 liberated before the trim heater is switched on is minimal.
- Flue gas and steam flow to the reboiler are based on the gas turbine with rapid start-up capability described by Eisfeld and Feldmuller (2013), as were the pilot-scale experiments.

Plant trends for the pilot-scale experiment are shown in figure 7.6a. As is the case with pilot-scale experiments, gas flow rate is considered to be proportional to the power output of the gas. Liquid flow rate is ramped up at the same rate to maintain a constant L/G ratio. Steam flow is introduced to the plant at t=14min and stabilises at 100% of baseload at t=35min.

Total CO_2 flow at the absorber inlet is assumed to be proportional to the gas flowrate (figure 7.6b).

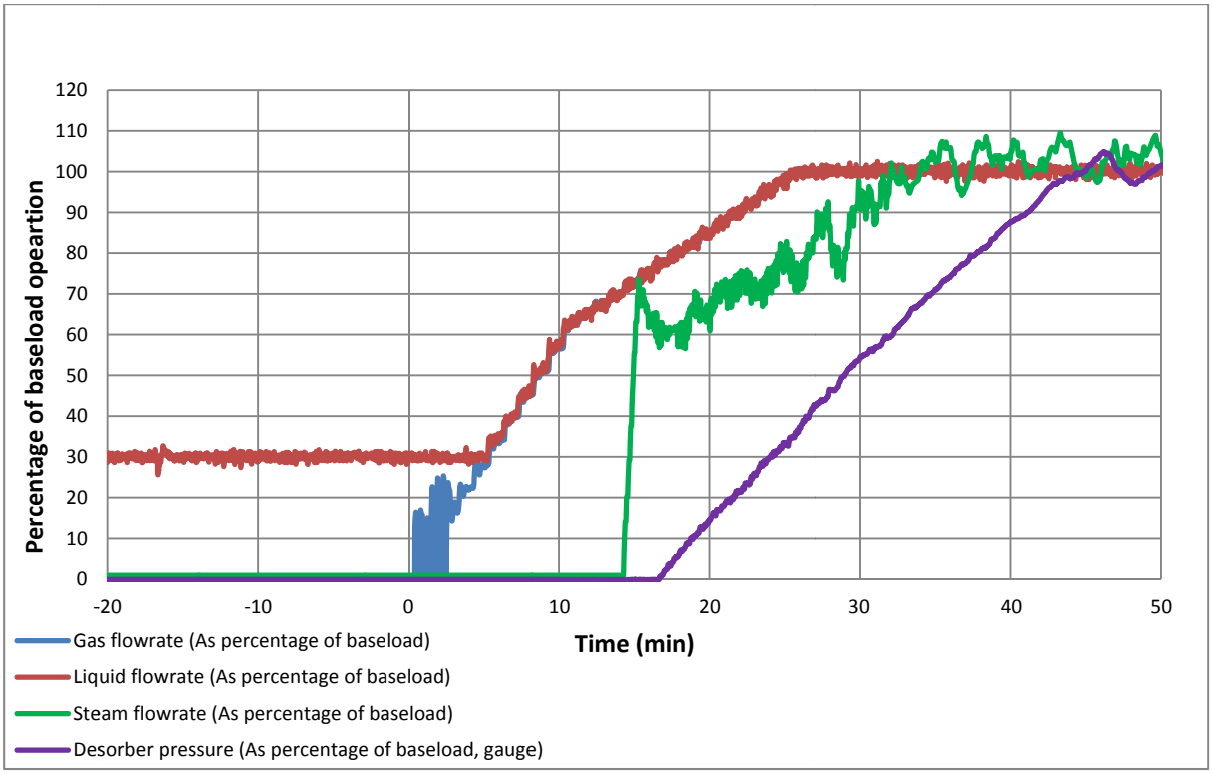

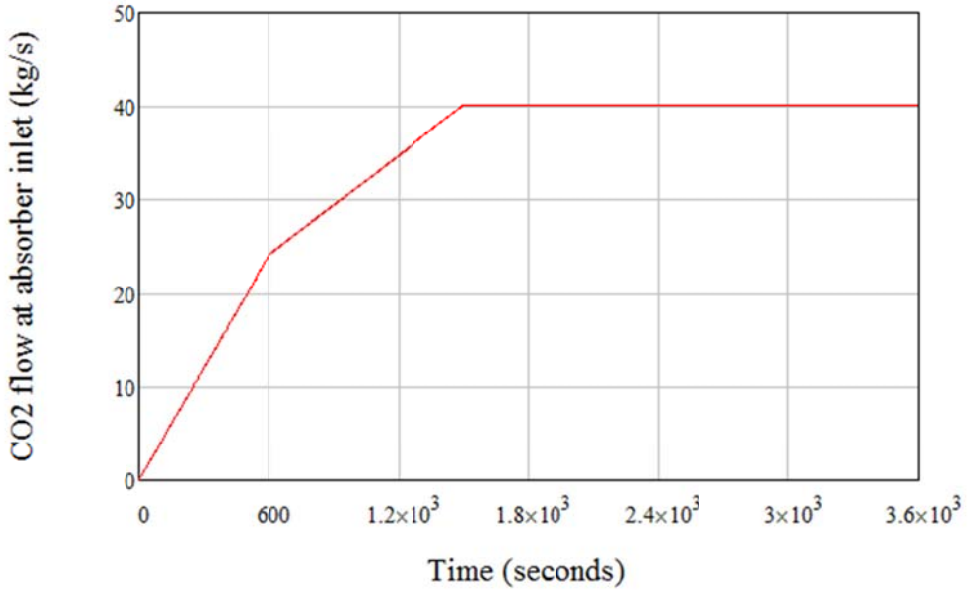

Figure 7.6a Plant trends for pilot plant startup
Figure 7.6 b CO_2 mass flow at absorber inlet as a function of time

The trend in CO_2 capture rate over the course of the startup operation is shown in figure 7.7, steadily decreasing before reaching an inflection point around t=85min, then increasing back to its baseload value. The capture rate trend in the regions before and after the inflection point can be approximated as two linear functions, allowing the rate of change in CO_2 capture rate for each region to be defined.

The time period between t=60min and t=80min, where both trim heater and reboiler are active, is used to approximate the rate of decline in CO_2 capture rate.

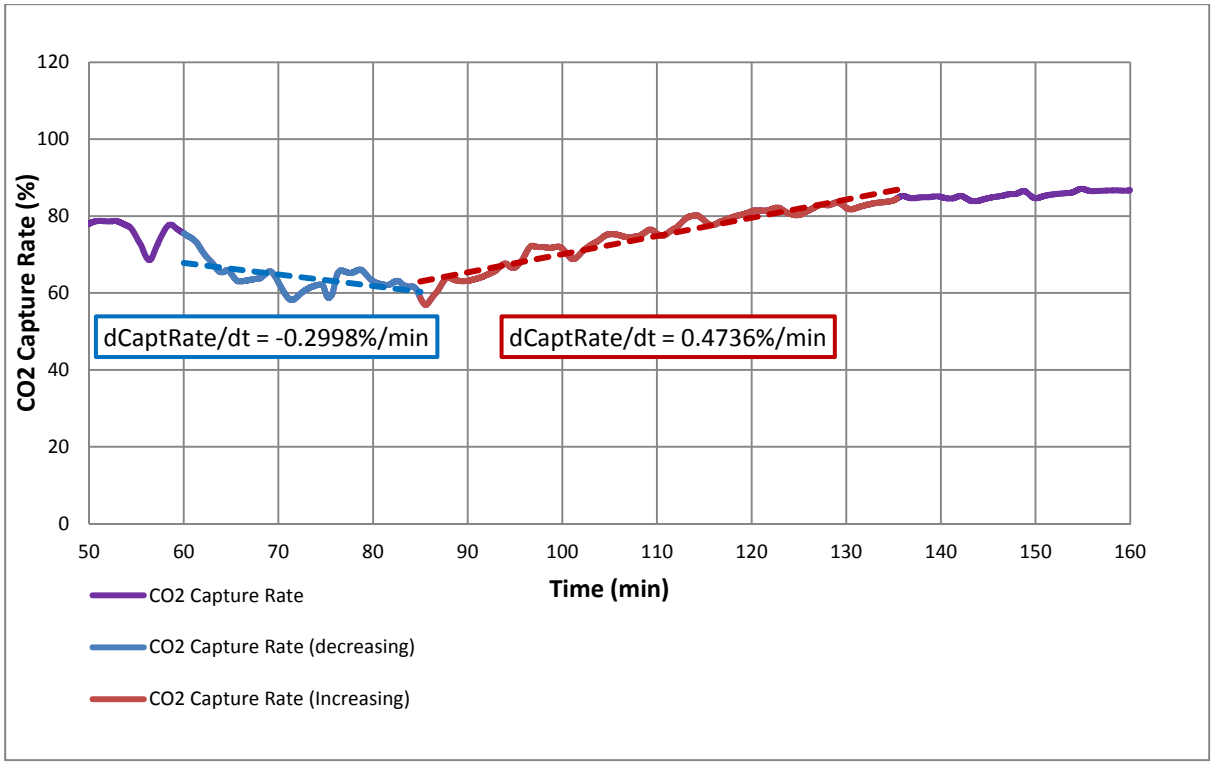

Figure 7.7 CO_2 capture rate trends for increasing and decreasing regions.

The estimated rate of decline in CO_2 capture rate for this case is 0.2998%/min, while the rate of increase after the inflection point is 0.4736%/min. These indicative values are likely to be conservative, as the Sulzer test campaign used low solvent loadings and a relatively high L/G flow ratio, both of which promote high capture rates and a more gradual decrease.

The time of the inflection point is a function of working lean solvent inventory. A generic case is displayed in figure 7.8. If the inflection point, CO_2 flowrate and capture rate as a function of time are known, the total CO_2 emissions before the plant returns to a capture rate of 90% can be determined by integrating over the region defined in figure 7.8.

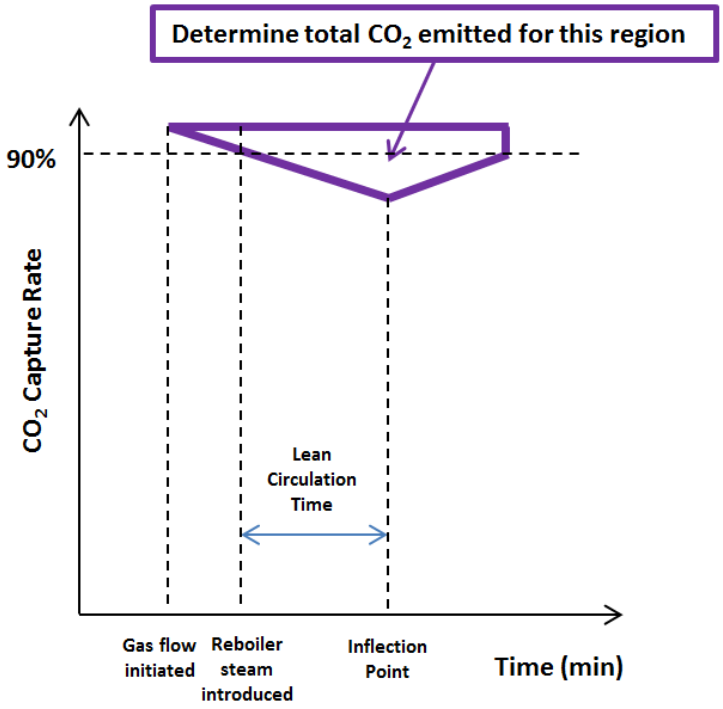

Figure 7.8 Illustration of the region over which the total startup emissions is calculated.

The inflection point is the sum of the lean solvent circulation time and the time at which the flow of steam to the reboiler reaches 100% of baseload. The end point occurs when the CO_2 capture rate reaches 90%. The total mass of CO_2 released before the capture rate returns to 100% can then be calculated via equation 7.13, where η_{CO2} is the CO_2 capture rate, t is time and m_{CO2} is the mass flowrate of CO_2 at time

$$Total\ CO_2 = \int_{t=0}^{t=InfPoint} (1-\eta_{CO2}) m_{CO2} dt + \int_{t=InfPoint}^{t=EndPoint} (1-\eta_{CO2}) m_{CO2} dt \qquad (7.13)$$

7.4.2 Impact of plant design on emissions

Inflection point and endpoint are dependent on lean solvent circulation time and hence, the total volume of working solvent in the lean tank. Using equation 7.11, total CO_2 emissions per startup operation are plotted as a function of working lean solvent tank volume in figure 7.9.

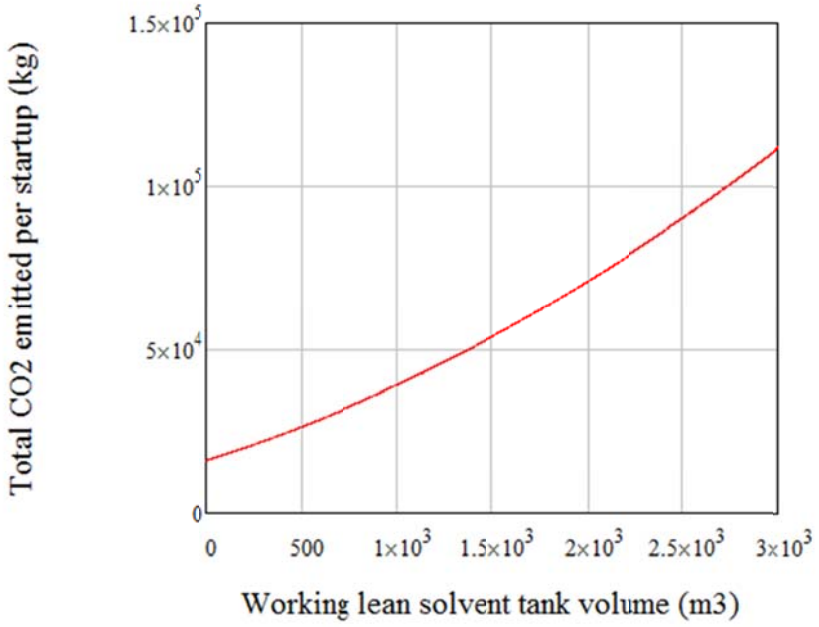

Figure 7.9 Total solvent emissions per startup event as a function of working lean solvent tank volume

Startup CO_2 emissions for a capture plant with an "ideal" lean solvent tank inventory of 1185m^3 and circulation time of 30mins will release a total of 44.53 tCO_2 per startup event, reaching 90% capture after approx 6540s (109min). For the corresponding period of time at baseload operation the capture plant would release 26.22 tCO_2 over this time, so an additional 18.60 tCO_2 is released as a result of each startup operation. If a lean solvent circulation time of 30min is taken to be the ideal situation and this additional 18.60tCO_2 is unavoidable, the additional CO_2 released per startup as a result of deviating from the design point can be calculated via equation 7.14. This is plotted in figure 7.10.

$$\Delta CO_2(TankVol) = TotalCO_2(TankVol) - TotalCO_2(1185m^3) \quad (7.14)$$

Where ΔCO_2 is the additional mass of CO_2 emitted as a result of increasing the working volume of the lean solvent tank.

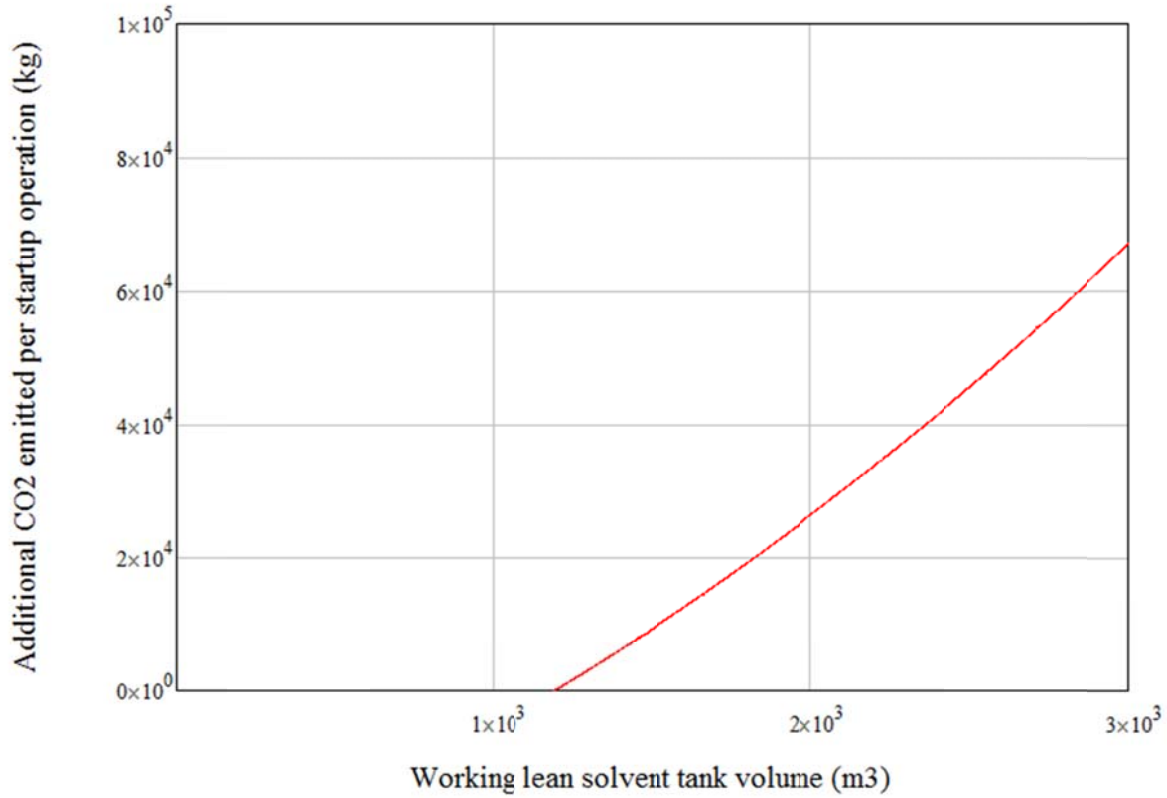

Figure 7.10 Additional CO_2 emitted per startup operation as a function of working lean solvent tank volume

This, however, only considers the startup operation itself. More useful conclusions can be made if the startup operation is considered within the context of a plant operating for a given period of time, then shutting back down again. A typical two-shifting power station will operate for 16 hours between 0600 and 2200 (DECC, 2014). For the purposes of this work two scenarios are considered – that of a two-shifting plant with 1x16hr shift per day, and that of a double two-shifting plant with 2x6hr shifts per day. The total CO_2 released per shift of x hours, as a function of solvent tank volume, can be calculated via equation 7.14. Endpoint is the time at which the CO_2 capture rate reaches 90% following a startup event, m_{CO2} is the mass flowrate of CO_2 and η_{CO2} is the CO_2 capture rate.

$$ShiftCO_2(TankVol) = [(ShiftTime - EndPoint(TankVol))m_{CO2}] + StartupCO_2(TankVol) \quad (7.14)$$

The total CO_2 released per either 16hr or 6hr shift are known, so the additional emissions per startup can be calculated as a percentage of the total emissions per shift. This is plotted in figure 7.12.

$$\Delta CO_{2,\%shift}(TankVol) = \frac{\Delta CO_2(TankVol)\cdot 100}{ShiftCO_2(TankVol)} \quad (7.15)$$

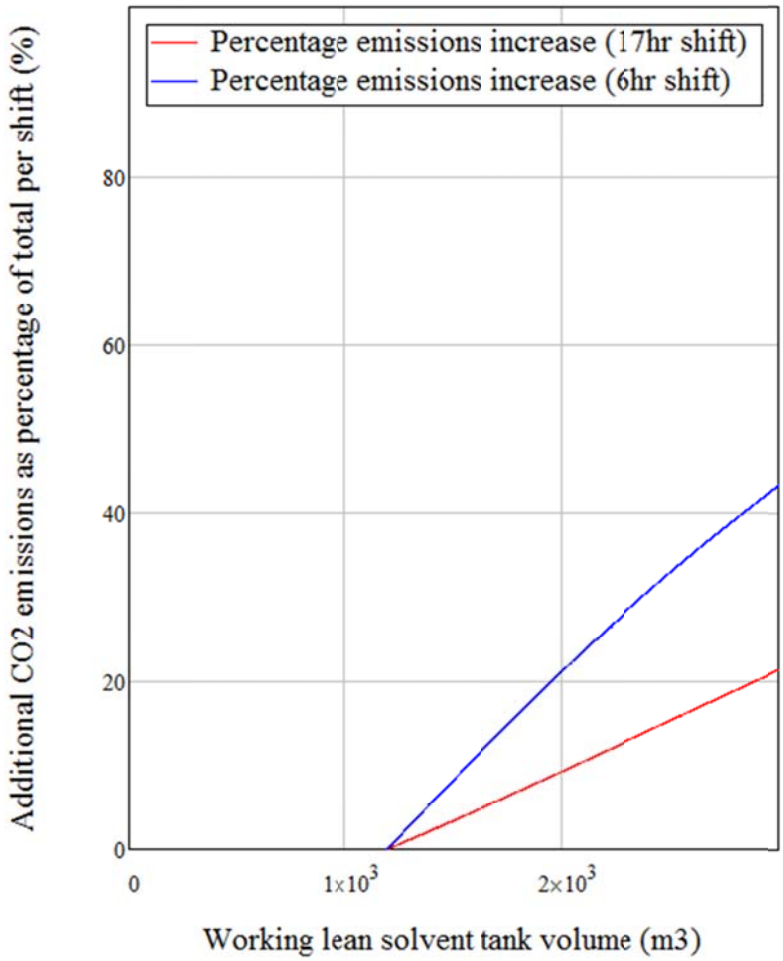

Figure 7.12 Additional percentage CO_2 emissions per shift for a two-shifting and double two-shifting plant

As figure 7.12 shows, the total CO_2 emissions per shift may be increased by up to approx. 20% for a 16hr shift and over 40% for a 6hr shift. It is imperative that the working lean solvent inventory and the associated solvent circulation time be taken into account when designing full-scale flexible CO_2 capture plant. Careful attention must also be paid to the probable mode of operation of the generation plant. To further illustrate this point, the potential additional emissions per year are calculated as a function of the number of daily startup operations.

$$\Delta CO_{2,year}(TankVol) = \Delta CO_2(TankVol) \cdot YearlyStartups \tag{7.16}$$

Where $\Delta CO_{2,year}$ is the total additional mass of CO_2 emitted per year. DECC (2014) estimated the total number of yearly hot start operations for a two-shifting plant to be 200, so the number of hot starts for a double two-shifting plant is estimated to be 400. The impact of increasing lean solvent inventory on total yearly CO_2 emissions could be up to 15000tCO_2 in the two-shifting regime, or 45000tCO_2 in the double two-shifting regime (figure 7.13a).

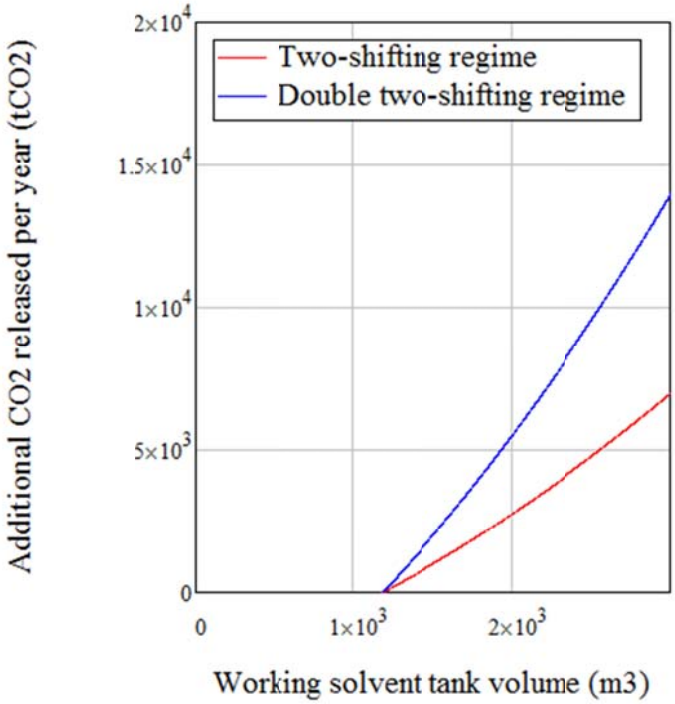

Figure 7.13 Additional yearly CO_2 emissions for two-shifting and double two-shifting regime

To illustrate the potential cost impact of these additional emissions, figure 7.14 shows the additional costs incurred per year as a function of CO_2 emissions costs for the range between £20 and £100. Note that as the scale-up and analysis of the rate of CO_2 capture rate reduction during start-up are based on a number of assumptions, and this is only intended to provide an indication of the order of magnitude of the additional cost incurred by a non-optimised plant.

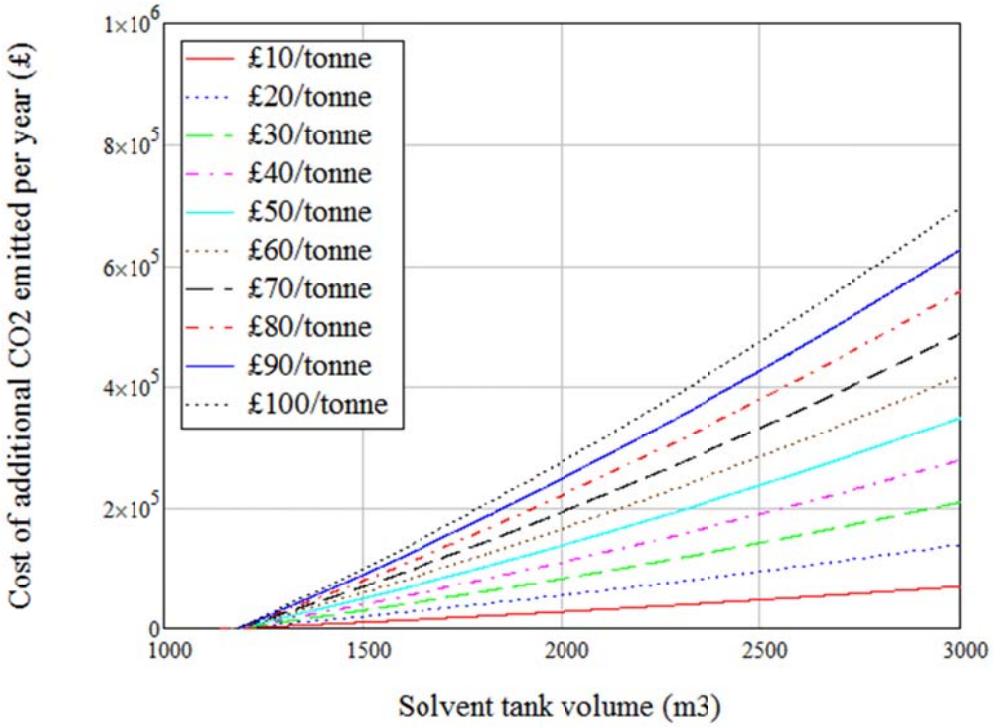

Figure 7.14 Additional yearly CO_2 costs for a plant operating in the two-shifting regime, with 200 start-ups per year

7.5 Conclusions

Lean solvent circulation time strongly affects the mass of CO_2 emitted to atmosphere during dynamic operations and hence, the potential financial penalties associated with CO_2 emissions. The most significant influence on lean solvent circulation time is the working volume of the main solvent tank. Increases in pipework length between desorber and absorber as a potential result of planning constraints are shown to be insignificant, as the working volume of the lean solvent tank can be modified to compensate for any increases in lean circulation time. By this metric, a retrofitted capture facility with planning restrictions on the placing of the absorber and desorber should be able to operate just as flexibly as a compact new-build.

However, the ability to modify lean solvent circulation time and total lean solvent inventory during operation will be useful to the operator of any flexible CO_2 capture facility. With this in mind, two desirable capabilities are proposed.

- Provide plant operators with the ability to modify the volume of solvent in the lean tank in anticipation of future dynamic operations.
- Install a section of pipework between the desorber outlet and absorber inlet which bypasses the lean solvent tank. During a startup event this could allow lean solvent to be introduced to the absorber much more rapidly, or act as a simplified version of solvent storage as proposed by Chalmers et al. (2009)

A circulation time of 30mins between desorber outlet and absorber inlet is selected as a compromise between rapid response to changes in reboiler steam input, and being able to continue to capture CO_2 during a reboiler steam shutdown event. The potential additional emissions costs resulting from increasing the solvent tank volume from this optimum level are significant, and could be of the order of magnitude of hundreds of thousands of pounds over the course of a year.

References

Aberdeenshire Council Infrastructure Services (2015). Full Planning Permission - National for Construction and Operation of a Carbon Capture, Compression and Conditioning Plant at Peterhead Power Station, Boddam, Aberdeenshire, AB423BZ. Aberdeenshire Council: Aberdeen, UK.

Basden M., Elridge, R.B., Farone, J., Feng, E., Hussey, D.S. and Jacobson, D.L. (2013). Liquid holdup profiles in structured packing determined via neutron radiography. *Industrial and Engineering Chemistry Research*, 52, 17263-17269

Ceccarelli, N., van Leeuwen, M., van Leeuwen, P., Maas, W., Ramos, A., van der Vaart, R. and Wolf, T. (2014). Flexibility of low-CO_2 gas power plants: Integration of the CO_2 capture unit with CCGT operation. *Energy Procedia,* 63, 1703-1726.

Chalmers, H., Leach, M., Lucquiaud, M. and Gibbins, J. (2009). Valuing flexible operation of power plants with CO_2 capture. *Energy Procedia,* 1, 4289-4296.

Department for Energy and Climate Change (2014). Technical Assessment of the Operation of Coal & Gas Fired Plants. Department for Energy and Climate Change: London, UK.

Eisfeld, T. and Feldmüller, A. (2013). Fast cycling and Fast Start Capability of Combined Cycle Power Plants with SGT5-4000F Gas Turbines. *IMechE Seminar: Demand Response and Flexible Operation in UK Power Stations,* Nottingham, 28 November 2013.

Gonzalez Diaz, A. (2016). Sequential Supplementary Firing in Natural Gas Combined Cycle Plants with Carbon Capture for Enhanced Oil Recovery. PhD Thesis, The University of Edinburgh.

Green, C.W., Farone, J., Briley, J.K., Elridge, R.B., Ketcham, R.A. and Nightingale, B (2007). Novel application of X-ray computed tomography: Determination of gas/liquid contact area and liquid holdup in structured packing. *Industrial and Engineering Chemistry Research,* 46, 5734-5753.

Herraiz, L.H. (2016). Selective Exhaust Gas Recirculation in Combined Cycle Gas Turbine Power Plants with Post-Combustion Carbon Capture. PhD Thesis, The University of Edinburgh.

Hume, S. (shume@epri.com), 13th July 2017. Question about pump flows and sizes. Email to B. BUSCHLE (b.buschle@ed.ac.uk)

Rezazadeh, F., Gale, W.F., Hughes, K.J. and Pourkashanian, M. (2015). Performance viability of a natural gas fired combined cycle power plant integrated with post-combustion CO_2 capture at part-load and temporary non-capture operations. *International Journal of Greenhouse Gas Control*, 39, 397-406.

Shell UK Ltd (2015). *Peterhead CCS project: Basic Design and Engineering Package*. Department for Business, Energy & Industrial Strategy

Shell UK Ltd (2015). *Peterhead CCS project: Appendices and Equipment List*. Department for Business, Energy & Industrial Strategy.

Spence, B. (2015, May 28th). *The Peterhead CCS Project: An Update*. In Global CCS Institute Webinar Series. Retrieved from https://www.slideshare.net/globalccs/the-shell-peterhead-ccs-project-an-update

Chapter 8. Conclusions and Recommendations for Future Work

8.1 Thesis overview

As established in chapters 1 and 2, CCS as applied to thermal fossil power stations can provide dispatchable low-carbon electricity on demand due to the operational flexibility of both the generation and capture plants, thereby significantly reducing the cost of decarbonising electricity generation. Deliberate variation of steam flow to the reboiler can add value to the capture process via optimising the CO_2 capture rate to capitalise on variable electricity selling price, or by providing a rapid change in power output to facilitate grid balancing or frequency response services.

However, gaps in current knowledge prevent the capture plant from operating dynamically in an optimised fashion. The vast majority of existing dynamic models are validated using steady-state data or remain un-validated, and it is not well known how differences in plant construction will affect plant response to changes in gas, solvent or steam flowrate. Model-predictive control has been identified as a promising option for advanced plant control systems, but will require reliable, continuous online measurements of solvent CO_2 loading as a control variable. These issues must be addressed if the economic and environmental performance of CCS is to be optimised in energy systems in which the generation plant must make frequent changes to its output.

On a smaller scale, there remains uncertainty about the nature of gas-liquid interactions in the absorber column. Existing commercial CFD software packages are unable to simulate the complex two-phase flow which exists inside the absorber column. At present, packings for CCS are designed using empirical trial-and-error methods and correlations which assume pseudo-first order reaction kinetics over the entire packed bed, when this is unlikely to be the case. Direct numerical simulations such as the open-source two phase level set (TPLS) solver are capable of rigorously modelling the gas-liquid interface and, with the addition of turbulence & mass transfer prediction and complex geometries (i.e. a unit cell of structured packing), will provide a comprehensive understanding of gas-liquid interactions and potentially the development of specialised structured packings for dynamic CCS. However, the TPLS code must be validated using experimental measurements.

This thesis uses experimental studies to improve current understanding of flexible plant operation and interfacial wave dynamics in the absorber column, as applied to post-combustion CO_2 capture using amine solvents.

8.2 Key Findings - Interfacial Wave Dynamics

For the purpose of DNS model validation, a wetted-wall column which is suitable for both mass transfer and liquid film thickness measurement experiments is constructed. Using fresh 30%wt MEA solution, a high-speed camera is used to observe the liquid film profile at four locations along the length of the column – 40mm, 80mm, 120mm and 160mm from the top of the column. Measurements are made at three liquid flow and four gas flow conditions, which include laminar and turbulent gas flows with and without mass transfer – 20l/min N_2, 80l/min N_2, 10.8l/min CO_2 and 43.2 l/min CO_2. Measurements are also made with quiescent ambient air, which acts as a "base case" against which other flow conditions can be compared. For all flow conditions, measured average film thickness is in agreement with the theoretical film thickness as predicted by the Kapitza equation (Kapitza, 1965) when the uncertainty, which does not exceed more than +/-10% of the measured average value, is taken into consideration. Measurements of wave length, amplitude, frequency, velocity and growth rate are made for all flow conditions where possible.

- For flow conditions in which there is no reactive absorption the coefficient of variation in wave peak amplitude is found to increase with gas Reynolds number. Increasing the gas Reynolds number results in a more irregular wave profile, with an increased frequency of short-term transient disturbances.
- Waves become saturated in amplitude and velocity once the liquid film has travelled 120mm down the column length. Temporal growth rates are determined for each non-reacting flow condition. An indicative trend that growth rate increases with increasing liquid Reynolds number is observed. Growth rate appears to be a weak function of countercurrent gas flow rate. However, the measurement uncertainty is significant and with this camera, growth rate measurements should only be used as part of a wider range of measurements to validate CFD models.

- Wavelength generally increases with greater liquid flowrate, but no significant sensitivity to gas flow conditions outside the bounds of the measurement uncertainty could be determined.
- The frequency of the regular wave pattern appears to be unaffected by changes in gas flowrate over short periods of time, but at higher gas-phase Reynolds numbers the regularity of short-term transient interfacial disturbances increases, decreasing the average frequency over time periods greater than 1.0 sec.
- The experimental data obtain shows reasonably good agreement with the low-dimensional model of Lavalle et al. (2017), but a camera with higher resolution will be required to capture the fine data in the capillary wave region preceding the main wave crest.

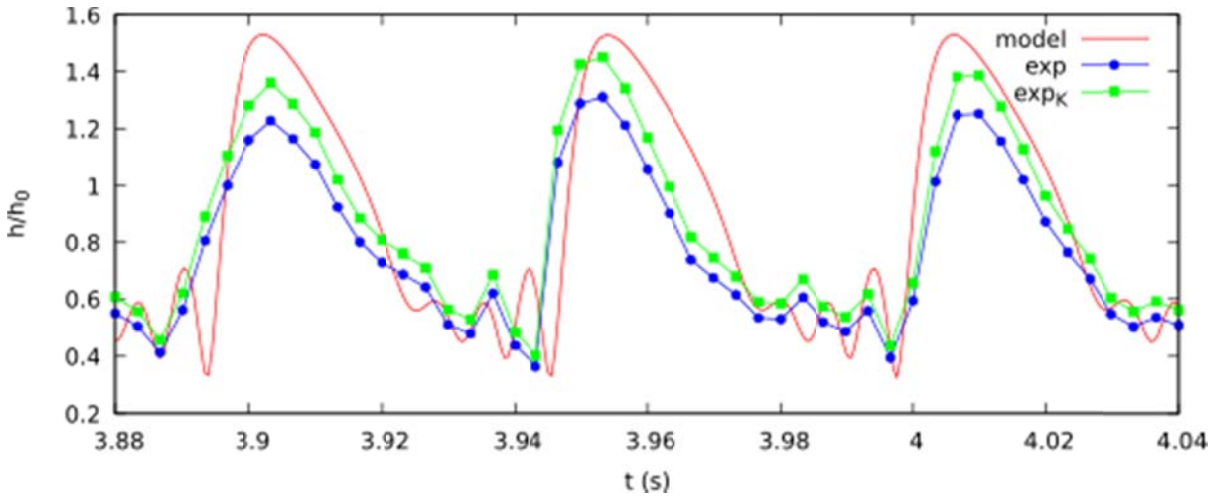

Fig. 8.1 Wave profile data, normalised with respect to the Nusselt (blue) and Kapitza (green) film thickness, compared with model predictions.

8.3 Key Findings – Dynamic Pilot-Scale Testing

In order to develop current understanding of dynamic operations involving the entire capture process, two pilot-scale test campaigns are implemented. Test campaign 1 is carried out using an absorption/desorption facility based at Sulzer Chemtech, with NGCC-equivalent flue gas. Test campaign 2 is carried out at the UKCCSRC's PACT amine facility, with PC-equivalent flue gas. 30%wt MEA is used as absorbent in both cases. The use of two separate test facilities allows the effect of differences in plant design on dynamic operating scenarios to be investigated. Test campaign 1 makes use of, in some dynamic scenarios, a novel online solvent sensor to provide continuous measurement of solvent CO_2 loading. In test campaign 2, two of these sensors are used to provide continuous in-situ measurements of rich and lean solvent CO_2 loading in real-time. Each capture plant is operated in response to changes in flue gas and reboiler steam flowrate which are designed to be representative of real NGCC and PC plant operation. Finally, knowledge of plant hydrodynamics and response times are used to demonstrate control of test facility 2 using online, in-situ measurements of lean solvent CO_2 loading.

- Dynamic datasets are obtained for five scenarios using NGCC-equivalent flue gas
  - Generation plant shutdown
  - Generation plant startup
  - Power output maximisation via capture plant decoupling
  - Power output maximisation via reboiler steam decoupling
  - Frequency response via regeneration steam increase
- Dynamic datasets are obtained for eight scenarios using PC-equivalent flue gas
  - Generation plant shutdown
  - Generation plant startup (standard)
  - Generation plant shutdown (repeat of previous scenario)
  - Generation plant startup with prioritisation of emissions reduction

    - Power output maximisation via reboiler "steam" decoupling
    - Power output maximisation via reboiler "steam" decoupling, with reduction of solvent flowrate
    - Frequency response via reboiler "steam" flow reduction
    - Capture plant ramping
- Solvent mixing and circulation times have a significant effect on the response to dynamic scenarios. These in turn are highly dependent on the design of the capture facility. Effective mixing is promoted when the majority of the solvent inventory resides in large vessels. Circulation times are dependent on the volume of solvent inventory relative to the baseload solvent flow rate.
    - As observed in test campaign 1, poor solvent mixing can result in large fluctuations in CO_2 capture rate following a return to baseload flow conditions. In cases where mixing is more effective, for example in test campaign 2, the return to baseload capture rate is more gradual but large fluctuations are not observed.
    - A large solvent inventory is desirable during reboiler steam decoupling events, as there remains a large reserve of lean solvent available for CO_2 absorption before the capture rate begins to drop significantly. However, a large solvent inventory implies longer circulation times, so the response in CO_2 capture rate to any changes made in reboiler heat input is delayed.
    - Interim solvent storage as described by Chalmers et al (2009) could facilitate the faster response times associated with a small solvent inventory while retaining a large reserve of lean solvent so a high capture rate can be maintained during reboiler shutdown events.
- Prioritisation of CO_2 emissions reduction during coal plant startup events can reduce total daily emissions by up to 18.6% if the plant is operating in a two-shifting dispatch pattern.
- A novel solvent sensor is used to provide continuous in-situ measurement of solvent CO_2 loading.
- Discrete knowledge of plant hydrodynamics, response times based on current plant conditions, continuous measurement of solvent composition and knowledge of upcoming changes in generation plant output will be required to optimise dynamic operation.
- Control of CO_2 capture rate during a reboiler steam flow decoupling event is demonstrated via online measurements of lean solvent CO_2 loading combined with knowledge of capture plant hydrodynamics and response times.

8.4 Key Findings - Capture plant scale-up

Those involved in the design and construction of CO_2 capture facilities have a considerable amount of freedom in adjusting the circulation time between desorber outlet and absorber inlet, by adjusting the working volume of solvent in the lean solvent tank. By the metrics laid out in this chapter, a capture plant which is subject to limitations in where the absorber and desorber can be placed should be no less likely to operate flexibly than a compact new-build or retrofitted plant.

- An optimum circulation time of 30mins between desorber outlet and absorber inlet is recommended, as a trade-off between allowing the plant to continue to capture CO_2 during steam shutdown events, and being able to respond rapidly during start-up operations or when steam is reintroduced.
- Plant operators can modify the volume of solvent in the lean tank depending on the dispatch pattern for that plant.
- A bypass loop between the outlet of the desorber and the inlet of the main solvent tank could be installed in the event that extremely rapid plant response is required, allowing the main solvent tank to be bypassed entirely.
- Significantly increasing the volume of lean solvent in the tank from the optimal volume which results in a 30min circulation time between desorber outlet and absorber inlet could increase the mass of CO_2 released during start-up operations by thousands or tens of thousands of tons.
- The associated cost of emissions as a result of this could run into the range of hundreds of thousands of pounds, depending on the carbon price. Therefore it is imperative that plant dynamic response times and its likely dispatch pattern be taken into consideration when designing CO_2 capture equipment.

8.5 Recommendations for Future Work

Wave measurements have been made at a variety of gas-liquid flow conditions using the wetted-wall column rig, so the next step in the short-term is to validate using the TPLS flow solver at its current level of complexity. This could be achieved using existing wave period and amplitude data for the flow condition with 20l/min counter-current N_2. Improvements could be made to both the practical test rig and the image analysis method in order to streamline the acquisition of wave measurements for researchers who are unfamiliar with its operation. Experimental data and the low-dimensional model of Lavalle et al. show reasonably close agreement, but an upgrade to the high-speed camera may be necessary to observe fine detail in the capillary wave region and obtain wave growth rate measurements with a lower range of uncertainty. Ultimately, the purpose of the test rig is to facilitate the validation of DNS models with turbulent gas flow and mass transfer so that gas-liquid interactions in the absorber column are well understood, allowing for the accurate sizing of absorption columns for CCS operations and potentially the development of specialized structured packings.

Active control of solvent flow rate, desorber pressure and reboiler heat input, combined with online rich and lean solvent composition measurements and prior knowledge of changes in generation plant output will form the basis of future capture plant control systems. Model-predictive control (MPC) and fuzzy logic control are promising alternatives to existing PID control systems for optimised dynamic capture plant operation. The next immediate steps in the development of plant control using online solvent measurements are as follows.

- Integrate the basic prediction method described in Chapter 6, section 6.4.6 with the Labview plant control system at UKCCSRC PACT or another pilot-scale facility.
- Enhance the prediction method by determining the contribution to changes in loading and capture rate from variations in other plant parameters (e.g. solvent flow, absorber temperature, nominal amine concentration), either via experimental or modelling studies.
- Attempt to use both rich and lean solvent measurements to make long-term predictions about changes in CO_2 capture rate and solvent working capacity.

In the long term, a standard procedure to determine the relative dependencies of critical capture plant operating parameters for use in advanced control systems should be developed, as differences in plant design have a significant effect on plant response to dynamic operations. The completion of these goals would represent a significant step towards the implementation of robust control systems for PCC, allowing the capture plant to be operated as cost-effectively as possible during flexible operation and reducing the operating costs of both CCS and the decarbonisation of electricity generation.

References

Lavalle, G., Vila, J.P., Lucquiaud, M. and Valluri, P. (2017). Ultraefficient reduced model for countercurrent two-layer flows. *Physical Review Fluids,* 2, 0104001.

Kapitza P.L. (1965). Wave Flow of Thin Layers of a Viscous Fluid. Collected Papers of P.L. Kapitza, 2, 662-708.

Appendix A – Wave profile visualisations

A.1 Results with no counter-current gas flow

A1.1 Measurement location = 40mm

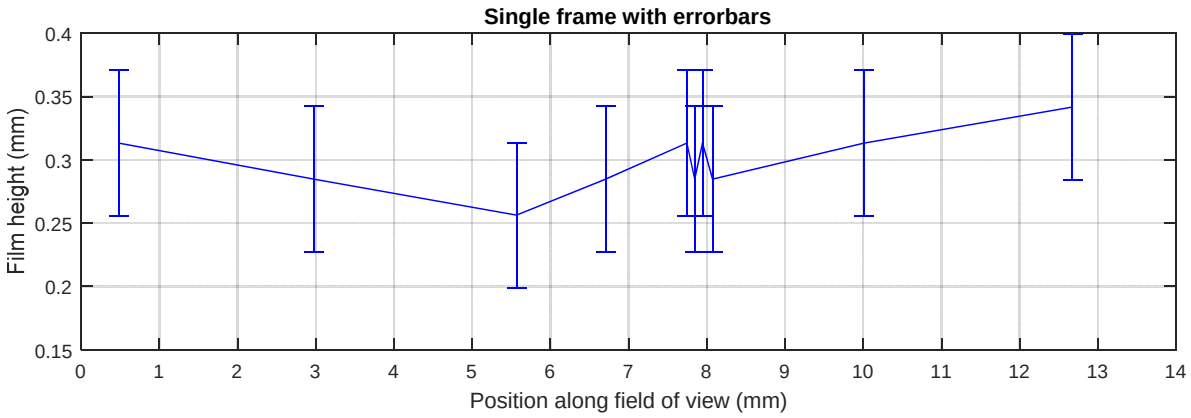

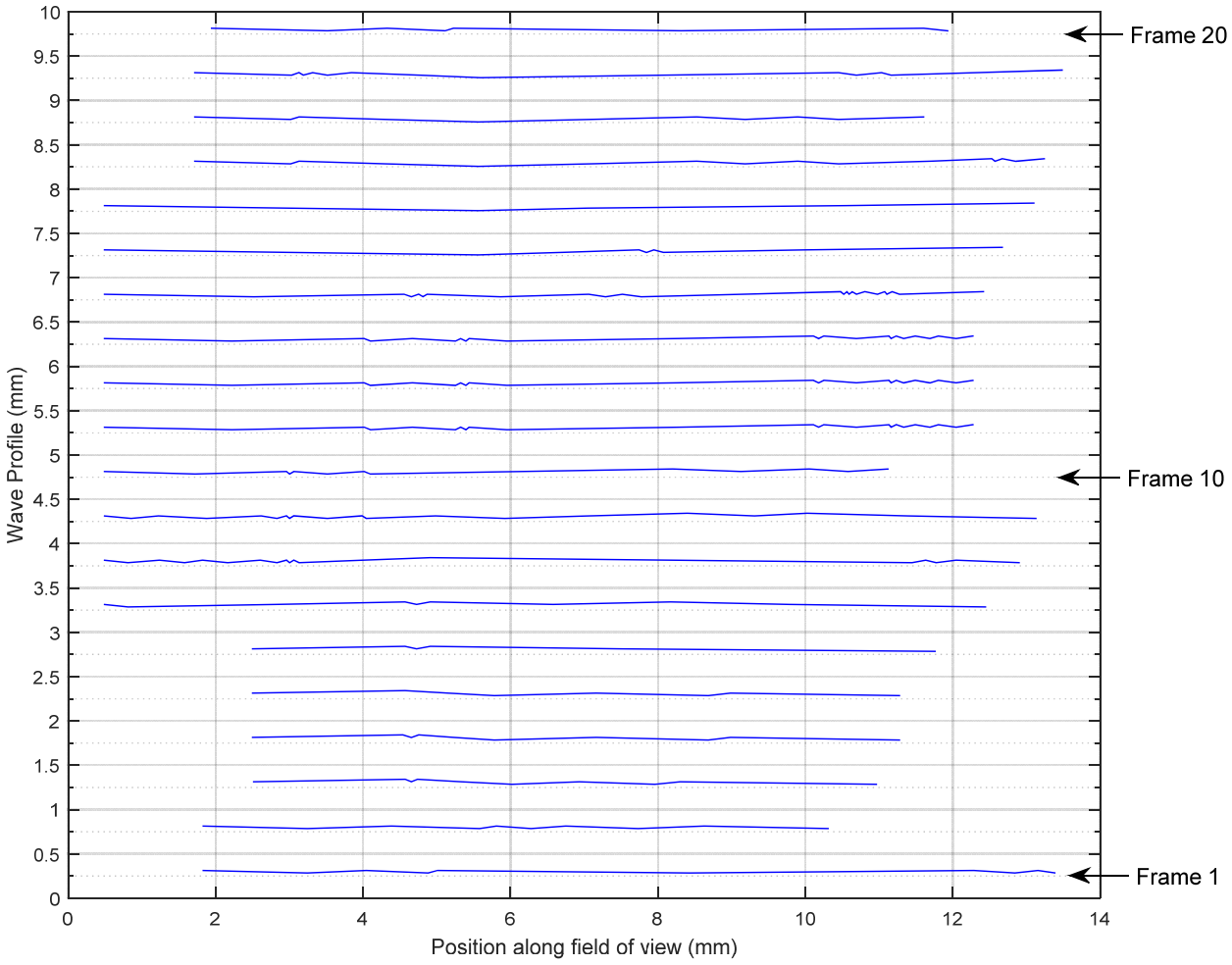

Fig. A1 Liquid flow condition 1, 40mm from top of column

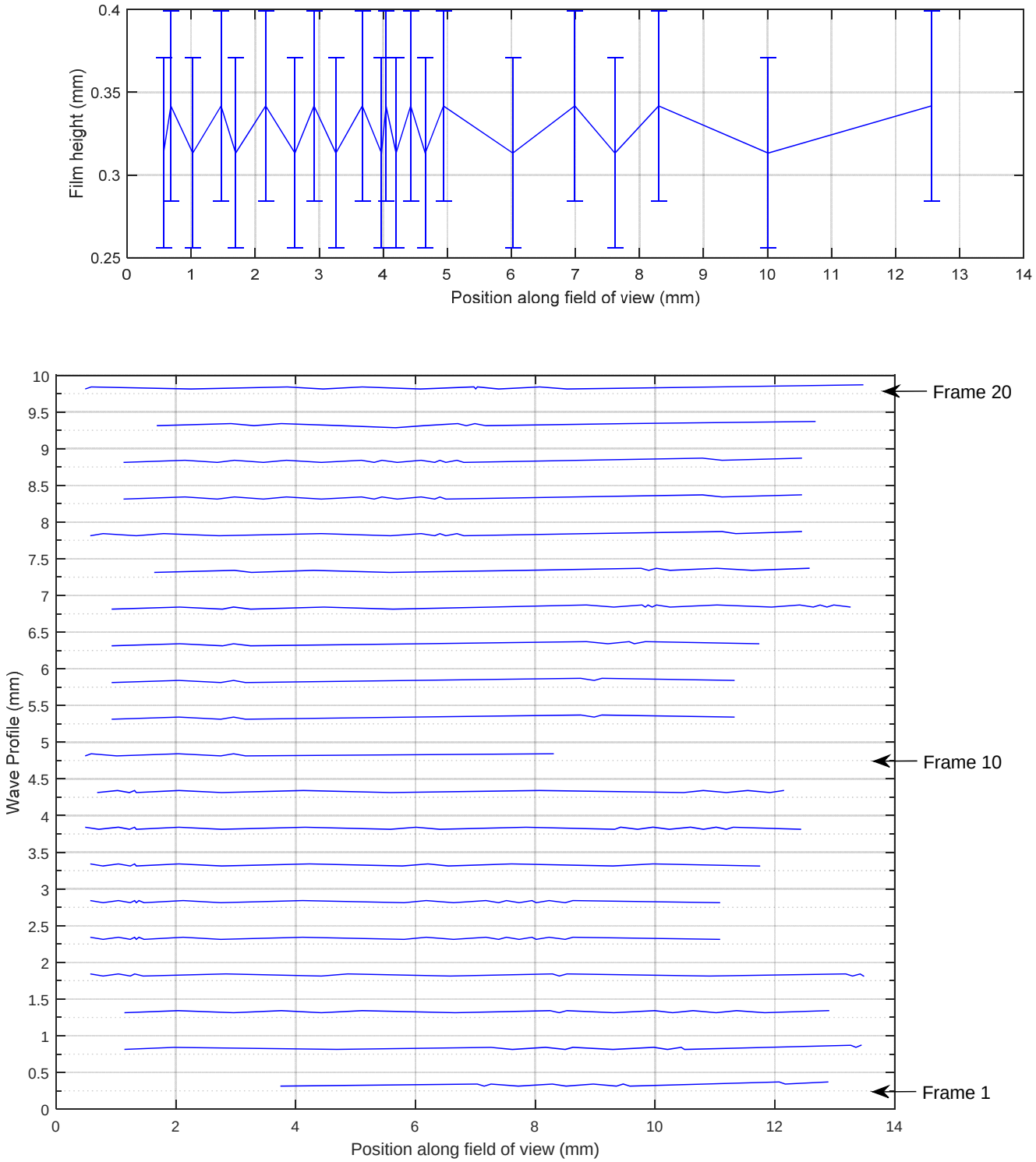

Fig. A2 Liquid flow condition 2, 40mm from top of column

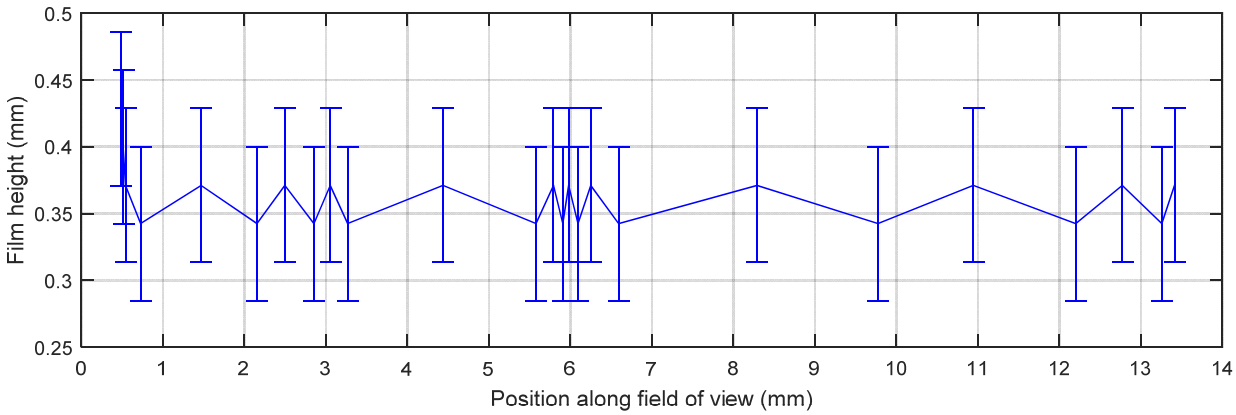
Film height (mm)
0.5
0.45
0.4
0.35
0.3
0.25
0
1
2
3
4
5
6
7
8
9
10
11
12
13
14
Position along field of view (mm)

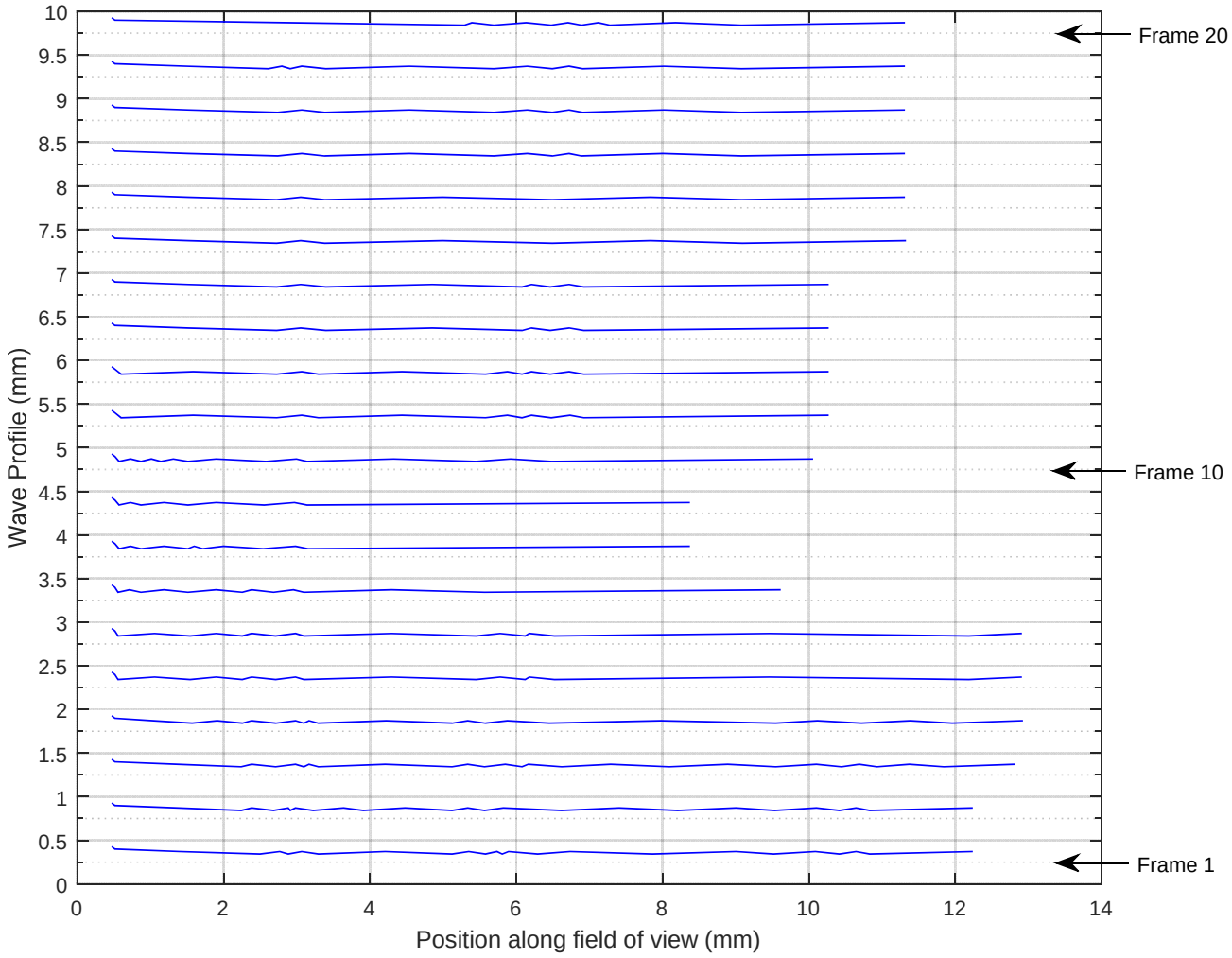

Fig. A3 Liquid flow condition 3, 40mm from top of column

N.B. For measurements made at liquid flow condition 3, the repeating pattern of a “high” liquid film around 0.5mm along the field of view is caused by a mark on the inside of the glass column.

A1.2 80mm from top of column

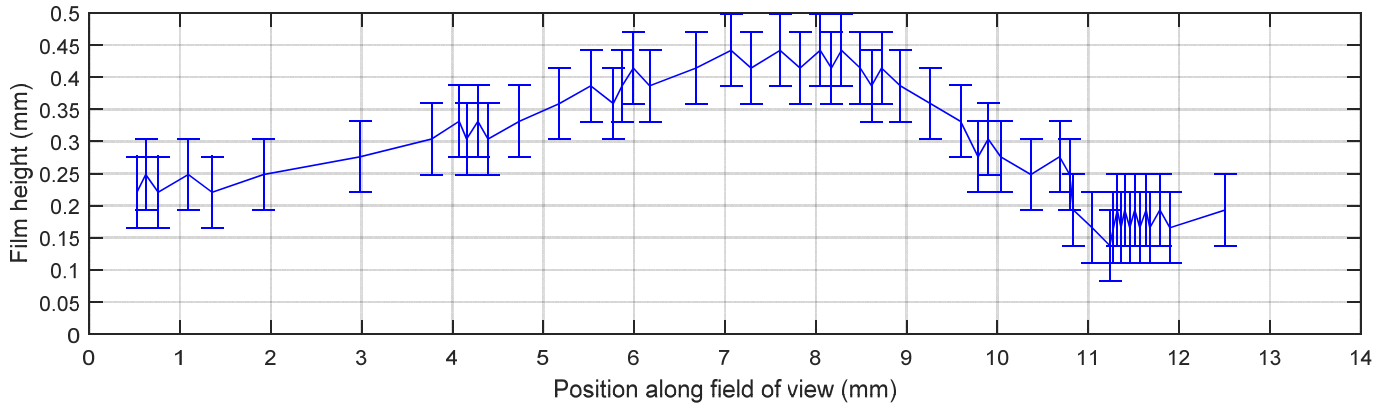

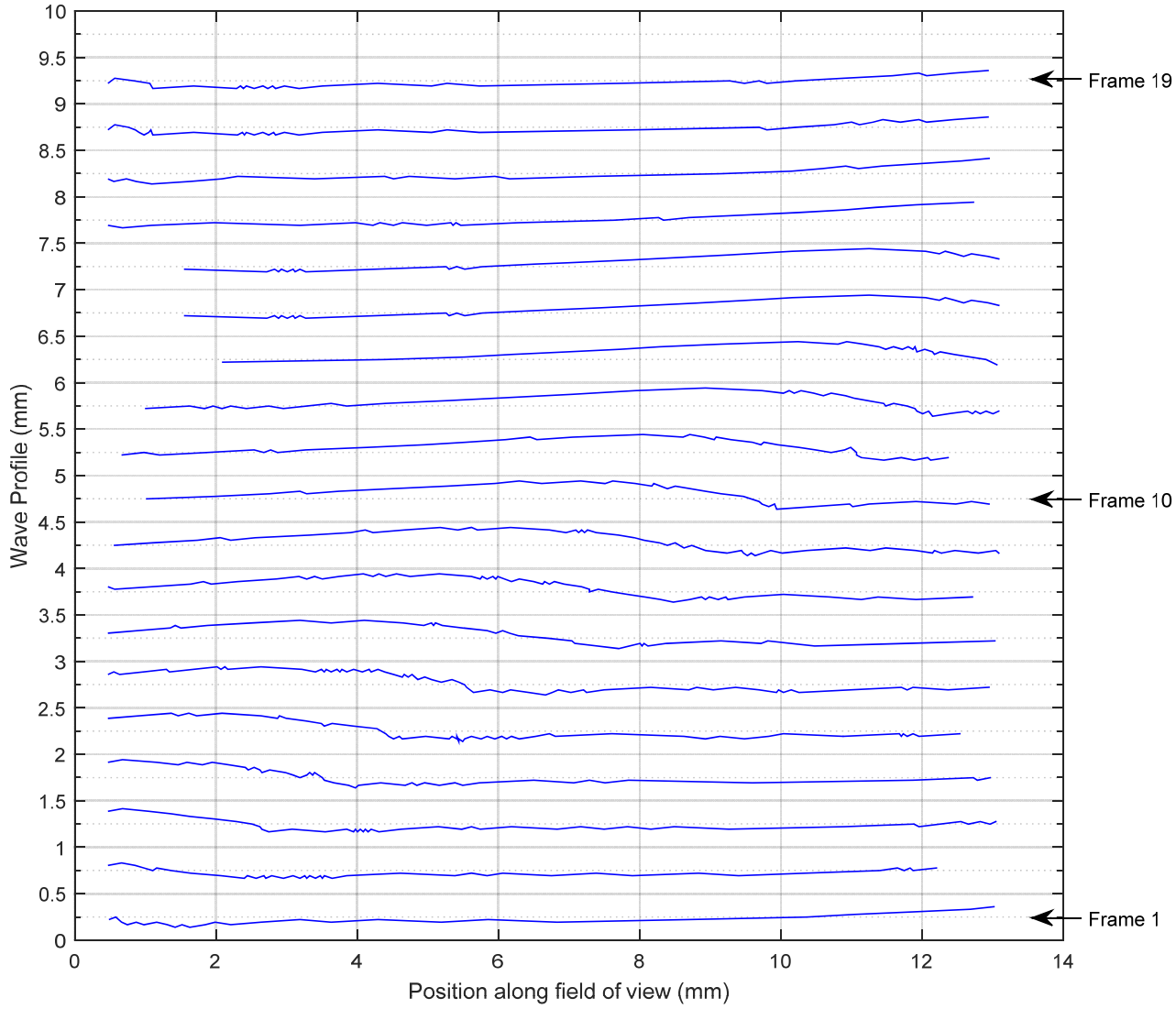

Fig. A4 Liquid flow condition 1, 80mm from top of column

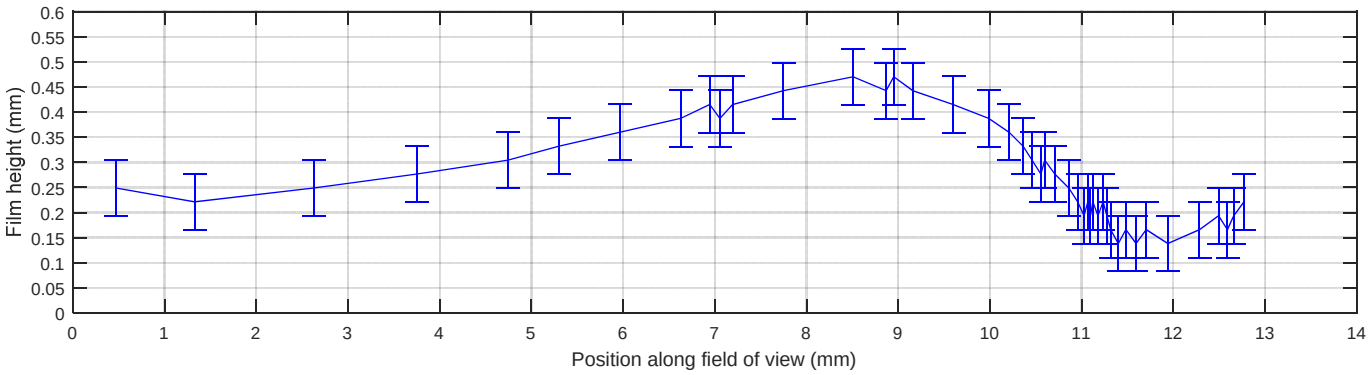

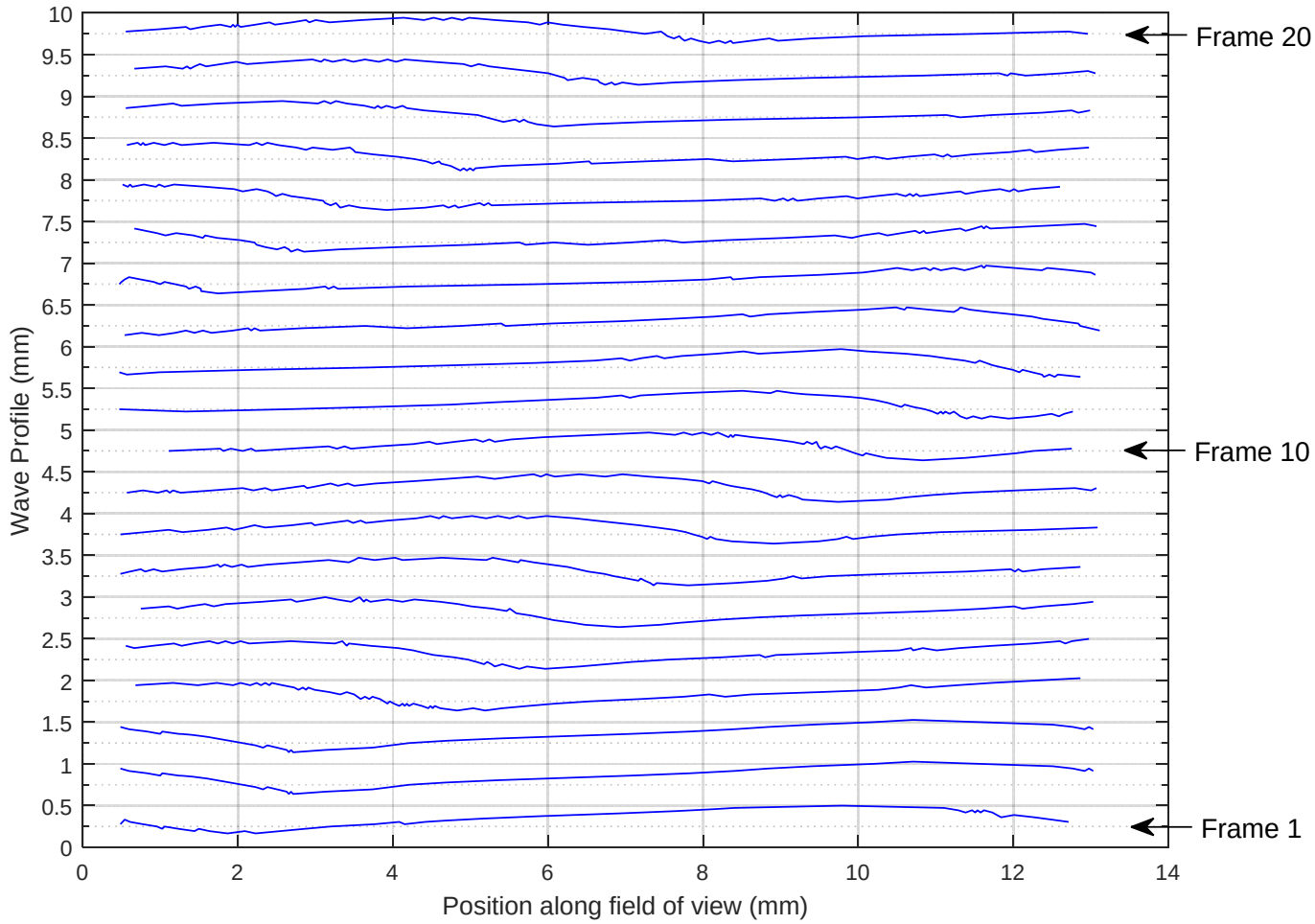

Fig. A5 Liquid flow condition 2, 80mm from top of column

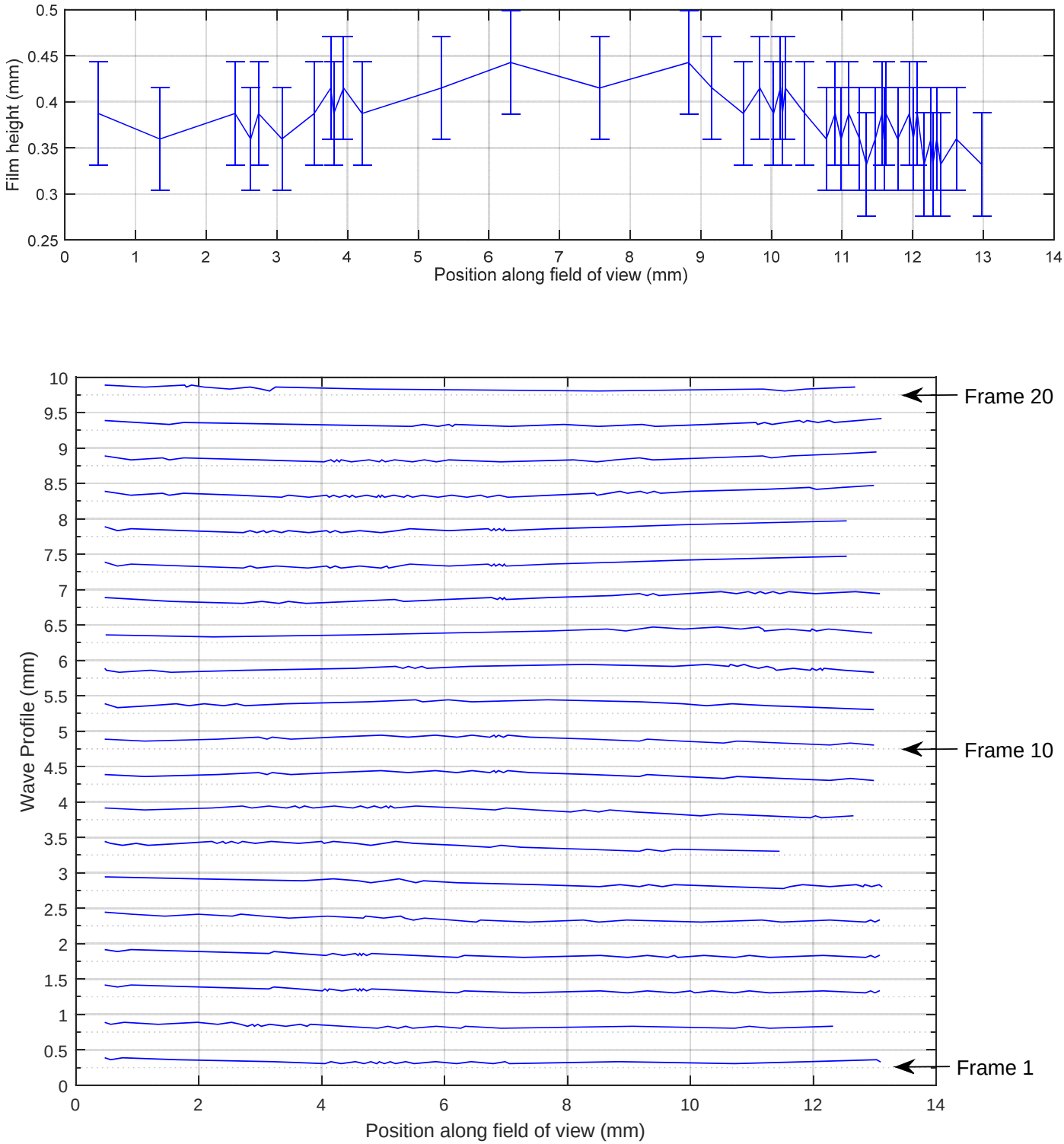

Fig. A6 Liquid flow condition 3, 80mm from top of column

A1.3 120mm from top of column

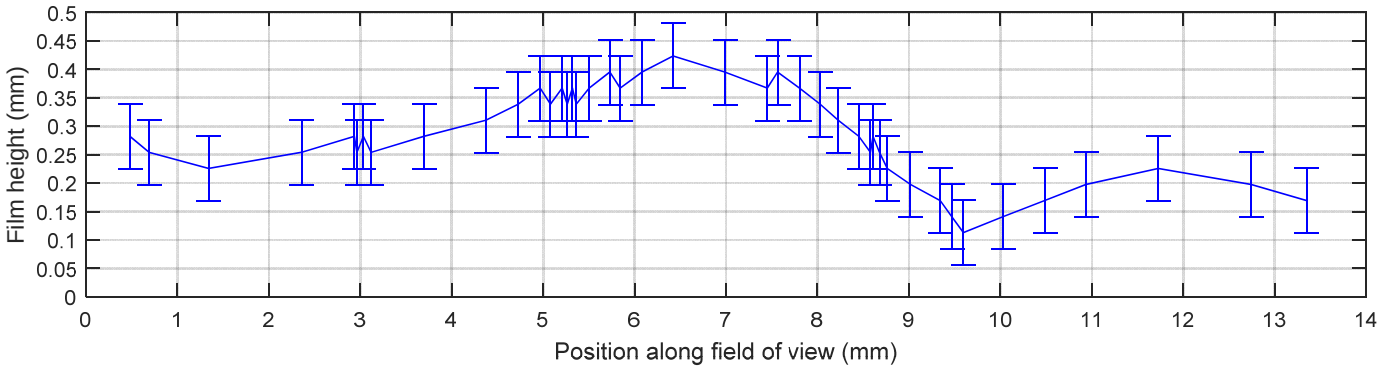

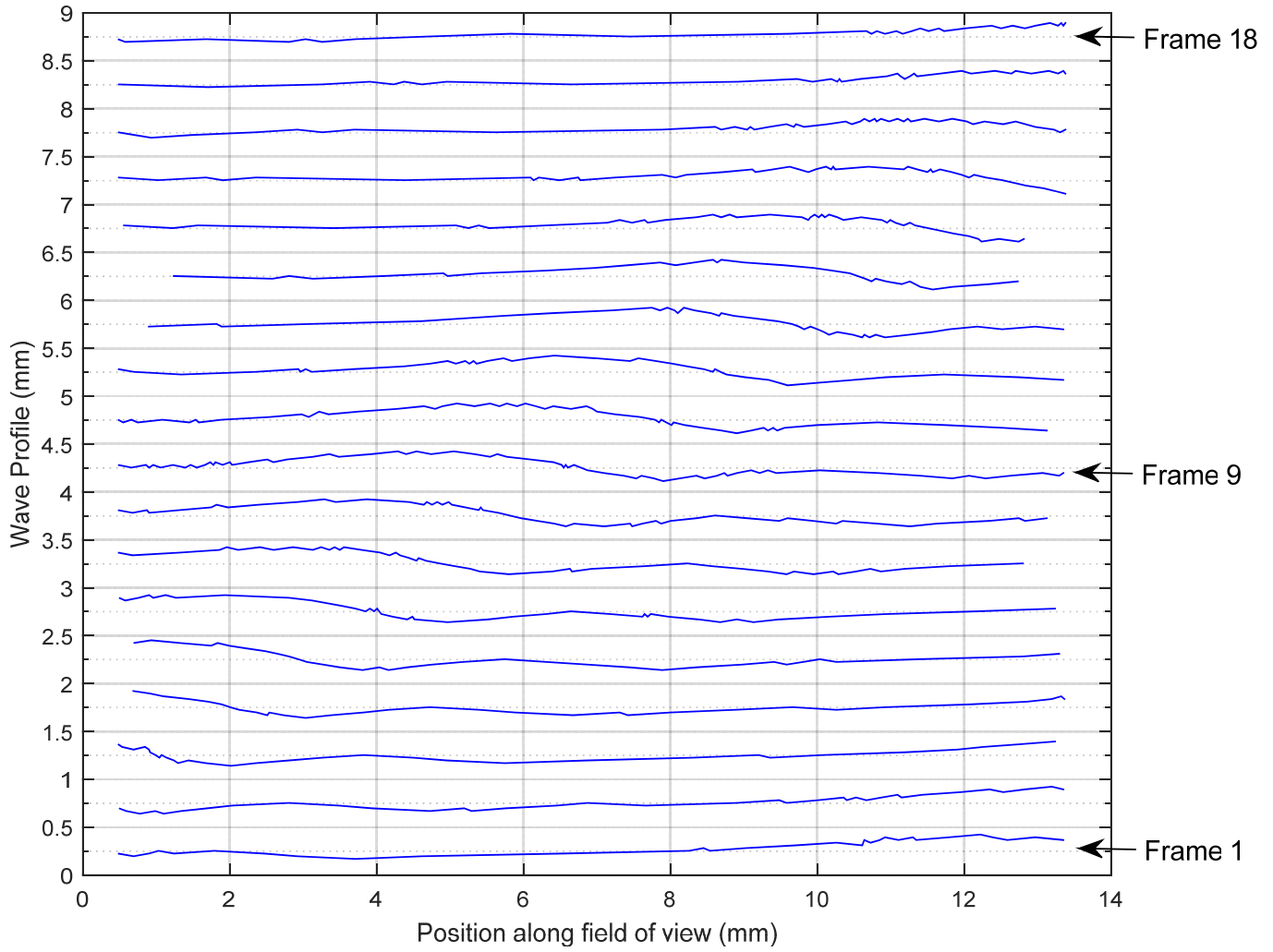

Fig. A7 Liquid flow condition 1, 120mm from top of column

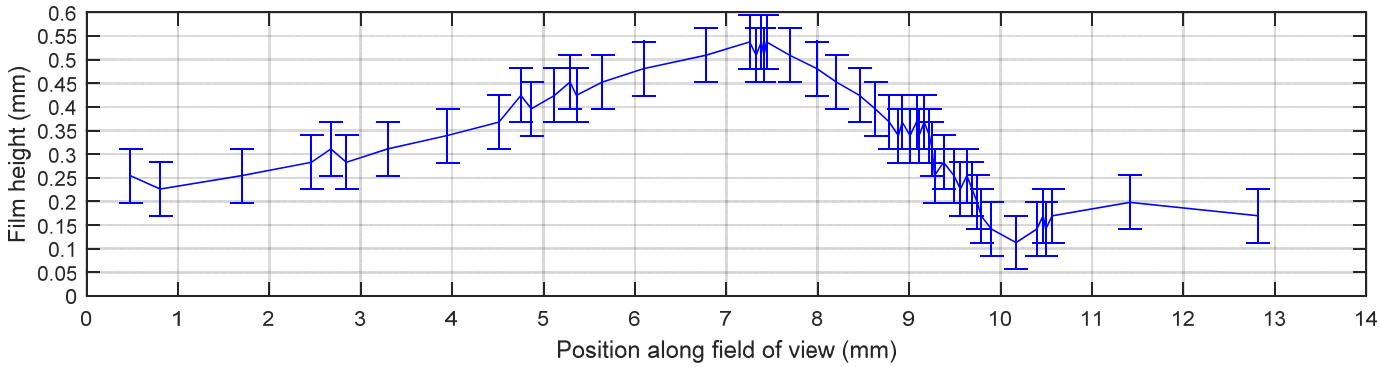

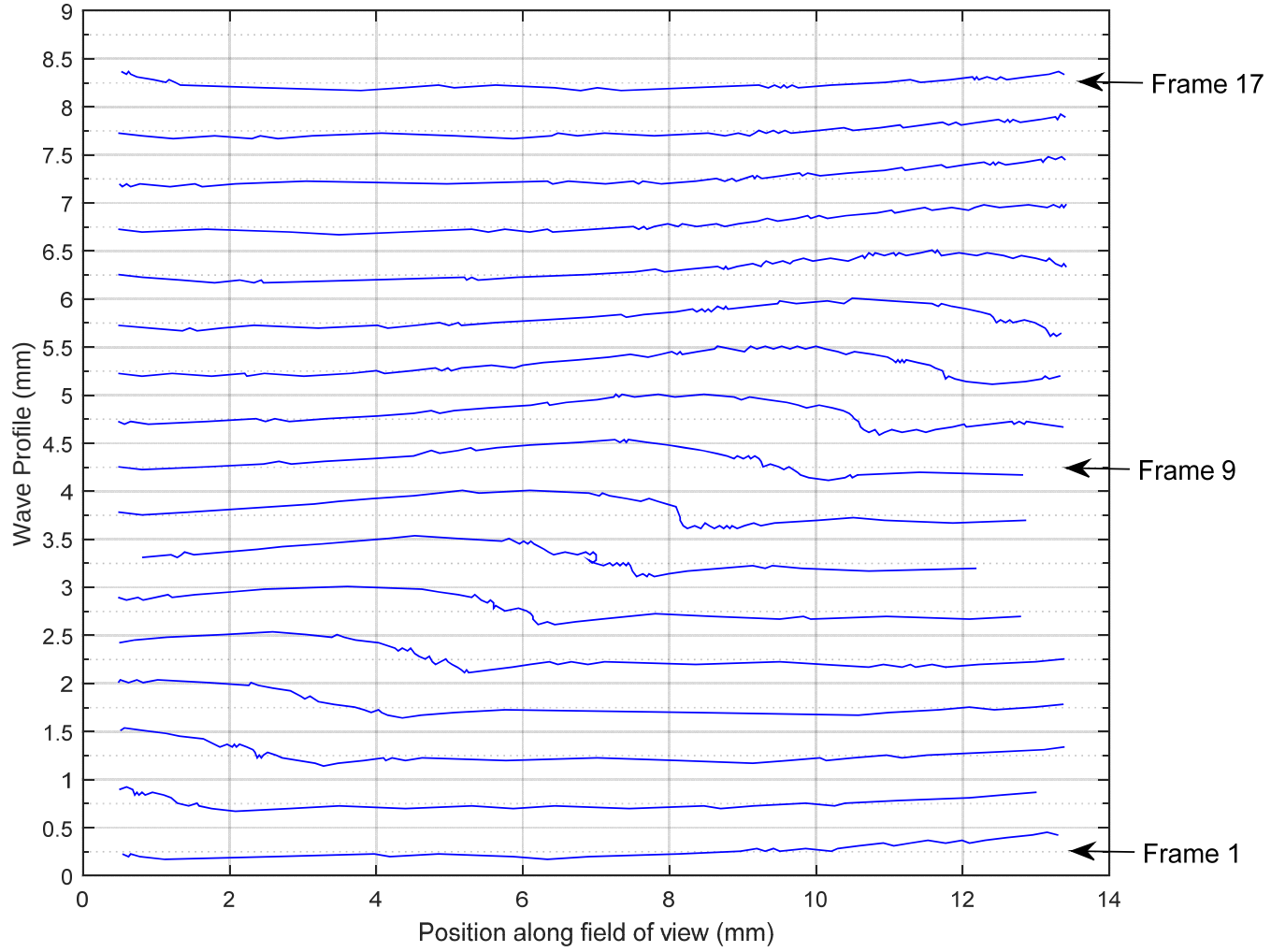

Fig. A8 Liquid flow condition 2, 120mm from top of column

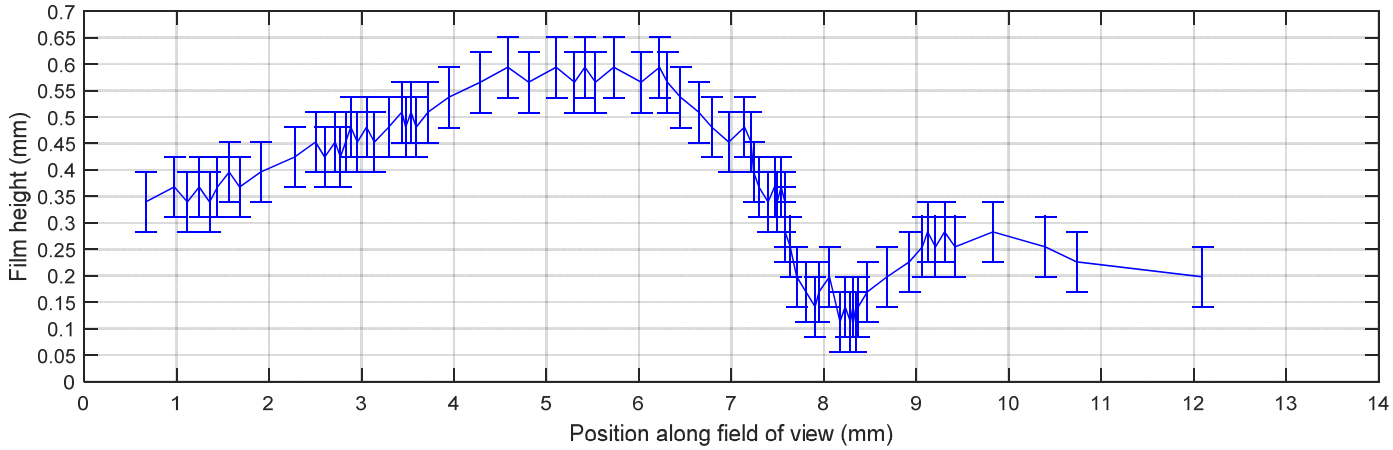

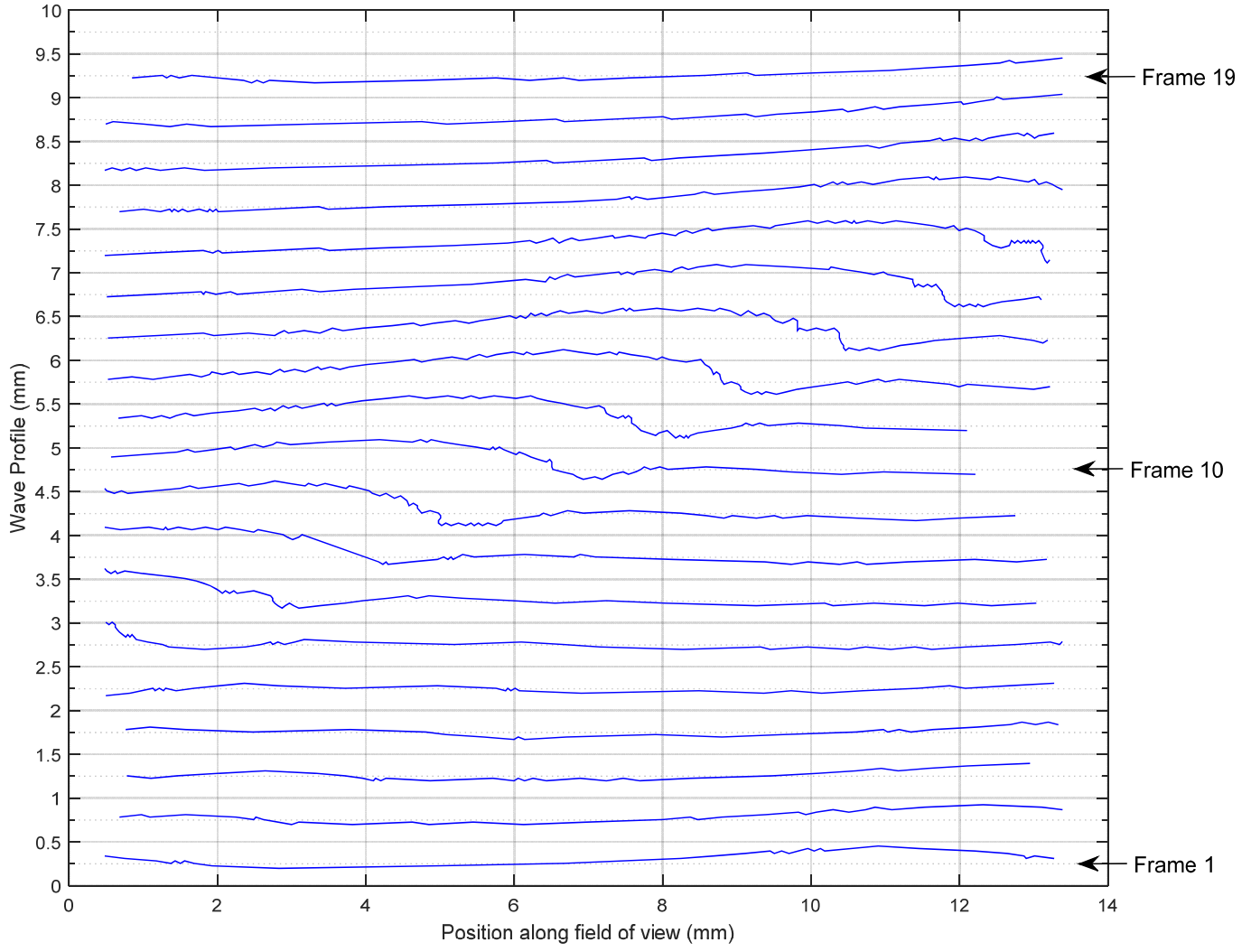

Fig. A9 Liquid flow condition 3, 120mm from top of column

A.2 Results with 20 l/min counter-current N_2

A2.1 40mm from top of column

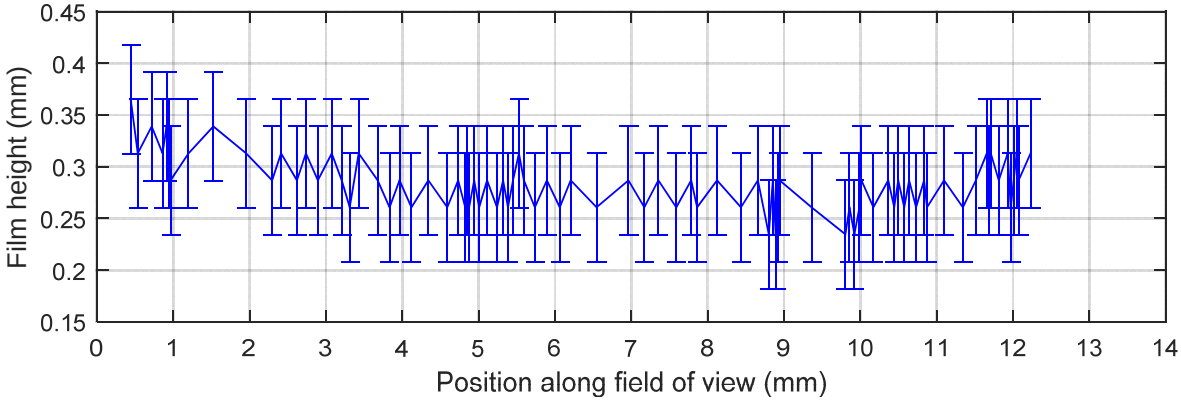

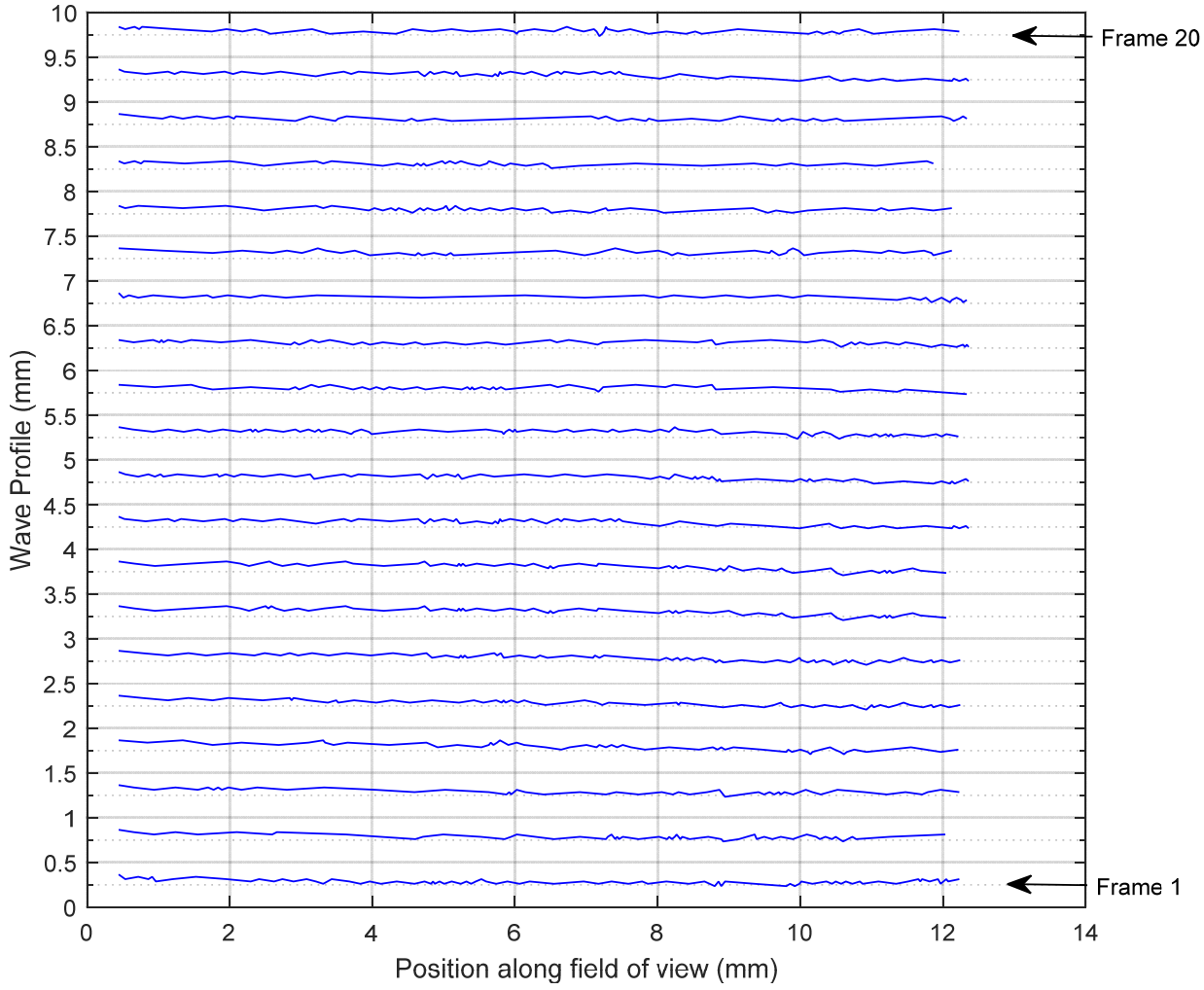

Fig. A10 Liquid flow condition 1, 40mm from top of column

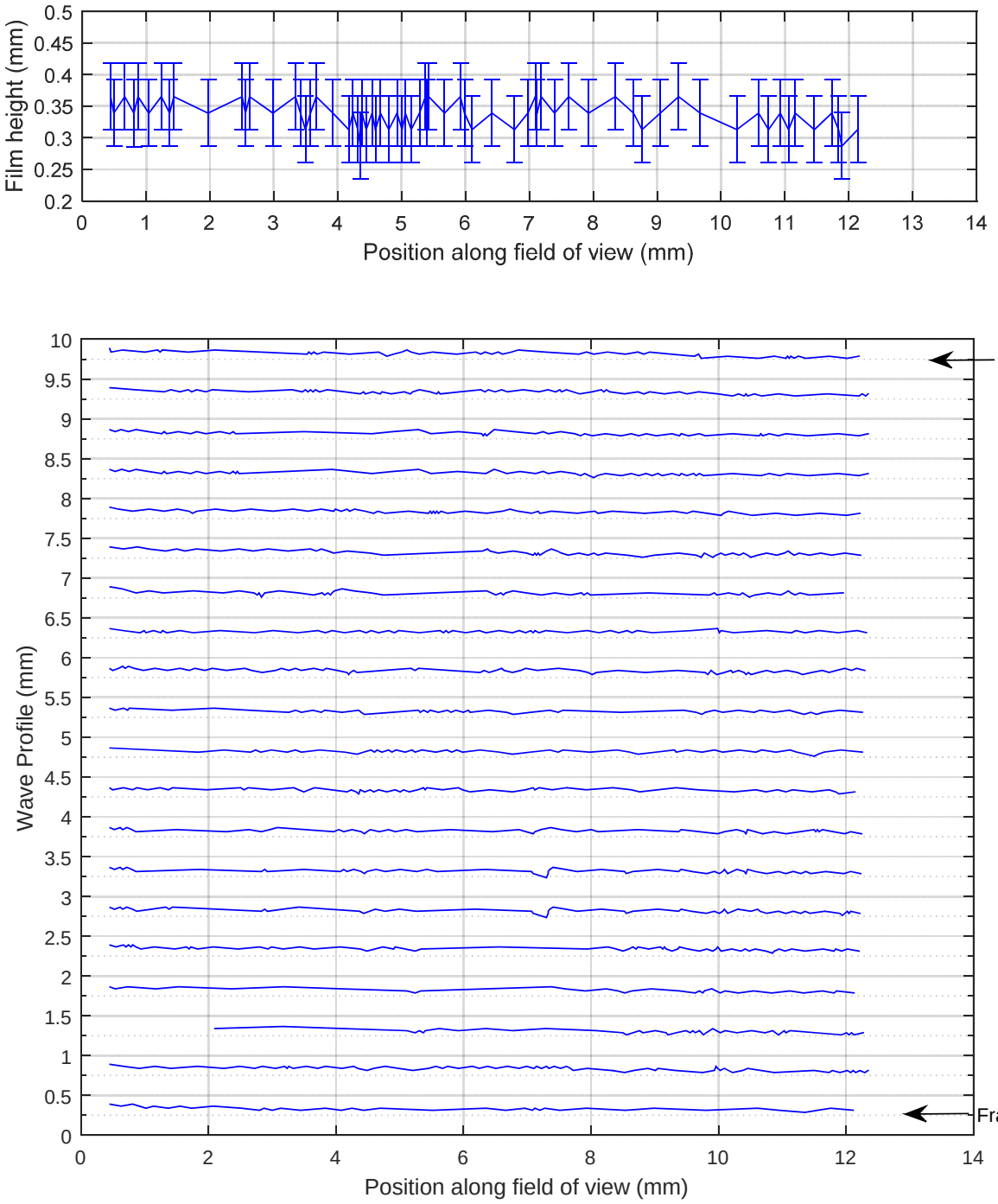

Fig. A11 Liquid flow condition 2, 40mm from top of column

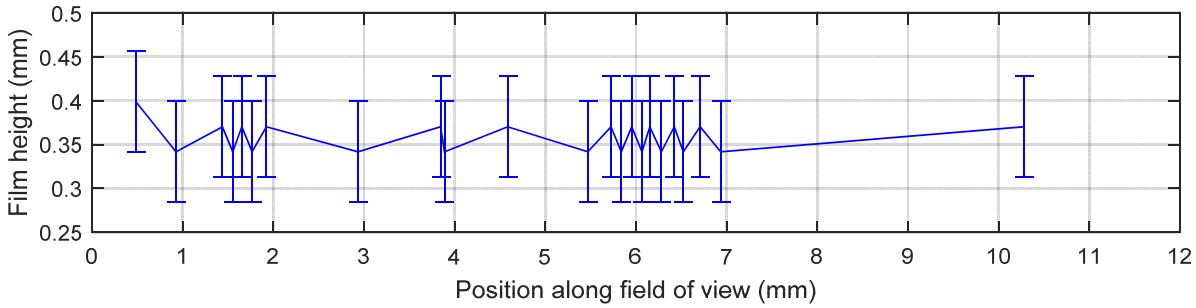

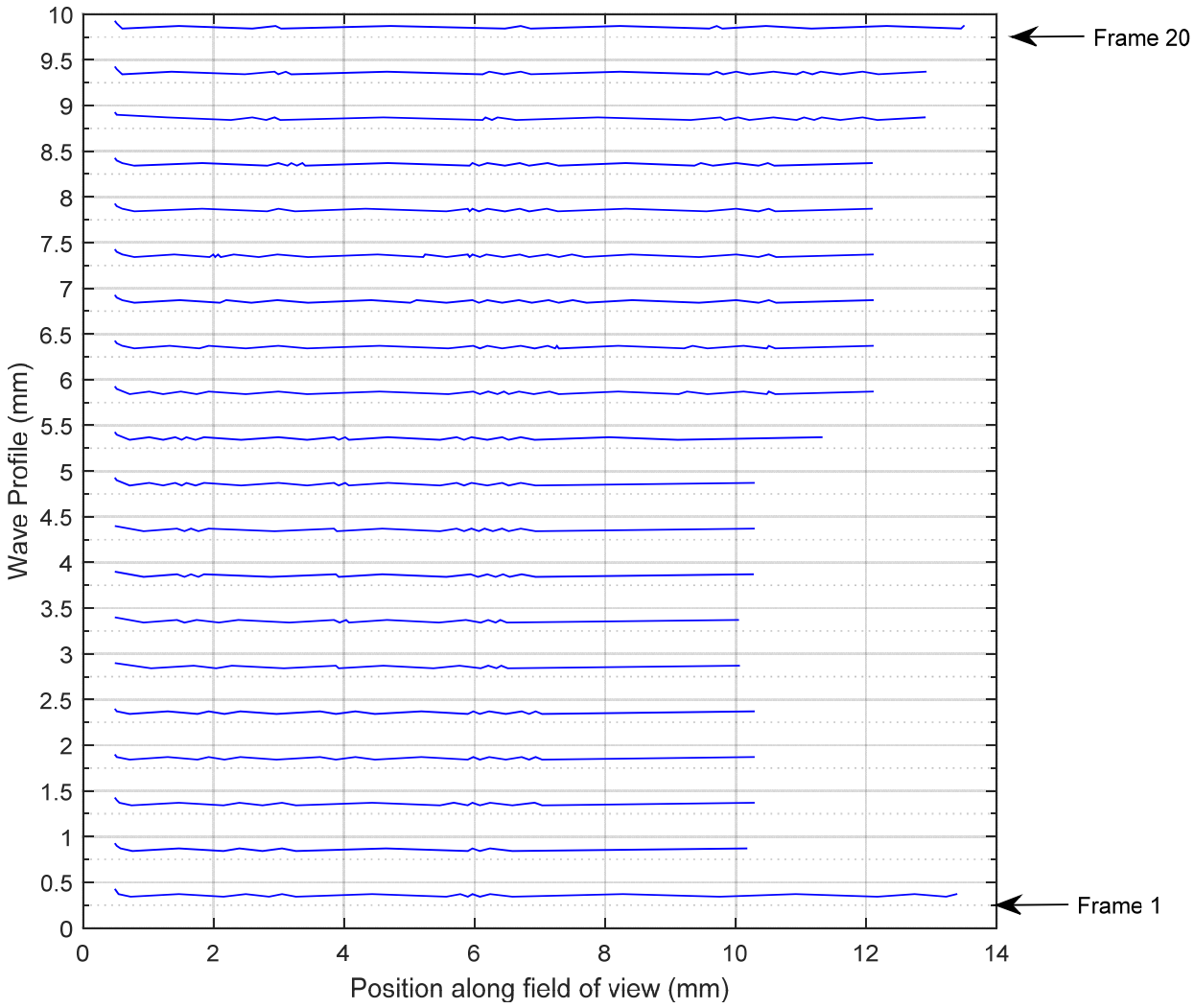

Fig. A12 Liquid flow condition 3, 40mm from top of column

A2.2 80mm from top of column

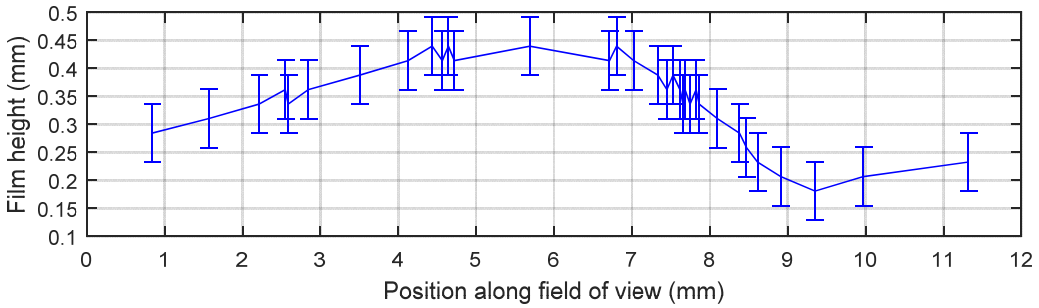

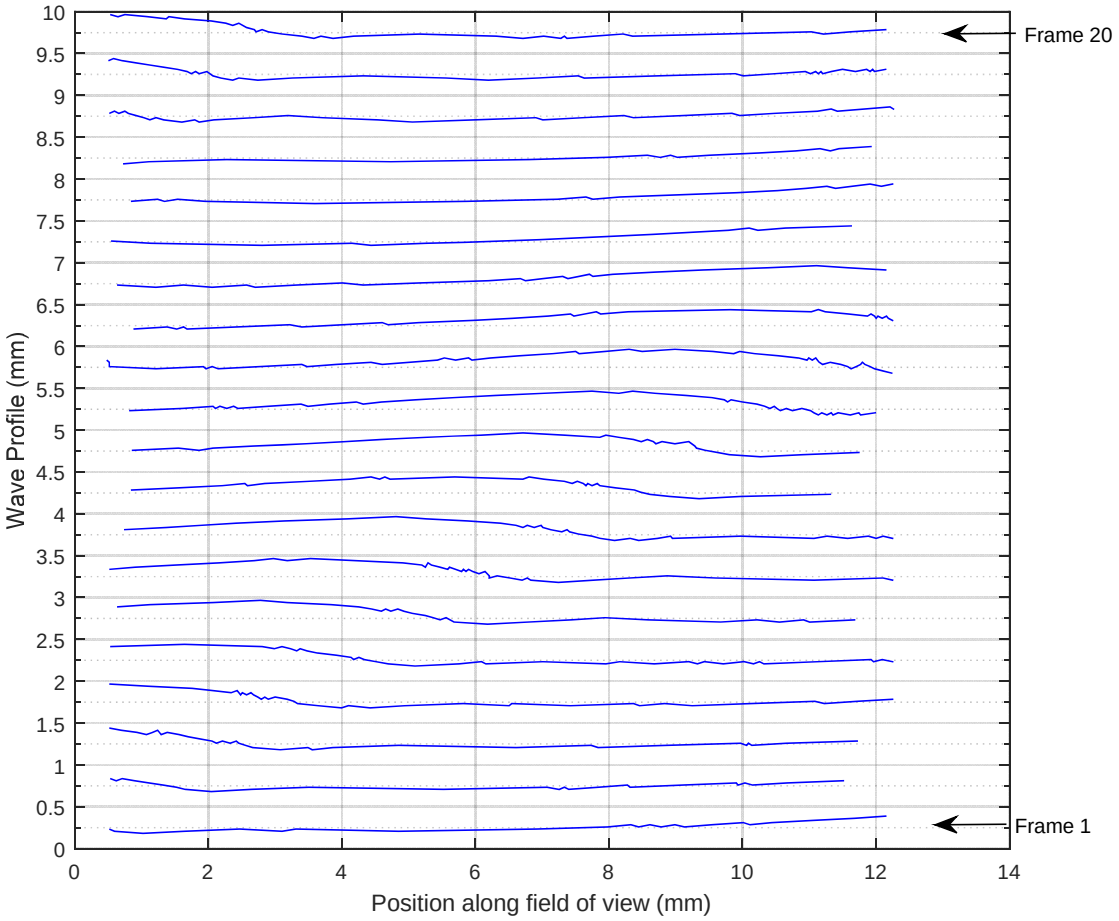

Fig. A13 Liquid flow condition 1, 80mm from top of column

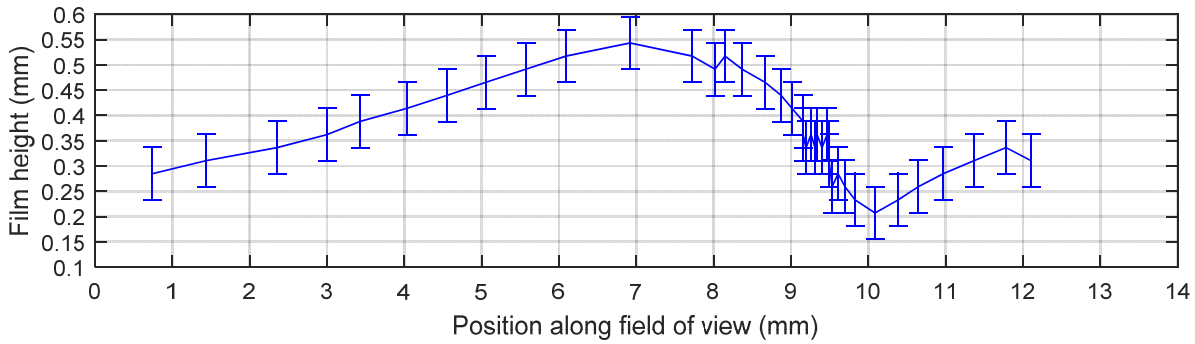

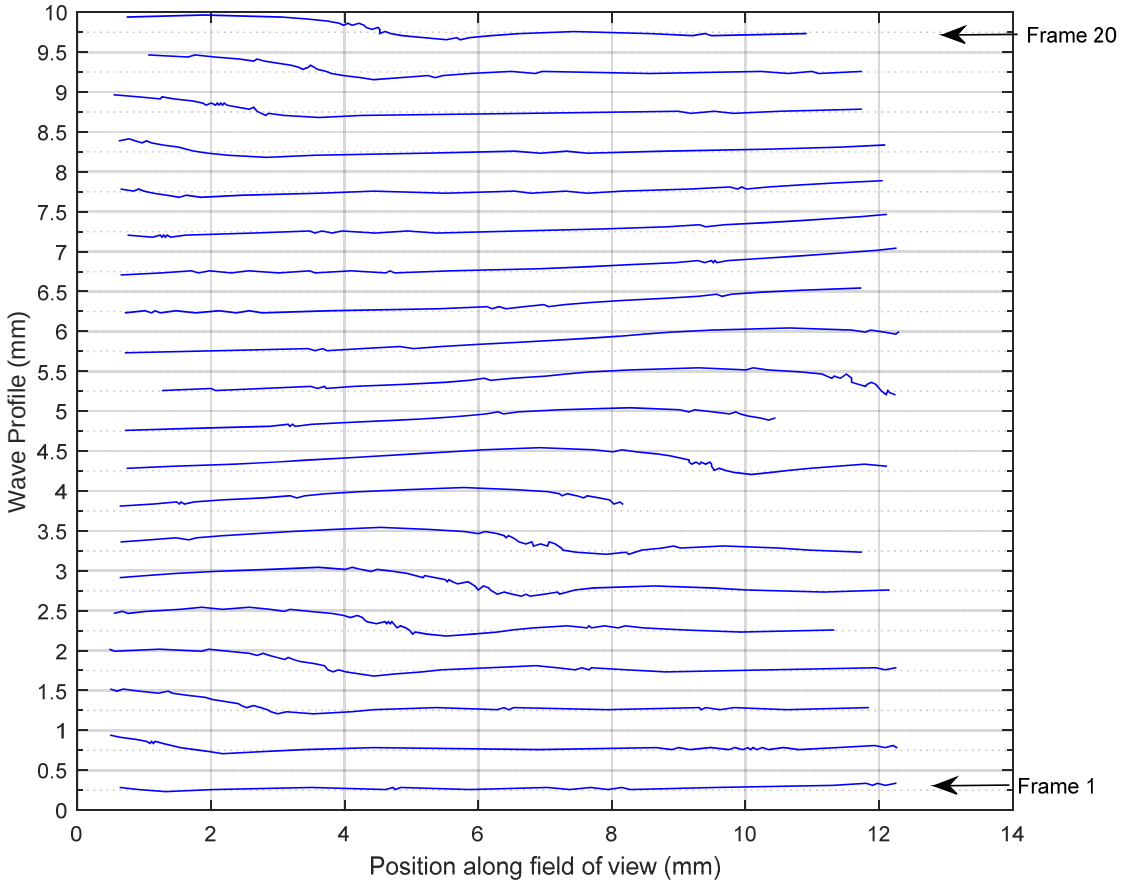

Fig. A14 Liquid flow condition 2, 80mm from top of column

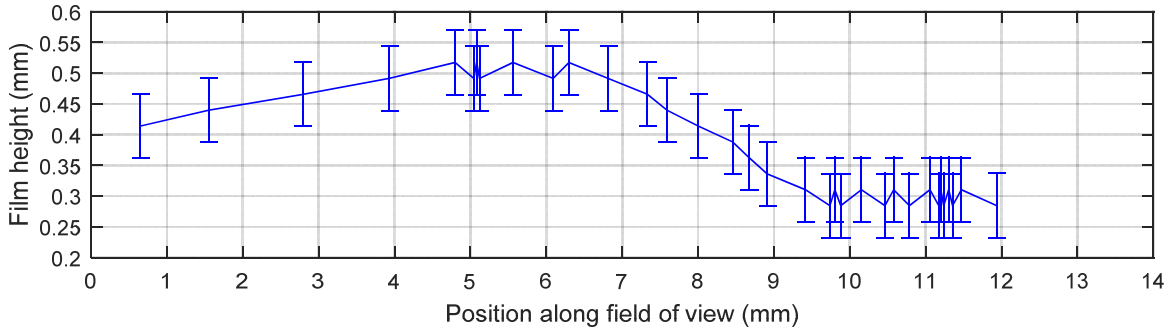

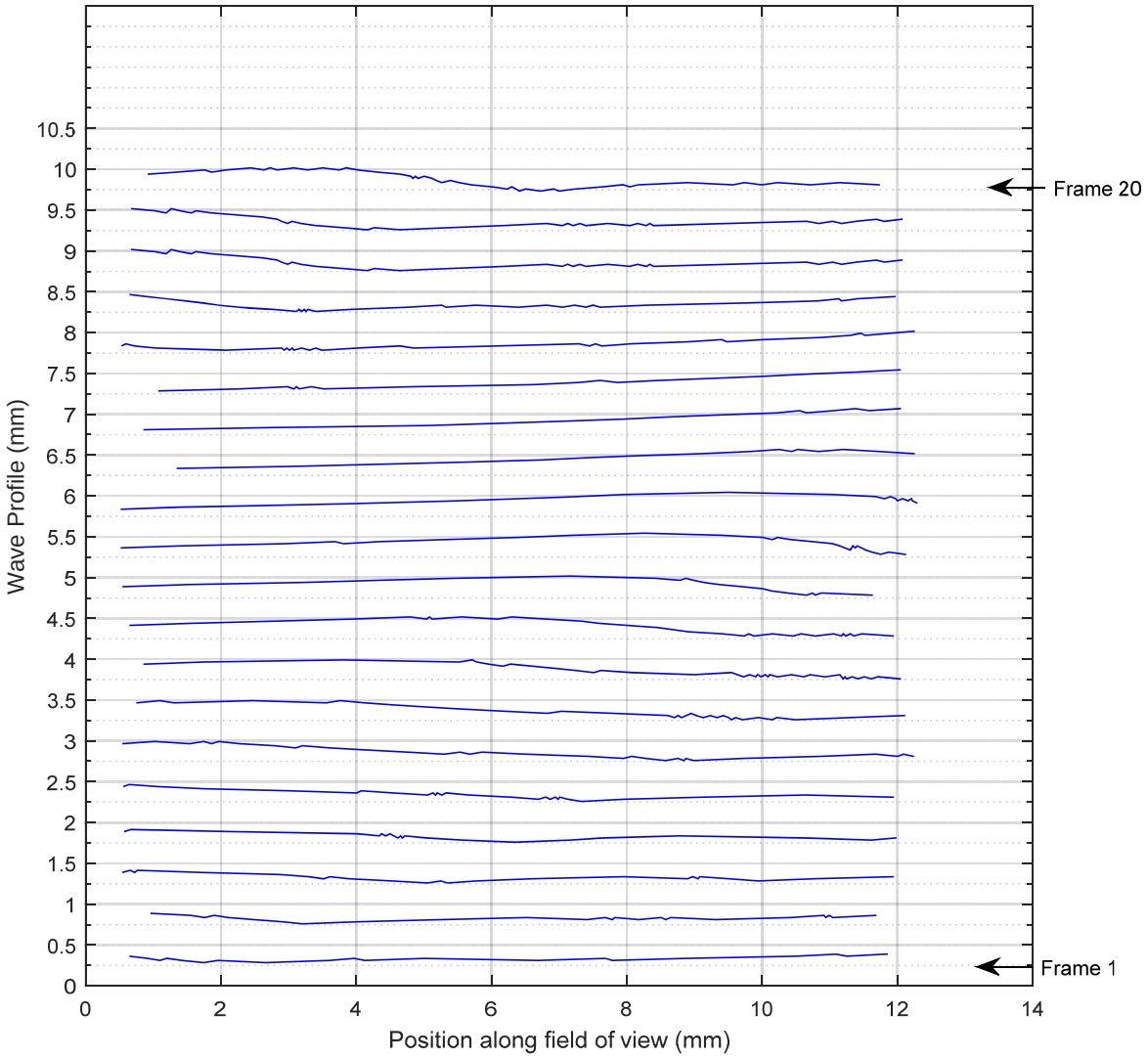

Fig. A15 Liquid flow condition 3, 80mm from top of column

A2.3 120mm from top of column

At this location with counter-current gas the presence of solvent droplets on the column walls makes it difficult to observe the full wave profile, but in some cases a reasonable wave profile can be discerned. At liquid flow condition two a double capillary wave is observed.

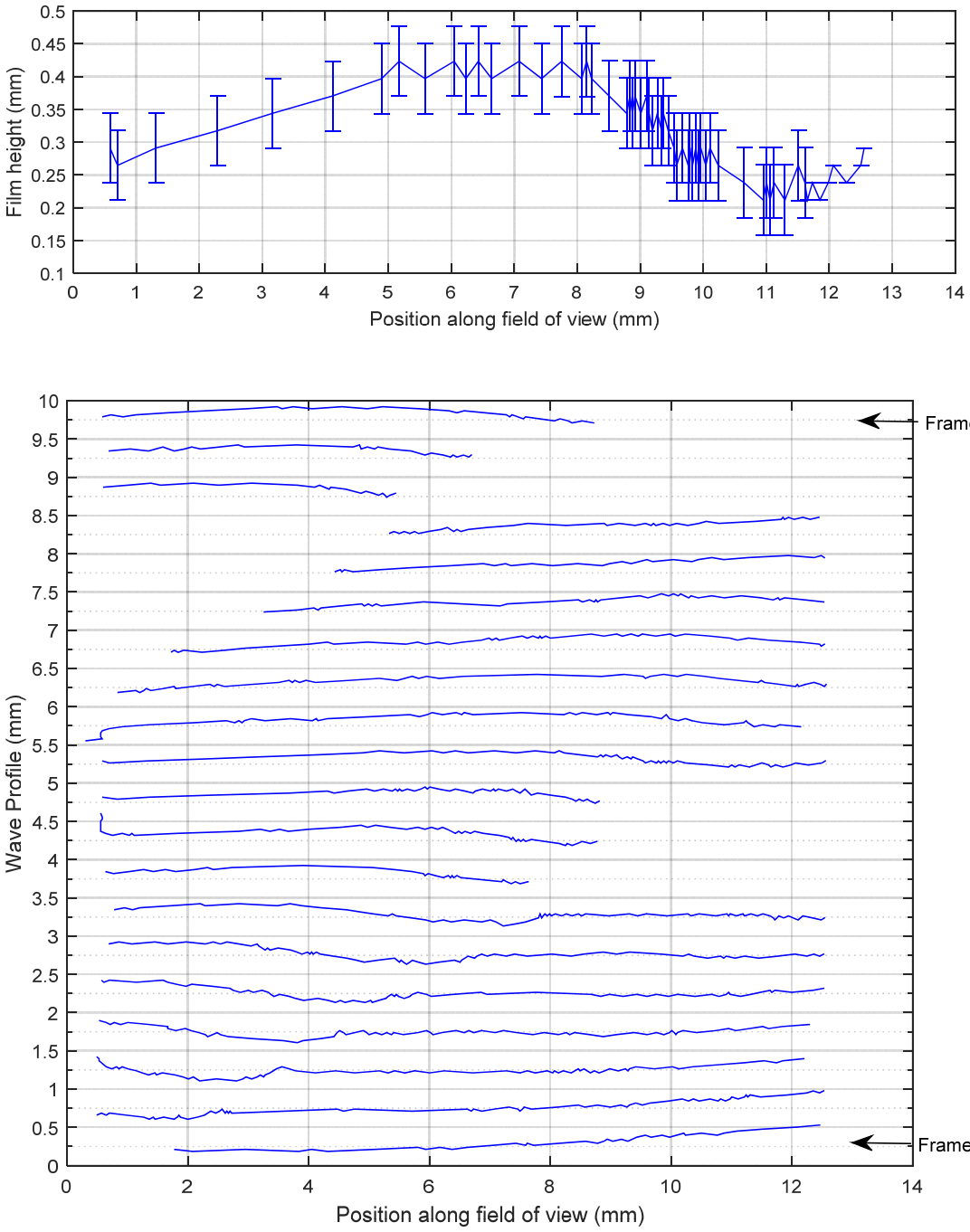

Fig. A16 Liquid flow condition 1, 120mm from top of column

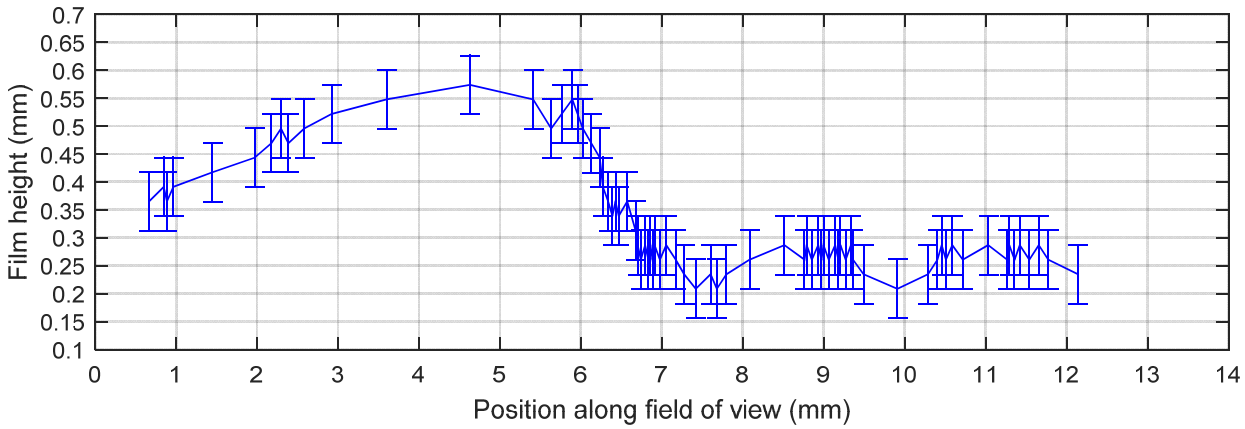

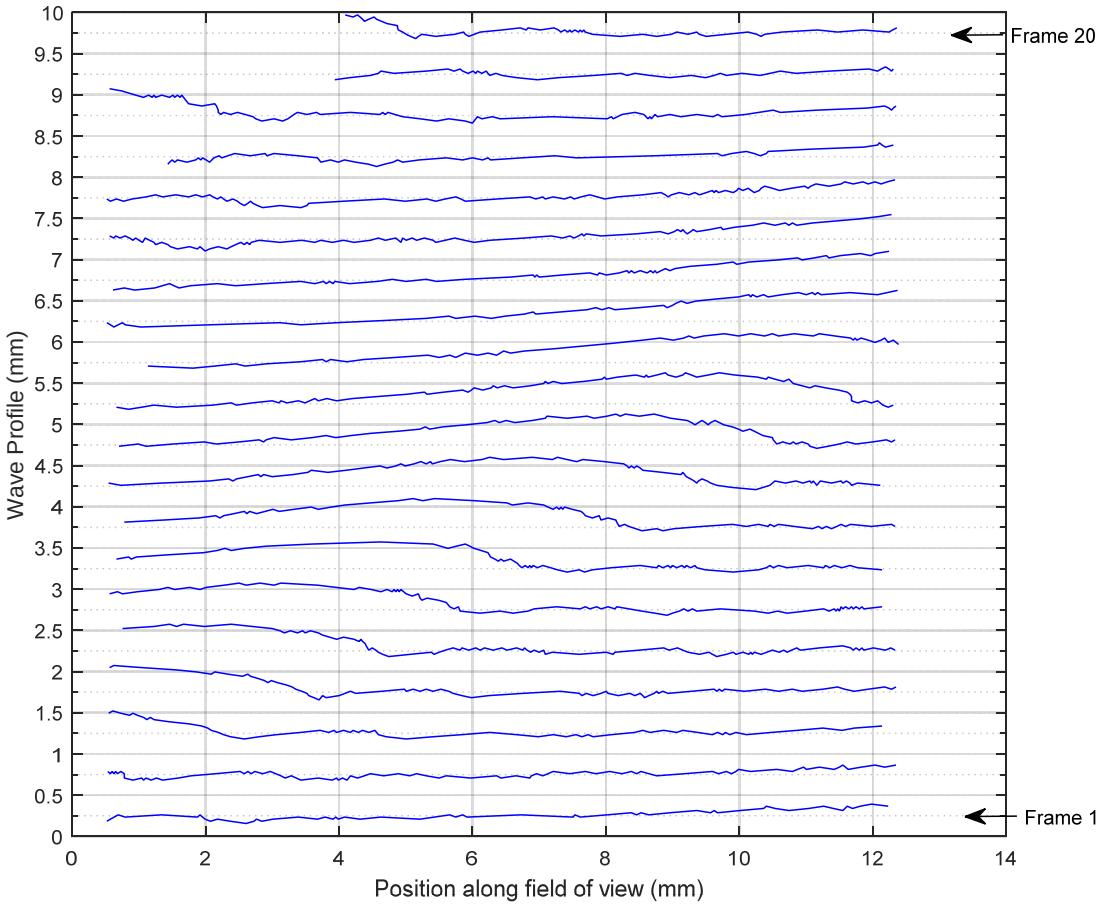

Fig. A17 Liquid flow condition 2, 120mm from top of column

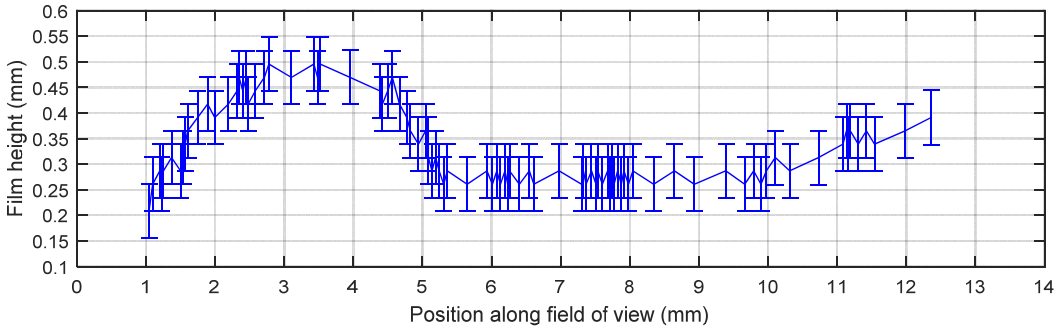

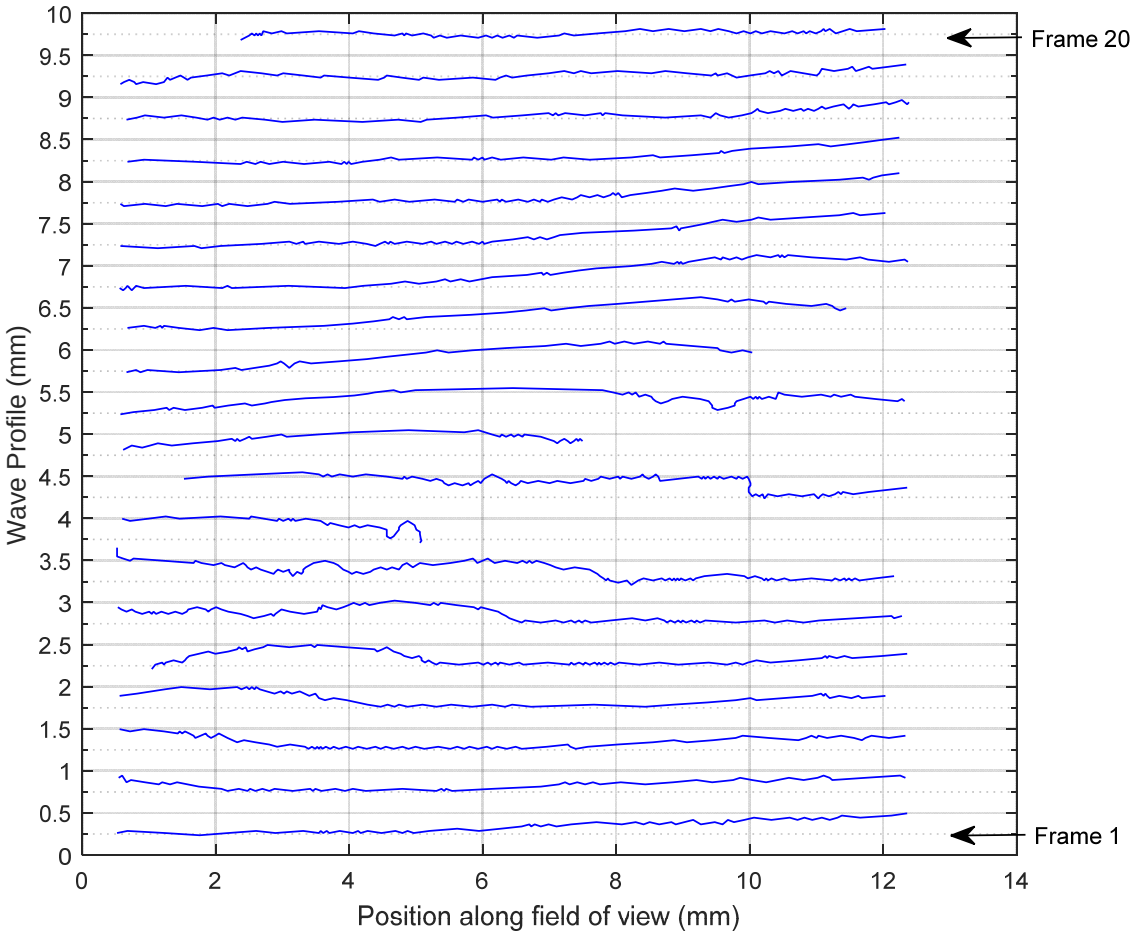

Fig. A18 Liquid flow condition 3, 120mm from top of column

A.3 Results with 80 l/min counter-current N_2

A3.1 40mm from top of column

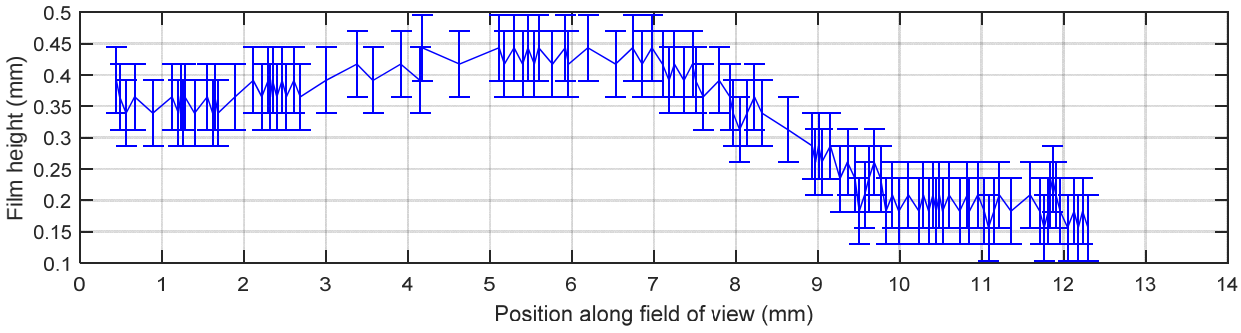

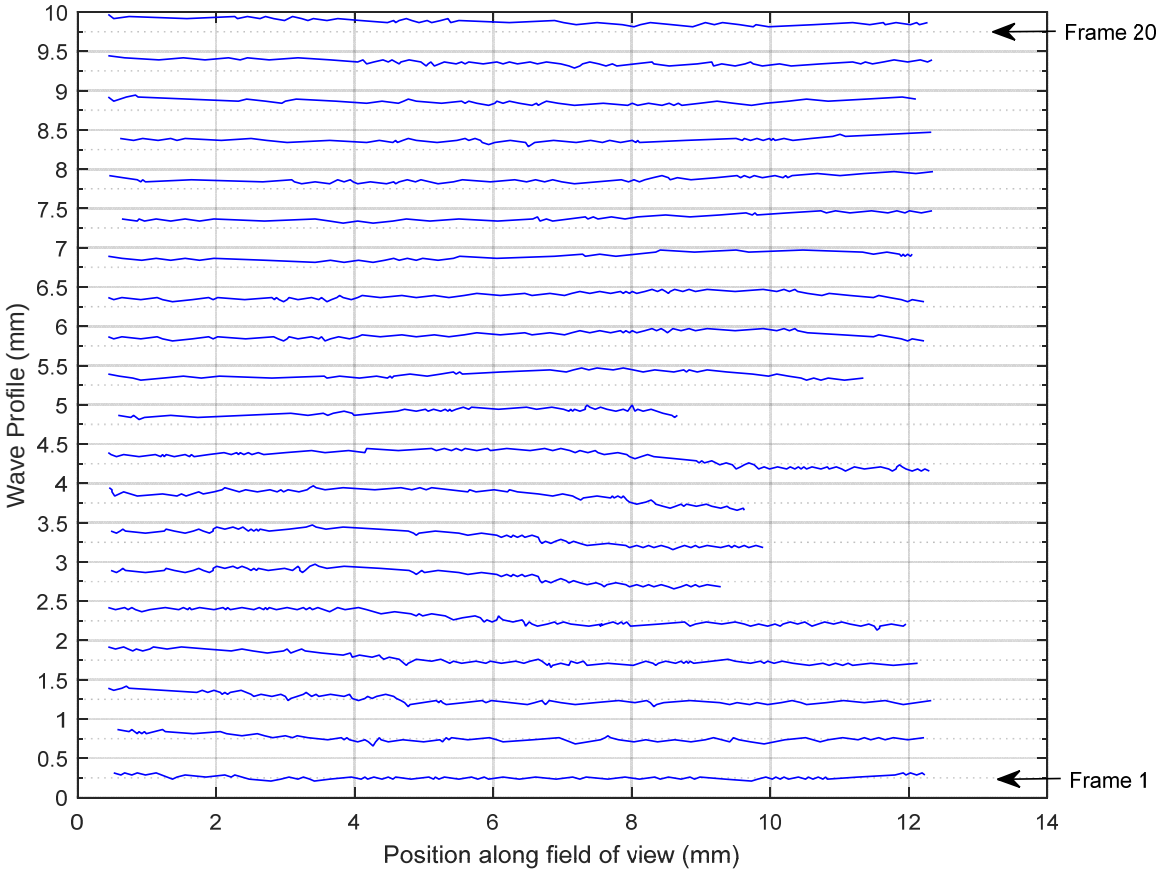

Fig. A19 Liquid flow condition 1, 40mm from top of column

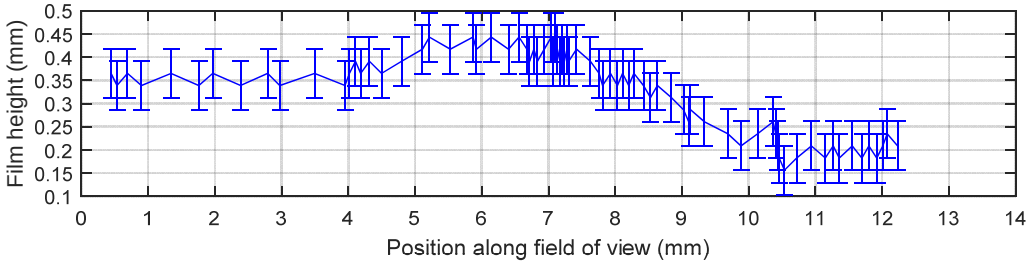

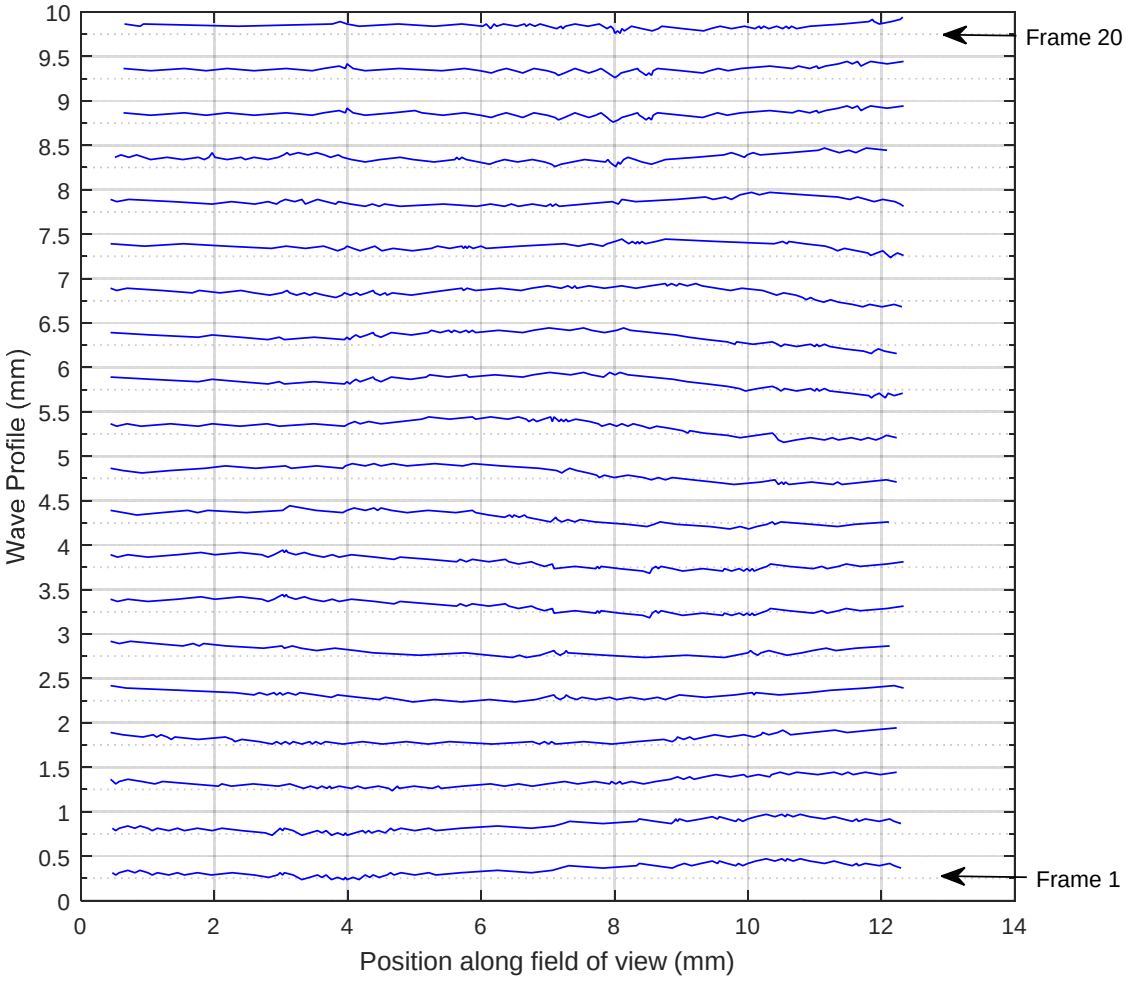

Fig. A20 Liquid flow condition 2, 40mm from top of column

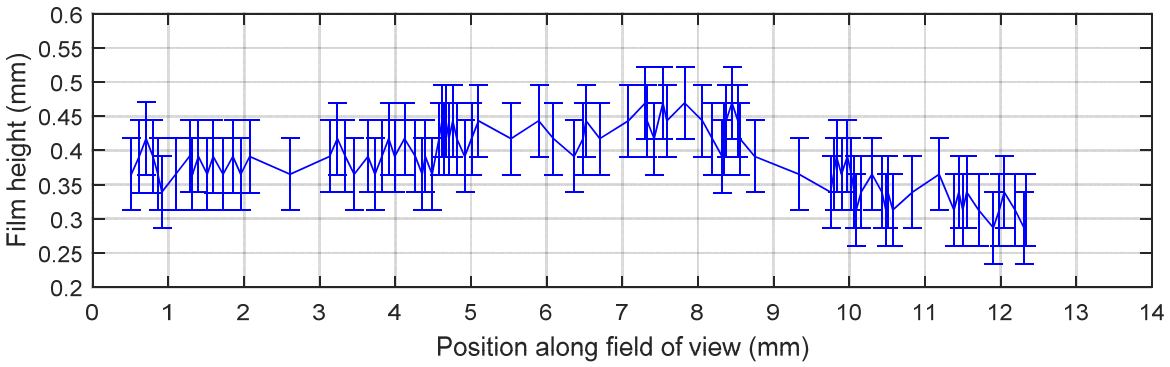

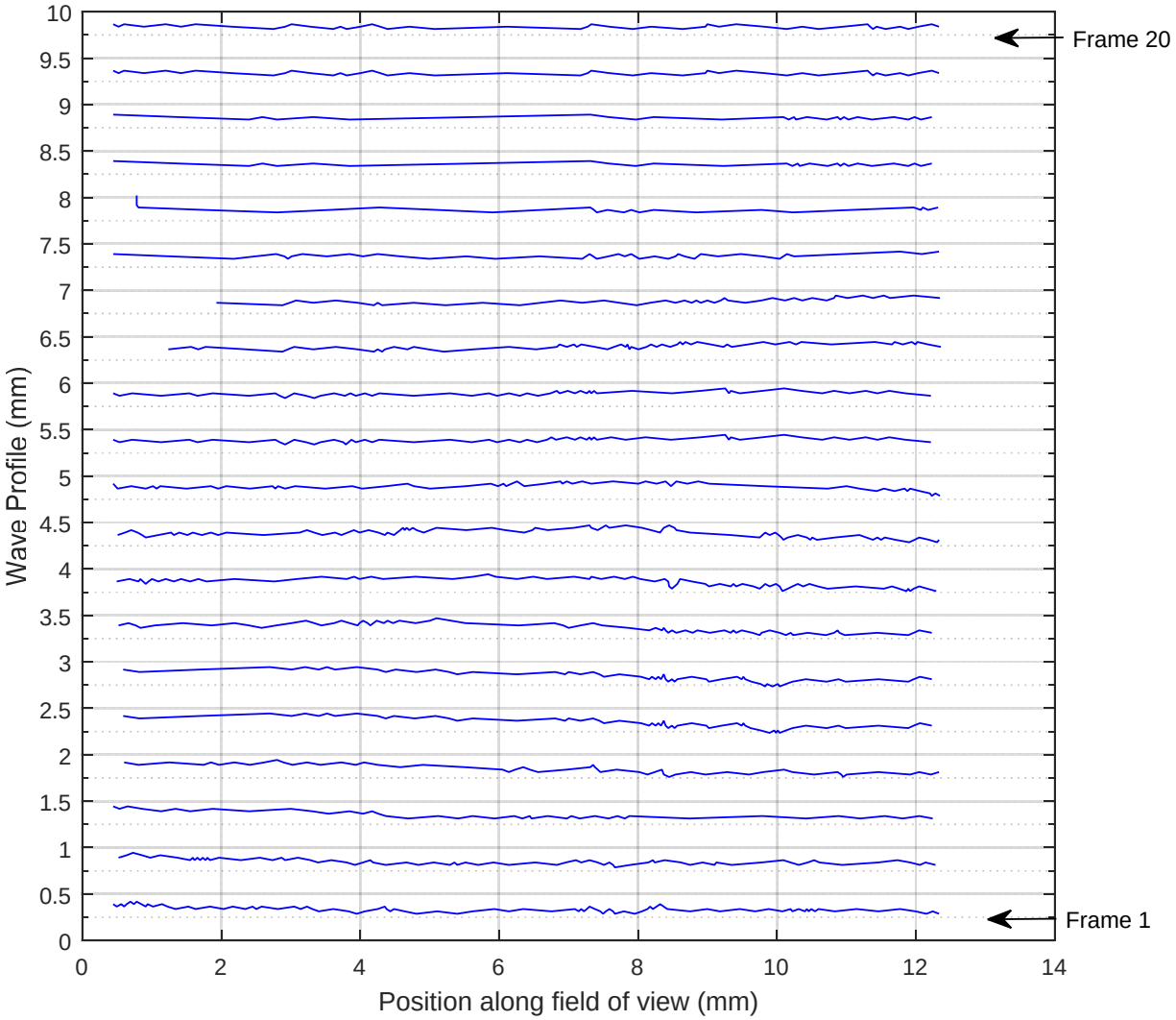

Fig. A21 Liquid flow condition 3, 40mm from top of column

A.3.2 80mm from top of column

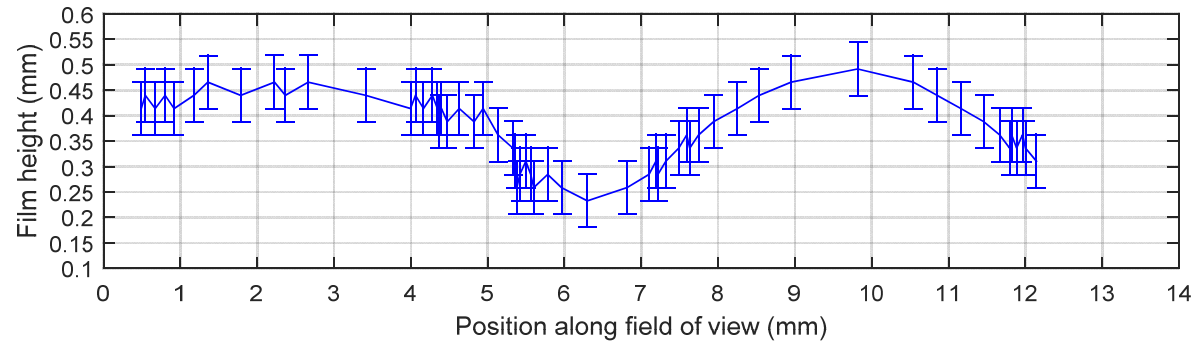

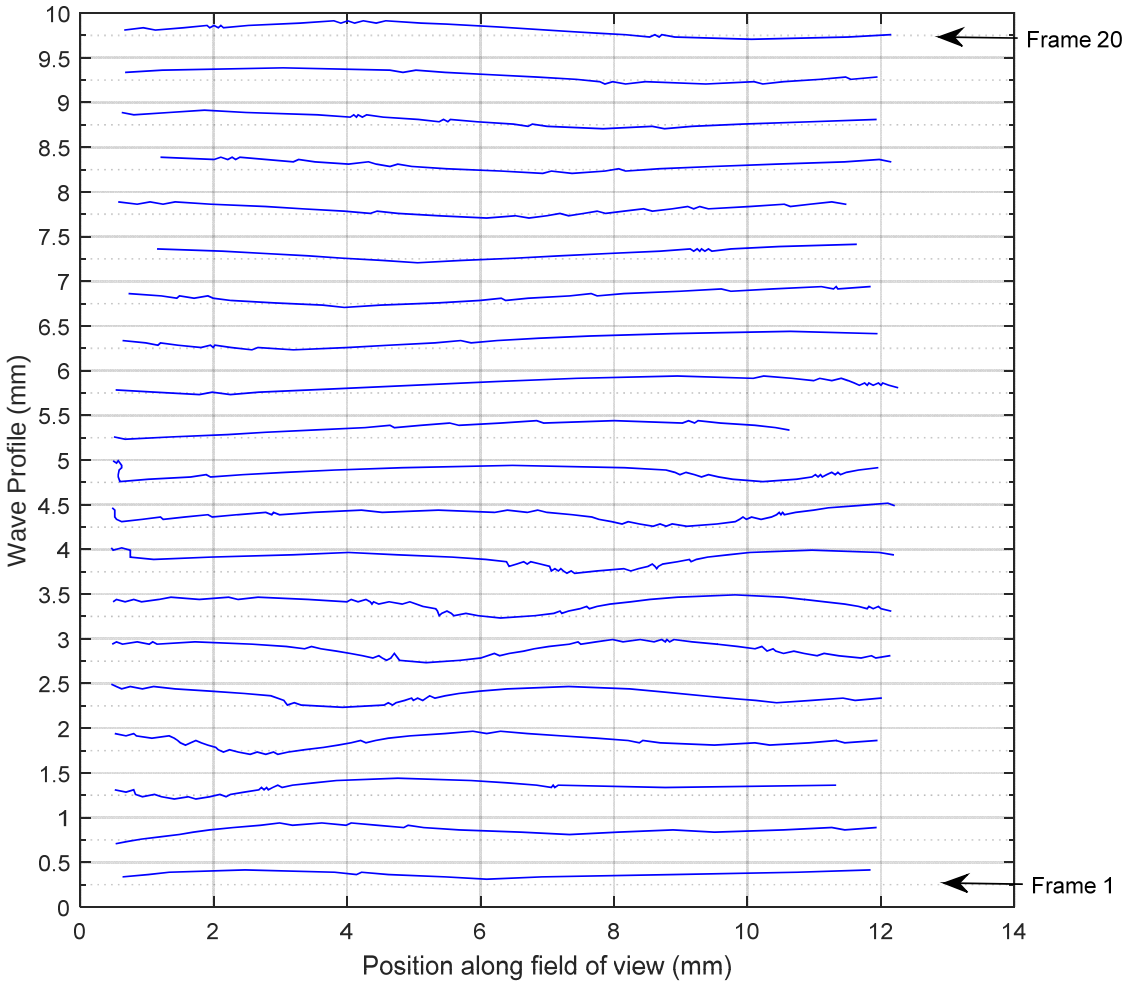

Fig. A22 Liquid flow condition 1, 80mm from top of column

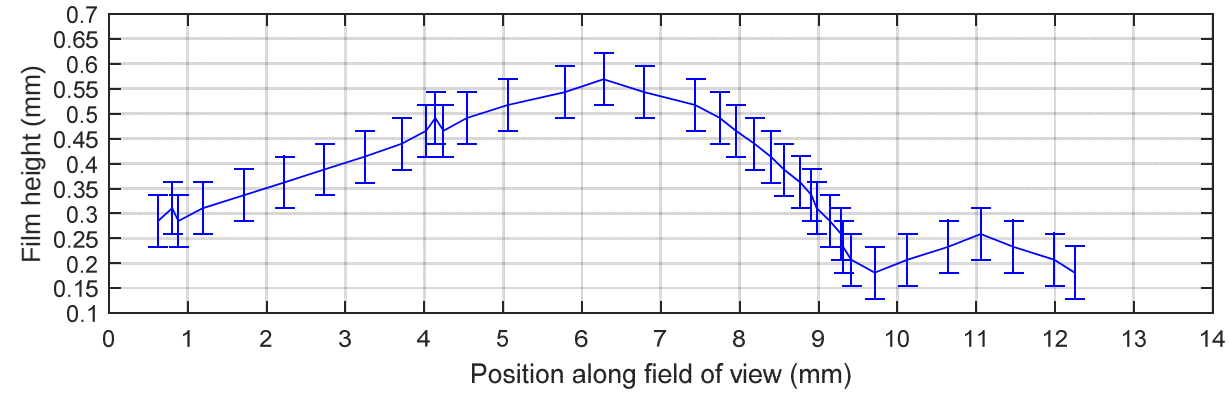

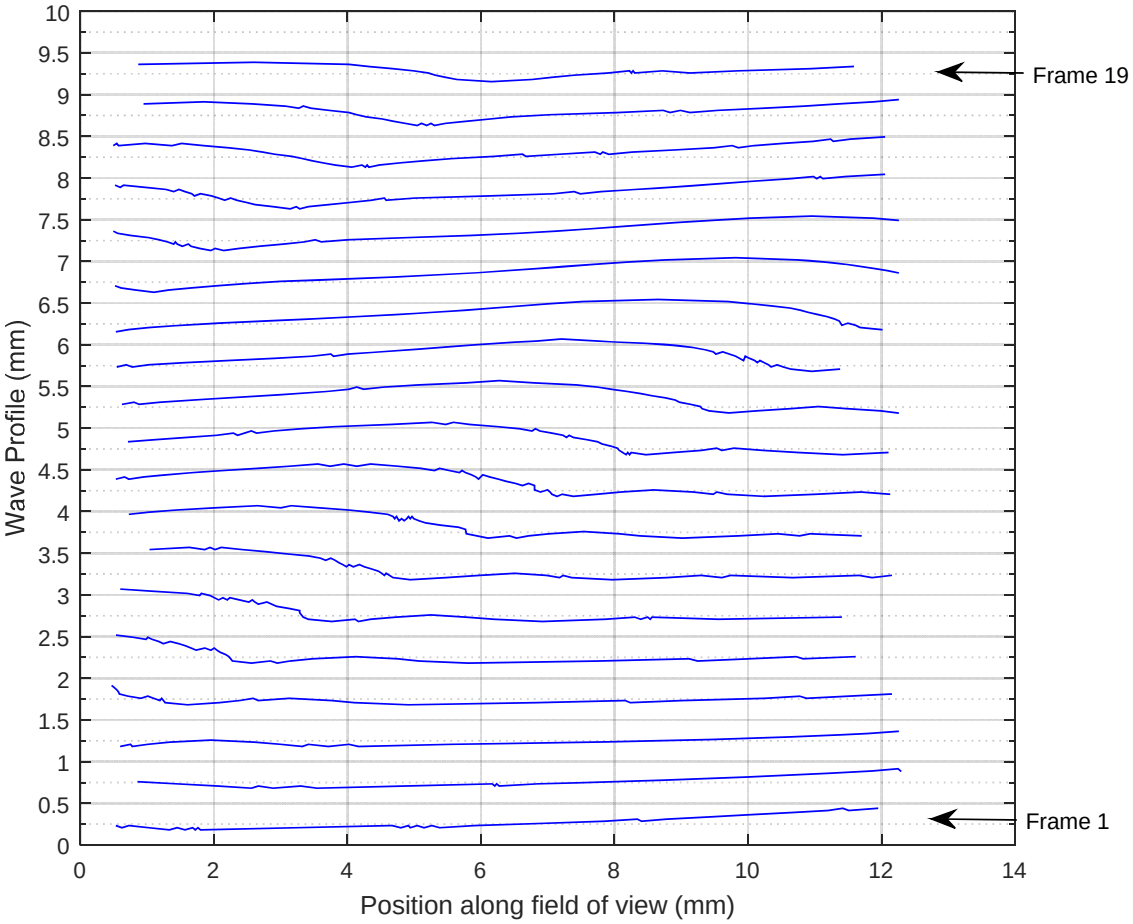

Fig. A23 Liquid flow condition 2, 80mm from top of column

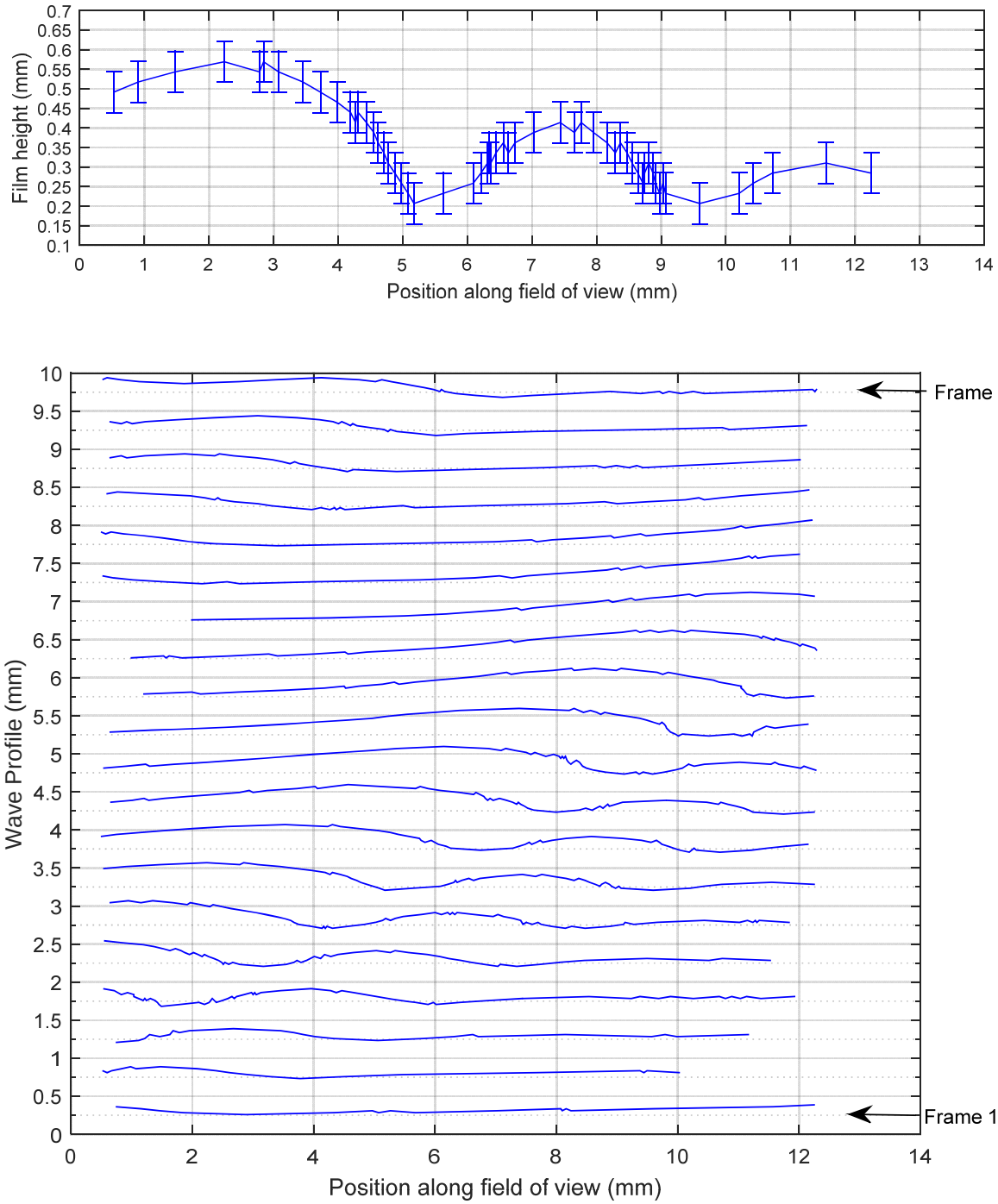

Fig. A24 Liquid flow condition 3, 80mm from top of column

A1.3.3 120mm from top of column

In this location with 80l/min N_2 the full wave profile is again obscured or distorted in places due to the presence of liquid droplets on the inner wall of the perspex tube.

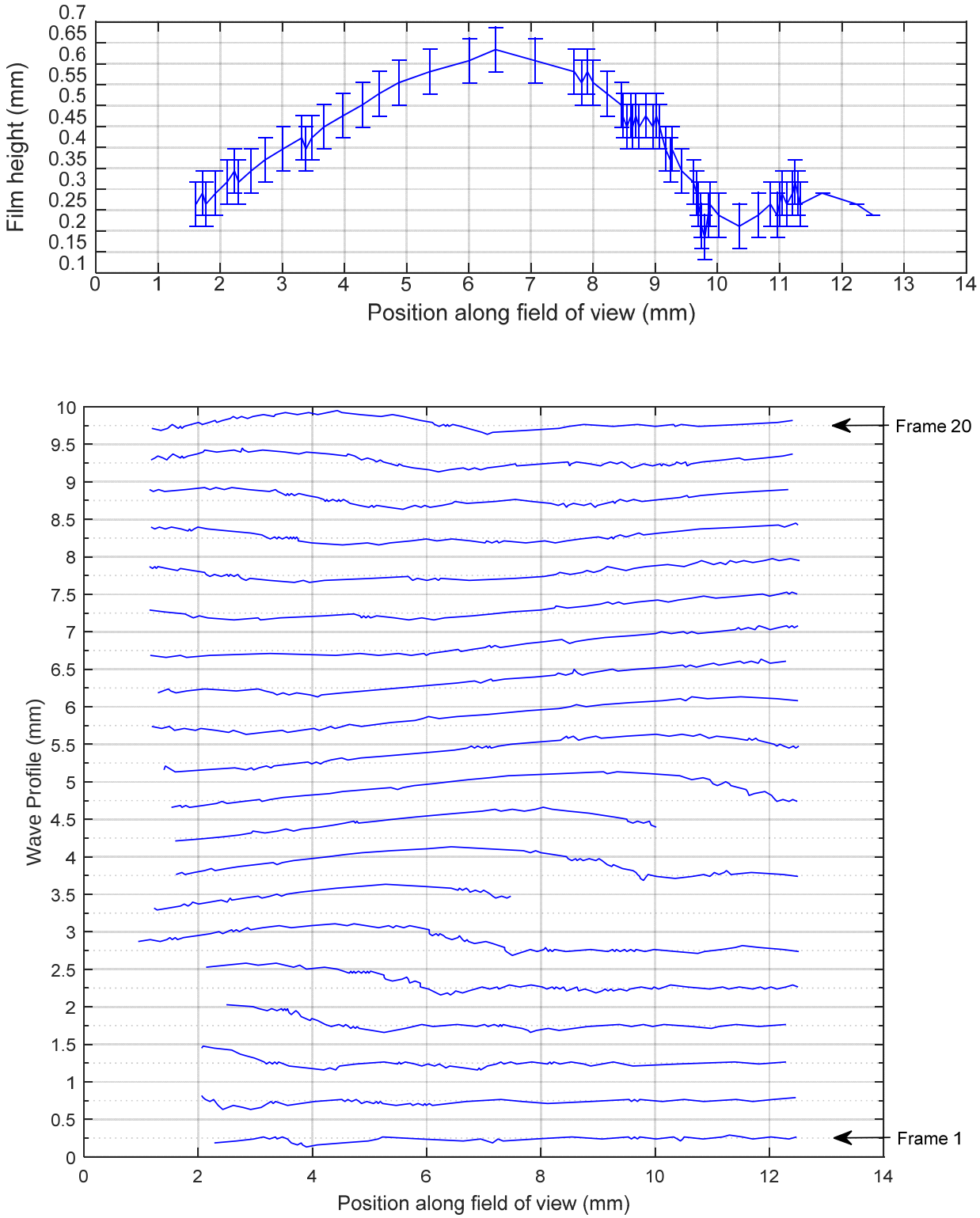

Fig. A25 Liquid flow condition 1, 120mm from top of column

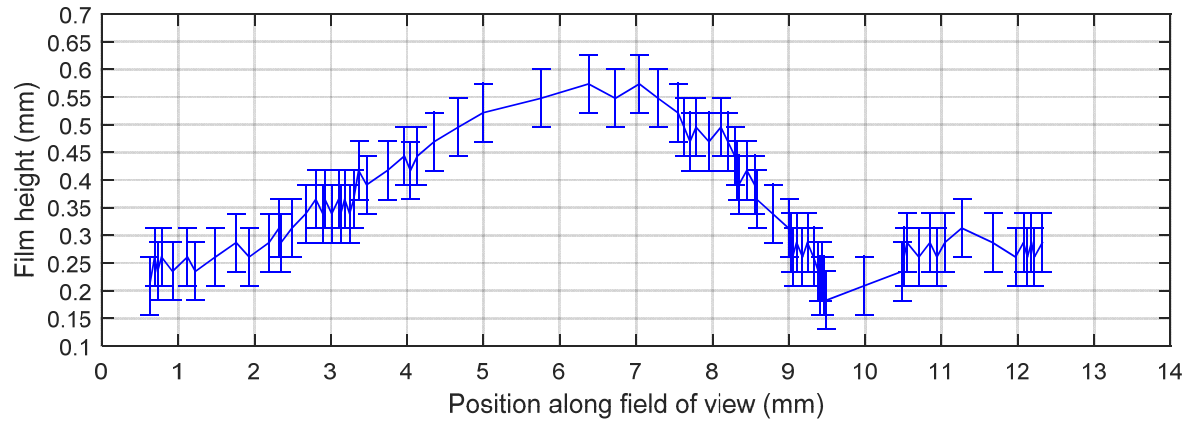

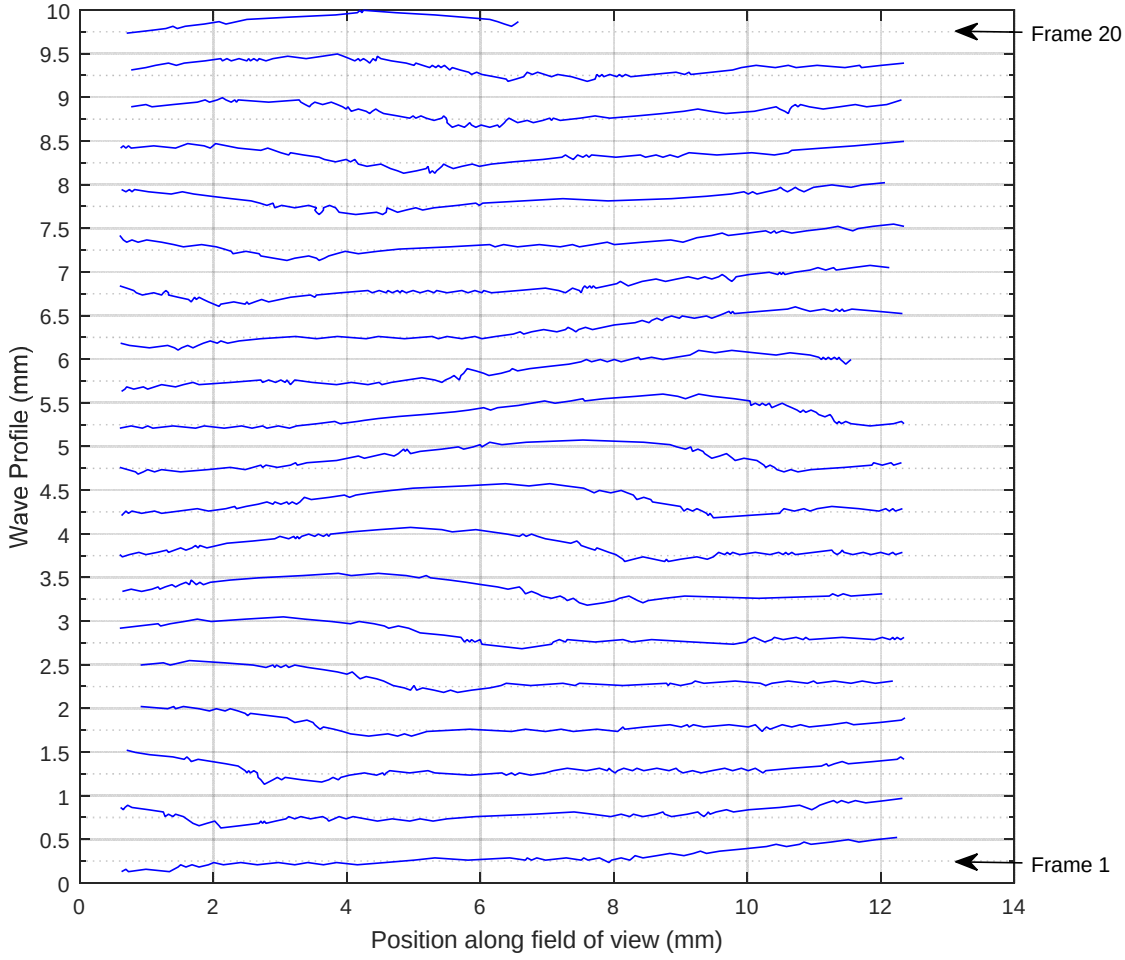

Fig. A26 Liquid flow condition 2, 120mm from top of column

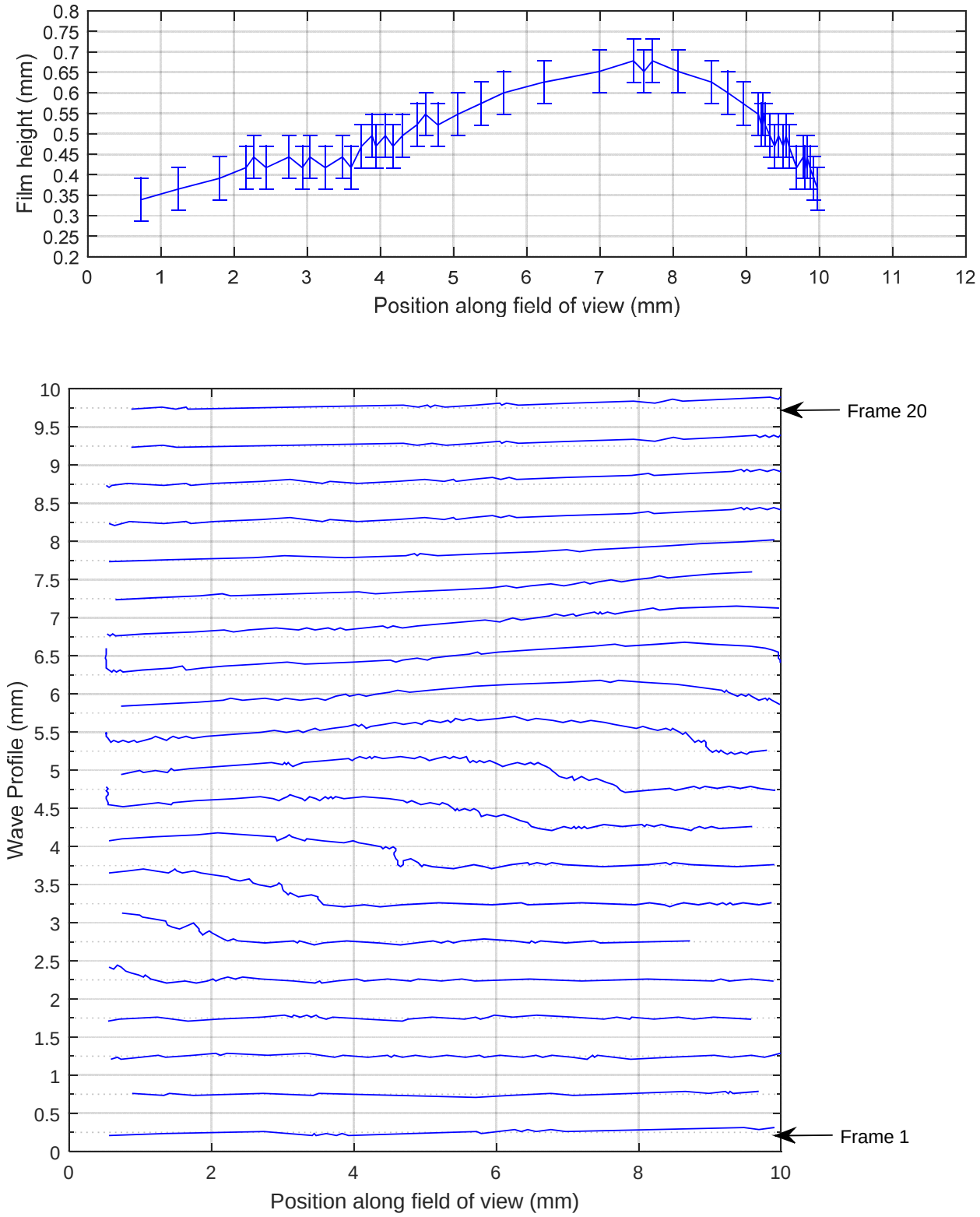

Fig. A27 Liquid flow condition 3, 120mm from top of column

A.4 Results with 20 l/min counter-current CO_2

A4.1 40mm from top of column

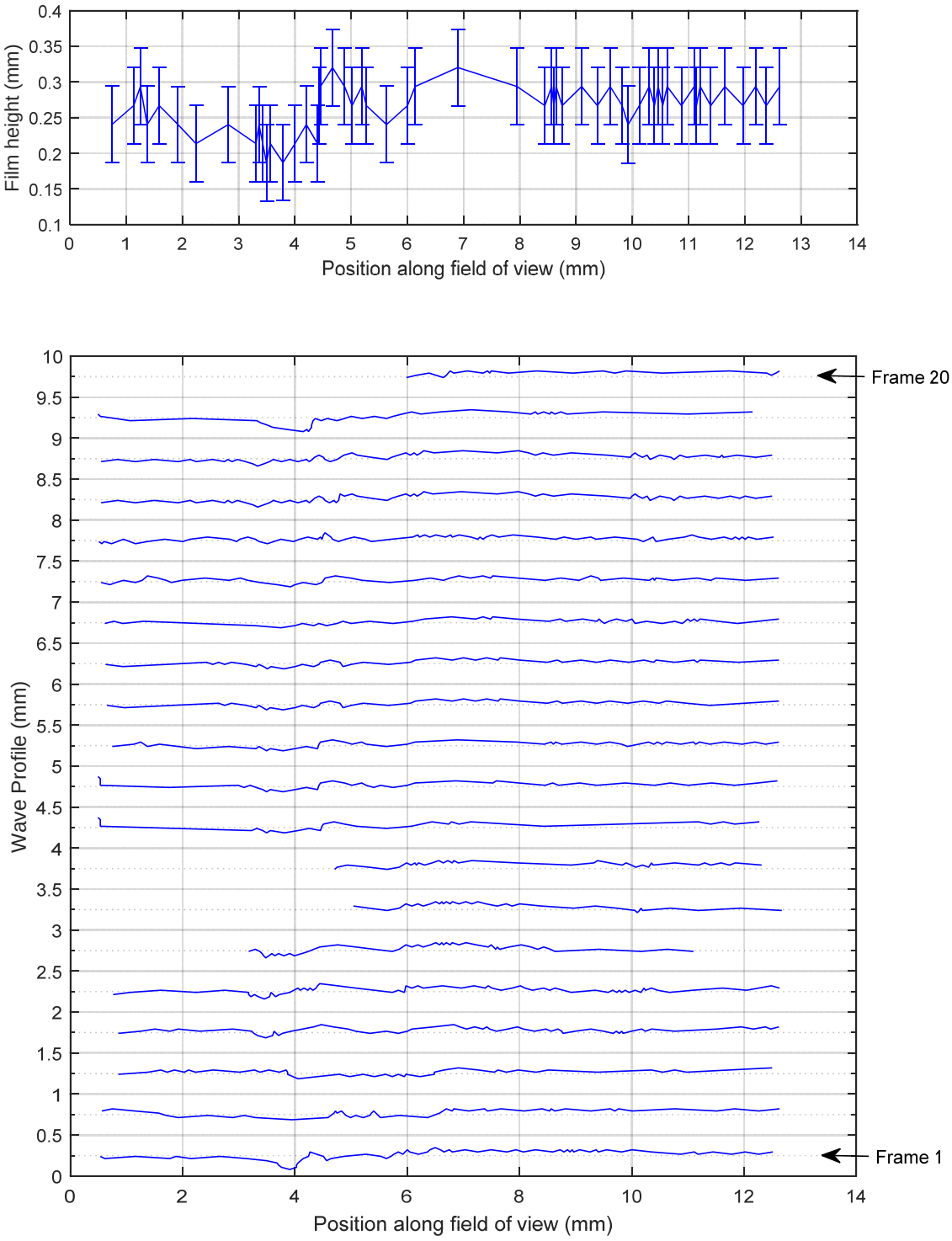

Fig. A28 Liquid flow condition 1, 40mm from top of column

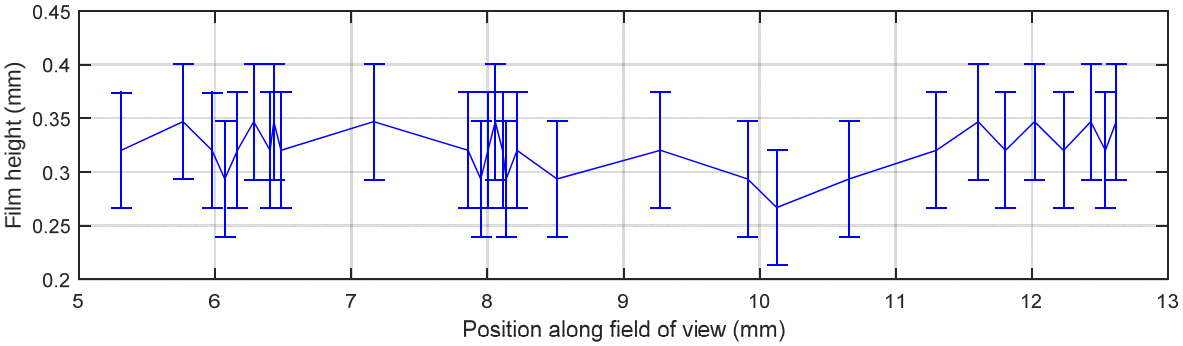

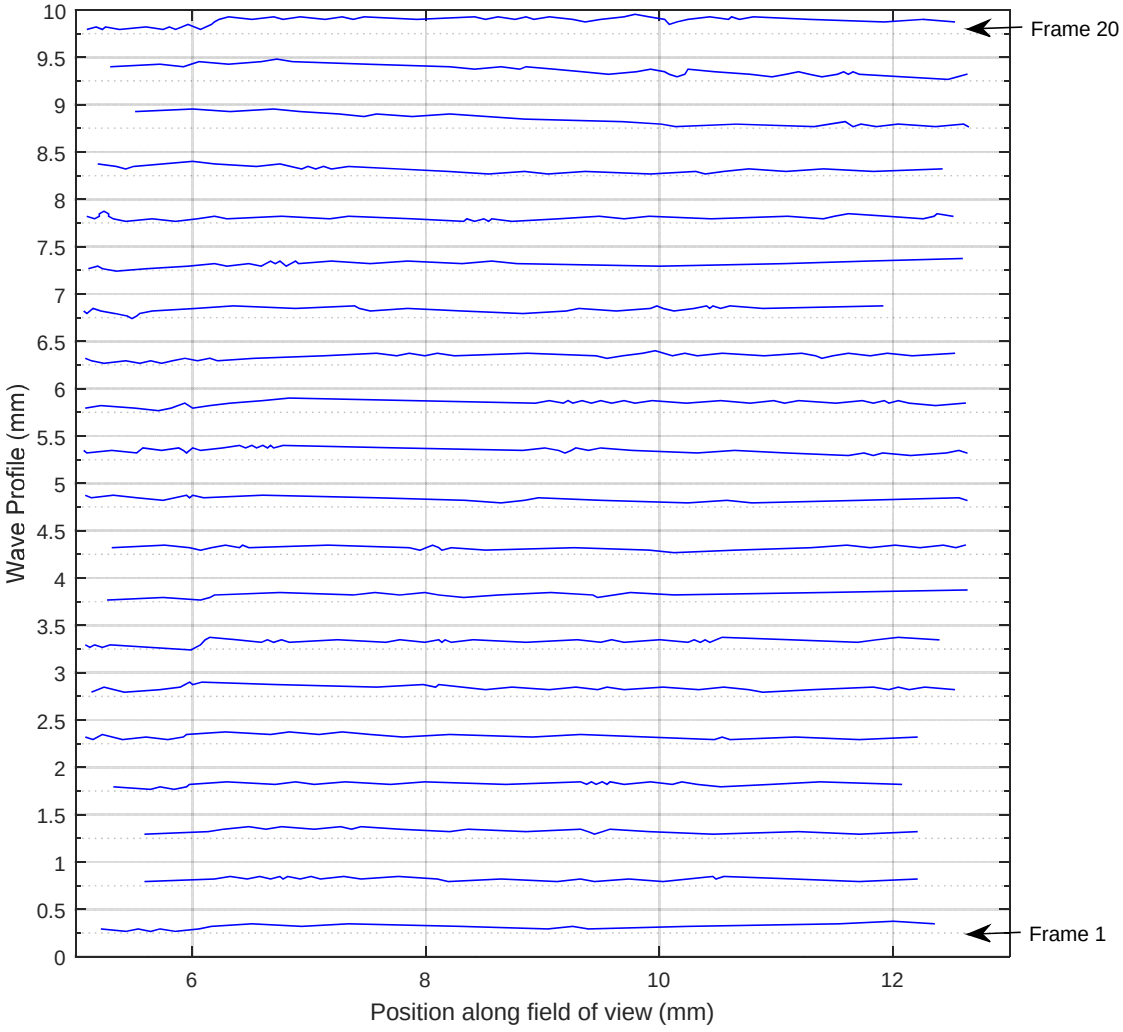

Fig. A29 Liquid flow condition 2, 40mm from top of column

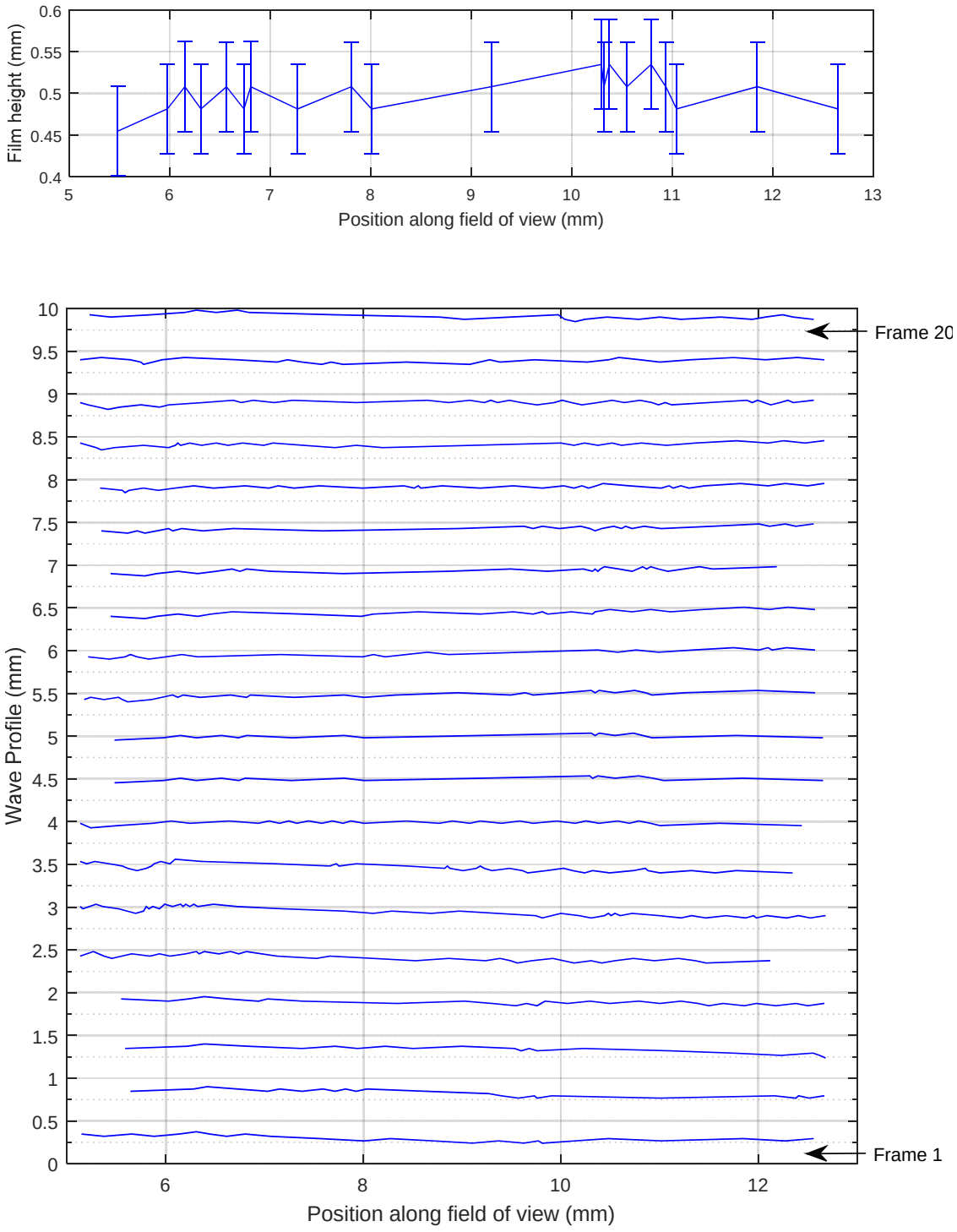

Fig. A30 Liquid flow condition 3, 40mm from top of column

A.4.2 80mm from top of column

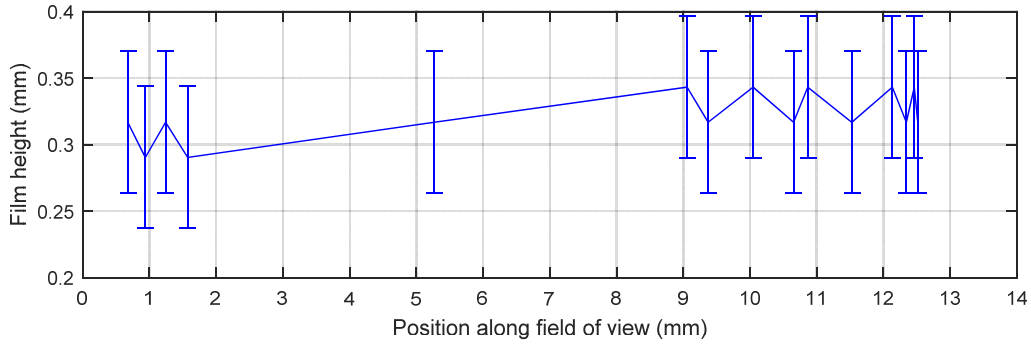

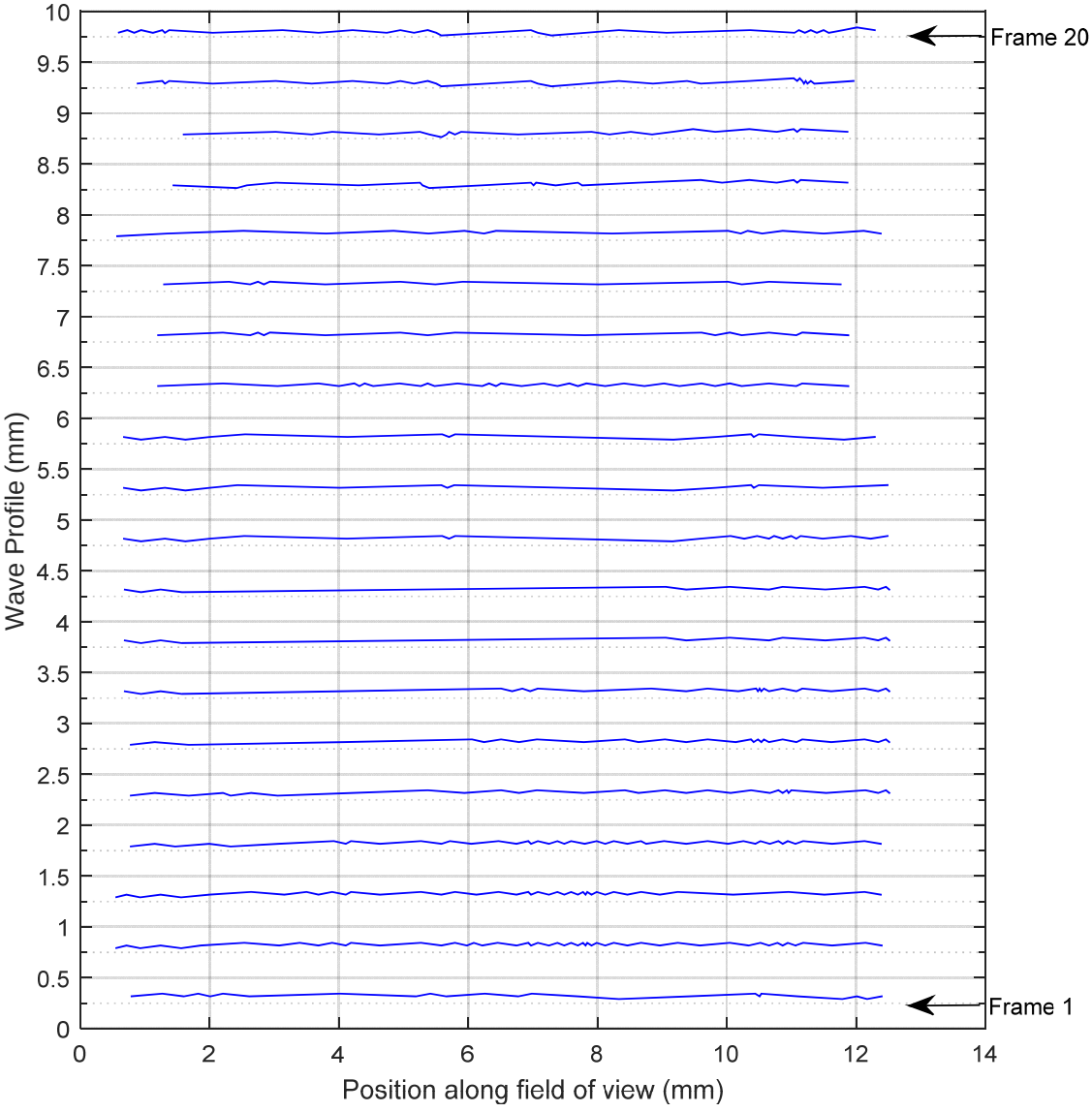

Fig. A31 Liquid flow condition 1, 80mm from top of column

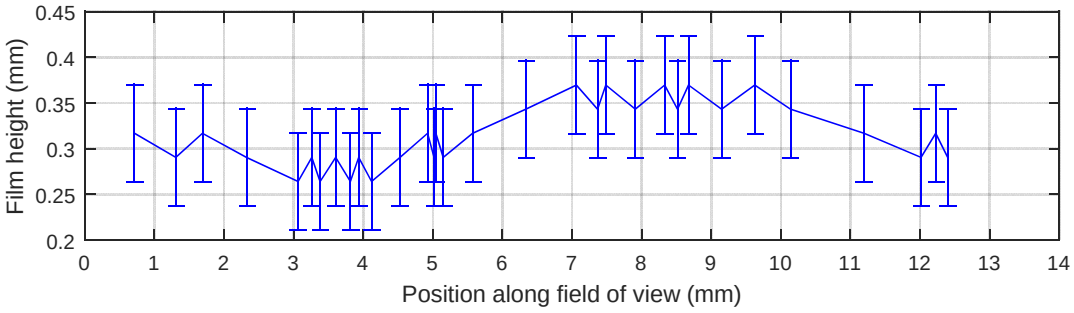

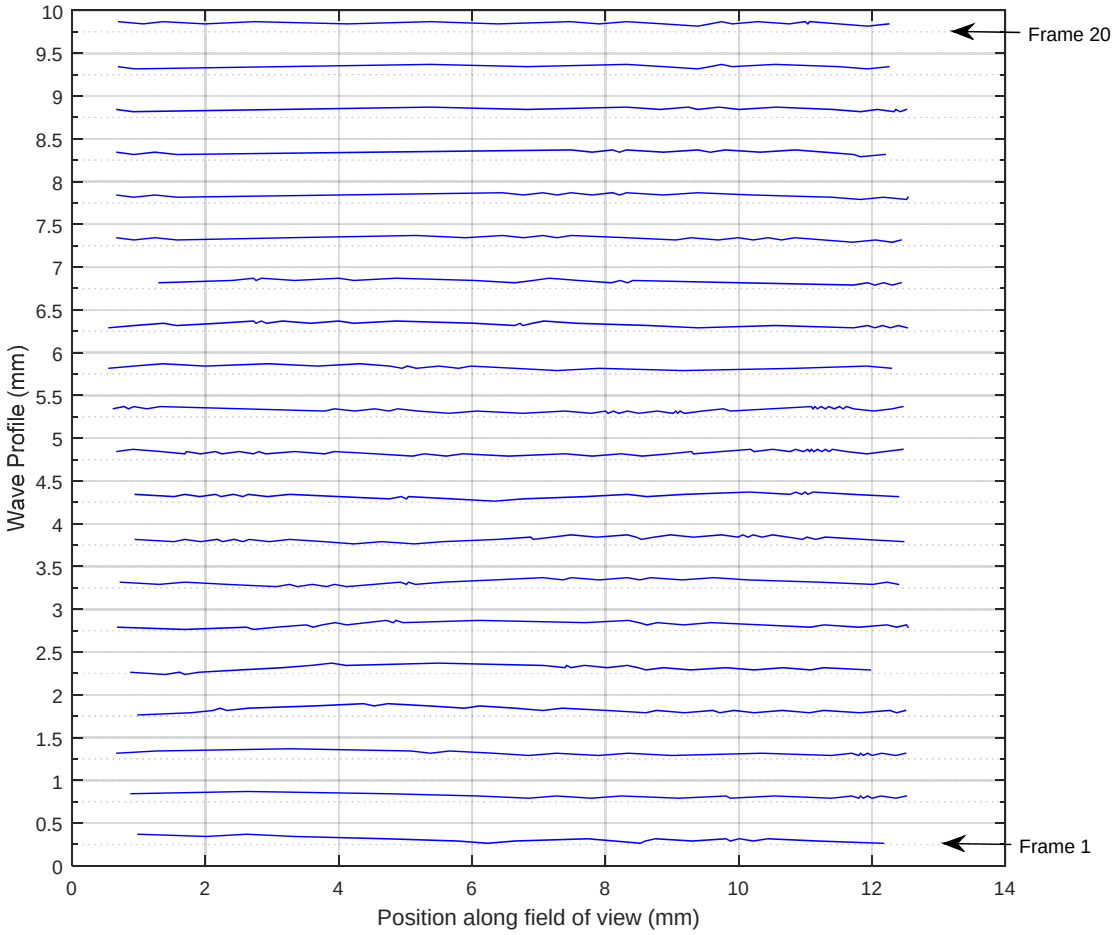

Fig. A32 Liquid flow condition 2, 80mm from top of column

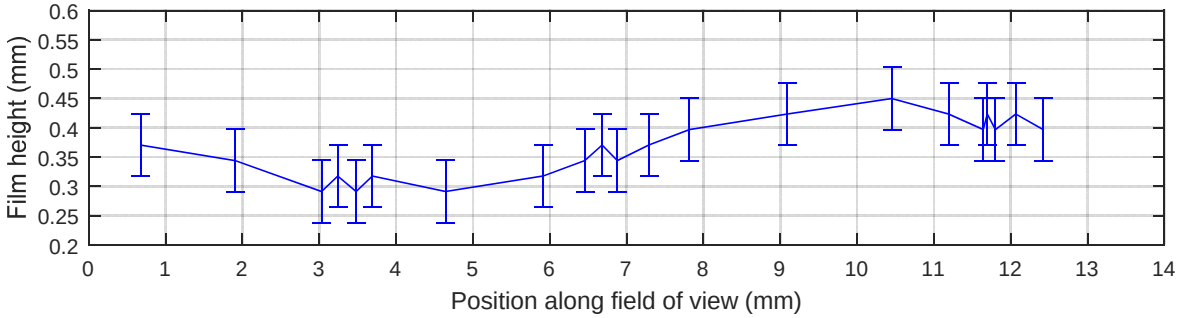

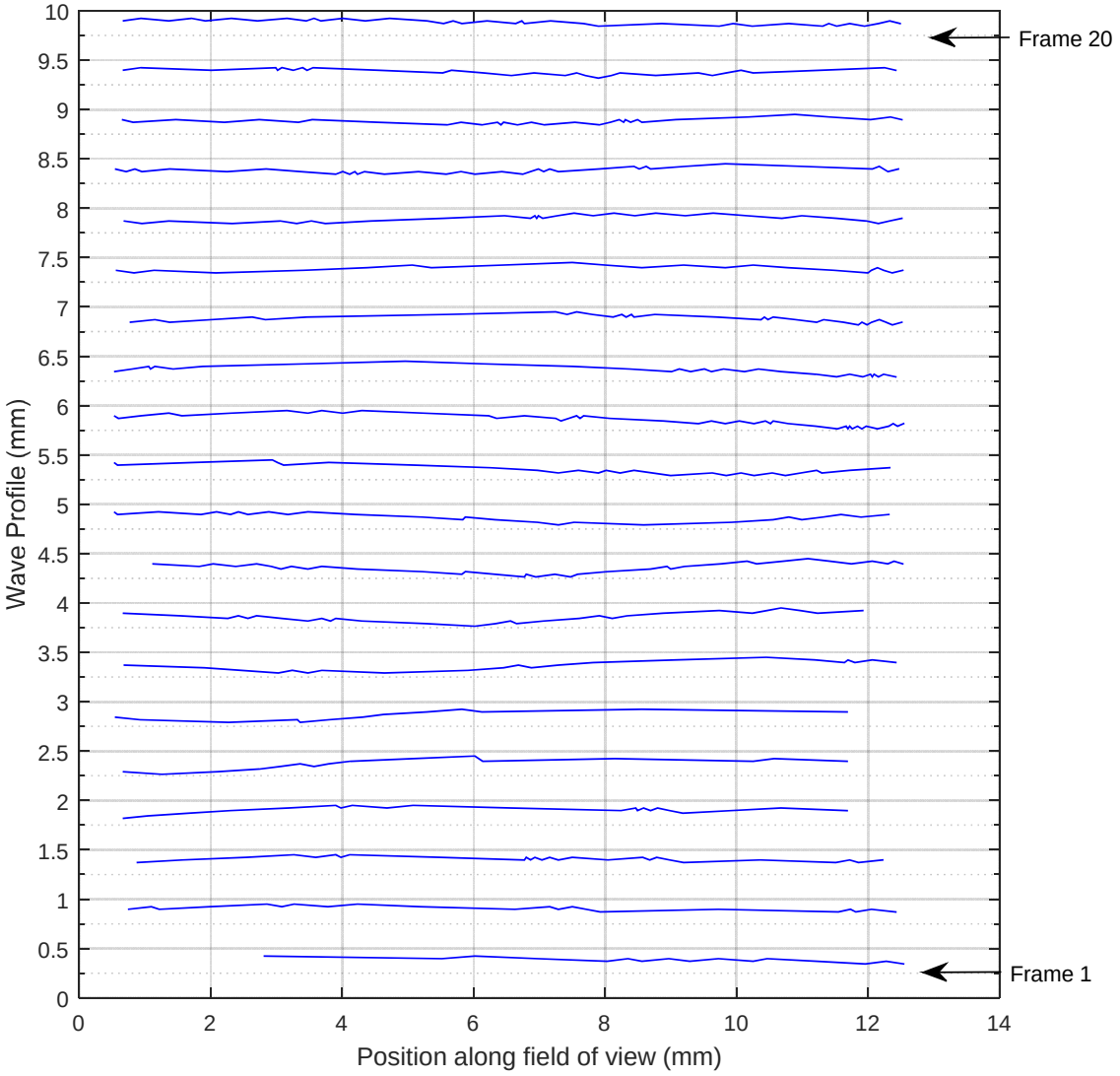

Fig. A33 Liquid flow condition 3, 80mm from top of column

A.4.3 120mm from top of column

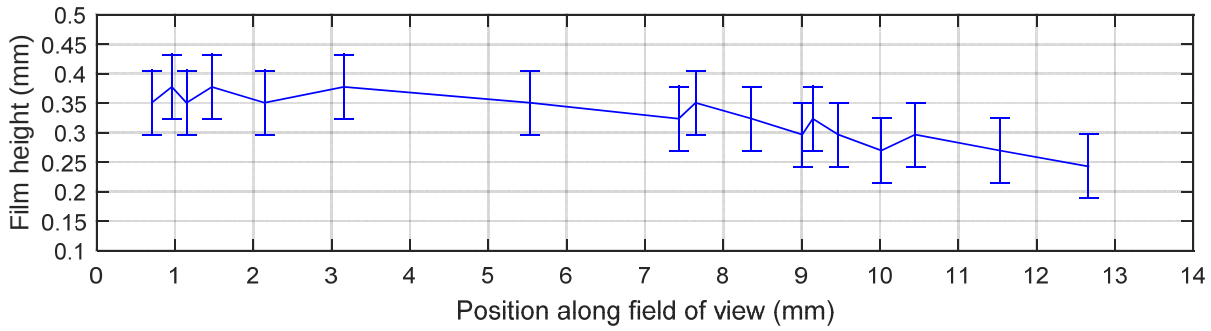

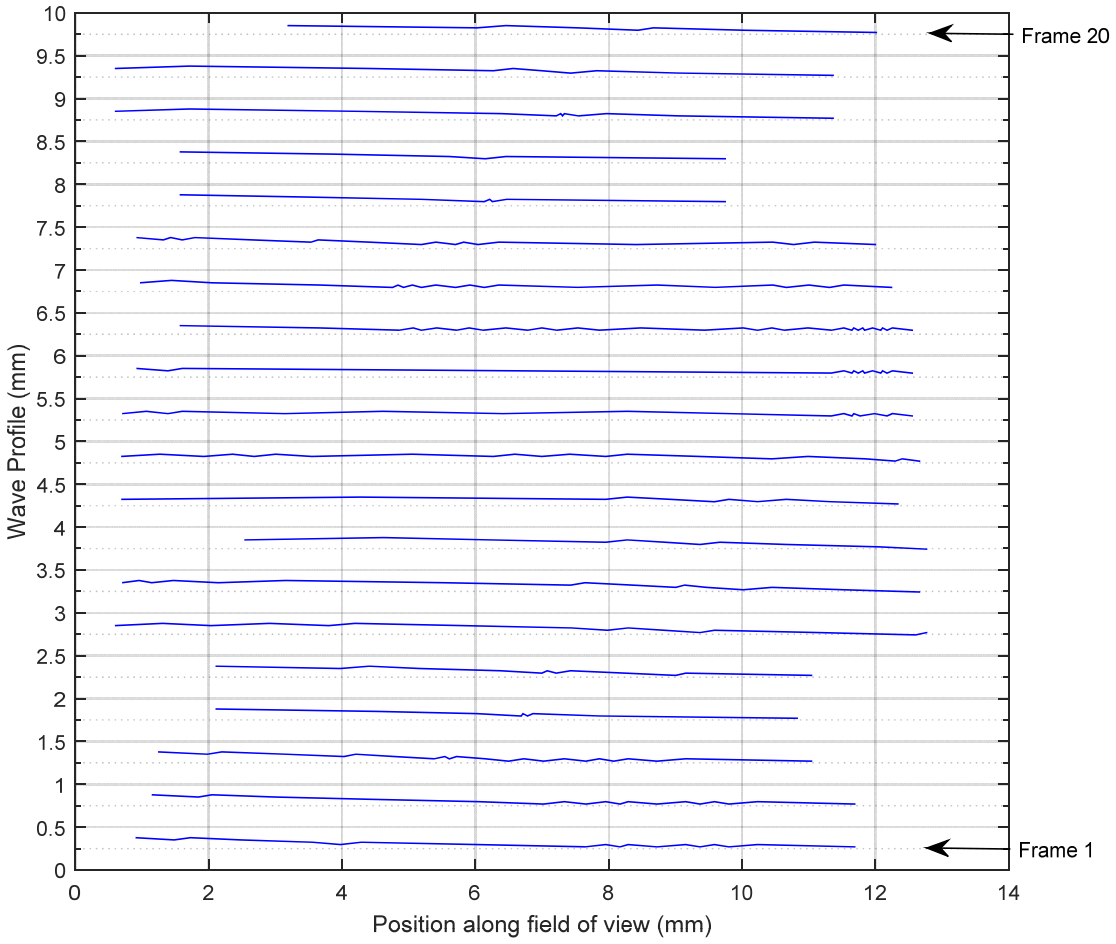

Fig. A34 Liquid flow condition 1, 120mm from top of column

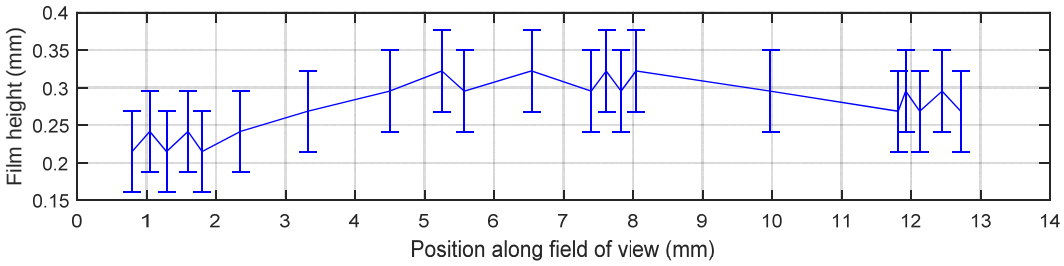

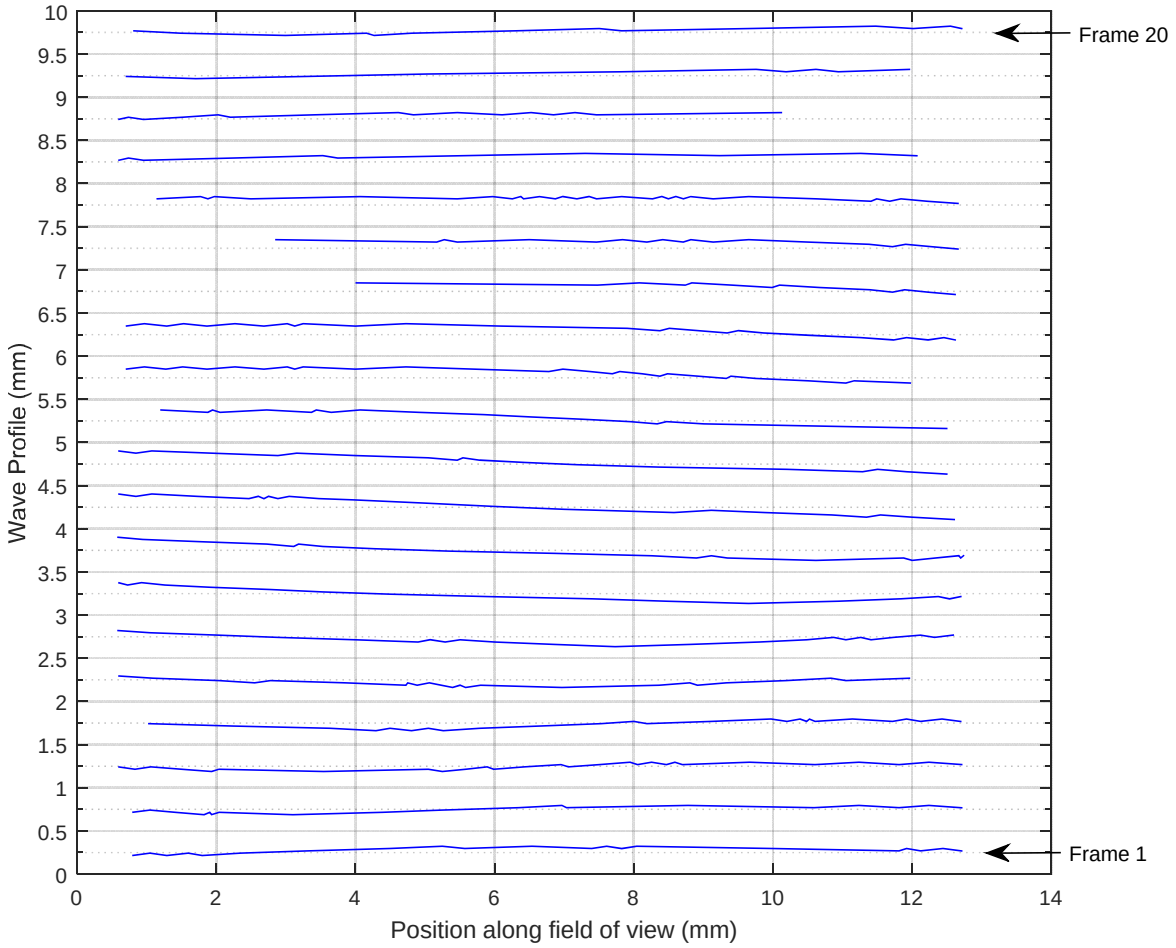

Fig. A35 Liquid flow condition 2, 120mm from top of column

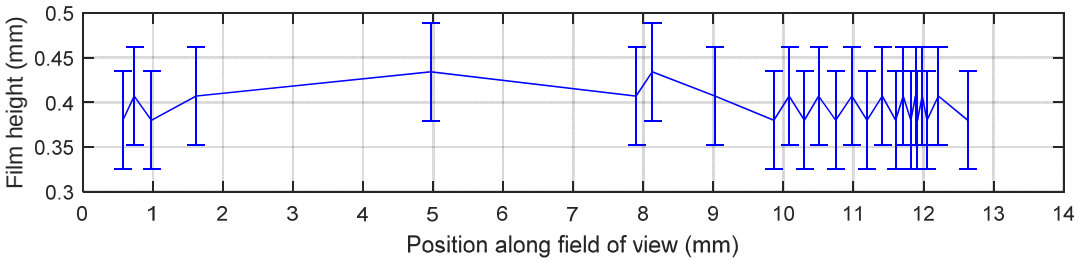

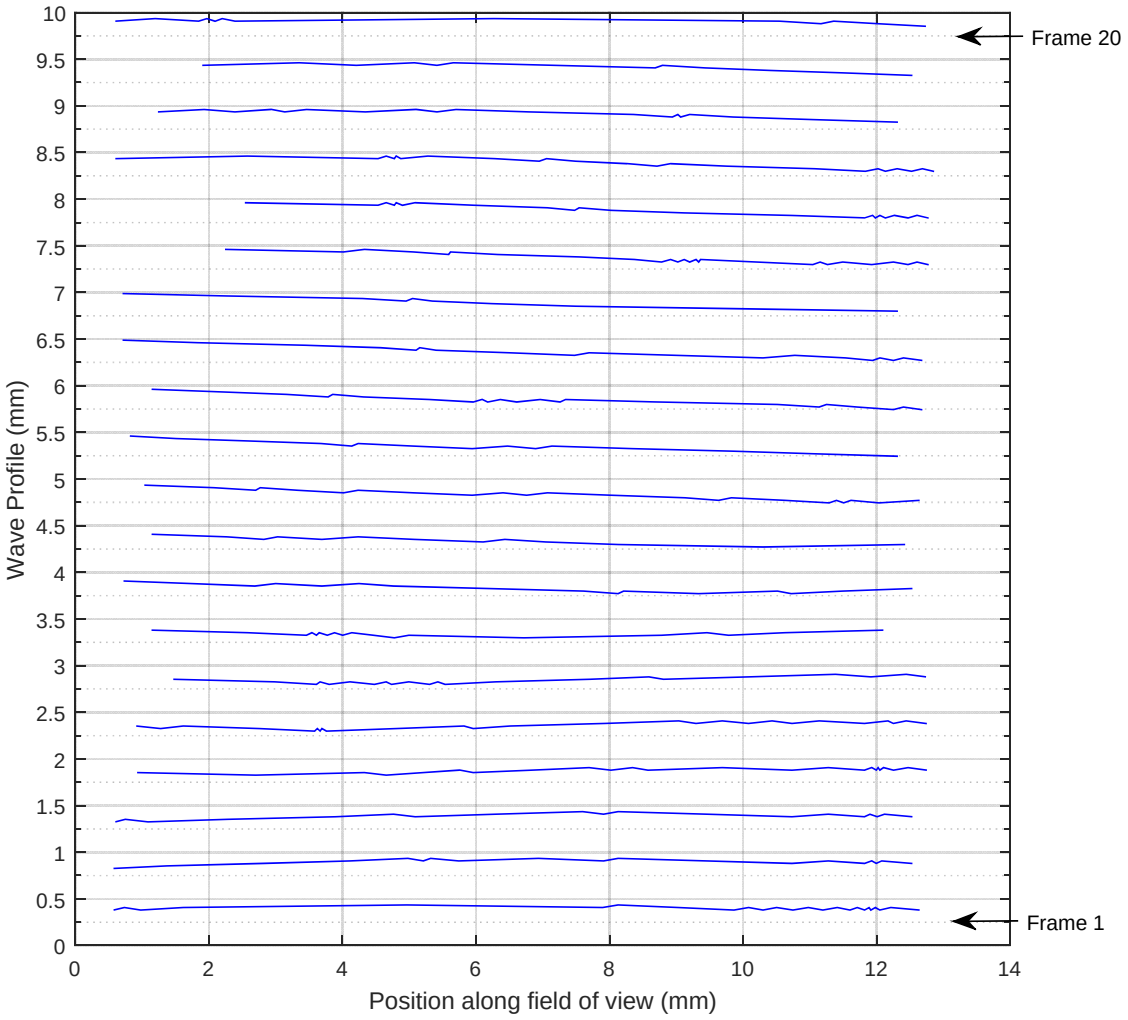

Fig. A36 Liquid flow condition 3, 120mm from top of column

A.5. Results with 80 l/min counter-current N_2

A.5.1 40mm from top of column

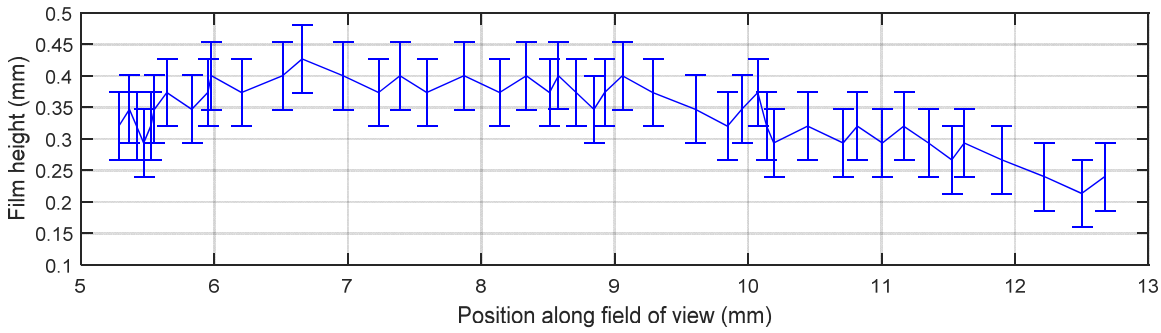

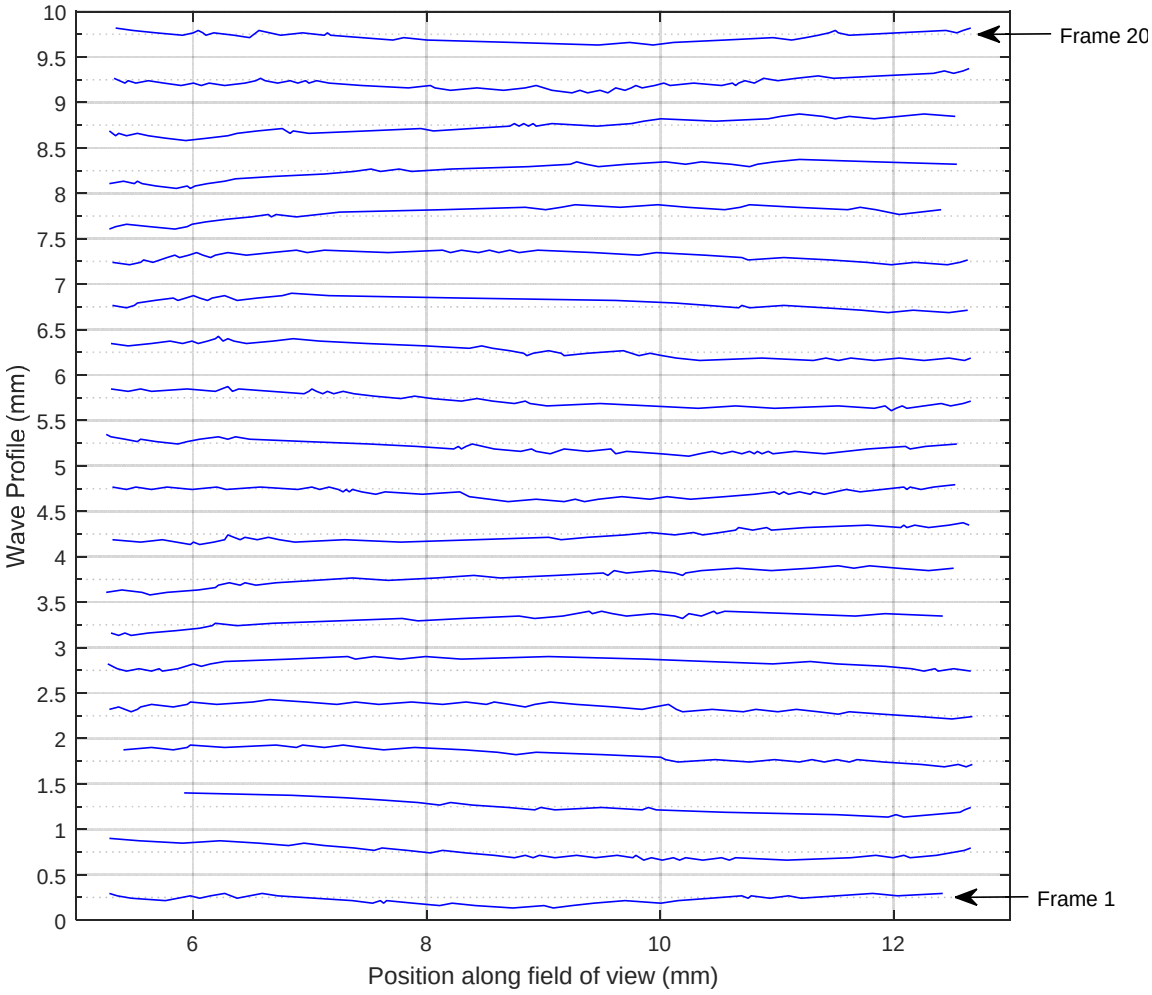

Fig. A37 Liquid flow condition 1, 40mm from top of column

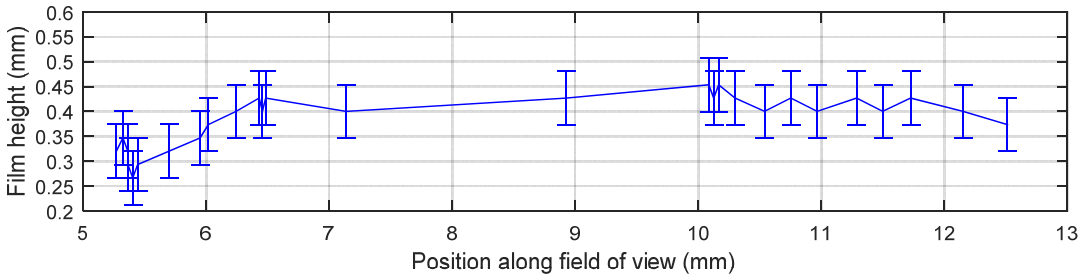

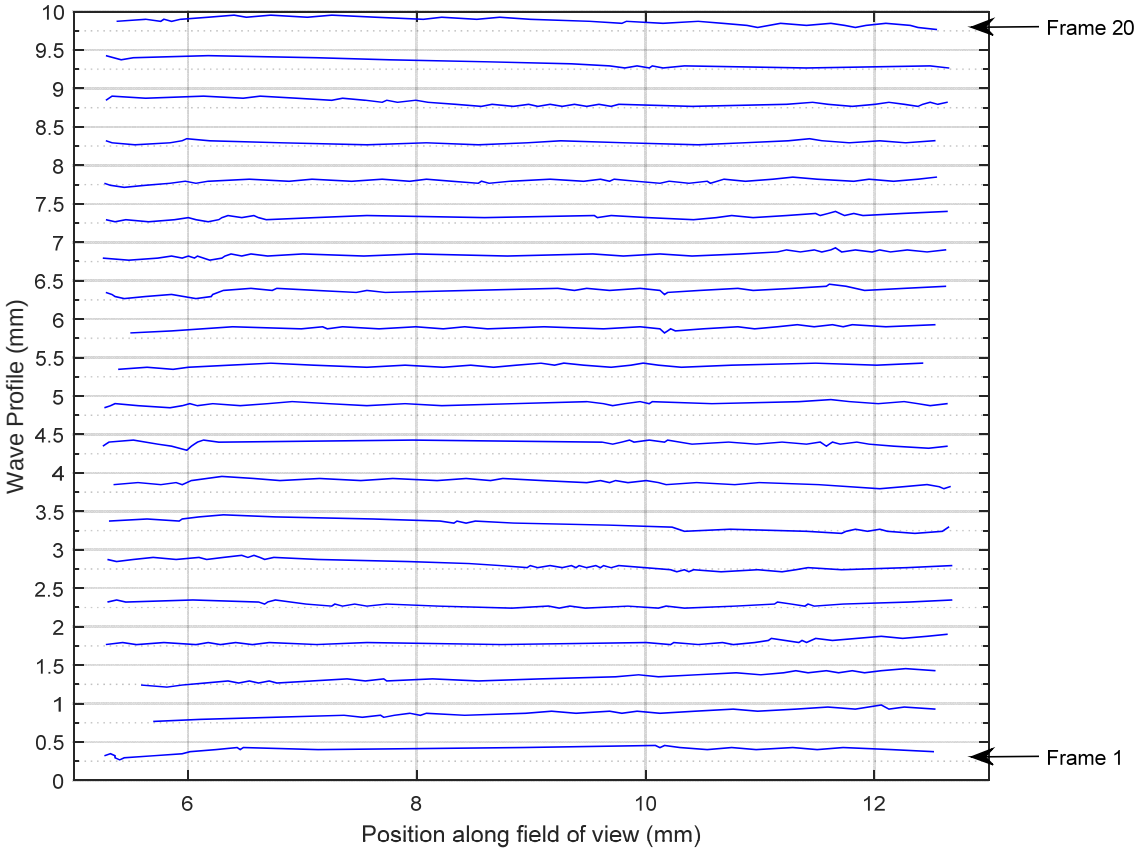

Fig. A38 Liquid flow condition 2, 40mm from top of column

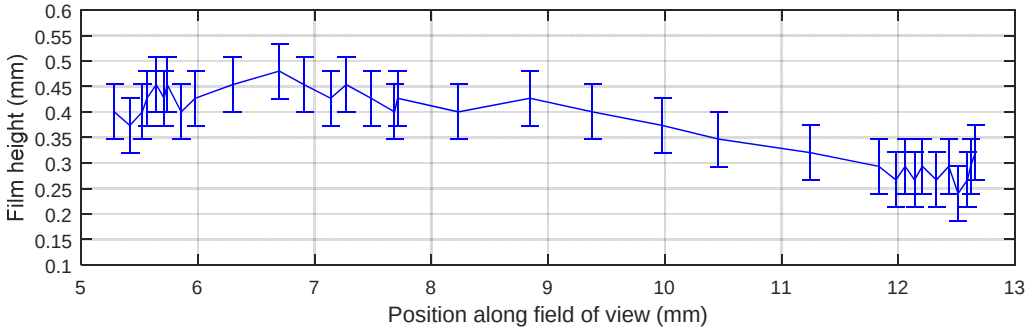

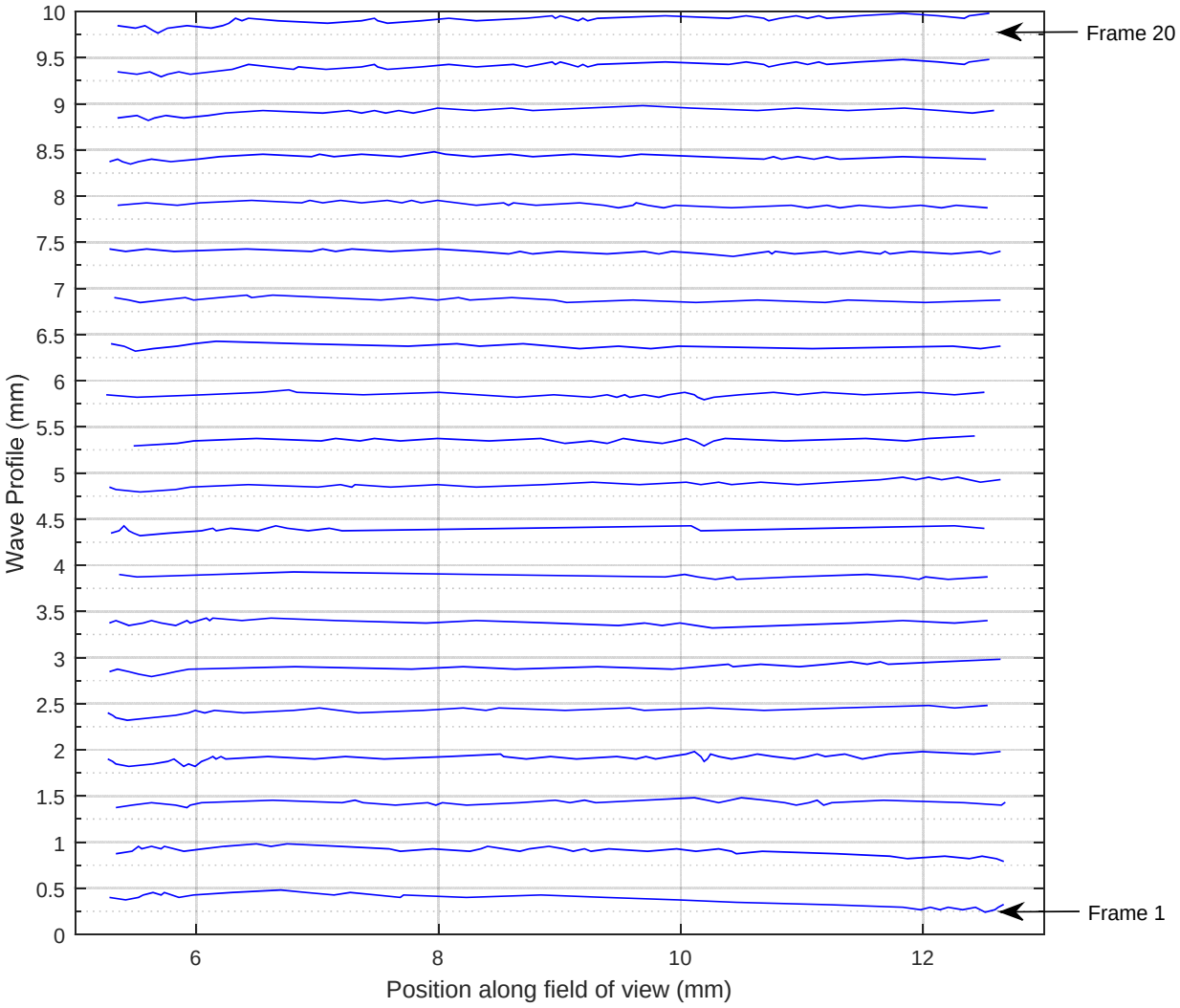

Fig. A39 Liquid flow condition 3, 40mm from top of column

A5.2 80mm from top of column

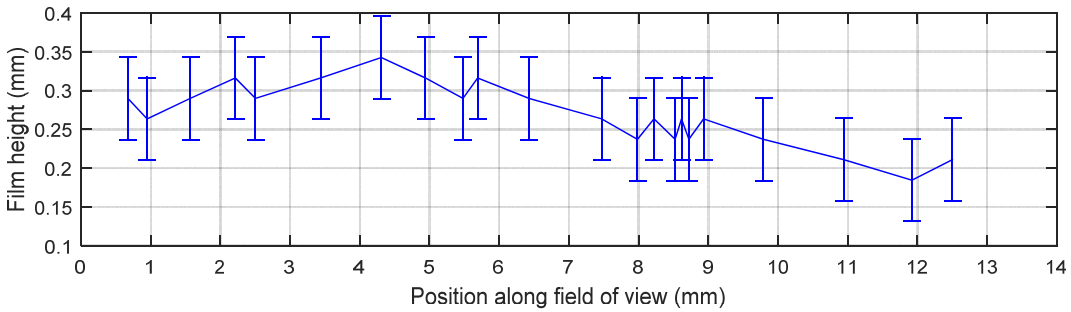

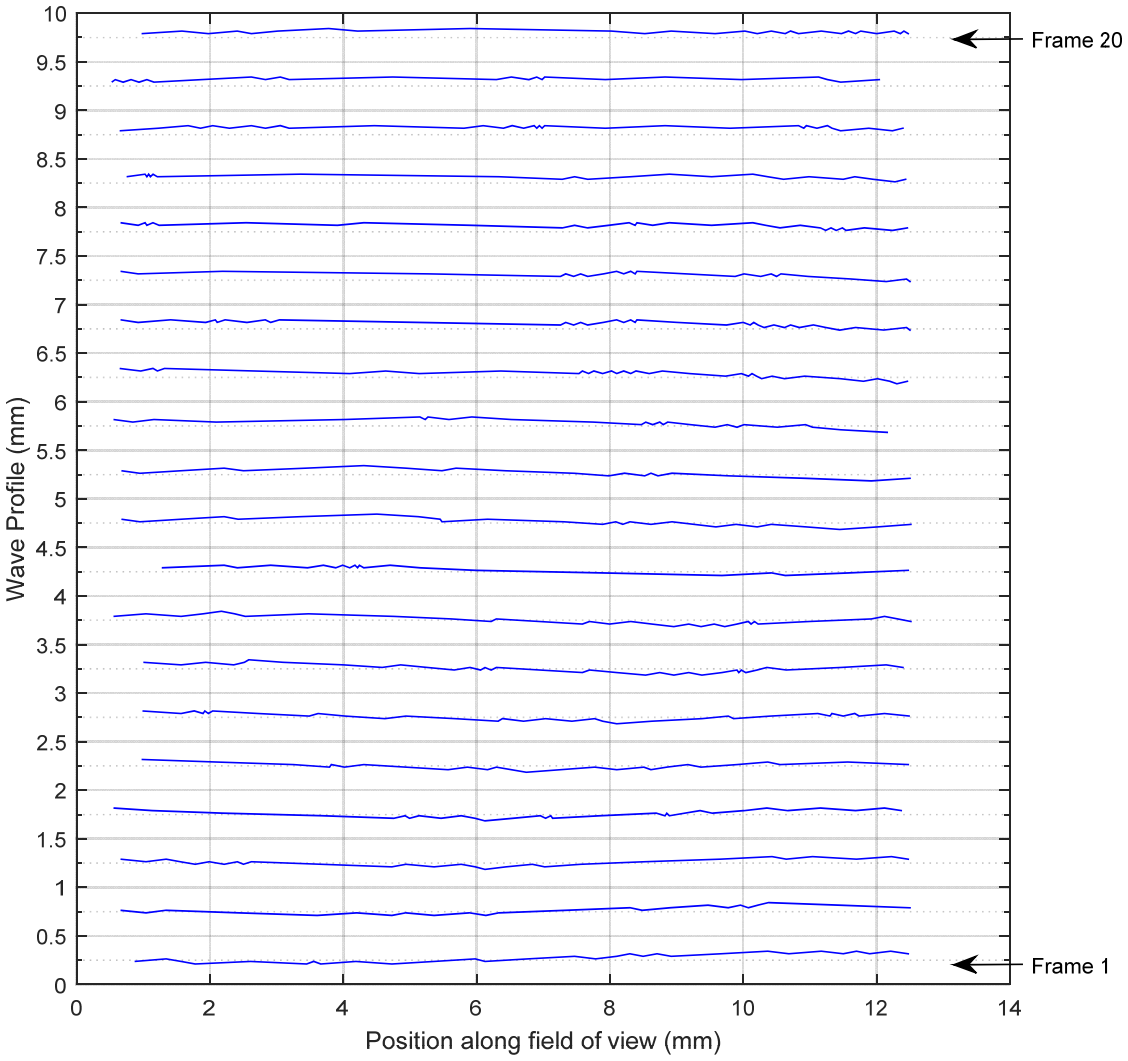

Fig. A40 Liquid flow condition 1, 80mm from top of column

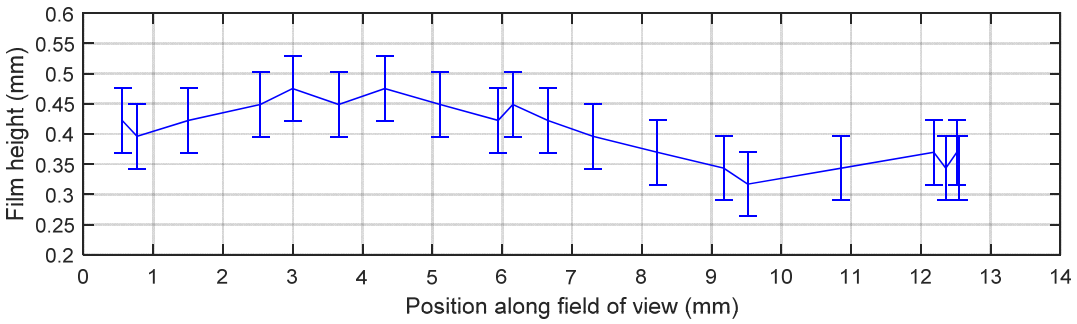

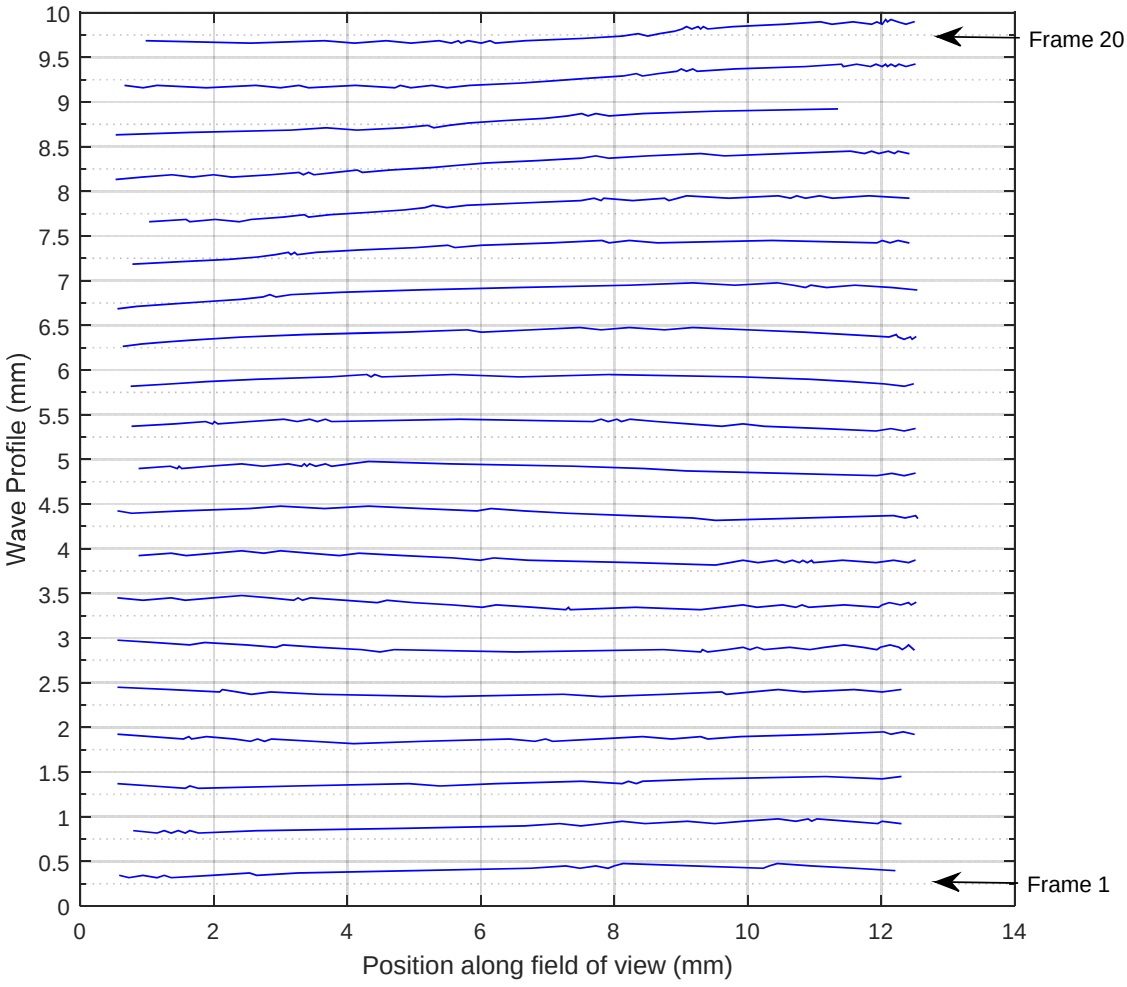

Fig. A41 Liquid flow condition 2, 80mm from top of column

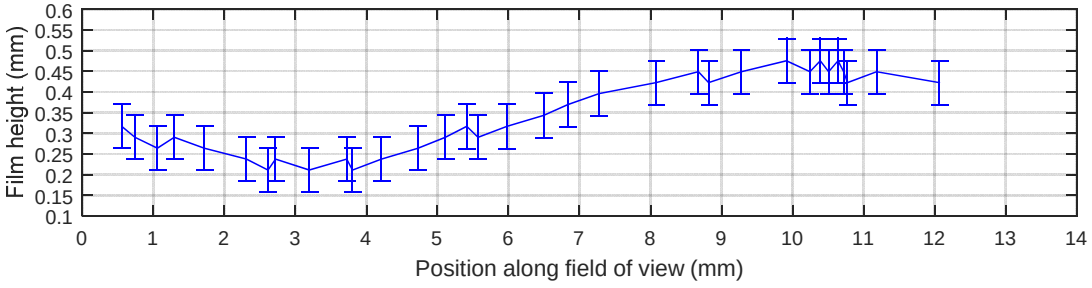

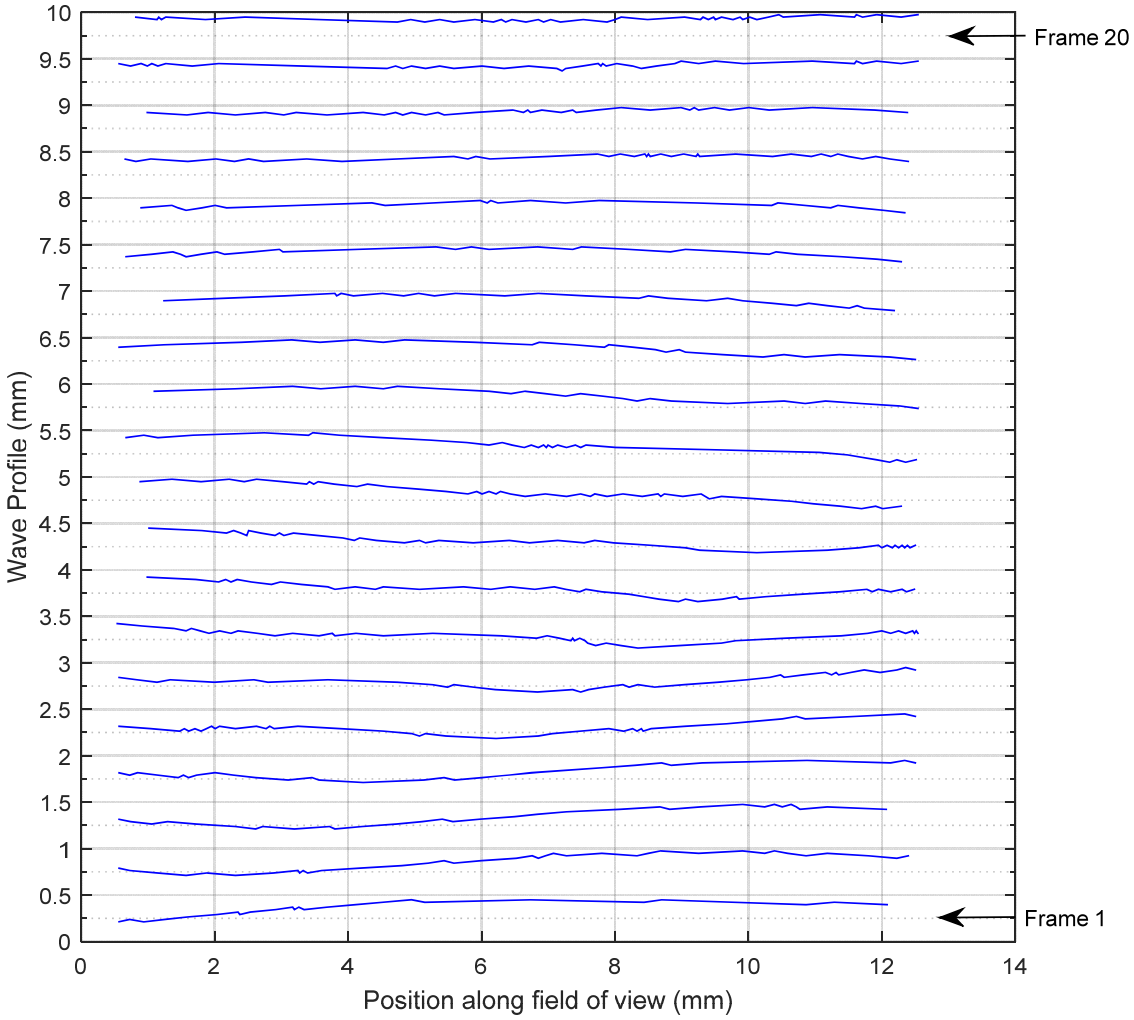

Fig. A42 Liquid flow condition 3, 80mm from top of column

A.5.3 120mm from top of column

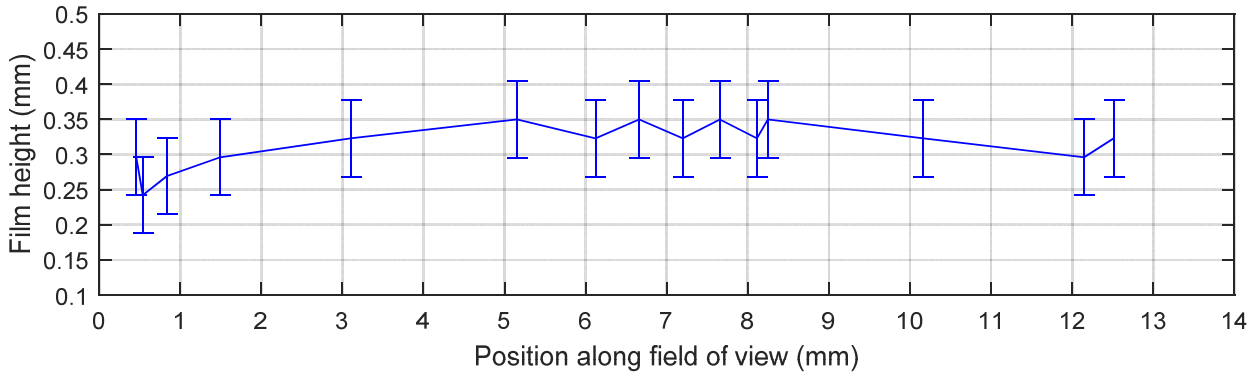

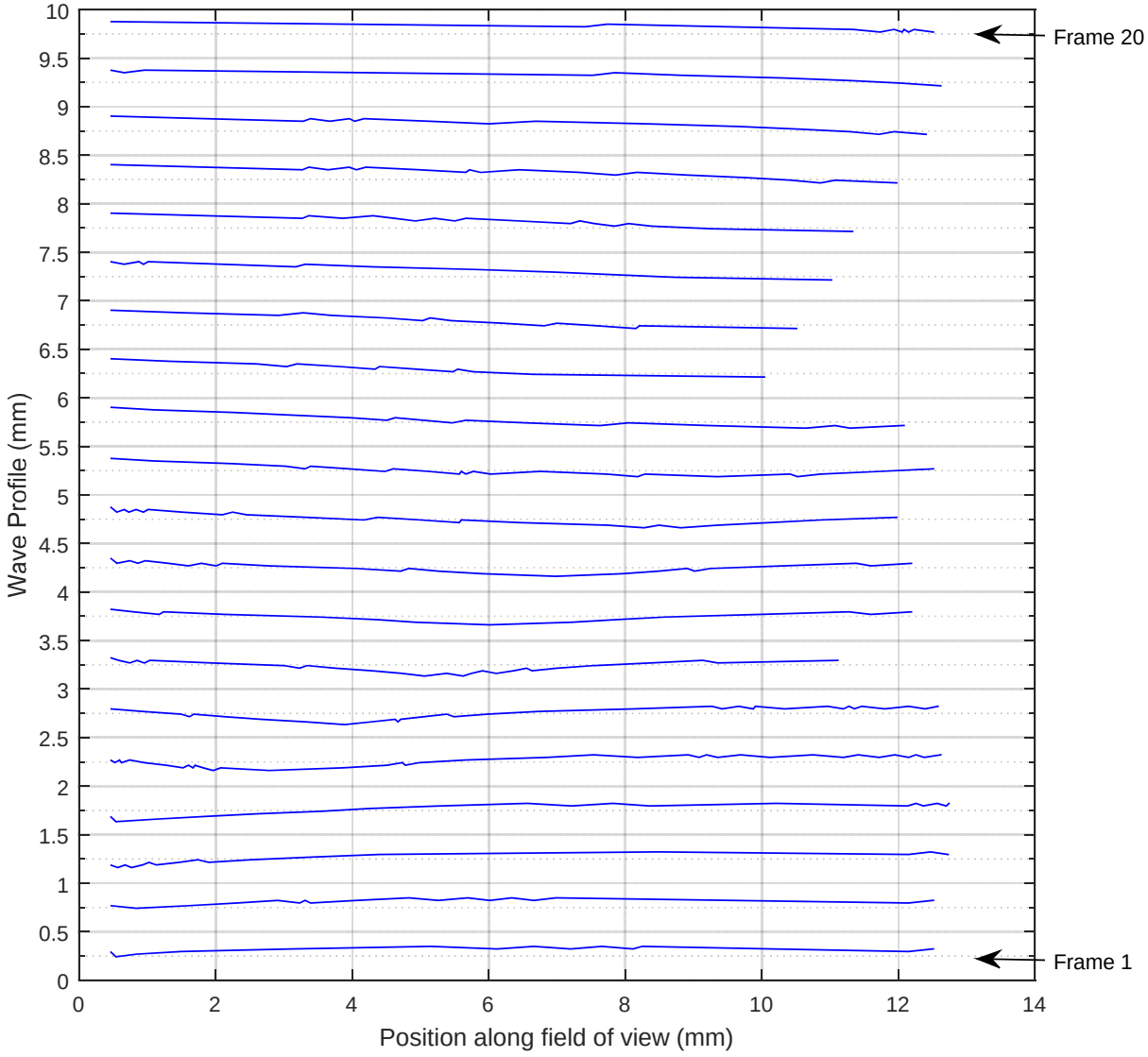

Fig. A43 Liquid flow condition 1, 120mm from top of column

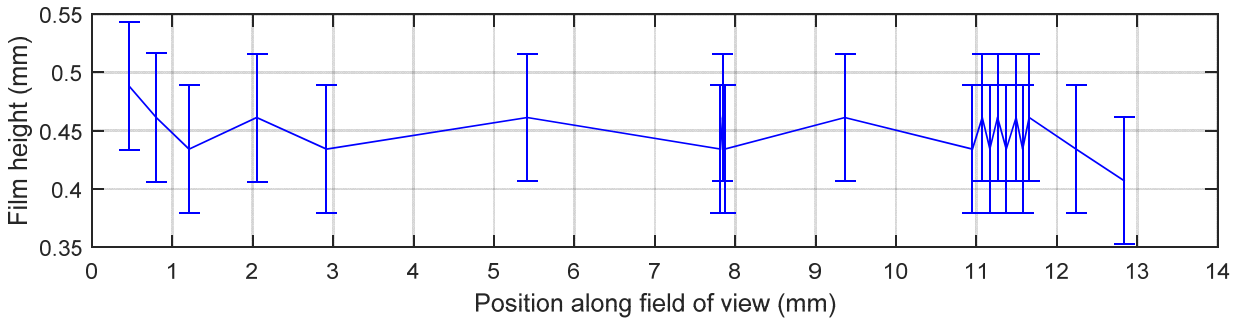

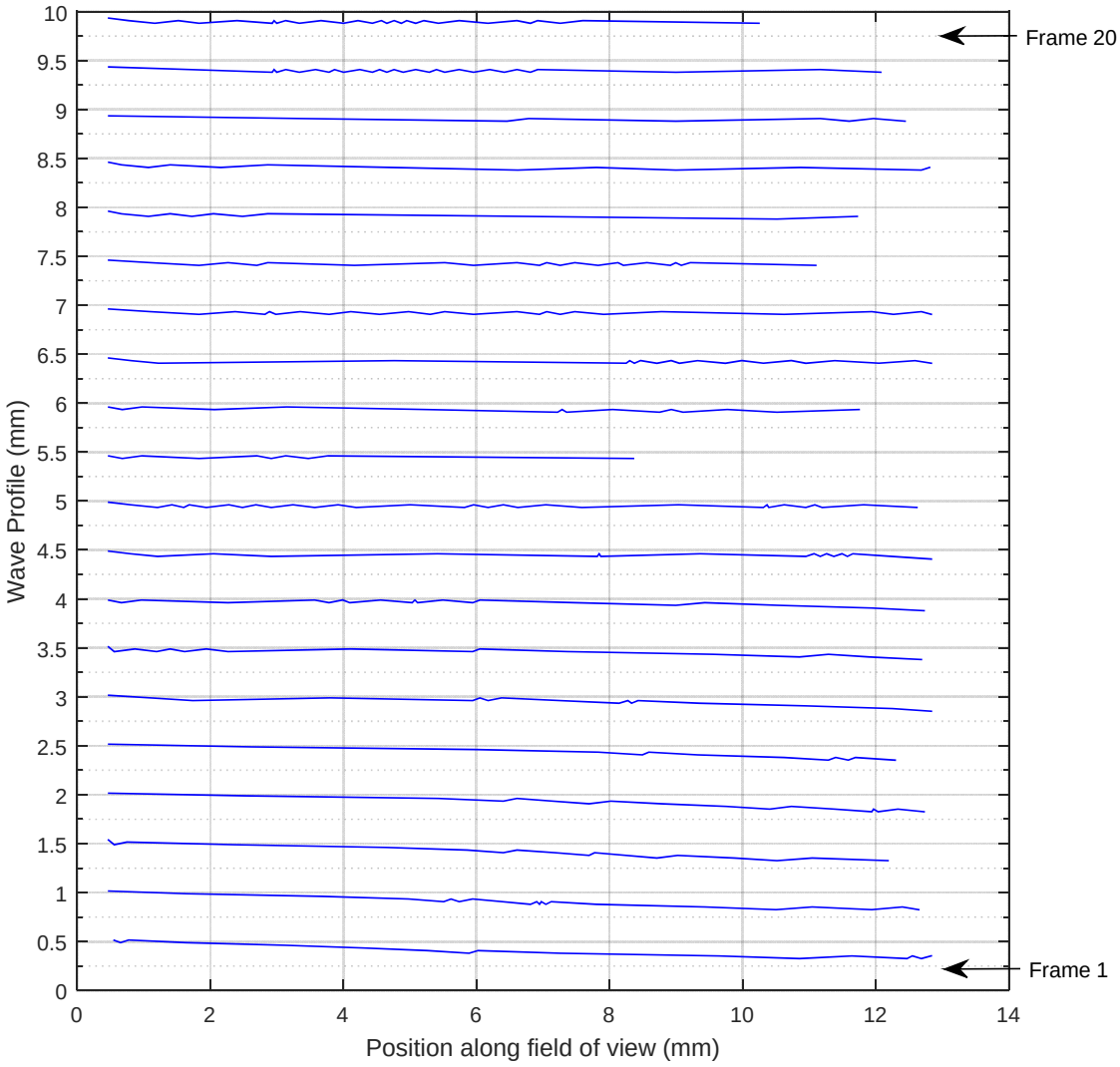

Fig. A44 Liquid flow condition 2, 120mm from top of column

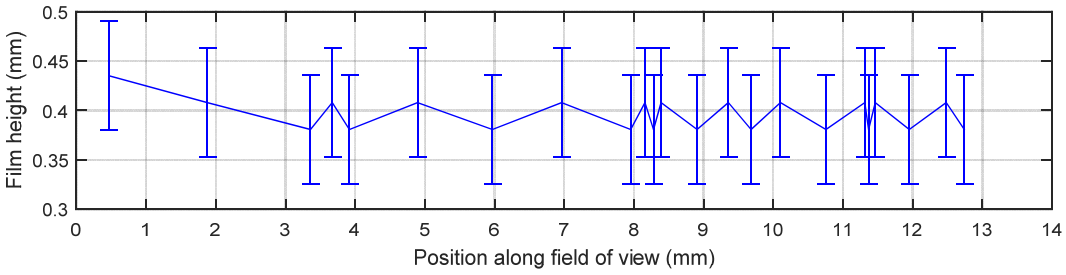

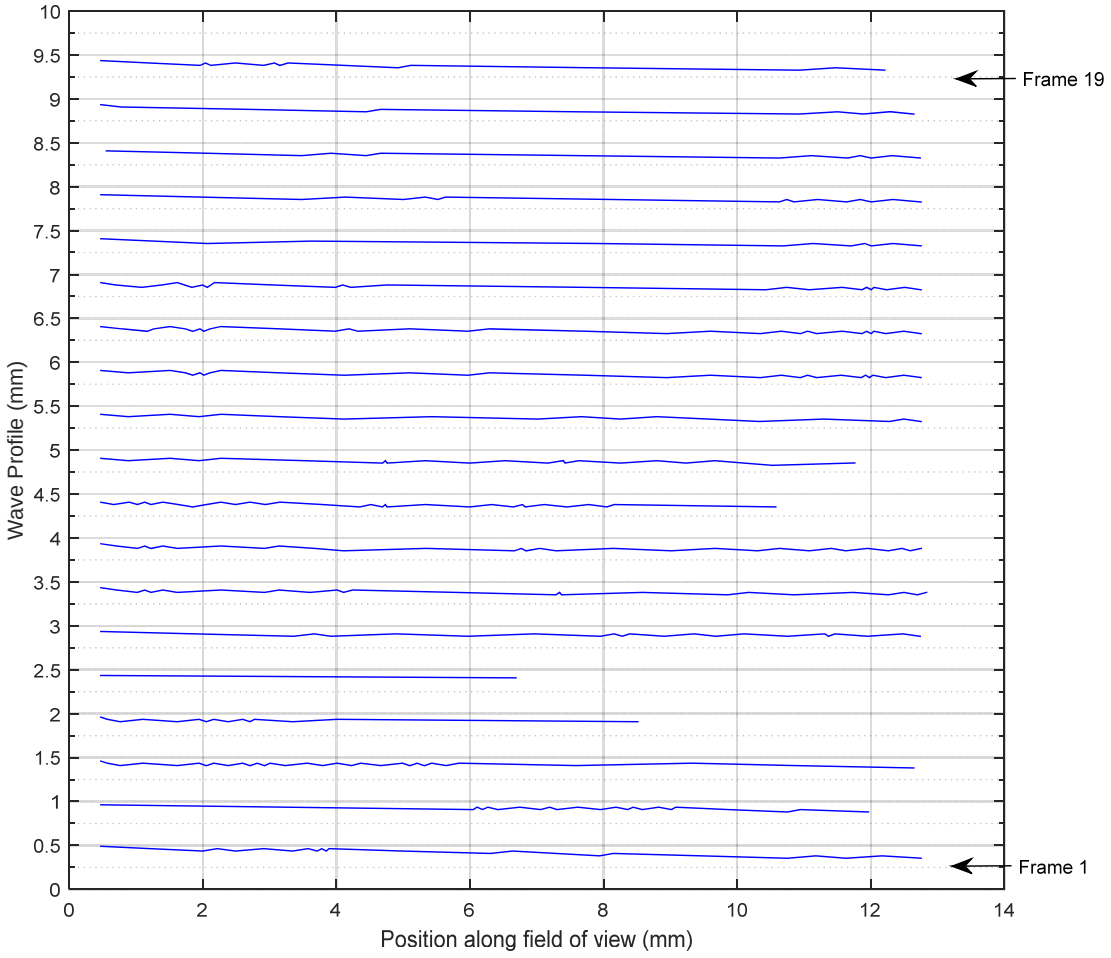

Fig. A45 Liquid flow condition 3, 120mm from top of column

Appendix B. Empirical coefficients for equation 4.17 (Jayarathna, 2013)

Coefficient	Value
p00	0.08788
p10	-0.4072
p01	-0.00002419
p20	0.8929
p11	0.002868
p02	-0.000000183
p30	0.1583
p21	-0.006328
p12	-0.000004862
p40	0.02552
p31	-0.0003935
p22	0.00001094

Table B1 Empirical coefficients for determination of loaded MEA solution surface tension

Appendix C. List of Symbols

a	Amplitude	(mm)
a_{eff}	Effective interfacial area for mass transfer	(m^2)
c	Concentration	(mol/l)
ΔC	Solvent CO_2 absorption capacity	(mol CO_2/kg solvent)
c_v	Coefficient of variation	(%)
d	diameter	(m)
d_{pix}	distance per pixel	(mm/pixel)
D	Diffusion coefficient	(m^2/s)
D_h	Hydraulic diameter	(m)
e	Euler's number	(-)
E	Reaction enhancement factor	(-)
f	Frequency	(waves/s)
FOV_v	Vertical field of view	(mm)
g	Acceleration due to gravity	(m/s^2)
G	Gas flow rate	(Nm^3/hr)
h	height	(m)
H	Henry's Constant	($mol/m^3 \cdot Pa$)
Ha	Hatta number	(-)
ΔH	Enthalpy of absorption	(kJ/mol)
k_2	Reaction rate constant	($mol^{1-(m+n)} \cdot l^{(m+n)-1} \cdot s^{-1}$)
k_g	Gas phase mass transfer coefficient	($mol/s \cdot Pa \cdot m^2$)
k_g'	Liquid phase mass transfer coefficient (gas phase units)	($mol/s \cdot Pa \cdot m^2$)
K_G	Overall mass transfer coefficient	($mol/s \cdot Pa \cdot m^2$)
Ki	Dimensionless kinetic parameter	(-)
k_L	Liquid side mass transfer coefficient	(m/s)
k_L^0	Physical liquid side mass transfer coefficient	(m/s)
L	Solvent flow rate	(l/hr)
L/G	Liquid/Gas flow ratio	(l/Nm^3)
L_h	Hydrodynamic entrance length	(m)
M	Molar mass	(kg/mol)
N	Flux	($mol/s \cdot m^2$)
$\dot{N}$	Molar flow rate	(mol/hr)
OD	Outer diameter	(m)
P	Pressure	(Pa)
q	Mass-specific heat duty	(GJ/t)
Q	Steam flow rate	(kg/hr)
Q_l	Volumetric liquid flow rate	(m^3/s)
r	Radius	(m)
R	Ideal gas constant	($J/K \cdot mol$)
Re	Reynolds number	(-)
S	Thickness of stagnant or semi-stagnant pool	(m)
STDEV	Standard deviation	(-)
t	Time	(s or min as specified)
T	Temperature	(K or ^oC as specified)
v	velocity	(m/s)
W	Channel width	(m)
x	x-position	(pixels)
X	mole fraction	(-)
xsect	Cross-sectional area	(m^2)

Greek Letters

α	CO_2 loading	(mol CO_2/mol MEA)
β	Channel angle	(^{o})
η	CO_2 capture rate	(%, mass basis)
δ	Film thickness	(m)
ν	Kinematic viscosity	(m^2/s)
μ	Dynamic viscosity	(Pa/s)
ρ	Density	(kg/m^3)
σ	Surface tension	(mN/m)
λ	Wavelength	(m)
ω	Wave growth rate	(-)
φ	Volume fraction	(-)

Indices

*	Equilibrium
‾	Average
abs	Absorption
AI	Reactant A at interface
AL	Reactant A in liquid phase
CO_2	Carbon dioxide
chamber	Contact chamber
column	Wetted-wall column
film	Liquid film
g	Gas phase
l	Liquid phase
laminar	Laminar flow regime
lean	Lean solvent
max	Maximum
MEA	Monoethanolamine
min	Minimum
N_2	Nitrogen
reb	Reboiler
ref	Reference
rich	Rich solvent
sens	Sensible
setpt	Setpoint
spat	Spatial
temp	Temporal
turbulent	Turbulent flow regime
vap	Vapourisation
wave	Single wave